

STRESS CORROSION CRACKING—THE SLOW STRAIN-RATE TECHNIQUE

A symposium sponsored by
ASTM Committee G-1 on Corrosion of
Metals in cooperation with the
National Association of Corrosion
Engineers TPC Committee T-3E on
Stress Corrosion Cracking of Metallic
Materials

AMERICAN SOCIETY FOR
TESTING AND MATERIALS
Toronto, Canada, 2-4 May 1977

ASTM SPECIAL TECHNICAL PUBLICATION 665
G. M. Ugiansky, National Bureau of Standards,
and J. H. Payer, Battelle Columbus
Laboratories, editors

List price \$39.75
04-665000-27



AMERICAN SOCIETY FOR TESTING AND MATERIALS
1916 Race Street, Philadelphia, Pa. 19103

Copyright © by American Society for Testing and Materials 1979
Library of Congress Catalog Card Number: 78-68418

NOTE

**The Society is not responsible, as a body,
for the statements and opinions
advanced in this publication.**

Foreword

The symposium on Stress Corrosion Cracking—The Slow Strain-Rate Technique was held 2-4 May 1977 in Toronto, Canada. The symposium was sponsored by ASTM Committee G-1 on Corrosion of Metals in cooperation with the National Association of Corrosion Engineers TPC Committee T-3E on Stress Corrosion Cracking of Metallic Materials. G. M. Ugiansky, National Bureau of Standards, represented ASTM Committee G-1, and J. H. Payer, Battelle Columbus Laboratories, represented NACE Committee T-3E. Ugiansky and Payer also served as editors of this publication.

Related ASTM Publications

**Intergranular Corrosion of Stainless Alloys, STP 656 (1978), \$24.00,
04-656000-27**

Stress Corrosion—New Approaches, STP 610 (1976), \$43.00, 04-610000-27

**Manual of Industrial Corrosion Standards and Control, STP 534 (1974),
\$16.75, 04-534000-27**

A Note of Appreciation to Reviewers

This publication is made possible by the authors and, also, the unheralded efforts of the reviewers. This body of technical experts whose dedication, sacrifice of time and effort, and collective wisdom in reviewing the papers must be acknowledged. The quality level of ASTM publications is a direct function of their respected opinions. On behalf of ASTM we acknowledge their contribution with appreciation.

ASTM Committee on Publications

Editorial Staff

Jane B. Wheeler, *Managing Editor*
Helen M. Hoersch, *Associate Editor*
Ellen J. McGlinchey, *Senior Assistant Editor*
Helen P. Mahy, *Assistant Editor*

Contents

Introduction	1
BACKGROUND AND INTERPRETATION OF THE SLOW STRAIN-RATE TEST TECHNIQUE	
Development of Strain-Rate Testing and Its Implications— R. N. PARKINS	5
Discussion	24
The Role of Film Rupture During Slow Strain-Rate Stress Corrosion Cracking Testing—R. B. DIEGLE AND W. K. BOYD	26
Anodic Dissolution and Crack Growth Rate in Constant Strain-Rate Tests at Controlled Potentials—M. HISHIDA, J. A. BEGLEY, R. D. MCCRIGHT, AND R. W. STAEHLE	47
Discussion	60
Evaluation of Slow Strain-Rate Stress Corrosion Tests Results— J. H. PAYER, W. E. BERRY, AND W. K. BOYD	61
Discussion	75
SLOW STRAIN-RATE TECHNIQUE FOR SPECIFIC ENVIRONMENTS AND APPLICATION	
Slow Strain-Rate Technique: Application to Caustic Stress Corrosion Cracking Studies—G. J. THEUS AND J. R. CELS	81
A Review of the Constant Strain-Rate Stress Corrosion Cracking Test—C. D. KIM AND B. E. WILDE	97
Discussion	112
Slow Strain-Rate Stress Corrosion Testing of Metals in Gaseous Atmospheres at Elevated Temperatures—G. M. UGIANSKY AND C. E. JOHNSON	113
Discussion	130
Slow Strain-Rate Testing in High Temperature Water— H. D. SOLOMON, M. J. POVICH, AND T. M. DEVINE	132
Dynamic Straining Stress Corrosion Test for Predicting Boiling Water Reactor Materials Performance—W. L. CLARKE, R. L. COWAN, AND J. C. DANKO	149
Discussion	168
Slow Strain-Rate Stress Corrosion Testing for Liquid Metal Fast Breeder Reactor Steam Generator Applications—M. E. INDIG	170
Stress Corrosion Cracking Test with Slow Strain Rate and Constant Current—R. S. ONDREJCIN	203
Discussion	221

Application of Slow Strain-Rate Technique to Stress Corrosion Cracking of Pipeline Steel— J. H. PAYER, W. E. BERRY, AND R. N. PARKINS	222
SLOW STRAIN-RATE TEST TECHNIQUE FOR SPECIFIC METALS AND ALLOYS	
Propagation of Stress Corrosion Cracks under Constant Strain-Rate Conditions— J. C. SCULLY	237
Discussion	252
Slow Strain-Rate Stress Corrosion Testing of Aluminum Alloys— G. M. UGIANSKY, C. E. JOHNSON, D. S. THOMPSON, AND E. H. GILLESPIE	254
Effect of Oxyanions and Chloride Ion on the Stress Corrosion Cracking Susceptibility of Admiralty Brass in Nonammoniacal Aqueous Solutions— A. KAWASHIMA, A. K. AGRAWAL, AND R. W. STAEHLE	266
Slow Strain-Rate Technique and Its Applications to the Environmental Stress Cracking of Nickel-Base and Cobalt-Base Alloys— A. I. ASPHAHANI	279
Stress Corrosion Cracking Susceptibility Index, I_{sc}, of Austenitic Stainless Steels in Constant Strain-Rate Test— SEIZABURO ABE, MASAO KOJIMA, AND YUZO HOSOI	294
Some Aspects of the Stress Corrosion Testing of Austenitic, Martensitic, Ferritic-Austenitic and Ferritic Types of Stainless Steel by Means of the Slow Strain-Rate Method— A. J. A. MOM, R. T. DENCHER, C. J. V.D. WEKKEN, AND W. A. SCHULTZE	305
Detection of Heat Treatment Effects on Environmentally Induced Degradation of a Martensitic Stainless Steel and a Nickel-Base Alloy by the Slow Strain-Rate Method— P. SUERY	320
Validity of the Slow Straining Test Method in the Stress Corrosion Cracking Research Compared with Conventional Testing Techniques— H. BUHL	333
Comparative Findings Using the Slow Strain-Rate, Constant Flow Stress, and U-Bend Stress Corrosion Cracking Techniques— W. J. DANIELS	347
Some Comparisons of the Slow Strain-Rate Method with the Constant Strain and the Constant Load Methods of Stress Corrosion Testing— J. F. ANDREW, J. T. HERON, AND J. STRINGER	362
SLOW STRAIN-RATE TEST TECHNIQUE EQUIPMENT AND PROCEDURES	
Design and Construction of an Inexpensive Multispecimen Slow Strain-Rate Machine— W. T. NUTTER, A. K. AGRAWAL, AND R. W. STAEHLE	375
Discussion	385

Multispecimen Test Facility for High Temperature, High Pressure Slow Strain-Rate Testing—F. F. LYLE, JR. AND E. B. NORRIS	388
Discussion	398
Portable Slow Strain-Rate Stress Corrosion Test Device—F. HAUSER, S. R. ABBOTT, I. CORNET, AND R. S. TRESEDER	399
A Bursting Tube, Slow Strain-Rate Stress Corrosion Test— BRYAN POULSON	408
General Discussion—Historical Note on the Slow Strain Testing of Solder—R. S. TRESEDER	425

SUMMARY

Summary	431
Index	435

Introduction

This symposium on the slow strain-rate technique (SSRT) for studying the stress corrosion behavior of metals was organized to assemble and make available the data, conclusions, experiences, and theories derived from the use of this test method. Use of the slow strain-rate technique has proliferated from use by only a few laboratories a decade ago to rather widespread use today by a large number of workers. Because of the rapid increase in use and interest in the SSRT, the need for a comprehensive treatment of the subject was recognized by the American Society for Testing and Materials (ASTM) and National Association of Corrosion Engineers (NACE) Committees concerned with stress corrosion cracking (SCC), Committees G-1 and T-3E, respectively.

The proceedings provide a convenient introduction for those unfamiliar with slow strain-rate tests for SCC and relevant information on the application of the technique for specific alloys of chemical environments. For those familiar with the technique a data base is also provided so that the results of slow strain-rate tests can be compared with results of other SCC tests, for example, constant load tests and constant strain tests. Based on the information presented, a greater appreciation can be gained for the strengths and limitations of the technique, and it can be used with the appropriate confidence or caution.

The symposium was organized to address from several vantage points the use of the slow strain-rate technique. A series of papers is concerned with the stress corrosion cracking process and the relationship of the slow strain-rate technique to relevant phenomena, for example, anodic dissolution, and passive film breakdown and repassivation. Interpretation of results is the primary topic of several papers. Other papers discuss the application of the SSRT to specific alloys or environments. In addition, several papers focus on equipment and procedures used in the test.

With the publication of the proceedings it is noted that the slow strain-rate technique can move more rapidly from the state of a "new" test method to

2 STRESS CORROSION CRACKING

that of a widely accepted and understood tool for the study of SCC. At the present time both the ASTM and the International Standards Organization (ISO) Committees concerned with corrosion are working on a standard test method for use of SSRT in stress corrosion testing.

The editors would like to specifically acknowledge the assistance of several contributors to this conference and proceedings. Professor R. H. Parkins is gratefully acknowledged for his contributions to this symposium as a keynote speaker, session chairman, and reviewer but more importantly for his leadership role in the development and application of slow strain rate technique for SCC. Dr. B. F. Brown, ASTM's publication committee representative, provided helpful guidance and support as did the ASTM staff and particularly Miss Jane B. Wheeler.

G. M. Ugiansky

National Measurement Laboratory, National
Bureau of Standards, Washington, D.C.
20234; editor.

J. H. Payer

Corrosion and Electrochemical Technology
Section, Battelle Columbus Laboratories,
Columbus, Ohio 43201; editor.

Background and Interpretation of the Slow Strain-Rate Test Technique

R. N. Parkins¹

Development of Strain-Rate Testing and Its Implications

REFERENCE: Parkins, R. N., "Development of Strain-Rate Testing and Its Implications," *Stress Corrosion Cracking—The Slow Strain-Rate Technique*, ASTM STP 665. G. M. Ugiansky and J. H. Payer, Eds., American Society for Testing and Materials, 1979, pp. 5-25.

ABSTRACT: The application of slow dynamic straining to specimens to facilitate stress corrosion cracking (SCC) now has been in use for more than a decade, and the test is beginning to emerge as one that has much more relevance than the rapid sorting test to which its early use was related. The importance of creep effects in constant load testing is considered, and it is shown that reasonable predictions of threshold stresses for SCC can be made from relevant creep data and that the effects of prior creep upon the incidence of cracking and of the phenomenon of non-propagating cracks below the threshold stress are all in agreement with the concept of the crack tip strain rate playing a major role, even under constant load conditions. The reasonable correlation between appropriate strain rate and constant load tests is therefore not surprising, nor is the reduction in threshold stress by dynamic straining, with or without cyclic loading, over that observed for constant loads.

KEY WORDS: stress corrosion cracking, strain rate, creep properties, nonpropagating cracks, threshold stress, corrosion fatigue, cyclic loads.

In most laboratory corrosion experiments an attempt is made to obtain data in a relatively short time, frequently by adopting some approach that increases the severity of the test. In stress corrosion testing [*I*],² this has usually been done by increasing the relative aggressiveness of the environment by altering its composition, temperature, or pressure; by stimulating the corrosion reactions galvanostatically or potentiostatically; by increasing the relative susceptibility of the alloy to cracking through changes in structure or composition; or by introducing a notch or precrack into the specimen. The application of slow dynamic straining to stress corrosion specimens comes into this category also in that it frequently facilitates

¹Professor and head, Department of Metallurgy and Engineering Materials, The University, Newcastle upon Tyne, England.

²The italic numbers in brackets refer to the list of references appended to this paper.

cracking in circumstances where, at constant load or constant total strain, cracking is not observed, shows poor reproducibility, or takes a prohibitively long time. Stress corrosion crack velocities usually fall in the range from 10^{-6} to 10^{-9} m/s, depending upon the system of metal and environment involved. These velocities imply that failure in laboratory specimens of usual dimensions should occur in not more than a few days. This was found to be so for any stressing mode if the system is one in which stress corrosion cracks are readily initiated, but it is common experience to find that many specimens do not fail in very extended periods of testing, which then are usually terminated at some arbitrarily selected time. The consequences are that considerable scatter may be associated with replicate tests, and the arbitrary termination of the test leaves an element of doubt concerning the outcome if it had been allowed to continue to a longer time. Just as the use of fatigue precracked specimens assists in stress corrosion crack initiation, so apparently does the application of slow dynamic strain, which has the further advantage that the test is not terminated after some arbitrary time, since the conclusion is always achieved by the specimen fracturing and the criterion of cracking susceptibility is then related to the mode of fracture. Thus, in the form in which it is commonly employed the slow strain-rate method will usually result in failure in not more than a few days, either by ductile fracture or by stress corrosion cracking (SCC), according to the susceptibility towards the latter. Metallographic or other parameters then may be assigned in assessing the cracking response. The fact that the test concludes in this positive manner in a relatively short period of time constitutes one of its main attractions.

The development of constant strain-rate stress corrosion testing [2] in Newcastle in the early 1960s arose from experiments designed to test ideas put forward by Coleman et al [3] who used a constant rate of loading to determine the stress at which cracks were just detected when the specimen was examined optically at low magnifications. Their specimens were loaded at the given rate to some arbitrary maximum stress and then removed from the corrosion cell and examined. This cycle was repeated until cracks were observed. The modifications to this approach introduced in Henthorne's work [2] were to perform the tests continuously, that is, without interruption for examination, using a different method of assessing cracking propensity, and to replace the constant loading rate by a constant deflection rate, modifications that not only simplified the constant loading rate test but also overcame some of its disadvantages. Early use of the test was in providing data whereby the effects of such variables as alloy composition and structure [4,5] or electrochemical parameters [6], including inhibitive additions to cracking environments [7], could be assessed. In recent years, understanding of the implications of slow dynamic strain testing has developed, and it now appears that this type of test may have much more

relevance than just that of an effective, rapid, sorting test, a point returned to later.

The Test Method

The forms of the test used at Newcastle have been described elsewhere [8]. It is sufficient here to state that they involve the use of plain, waisted, tension specimens strained in relatively stiff frame machines, which are also used in testing fatigue precracked specimens, although the latter are tested also in cantilever bend in machines that allow the lever arm to be deflected, and hence the plastic zone strained, over a range of rates. The choice of the latter is critical, and it is important to realize that the same strain rate does not produce the same response in all systems. Clearly, if the strain rate were too high, ductile fracture by void coalescence would occur before the necessary corrosion reactions could take place to promote SCC; or, with precracked specimens, K_{Ic} would be reached or plastic collapse would occur before SCC were initiated. However, it is also possible for the strain rate to be too low for SCC to be produced since the range of strain rates over which SCC is observed can vary from one system to another. For many systems it has been found that a tensile strain rate in the region of 10^{-5} to 10^{-6} s⁻¹ will promote SCC, but the absence of cracking in tests conducted at such rates should not be taken as an indication of immunity to cracking for a given system until tests have also been conducted at faster and slower strain rates. It is important to remember also that once necking begins in a ductile metal stressed in tension the effective strain rate in the necked region may increase by as much as an order of magnitude. This can cause the strain rate to move into, or out of, the critical range. This point may be particularly important when the strain rate is being varied from test to test. It may lead to a situation where precracked rather than plain specimens are more appropriate, since with the former the strain rate will remain sensibly constant if the plastic zone size remained the same. This requirement may be met easier with a precracked rather than a plain specimen.

The method of assessing the results where SCC is observed can be by a variety of parameters. The usual means of indicating the severity of SCC from nominally static tests, by the time to failure at a given stress or the threshold stress or stress intensity if tests are conducted over a range of initial stresses, may appear inappropriate in constant strain-rate tests. An examination of the test however indicates a number of readily measurable and quantifiable parameters that can be used in expressing SCC susceptibility, and some of these are related to those used in static tests. The effects of SCC are reflected in the load-deflection curve that may be recorded during a strain-rate test. Since stress corrosion failure is usually

8 STRESS CORROSION CRACKING

associated with relatively little macroscopic plastic deformation during crack propagation, a comparison of the load-deflection curves for specimens with and without SCC will usually reveal marked differences. Figure 1 shows such curves, from which it is apparent that not only is the elongation to fracture dependent upon the presence or otherwise of stress corrosion cracks, but so also is the maximum load achieved. The latter may be used therefore for expressing crack susceptibility, as may also the usual measures of ductility, elongation, or reduction of area. However, the variations in these quantities in circumstances of varying cracking severity are not always large enough for significant distinction to be made and measurements of ductility are not invariably easy, especially if the final fracture of the specimen does not follow a simple path and the fitting together of the broken pieces is not easy. In such cases a combination of load and ductility may provide a useful basis of comparison, since the area under the load-extension curve, as is apparent from Fig. 1, can be used for assessing cracking susceptibility [9].

The fact that the elongation to fracture varies with the severity of SCC means that, for a constant elongation rate, the time to failure should also vary with severity of cracking. This is found to be so and the time to failure in constant strain rate tests, which is a quantity usually easily measured, probably has as much significance as it does in any other type of stress corrosion test. Consequently, time to failure is frequently used for assessing constant strain-rate test results, the latter usually being normalized

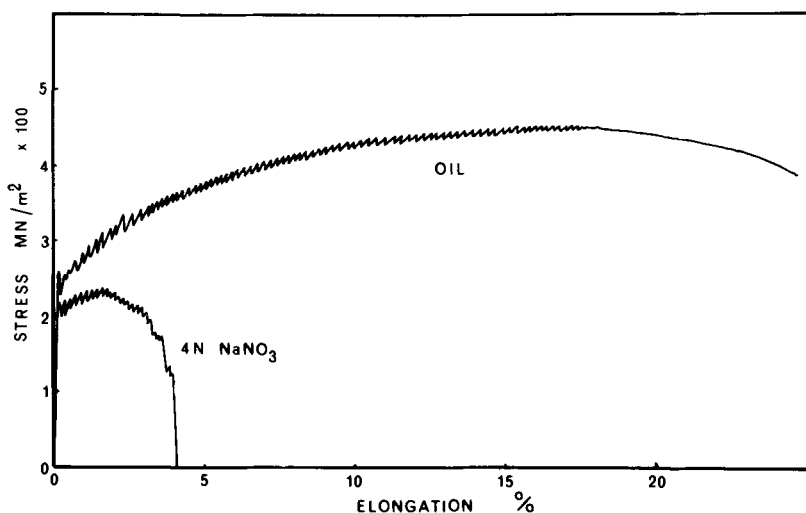


FIG. 1—Nominal stress-elongation curves for C-Mn steel in constant strain-rate tests in boiling 4 N sodium nitrate (NaNO_3) and in oil at the same temperature.

by dividing by the time to failure at the same strain rate in a test in an inert environment at the same temperature as that employed in the stress corrosion test, so that increasing susceptibility is marked by increasing departure of this ratio from unity.

The measurement of stress corrosion crack velocities, especially on precracked specimens, has been used more often in the last decade for assessing cracking susceptibility. Crack velocities may be derived from slow strain rate tests, using, for example, the potential drop method with precracked specimens in which the resistivity of the uncracked portion of the specimen is monitored as the crack extends, but also by using simple optical methods on initially plain specimens. The latter usually develop many cracks during a stress corrosion test and sectioning of the fractured specimen along a diametral plane and microscopical measurement of the largest detectable crack, and its division by the test time gives an average crack velocity that is usually in good agreement with velocities measured by more sophisticated methods [10].

Comparison with Results from Other Test Methods

For the slow strain-rate method to have credence, it is not unreasonable to expect that it should give results for cracking propensities that are comparable with those obtained by other methods, for given systems of metal and environment. Figure 2 shows some results from tests upon some low alloy ferritic steels immersed in boiling 4 N ammonium nitrate (NH_4NO_3), the various alloying elements producing a range of cracking susceptibilities, as measured by the threshold stress determined from constant strain tests. To allow for the influence of the alloying upon the mechanical properties of the steels, the stress corrosion test results have been normalized by dividing the threshold stress for each steel by its yield strength. The same steels were also tested in dynamic strain tests in 4 N NH_4NO_3 and silicone oil at the same temperature, so the cracking susceptibility may be expressed as a time to failure ratio. While the results shown in Fig. 2 indicate some scatter, the general trend is clear in that the results from the two types of tests show reasonable agreement in placing the steels in essentially the same order of merit, particularly so when the differences are relatively large.

An example of the use of strain-rate testing in comparing the effects of structural variations in a carbon-manganese (C-Mn) steel upon SCC propensities provides additional evidence of the correspondence between results from this method of testing and that involving constant strain [11]. Figure 3 shows the initial applied stress-time to failure curves for a steel after quenching and tempering at various temperatures, while Fig. 4 shows the time to failure ratios from slow strain-rate tests upon similarly treated specimens tested in the same environment. A comparison of these

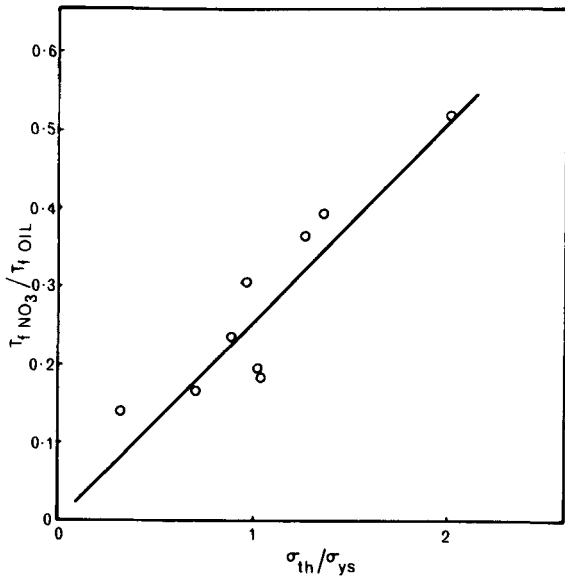


FIG. 2—Relationship between time to failure ratio from slow strain-rate tests and the normalized threshold stress from constant strain tests on low alloy ferritic steels in boiling 4 N NH_4NO_3 .

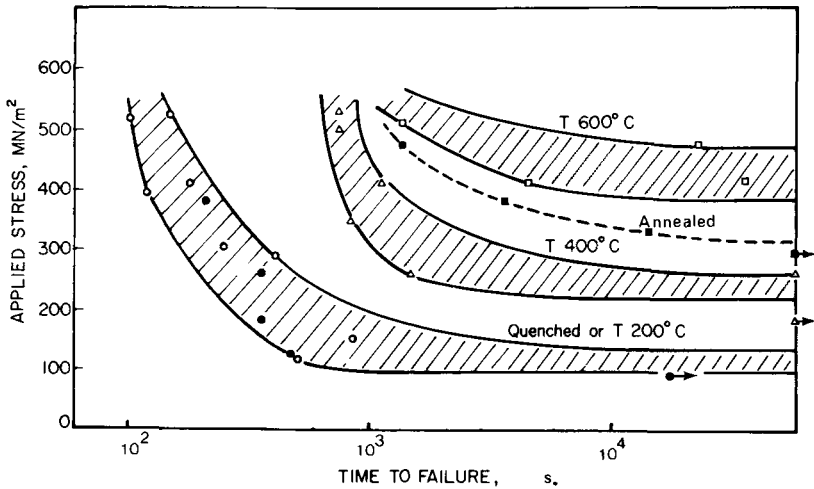


FIG. 3—Initial applied stress-time to failure curves in constant strain tests upon a C-Mn steel in a boiling nitrate solution after various heat treatments [11].

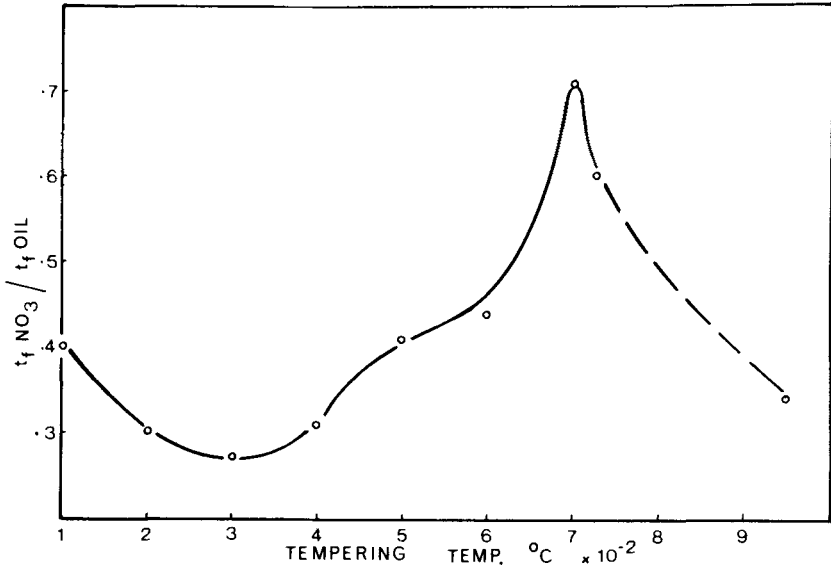


FIG. 4—Slow strain-rate test results upon a C-Mn steel in a boiling nitrate solution after various heat treatments for comparison with Fig. 3 [11].

figures shows that essentially the same susceptibility trends are observed as a function of heat treatment for both types of test.

Of course, it is also possible to produce results that do not show good correlation between the cracking propensities determined in constant strain rate and other methods of testing. For example, it is extremely difficult, and indeed sometimes impossible, to promote stress corrosion cracking in constant strain tests upon a carbon steel in boiling sodium hydroxide (NaOH), yet relatively easy to do so in constant strain-rate tests. But such results may be in fact no more than a demonstration of the importance of strain rate, as opposed to stress *per se*, in real situations and this, together with the reasonable correlation from tests where positive results are given by both the methods of testing being compared, suggest that strain rate may be significant in its own right.

Significance of Strain Rate in SCC

Relation to Constant Strain and Constant Load Tests

It may be thought that laboratory tests involving the pulling of specimens to failure at a slow strain rate shows little relation to the conditions in constant load or constant strain tests or to service failure conditions. In fact in nominally static laboratory tests or in service failures, crack

propagation also occurs under conditions of slow dynamic strain to a greater or lesser extent, depending upon the initial value of stress, the point in time at which a crack is initiated, and various metallurgical parameters that govern creep. Although creep is apt to be considered as a high temperature phenomenon in most engineering materials, it does occur at low temperatures and when any structure is loaded. The rate of creep diminishes due to exhaustion as time elapses after stress is applied, unless stress corrosion crack propagation results in an effective increase in stress that accelerates creep. It may be expected therefore that, if creep or strain rate is the controlling parameter in SCC, the cracking response will depend upon the delay time between the application of stress and the establishment of the electrochemical conditions for cracking.

Figure 5 refers to tests upon fatigue precracked specimens of a C-Mn steel loaded as cantilevers in a carbon trioxide-hydrocarbonate ($\text{CO}_3\text{-HCO}_3$) solution which, at appropriate potentials, promotes intergranular SCC in such steels. Measurement of the deflections of the loading beam as a function of time indicates the creep and cracking response of the specimen in the crack tip region. If the potential is established in the cracking range before or at the time of loading, the beam deflection responds in the

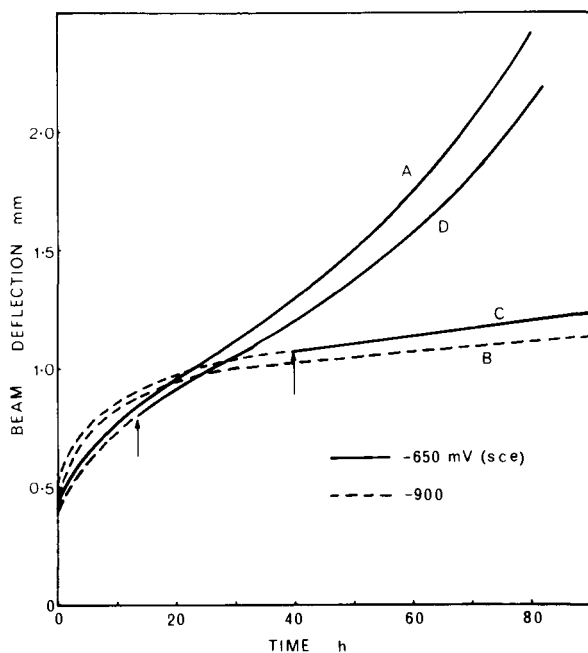


FIG. 5—Beam deflection-time curves for constant load cantilever beam tests upon a C-Mn steel in $1\text{ N Na}_2\text{CO}_3 + 1\text{ N NaHCO}_3$ at 75°C and the effects of cracking (-650 mV) and non-cracking potentials (-900 mV) [13].

manner shown in Curve A. The interpretation of the shape of this curve is that initially the beam deflection rate diminishes at a relatively rapid rate as the creep in the plastic zone at the crack tip tends to exhaustion. After a stress corrosion crack has been initiated and propagated to some extent the constant load condition leads to an increase in stress and additional creep, so that the beam deflection rate begins to accelerate under the joint actions of crack propagation and creep in the metal beyond the crack tip. If, for an identical stress intensity, the potential is not held in the SCC range, the beam deflection curve simply reflects the creep behavior of the specimen after loading, without the attendant complication of crack propagation. This is shown in Curve B in Fig. 5, so that SCC is reflected in the differences between Curves A and B. If an experiment were now being conducted in which the potential were initially held outside the cracking range, at -950 mV, for more than a day after the load was applied, and then the potential would be moved to a value (-650 mV) inside the SCC range the beam deflection curve (C in Fig. 5) indicates that SCC has not occurred, since it is essentially the same as that obtained when the potential is maintained at -950 mV throughout. Metallographic examination confirmed that no intergranular stress corrosion crack had propagated from the tip of the transgranular fatigue precrack, despite the fact that the stress intensity at the crack tip was essentially the same as that which had produced cracking in the test that produced Curve A. One obvious explanation of this result was that by the time the potential was changed to one that should promote cracking, the creep rate had diminished to a value below that which initiates or sustains cracking. A further experiment therefore was conducted in which the potential was changed from -950 to -650 mV before the creep rate had fallen to such a low value as that which obtained in the experiment that produced Curve C. As Curve D indicates, this resulted in a stress corrosion crack being propagated, as was confirmed by metallographic examination.

The results from this series of experiments conform with expectations if the controlling parameter in constant load tests is in fact the effective creep rate, but the result is not a peculiarity of this system. Thus, in constant load tests upon a magnesium-aluminum (Mg-Al) alloy immersed in a $\text{CrO}_4\text{-Cl}$ solution [12], the threshold stress for plain specimens was raised from 146 to 164 MN/m^2 by delaying the establishment of the electrochemical requirements for cracking for only 3 h after load application. The times to failure at stresses above 164 MN/m^2 were increased by about an order of magnitude as the result of a similar delay.

Threshold Stress from Creep Data

As a further test of the concept of the strain rate being important in constant load tests, it should be possible to calculate the threshold stress

for SCC from appropriate creep data, if the limiting creep rate below which SCC will not occur can be defined. These predicted threshold stresses should be in reasonable agreement with observed values. From experiments of the type reflected in Fig. 5, and others, the critical time in relation to the establishment of cracking conditions for a C-Mn steel in a $\text{CO}_3\text{-HCO}_3$ solution is about 17 h after loading, that is, the creep rate at that time determines whether or not cracking occurs. It may be expected therefore that the value of the average creep rate up to the end of that period will be related to whether or not cracking occurs. By analyzing the data along these lines for a given structural condition of a steel, it should be possible to define a limiting average creep rate for SCC and then to use that for predicting the threshold stresses for other structural conditions for which equivalent creep data is available. One of the ways in which the structural condition of C-Mn steels can be varied to influence creep response is by subjecting the steel to different strain aging treatments, to which the following results refer.

Figure 6 shows the average beam deflection rate between 1 and 17 h after loading specimens at various net section stresses for a C-Mn steel plastically deformed 5 percent and then aged for 1 h at 150°C prior to immersion in the stress corrosion test solution at 75°C . The effect of stress, σ , upon creep rate, $\dot{\epsilon}$, is usually expressed in the form of a power law which, in logarithmic form, is

$$\log \dot{\epsilon} = \log a + b \log \sigma$$

where a and b are constants. In Fig. 6, for convenience, the results are shown in semilogarithmic form, while the line shown refers to the regression equation for the data which, of course, should not be a straight line for this particular plot. However, no great error is involved for present purposes in showing the regression line as a straight line on a semilogarithmic plot over a very restricted range of stresses. In the structural condition of the steel to which Fig. 6 refers, the threshold net section stress below which SCC did not occur was 280 MN/m^2 . From Fig. 6, this corresponds to an average limiting beam deflection of $5 \times 10^{-10} \text{ m/s}$. The latter figure was used to calculate the threshold net section stresses from the regression equations for the creep response of the same steel after plastically deforming the steel different amounts and aging for 1 h at 150°C . A comparison of the threshold net section stresses so determined and those obtained experimentally is apparent from Fig. 7, which shows reasonable agreement in terms of the general trend of the curve and adds further weight to the suggestion that even in constant load tests the controlling parameter in relation to SCC is the strain rate.

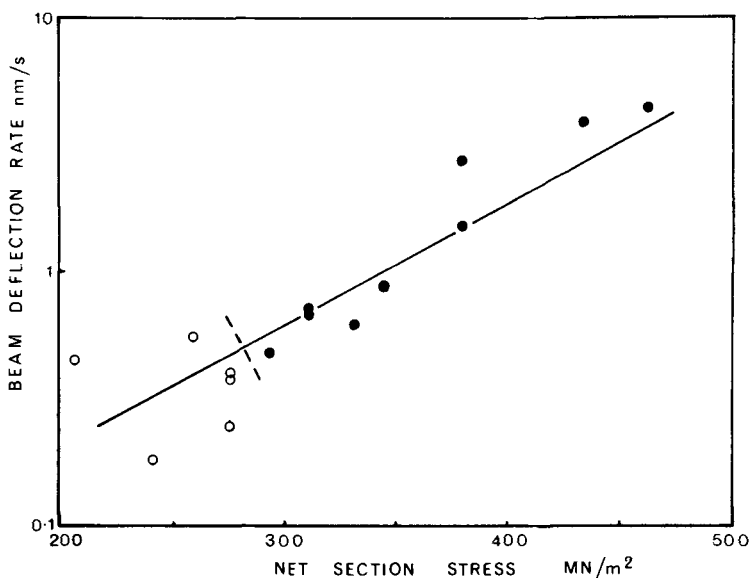


FIG. 6—Average beam deflection rate between 1 and 17 h after the start of stress corrosion tests as a function of initial applied net section stress for C-Mn specimens previously deformed 5 percent and aged 1 h at 150°C. The dots refer to specimens found to contain stress corrosion cracks after testing; the circles refer to specimens that did not crack. The line is from the regression equation for the data.

Significance of Nonpropagating Stress Corrosion Cracks

There is a further expectation from this suggestion which, if proven, would provide further support. In constant strain or constant load tests below the threshold stress it may be expected that stress corrosion cracks will initiate but later cease to propagate, if the rate of crack advancement is not sufficient to maintain the crack tip strain rate above the limiting value for SCC. Following the initial stress application, the creep rate will diminish as work hardening occurs, but if a crack is initiated this will increase the local stress intensity and enhance creep in the associated plastic zone. Which of these opposing effects dominates will determine whether or not crack propagation is sustained. If crack extension maintains the creep rate above the limiting value, cracking will continue and total failure will ensue, the conditions that were obtained above the threshold stress. But if the rate of crack extension is not sufficient to maintain the creep rate above the limiting value, then the crack will cease to grow. This may be expected at some stresses below the threshold stress. If specimens tested below the latter are examined, they may be found to contain non-propagating cracks, these having been observed in a Mg-Al alloy tested in a $\text{CrO}_4\text{-Cl}$ solution [12] and in a C-Mn steel tested in $\text{CO}_3\text{-HCO}_3$ solution.

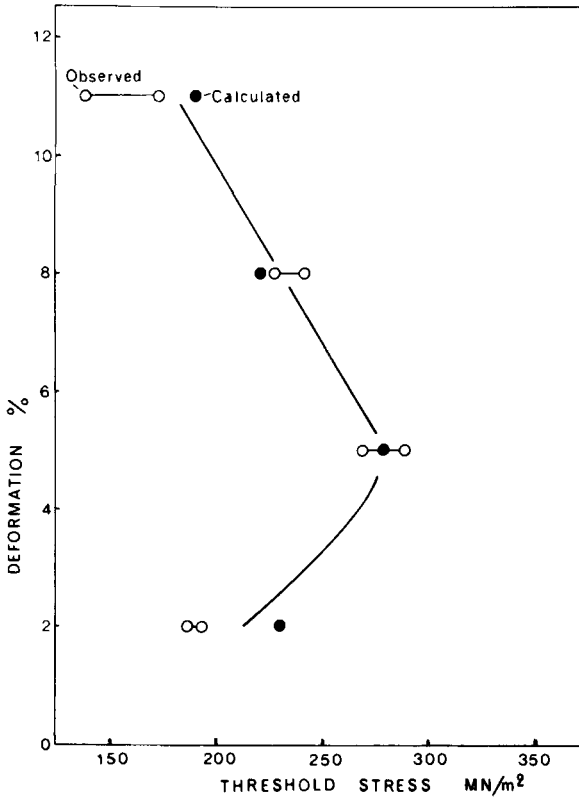


FIG. 7—Observed and calculated values of the threshold net section stresses for SCC of C-Mn steel in $\text{CO}_3\text{-HCO}_3$ solution at 75°C and -650 mV (SCE) after various prior deformations and aging for 1 h at 150°C .

The lengths of these nonpropagating cracks may be expected to be a function of the initial applied stress, being largest at stresses close to the threshold stress and decreasing as the initial stress is decreased to some value below which the creep rate is never sufficient to facilitate crack initiation. Figure 8 shows the maximum nonpropagating crack lengths as a function of initial applied stress for a C-Mn steel tested in a $\text{CO}_3\text{-HCO}_3$ solution and conforms to the expected results. Moreover, these nonpropagating cracks can be made to propagate again by a small load increment, which causes plastic strain in the crack tip region and reinitiates creep [12,13].

Concept of Threshold Strain Rates

There are various indications that even in constant load or constant strain tests strain rate effects are operative and define the limiting cracking

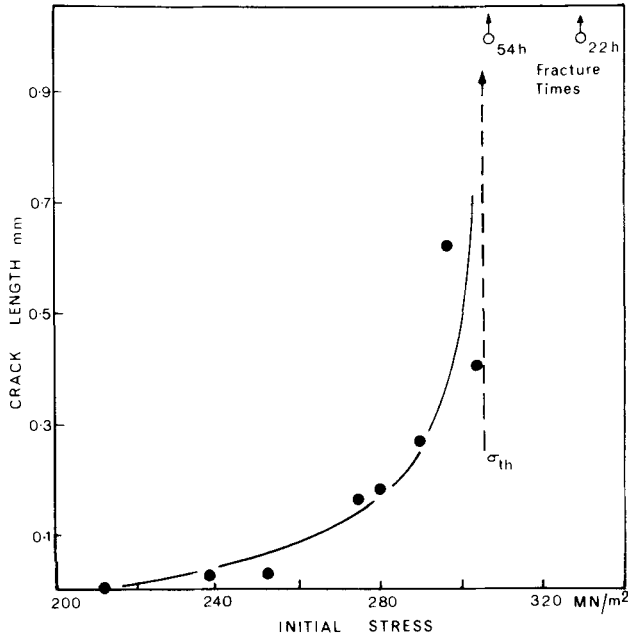


FIG. 8—Maximum intergranular crack lengths for different initial applied stresses below the threshold stress (σ_{th}) for a 0.05 percent carbon steel in CO_3-HCO_3 solution at $90^\circ C$ and $-650 mV (SCE)$ [13].

conditions. These indications suggest that if specimens were subjected to different strain rates instead of constant loads, it should be possible to define a minimum strain rate below which cracking is not observed as well as a maximum rate above which ductile failure would occur because of insufficient time for the electrochemical reactions that are associated with SCC. Figure 9 shows the results [12] from tension tests on a magnesium base alloy immersed in a CrO_4-Cl solution. These results from the reductions in the maximum load at failure, indicate that SCC only occurs within a restricted range of strain rates. Above or below this range the material fails in a normal ductile fashion, despite the fact that the stresses reach the ultimate tensile strength, that is, well in excess of the threshold stress for SCC, in the presence of an environment that readily promotes cracking at appropriate strain rates. Essentially similar effects may be seen in the results from some tests upon precracked cantilever beam specimens of a C-Mn steel immersed in a CO_3-HCO_3 solution. In those tests, instead of constant loading, specimens were subjected to different deflection rates, having previously been deflected to produce effectively the same preload. After this initial deflection, the specimens were allowed to creep under noncracking conditions until the creep rate fell below that which was

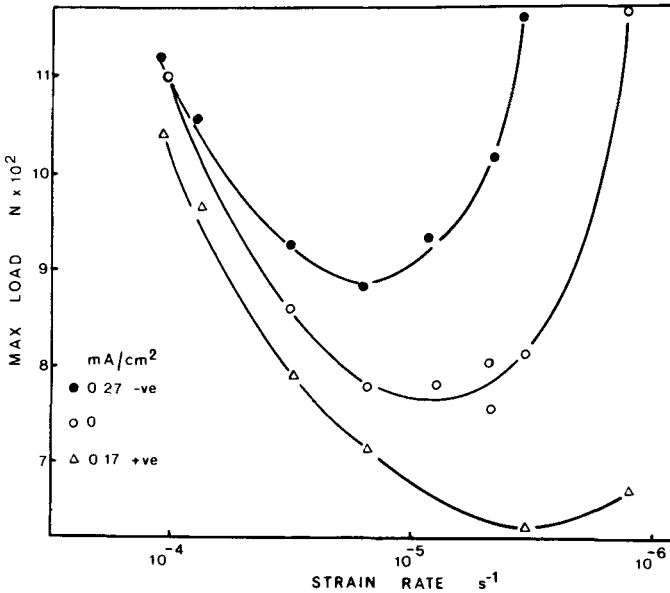


FIG. 9—Effects of various strain rates upon the cracking response of a Mg-Al alloy in a $\text{CrO}_4\text{-Cl}$ solution at various applied current densities [12].

subsequently applied when the potential was moved to a value at which SCC would occur. By restricting the total deflection during the cracking phase of the experiment, the effective load changes during the tests, monitored by strain gages attached to the loading beam, were contained within a few percent of the initial load. Figure 10 shows the results of these tests and clearly indicates a lower limiting beam deflection rate below which crack propagation is not observed and above which the crack velocity remains essentially constant irrespective of deflection rate up to a value where a transition from intergranular to transgranular fracture is observed due to the incidence of ductile failure. The limiting strain rates within which SCC is observed are dependent upon the environmental conditions [8,12,13], as would be expected if the concept of a critical range of strain rates for SCC was related to achieving a critical balance between the rate at which bare metal is created by straining and the rate at which the crack tip is rendered inactive by electrochemical reactions.

There is a further implication arising from both the applied strain rate effects and the nonpropagating cracks observed in constant load tests just discussed. This is that the threshold stress for SCC should be less in applied strain-rate tests than in constant load tests, because the nonpropagating cracks that form in constant load tests below the threshold stress will continue to propagate if an appropriate strain rate is maintained.

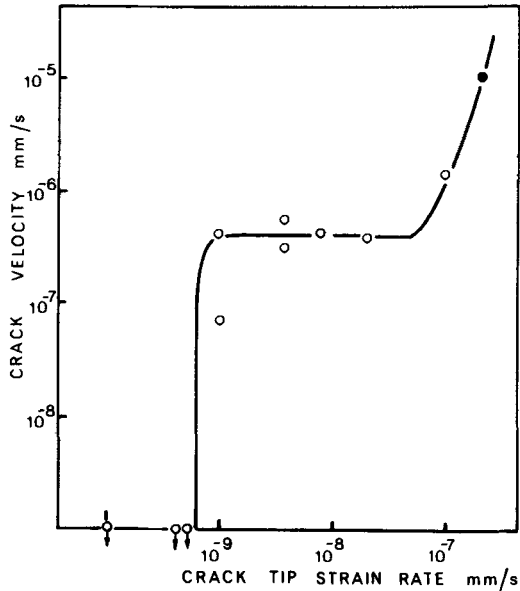


FIG. 10—Intergranular crack velocities for various applied crack tip strain rates in C-Mn steel immersed in $\text{CO}_3\text{-HCO}_3$ solution at 75°C and -650 mV (SCE) .

Figure 11 shows that the threshold net section stress is reduced from 455 MN/m^2 under constant load conditions to 360 MN/m^2 at a constant deflection rate. The markedly better reproducibility of the crack velocities determined from constant deflection rate experiments as compared to those from constant load tests is also noteworthy.

Interface of Stress Corrosion and Corrosion Fatigue

There is an obvious extension of these arguments on the importance of strain-rate effects in SCC to low frequency corrosion fatigue (CF), the interface between these modes of failure obviously becoming ill defined when the strain rates associated with load cycling approach the regimes involved in SCC. Indeed it is conceivable that the reduction in threshold stress resulting from applied strain rates, as opposed to static loads (Fig. 11), could be reduced even further with cyclic loading. Thus, load cycling can promote additional creep beyond that observed with static loading [14]. Figure 12 shows that the removal and replacement of the load applied to a precracked specimen promote plastic displacements in the crack tip region, the magnitude and time dependence of which are a function of frequency, load change, and temperature. By appropriate choices of these variables, average creep rates may be sustained over extended periods

20 STRESS CORROSION CRACKING

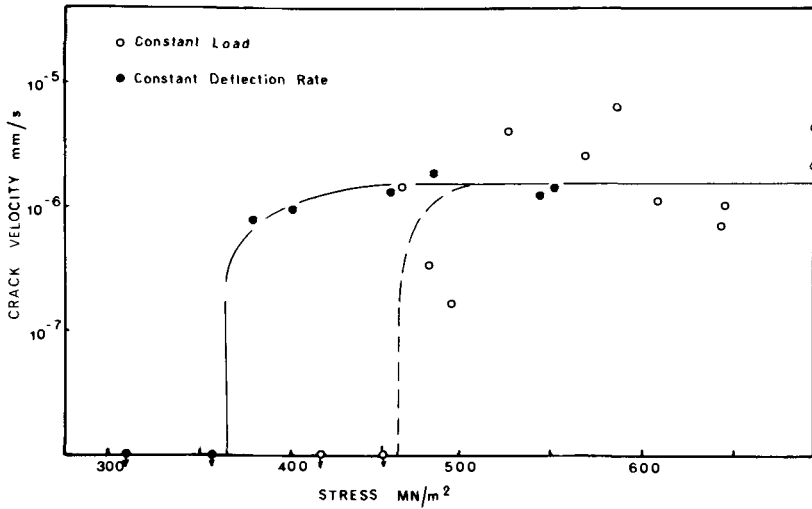


FIG. 11—Stress corrosion crack velocities observed in a C-Mn steel immersed in CO_3-HCO_3 solution at $75^\circ C$ and -650 mV for different initial net section stresses in constant load and constant beam deflection rate tests.

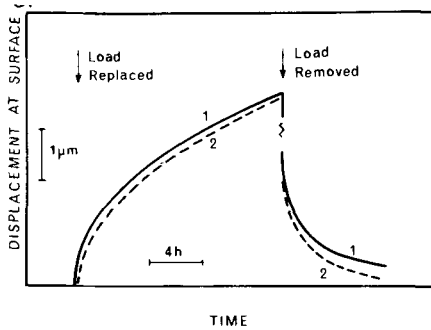


FIG. 12—Time dependent plastic displacement measured at the surface of a precracked C-Mn steel specimen subjected to loading and unloading at $75^\circ C$ (the instantaneous, elastic, displacement has been removed from the curves, which refer to successive load cycles, following a few earlier load cycles [14]).

(Fig. 13) simply by loading and unloading, whereas with static loading the creep rate would fall to values below those needed to promote SCC. It follows that cyclic loading may produce SCC at significantly lower stresses than those involved with static loading and even below those stresses that promote the formation of nonpropagating cracks under static conditions.

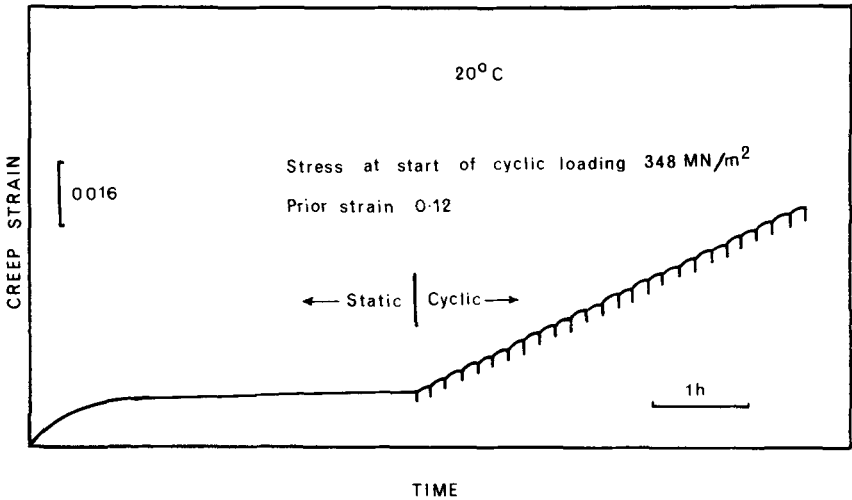


FIG. 13—Envelope creep curve resulting from load cycling to a maximum stress of 348 MN/m² after creep exhaustion under static load at same stress, cycle period, 600 s; unloading time, 60 s [14].

The intergranular SCC of C-Mn steels in CO₃-HCO₃ solutions at -650 mV saturated calomel electrode (SCE) and 75°C transforms to a transgranular mode with cyclic loading at high frequencies or relatively high values of the initial stress intensity range, ΔK_i , for a given initial mean stress intensity, K_m . However as the frequency of cycling is reduced so also is the limiting mean stress intensity for intergranular cracking [10]. Figure 14 shows the regime in which intergranular cracking is observed at a frequency of 11 Hz, the threshold stress intensity for corrosion fatigue being the same as that for SCC. However, if the frequency were reduced to 0.19 Hz, then the intergranular cracking regime would be considerably extended (Fig. 15), both in the sense of the value of ΔK_i at which the transition from intergranular to transgranular cracking occurred at relatively high K_m values and in extending the intergranular cracking to much lower values of the mean stress intensity. Insofar as these effects are observed at relatively small values of ΔK_i , the implications for service conditions, in which nominally static circumstances are assumed but in which in reality small changes in stress occur, may be very considerable.

Conclusions

It would appear that strain-rate testing for SCC is moving out of the phase where it was considered to be a rapid, *ad hoc* sorting test, into one in which its significance to service failures is more realistic than was at one

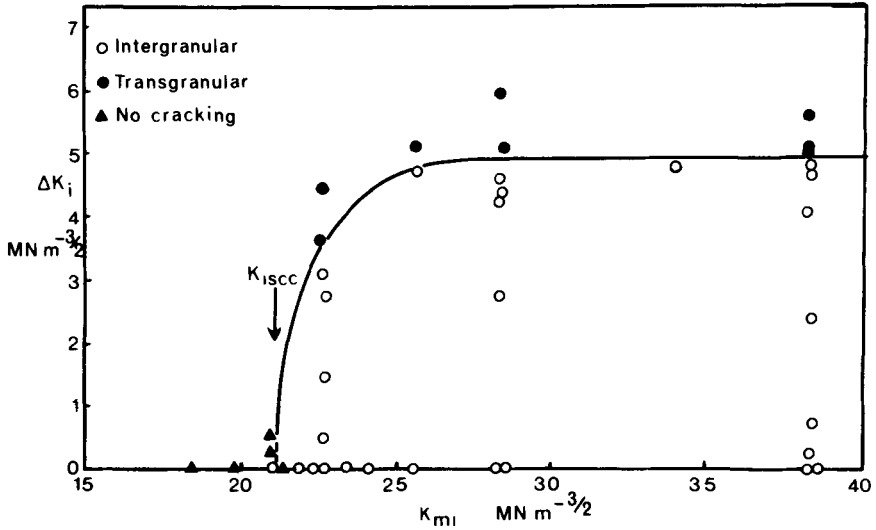


FIG. 14—Modified Goodman diagram indicating the loading parameters for which intergranular and transgranular cracking were observed for a C-Mn steel immersed in a CO_3-HCO_3 solution at $75^\circ C$, -650 mV (SCE), 11 Hz and $R > 0$ [10].

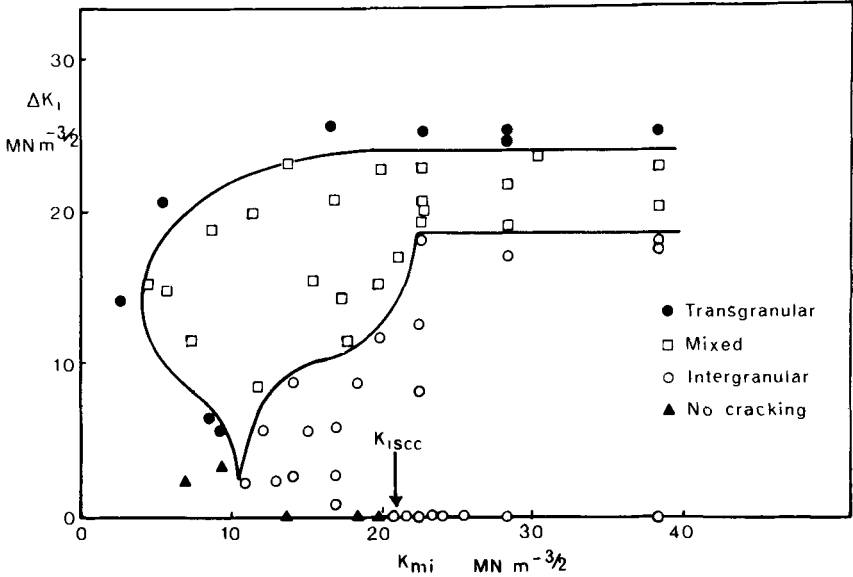


FIG. 15—Modified Goodman diagram indicating the loading parameters for which intergranular and transgranular cracking were observed for a C-Mn steel immersed in a CO_3-HCO_3 solution at $75^\circ C$, -650 mV (SCE), 0.19 Hz and $R > 0$ [10].

time thought likely. The relevance of strain-rate effects in static load tests with their overtones for nonpropagating cracks, the concept of an electrochemically dependent range of strain rates within which SCC occurs, and the significance of load cycling in sustaining creep and hence cracking, all support this conclusion. The objection that has been raised sometimes against strain-rate testing, is that it does not provide data that the designer can employ, no longer appears relevant, or even correct. In other circumstances, creep rate is considered to be as much an engineering design parameter as is stress or stress intensity, and where the creep rate is controlling in SCC it is important to recognize this, if the incidence of failure of structures designed on the basis of other criteria is to be reduced. Of course it is possible to imagine circumstances in which strain-rate effects will be less significant than in the systems discussed in this paper, for example where cracking is the result of elastic interactions or where localized corrosion can proceed significantly even in the absence of stress or strain rate effects, but may be accelerated by the latter. Nevertheless, indications are now emerging, especially for SCC in the lower strength, ductile alloys, that strain-rate effects and hence testing are relevant to environment sensitive fracture.

Acknowledgments

The contributions of a number of my former research colleagues, notably M. Henthorne, M. J. Humphries, W. R. Wearmouth, G. P. Dean, and G. P. Marsh, in the development of this method of testing and of its understanding must be gratefully recorded. In addition, the financial support of the Science Research Council (U.K.) and of the Pipeline Research Committee of the American Gas Association (Project NG18) is acknowledged with gratitude.

References

- [1] Parkins, R. N., Mazza, F., Royuela, J. J., and Scully, J. C., *British Corrosion Journal*, Vol. 7, 1972, p. 154.
- [2] Henthorne, M., Ph.D. thesis, University of Newcastle upon Tyne, England, 1965.
- [3] Coleman, E. G., Weinstein, D., and Rostoker, W., *Acta Metallurgica*, Vol. 9, 1961, p. 491.
- [4] Henthorne, M. and Parkins, R. N., *Corrosion Science*, Vol. 6, 1966, p. 357.
- [5] Henthorne, M. and Parkins, R. N., *British Corrosion Journal*, Vol. 5, 1967, p. 186.
- [6] Humphries, M. J. and Parkins, R. N., *Proceedings*, Conference on Fundamental Aspects of Stress Corrosion Cracking, Ohio State University, National Association of Corrosion Engineers, 1969, p. 384.
- [7] Humphries, M. J. and Parkins, R. N., *Corrosion Science*, Vol. 7, 1967, p. 747.
- [8] Parkins, R. N., Paper presented at NATO Advanced Study Institute, Copenhagen, 1975, to be published by Noordhoff, Netherlands.
- [9] Flis, J. and Scully, J. C., *Corrosion*, Vol. 24, 1968, p. 326.

- [10] Parkins, R. N. and Greenwell, B. S., *Metal Science*, Vol. 11, p. 405.
- [11] Parkins, R. N., Slattery, P. W., Middleton, W. R., and Humphries, M. J., *British Corrosion Journal*, Vol. 8, 1973, p. 117.
- [12] Wearmouth, W. R., Dean, G. P., and Parkins, R. N., *Corrosion*, Vol. 29, 1973, p. 251.
- [13] Parkins, R. N., 5th Symposium on Line Pipe Research, American Gas Association, Cat. No. L30174, 1974, U1-40.
- [14] Evans, J. T. and Parkins, R. N., *Acta Metallurgica*, Vol. 24, 1976, p. 511.

DISCUSSION

*Andrew Madeyski*¹—Is the effect of the strain rate on the SCC related exclusively to the passivating film rupture and the electrochemical surface reactions, or is it affected also by such phenomena as strain aging and stress-assisted impurity diffusion in some metals?

R. N. Parkins (author's closure)—In constant load or constant strain tests the critical strain rate for SCC may be influenced by physico-metallurgical phenomena, such as strain aging or stress-assisted diffusion. However, when the strain rate is controlled by direct application, as in slow strain-rate testing, these physico-metallurgical effects are overridden, and the critical strain rate for cracking should be governed by electrochemical considerations. The exception may be where the cracking mechanism involves the ingress of hydrogen into the metal, since hydrogen reduced ductility is known to be strain rate dependent. This may be related to the effect of the strain rate upon the transport of hydrogen.

*I. L. W. Wilson*²—Referring to the topic covered in Dr. Parkins' last two figures, that is, corrosion fatigue of precracked specimens with a high mean load, so that one is above any threshold effects, if the frequency were constant and the alternating stress decreased, then the strain rate would decrease. It is possible that, as one is approaching the normal ΔK_{th} for a material, where the crack growth rate rapidly approaches zero, the "strain rate" at the crack tip is approaching the value where maximum environmental susceptibility is observed. At this point, the value of the crack growth rate could increase with decreasing values of ΔK (with some limiting value). I have seen data³ which indicates this behavior. Has Dr. Parkins seen this behavior in his own testing? It has the obvious implication that ΔK_{th} for corrosion fatigue will be a sensitive function of frequency, etc. of test.

¹Westinghouse Electric Corporation, R & D Center, Pittsburgh, Pa. 15235.

²Westinghouse Electric Corporation, R & D Center, Pittsburgh, Pa. 15235.

³Bamford, W. H., Scott, K. V., and Ceschini, L. J., Quarterly Progress Report #4, March-May 1977, Heavy Section Steel Technology Program, Westinghouse Electric Corporation (to be issued).

R. N. Parkins (author's closure)—We have some experimental data which show quite clearly that corrosion-fatigue crack growth rates do not simply increase with the severity of stressing. Thus, as K_{\max} is increased, the crack velocity may pass through a maximum under certain environmental conditions. We have also observed that as the maximum net section stress ratio is varied, the crack velocity may pass through a maximum for constant values of ΔK . Clearly there are some complex interactions between those parameters that are used for quantifying the stressing conditions in cyclic loading and the crack velocity, and these may be expected to show frequency dependence also where time dependent electrochemical reactions are involved in the crack growth.

R. B. Diegle¹ and W. K. Boyd¹

The Role of Film Rupture During Slow Strain-Rate Stress Corrosion Cracking Testing

REFERENCE: Diegle, R. B. and Boyd, W. K., "The Role of Film Rupture During Slow Strain-Rate Stress Corrosion Cracking Testing," *Stress Corrosion Cracking—The Slow Strain-Rate Technique*, ASTM STP 665, G. M. Ugiansky and J. H. Payer, Eds., American Society for Testing and Materials, 1979, pp. 26-46.

ABSTRACT: The unique nature of the slow strain-rate technique for stress corrosion testing is discussed in terms of its ability to maintain repetitive rupture of corrosion films. It is first shown that the surfaces of alloys of engineering importance tend to be covered with films under electrochemical conditions that promote stress corrosion cracking (SCC). The relevance of this observation to conditions prevailing directly at the stress corrosion crack tip is considered next, and it is shown that a film-covered tip is a likely probability in several alloy-corrodent systems. It is proposed that film rupture can be considered a prerequisite for the operation of the two major proposed SCC mechanisms, namely, anodic dissolution and hydrogen embrittlement. The predominance of intergranular or transgranular cracking is ascribed to the morphology of slip within the alloys and possibly to the effect of solute segregation on corrosion kinetics. It is concluded that the success of the slow strain-rate technique as a severe test of SCC susceptibility results from its ability to expose the crack tip region to the aggressive environment through film rupture.

KEY WORDS: corrosion prevention, stress corrosion cracking, corrosion, cracks, hydrogen embrittlement, intergranular corrosion, transgranular corrosion

The objective of this paper is to consider the effects that mechanical properties of corrosion films have on the phenomenon of stress corrosion cracking (SCC). For this paper, the term "influence" means exerting an effect on the rate of stress corrosion cracking. Generally, SCC will be considered to mean cracking under the combined effect of a static tensile stress and corrosion and in the absence of large scale plastic deformation; however, the concepts presented also will be applicable to hydrogen-related phenomena such as hydrogen embrittlement and sulfide stress cracking. "Corrosion film"

¹Senior research metallurgist and senior research leader, respectively, Battelle Columbus Laboratories, Columbus, Ohio 43201.

denotes any reaction product of the metal or alloy with the corrodent, or any residual layer, that markedly polarizes the anodic or cathodic partial reactions and thereby reduces the corrosion rate. Note that this definition includes films other than those formed strictly within the passive potential region of polarization behavior.

It is believed that the success exhibited by the constant strain-rate technique in laboratory investigations of SCC is related directly to the presence of corrosion films on engineering alloys. Indeed there is ample evidence that exposed surfaces of almost, if not all, alloys undergoing SCC are covered with some type of corrosion product layer. Evidence for such films first will be considered, and then the influence of slow strain-rate testing on their integrity will be discussed. Although the concept of an anodic film rupture SCC mechanism is implicit in any consideration of the slow strain-rate technique, it will be shown that the ideas presented are applicable to cracking mechanisms other than the classical brittle film rupture model.

Evidence of Reaction Films on Alloys During SCC

Stress corrosion cracking is experienced by many different types of alloys in a wide variety of environments, yet laboratory evidence suggests at least one common factor: the alloys are covered by corrosion films under conditions causing SCC. These films may differ in various alloy-corrodent systems; in some cases they may consist of oxide or hydroxide phases and in others of noble metal layers, but they have been found on the great majority, if not all, alloys undergoing SCC. To illustrate the generality of this statement, and to set the stage for a later section on the role of applied strain in initiating and propagating stress corrosion cracks, a very brief review of film formation will be given for the following alloy-corrodent systems: (a) brass in ammoniacal tarnishing solutions, (b) austenitic stainless steels in chloride and acidic solutions, (c) low strength ferritic steels in alkaline and nitrate solutions, (d) aluminum-base alloys in chloride solutions, (e) titanium and titanium alloys in chloride solutions, and (f) noble metal alloys in chloride solutions.

Brasses

Exposure of stressed alpha-brass (70Cu-30Zn) to certain ammonia-containing electrolytes results in SCC in the presence of a black tarnish film. X-ray and electron diffraction analysis [1-3]² indicated that this film is principally crystalline cuprous oxide (Cu₂O). Examination by electron microscopy of stripped flakes showed that the tarnish consists of small platelets about 500 Å in diameter and 100 Å thick. Room temperature

²The italic numbers in brackets refer to the list of references appended to this paper.

plastic deformation experiments demonstrated that the tarnish layer is quite brittle [1]. It can grow to extreme thicknesses, causing intergranular penetration of polycrystalline brass during long exposure periods [4]. According to one model [5], the advancing stress corrosion crack rapidly penetrates the brittle tarnish layer, and propagation then ceases temporarily because of plastic blunting at the crack tip in the ductile metal. However, more recent analysis by Auger spectroscopy of fracture surfaces of specimens broken open during SCC [6] suggests that the oxide film present directly at the leading edge of the crack is quite thin, and that the characteristic thicker Cu_2O tarnish layer forms on crack walls only after the crack tip has passed. In another study [7], electron diffraction analysis was used to show the presence of a mechanically weak, thin surface layer of Cu_2O within the crack. Thus, the morphology of the crack tip film has undergone a transition in the literature from that of a thick, black brittle tarnish to a thin, almost colorless layer, but available experimental evidence nevertheless still indicates that the crack tip is apparently covered with some type of film during SCC.

Austenitic Stainless Steels

Austenitic stainless steels owe their good corrosion resistance to the presence of a thin, tenacious, chromium-containing passive film. The film formed in sulfuric acid (H_2SO_4) at passive potentials is reported to be amorphous and less than 100 Å thick [8]. Although its exact structure and composition were not determined, reflection electron diffraction suggests that it is a type of hydrous oxide; this supports the results of previous research that utilized tritium tracer techniques [9-11]. Electron spectroscopy for chemical analysis (ESCA) indicated that the film composition depends somewhat on the formation conditions, especially potential and time of application; that is, enrichment of chromium relative to nickel and iron occurs at potentials below 0.4 V (saturated calomel electrode (SCE)), whereas the chromium/iron ratio decreases with increasing polarization time at more oxidizing potentials.

Although Barnartt and van Rooyen initially interpreted potential-current data from stainless steel in boiling magnesium chloride (MgCl_2) as indicating that the steel was film-free [12], subsequent investigations were interpreted differently. Latanision and Staehle suggested, because of the noble nature of nickel and the rise in potential customarily observed at the onset of SCC, that enrichment of nickel on the surface provided a film [13]. However, Rockel and Staehle later explained the data of Barnartt and van Rooyen as indicating conventional active-passive behavior [14]. Subsequent investigations support the concept of a filmed surface: Montuelle et al [15] have detected magnetite (Fe_3O_4), and Davis and Wilde [16] also have shown that the surface film is not elemental nickel, but rather an oxidized layer.

Low Strength Ferritic Steels

Humphries and Parkins confirmed that low strength ferritic steels (mild steels) are film covered during SCC in caustic and nitrate electrolytes [17]. X-ray diffraction patterns indicated that in caustic electrolyte at -0.710 V (saturated hydrogen electrode (SHE)), a potential that readily causes SCC, the film is Fe_3O_4 , and that at more oxidizing potentials the proportion of ferric iron increases. Other experiments simulating crack tip electrochemical conditions demonstrated that an extremely thin layer ($\sim < 33$ Å) of Fe_3O_4 is expected to exist at the tip [18].

Films formed in nitrate solutions on surfaces external to stress corrosion cracks have been investigated by a variety of workers [17,19-22]. X-ray results indicate that Fe_3O_4 is present at the extreme ends of the potential range in which SCC occurs, although no visible layer was observed at intermediate potentials [19]. Visible films were detected from -0.560 to 1.340 V (SHE) in ammonium nitrate (NH_4NO_3) and from -0.160 to 1.340 V (SHE) in sodium nitrate (NaNO_3) [20]. Fe_3O_4 was detected at active potentials, and alpha-ferric oxide ($\alpha\text{-Fe}_2\text{O}_3$) was found at noble potentials.

Aluminum-Base Alloys

A wealth of information has been generated on the nature of the films developed on aluminum, as comprehensively reviewed by Godard [24]. Hart reports a thickness of $55\ 000$ Å after 20 days immersion of pure aluminum in distilled water, with the growth rate decreasing with time [25]. The initial corrosion product was proposed to be alumina trihydrate [$\text{Al}(\text{OH})_3$], which ages with time to become hydrated aluminum oxide ($\text{Al}_2\text{O}_3 \cdot \text{H}_2\text{O}$). Vedder and Vermilyea [26] found that a thin amorphous oxide is next to the metal surface after immersion in water, and that the oxide surface is hydrolyzed either to soluble species or a porous hydroxide layer.

However, pure aluminum does not undergo SCC, but aluminum-base alloys such as the 2000 (aluminum-copper-magnesium-silicon), 5000 (aluminum-magnesium-manganese), and 7000 (aluminum-zinc-magnesium) series do exhibit SCC. Relatively little published information exists describing the detailed nature of corrosion films on such alloys, research instead having centered on interrelationships between alloy microstructure and SCC susceptibility. Nevertheless it is certain that such alloys are film covered in corrosive environments due to the very reactive nature of the major component, aluminum, and of other reactive alloying elements such magnesium and zinc. Indeed, it is the presence of these films that renders this very reactive metal useful in structural applications.

Titanium and Titanium Alloys

Titanium, like aluminum, is a very reactive metal, which owes its

usefulness in engineering applications to the presence of a stable oxide film. The film formed on clean titanium upon exposure to room temperature air is 12 to 16 Å thick, reaching 50 Å after 70 days [27]. Its thickness varies in aqueous solution with temperature, pH, and electrode potential. The film composition has been reported to be predominantly titanium oxide (TiO) near the metal/oxide interface, Ti₂O₃ in the interior, and titanium dioxide (TiO₂) at the outer surface [28]. It has been proposed that titanium, which exhibits passivity in numerous electrolytes [29], is covered with rhombohedral TiO₂ at the onset of passivation and the tetrahedral form at more anodic potentials [30]. Both rutile and anatase were detected on titanium immersed in electrolytes such as boiling concentrated nitric acid (HNO₃), boiling 20 percent chromic acid (Cr₂O₃), and high temperature water [31].

Alpha-titanium alloys fail by SCC in liquid nitrogen tetroxide (N₂O₄) containing no free nitric oxide. A black film develops on exposure, which electron optical techniques have shown to be the rutile modification of TiO₂ [32,33]. It grew to several microns in thickness on specimens that were plastically deformed. No detailed information was found on the nature of the TiO₂ film formed in chloride solutions, which also produce SCC.

Noble Metal Alloys

As an example of this alloy class, gold-copper and silver-gold will be considered, which undergo SCC in aqueous ferric chloride (FeCl₃) and aqua regia. Graf proposed that the crack sides become covered with the more noble component, in these examples gold, due to preferential dissolution of the less noble component by FeCl₃ [34]. In aqua regia, which dissolves both components, the gold is presumed to precipitate partially at high ionic concentration onto the base component of the alloy. Considerable experimental evidence involving a variety of optical and analytical techniques demonstrates the formation of gold-rich layers on specimens exposed to solutions producing SCC [35-39].

The preceding discussion was not intended to be an exhaustive review of film formation on alloys susceptible to SCC. Rather, it was presented to emphasize that corrosion film layers are present on exposed alloy surfaces under a wide variety of corrosive conditions, including many that cause SCC, and that their presence may very well be a contributing factor in the overall SCC process.

Is the Crack Tip Unfilmed?

The statement in the preceding paragraph can be challenged on the following premise, that is, it can be argued that the electrochemical conditions of more active potential and reduced pH prevailing deep within stress corrosion

cracks may render films unstable, such that the crack tip is unfiled and the role of the film is merely to passivate the crack sides. In such instances, mechanical properties of the film would be important only during crack initiation, but not during propagation.

It is conceivable that the tips of propagating stress corrosion cracks in certain alloys are indeed unfiled. For example, precipitation hardened aluminum-zinc-magnesium alloys have been observed to crack at nominal rates up to 10^{-2} cm/s [40]. A Faraday's law calculation assuming a purely electrochemical SCC mechanism, namely, no propagation except by dissolution, would require a current density of about 290 A/cm². This equivalent corrosion rate is about 29 times greater than the maximum of 10 A/cm² observed for aluminum [41]. This apparent discrepancy demonstrates that an unfiled tip would not be inconsistent with certain observed crack propagation rate data; that is, if the tip *were* unfiled, it would not corrode at a rate which exceeds the maximum observed crack propagation rate. However, an alternative mechanism would be needed to account for this large discrepancy, such as propagation by mechanical as well as electrochemical means.

It seems less likely that an unfiled crack tip could exist in certain other alloy-corrodent systems for which it also has been postulated. For example, corrosion rate data obtained from straining electrode experiments involving iron in sodium hydroxide (NaOH) electrolyte were interpreted as reflecting the corrosion rate on unfiled iron [42]. The close agreement between these rates and those required to account for observed crack propagation rates in caustic electrolyte, Table 1, was considered evidence for a bare crack tip.

TABLE 1—*Influence of potential on incidence and penetration of cracks in 0.1 percent C steel in 10 M NaOH at 121°C. Strain rate 1.5 percent/min [42].*

Potential, V (SHE)	Incidence of Attack	Penetration		
		Current Density Over Bare Surface, mA/cm ²	Calculated From Cur- rent Density, μm	Measured Microscop- ically, μm
-0.50	some short, blunt pits; no cracks	...	0	0
-0.55	a few cracks	33	10	17 to 29
-0.60	a few cracks	77	25	23 to 29
-0.65	a few cracks	74	25	26 to 34
-0.70	many cracks—about ½ of grain boundaries penetrated	89	30	29 to 37
-0.75	many cracks over ⅓ of surface	120	40	29 to 40
-0.80	many cracks—almost every grain boundary penetrated	154	50	31 to 40
-0.825	a few cracks	73	25	7 to 14
-0.85	a few cracks and pits	110	37	3 to 9
-0.90	no cracks	...	0	0

However, it was subsequently proposed [43] that the current densities obtained by Hoar and Jones [42] in the higher strain-rate range do not represent steady state, hence bare surface values, but were in fact still increasing (see Fig. 1). The "bare surface" current densities reported in Table 1 were therefore considered to be average corrosion rates on electrodes experiencing repetitive film rupture and repair during straining. Additional data generated at a much higher strain rate of 57 s^{-1} indicated that the current density on unfilmed iron in caustic electrolyte exceeds 1 A/cm^2 [23]; such a large value corresponds to a cracking rate of 1.3 mm/h , which is about an order of magnitude greater than the maximum rate observed [17, 42, 44]. It is therefore unlikely that caustic SCC proceeds with a continuously unfilmed crack tip.

It should be noted that the preceding reasoning presupposes a relatively

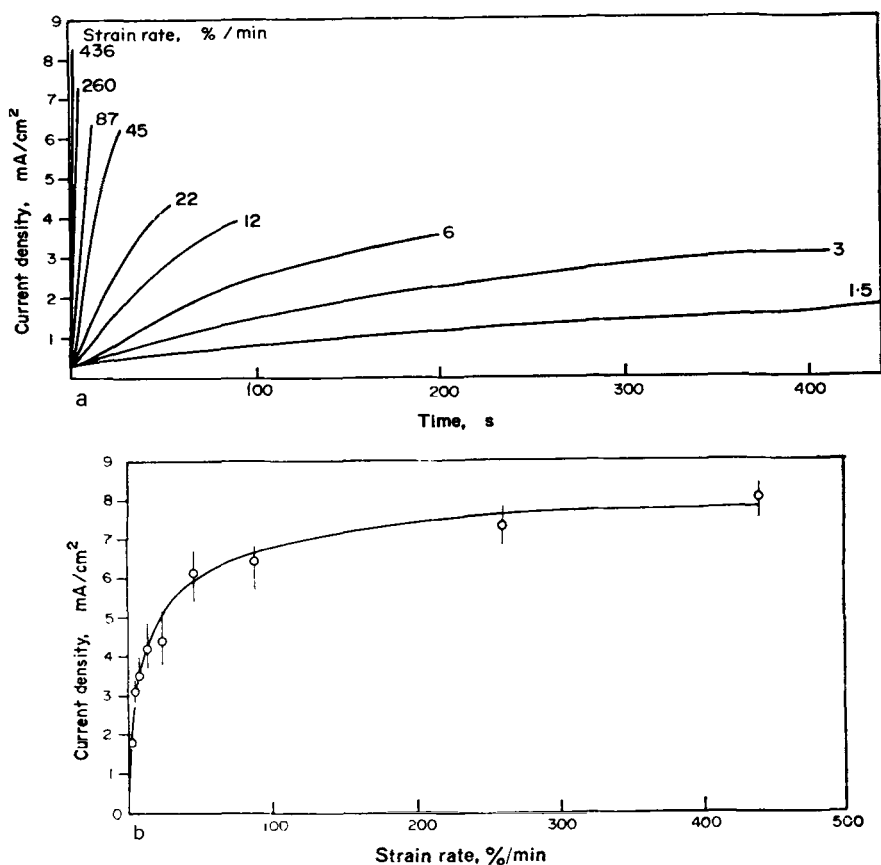


FIG. 1—Results of current density measurements made on slowly straining 0.1 C steel electrodes in 10 M NaOH at -0.700 V (SHE) : (a) potentiostatic current density-time curves, (b) limiting current density versus applied strain rate [42].

constant rate of crack advance, namely, no long periods of crack arrest. If a crack advances in rapid bursts of anodic dissolution separated by periods of inactivity, then almost any *nominal* crack propagation rate could be postulated to result from corrosion at a bare crack tip. Unfortunately, experimental techniques are not yet sufficiently refined to determine unambiguously the microscopic nature of crack advance in macroscopic sized specimens.

Neither does the fact that SCC sometimes occurs at potentials within the active region of polarization behavior constitute evidence that the crack tip is unfilmed. The term "active," when used in reference to current-potential behavior, is a relative term; that is, it only means that the oxidation rate is large relative to that in the passive potential region, and it in no way implies the absence of a protective film. For example, rapid straining experiments under simulated crack tip conditions of electrolyte chemistry and potential have produced large anodic current transients at active as well as passive potentials. Typical data from one such set of experiments is shown in Fig. 2 [45]. The lower set of curves illustrates polarization behavior of Type 304 stainless steel in pH 2 sodium chloride (NaCl); active dissolution is evident at about -75 to -100 mV (SHE), followed by passivity over a narrow potential range and transpassivity beginning at 25 mV (SHE). Curve III indicates the maximum anodic current density obtained directly after straining. It is evident that large current increases occurred *throughout* the active potential range, and therefore that significant polarization due to a film was present even at these active potentials. The upper curves, denoting the integrated anodic charge density, again reflect the depolarizing effect of strain throughout (and slightly cathodic to) the anodic potential range. Similar behavior was observed for iron strained at high rates in an NaOH electrolyte [23] and the results of these two studies are summarized in Table 2. It is apparent that although corrosion films are poorly developed at active potentials compared to those at passive potentials, they are not absent.

A final word on the presence of films relates to statements occasionally found in the literature to the effect that a "specimen was filmed because it was covered by a visible layer," or that a "specimen was bright and shiny and therefore not covered by a corrosion product film." Many alloys, for example, stainless steels, form protective films that are not always visible to the unaided eye. Therefore, the apparent absence of a film does not constitute a bare specimen, nor does a heavy corrosion product necessarily constitute an electrochemically protective layer. Abrasion and rapid straining experiments are useful means for assessing the presence and protective nature of corrosion films.

Utility of the Slow Strain-Rate Technique

As stated earlier, the success of the slow strain-rate technique in producing

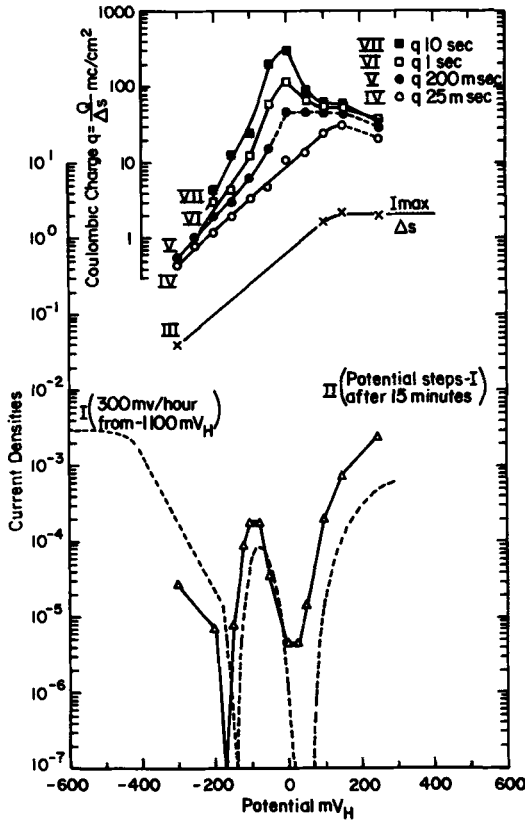


FIG. 2—Polarization behavior and straining electrode parameters of Type 304 stainless steel in 2 M NaCl adjusted to pH 2 [45].

SCC in laboratory investigations results from the film-covered nature of alloys in corrodents that cause SCC. It is proposed that the role of strain is either to promote repetitive film rupture, or possibly to maintain (through enhanced dissolution) a transition film of poor protective quality [46], which in turn facilitates crack initiation and propagation by one of a number of proposed mechanisms as discussed below.

Classic Film Rupture

All SCC models based on electrochemical dissolution require a concentration of the anodic reaction at the crack tip to maintain the crack geometry. Insufficient anodic activity at the tip relative to the sides would result in blunting the crack and eventual crack arrest or pitting. The role of strain according to such models is to rupture the corrosion film locally at the crack

TABLE 2—Effect of applied strain on producing anodic dissolution of electrodes polarized at active potentials.

Alloy	Electrolyte	Applied Strain Rate, %/min	Potential, ^a i_{max} ,		Reference
			mV (SHE)	A/cm ²	
T304 S.S.	0.02 M NaCl, pH 4	750	0	0.2	45
	2 M NaCl, pH 2	750	-90	0.3	45
	1 N HCl	750	-20	0.4	45
Iron	35% NaOH	3.4×10^5	-800	0.45	23

^aPotential at peak of active loop.

tip, thereby depolarizing the anodic reaction and promoting forward rather than lateral growth. The importance of repetitive film rupture is illustrated in Fig. 3 [47], which shows cracks in a single crystal of brass that was alternately strained and corroded. The specimen was dry while it was being deformed plastically in tension, and it was free of external stress during immersion in a tarnishing solution. The role of stress-induced strain in producing film rupture is clear. As would be expected from these results, the slow strain-rate technique produces SCC of brass in tarnishing solutions; rapid intergranular attack occurs under the same conditions as those producing a large increase in corrosion current due to film rupture on electrode surfaces [48].

Strain at the crack tip has been considered necessary to produce SCC by a number of workers. Logan proposed that it was needed to confine the bulk of corrosion to a very narrow crack front through film rupture [49]. Vermilyea

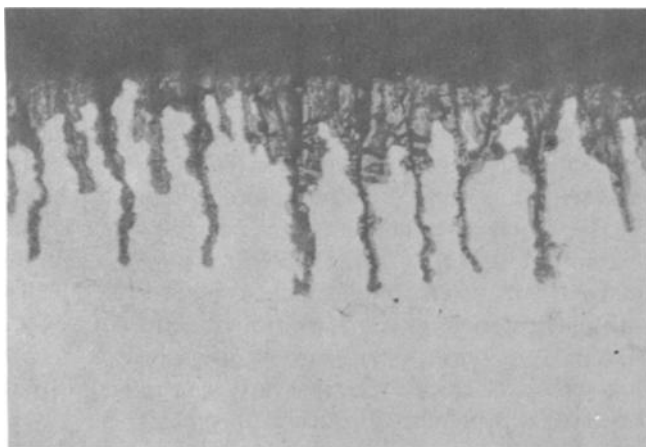


FIG. 3—Transverse section through an α -brass single crystal that has been immersed in a tarnishing solution and stressed intermittently for 50 cycles [47]. By permission of National Association of Corrosion Engineers.

modeled the relationships between corrosion and strain and proposed that film ductility determines the amount of strain required for rupture [50,51]. The proposed time dependence of corrosion and strain are shown in Fig. 4; when corrosion has proceeded to a depth L after film rupture, a sufficient increment of strain, ϵ_c , occurs in the ensuing strain transient to re-rupture the film and continue the cycle. Scully proposed an analogous constant charge criterion whereby it is necessary, after strain-induced film rupture at the crack tip, for a minimum amount of charge to pass via metal dissolution to maintain repetitive film rupture [52].

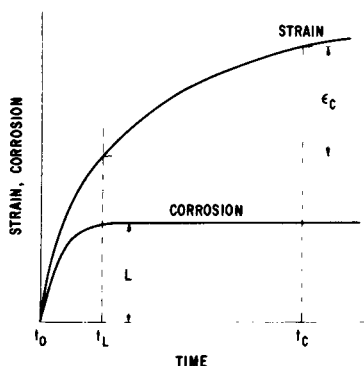


FIG. 4—Time dependence of strain and corrosion following film rupture [50]. By permission of National Association of Corrosion Engineers.

In another strain-related model, three fundamental criteria for crack growth were proposed [53]: (a) application of strain must accelerate corrosion, (b) the SCC mechanism must produce a crack that lengthens much faster than it widens, and (c) each increment of strain must produce sufficient crack advance to produce another equal increment of strain. It was also necessary that anodic activity be concentrated on a small fraction of the crack tip surface, for example, by film rupture at highly localized sites. This theory led to the requirement that the ratio of corrosion rate at the crack tip, \dot{l} , to local strain rate, $\dot{\epsilon}$, or $\dot{l}/\dot{\epsilon}$, must exceed a critical value in the range of $2 \cdot 10^{-7}$ cm for several systems that exhibit SCC (see Table 3). However, this is not a sufficient criterion, as is evident from data from Fe-50Ni in 42 percent MgCl₂ and alpha brass in pH 3.6 Mattson's solution. Nevertheless, the agreement is sufficiently good to warrant further investigation of this model, especially because it is predictive in nature.

Hydrogen Embrittlement

According to another theory, crack advance occurs by fracture of a zone of metal at the crack tip that is embrittled by cathodically generated hydrogen.

TABLE 3—Data from straining electrode experiments indicating correspondence between I/ϵ criterion and susceptibility to SCC [53].

Metal	Environment	Potential, V (SHE)	Strain Rate, s^{-1}	I/ϵ , ^a cm	Susceptibility to SCC	Reference (from original paper)
Type 304 stainless	42% MgCl ₂ , 154°C	-0.14	6.7×10^{-4}	1.2×10^{-5}	yes	10
Fe-5Ni	42% MgCl ₂ , 154°C	-0.182	6.7×10^{-4}	8×10^{-6}	yes	11
Fe-50Ni	42% MgCl ₂ , 154°C	-0.103	6.7×10^{-4}	2.4×10^{-6}	no	11
Type 304 stainless	pH 2.5 H ₂ SO ₄ , 289°C	0	3.7×10^{-4}	2.6×10^{-5}	yes	12
0.1% carbon steel	10 M NaOH, 121°C	-0.7	7×10^{-2} to 10^{-3}	4×10^{-6} to 10^{-4}	yes	5
0.1% carbon steel	pH 4.8, 4 N NaNO ₃ , 102°C	-0.14	1.3×10^{-3}	2.3×10^{-3}	yes	13
0.1% carbon steel	7 N NH ₄ NO ₃ , boiling	+0.4	3×10^{-3}	3.3×10^{-3}	yes	14
Ta, Al, Fe	1% ammonium borate, 25°C	-0.3 to 0	4.8×10^{-3}	4.2×10^{-8}	no	15
Zr, Type 304 stainless, nitchrome, 80Ni-20Cr, 16Cr-14Ni-bal, Fe	M Na ₂ SO ₄ , 25°C M NaH ₂ PO ₄ , 25°C	0 to 0.6	4.8×10^{-3}	to	no	
α brass	Mattson's solution, pH 7.3, 25°C	+0.25	1.1×10^{-3}	1.7×10^{-7}	yes	16
	Mattson's solution, pH 3.6	+0.18	1.1×10^{-3}	4.5×10^{-5} 5.5×10^{-7}	yes no	

^aCurrent densities were converted approximately to metal removal rates by dividing by 3×10^4 .

Hydrogen is presumed to promote crack advance by one of at least six proposed mechanisms [54]: (1) formation of a brittle hydride phase, (2) development of high pressure within internal voids and microcracks, (3) dislocation pinning, (4) facilitation of plastic flow, (5) surface energy reduction, and (6) lattice decohesion. One role of film rupture in crack advance by hydrogen embrittlement would be to maintain sufficient hydrogen generation for embrittlement to occur. Thus, film rupture would involve two effects: (1) depolarizing the anodic reaction, thereby increasing the rate of hydrogen generation at cathodic sites, and (2) reducing the pH within cracks due to hydrolysis of metallic ions, thereby facilitating hydrogen ion reduction within the crevices and making hydrogen available for localized embrittlement near the crack tip. It is also conceivable that the film itself is in some cases a brittle hydride phase, such that rupture not only directly advances the crack but also increases the rate of corrosion for formation of additional hydride.

Film Rupture during Slow Straining

Role of Film Rupture

If the effectiveness of the slow strain-rate technique derives from its ability to maintain accelerated dissolution at a crack tip through repetitive film rupture, it follows that film ductility must be an important parameter of the corroding system. If other factors are held constant, such as repassivation time and amount of crack propagation per rupture event (by whatever operative mechanism), it is apparent that a relatively brittle film would result in faster crack propagation because of its greater frequency of rupture. Crack propagation rate should therefore exhibit some type of inverse relationship with film ductility. In practice it is not possible to test the validity of this expected relationship, because it is not yet possible to vary film ductility independently of other system parameters.

When a filmed electrode is slowly strained, as during slow strain-rate SCC testing, the film first elongates and thins, and then it ruptures. Experiments involving deformation of anodic films on aluminum, iron, stainless steel, and other alloys have shown that typical fracture strains range from about 10^{-4} to 10^{-2} [18,55-60]. For films which grow to a thickness characteristic of the electrode potential, such as Al_2O_3 , chromium oxide (Cr_2O_3), and Fe_3O_4 under certain conditions, the total corrosion that occurs during straining is approximately the same regardless of whether the films thin or rupture. However, the manner of film deformation determines whether SCC occurs. That is, if a film undergoes extensive deformation before it ruptures, it is impossible for cracks to initiate; an incipient crack will be blunted by the large amount of strain in the substrate relative to the amount of forward propagation after film rupture. Conversely, if the film is brittle a better

chance for SCC exists, because a larger amount of localized corrosion occurs per unit amount of substrate strain due to the higher frequency of rupture events.

Although a relatively "brittle" (admittedly this is a nebulous term) film is necessary for initiation and propagation of stress corrosion cracks, it is not a sufficient condition. That is, if ruptures developed in a random fashion over the electrode surface, the net effect would be uniform dissolution of the electrode without cracking. It is necessary that film ruptures be localized at a relatively few specific sites to permit cracks to initiate. These sites might be grain boundaries favorably oriented to the applied stress in the case of intergranular SCC (IGSCC) or active emergent slip steps during transgranular SCC (TGSCC). It is not yet clear why certain sites are favored for crack initiation in a given alloy-corrodent system. For example, for alloys in which dislocation cross slip readily occurs, such as low strength ferritic steels, it is conceivable that dislocations pile up at high angle grain boundaries because other obstacles are easily bypassed. Thus plastic strain might cause severe grain boundary shear, thereby localizing film rupture to these sites and favoring initiation of IGSCC. Although preferential grain boundary deformation has not been reported for mild steel under SCC conditions, it has been observed for Inconel 600 as shown in Fig. 5 [61], which also exhibits IGSCC.

It is also possible for films to grow more rapidly over grain boundaries than within grains, perhaps because of chromium depletion or equilibrium solute segregation to the boundaries causing them to become "active paths" for preferential crack initiation and propagation. Increased rate of film growth over grain boundaries is illustrated in Fig. 6, representing sensitized Type 304 stainless steel exposed in pure water at 289°C [62]. IGSCC would be favored because of the greater amount of crack propagation following film rupture at boundaries than at intragranular sites. Another conceivable effect of grain boundary segregation would be to alter locally the protective or mechanical properties of films through incorporating impurity elements in them. Such changes in film properties would be expected to influence anodic activity at the grain boundaries, and hence the tendency for IGSCC.

Transgranular SCC would prevail if, for example, an active slip system intersected the specimen surface and localized film rupture to this type of site. Alloys in which large slip offsets occur are those with low stacking fault energy, and some correlation between low stacking fault energy and susceptibility to TGSCC has been observed, as reviewed by Parkins [63]. Impurity segregation to active slip planes, thereby rendering them anodic to the surrounding matrix, is another example of conditions that might promote TGSCC.

The preceding considerations indicate why the slow strain-rate technique is a more positive SCC testing procedure than constant strain or constant load tests. During constant strain and constant load testing, each crack ad-

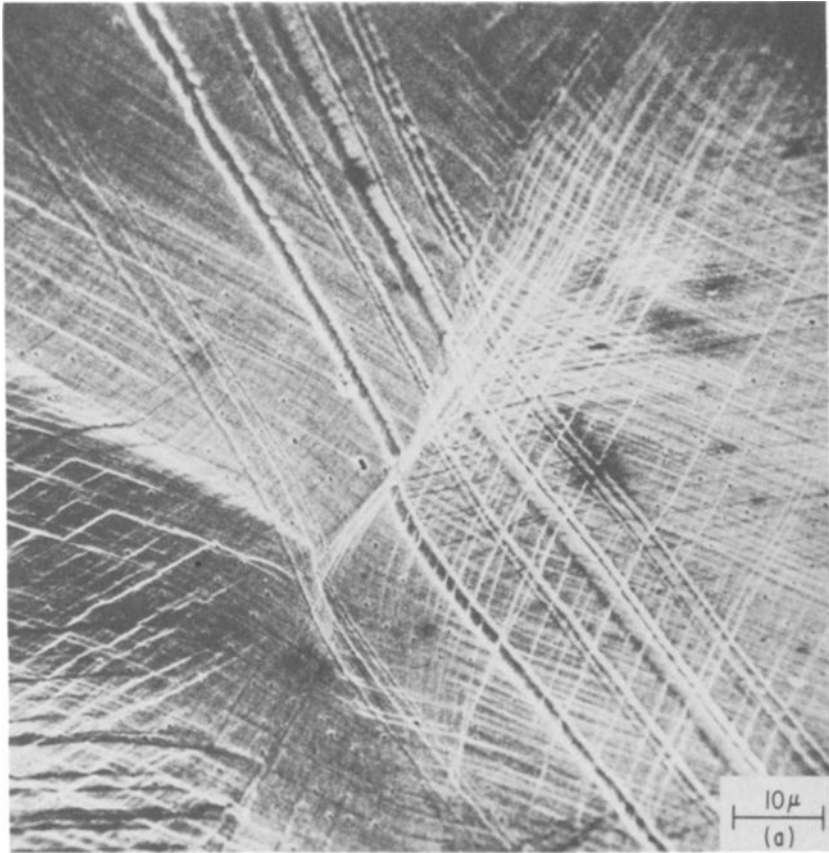


FIG. 5—Electron scanning micrograph of the deformed surface of solution annealed and quenched Inconel-600, pulled to 42 percent axial strain. The loading direction is parallel to the scribed lines [61].

vance following film rupture must be large enough to cause sufficient plastic strain at the crack tip to produce successive rupture. Borderline SCC conditions may not satisfy this condition, and therefore cracking under marginal conditions is sometimes not observed by these procedures. However, the slow strain-rate technique will always cause repetitive film rupture due to continuous application of strain. Therefore, SCC *must* occur if this film rupture is localized and dissolution is sufficiently intense.

Potential Dependence

The slow strain-rate technique, like other methods of SCC testing, usually produces cracking within a well defined range of electrode potential. Typical

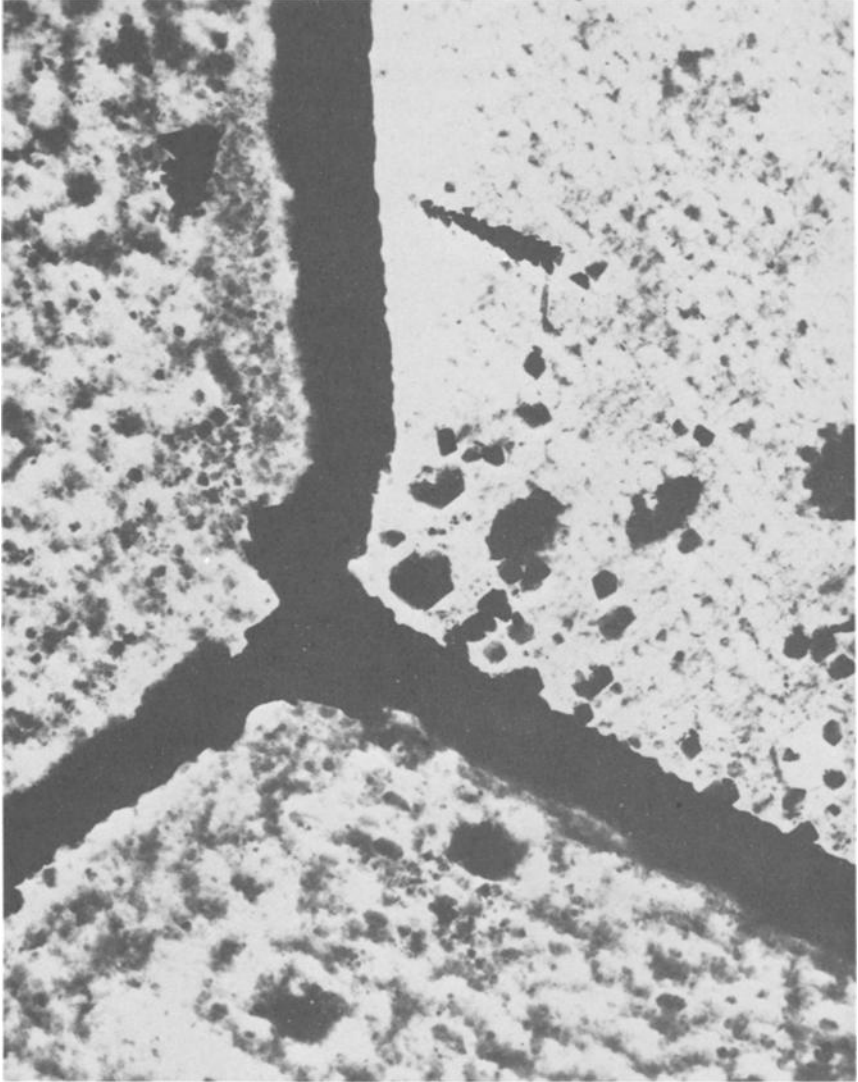


FIG. 6—Transmission electron micrograph of the corrosion product formed during 48 h in pure water at 289°C on sensitized Type 304 stainless steel. The metal has been dissolved in bromine-methanol solution [62].

potential dependence is shown for mild steel in caustic electrolyte in Fig. 7 [17]. In some cases the potential range of SCC susceptibility encompasses primarily the active-passive transition region of polarization behavior, but in others, such as SCC of mild steel in nitrate solution, the range is considerably broader. The influence of electrode potential has been discussed by others [49, 64-67] and therefore will be only summarized here. Essentially, crack formation and propagation depend on a critical balance between activity and passivity at the crack tip. That is, film rupture must produce sufficient dissolution to advance the crack, yet the crack sides must remain relatively passive. Only in a certain range of potential will this balance between electrochemical activity on fresh surface and relative passivity on crack walls be achieved, which is the critical cracking potential range. It is worth noting that a potentiodynamic polarization technique has been developed to capitalize on the preference of SCC for a critical potential range, and this has been used to predict *a priori* the susceptibility of mild steel for SCC in carbonate solutions [68].

Strain-Rate Dependence

Stress corrosion cracking during slow strain-rate testing is sometimes observed only within a specific range of applied strain rate. This range depends on the particular system under consideration; for Ti-5Al-2.5Sn in NaCl solution it is about 10^{-5} to 10^{-4} s^{-1} in unnotched specimens, and 10^{-6} to 10^{-5} s^{-1} for notched specimens [69]. The strain-rate dependence for line pipe steel in carbonate-bicarbonate electrolyte is shown in Fig. 8 [70]. It is evident that at the most aggressive potential of -0.700 V a lower limit is not

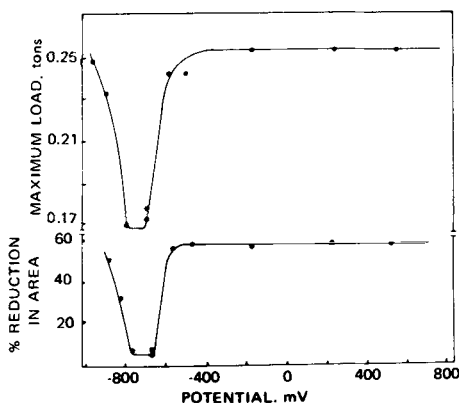


FIG. 7—Mechanical properties of mild steel, strained at $4.2 \times 10^{-6} \text{ s}^{-1}$ in boiling 35 percent NaOH, as a function of potential [17]. By permission of National Association of Corrosion Engineers.

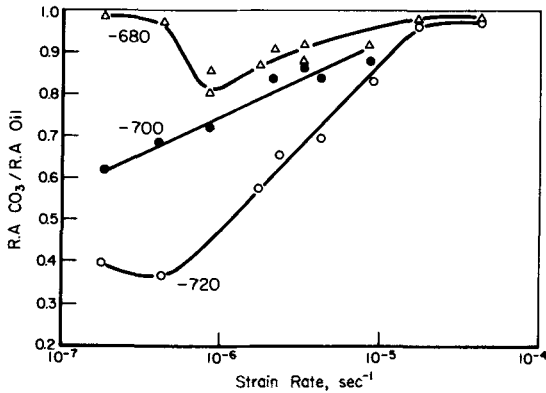


FIG. 8—Effects of strain rate upon the stress corrosion susceptibility of line pipe steel in 79°C (175°F) 2 N CO₃/HCO₃ solution at various potentials [70]. Courtesy of Pipeline Research Committee of American Gas Association.

apparent in the strain-rate range investigated, but at potentials slightly anodic and cathodic to this value a lower limit exists.

The existence of an upper limit on strain rate is easily understood. It results from insufficient crack advance relative to the amount of strain occurring in the substrate, such that a crack geometry cannot be developed and maintained. The reason for a lower strain rate limit is less obvious. It is sometimes stated that it results from an insufficient strain rate to maintain an "active crack tip." However, as has already been discussed, in theory a stress corrosion crack tip need not always be "active" in the sense of being continuously unfiled to undergo accelerated dissolution. Indeed, if reducing the strain rate does not significantly increase the number of sites on the electrode surface at which the film is rupturing (and there is no obvious reason why it should), and if the rate of film dissolution into the electrolyte is nil, then logically there should be no lower strain-rate limit. That is, the crack propagation rate should decrease indefinitely with decreasing strain rate, because although the frequency of film rupture decreases, film rupture nevertheless still proceeds and is still localized to a few sites.

There are several possible explanations for the existence of a lower limit on strain rate. The first results from the fact that in almost all electrolytes causing SCC, the corrosion film dissolves at a finite rate. This dissolution continuously removes old film that has been stressed in tension due to the deforming substrate, and replaces it with fresh film in which no stress exists other than the inherent growth stress. At strain rates in the SCC range, the above stress relief may be slow relative to the rate of increase of stress due to straining, such that the fracture stress of the film can be attained and periodic film rupture can occur. At very slow strain rates, however, the rate of stress increase in the film may be slow compared to the dissolution-

induced stress relief, and film rupture may be either impossible or too infrequent to cause SCC. Thus, incipient crack initiation sites are continuously removed by anodic dissolution. Alternatively, if cracking depends on a poorly protective transition film being maintained at the crack tip, then application of very slow strain rates may permit a more protective film to establish itself and thereby stifle dissolution. A third possibility derives from the observation that ionic mobility apparently facilitates deformation of corrosion films [71, 72], and that conceivably the reverse may occur. If stress relief results from increased ionic mobility created by deformation of a growing film, as would be expected if both cations and anions diffuse, then sufficient stress relaxation may occur at very low strain rates to reduce or suppress film rupture. Providing that this deformation-enhanced diffusivity does not increase proportionately with strain rate, the tensile stress in the film at a given strain would increase with increasing strain rate. Thus at a critical lower strain-rate limit the stress in the film would reach the fracture stress, and film rupture would commence.

Summary

Stress corrosion cracking proceeds in many alloy-corrodent systems under conditions favoring film formation on exposed surfaces. Although it has been proposed that certain alloys such as aluminum-zinc-magnesium may stress corrode under film-free conditions directly at the crack tip, numerous other alloys are likely covered by some type of corrosion film at the tip. Repetitive rupture of such films exposes the alloy surface and permits crack advance by proposed mechanisms such as dissolution or hydrogen embrittlement. Cracking morphology, intergranular versus transgranular, is determined either by active path corrosion, or by whether slip is localized at grain boundaries or intragranularly such as at emergent slip steps. The success of the slow strain-rate technique as a severe test of SCC susceptibility is ascribed to its ability to repeatedly expose the crack tip metal to the aggressive corrodent by film rupture.

References

- [1] Forty, A. J., and Humble, P., *Philosophical Magazine*, Vol. 8, 1963, p. 247.
- [2] Johnson, H. E. and Leja, J., *Corrosion*, Vol. 22, 1966, p. 178.
- [3] Hoar, T. P. and Booker, C. J. L., *Corrosion Science*, Vol. 5, 1965, p. 821.
- [4] Pugh, E. N. in *Environment-Sensitive Mechanical Behavior*, Gordon and Breach, New York, 1966, pp. 351-401.
- [5] McEvily, A. J., Jr. and Bond, A. P., *Journal of the Electrochemical Society*, Vol. 112, 1965, p. 131.
- [6] Pinchback, J. R., Clough, S. P., and Heldt, L. A., *Metallurgical Transactions*, Vol. 6A, 1975, p. 1479.
- [7] Birley, S. S. and Tromans, D., *Corrosion*, Vol. 27, 1971, p. 297.
- [8] Okamoto, G., *Corrosion Science*, Vol. 13, 1973, p. 471.
- [9] Schwabe, K., *Journal of the Electrochemical Society*, Vol. 110, 1963, p. 667.

- [10] Okamoto, G. and Shibata, T., *Proceedings*, Third International Congress on Metallic Corrosion, Vol. 1, MIR Moscow, 1969, p. 396.
- [11] Kudo, D., Shibata, T., Okamoto, G., and Sato, N., *Corrosion Science*, Vol. 8, 1968, p. 809.
- [12] Barnartt, S. and van Rooyen, D., *Journal of the Electrochemical Society*, Vol. 108, 1961, p. 222.
- [13] Latanision, R. M. and Staehle, R. W., *Proceedings*, Conference on Fundamental Aspects of Stress Corrosion Cracking, R. W. Staehle and D. van Rooyen, Eds., National Association of Corrosion Engineers, Houston, 1969, p. 214.
- [14] Rockel, M. and Staehle, R. W., unpublished results.
- [15] Montuelle, J., Cunha-Beb, N., Berge, P., and Colin, D., Rapport Euratom No. 2064 C.N.R.S.
- [16] Davis, J. A. and Wilde, B. E., *Journal of the Electrochemical Society*, Vol. 117, 1970, p. 1348.
- [17] Humphries, M. J. and Parkins, R. N., *Proceedings*, Conference on Fundamental Aspects of Stress Corrosion Cracking, R. W. Staehle and D. van Rooyen, Eds., National Association of Corrosion Engineers, Houston, 1969, p. 384.
- [18] Diegle, R. B. and Vermilyea, D. A., *Corrosion*, Vol. 32, 1976, p. 411.
- [19] Szklarska-Smialowska, Z., *Corrosion*, Vol. 20, 1964, p. 1981.
- [20] Parkins, R. N. and Usher, R., *First International Congress on Metallic Corrosion*, Butterworths, London, 1962, p. 289.
- [21] Parkins, R. N., *Journal of the Iron and Steel Institute*, Vol. 172, 1954, p. 149.
- [22] Galvele, J. and Hoar, T. P., unpublished work quoted in Ref 17.
- [23] Diegle, R. B. and Vermilyea, D. A., *Journal of the Electrochemical Society*, Vol. 122, 1975, p. 180.
- [24] Godard, H. P. in *The Corrosion of Light Metals*, R. T. Foley, N. Hackerman, C. V. King, F. C. LaQue, and H. H. Uhlig, Eds., Wiley, New York, 1967, p. 3.
- [25] Hart, R. K., *Transactions*, Faraday Society, Vol. 53, 1957, p. 1020.
- [26] Vedder, W. and Vermilyea, D. A., *Transactions*, Faraday Society, Vol. 65, 1969, p. 561.
- [27] Andreeva, V. V., *Corrosion*, Vol. 20, 1964, p. 35t.
- [28] Tomashov, N. D., Altovskii, R. M., and Takushnerev, M., *Doklady Akademii Nauk (USSR)*, 1961, Tom. 141, Table 1, p. 2.
- [29] Rivolta, B., *Metallurgia Italiana*, Vol. 50, 1958, pp. 173, 255.
- [30] Cotton, J. B., *Werkstoffe und Korrosion*, Vol. 11, 1960, p. 152.
- [31] Koizumi, T. and Nakayama, T., *Proceedings*, Third International Congress on Metallic Corrosion, MIR, Moscow, 1969, p. 451.
- [32] Sedriks, A. J., *Transactions*, American Institute of Mining, Metallurgical, and Petroleum Engineers, Vol. 239, 1967, p. 916.
- [33] Sedriks, A. J., Slattery, R. W., and Pugh, E. N., *Proceedings*, Conference on Fundamental Aspects of Stress Corrosion Cracking, R. W. Staehle and D. van Rooyen, Eds., National Association of Corrosion Engineers, Houston, 1969, p. 673.
- [34] Graf, L., *Proceedings*, Conference on Fundamental Aspects of Stress Corrosion Cracking, R. W. Staehle and D. van Rooyen, Eds., National Association of Corrosion Engineers, Houston, 1969, p. 187.
- [35] Bakish, R. and Robertson, W. D., *Journal of the Electrochemical Society*, Vol. 103, 1956, p. 320.
- [36] Bakish, R. and Robertson, W. D., *Transactions*, American Institute of Mining, Metallurgical, and Petroleum Engineers, Vol. 206, 1956, p. 1277.
- [37] Pickering, H. W. and Swann, P. R., *Corrosion*, Vol. 19, 1963, p. 373.
- [38] Pickering, H. W. and Wagner, C., *Journal of the Electrochemical Society*, Vol. 114, 1967, p. 698.
- [39] Pickering, H. W., *Proceedings*, Conference on Fundamental Aspects of Stress Corrosion Cracking, R. W. Staehle and D. van Rooyen, Eds., National Association of Corrosion Engineers, Houston, 1969, p. 159.
- [40] Beck, T. R., Blackburn, M. J., and Speidel, M. O., Contract NAS 7-489, Quarterly Progress Report No. 11, March 1969.
- [41] Kaesche, H., *Die Korrosion der Metalle*, Springer Verlag Berlin, Heidelberg, 1966.
- [42] Hoar, T. P. and Jones, R. W., *Corrosion Science*, Vol. 13, 1973, p. 725.

- [43] Diegle, R. B. and Vermilyea, D. A., *Corrosion*, Vol. 32, 1976, p. 353.
- [44] Bohnenkamp, K., *Proceedings*, Conference on Fundamental Aspects of Stress Corrosion Cracking, R. W. Staehle and D. van Rooyen, Eds., National Association of Corrosion Engineers, Houston, 1969, p. 374.
- [45] Staehle, R. W., Turluer, G., and McCright, D., EPRI Progress Report for January-June, 1975, Project Rp. 311-1.
- [46] Parkins, R. N., private communication.
- [47] Forty, A. J. and Humble, P. H., *Second International Congress on Metallic Corrosion*, National Association of Corrosion Engineers, Houston, 1966, p. 80.
- [48] Podesta, J. J., Rothwell, G. P., and Hoar, T. P., *Corrosion Science*, Vol. 11, 1971, p. 241.
- [49] Logan, H. L., *Journal of Research*, National Bureau of Standards, Vol. 48, 1952, p. 99.
- [50] Vermilyea, D. A., *Proceedings*, International Conference on Stress Corrosion Cracking and Hydrogen Embrittlement of Iron Base Alloys, Firminy, France, 1973, to be published by National Association of Corrosion Engineers.
- [51] Vermilyea, D. A., *Journal of the Electrochemical Society*, Vol. 119, 1972, p. 405.
- [52] Scully, J. C., *Corrosion Science*, Vol. 15, 1975, p. 207.
- [53] Vermilyea, D. A. and Diegle, R. B., *Corrosion*, Vol. 32, 1976, p. 26.
- [54] *Proceedings*, International Conference on Stress Corrosion Cracking and Hydrogen Embrittlement of Iron Base Alloys, Firminy, France, 1973, to be published by National Association of Corrosion Engineers.
- [55] Bradhurst, D. H. and Leach, J. S. L., *Transactions*, British Ceramic Society, Vol. 62, 1963, p. 793.
- [56] Grosskreutz, J. C., *Journal of the Electrochemical Society*, Vol. 116, 1969, p. 1232.
- [57] Block, R. J., *Journal of the Electrochemical Society*, Vol. 117, 1970, p. 788.
- [58] Cochran, N. J. and Block, R. J., *Journal of the Electrochemical Society*, Vol. 117, 1970, p. 225.
- [59] Bubar, S. F. and Vermilyea, D. A., *Journal of the Electrochemical Society*, Vol. 114, 1967, p. 882.
- [60] Harrison, P. L., *Corrosion Science*, Vol. 7, 1967, p. 789.
- [61] Lee, D. and Vermilyea, D. A., *Metallurgical Transactions*, Vol. 2, 1971, p. 2565.
- [62] Indig, M. E. and Vermilyea, D. A., *Proceedings of the Fifth International Symposium on Metallic Corrosion*, Paper D-28, Tokyo, May 1972.
- [63] Parkins, R. N., *Metallurgical Review*, Vol. 9, 1964, p. 201.
- [64] Hoar, T. P. and Hines, J. G., *Journal of the Iron and Steel Institute*, Vol. 177, 1954, p. 248; Vol. 182, 1956, p. 124.
- [65] Hines, J. G. and Hoar, T. P., *Journal of the Iron and Steel Institute*, Vol. 184, 1956, p. 166.
- [66] Hoar, T. P., and Hines, J. G., *Proceedings*, Eighth Meeting CITCE, Madrid, 1956, Butterworths, London, 1958, p. 273.
- [67] Hines, J. G. and Hoar, T. P., *Journal of Applied Chemistry*, Vol. 8, 1958, p. 764.
- [68] Sutcliffe, J. M., Fessler, R. R., Boyd, W. K., and Parkins, R. N., *Corrosion*, Vol. 28, 1972, p. 313.
- [69] Powell, D. J. and Scully, J. C., *Corrosion*, Vol. 24, 1968, p. 151.
- [70] Berry, W. E., *Proceedings*, Fifth Symposium on Line Pipe Research, Vol. 1, Houston, 20-22 Nov. 1974.
- [71] Bradhurst, D. H. and Leach, J. S. L., *Journal of the Electrochemical Society*, Vol. 113, 1966, p. 1245.
- [72] Leach, J. S. L. and Neufeld, P., *Proceedings*, British Ceramic Society, No. 6, 1966, p. 49.

M. Hishida,¹ J. A. Begley,² R. D. McCright,³ and R. W. Staehle²

Anodic Dissolution and Crack Growth Rate in Constant Strain-Rate Tests at Controlled Potentials

REFERENCE: Hishida, M., Begley, J. A., McCright, R. D., and Staehle, R. W., "Anodic Dissolution and Crack Growth Rate in Constant Strain-Rate Tests at Controlled Potentials," *Stress Corrosion Cracking—The Slow Strain-Rate Technique*, ASTM STP 665, G. M. Ugiansky and J. H. Payer, Eds., American Society for Testing and Materials, 1979, pp. 47-60.

ABSTRACT: A theoretical analysis is presented of the constant strain-rate test. The rate of reduction of the cross-sectional area caused by straining is compared with the loss of cross section due to metal dissolution or crack growth, or both. The relationship between the environmental deterioration rate and the strain at which a maximum load is obtained in a constant strain rate test is developed as a function of strain rate. Experimental results of constant strain-rate tests of Type 304 stainless steel conducted in a 10 *N* sulfuric acid (H₂SO₄) + 0.1 *M* sodium chloride (NaCl) solution at various rates are discussed. Measured and calculated crack growth rates show good agreement.

KEY WORDS: stress corrosion cracking, constant strain rate tests, Type 304 stainless steel, sensitization, anodic dissolution, polarization curves, sulfuric acid, experimental data, theoretical analysis

During constant strain-rate tests, various mechanical properties, such as yield stress, ultimate tensile stress, elongation, and reduction in area, are measured. Ratios of these mechanical properties obtained in a corrosive environment to those obtained in an inert environment are taken to indicate the presence and relative severity of an environmental effect. More complex indices are sometimes used to reflect stress corrosion cracking susceptibility [1].⁴

¹Metallurgist, Toshiba Research and Development Center, Kawasaki, 210 Japan.

²Associate professor and professor, respectively, The Ohio State University, Columbus, Ohio 43210.

³Metallurgist, Lawrence-Livermore Laboratory, University of California, Livermore, Calif. 94550.

⁴The italic numbers in brackets refer to the list of references appended to this paper.

In this paper, a theoretical analysis is developed to provide a better understanding of the constant strain-rate test. The rate of reduction in cross-sectional area caused by constant straining is compared with the environmental deterioration rate, that is, the loss of cross section due to metal dissolution or crack growth, or both. This comparison leads to a relationship between the environmental deterioration rate and the strain at which a maximum load is obtained in a load-strain diagram at constant strain rates. Experimental results from constant strain-rate tests of Type 304 stainless steel conducted in a 10 *N* sulfuric acid (H₂SO₄) + 0.1 *M* sodium chloride (NaCl) solution at strain rates of 2×10^{-5} , 2×10^{-6} , and $4 \times 10^{-7} \text{ s}^{-1}$ are compared with theoretical predictions.

Theoretical Analysis

Consider a bar-type tension specimen with a gage length, L_0 , and a radius, r_0 . The load on a specimen which increases with time, t , and reaches a maximum load, P_m , in a constant strain rate test is expressed by

$$P(t) = A(t) \cdot \sigma(t) \quad (1)$$

where $A(t)$ is the area of cross section of the specimen at time t and $\sigma(t)$ is the true stress on the specimen. The stress-strain curves of many materials fit a power expression of the form

$$\sigma = K\epsilon^n \quad (2)$$

where K is the stress at $\epsilon = 1.0$, and n , the strain hardening coefficient, is the slope of a log-log plot of Eq 2. This equation is only valid from the beginning of plastic flow to the maximum load at which point the specimen begins to neck down.

The area of cross section can be written as

$$A(t) = \pi \cdot r(t)^2 \quad (3)$$

where $r(t)$ is the radius of cross section. The time differential of $A(t)$ is

$$\frac{dA(t)}{dt} = 2\pi \cdot r(t) \frac{dr(t)}{dt} \quad (4)$$

The decrease of $r(t)$ with time is caused not only by deformation but also by environmental deterioration effects such as metal dissolution or crack growth, or both. Therefore, $dr(t)/dt$ can be considered to consist of two terms. The term for constant straining deformation is calculated from a constancy of volume relationship

$$L(t) \cdot \pi r(t)^2 = L_0 \cdot \pi r_0^2 \quad (5)$$

Differentiating Eq 5 with respect to time gives

$$\begin{aligned} \frac{dL(t)}{dt} \cdot \pi r(t)^2 + L(t) \cdot 2\pi r(t) \frac{dr(t)}{dt} &= 0 \\ \frac{dr(t)}{dt} &= \frac{-r(t)}{2L(t)} \frac{dL(t)}{dt} \end{aligned} \quad (6)$$

A constant strain rate is assumed to be $\dot{\epsilon}$, hence

$$L(t) = L_0(\dot{\epsilon}t + 1) \quad (7)$$

and

$$\frac{dL(t)}{dt} = L_0 \cdot \dot{\epsilon} \quad (8)$$

Substituting Eqs 7 and 8 into Eq 6 results in

$$\frac{dr(t)}{dt} = -\frac{r(t) \cdot \dot{\epsilon}}{2(\dot{\epsilon}t + 1)} \quad (9)$$

On the other hand, a partial term for environmental deterioration rate is defined as

$$\frac{dr(t)}{dt} = -\dot{\gamma} = -(\dot{\gamma}_a + \dot{\gamma}_c) \quad (10)$$

where $\dot{\gamma}_a$ is a metal dissolution rate and $\dot{\gamma}_c$ is a crack growth rate. In this derivation, $\dot{\gamma}$ is assumed to be independent of time and stress. Therefore, the total rate of reduction of area is

$$\frac{dr(t)}{dt} = -\frac{r(t) \cdot \dot{\epsilon}}{2(\dot{\epsilon}t + 1)} - \dot{\gamma} \quad (11)$$

In this development, a constancy of volume relationship and a strain rate constancy over the specimen gage section are applied, and the approximations may not make much deviation from this story until local elongation commences. This local elongation may fairly occur after the maximum load during constant strain rate tests.

Therefore, the differential form of Eq 1 is useful. It is given by

$$\begin{aligned} \frac{dP(t)}{dt} &= A(t) \frac{d\sigma(t)}{dt} + \sigma(t) \cdot \frac{dA(t)}{dt} \\ &= \pi r(t)^2 \frac{d\sigma(t)}{dt} + \sigma(t) \cdot 2\pi r(t) \frac{dr(t)}{dt} \end{aligned} \quad (12)$$

Substituting Eqs 2, 4, and 11, and also the definition of true strain

$$\epsilon = \ln(\dot{\epsilon}t + 1) \quad (13)$$

into Eq 12 leads to Eq 14

$$\begin{aligned} \frac{dP}{dt} &= \pi r(t)^2 \cdot K \cdot n \{ \ln(\dot{\epsilon}t + 1) \}^{n-1} \frac{\dot{\epsilon}}{(\dot{\epsilon}t + 1)} \\ &+ K \{ \ln(\dot{\epsilon}t + 1) \}^n \cdot 2\pi r(t) \left(-\frac{r(t) \cdot \dot{\epsilon}}{2(\dot{\epsilon}t + 1)} - \dot{\gamma} \right) \\ &= P \left\{ \frac{n\dot{\epsilon}}{(\dot{\epsilon}t + 1) \ln(\dot{\epsilon}t + 1)} - \frac{\dot{\epsilon}}{(\dot{\epsilon}t + 1)} - \frac{2\dot{\gamma}}{r(t)} \right\} \end{aligned} \quad (14)$$

The variation of the gage section radius with time, $r(t)$, can be obtained by solving differential Eq 11. The solution is

$$r(t) = \frac{r_0 + \frac{2}{3} \frac{\dot{\gamma}}{\dot{\epsilon}}}{(\dot{\epsilon}t + 1)^{1/2}} - \frac{2}{3} \frac{\dot{\gamma}}{\dot{\epsilon}} (\dot{\epsilon}t + 1) \quad (15)$$

Substituting Eq 15 into Eq 14 results in a relationship between the time to maximum load, the environmental deterioration rate, and the strain rate.

$$\frac{n\dot{\epsilon}}{(\dot{\epsilon}t_m + 1) \ln(\dot{\epsilon}t_m + 1)} - \frac{\dot{\epsilon}}{(\dot{\epsilon}t_m + 1)} - \frac{2\dot{\gamma}_m(\dot{\epsilon}t_m + 1)^{1/2}}{r_0 - \frac{2}{3} \frac{\dot{\gamma}_m}{\dot{\epsilon}} \{ (\dot{\epsilon}t_m + 1)^{3/2} - 1 \}} = 0$$

Thus

$$\frac{\dot{\gamma}_m}{r_0 \dot{\epsilon}} = \frac{1}{\frac{2(\dot{\epsilon}t_m + 1)^{3/2} \ln(\dot{\epsilon}t_m + 1)}{n - \ln(\dot{\epsilon}t_m + 1)} + \frac{2}{3} \{ (\dot{\epsilon}t_m + 1)^{3/2} - 1 \}} \quad (16)$$

The term $\dot{\gamma}_m/r_0\dot{\epsilon}$ is dimensionless.

Equation 16 is plotted in Fig. 1 for a strain hardening exponent, n , of 0.59. This value is the measured value for the Type 304 stainless steel used in this study. Equation 16 thus permits the calculation of the total rate of loss of cross-sectional area in a constant strain-rate test. If cracking occurs, the crack growth rate may be calculated provided that either the general corrosion rate is negligible or can be reasonably estimated.

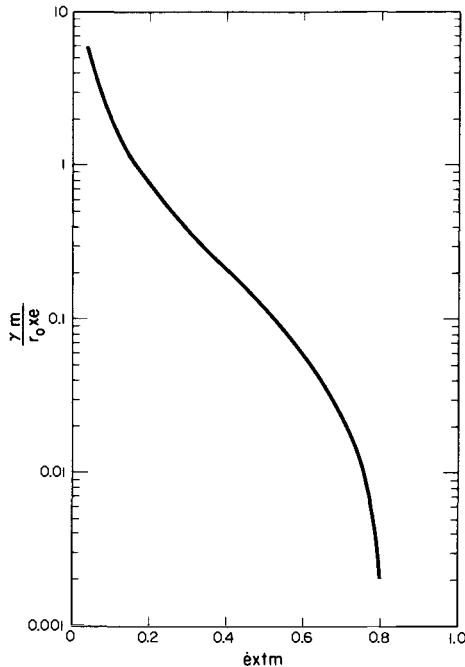


FIG. 1—Relationship between the dimensionless environmental deterioration rate $\dot{\gamma}_m/\tau_0\dot{\epsilon}$ and the strain at which a maximum load is obtained in a load-strain diagram of constant strain-rate tests, calculated from Eq 16.

Results and Discussions

The following paragraphs describe the results of constant strain-rate tests of Type 304 stainless steel in a 10 N H₂SO₄ + 0.1 M NaCl solution along with polarization curve data. Figure 2 shows an experimental cell used. Measured environmental deterioration rates are compared with computed values.

Polarization Curves

Polarization curves of Type 304 stainless steel obtained in 10 N H₂SO₄ + 0.1 M NaCl are shown in Fig. 3. Corrosion potentials and active peak currents of annealed and sensitized specimens were almost the same. A significant difference was observed in the active to passive transition region. The transition potential region of the sensitized specimen, especially for the 20-h heat treatment, was broad and the current density decreased gradually from the active peak current to the passive current. From the passive potential range to the transpassive range, there are no meaningful differences except perhaps a mild increase in the transition potential region.

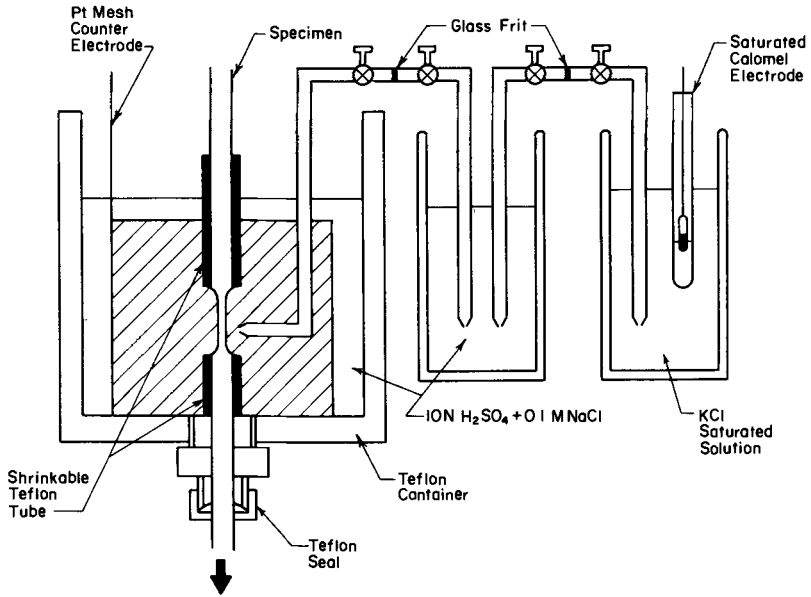


FIG. 2—Experimental cell.

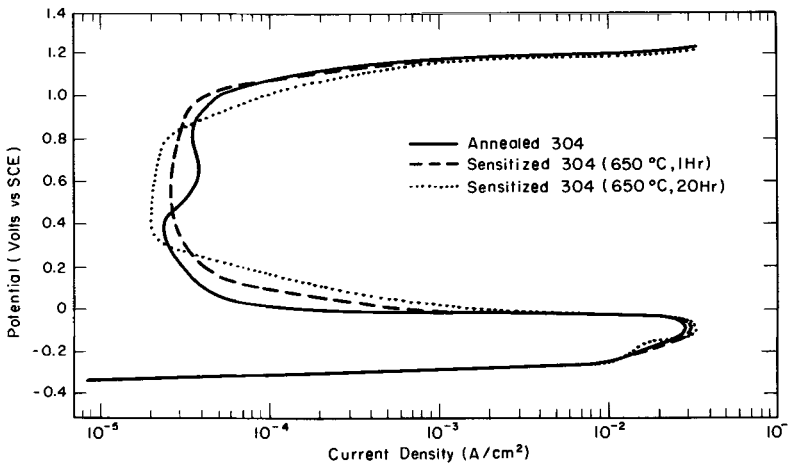


FIG. 3—Polarization curves of annealed Type 304 stainless steel and sensitized (650°C, 1 h and 650°C, 20 h) Type 304 stainless steels in 10 N H₂SO₄ + 0.1 M NaCl at room temperature. Scanned at 20 mV/min.

Calculated Environmental Effects in Constant Strain Rate Tests

Figure 4 shows $\dot{\gamma}_m$, calculated environmental deterioration rates, from maximum loads and times to maximum load, t_m , of the constant strain-rate tests. As shown in Fig. 4, potentials in the active and transpassive regions resulted in high $\dot{\gamma}_m$ values. No significant effect of sensitizing heat treatments on $\dot{\gamma}_m$ was found at a strain rate of $2 \times 10^{-5} \text{ s}^{-1}$ so far. At a strain rate of $2 \times 10^{-6} \text{ s}^{-1}$, a cathodic potential also showed high $\dot{\gamma}_m$ values. A specimen sensitized for 20 h exhibited a high susceptibility to environmental deterioration in the active to passive transition region. The fact coincides with polarization measurement results.

The shape of the environmental deterioration rate curve of Fig. 1 and the fact that the chosen strain hardening exponent is most suitable for intermediate strain ranges suggest that the most reliable calculations will occur in the range of $0.06 < \dot{\gamma}_m/r_0\dot{\epsilon} < 0.60$. Thus the optimum strain rate is keyed to $\dot{\gamma}_m$. For example, in the present tests, $\dot{\gamma}_m$ is on the order of 10^{-6} mm/s , and a mid-range value of $\dot{\gamma}_m/r_0\dot{\epsilon}$ is obtained with a strain rate of $4 \times 10^{-6} \text{ s}^{-1}$ for a 1.27-mm radius specimen.

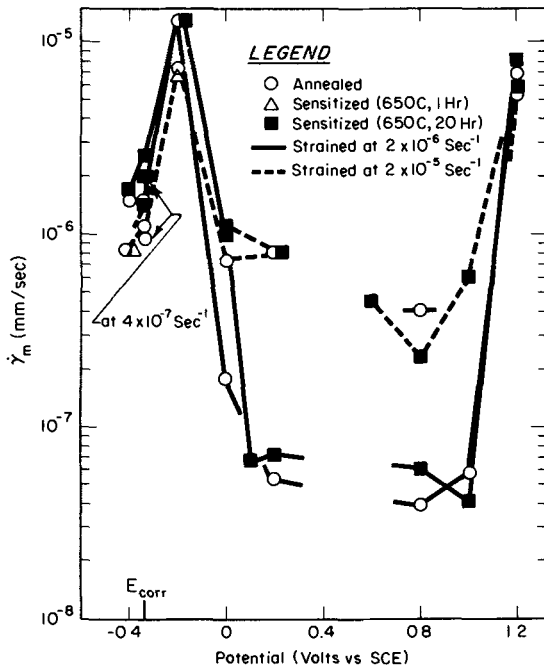


FIG. 4—Change of environmental deterioration rates with potential. Calculated from constant strain-rate test results.

Anodic Dissolution Rates

The term $\dot{\gamma}_m$ consists of both general anodic dissolution rates, $\dot{\gamma}_a$, and rates of crack growth, $\dot{\gamma}_c$. The rate of loss of cross section due to metal dissolution can be estimated from current densities. Electrochemical equivalencies of Type 304 stainless steel at various applied potentials are calculated on the basis of Pourbaix diagrams and a composition of 18Cr-8Ni-74Fe. In converting $\dot{\gamma}_m$ to an equivalent current density, the molecular weight chosen was 55.4 g/mole and the density was set equal to 8.0 g/cm³. Table 1 shows corresponding $\dot{\gamma}_a$ calculated from $\dot{\gamma}_m$, $\dot{\gamma}_a$ from observed current densities at a strain of 7.2 percent during the constant strain rate tests, and current densities in polarization tests. At potentials in the active and transpassive regions, $\dot{\gamma}_a$ calculated from environmental deterioration rates agrees well with $\dot{\gamma}_a$ from current densities observed in the constant strain-rate tests or the current densities observed in polarization tests. In the passive region, the calculated $\dot{\gamma}_a$ was much higher than current density measurements at a strain of 7.2 percent and the current densities in polarization tests. Dynamic straining may be expected to result in film rupture and therefore higher corrosion rates. Hence the calculated $\dot{\gamma}_a$ should not correspond to passive current densities in the polarization tests. The discrepancy between the calculated $\dot{\gamma}_a$ values and the equivalent current densities measured in the slow strain-rate

TABLE 1—Comparison of current densities in constant strain rate tests conducted at various potentials.

Potential mV versus SCE	Specimen	$\dot{\epsilon} = 2 \times 10^{-5} \text{ s}^{-1}$		$\dot{\epsilon} = 2 \times 10^{-6} \text{ s}^{-1}$		Current Density in Polarization Curves, (mA/cm ²)
		Cal. $\dot{\gamma}_a$	Ob. $\dot{\gamma}_a$	Cal. $\dot{\gamma}_a$	Ob. $\dot{\gamma}_a$	
-200	AN	23	16	40	19	16
	SM	20				17
	SH			40	17	14
0	AN	2.2	0.13	0.55	0.68	0.20
	SH	3.3	0.085	3.0	3.5	2.5
+100	SH			0.20	0.008	0.26
+200	AN	2.4	0.10	0.16	0.04	0.03
	SH	2.4	0.060	0.22	0.008	0.070
+600	SH	1.9	0.089			0.020
+800	AN	1.6	0.048	0.16	0.044	0.035
	SH	0.94	0.080	0.24	0.013	0.025
+1000	AN			0.24	0.20	0.040
	SH	2.5	0.10	0.16	0.007	0.090
+1200	AN	26	21	33	21	15
	SH	29	27	39	25	20

NOTE—

AN = annealed, SM = sensitized (650°C, 1 h), and SH = sensitized (650°C, 20 h).

Cal. $\dot{\gamma}_a$ was an environmental deterioration rate obtained in constant strain rate tests (neglecting crack growth). Converted to equivalent current density.

Ob. $\dot{\gamma}_a$ was the current density observed at a strain of 7.2 percent in the constant strain rate tests.

tests are more difficult to explain. The current density at a strain of 7.2 percent may not represent the overall behavior.

Figures 5 and 6 show scanning electron microscope (SEM) fractographs of the constant strain rate specimens. At -400 mV (versus saturated calomel electrode (SCE)), in the cathodic potential range, shallow secondary cracks were observed at a strain rate of $2 \times 10^{-5} \text{ s}^{-1}$. The cracking seemed to be intergranular. These secondary cracks were not observed at a strain rate of $2 \times 10^{-6} \text{ s}^{-1}$. At open circuit potential, secondary intergranular cracks were observed at both strain rate tests. At -200 mV (versus SCE), that is close to the active peak potential, severe general anodic dissolution occurred. After tests in the passive potential region at 200 mV (versus SCE), the fracture surface and outside surface of the specimens were very similar to those of specimens tested in air. There was no secondary cracking and only a ductile fracture mode was observed. At 1200 mV (versus SCE), in the transpassive potential region, severe anodic dissolution was also observed. However, the corrosion morphology was different from the specimens tested near the active peak. Some evidence of intergranular attack was observed on the specimen surfaces. Thus, these surface observations support a separability of $\dot{\gamma}_a$ from $\dot{\gamma}_m$ and that of $\dot{\gamma}_c$ from $\dot{\gamma}_m$ depending on the applied potentials.

Crack Growth Rates

At corrosion potentials and at potentials in the cathodic region, metal dissolution can be neglected. Therefore, the environmental deterioration rates, $\dot{\gamma}_m$, are equal to crack growth rates. Figure 7 shows the calculated crack growth rates as a function of strain rate and heat treatment.

The calculated crack growth rates were compared to measured values. The specimens were mounted after failure and polished to mid-diameter. Average depths of major cracks were measured on the cross section. The average crack growth rate was then calculated from the average depth and time to failure. Table 2 shows the results. The average measured crack growth rates correspond quite well with the calculated growth rates.

The rationale for assuming a constant crack growth rate is based upon the fracture mechanics approach to stress corrosion cracking. The Stage II region of crack growth is independent of the applied stress intensity. The constant strain rate tests were certainly beyond the realm of linear elastic fracture mechanics. However the concept of a plastic crack tip singularity [2,3] has led to the successful J_{Ic} elastic-plastic fracture criterion [4,5]. The plastic singularity concept should apply equally well to other crack tip processes such as stress corrosion cracking. Hence the assumption of Stage II cracking is reasonable in the fully plastic constant strain rate tests. A further verification of this hypothesis is shown in Fig. 7 where the crack growth rates are shown to be independent of the applied strain rates from $4 \times 10^{-7} \text{ s}^{-1}$ to $2 \times 10^{-5} \text{ s}^{-1}$.

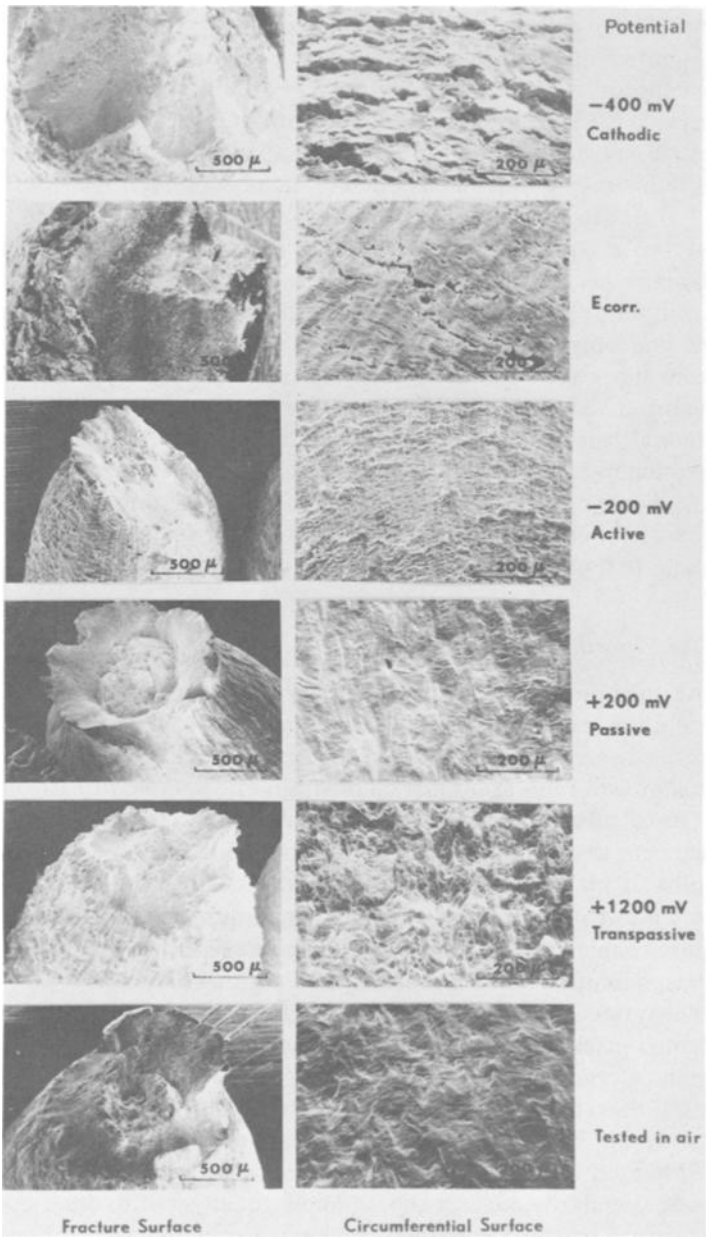


FIG. 5—SEM fractographs and circumferential surfaces of annealed Type 304 stainless steel after constant strain-rate tests conducted at various potentials in a 10 N H₂SO₄ + 0.1 M NaCl solution at room temperature at $2 \times 10^{-5} \text{ s}^{-1}$.

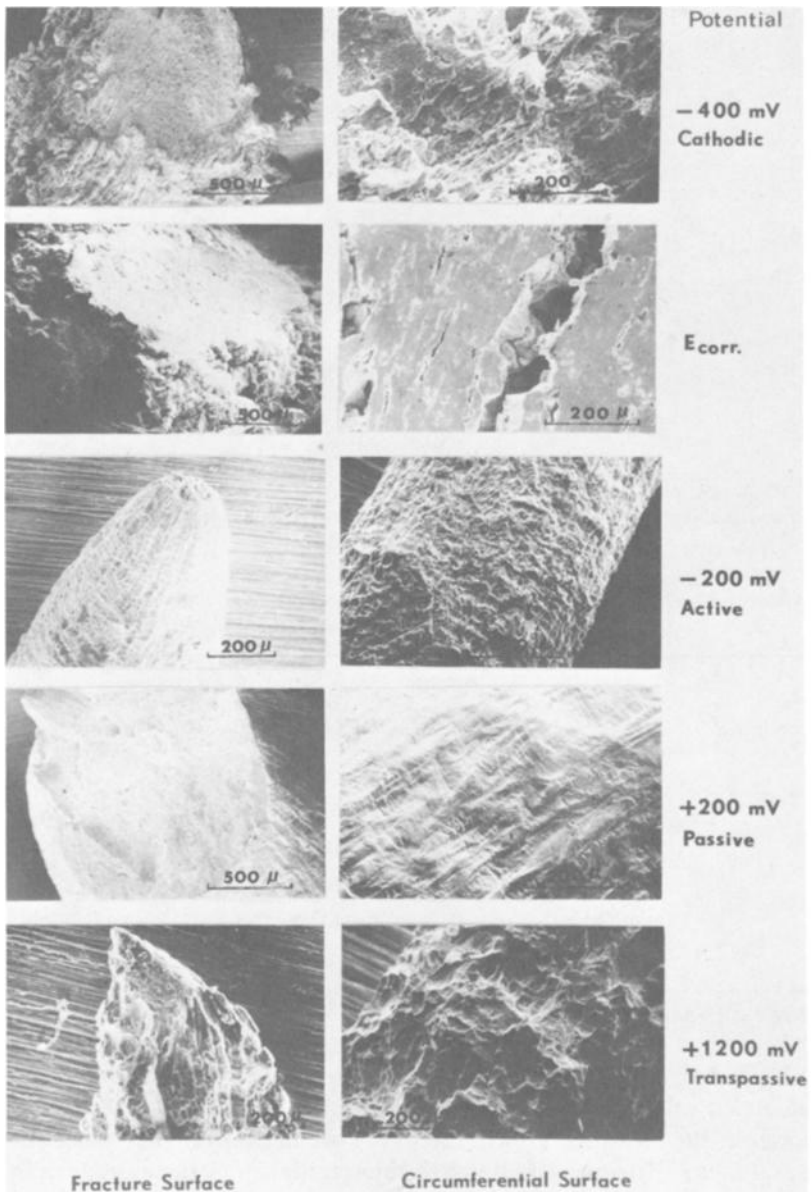


FIG. 6—SEM fractographs and circumferential surfaces of annealed Type 304 stainless steel after constant strain-rate tests conducted at various potentials in a 10 N H_2SO_4 + 0.1 M NaCl solution at room temperature at $2 \times 10^{-6} s^{-1}$.

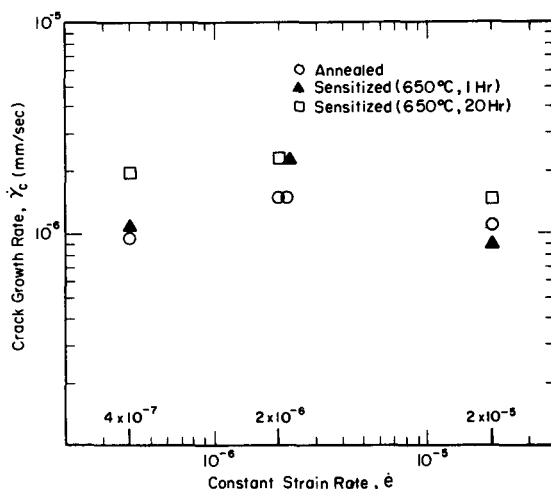


FIG. 7—Calculated crack growth rates in constant strain-rate tests conducted at the open circuit potential in a 10 N H_2SO_4 + 0.1 M NaCl solution at room temperature. Type 304 stainless steel.

TABLE 2—Crack depths and average crack growth rates measured in constant strain rate tests at the open circuit potential.

Strain Rate	Specimen	Average Depth of Crack, mm	Time to Failure, h	Average Crack Growth Rate	$\dot{\gamma}_c$ mm/s
$2 \times 10^{-5} s^{-1}$	annealed	0.05	10.0	1.3×10^{-6}	1.1×10^{-6}
	sensitized (650°C, 20 h)	0.08	10.7	2.1	1.5×10^{-6}
$2 \times 10^{-6} s^{-1}$	annealed	0.33	55.2	1.6	1.5×10^{-6}
	sensitized (650°C, 20 h)	0.52	42.0	3.4	2.6×10^{-6}
$4 \times 10^{-7} s^{-1}$	annealed	0.73	137.3	1.5	9.7×10^{-7}
	sensitized (650°C, 20 h)	0.84	83.8	2.8	2.0×10^{-6}

NOTE— $\dot{\gamma}_c$ calculated via Eq 16.

The average measured crack growth rates were slightly higher than the calculated values. The difference is within the bounds of expected scatter. However, the measured growth rates are systematically higher, suggesting a causal factor. The measured growth rates are taken as the average over the entire test time whereas the calculated values are based on crack growth rates up to the time to maximum load. Beyond maximum load, some Stage III crack growth may be observed thus giving a small increase in the overall average measured growth rates.

The development of reliable stress corrosion crack growth rates in the con-

stant strain-rate test is an important technological goal. The concept of a unique plastic crack tip field make this goal reasonable. The reported results are very encouraging. Conventional linear elastic fracture mechanics stress corrosion tests will be conducted to provide a definitive comparison with the constant strain-rate results.

Summary and Conclusions

A theoretical analysis of the constant strain-rate test was conducted, and constant strain-rate tests of Type 304 stainless steel were performed over a range of applied potentials and strain rates in a solution of 10 N H₂SO₄ + 0.1 M NaCl. Both annealed and sensitized material was studied.

Following conclusions were obtained.

1. The environmental deterioration rate, that is, the rate of loss of cross section due to both anodic dissolution and crack growth, can be computed from the time to maximum load, the strain hardening exponent, and the strain rate in a constant strain-rate test.

2. Intergranular cracking was observed at open circuit potentials. Computed and measured crack growth rates were in good agreement. The average value was on the order of 1.5×10^{-6} mm/s.

3. For the given test solution, sensitizing treatments only show a slight tendency to increased stress corrosion crack growth rates. This fact is suggestive of sensitization effects on the cracking.

4. In the active and transpassive potential regions, the environmental deterioration rate was almost completely a result of anodic dissolution. No significant cracking was observed.

5. A rationale has been given to indicate that stress corrosion crack growth rates in the constant strain-rate test should correspond with results of fracture mechanics tests. Confirming tests are needed.

Acknowledgments

The authors would like to thank R. V. Farrar for the scanning electron microscopic work. Mamoru Hishida, who is on a leave of absence from Toshiba Electric Co., Ltd., Japan, would like to thank EPRI for allowing him to participate in this project.

References

- [1] Hishida, M. and Nakada, H., *Corrosion*, Vol. 33, 1978, p. 332.
- [2] Hutchinson, J. W., *Journal of the Mechanics and Physics of Solids*, Vol. 16, 1968, p. 337.
- [3] Rice, J. R. and Rosengren, G. F., *Journal of the Mechanics and Physics of Solids*, Vol. 16, 1968, p. 1.
- [4] Begley, J. A. and Landes, J. D. in *Fracture Toughness, ASTM STP 514*, American Society for Testing and Materials, 1972, p. 1.

- [5] Landes, J. D. and Begley, J. A. in *Fracture Toughness, ASTM STP 514*, American Society for Testing and Materials, 1972, p. 24.

DISCUSSION

*H. D. Solomon*¹—Your model does not take grain size into account, so how can it predict intergranular crack growth due to dissolution? If applicable to intergranular cracking, the crack growth due to dissolution should be dependent upon grain size since the grain size determines the crack path and total area that must be dissolved for a given depth of attack. If the model is not applicable for intergranular attack, what, if any, should be the influence of sensitization heat treatments?

M. Hishida, J. A. Begley, R. D. McCright, and R. W. Staehle (authors closure)—In our model, we tried to quantify whole environmental deterioration effects during constant strain rate tests, not to predict intergranular crack growth. Before we started the experiments, we expected that sensitization heat treatments could play a significant role in cracking; however, the test results showed our expectation was wrong. The treatments slightly increased crack growth and anodic dissolution only in a certain potential range. In this solution (10 N H₂SO₄ + 0.1 M NaCl), even an annealed Type 304 steel exhibited intergranular cracking. Therefore, we assumed chromium carbides or chromium depleted zone at grain boundaries due to sensitization assist reactions, but they are not of primary importance for cracking in this system.

¹General Electric Company, Corporate Research and Development Center, Schenectady, N. Y. 12301.

J. H. Payer,¹ W. E. Berry,¹ and W. K. Boyd¹

Evaluation of Slow Strain-Rate Stress Corrosion Tests Results

REFERENCE: Payer, J. H., Berry, W. E., and Boyd, W. K., "Evaluation of Slow Strain-Rate Stress Corrosion Tests Results," *Stress Corrosion Cracking—The Slow Strain-Rate Technique*, ASTM STP 665, G. M. Ugiansky and J. H. Payer, Eds., American Society for Testing and Materials, 1979, pp. 61-77.

ABSTRACT: Slow strain-rate technique provides a rapid and reliable method to determine stress corrosion cracking (SCC) susceptibility of metals and alloys for a broad range of applications. Procedures are discussed for using the technique to (a) determine if an alloy is susceptible to SCC, (b) express SCC severity quantitatively, (c) rank alloys with respect to SCC susceptibility, and (d) evaluate the consequences of SCC susceptibility. Metallography or fractography is essential to confirm the presence or absence of SCC. Once SCC is confirmed, a number of parameters are available to express SCC severity quantitatively. Slow strain-rate technique is a conservative measure in that alloys exhibiting SCC in the test can be acceptable in service if stresses are controlled; however, no SCC in the test indicates no SCC in service under the conditions tested.

KEY WORDS: stress corrosion cracking, potential, oxidizers, reducing agents, materials selection, failure analysis, metallography, fractography, carbon steels, carbon dioxide-carbon monoxide, stainless steels, high temperature, crack velocity, ductility

The slow strain-rate technique is a method used to evaluate susceptibility of metals and alloys to stress corrosion cracking (SCC). Primary advantages of the technique are (a) slow strain rate provides a rapid laboratory method to evaluate SCC susceptibility in solutions of practical interest, and (b) the results are positive in that failure occurs either in a ductile manner or prematurely in a brittle mode, if SCC occurs. The relative merits of slow strain rate, constant load, and constant strain SCC tests were presented and compared by Parkins, [1].² Equipment for slow strain-rate experiments,

¹Associate manager, Corrosion and Electrochemical Technology Section, manager, Corrosion and Electrochemical Technology Section, and research leader, Chemistry Department, respectively, Battelle's Columbus Laboratories, Columbus, Ohio 43201.

²The italic numbers in brackets refer to the list of references appended to this paper.

methods to measure SCC severity, and important experimental parameters also were discussed previously [2]. The purpose of this paper is to discuss evaluation of slow strain-rate test results.

As documented by many papers in this publication, slow strain-rate technique was applied successfully to determine SCC susceptibility for a broad range of metal/solution combinations. Acceleration of the SCC process is achieved through imposing slow strain rate on the metal with no need to adjust solution concentration, composition, or temperature beyond the range of interest. When SCC is observed, the mode of cracking is characteristic of the metal/solution combination, that is, carbon steel in concentrated hydroxide (OH) solutions exhibits intergranular SCC while carbon steel in carbon dioxide-carbon monoxide-water (CO₂-CO-H₂O) solutions exhibits transgranular SCC.

Results of slow strain-rate tests are applied to the study of four basic questions where SCC is a consideration.

1. Is the alloy susceptible to SCC for a specific combination of solution, temperature, and oxidizing conditions?
2. If susceptible, how does SCC severity change with environmental conditions?
3. What is the ranking of susceptible alloys with respect to SCC severity?
4. What are the consequences of SCC susceptibility?

Procedures to address these questions are presented here. In many instances, interpretation is straightforward and unambiguous; for others, technical judgment is necessary and supplemental data are required.

Determination of SCC Susceptibility

Often a primary concern is to determine whether or not an alloy is susceptible to SCC for a given operating condition. This may be as input to selection of candidate materials of construction for a new process or to evaluate the effects of altering operating conditions of an existing process. In the former case, the concern is to avoid susceptible alloys, while in the latter the concern is integrity of existing equipment when solution, temperature, or oxidizing conditions are altered. A third application in this category is to provide information for determination of mode of failure in a failure analysis. Results of slow strain-rate tests can be used as evidence to determine if SCC is an operable failure mode for conditions of interest.

Clear Indication of SCC Susceptibility

In our laboratory, metallography or fractography is always used to verify the presence or absence of SCC after slow strain-rate tests. Examples are given below for unambiguous SCC indications, unambiguous nonSCC indications, and ambiguous indications. The issue for the latter, where

shallow surface events are observed, is whether the events are nonpropagating surface phenomena and of no consequence to metal integrity or are the result of testing near conditions to promote severe SCC. Severity of SCC is a function of metal/environment parameters, for example, concentration, temperature, and oxidizing condition, and borderline conditions between a region of severe SCC and a region of no SCC can result in shallow surface events which are difficult to interpret.

Severe SCC is clearly indicated in Fig. 1. Both pieces of a carbon steel specimen tested at a slow strain rate of $2.5 \times 10^{-6}/s$ in a CO_2 - CO - H_2O solution at ambient temperature exhibited numerous secondary cracks along the gage length and perpendicular to applied stress.³ The typically ductile steel exhibited limited necking in the fracture region because of deep stress corrosion cracks. Reduction of area (ROA) for this steel in a



FIG. 1—Severe SCC of carbon steel in slow strain-rate test in CO_2 - CO - H_2O at ambient temperature (original diameter, 2.5 mm).

³ See p. 222.

solution that does not promote SCC was 59 percent, while ROA of 28 percent was measured for the specimen shown. Stress corrosion cracks examined by optical metallography were found to propagate in a transgranular mode.

A scanning electron micrograph looking directly at the fracture surface of carbon steel pulled to failure at a slow strain rate of $2.5 \times 10^{-6}/s$ in 5.75 M sodium hydroxide (NaOH) at 93°C is shown in Fig. 2 [3]. Secondary cracks along the gage length near the fracture are shown at the top of the micrograph. The transition from brittle, intergranular propagation in the SCC region to ductile, dimpled propagation in the mechanical region at the bottom of the micrograph is apparent. Secondary cracks were completely intergranular. The unambiguous evidence indicating SCC susceptibility included loss of ductility, crack propagation by brittle mode, and numerous secondary cracks along the gage length oriented perpendicular to applied stress. Many other metal/solution combinations exhibit severe SCC, including sensitized austenitic stainless steel in high temperature oxygenated water and Inconel alloy 600 in a caustic-coal sulfur solution at 300°C.

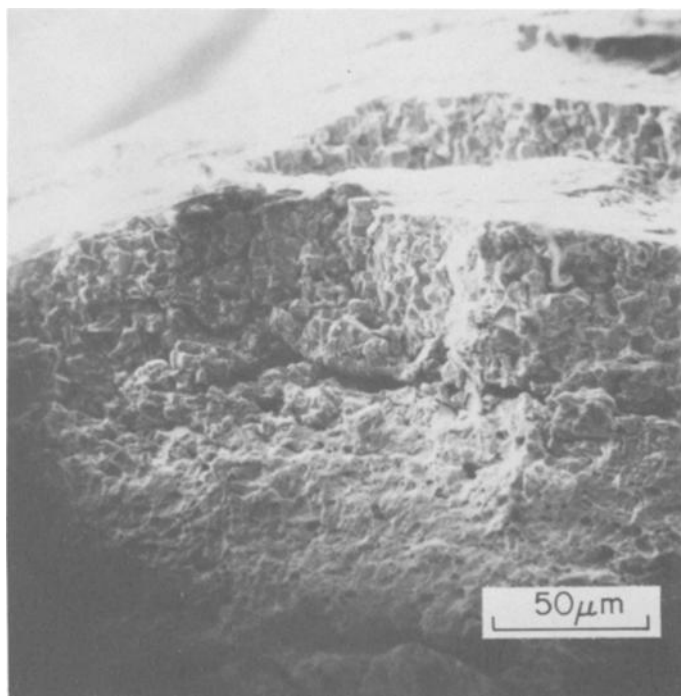


FIG. 2—Scanning electron micrograph of fracture surface of steel after slow strain-rate tests in 5.75 M NaOH at 93°C and -1.0 V (SCE).

Interpretation of Shallow Penetration

Results are not always as straightforward as those just presented. Shallow penetrations along the gage length, observed after slow strain-rate tests can result from stress corrosion or other causes. Events resulting in shallow penetrations are listed in Table 1, where they are grouped into those which are SCC related and those which are not. Penetrations of several grain diameters or more are readily interpreted by using optical metallography. Shallower penetrations can be difficult to interpret.

Shallow penetrations associated with stress corrosion indicate borderline conditions between regions of severe SCC and no SCC. For a given alloy, specific environments promote SCC and critical ranges of concentration, oxidizing conditions, and temperatures exist within which SCC will occur. For example, SCC of carbon steel in 1 *N* sodium carbonate (Na_2CO_3)-1 *N* sodium bicarbonate (NaHCO_3) at 92°C occurs over a narrow range of oxidizing potentials [4,5]. Severe SCC is observed at -0.65 V (saturated calomel electrode (SCE)), and decreasing SCC severity is observed over a range of approximately 100 mV at more positive or more negative potentials. At potentials more positive (noble) than the critical SCC range, steel is passive and no SCC is observed. While on moving to potentials more negative (active) than the critical SCC range, steel first exhibits pitting corrosion and, at still more negative potentials, no corrosion because of cathodic protection.

Similarly, critical concentrations and temperature ranges were determined for caustic SCC of carbon steel [6]. At the extremes of the critical SCC range, shallow penetrations are observed as opposed to deep intergranular penetrations observed in midrange.

In addition to solution parameters resulting in borderline SCC severity,

TABLE 1—Events resulting in shallow penetrations.

<i>Events related to SCC</i>
borderline ^a oxidizing condition
borderline solution composition
borderline metal composition or microstructure
borderline strain rate
<i>Events unrelated to SCC</i>
mechanical tear
cracks not perpendicular to applied load
pits
nonpropagating intergranular attack
cracks in corrosion product

^aNear the extremes but within the range of conditions which promote SCC.

metal composition and microstructure can contribute. Furthermore, applied slow strain rates within a given range are necessary for severe SCC.

Several events listed in Table 1 can result in shallow surface penetrations not related to SCC. Mechanical tears are observed, generally close to the fracture surface in a highly deformed region. These tears can sometimes be associated with inclusions or other heterogeneities in the metal. Broad shallow notches are also observed. Other cracks are observed that are oriented, not perpendicular, but at 45 deg to the direction of applied load. For mild and carbon steels, these types of cracks are often associated with conditions which promote hydrogen entry into the steel.

Three forms of corrosion (not SCC) related penetrations are observed: pitting corrosion, intergranular corrosion, and cracks in corrosion products. Corrosion pits are generally distinguishable from shallow stress corrosion cracks by their greater width to depth ratio. Nonpropagating intergranular corrosion is observed and can require further testing to distinguish it from shallow SCC. Cracks in thick, corrosion products not penetrating into the metal substrate can appear to be secondary cracks along the gage length. Metallographic cross sections through specimens provide a method to distinguish between SCC and nonSCC events.

A montage of metallographic cross sections to illustrate some of these events is presented in Fig. 3. Penetrations from the top of each micrograph into an unetched steel cross section (white in the figure) are shown. All micrographs are of carbon steel after slow strain-rate tests in CO_2 - CO - H_2O solutions at ambient temperature. The different results were obtained as partial pressures of CO_2 and CO were varied from test to test.

A range of SCC behavior was observed from clearly indicated SCC (bottom of the figure) to clearly indicated lack of SCC (top of the figure). The lower two micrographs show secondary stress corrosion cracks along the gage length. The upper two micrographs show penetration not related to SCC; broad, hemispherical corrosion pits on the upper right and a penetration oriented at 45 deg to applied load on the upper left. Two examples of shallow, notch penetrations which are difficult to interpret are also shown. In themselves, these latter penetrations are of little or no consequence; however, if they indicate that conditions are on the boundary of a severe SCC range they are quite significant.

Interpretation of shallow penetrations is often difficult, and further tests to broaden the data base may be necessary to minimize ambiguity. Interpretation can be guided by corroborative evidence, that is, behavior of the alloy in similar environments and dissolution behavior of the alloy in solutions of interest over a range of oxidizing conditions.

Measurement of SCC Severity

An indication of whether or not a metal in a given environment is

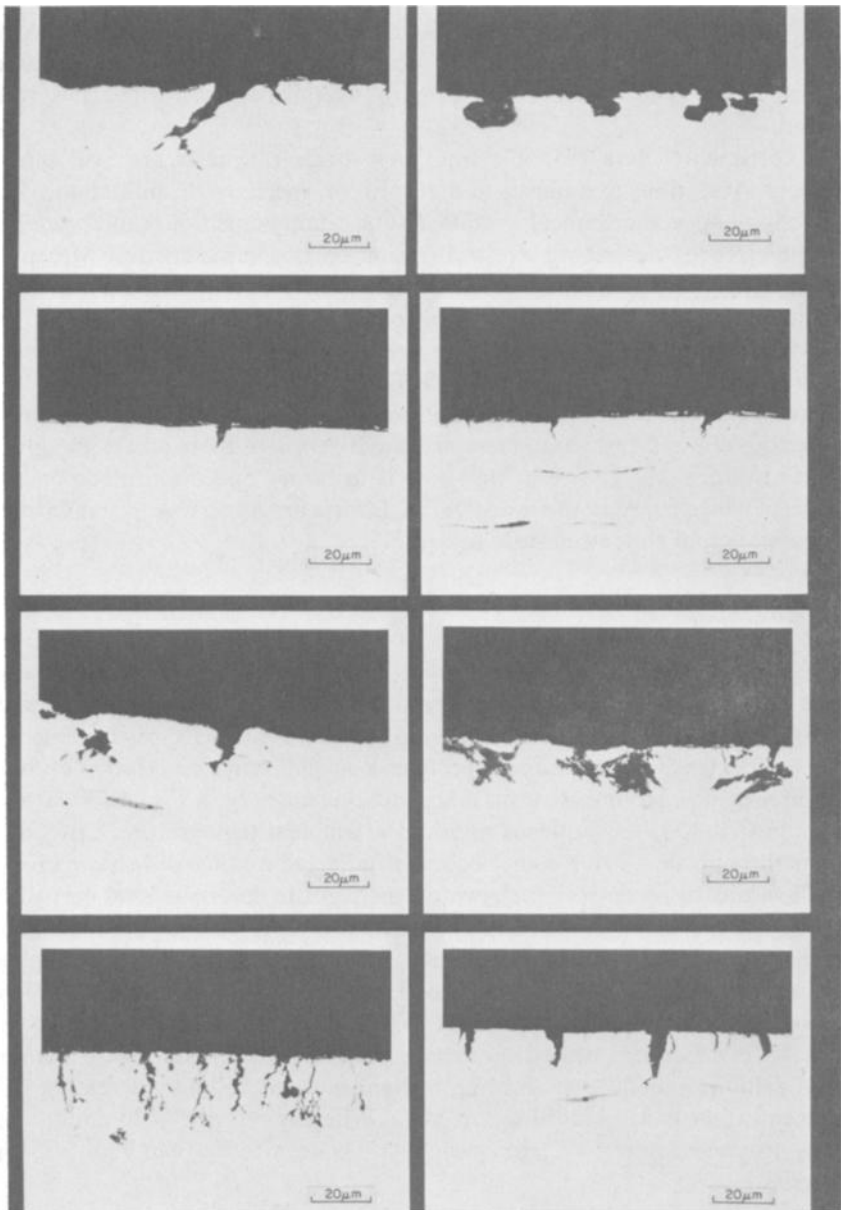


FIG. 3—Montage of metallographic cross sections through steel after slow strain-rate tests in $\text{CO}_2\text{-CO}$ aqueous solutions showing SCC and nonSCC events.

susceptible to SCC may be all the information required for some instances, however other applications require a quantitative description of SCC severity. Such a quantitative parameter is required to express severity of SCC as a function of controlling factors of the stress corrosion process, for example, solution concentration, oxidizing potential, and temperature. Then, methods to reduce SCC susceptibility can be investigated and evaluated.

Experimental data available from slow strain-rate tests are load versus time curves, time to failure, and results of specimen examination. The latter includes mechanical results (ROA and elongation) and metallographic results describing stress corrosion crack characteristics. Measures of severity are based upon metallography, ductility, time-to-failure, load versus elongation behavior, or hybrid combinations of these.

Metallography and fractography are the only acceptable methods to confirm the presence or absence of SCC. Once confirmation is obtained by either of these techniques, several parameters are available to express severity. While some parameters are more sensitive than others for given circumstances, the choice at this time is arbitrary and often made on the basis of convenience to the investigator. Efforts are underway to standardize presentation of slow strain-rate test results.

Metallography

Metallographic examination is essential to interpretation of slow strain-rate results and can provide both qualitative and quantitative descriptions of SCC severity. Both optical metallography and scanning electron microscopy are used extensively to examine specimens. A qualitative description of SCC severity in slow strain-rate tests is shown schematically in Fig. 4 for carbon steel in $\text{CH}_4\text{-CO}_2\text{-CO}$ aqueous solutions at ambient temperature. Cross sections through slow strain-rate specimens indicated a range of behavior from shallow pits or no corrosion shown on the right to severe general corrosion shown on the left. Between the two extremes, SCC was observed. In general, forms shown on the left were favored by increased corrosivity, higher concentration of CO_2 or O_2 , lower concentrations of CO , and more positive (anodic) corrosion potential. The effect of varying any of the above on SCC severity is dependent upon the starting conditions. For example, if carbon steel exhibits general corrosion for a given set of conditions, increasing CO concentration can promote severe SCC. Whereas starting with conditions that promote severe SCC, increasing CO concentration can reduce SCC severity.

Quantitative parameters based on metallographic examination are available from stress corrosion crack characteristics. From the fracture surface, area of stress corrosion can be expressed as percent total area; however, in practice the SCC area is often difficult to measure accurately. Secondary

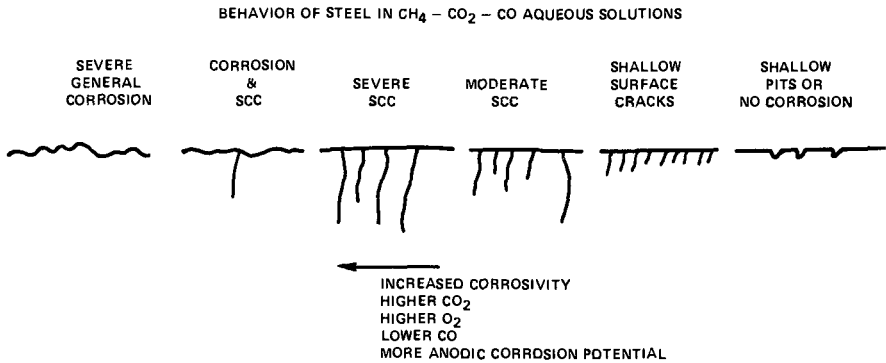


FIG. 4—Range of corrosion behavior of carbon steel in CH₄-CO₂-CO aqueous solutions.

cracks along the gage length provide useful parameters: crack length, crack velocity, and crack frequency.

Crack velocity based on length of secondary cracks along the gage length of slow strain-rate specimens was found to be a sensitive parameter for SCC severity of carbon steel in caustic solutions. Apparent crack velocity can be calculated from crack length divided by time-to-failure. Results of six slow strain-rate tests in 5.75 M NaOH at 93°C over a range of oxidizing conditions are presented in Fig. 5 along with anodic potentiodynamic polarization curves determined at fast and slow scan rates [3]. Crack velocity was greatest (1.3×10^{-6} mm/s) indicating most severe SCC at -1.0 V (SCE). The critical potential range for SCC was indicated by differences between the fast and slow scan rate polarization curves and magnitude of current measured during the fast scan. Velocity of SCC was related directly to anodic current density from the fast scan curve.

Ductility

Measurement of specimen ductility in slow strain-rate tests provides a convenient parameter for SCC severity. Reduction of area or elongation can be used. A comparison, explicit or implied, is made between ductility under conditions of interest and under conditions which do not promote SCC. Loss in ductility is attributed to SCC with more severe SCC corresponding to greater loss of ductility.

It is essential to confirm SCC by metallography when using these parameters. Severe loss of ductility can result from causes other than SCC, for example, hydrogen in the metal. Cathodic charging of hydrogen on steel in caustic solutions during slow strain-rate tests results in a severe loss of ductility but no SCC. Interpretation of results where hydrogen coexists with or is a causative agent of SCC must be made carefully.

An example of the use of reduction of area to express SCC severity is

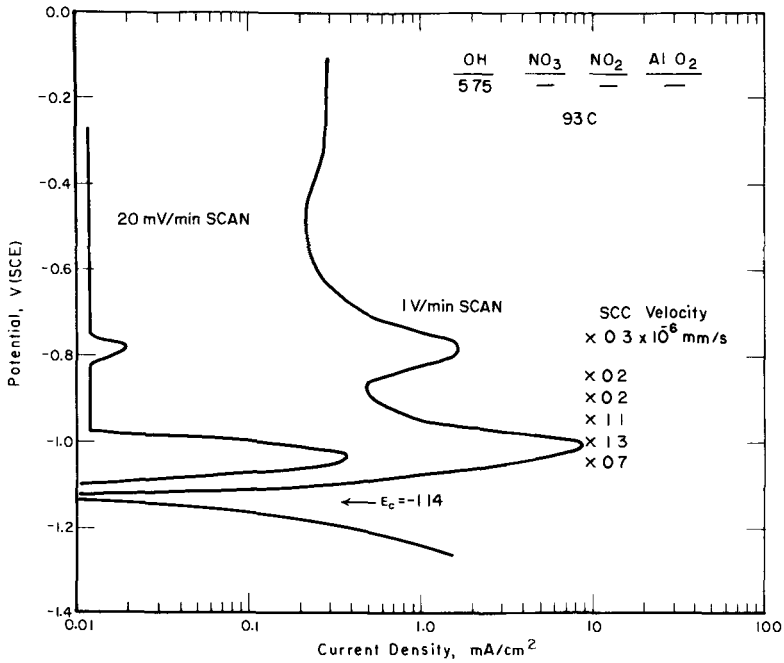


FIG. 5—Fast and slow scan-rate polarization curves of steel in 5.75 M NaOH and SCC velocities from slow strain-rate tests.

presented in Fig. 6. The two solid lines represent the scatter band of ROA as a function of applied potential for carbon steel in 33 weight percent NaOH at 92°C [5]. The critical potential range for SCC is delineated by the dip in the curves. Stress corrosion was most severe at -0.94 V (SCE) and was observed over a range of approximately 100 mV. No SCC was observed at potentials outside of this range.

Time-to-Failure

Times-to-failure (TTF) in slow strain-rate tests are typically on the order of 20 to 50 h and depend upon the metal and strain rate. Stress corrosion severity can be expressed as the ratio of TTF when SCC was observed to a baseline TTF for the metal tested at the same temperature and strain rate in a solution that does not promote SCC. A ratio of 1 indicates no SCC while ratios less than 1 indicate SCC susceptibility. Decreasing TTF ratios correspond to increasing SCC severity.

Plots of TTF in slow strain-rate tests versus applied potential for carbon steel and a series of steels with minor alloy additions were used to identify the effect of alloy additions on SCC susceptibility in nitrate solutions [4].

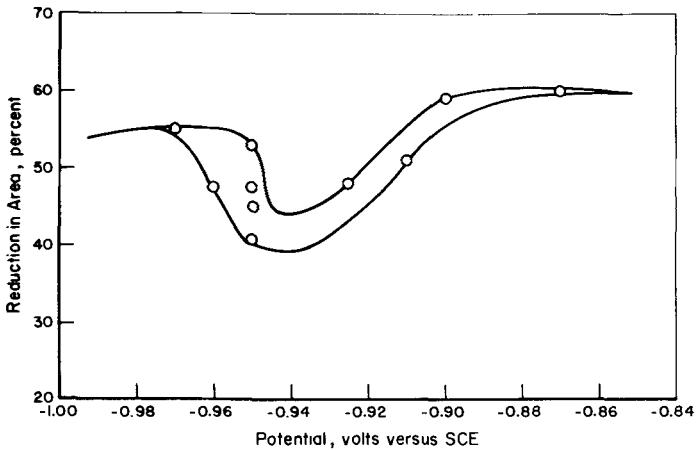


FIG. 6—ROA versus potential for carbon steel in 33 weight percent NaOH at 92°C.

General shape of the curves were similar to those shown for ROA versus potential in Fig. 6. A dip in the curve identifies the critical potential range for SCC and the minimum in the curve identifies the most severe SCC. Based on these results, beneficial and detrimental elements for SCC of carbon steel in nitrate solutions were determined.

Load versus Elongation Curves

Applied tensile load versus specimen elongation during slow strain-rate tests are shown in Fig. 7 for a specimen exhibiting SCC and another with no SCC. Specimen elongation is related directly to time because a constant cross-head extension is imposed throughout the test. Initially, load increases linearly with elongation within the elastic range. A break in this linear portion occurs at the yield point with load continuing to increase with elongation until the onset of necking. Beyond necking, load decreases and goes to zero at failure.

Typically, SCC severity is expressed as the ratio of a parameter from the SCC curve to a parameter of the baseline curve. As before, a ratio of 1 indicates no susceptibility and lower ratios indicate increasing SCC severity. Several parameters that are available for comparison are identified in Fig. 7: maximum load (L), total elongation (e), area under the curve (A), and failure load (F).

In addition to these parameters, hybrid combinations have been used to express SCC severity. An example which has been found to be quite sensitive to changes in SCC severity is the true failure stress determined by dividing the failure load by specimen cross-sectional area at failure. Other complex parameters have been developed.

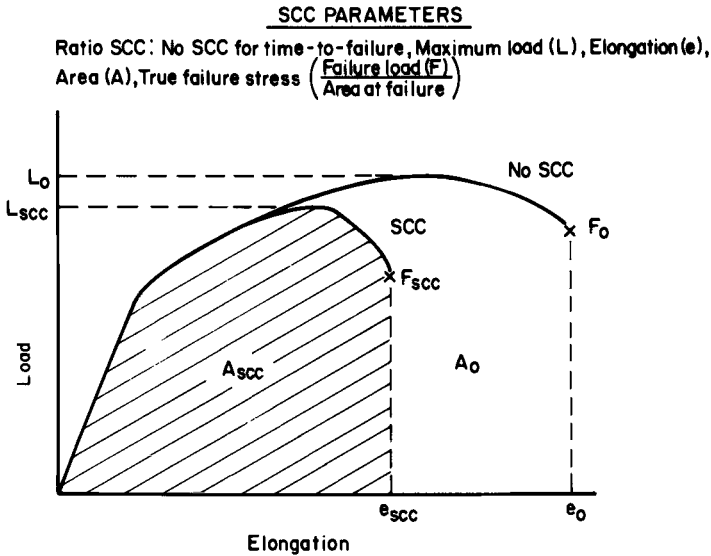


FIG. 7—Applied load versus specimen elongation curves for slow strain-rate tests with and without SCC.

In summary, once SCC is confirmed by metallography or fractography a number of parameters are available to express quantitatively SCC severity. No single parameter has been found to be optimum, but rather a selection is made based upon sensitivity required and data available. While the selection of a SCC parameter is left to the investigator, efforts are underway to standardize presentation of slow strain-rate data by expressing increasing SCC severity by decreasing values of the SCC parameter.

Ranking of Susceptible Alloys

It was shown that slow strain-rate tests can be used to determine if an alloy is susceptible to SCC. Using this as a basis, one can divide alloys into go and no-go categories with respect to SCC for a given application. Further, for an alloy, several parameters are available to express quantitatively SCC severity as a function of solution composition, temperature, and oxidizing potential. The next issue to be discussed is whether slow strain-rate tests can be applied to ranking of alloys which are susceptible to SCC.

For similar alloys, that is, minor compositional or microstructural differences, slow strain-rate tests can establish ranking with respect to SCC susceptibility. The effects of minor alloying additions on SCC susceptibility of carbon steel in caustic and nitrate solutions were determined by slow strain-rate tests [4]. Two cautions are pertinent. First, the parameter selected to express SCC severity should not change appreciably for the no

SCC-baseline condition, for example, large differences in ductility as a function of alloy additions would make ranking based on ratios of reductions of area risky. Secondly, tests should be run over a broad enough range of oxidizing conditions to substantiate the effect. For carbon steels, a critical potential range for SCC is observed and sufficient tests are necessary to determine whether an alloying addition merely shifts the critical potential range with no change of SCC severity within the range or the alloy addition truly reduces severity by decreasing SCC severity within the critical potential range.

The effects of thermal history on SCC susceptibility of austenitic stainless steels and nickel alloys in high temperature aqueous solutions of interest in nuclear power generation have been studied extensively using slow strain-rate technique. Microstructural effects, for example, degree of sensitization, for an alloy are measured and a quantitative ranking of susceptibility developed based on a slow strain-rate test parameter.

Slow strain-rate results as a function of heat treatment are presented in Table 2. Times-to-failure and ROAs for AISI 304 and AISI 304L stainless

TABLE 2—*Slow strain-rate test results as a function of heat treatment.*

288°C - 100 ppm O ₂ - 3 × 10 ⁻⁶ in./in. · s				
Material	Heat Treatment Condition	TTF, h	ROA, %	Notes
AISI 304	mill anneal	62.4	61	no SCC
	4 h/677°C	26.4	15	SCC
	7 h/620°C	56.3	60	SCC
AISI 304L	24 h/620°C	26.2	28	SCC
Alloy 600	mill anneal	77.9	59	no SCC
	7 h/620°C	81.8	62	no SCC

Conversion factor—3 × 10⁻⁶ in./in. · s = 3 × 10⁻⁶ mm/mm · s.

steels and Inconel alloy 600 tested in high purity water with 100 ppm O₂ at 288°C are presented with results of metallographic examination for SCC. A 4 h/677°C thermal treatment results in increased SCC severity compared to a 7 h/620°C thermal treatment for AISI 304 stainless steel. The 24 h/620°C treatment of AISI 304L stainless steel results in SCC severity equivalent to the most severe treatment for AISI 304 stainless steel.

For dissimilar alloys, results of slow strain-rate tests for susceptible alloys can be used only as a rough comparison. Alloys exhibiting severe SCC would be ranked lower than those exhibiting minor SCC, but distinction between alloys with similar SCC severity is not advised.

Consequences of SCC Susceptibility

The final issue to be discussed is that of the consequences of SCC susceptibility. Slow strain-rate technique has been found to be a conservative test. Where no SCC susceptibility was found in the test, no SCC is predicted in service for the conditions tested. Conversely, where susceptibility is found in slow strain-rate tests, an alloy may be acceptable for an application and no SCC failures experienced if stresses are insufficient to sustain SCC. It must be recognized in the latter case, however, that the metal/solution combination is susceptible to SCC and that failures can occur given appropriate stresses.

An evaluation of the consequences of SCC susceptibility is a complex engineering decision with many contributing factors. Of primary consideration are the consequences of failure with regard to safety, loss of product or service, and ease of repair. The economics of alternate materials of construction and changes in service conditions to avoid SCC susceptibility are other primary considerations.

The occurrence of strains in service comparable to those imposed on a metal during slow strain-rate tests is not as rare as might at first be expected. While most designs do not anticipate appreciable plastic strain in service, strains on the order of creep rates are of interest here and can result in SCC. These strains can result from the additive effects of operating loads, pressure fluctuations, thermal stresses, and residual stresses during normal operation, start-up, or shut down. Service failures have been observed in a variety of applications where nominal stresses were well below the yield stress of the metal.

Conclusions

Slow strain-rate technique provides a rapid and reliable method to determine SCC susceptibility of metals and alloys for a broad range of applications. Metallography or fractography is essential to confirm the presence or absence of SCC susceptibility. Once SCC susceptibility is confirmed, a number of parameters are available to express SCC severity quantitatively. These parameters can be used to measure the effect of solution composition, temperature, and oxidizing condition on SCC severity and to rank similar alloys with respect to SCC resistance. For dissimilar alloys, rough ranking only is advisable.

Slow strain-rate technique is conservative. No SCC in the test indicates no SCC in service under the conditions tested; conversely, where SCC is observed in the test, the alloy may be acceptable in service if stresses can be controlled to avoid SCC. In the latter case it must be recognized that the metal/solution combination is susceptible to SCC and failures could occur with the appropriate stresses.

Acknowledgments

Much of the data presented here is from research projects sponsored at Battelle Columbus Laboratories. In particular, the support of the Pipeline Research Committee of the American Gas Association and Rockwell International Corporation, Atomics International Division, Rockwell Hanford Operations is gratefully acknowledged. The contributions of Professor R. N. Parkins, University of Newcastle-Upon-Tyne, to the development of experimental procedures and our discussions regarding this paper also are gratefully acknowledged.

References

- [1] Parkins, R. N., *Proceedings of Specialists Meeting on Stress Corrosion Testing Methods*, NATO Advisory Group for Aerospace Research and Development, Brussels, Belgium, Oct. 1971.
- [2] Payer, J. H., Berry, W. E., and Boyd, W. K. in *Stress Corrosion—New Approaches*, ASTM STP 610, American Society for Testing and Materials, 1976, pp. 82-93.
- [3] Payer, J. H., Moore, E. L., and Boyd, W. K., "Corrosion of Carbon Steel in Synthetic Nuclear Wastes," *Corrosion*, submitted for publication.
- [4] Parkins, R. N., *Fifth Symposium on Line Pipe Research*, American Gas Association, Inc., Houston, Tex., Paper U, Nov. 1974, pp. 1-43.
- [5] Berry, W. E., *Fifth Symposium on Line Pipe Research*, American Gas Association, Inc., Houston, Tex., Paper V, Nov. 1974, pp. 1-40.
- [6] Reinoehl, J. E. and Berry, W. E., *Corrosion*, Vol. 28, 1972, p. 151

DISCUSSION

*Andrew Madeyski*¹—When using the ratio of the final load to the final cross-section area as a parameter for evaluation of susceptibility to SCC, it should be realized that this parameter may express not only a purely geometric factor, but also the degree of degradation of the remaining material due, for instance, to the accumulation of hydrogen ("hydrogen embrittlement").

J. H. Payer, W. E. Berry, and W. K. Boyd (authors' closure)—Thank you for reemphasizing an important consideration. Whatever parameter is selected to express severity of SCC, the implicit or explicit assumption is made that the extent of SCC is the only factor that affects the parameter. The validity of this assumption should be analyzed by the investigator. As is pointed out, hydrogen in the metal reduces ductility and a false indication of SCC severity can be made. Other phenomena, for example, intergranular corrosion, also can affect results.

¹Westinghouse Electric Corporation, Research and Development Center, Pittsburgh, Pa. 15235.

*I. L. W. Wilson*²—(1). On Fig. 4 (CO/CO₂ schematic), you list the parameters which cause the various forms of attack. Could you add the effect of strain rate, other parameters being fixed, to this figure?

(2). Assume you are forced to select (for example) three alloys for a given application and each alloy shows exactly the same profile for SCC susceptibility versus strain rate but with the nadir of the curve at a different strain rate for each material. How then do you select the best alloy?

J. H. Payer, W. E. Berry, and W. K. Boyd (authors' closure)—(1) While SCC is a function of strain rate, it could not be included directly on this figure. For this study, a strain rate ($2.5 \times 10^{-6} \text{ s}^{-1}$) was selected which resulted in severe SCC under some environmental conditions. Less severe SCC was observed as environmental conditions were changed. The interest was in the effect of environmental changes only and not the effects of strain rate, steel composition, or steel metallurgical structure.

(2) If no other information on SCC susceptibility of the three alloys were available, a technical judgment would be made for the anticipated strain rates likely to be encountered in service. Unfortunately strain rates of interest, typically on the order of 10^{-6} s^{-1} , are (a) difficult to predict or measure, and (b) difficult to prevent. It is more likely that a range of strain rates will be experienced in service, which makes selection based on the strain-rate dependence tenuous. A selection based on differences in susceptibility as a function of environmental conditions (solution chemistry, temperature, and oxidizing potential), or metallurgical structure and composition would be favored. If strain rates and environmental conditions used in slow strain-rate tests for each alloy are experienced in service, none of the alloys would be suitable.

*W. J. Baxter*³—What are your reasons for stating that the cracks which develop at 45 deg to the tensile axis are not stress corrosion cracks? Are they not transgranular cracks initiated by transgranular slip along the direction of maximum shear stress?

J. H. Payer, W. E. Berry, and W. K. Boyd (authors' closure)—The point to be made is that cracks at 45 deg to the tensile axis do not necessarily indicate SCC susceptibility for the metal. For example, these cracks have been observed for carbon steel in caustic solutions under conditions of cathodic charging. They are not intergranular stress corrosion cracks observed within the critical potential range for steel in caustic solutions, and they do not indicate susceptibility to hydrogen stress cracking. The combination of hydrogen charging and substantial plastic deformation are not experienced in service; if they were, cracking would be predicted.

*W. J. Daniels*⁴—I agree that the slow strain-rate test is a conservative

²Westinghouse Electric Corporation, Research and Development Center, Pittsburgh, Pa. 15235.

³General Motors Research Laboratories, Warren, Mich. 48090.

⁴Monsanto Company, St. Louis, Mo. 63166.

test if you find cracks or other failure mechanisms. But what can you conclude if you do not find cracks in your test grid of experimental conditions (electrochemical potential, strain rate, temperature, metal conditions, or solution composition)?

Do you recommend the use of other SCC test techniques (U-bend, constant flow stress tests, for example) to augment or complement the slow strain-rate technique results?

J. H. Payer, W. E. Berry, and W. K. Boyd (authors' closure)—Our experience has shown that the slow strain-rate test is a conservative test. We know of no instances where a SCC failure of a metal/environment combination in service could not be duplicated in slow strain-rate tests, if the environment can be duplicated in the laboratory. Furthermore, no SCC in the slow strain-rate test indicates that no SCC is anticipated in service, *under the conditions tested*.

Slow strain-rate technique is a powerful tool for the study of SCC, but it is obviously not the only technique. Selection of test method(s) is made based on metal, environment, and application.

Slow Strain-Rate Technique for Specific Environments and Application

Slow Strain-Rate Technique: Application to Caustic Stress Corrosion Cracking Studies

REFERENCE: Theus, G. J. and Cels, J. R., "Slow Strain-Rate Technique: Application to Caustic Stress Corrosion Cracking Studies," *Stress Corrosion Cracking—The Slow Strain-Rate Technique*, ASTM STP 665, G. M. Ugiansky and J. H. Payer, Eds., American Society for Testing and Materials, 1979, pp. 81-96.

ABSTRACT: This paper describes slow strain-rate test equipment, operable at elevated temperatures and pressures, that includes electrochemical potential control capability. Applications in caustic stress corrosion cracking (SCC) studies of both nuclear steam generator and fossil boiler materials are presented. Electrochemical potential regions for stress corrosion cracking of Inconel alloy 600, Incoloy alloy 800, and Type 304 stainless steel are compared to results obtained using constant load specimens. Tests with titanium stabilized Alloy 800 (Sanicro 30) tubular specimens also demonstrate the effect of potential on cracking mode. A comparison of SCC test results, using both long term exposure tests and short term straining electrode tests, is made between a mild steel and its weld metal. In these examples, favorable comparisons are obtained with tests using conventional methods, proving the value and usefulness of the slow straining device in accelerating SCC studies and in defining more accurately conditions under which SCC can occur.

KEY WORDS: stress corrosion cracking, alloys, stainless steels, carbon steels, base metal, weld metal, slow strain-rate tests, electrochemical potential

Since the turn of the century, the utility industry has been plagued with many corrosion problems. Among the most persistent is caustic stress corrosion cracking (SCC) of heat exchanger materials. Not only is caustic embrittlement of mild steels a historical problem, as evidenced by the literature of 25 years ago [1,2],² but it also remains a subject of current concern to design and corrosion engineers [3-6]. The change to stainless steels and high nickel alloys for steam generator tubes in nuclear steam generators of light water reactors has not eliminated problems with caustic

¹Corrosion group supervisor and research specialist, respectively, Corrosion Technology Section, Babcock & Wilcox, Research and Development, Alliance, Ohio 44601.

²The italic numbers in brackets refer to the list of references appended to this paper.

SCC. Again, the literature contains summaries of field failures and their suspected causes [7-10] (many of which are associated with caustic contaminants) as well as papers reviewing various aspects of caustic cracking of austenitic alloys [11-14].

The usual laboratory experiments for assessing an alloy's resistance to caustic SCC are to expose severely stressed specimens (beyond yield stress) at their open circuit potential to a concentrated caustic solution at an elevated temperature. A data point is recorded after failure or after exposure for a predetermined time. More recently, potentiostatic methods are being employed to accelerate the failure times and define more accurately the electrochemical and environmental chemistry conditions within which caustic SCC is possible. However, if cracks are not detected in either type of experiment, there is always the question of whether the test duration was long enough. This is particularly troublesome in testing related to the utility industry where components are designed for a 30 to 40-year life.

In the late 1960s, Parkins [4,5,15] described a test arrangement wherein he immersed a tension specimen (polarized or at open circuit) in an aqueous solution and pulled it at a slow constant extension rate. One of the most attractive features of this method is that failure always occurs: brittle failure and numerous secondary cracks if the imposed test conditions (electrochemical potential, electrolyte, temperature, strain rate, material, metallurgical condition, etc.) are conducive to SCC or ductile rupture if the imposed conditions are not. Since the resulting data from the slow strain-rate method appear to agree with long term open circuit tests, constant potential tests, and limited field experience (when the correlations can be made), it provides corrosion engineers with a greater degree of confidence in choosing compatible material/environment combinations.

Not only can this method satisfy pass/fail criteria, but it can also provide data to judge the relative degree of SCC susceptibility among test variables. Conditions that cause SCC result in a lower maximum load and a loss of ductility. Therefore, by comparing maximum load, reduction in area, or elongation, as well as noting the degree of secondary cracking, a particular variable can be judged to retard or accelerate cracking.

This paper describes slow strain-rate test equipment, operable at elevated temperatures and pressures, that includes electrochemical potential control capability. Applications in caustic SCC studies of both nuclear steam generator and fossil boiler materials are presented. Electrochemical potential regions for SCC of Inconel alloy 600, Incoloy alloy 800, and Type 304 stainless steel are compared to results obtained using constant load specimens. Tests with titanium-stabilized Alloy 800 (Sanicro 30) tubular specimens also demonstrate the effect of potential on cracking mode. A comparison of SCC test results, using both long term exposure tests and short term straining electrode tests, is made between a mild steel and its weld metal. In these examples, favorable comparisons are obtained with

tests using conventional methods, proving the value and usefulness of the slow straining device in accelerating SCC studies and in defining more accurately conditions under which SCC can occur.

Equipment, Experimental Procedure, and Test Materials

The equipment and experimental procedure for these tests were extensively described previously [16] but are briefly reviewed here. Figure 1 presents a schematic drawing of the entire straining electrode/autoclave assembly, and Fig. 2 is a schematic drawing of the tension specimen arrangement within the autoclave.

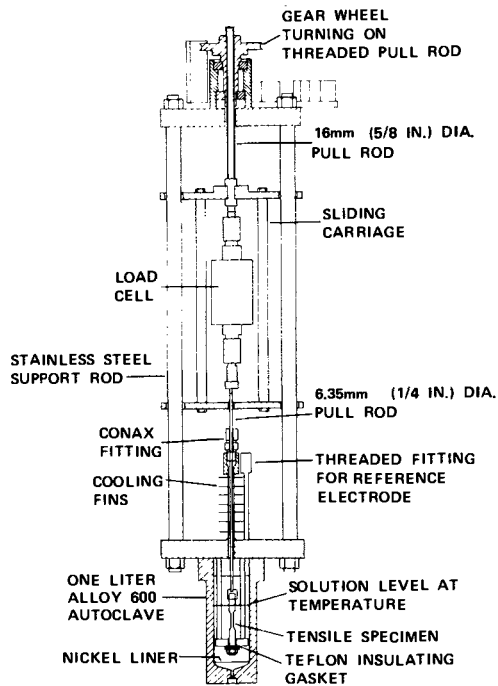


FIG. 1—Straining electrode assembly.

Slow Strain-Rate Test Assembly

The constant strain-rate test assembly is supported by the floor stand of a 1 litre autoclave. A direct current motor is mounted on the top framework of the assembly and is connected to a pull rod through a gear reduction train. The motor is controlled by a silicon controlled rectifier (SCR) power supply, and the travel speed of the pull rod can be varied between 3.3×10^{-5} mm/s (1.3×10^{-6} in./s) and 5.3×10^{-4} mm/s (2.1×10^{-5}

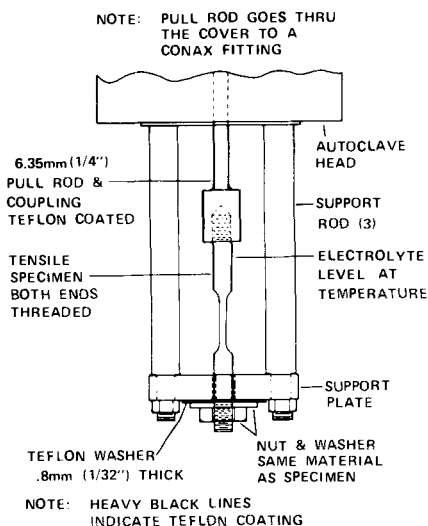


FIG. 2—Straining electrode specimen assembly.

in./s) without gear changes. This corresponds to a strain rate of $3 \times 10^{-6} \text{ s}^{-1}$ to $4.8 \times 10^{-5} \text{ s}^{-1}$ for the regular tension specimens and a strain rate of $2.6 \times 10^{-6} \text{ s}^{-1}$ to $4.2 \times 10^{-5} \text{ s}^{-1}$ for the tubular-type tension specimens, both described in detail later. The carriage is connected to the top pull rod, and the load cell is connected to the carriage and a second pull rod which enters the autoclave. The entire carriage assembly slides on the support rods. A recorder plots the load cell output versus time (thus total strain).

Autoclave Assembly

The carriage assembly pull rod enters the autoclave through a trifluoroethylene resin seal in a high pressure fitting mounted on the autoclave head. Three support columns are connected between the inside of the autoclave head and the specimen support plate. The threaded tension specimen is coupled on one end to the pull rod and the other end is secured to the support plate. A trifluoroethylene resin washer electrically insulates the tension specimen from the support plate. In addition, heat shrinkable trifluoroethylene resin is used to coat the nontest areas of the tension specimen to decrease the magnitude of current flow during an experiment. Tests with Sanicro 30 were conducted with tubular tension specimens, and adapters were used to connect the specimen to the pull rod and support plate. The autoclave, its head, the pull rods, and the specimen support assembly are

made of stress relieved Alloy 600. A nickel Alloy 200 liner is used to contain the test solution.

Electrochemical Equipment

A potentiostat controlled the specimen's potential using the autoclave as the counter electrode. A high purity nickel wire (inserted through a high pressure fitting) served as an internal reference electrode which behaves like a hydrogen reference electrode in a solution with an atmosphere of 5 percent hydrogen (H_2)-95 percent nitrogen (N_2) cover gas [17]. However, it is not a standard hydrogen electrode because the hydrogen activity and partial pressure are not known for these test conditions. The alloys tested under these experimental conditions also behave similarly to the reference electrode when at open circuit. Thus E_{corr} for the alloys is $\sim 0 \text{ mV}_{\text{Ni}(H_2)}$.

Materials and Specimens

Round tension specimens, schematically shown in Fig. 3, were machined from rods of Alloy 600, Alloy 800, and Type 304 stainless steel. Tension

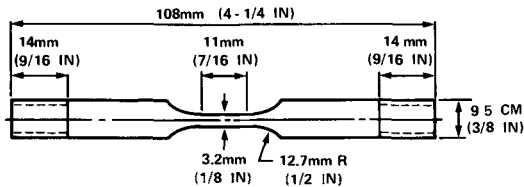


FIG. 3—Tension specimen.

specimens were also machined from trepanned steam drum material for the tests on the mild steel and weld metal. Figure 4 is a schematic of the tubular tension specimen used for tests of titanium stabilized Alloy 800. Table 1 lists the composition and Table 2 reports the mechanical properties of the test materials. All materials were tested in the as-received (that is, mill annealed) condition.

Test Solutions

Comparative tests on Alloy 600, Alloy 800, and Type 304 stainless steel were conducted in a 10 percent sodium hydroxide (NaOH) solution at 288°C (550°F) using a 5 percent H_2 -95 percent N_2 cover gas with and without an applied potential. Tests on titanium stabilized Alloy 800 were also conducted at 288°C (550°F) in 10 percent NaOH with a 5 percent H_2 -95 percent N_2 cover gas and with an applied potential.

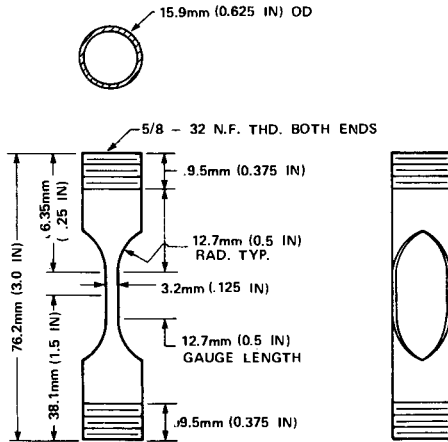


FIG. 4—Tubing-type tension specimen.

Controlled potential tests are often necessary to induce cracking of some of these alloys. Additionally, the corrosion morphology of a particular alloy can be altered by changing the test potential. Thus, potential control tests often lead to a better understanding of the field conditions that caused SCC.

Comparative tests between mild steel base metal and weld metal were conducted in boiling (127°C, 260°F) 35 percent NaOH at the open circuit potential with air originally over the test solution.

Test Procedure

The test procedure for the slow strain-rate tests is outlined below.

1. Prepare test solutions in the nickel Alloy 200 liner with reagent grade NaOH and deionized water.
2. Degrease and ultrasonically clean the specimens.
3. Bolt the autoclave head with the mounted specimen onto the autoclave.
4. Deaerate the solution with the gas mixture (5 percent H₂-95 percent N₂) for at least 19 h.
5. Increase the gas pressure to 1.38 N/m² (13.6 atm, 200 psi) for the high temperature tests. Leave at atmospheric pressure for the boiling 35 percent NaOH tests.
6. After the system has stabilized at the test temperature, apply the test potential for potentiostatic tests.
7. Start the straining test at a pull rate of 3.3×10^{-4} mm/s (1.3×10^{-5} in./s) until a load of about 160 kg (350 lb) is reached. Decrease the

TABLE 1—Chemical composition of the test materials (weight percent).

Alloy	Heat	C	Mn	S	Si	Cr	Ni	Fe	Cu	Ti	Al
Alloy 600	A	0.08	0.36	0.003	0.16	15.76	bal	8.91	0.31
	B	0.04	0.38	0.006	0.11	15.71	bal	8.60	0.03
Alloy 800	A	0.07	0.68	0.003	0.29	19.20	30.89	47.36	0.65	0.39	0.47
	B	0.06	0.81	0.007	0.30	20.36	32.45	44.95	0.27	0.38	0.39
Type 304 stainless steel	A	0.06	1.58	0.017	0.70	19.00	8.43	bal	0.10
	B	0.07	1.09	0.008	0.52	18.55	9.45	bal	0.44
Mild steel	base metal	0.32	0.79	0.034	0.23	0.03	...	bal	0.04	...	0.03
	weld metal	0.07	1.34	0.014	0.43	0.05	...	bal	0.19	...	0.02
Sanicro 30	...	0.015	0.61	0.003	0.56	22.0	33.7	bal	0.01	0.46	0.38

TABLE 2—Mechanical properties of the test materials.

Alloy	Heat	Yield Strength, ksi	Tensile Strength, ksi	Elongation, (% in 2 in.)	Reduction of Area, %
Alloy 600	A	53	108	42	63
Alloy 800	A	48	90.5	45	...
Type 304 stainless steel	A	41	93.6	43	77
Mild steel	base metal	39.5	74.3	30	53.6
	weld metal	70.1	86.2	25	65.4
Sanicro 30	...	47	94.4	44	not available

Conversion factors—

1 ksi = 6.89 MPa, and

1 in. = 25.4 mm.

pull rate for the remainder of the tests by approximately an order of magnitude.

Test procedures and specimen types for the comparison static tests are described elsewhere [17] and in ASTM Recommended Practice for Making and Using U-Bend Stress Corrosion Test Specimens (G 30-72).

All specimens were examined with an optical microscope at approximately $\times 100$. Cross sections of selected specimens were metallographically examined to determine cracking mode.

Results and Discussion

Alloy 600, Alloy 800, and Type 304 Stainless Steel

Comparative tests on Alloy 600, Alloy 800, and Type 304 stainless steel in 10 percent NaOH solution at 288°C (550°F) using the slow strain-rate test method and the conventional method are presented in Table 3. The data show the effect of potential on the mode of failure, that is, ductile rupture with no secondary cracks or brittle fracture with numerous secondary cracks. Figure 5 presents the slow strain-rate data for Alloy 600 and Alloy 800 and further demonstrates the effect of potential on the reduction of area. The data in Table 3 for the static load test are graphically shown in Figs. 6, 7, and 8, which were obtained in earlier tests [13,17] or previously unpublished tests.

For Alloy 600, both sets of data show that SCC does not occur under the conditions of the test until a potential more noble than 120 mV_{Ni(H₂)} is applied to the specimens. Cracking appears to be more severe in both types of experiments at an applied potential of around 250 mV_{Ni(H₂)}. For the constant strain-rate tests, this is shown by the smallest value for the reduction of area while for the static load tests, the most severe condition is

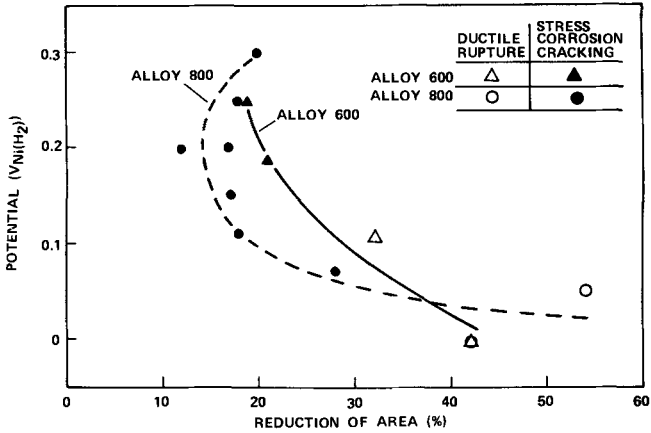


FIG. 5—Effect of potential versus reduction of area on Alloy 600 and Alloy 800 in 10 percent NaOH at 288°C (550°F) using the slow strain-rate test technique.

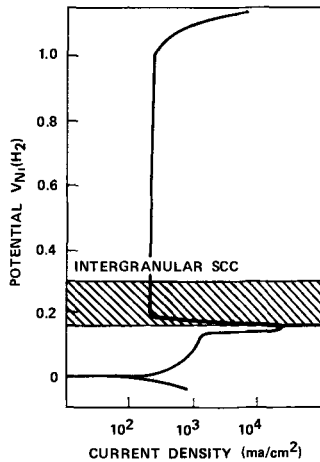


FIG. 6—Cracking zone for Alloy 600 in 10 percent NaOH at 288°C (550°F) using static specimens.

indicated by the deepest crack penetration in a fixed test time. The static load tests also show that SCC ceases at a potential of around 350 mV_{Ni(H₂)}. The corresponding tests at the higher potentials using the constant strain-rate method have not been conducted.

For Alloy 800, no cracking was observed with either test technique below a potential of 50 mV_{Ni(H₂)}. Using the statically loaded specimens, previous data [13,17] had shown a very narrow cracking region. However, more recent static load data and data obtained with the constant strain-rate technique show that the cracking region is much broader between 50 mV_{Ni(H₂)}

TABLE 3—Effect of potential on the failure mode.

Material ^a	Specimen Potential ^b	Slow Strain-Rate Method			Static Method Results
		Reduction of Area, %	Failure Mode		
Alloy 600 ^c	open circuit	42		no cracks	...
	110	32	ductile rupture	no cracks	
	120	...	ductile rupture	fine intergranular cracks	
	125	fine intergranular cracks	
	150	fine intergranular cracks	
	190	21	intergranular SCC	large intergranular cracks	
	200	large intergranular cracks	
	250	19	intergranular SCC	...	
	270	very large intergranular cracks	
	300	large intergranular cracks	
	350	no cracks	
400	no cracks		
700	general wastage		
Alloy 800	open circuit	42	ductile rupture		...
	40	no cracks	

50	54	ductile rupture	no cracks	...
60
70	28	transgranular SCC	fine transgranular cracks	...
80	large transgranular cracks	...
100
110	18	transgranular SCC
150	17	transgranular SCC
180	fine transgranular cracks	...
200	12	transgranular SCC
200	17	transgranular SCC
250	18	transgranular SCC
300	20	transgranular SCC
750 to 850	large intergranular cracks	...
0 to 80	large mixed transgranular and intergranular cracks	...
80	22	intergranular and transgranular SCC
80 to 130	large mixed transgranular and intergranular cracks	...
130 to 180	large mixed transgranular and intergranular cracks	...

Type 304

^a All materials tested in the mill annealed condition.^b 10 percent NaOH, 288°C (550°F), cover gas of 5 percent H₂—95 percent N₂.^c All slow strain specimens were Heat A and all static specimens were Heat B for all three alloys.

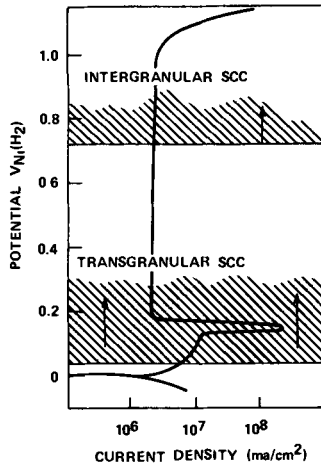


FIG. 7—Cracking zones for Alloy 800 in 10 percent NaOH at 288°C (550°F) using static specimen.

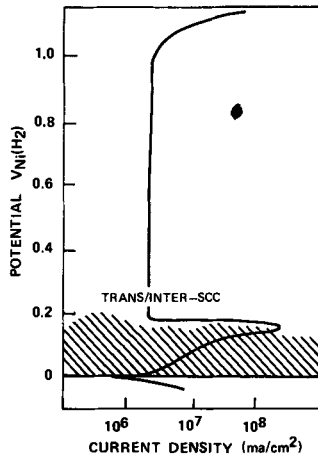


FIG. 8—Cracking zone for Type 304 stainless steel in 10 percent NaOH at 288°C (550°F) using static specimen.

and, at least, 300 $mV_{Ni(H_2)}$. Statically loaded specimens show the most damaging potential for stress cracking of Alloy 800 to be at approximately 100 $mV_{Ni(H_2)}$ while the constant strain-rate tests indicate that a potential of 200 $mV_{Ni(H_2)}$ causes the greatest amount of damage.

Limited tests on Type 304 stainless steel using both test techniques agree: this alloy will crack between the open circuit potential and, at least, a potential of 180 $mV_{Ni(H_2)}$.

For the three alloys tested, the cracking mode is also in agreement for both types of tests where the comparisons can be made (see Table 3). Alloy 600 cracked intergranularly, Alloy 800 cracked transgranularly, and Type 304 stainless steel had a mixed mode of failure.

Titanium Stabilized Alloy 800

A limited number of constant strain-rate tests on Sanicro 30 (titanium stabilized Alloy 800) specimens in 10 percent NaOH at 288°C (550°F) with a 5 percent H₂-95 percent N₂ cover gas were conducted to determine the failure mode as a function of potential. This information along with the percent elongation of the specimens is presented in Fig 9. Preliminary re-

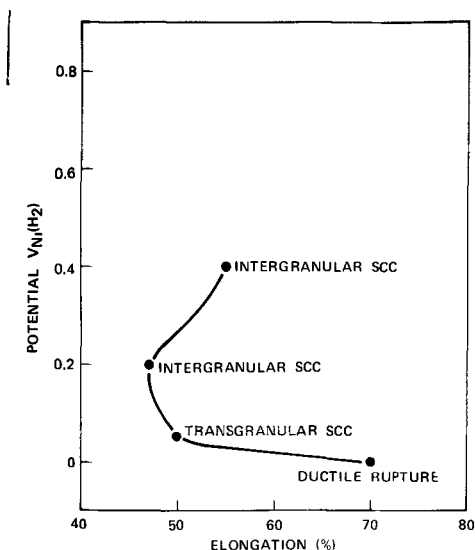


FIG. 9—Effect of potential on percent elongation and failure mode on Sanicro 30 in 10 percent NaOH at 288°C (550°F) using the slow strain-rate test technique.

sults show that the failure mode changes from ductile rupture at the open circuit potential to transgranular SCC at mildly anodic (that is, 50 mV_{Ni(H₂)}) potentials to intergranular stress corrosion cracking at intermediate anodic potentials (200 to 400 mV_{Ni(H₂)}).

Data for unstabilized Alloy 800 were previously reported (Table 3) and shown graphically in Fig 7. These data showed Alloy 800 to crack transgranularly at potentials from 50 mV_{Ni(H₂)} to at least 300 mV_{Ni(H₂)} and not to crack intergranularly until a potential of approximately 800 mV_{Ni(H₂)} was applied. Perhaps the alloy composition (namely, titanium to carbon plus

nitrogen ratio) or stress level has an important role in cracking morphology and cracking potentials [18,19].

Carbon Steel: Base Metal/Weld Metal Comparison

Tests were conducted in 127°C (260°F) undeaerated (open to air) 35 weight percent NaOH solution under open circuit conditions in order to compare the relative susceptibility to caustic SCC of carbon steel base metal with its weld metal. Similar solutions do induce SCC in mild steels [4].

U-bend specimens (12.70 mm (0.5 in.) wide by 19.05 mm (0.75 in.) leg by 12.70 mm (0.5 in.) span between legs by 03.18 mm (0.125 in.) thick) and round tension specimens were machined from carbon steel base metal and weld metal. These materials had been trepanned from a steam drum.

Two types of tests were conducted. The first was simple exposure of the U-bend specimens to the 35 weight percent NaOH solution to see whether cracking would occur. The second type of test employed the straining electrode machine and was used to determine the relative susceptibility of the two materials to caustic SCC.

The U-bend specimens were exposed to the test solution for 40 days with inspections every ten days. The inspections consisted of ultrasonically cleaning the specimens in distilled water to remove loose corrosion products and stereoscopic examination of the cleaned specimens at $\times 10$ and $\times 70$. The base metal specimen was found to be cracked at the final examination. Cracking was obvious before the specimens were cleaned and the cracks were severe. The weld metal specimen was not cracked, but showed gross wastage attack as opposed to less wastage attack on the base metal specimens.

In the straining electrode tests, the base metal failed by SCC as evidenced by numerous secondary cracks and the extremely low reduction in area ("brittle" failure). The weld metal failed in a ductile manner, had a significantly higher reduction in area, and no secondary cracks were observed. Results from both types of tests are summarized in Table 4. Both types of tests show that the base metal is susceptible to SCC in undeaerated 35 percent NaOH solution at 127°C (260°F). However, the slow strain-rate test shows that it is highly unlikely that the weld metal is susceptible to SCC under these same conditions. This conclusion cannot be drawn as readily from the U-bend tests since there is always the question in long term exposure tests that the test time was not of sufficient duration.

Summary and Conclusions

Slow strain-rate test equipment and three applications of the test to caustic SCC studies have been described. The equipment system has the capability to test metals potentiostatically at high temperatures and pres-

TABLE 4—Caustic SCC of mild steel: comparison of base and weld metal. ^a

Material	Constant Strain Rate Tests		
	Reduction of Area, %	Surface Examination	U-bend Tests
Base metal	16	numerous secondary cracks	severe cracking between 30th and 40th day of exposure
Weld metal	55	no secondary cracks	no cracking after 40 days exposure

^a 35 percent undeaerated NaOH (open to air) at 127°C (260°F).

sures. The results obtained from the three distinct studies have been compared to results obtained using other SCC test methods.

In tests on Alloy 600, Alloy 800, and Type 304 stainless steel the failure modes, the applied electrochemical potentials for SCC, and the potential for maximum cracking are in excellent agreement in comparisons between the constant strain-rate tests and the statically loaded tests. Similar agreement was found in the carbon steel base metal/weld metal tests. Test results on stabilized Alloy 800 (Sanicro 30) did not completely agree with test results on Alloy 800 in that the potential regions of the cracking modes (intergranular versus transgranular) did not always agree. However, the difference in results may be due to a difference in material composition or stress level and, therefore, this comparison may not be valid.

Acknowledgments

The authors thank J. V. Monter and J. P. Sorenson for performing the corrosion experiments, C. M. Chen for directing part of the research program, T. A. McNary for his helpful suggestions, and the Babcock & Wilcox Company for permission to publish the information.

References

- [1] Schmidt, H. W., Gegner, P. J., Heinemann, G., Pogacar, C. F., and Wyche, E. H., *Corrosion*, Vol. 7, 1951, p. 295.
- [2] Houdrement, E., Bennek, H., and Wentrup, H., *Stahl und Eisen*, Vol. 60, 1940, pp. 575, 791.
- [3] Robinson, F. P. A. and Nel, L. G., *Second International Congress on Metallic Corrosion*, National Association of Corrosion Engineers, Houston, Tex., 1963, p. 172.
- [4] Humphries, M. J. and Parkins, R. N., *Corrosion Science*, Vol. 7, 1967, p. 747.
- [5] Parkins, R. N., *Proceedings of Conference: Fundamental Aspects of Stress Corrosion Cracking*, National Association of Corrosion Engineers, Houston, Tex., 1969, p. 361.
- [6] Grafen, H. and Kuron, D., *Archiv fur Eisenhuettenwesen*, Vol. 36, 1965, p. 285.

- [7] Bush, S. H. and Dillon, R. L., "Stress Corrosion in Nuclear Systems," paper presented at the International Conference on Stress Corrosion Cracking and Hydrogen Embrittlement of Iron Base Alloys, Firminy, France, June 1973.
- [8] Weeks, J. R., *Nuclear Technology*, Vol. 28, 1976.
- [9] Cheng, C. F., *Journal of Nuclear Materials*, Vol. 56, 1975, p. 11.
- [10] Hare, M. G. and Stevens-Guille, P. D., "Steam Generators: The Long Road to Maturity," AECL-5089, Atomic Energy of Canada Limited, 1976.
- [11] Latanision, R. M. and Staehle, R. W., *Proceedings*, 1967 Conference on Fundamental Aspects of Stress Corrosion Cracking, National Association of Corrosion Engineers, Houston, Tex., 1969, p. 214.
- [12] Theus, G. J. and Staehle, R. W., "Review of Stress Corrosion Cracking and Hydrogen Embrittlement in Austenitic Fe-Cr-Ni Alloys," paper presented at the International Conference on Stress Corrosion Cracking and Hydrogen Embrittlement of Iron Base Alloys, Firminy, France, June 1973.
- [13] Theus, G. J., *Nuclear Technology*, Vol. 28, 1976, p. 388.
- [14] van Rooyen, D., *Corrosion*, Vol. 31, 1975, p. 327.
- [15] Parkins, R. N., in *The Theory of Stress Corrosion Cracking in Alloys*, J. C. Scully, Ed., North Atlantic Treaty Organization, Scientific Affairs Division, Brussels, 1971, p. 499.
- [16] Cels, J. R., *Corrosion*, Vol. 34, 1978, p. 198.
- [17] Cels, J. R., *Journal of the Electrochemical Society*, Vol. 123, 1976, p. 1152.
- [18] Wilson, I. L. W. and Aspden, R. G., "The Influence of Specimen Type and Metallurgical Structure on the Caustic Stress Corrosion Cracking of Some Stainless Alloys," paper presented at NACE Corrosion/75, National Association of Corrosion Engineers, Toronto, April 1975.
- [19] Chen, C. M., Emanuelson, R. H., and Theus, G. J., "Stress Corrosion Cracking Tests on Stabilized Alloy 800," to be presented at NACE Corrosion/79, National Association of Corrosion Engineers, Atlanta, March 1979.

C. D. Kim¹ and B. E. Wilde¹

A Review of the Constant Strain-Rate Stress Corrosion Cracking Test

REFERENCE: Kim, C. D. and Wilde, B. E., "A Review of the Constant Strain-Rate Stress Corrosion Cracking Test," *Stress Corrosion Cracking—The Slow Strain-Rate Technique*, ASTM STP 665, G. M. Ugiansky and J. H. Payer, Eds., American Society for Testing and Materials, 1979, pp. 97-112.

ABSTRACT: A review of six years operational experience in using the slow strain test procedure has indicated several unique advantages associated with dynamic strain techniques and also identified an area of limitation.

The chief advantage of the dynamic slow strain test procedure is that it is much more aggressive in producing stress corrosion cracking (SCC) than conventional constant-strain or constant-load tests, so that the testing time is considerably reduced. The procedure reduces the incubation period for crack nucleation by virtue of continuous straining above the elastic limit on smooth surfaces, and avoids the pitfalls associated with reducing incubation times by means of precracking and other methods. With the latter methods, marked chemical inhomogeneities in an environment have been observed so that spurious results are obtained.

The slow strain test is also ideally suited, on a "go-no-go" basis, for rapid sorting or screening of environment/metal or environment/metallurgical-condition combinations which can produce SCC. However, the test is not suitable for ranking materials with regard to their resistance to SCC when the strength levels and microstructure vary widely. Furthermore, because of the test severity, discretion must be exercised in translating susceptibility to SCC observed in the laboratory to anticipated performance in service.

KEY WORDS: stress corrosion cracking, hydrogen-induced cracking, strain rate, steels, ammonia, nitrate, caustic, carbonate-bicarbonate

Over the past several years U.S. Steel Research has been using a slow strain-rate test method to study the stress corrosion behavior of steels in various environments. It has been found that this method is very effective in producing stress corrosion cracking (SCC) in relatively short time periods. The main feature of this test method is the use of dynamic strain to stress the specimen, in contrast to the more conventional SCC tests which are conducted under a static stress condition. Although this procedure has been in

¹Associate research consultant and section supervisor, respectively, Research Laboratory, United States Steel Corporation, Monroeville, Pa. 15146.

use for five or more years, the slow strain test is still unfamiliar to many workers, and the practical significance and limitations of this test are not yet fully understood. In the present work, some observations made during the use of the slow strain test are presented, and the advantages and disadvantages of this test method compared with other SCC test methods are described.

Slow Strain Test Method

The concept of using dynamic strain in a SCC test was originally advanced by Parkins [1]² in his study of SCC behavior of carbon steels in hot nitrate solutions and subsequently was adopted by our laboratory for the study of SCC in line-pipe steels. In essence, this test method involves the application of a relatively slow strain rate to a specimen subjected to appropriate environmental conditions.

The apparatus for the slow strain test is similar to an ordinary tension testing machine, but its drive mechanism produces much slower crosshead speeds than those encountered in a tension test. Figure 1 is a general view of the slow strain test apparatus. In brief, it consists of a fixed stiff frame, a carriage, a drive mechanism, and a load cell and recorder (usually incorporated for continuous monitoring of the load on the specimen). Using an electric synchronous motor and suitable gear reducer, the carriage can be pulled downward at a constant rate in the range 10^{-7} to 10^{-3} cm/s. The bottom end of the specimen is coupled to the lower crosshead at the bottom of the carriage, while the top end is connected by means of a load cell to the cross beam of the fixed frame. Thus the downward movement of the carriage pulls the specimen in tension to fracture.

Although a variety of specimen sizes and shapes, including precracked specimens, can be employed with this test, a long smooth tension specimen is used most frequently. A typical specimen has a total length of 20.32 cm (8 in.), with the gage section—1.27 cm in length and 0.318 cm in diameter (0.5 by 0.125 in.)—in the middle. The specimen is inserted in a test cell with both ends outside the cell for connection to the crossheads. The test cell is usually constructed of trifluoroethylene resin or stainless steel, and pressure fittings are used to seal the specimen.

The strain rate used in this test is usually of the order of 10^{-6} s⁻¹ and is lower than that employed in straining electrode experiments (about 10^{-3} s⁻¹) conducted by Hoar and West [2] and by various other workers, where the purpose was to measure current transients during straining. Further, the present slow strain test should not be confused with that adopted by Coleman et al [3], where a constant rate of loading was used to determine the stress at which cracks were just detected.

²The italic numbers in brackets refer to the list of references appended to this paper.

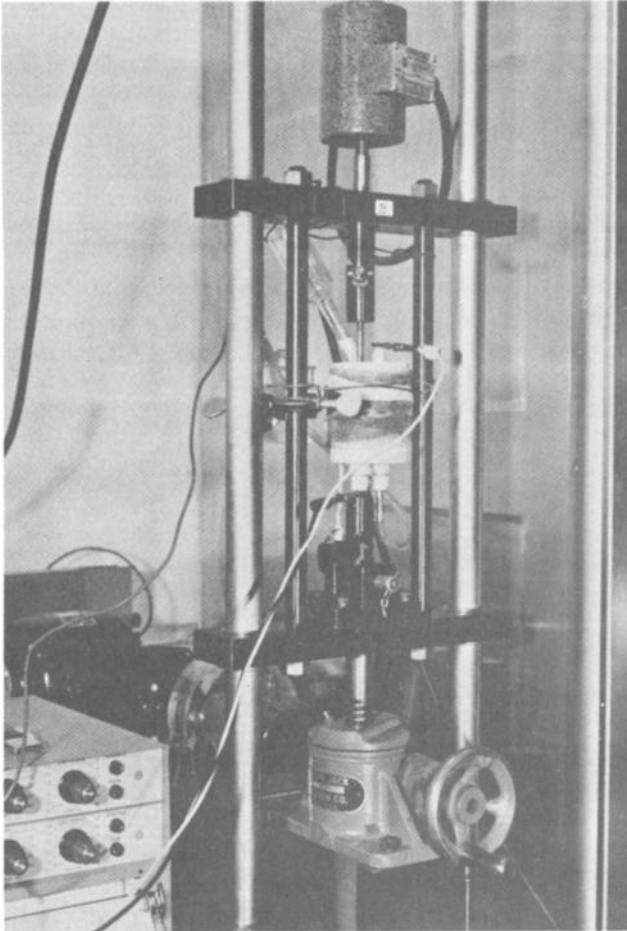


FIG. 1—General view of slow straining test apparatus.

Assessment of Results From Slow Strain Testing

Because the specimen is continuously strained in tension until fracture, the test always causes rupture, either by SCC or some other mechanism. Thus it is necessary to examine the specimen to determine whether or not SCC has occurred during the test. Visual inspection at $\times 30$ magnification is usually sufficient to determine the presence or absence of SCC, but cross-section metallographic and scanning electron microscopic (SEM) examination have been employed routinely to confirm the presence of SCC. In the absence of SCC, the fracture has a typical cup-and-cone character. In the presence of SCC, however, the ductility of the specimen is markedly decreased, and for many steels, secondary cracks are commonly observed near the main frac-

ture, as seen in Fig. 2. The SEM examination has proved very useful in identifying SCC, because it reveals the readily visible quasicleavage fracture mode associated with SCC or the dimple fracture mode indicative of the absence of SCC, Fig. 3. Such examination of specimens, however, reveals only whether SCC has occurred; it does not provide any quantifiable index for comparison of SCC susceptibility.

In conventional static tests, comparative SCC data are commonly expressed in terms of (a) the threshold stress below which SCC does not occur in an arbitrary period of time or (b) the time-to-failure at a given applied stress (T_F). With the slow strain test, similar expression of the severity of SCC is, unfortunately, not as simple (and probably not applicable) because the specimen is exposed to a continually changing stress during straining.

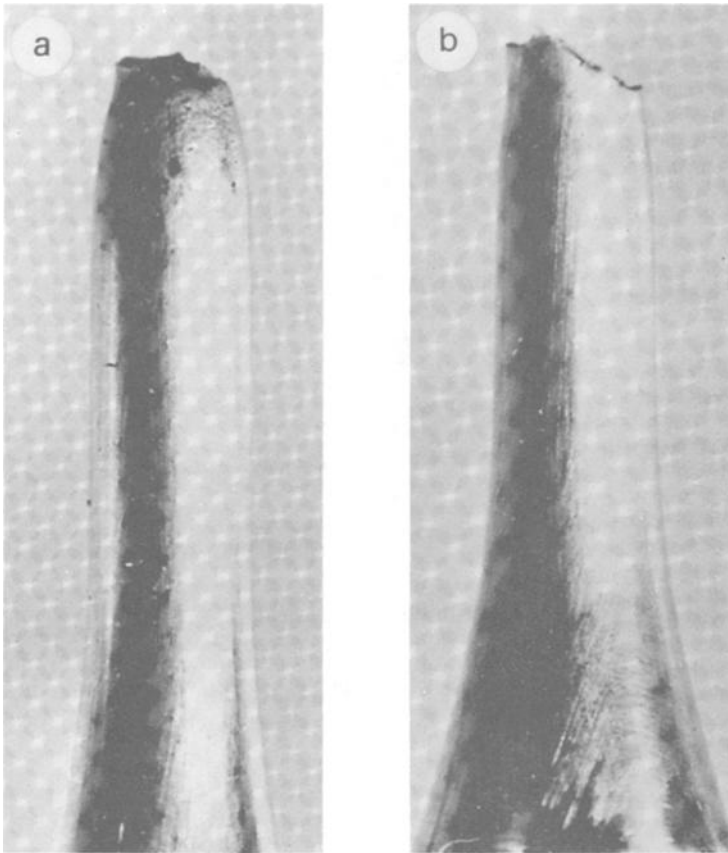


FIG. 2—Macrophotographs showing complete ductility and SCC on A517 Grade F steel. (a) Testing in air-contaminated metallurgical-grade ammonia. (b) Tested in water-inhibited air-contaminated metallurgical-grade ammonia. $\times 4$. (From Ref 7.)

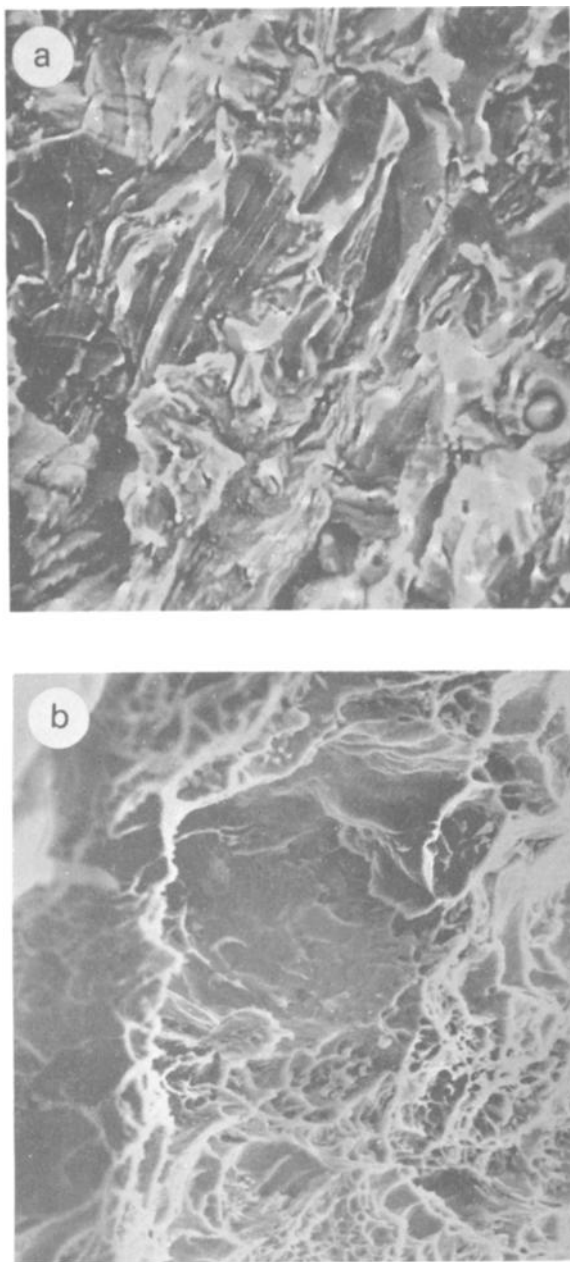


FIG. 3—Scanning electron micrographs of fracture surface on ERW Grade $\times 46$ line-pipe steel. (a) Tested in air-contaminated metallurgical-grade ammonia; note quasicleavage mode. (b) Tested in water-inhibited air-contaminated metallurgical-grade ammonia; note ductile dimple fracture mode and complete absence of quasicleavage mode. $\times 1000$. (From Ref 5.)

However, the following parameters can be considered, under certain limited conditions, as a comparative index for ranking SCC when the slow strain test is used: T_F , percent reduction of area (percent RA), maximum load (L_{max}), plastic strain to fracture (E_p), and percent elongation. Parkins [4] has used a number of these parameters to quantify susceptibility to SCC. Figure 4 shows the influence of applied electrode potential on the SCC of mild steel in 2 N ammonium carbonate ($(NH_4)_2 CO_3$) at 75°C (167°F), where percent RA is used as the index of cracking susceptibility. Because the specimen is strained continuously at a given rate, T_F is related directly to the percent elongation. Both percent elongation and RA are ductility parameters, and these two should be able to quantify SCC propensity in some manner. Figure 5 shows the relation of percent RA to T_F for an 0.07C steel in boiling 35 percent sodium hydroxide (NaOH).

However, our experience has indicated that such simple relationships between percent RA or T_F and cracking susceptibility are confined to studies where the mechanical properties of the steels investigated are quite similar. For example, if one tries to relate T_F to a ductility index for a range of steels differing widely in yield strength, a complicated, poorly understood relationship is observed, as shown in Fig. 6 for line-pipe steels exposed to boiling 1 M ammonium nitrate ($NH_4 NO_3$).

The problem of precisely indexing the data from the slow strain test is perhaps best illustrated in Fig. 7(a) and (b). Figure 7(a) shows a specimen of ASTM A517 Grade F alloy steel (yield strength = 110 ksi or 760 MPa) after testing in air-contaminated liquid ammonia. Note the low degree of ductility as evidenced by the low percent RA and the presence of few secondary cracks. Figure 7(b) shows a specimen of A202 Grade B carbon steel (yield strength = 68 ksi or 470 MPa) tested under the same conditions, again show-

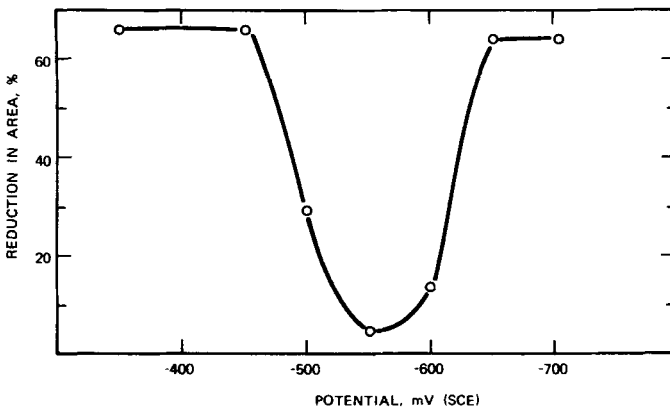


FIG. 4—Effect of applied potential on the cracking of mild steel in 2 N $(NH_4)_2 CO_3$ at 75°C (167°F). (From Ref 4.)

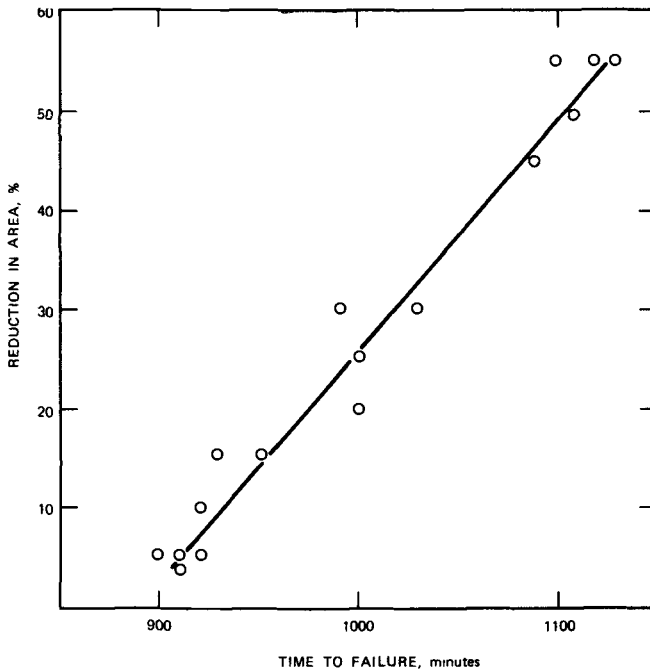


FIG. 5—Results for annealed 0.07 percent carbon steel tested in boiling 35 percent NaOH in constant strain-rate test, showing that time to failure (and hence, cracking propensity) is related to reduction of area. (From Ref 8.)

ing clear evidence of SCC. However, for the latter specimen, the percent RA was indistinguishable from the value determined in air, even though the gage length is riddled with cracks. Thus the question of which material is most susceptible to cracking is difficult to answer quantitatively.

In addition to the problems discussed above, it appears that the slow strain test is so severe that it can produce SCC on materials that have performed satisfactorily for years under conventional loading conditions, as illustrated, for example, by the behavior shown in Fig. 7(b) for A202 Grade B steel. Although susceptible to SCC in the laboratory, this steel has evidenced no SCC in service when used in railroad cars and over-the-road tank trucks. Therefore, slow strain testing at our laboratory has been limited to a very severe, rapid “go-no-go” test of material/environment interactions in which visual inspection and the presence of a quasicleavage mode of fracture on the fracture face are used as the criteria for the presence of SCC. By using the slow strain test in this way, significant accomplishments may be achieved in desirably short time periods, as was done, for example, in evaluating the suitability of electric resistant welded (ERW) line-pipe steels for ammonia pipelines [5].

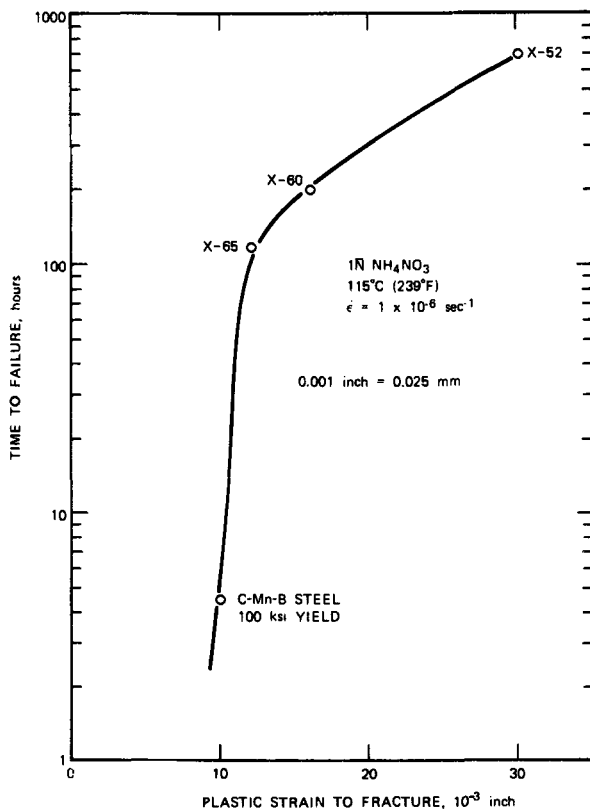


FIG. 6—Relation between environmental ductility and time-to-fracture for steels of varying strength.

Role of Dynamic Strain in SCC Process

Most SCC tests are conducted under a static stress condition by use of either a constant load or a constant strain. The use of a dynamic strain is relatively new and has been employed by only a few laboratories. As most field failures due to SCC appear to occur under static load conditions, the use of dynamic-strain tests might appear unrealistic. However, examination of the various SCC mechanisms reveals that dynamic strain always is involved in the process, plays an important role in the initiation and propagation of SCC and, in fact, is probably the best way in which to accelerate the cracking process, as will be discussed later.

The importance of film formation and film rupture during the SCC process has long been recognized. The formation of a film on a metal surface reduces the reactivity of the underlying metal, and rupture of the film must occur before the crack can initiate. According to the film-rupture theory,

rupture takes place during straining by slip-steps emerging at the surface; localized corrosion then occurs at the small area of freshly exposed metal to initiate a crack [6]. During a static test there is no way of sustaining the rate of slip-step emergence other than by increasing the applied stress or strain—that is, in a static-load test, the driving force for slip relaxes with time. However, when dynamic strain is applied in the slow strain test, slip-step emergence is induced artificially at a relatively constant rate which always ensures film rupture. Furthermore, the strain rate, and hence the rate of slip-step emergence, can be readily controlled in the slow strain test, thereby providing a degree of control of the severity of cracking.

This latter feature is of great importance for the following reasons. All SCC processes occur in two distinct stages—incubation and propagation. The incubation stage often occupies 90 percent of the test duration and therefore is the stage which most investigators try to minimize or eliminate, and hence resist the use of smooth specimens. Several popular techniques are utilized to minimize the incubation period, namely, (a) fatigue precracking, (b) potentiostatic control at potentials somewhat divorced from reality, and (c) manipulation of the severity of the corrosive environment. However, each technique results in unrealistic changes in the environment producing cracking. For example, the use of precracked specimens encourages acidification of the environment due to crevice corrosion. This may lead to an undue emphasis on hydrogen-embrittlement processes rather than anodic-dissolution reactions which may be operative on a smooth surface. In this regard, dynamic strain is preferred as a means of accelerating cracking, because in this method only the slip-step emergence rate is altered.

Dynamic strain also plays a very important role during crack propagation by maintaining localized corrosion at an active crack tip, while the sides of the crack are rendered inactive by filming. The maintenance of an active condition depends not only on the electrochemical conditions in the crack but also on the rate at which fresh metal is exposed by dynamic strain [6]. The need for dynamic strain to be present was recently demonstrated by Parkins in his work [4] on the SCC of a carbon-manganese (C-Mn) steel in an aqueous solution of sodium carbonate and bicarbonate. In this work, fatigue-precracked cantilever-beam specimens were loaded to a predetermined value, and cracking was measured by cross-section metallography after a given time of exposure and deflection of the beam. When C-Mn steel is exposed in an aqueous solution containing sodium carbonate and bicarbonate, SCC occurs only in a narrow range of potentials and does not occur when the potential is maintained in the noncracking range. When the specimen was loaded and the potential kept at a noncracking value, the beam-deflection rate was initially fast. However, as the creep in the plastic zone at the crack tip became exhausted, the rate gradually decreased and no SCC was produced, as illustrated by Curve A in Fig. 8. When the potential was maintained at a cracking value, the beam-deflection rate diminished at

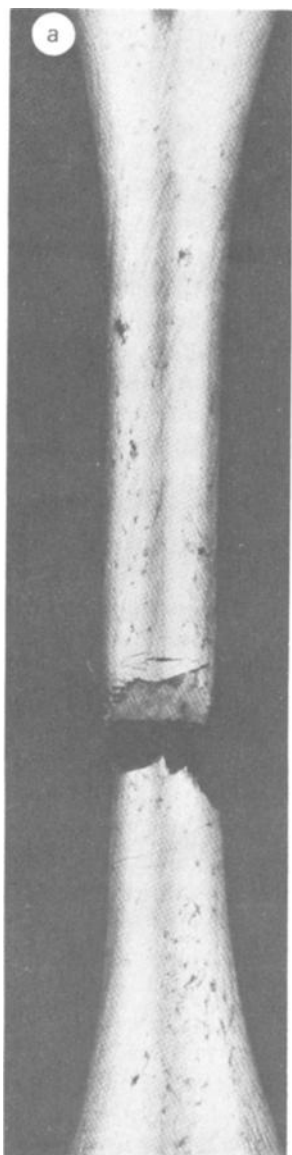


FIG. 7—(a) *ASTM A517 Grade F steel tested in liquid ammonia. $\times 6$.*

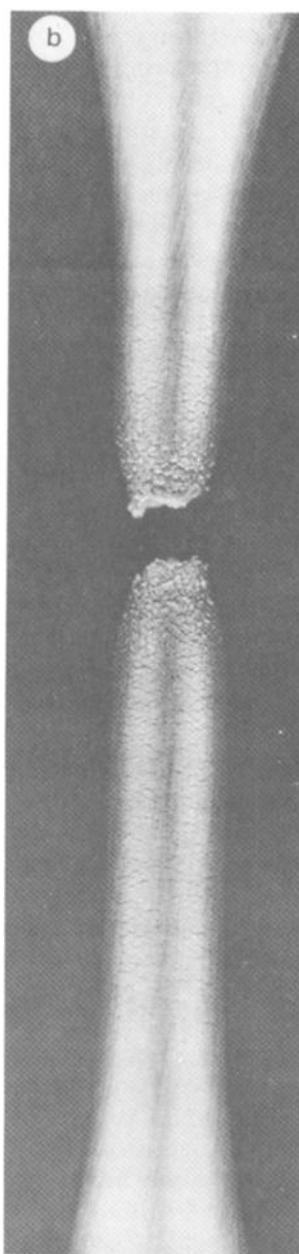


FIG. 7—(b) *A202 Grade B steel tested in liquid ammonia (SPL No. A202B No. 2). $\times 6$.*

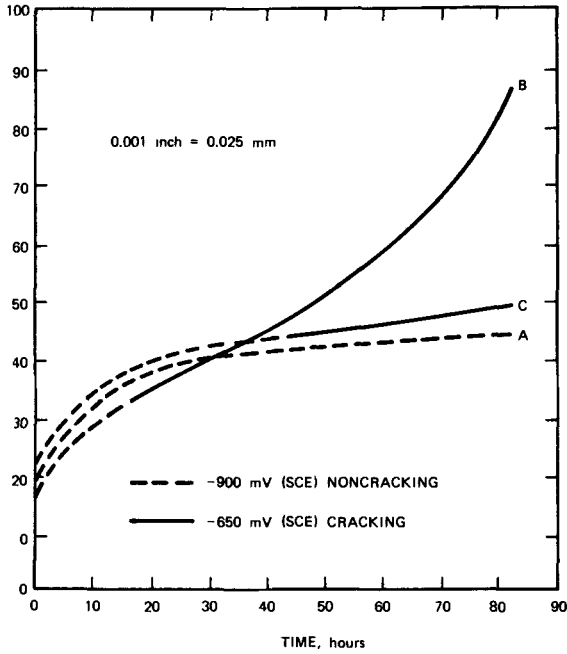


FIG. 8—Effects of time of change of potential on beam-deflection behavior of precracked pipeline steel specimens immersed in 1 N Na_2CO_3 + 1 N NaHCO_3 at 75°C (167°F).

the early stage, but after SCC initiated and propagated, the deflection rate slowly increased until failure, Curve B in Fig. 8. However, when the cracking potential was applied after the initial transient of the deflection rate, no SCC was produced (Curve C in Fig. 8) indicating that SCC did not take place at the lower deflection rate. Thus, it can be seen that the SCC process is controlled not only by the electrochemical condition but also by dynamic strain, and that SCC does not take place unless the appropriate combination of dynamic strain and electrochemical condition for SCC is met. Although the role of stress may be considered as simply that of maintaining the crack open to allow an inflow of fresh solution during the SCC process, the most important role of the applied stress is not stress *per se*, but the dynamic strain that it produces.

The direct application of dynamic strain makes the slow strain test a more severe test for SCC than static tests. For example, when a line-pipe steel (X-52) was tested under constant load in a boiling caustic solution or a hot aqueous solution of sodium carbonate and bicarbonate, no SCC was produced. However, under the same environmental conditions, the slow strain test was able to produce SCC in a relatively short time. Another example of the accelerating effect of dynamic strain can be seen in the SCC behavior of

steels in anhydrous ammonia; in this environment, static tests usually require many months for SCC to occur, but the slow strain test requires only about two days to produce severe SCC.

Selection of Strain Rate

Under a static load condition, onset of localized corrosion in the form of pits gives rise to an increase in stress in metal under the pits and thereby induces slip-step emergence at the surface, thus creating an active condition. However, with the slow strain-rate test, the active condition of the metal surface is always maintained by dynamic strain. Strain rate is an important experimental parameter in the slow-strain test. Although this test method is very effective in producing SCC in systems where cracking is difficult to produce in a static test, a specific range of strain rate must be employed before SCC can occur. For example, when the test is performed at too high a strain rate, the specimen fails by tensile rupture since there is not enough time for SCC to develop. At high strain rates, even if initiation of SCC takes place, the cracks become blunted due to dynamic strain before any significant amount of localized corrosion can occur at the crack tip, and consequently no SCC is observed. On the other hand, when a test is conducted at too low a strain rate, SCC may not occur because the corrosion reaction is obstructed by the film formation, and the active condition at the crack tip cannot be maintained if the film-rupture rate is below a critical value. Thus, the slow strain test does not produce SCC at either extreme of strain rates but will produce SCC in a critical range of strain rates characteristic of each material.

The influence of strain rate on SCC behavior is shown in Fig. 9 for an ASTM A517 Grade F steel tested at various strain rates in air-contaminated liquid ammonia [7]. The most severe SCC was produced at a strain rate of about 10^{-6} s^{-1} , as seen in Fig. 9. Past experience has shown that steels generally evidence severe SCC at a strain rate of about 10^{-6} s^{-1} regardless of the test environment (for example, ammonium nitrate solution, concentrated caustic solution, sodium carbonate and bicarbonate solution, and anhydrous liquid ammonia). It is important to appreciate that at extremely low strain rates, film formation protects the metal surface from an active condition, and as a result, SCC susceptibility is suppressed.

A similar dependency of cracking susceptibility on strain rate would not be observed for hydrogen-induced cracking. The reason is that hydrogen-induced cracking, unlike SCC, does not require a film-rupture event, but is caused by occluded hydrogen in the steel. During the corrosion reaction for hydrogen cracking, the cathodic partial reaction produces hydrogen on the steel surface, some of which is adsorbed by steel up to the saturation limit. As the testing period is increased by reducing the strain rate, the specimen becomes more susceptible to hydrogen cracking. Because of this varying response to strain rate, as shown schematically in Fig. 10, the slow strain test

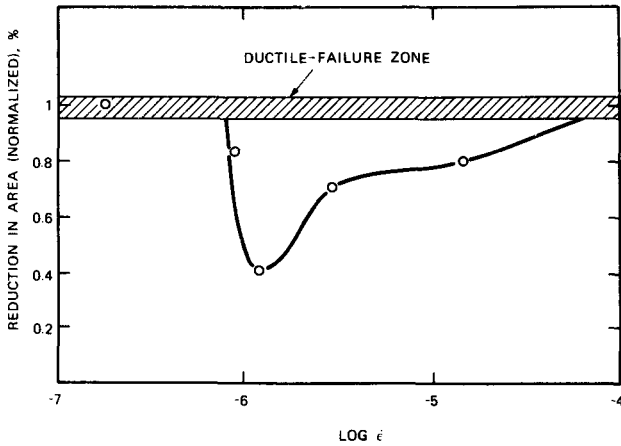


FIG. 9—Effect of strain rate on SCC behavior of A517 Grade F steel tested in air-contaminated ammonia. (From Ref 7.)

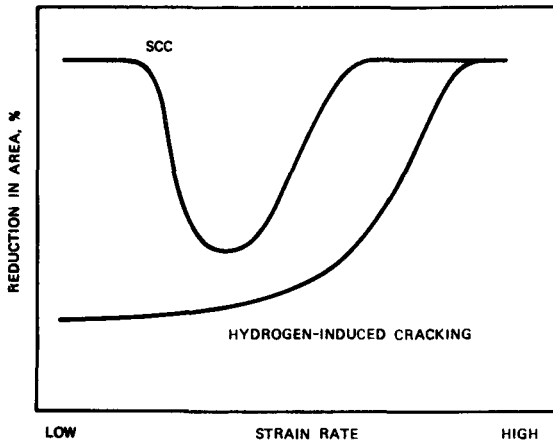


FIG. 10—Schematic presentation of the effect of strain rate on SCC and hydrogen-induced cracking.

can be used conveniently to determine whether the failure mechanism for a given cracking environment is SCC or hydrogen-induced cracking.

New Developments

Currently, work is in progress in Europe to develop dynamic-strain procedures which will extend the applicability of the smooth-bar uniaxial procedure used at U.S. Steel Research. For example, using a prenotched cantilever-beam specimen, Parkins [8] has studied the SCC behavior of line-

pipe steels in terms of threshold strain rate for crack growth and also Stage II plateau velocities. With this procedure, material parameters that influence the SCC performance of widely dissimilar steels can be measured readily. Typical data obtained by Parkins in his study of SCC in line-pipe steels are presented in Figs. 11 and 12.

Summary

A review of several years operational experience in using the slow strain test procedure has indicated several unique advantages associated with dynamic-strain techniques and also has identified areas of application where the value of the slow strain test is limited. The advantages and disadvantages of this test procedure are summarized as follows.

1. The dynamic slow strain test procedure is much more aggressive in producing SCC than conventional constant-strain or constant-load tests, so that testing time is reduced considerably.

2. The slow strain test is ideally suited for rapid identification of environment/metal combinations which will produce SCC. As a "go-no-go" test to identify metal/environment or metallurgical-condition/environment combinations for producing SCC, the slow strain test is always satisfactory.

3. The slow strain test can be used for quantitative ranking of SCC properties of steels having similar microstructures and strength levels. However, such ranking is difficult when applied to groups of steels having widely different strength levels and structures.

4. The slow strain test can produce SCC on materials that have performed satisfactorily in the field. The reason for this anomaly is believed to be that the slow strain-rate test imposes much higher stresses on these steels than actually are present in the steel in a postweld-heat-treated vessel under load conditions.

5. On the basis of several years experience, it has been found that visual inspection of the specimen after test, coupled with high-magnification scanning-electron fractographic analysis of the fracture face, yields unambiguous evidence of the presence or absence of SCC. In the presence of SCC, quasicleavage always occurs, whereas in the absence of SCC, a dimple mode of fracture occurs.

Acknowledgments

The authors are indebted to A. W. Loginow of U.S. Steel Research for helpful discussions.

Authors' Note

It is understood that the material in this paper is intended for general in-

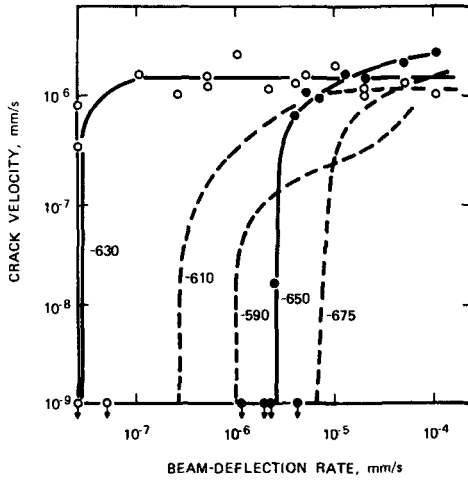


FIG. 11—Effects of different potentials on the applied beam deflection rate—crack velocity curves for a carbon steel in 1 N Na₂CO₃ + 1 N NaHCO₃ at 75°C (167°F). (From Ref 8.)

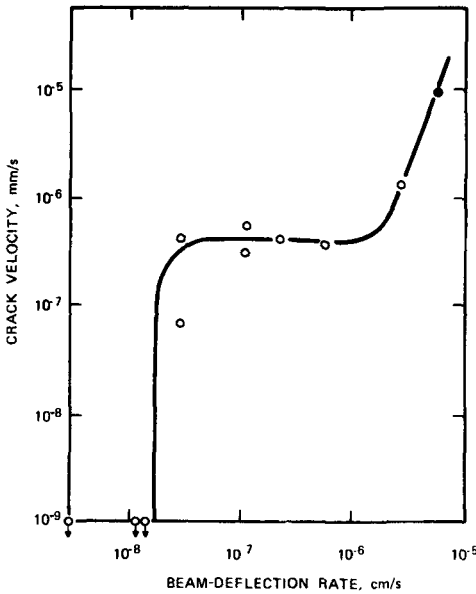


FIG. 12—Effects of various applied beam deflection rates on the stress corrosion crack velocity for a carbon steel in 1 N Na₂CO₃ + 1 N NaHCO₃ at 75°C (167°F). (From Ref 8.)

formation only and should not be used in relation to any specific application without independent examination and verification of its applicability and suitability by professionally qualified personnel. Those making use thereof or relying thereon assume all risk and liability arising from such use or reliance.

References

- [1] Parkins, R. N., in *Fundamental Aspects of Stress Corrosion Cracking*, R. W. Staehle, A. J. Forty, and D. van Rooyen, Eds., National Association of Corrosion Engineers, Houston, 1969, p. 361.
- [2] Hoar, T. P. and West, J. M., *Proceedings of the Royal Society*, A268, 1962, p. 304.
- [3] Coleman, E. G., Weinstein, D., and Rostoker, W., *Acta Metallurgica*, Vol. 9, 1961, p. 491.
- [4] Parkins, R. N., "The Controlling Parameters in Stress Corrosion Cracking," 5th Symposium on Line Pipe Research, Houston, 20-22 Nov. 1974.
- [5] Kim, C. D., Wilde, B. E., and Phelps, E. H., *Corrosion*, Vol. 31, 1975, p. 255.
- [6] Wilde, B. E., "Proceedings of USA/Japanese Seminar on Passivity," Honolulu, Hawaii, 12-16 March 1975.
- [7] Wilde, B. E. and Deegan, D. C., *Corrosion*, in press.
- [8] Parkins, R. N., "Constant Strain Rate Stress Corrosion Testing," submitted for publication in *Corrosion*.

DISCUSSION

*R. N. Parkins*¹—I wonder if there is any justifiable reason for expecting to rank or compare steels of very different microstructures and mechanical properties by strain-rate testing? Thus, your steel with a tempered martensitic structure is likely to be much more sensitive to the presence of cracks than the relatively ductile ferrite-pearlite steels. Consequently the former steel is likely to fail soon after the initiation of cracking, that is, with lower T_F or RA than the latter steel. A better means of comparison might be crack velocity, rather than the more easily measured quantities such as T_F or reduction of area.

C. D. Kim and B. E. Wilde (authors' closure)—We agree with your idea of using crack-velocity techniques as possibly being a more meaningful way of ranking widely differing steels. We simply wished to document the difficulty in ranking SCC performance of steels having widely different strengths and structures with the more common uniaxial slow strain-rate test for the new workers in the field.

¹University of Newcastle, England.

G. M. Ugiansky¹ and C. E. Johnson¹

Slow Strain-Rate Stress Corrosion Testing of Metals in Gaseous Atmospheres at Elevated Temperatures

REFERENCE: Ugiansky, G. M. and Johnson, C. E., "Slow Strain-Rate Stress Corrosion Testing of Metals in Gaseous Atmospheres at Elevated Temperatures," *Stress Corrosion Cracking—The Slow Strain-Rate Technique*, ASTM STP 665, G. M. Ugiansky and J. H. Payer, Eds., American Society for Testing and Materials, 1979, pp. 113-131.

ABSTRACT: A total of six different alloys—stainless steel (SS) Types 310, 310S, 347, and 446, and nickel alloys 800 and 671—were tested using the slow strain-rate test technique in oxidizing/sulfidizing and in oxidizing/sulfidizing/carburizing simulated coal gasification environments, and in helium (and other inert environments) at both 450 and 600°C at a strain rate of 10^{-6} /s. Of the six alloys, four (Types 310 stainless steel and 310S stainless steel, nickel alloy 800, and nickel alloy 671) were found to be susceptible to cracking at 600°C by possibly different mechanisms, however, all were detected by the slow strain-rate technique.

For cracking, the nickel alloy 671 required no reactive environment; it suffered internal cracking in helium and all other test environments used. However, the stainless steel Type 310, Type 310S, and nickel alloy 800, all of which failed through surface initiated cracking, required increasingly severe environments for cracking. The Type 310 stainless steel required very little reactive environment; it cracked not only in the simulated coal gasification gases but also in low vapor pressure O₂ or water (H₂O) environments, or both (for example, helium), as did the Type 310S stainless steel, although with greater ductility than the Type 310 stainless steel. The nickel alloy 800 required the rather reactive environment of the simulated coal gasification gases; it did not crack in the low vapor pressure O₂ and H₂O environments.

The detection of the environmentally independent failure of Alloy 671 shows that the use of the slow strain-rate technique need not be limited to use for testing for susceptibility to cracking by stress corrosion cracking. The slow strain-rate technique is shown to be a viable testing method for detecting an alloy's propensity to premature failure in simulated coal gasification environments.

KEY WORDS: austenitic stainless steels, coal gasification, elevated temperatures, ferritic stainless steels, gaseous environments, nickel alloy 671, nickel alloy 800,

¹ Metallurgist and physical science technician, respectively, National Measurement Laboratory, National Bureau of Standards, Washington, D.C. 20234.

oxidizing/sulfidizing gas, oxidizing/sulfidizing/carburizing gas, premature failure, slow strain-rate test technique, stress corrosion cracking, Type 310 stainless steel, Type 310S stainless steel, Type 347 stainless steel, Type 446 stainless steel.

Although the slow strain-rate method has not been adopted as a standard test method for determining the susceptibility of alloys to stress corrosion cracking (SCC),² various forms of the method have been used successfully for mechanistic studies and for alloy evaluation purposes as is readily evident from the many papers in this volume. Parkins [1]³ gives a particularly good review of the development of the technique. All of the other papers in this volume deal with the SCC susceptibility of metals and alloys in liquid environments. However, in this paper the results of an investigation of the susceptibility of metals and alloys in gaseous atmospheres at elevated temperatures are presented.

The study of the susceptibility of alloys to SCC in gaseous environments at elevated temperatures was initiated primarily due to the energy shortage in the United States and the subsequent efforts being made to alleviate that problem by developing a technology and an industry to convert the nation's abundant coal reserves to both high and low BTU gas. It is in this industry that alloys will be used in a combination of gaseous compositions and at elevated temperatures in which their susceptibility to failure by an environmentally sensitive cracking mechanism (SCC as defined previously) is completely unknown. Therefore, in the hope of avoiding the appearance of SCC problems in coal gasification plants after they have become operational (as was experienced in the nuclear industry), this work was begun to evaluate the slow strain-rate technique for determining the susceptibility of alloys to SCC in environments of relevance to coal gasification technology.

In order to establish the usefulness of the slow strain-rate technique for coal gasification systems, it was first necessary to evaluate the test with a specimen/gaseous environment system of known susceptibility to SCC. For this purpose, brass was tested in an atmosphere of anhydrous ammonia (NH_3) saturated with water (H_2O) vapor and in dry helium. The results of these tests were compared with the results of Takano [4] for brass in aqueous ammoniacal environments.

²Some people disagree with the use of the term SCC as applied in this paper to elevated temperature/gaseous phenomena. However, the term SCC is used here under the broad definition given by Logan [2]: "... the spontaneous failure of a metal resulting from the combined effects of corrosion and stress." The term "corrosion" is taken to mean "destruction or deterioration of a material because of reaction with its environment" as defined by Fontana and Greene [3]. Using these definitions, the term SCC can be used appropriately to define cracking phenomena in gaseous environments where chemical reaction of the gas with the metal results in an increased susceptibility to cracking as compared with the behavior of the same metal in a completely inert environment.

³The italic numbers in brackets refer to the list of references appended to this paper.

The results of the tests of the brass specimens in NH_3 saturated with H_2O vapor at 23°C [5,6] showed that the slow strain-rate technique was valid for SCC in an alloy/gaseous environment system of known susceptibility to SCC; that is, the results were similar to the results obtained by Takano [4] in aqueous ammoniacal environments.

After the evaluation of the slow strain-rate results for the brass/water saturated NH_3 system was completed, it was possible to extend the test to systems of more relevance to coal gasification systems as described next.

Experimental Procedures

Materials and Specimen Description

The compositions and heat treatments of the six alloys used in this investigation are given in Table 1. Four of the alloys (Type 310 stainless steel, Type 310S stainless steel, Type 347 stainless steel, and nickel alloy 800) have an austenitic structure; one alloy (Type 446 stainless steel) is ferritic; and one (nickel alloy 671, essentially 50Ni-50Cr) has an austenitic structure with a secondary α -chromium phase. The heat treatments of these alloys were performed by the suppliers prior to the machining of the specimens.

The machined specimens were 58 cm long by 9.5 mm in diameter and threaded on both ends for attachment to universal couplings outside of the test cell. The effective gage length was 2.5 cm, with a corresponding reduced diameter of 4 mm. Before testing, the reduced area of the specimens was polished using 320, 400, and 600 grit silicon carbide paper, respectively, followed by a final polish using crocus cloth. The surface was finally cleaned with acetone and alcohol and air dried.

Test Facility

The slow strain-rate test facility is capable of testing four specimens simultaneously with automatic digital data acquisition and storage. The facility is depicted schematically in Fig. 1. A range of strain rates from $10^{-3}/\text{s}$ to $10^{-7}/\text{s}$ (over a 2.5-cm gage length) was achieved through the use of different gear ratios, reduction gear boxes, and a variable speed motor. The tensile load on the specimen was measured by a load cell with a maximum capacity of 900 kg and an output of $39.6 \mu\text{V}/\text{kg}$. Linear voltage differential transformers (with an output of $13.33 \text{ V}/\text{m}$) were used for measuring the elongation of the specimens. The elongation was also measured by the use of gage marks on the reduced section of the specimen. Additionally, reduction of area measurements were made on the specimens by measuring the diameter of the reduced section before and after testing. The load cells and differential transformers were sequentially scanned, and their outputs were read on a digital multimeter. The digital multi-

TABLE 1—Alloy compositions, weight percent.^a

Alloy	C	Mn	Si	S	P	Cb + Ta	Ti	Cu	Mo	Ni	Cr	Fe	Heat Treatment
Type 310 stainless steel	0.08	1.78	0.48	0.02	0.028			0.17	0.10	19.59	24.84	bal	cold drawn, annealed 1040 to 1150°C, water quench, pickled (HNO ₃ - HF)
Type 310S stainless steel	0.06	1.68	0.72	0.011	0.017			0.14	0.11	19.60	24.67	bal	same as Type 310 stainless steel
Type 347 stainless steel	0.06	1.45	0.69	0.01	0.024	0.66		0.28	0.43	9.49	18.21	bal	cold drawn, annealed 980 to 1090°C, water quench, pickled (HNO ₃ - HF)
Type 446 stainless steel	0.11	0.52	0.47	<0.005	0.035			0.03	0.13	0.59	25.77	bal	cold drawn, annealed 790 to 870°C, water quench, pickled (HNO ₃ - HF)
Nickel alloy 800	0.04	0.93	0.29	0.01	0.005		0.38	0.54	0.08	32.51	20.02	bal	cold drawn, solution annealed 980 to 1040°C, pickled
Nickel alloy 671	0.06					0.30				50.27	46.74		cold drawn, solution annealed 1150°C, pickled

^a From quantitative analyses.

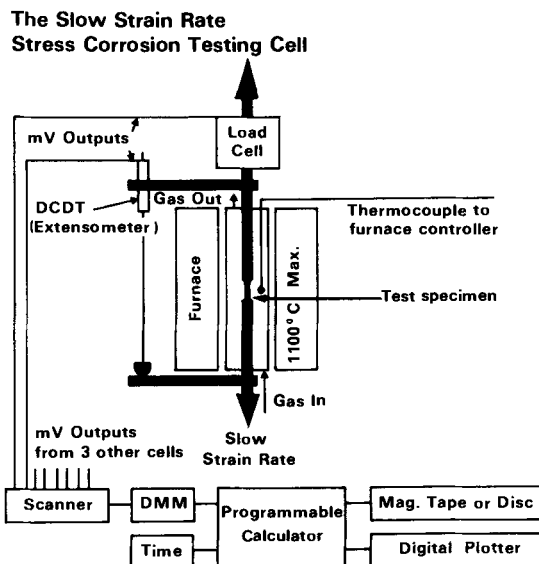


FIG. 1—Schematic of the slow strain-rate stress corrosion testing system.

meter readings were then stored in a programmable calculator until the tests were finished. Then the data were transferred to magnetic tape or flexible magnetic disk memory for later use in constructing stress-strain curves or other curves of tensile strength, elongation, or reduction of area versus strain rate using a digital x - y plotter.

The test cells were Type 304 stainless steel tubes (38 cm long by 5 cm in diameter) sealed on both ends with Type 304 stainless steel plates using gaskets. The cells were mounted in furnaces capable of producing test temperatures up to 1100°C. Ports for entrant and exit gases, thermocouple, and specimens were available on the end plates of the test cells. The specimens were pulled through sliding seals of trifluoroethylene resin or through high vacuum O-ring couplings. These seals are limited in use to below 300°C; but since the seals are located outside of the furnace, their temperature was kept below 300°C by the use of forced air cooling.

Test Procedure and Test Gases

The specimens were positioned in the test cell so that the reduced area of the specimen was in the center of the cell and furnace. The cells were purged with either nitrogen, argon, or helium. The test gas was introduced into the cells and the furnaces were brought up to test temperature. The gas flow through the cells was 10 volume changes/h (2.2 cm³/s for each

cell). The specimens were preloaded to 100 kg to remove the slack from the system and to produce a positive output from the load cell. Data were taken at predetermined intervals of load change (approximated by dividing the expected maximum load by the number of data registers available), usually 0.3 or 0.4 mV corresponding to 7.5 or 10 kg. Tests were conducted at temperatures ranging from 23 to 1040°C.

The test gases used consisted of helium, argon, hydrogen sulfide (H₂S) plus steam, H₂S saturated at 23°C with H₂O vapor, and gaseous mixtures of carbon monoxide (CO), carbon dioxide (CO₂), hydrogen (H₂), methane (CH₄), H₂S, and H₂O. The helium and argon environments were used as "normalizing" environments. Results for specimens tested in these normalizing environments were compared to results for specimens tested in the other gaseous environments. The H₂S plus steam and H₂S saturated at 23°C with H₂O vapor were used as initial simplified coal gasification type environments because of the high probability of SCC in those environments as based on the known susceptibility to SCC of austenitic stainless steels in sulfidic environments found in oil refineries. The gaseous mixtures of CO, CO₂, H₂, CH₄, H₂S, and H₂O were used to simulate possible coal gasification environments. The inlet gas compositions and the calculated equilibrium compositions of the simulated coal gasification environments are given in Table 2.

TABLE 2—Gas compositions.^a

	Oxidizing/Sulfidizing Gas ^b		Oxidizing/Sulfidizing/Carburizing Gas ^c			
	Input	Equilibrium	Input	Equilibrium	Input	Equilibrium
	1 atm, 25°C	1 atm, 450°C	1 atm, 600°C	1 atm, 25°C	1 atm, 450°C	1 atm, 600°C
CO	11.6	1.2	9.2	26.0	1.1	12.5
CO ₂	15.4	24.9	20.6	14.8	22.0	20.0
H ₂	13.0	16.0	36.3	26.0	12.8	32.7
CH ₄	10.0	12.5	2.9	10.0	11.2	5.5
H ₂ S	1.0	1.0	0.9	1.0	1.0	0.9
H ₂ O	49.0	44.4	30.3	22.2	34.3	19.4
C	17.6	9.0
log P _{O₂}		-28.995	-23.919		-29.026	-24.216
log P _{S₂}		-10.260	-8.878		-10.086	-8.751
log a _c		-0.043	-0.288		+0.017	+0.038

Note—The major difference between the two mixtures is the deposition of carbon from the oxidizing/sulfidizing/carburizing gas at both temperatures, the oxidizing and sulfidizing potentials being similar at each temperature.

^aThe gas mixtures are two of twelve mixtures being used at Battelle's Columbus Laboratories and Argonne National Laboratory.

^bThis mixture corresponds to Battelle's "Gas Mixture 1A" [7].

^cThis mixture corresponds to Battelle's "Gas Mixture 3A" [7].

Results and Discussion

Coal gasification candidate materials of stainless steel Types 310, 310S, and 347 and nickel alloy 800 were initially tested at 540°C, over a range of strain rates from 10^{-4} to 10^{-7} /s, in an environment of helium and in corrosive environments of H₂S plus steam and H₂S saturated at 23°C with H₂O vapor. The results of the tests of these alloys in helium and in the gaseous H₂O/H₂S can be seen in Fig. 2. Type 310S stainless steel, Type 347 stainless steel, and nickel alloy 800, failed with relatively high ductility in both the helium and in the gaseous H₂O/H₂S (Fig. 2). However, the Type 310 stainless steel was found to fail prematurely by intergranular cracking with low elongation and little reduction of area when tested in either environment. Numerous secondary cracks also were observed along the reduced area of the specimen. This brittle (in appearance) type fracture of Type 310 stainless steel was found to be related to strain rate induced sensitization of the grain boundaries. The test temperature of 540°C is well within the range of temperature (450 to 870°C) in which sensitization of Type 310 stainless steel is known to occur. Even when testing Type 310 stainless steel in dry helium or argon, the specimens fractured in the brittle manner when tested at 540°C and a strain rate of 10^{-6} /s. Since a visible oxide film was present on all specimens tested, regardless of environment, and the cracks initiated at the surface (Fig. 3), we believe that the embrittlement is due to oxidation of the chromium depleted (that is, sensitized) grain boundary region. When testing at temperatures below the temperature range for sensitization, the specimen fracture was ductile in appearance with higher elongation and reduction of area results even though tested at

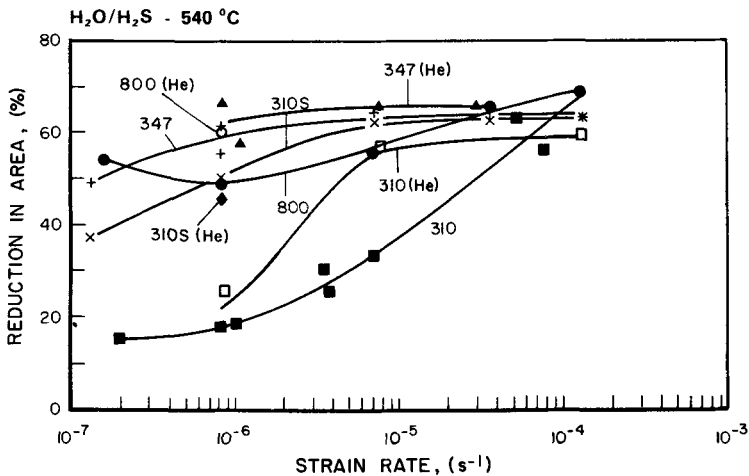


FIG. 2—Ductility as reduction of area versus strain rate for four alloys tested in gaseous H₂O/H₂S at 540°C.

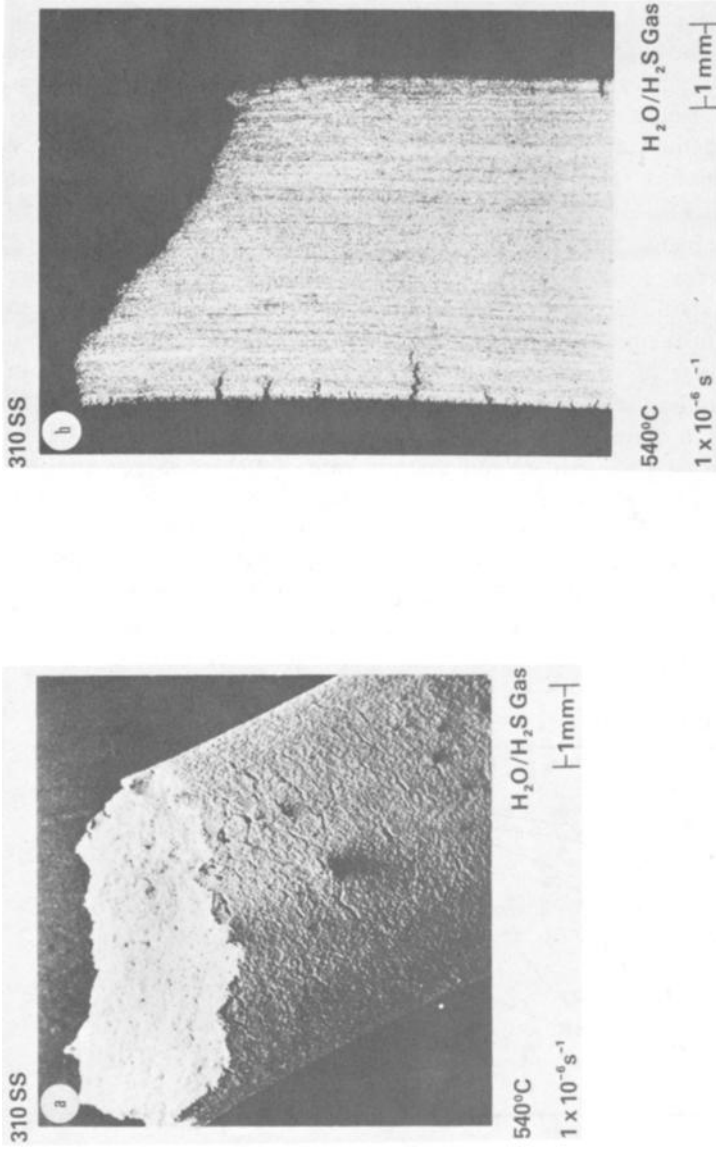


FIG. 3—A specimen of Type 310 stainless steel after testing in H₂O/H₂S at 540°C and a strain rate of 10⁻⁶/s. Cracks are seen to initiate at the surface of the specimen in the scanning electron micrograph (a) and in the optical micrograph of the cross section of the specimen (b).

a slow strain rate of 10^{-6} /s. Even when the Type 310 stainless steel specimen was heat treated at 540°C for a time equivalent to the time required for specimen failure when tested at a strain rate of 10^{-6} /s, the Type 310 stainless steel specimen failed in a ductile manner when subsequently tested at a higher strain rate (10^{-4} /s). This test showed the need for simultaneous application of the slow strain rate (10^{-6} /s) and the sensitization temperature for premature intergranular fracture. Regardless of the precise mechanism, the slow strain-rate technique enabled the detection of this premature failure.

The coal gasification candidate materials Types 310, 310S, 347, and 446 stainless steels, and nickel alloys 800 and 671 were tested in simulated coal gasification environments (Table 2) at temperatures of 450 and 600°C at a strain rate of 10^{-6} /s; they were also tested in an environment of ultrapure helium at the same temperatures and strain rate. The resulting stress-strain curves for these tests are shown in Figs. 4 through 9.

Type 310 stainless steel was found to be susceptible to cracking at 600°C (but not at 450°C) in all three gaseous environments. As can be seen in Fig. 4, the ductility was lowest in the oxidizing/sulfidizing environment. Examples of fractures of Type 310 stainless steel in the oxidizing/sulfidizing gas at both 450 and 600°C are shown in Fig. 10. As in the case of testing the alloys in $\text{H}_2\text{O}/\text{H}_2\text{S}$ gases at 540°C , the Type 310S stainless steel specimens were much more ductile than the Type 310 stainless

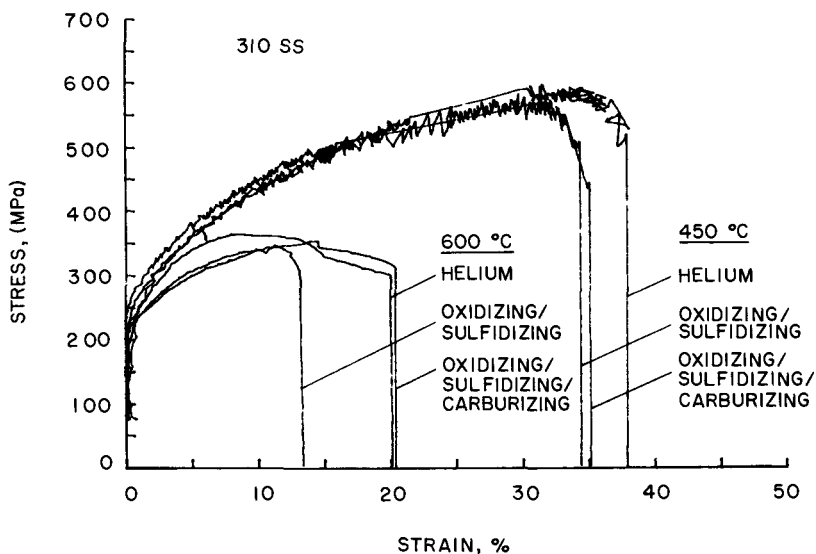


FIG. 4—Stress-strain curves for Type 310 stainless steel tested at 450 and 600°C (840 and 1100°F) in helium and in oxidizing/sulfidizing and oxidizing/sulfidizing/carburizing coal gasification environments at a strain rate of 10^{-6} /s.

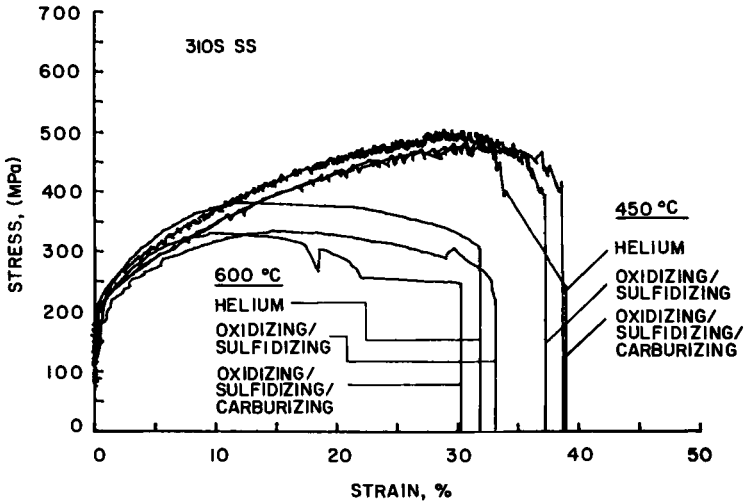


FIG. 5—Stress-strain curves for Type 310S stainless steel tested at 450 and 600°C (840 and 1100°F) in helium and in oxidizing/sulfidizing and oxidizing/sulfidizing/carburizing coal gasification environments at a strain rate of 10^{-6} /s.

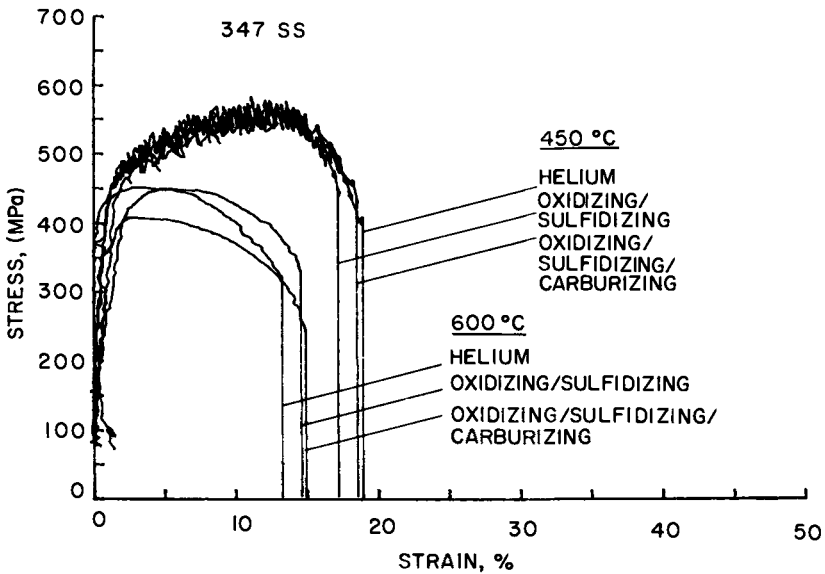


FIG. 6—Stress-strain curves for Type 347 stainless steel tested at 450 and 600°C (840 and 1100°F) in helium and in oxidizing/sulfidizing and oxidizing/sulfidizing/carburizing coal gasification environments at a strain rate of 10^{-6} /s.

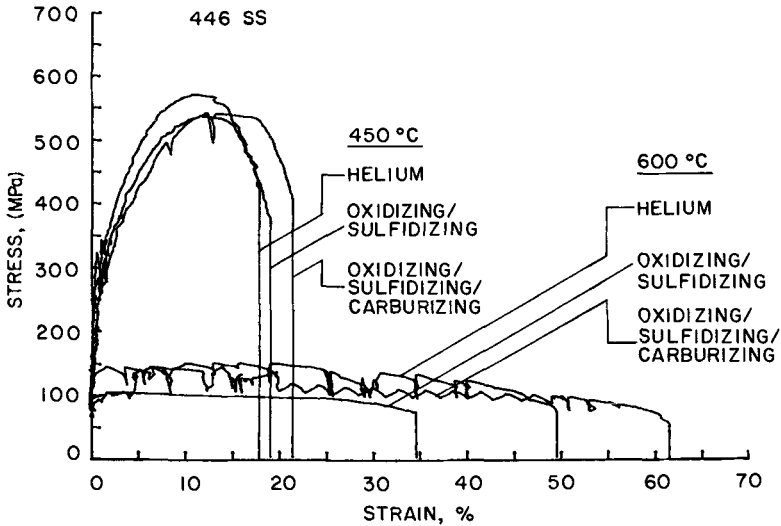


FIG. 7—Stress-strain curves for Type 446 stainless steel tested at 450 and 600°C (840 and 1100°F) in helium and in oxidizing/sulfidizing and oxidizing/sulfidizing/carburizing coal gasification environments at a strain rate of 10^{-6} /s.

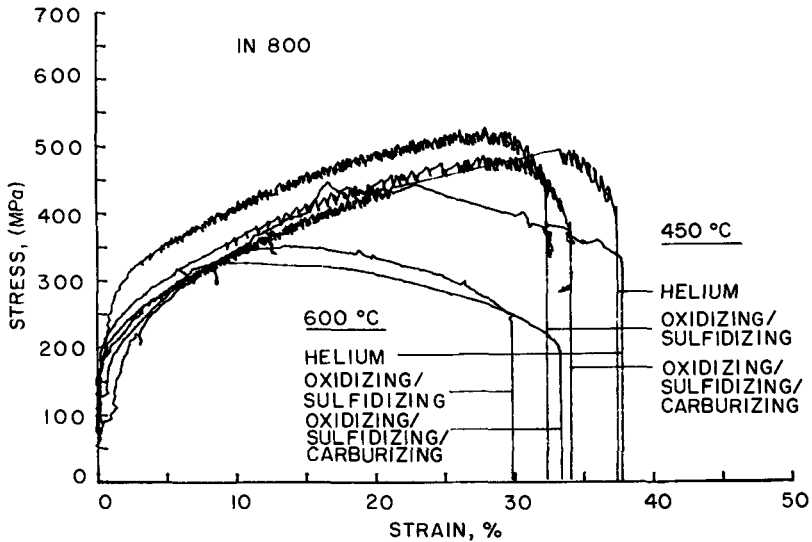


FIG. 8—Stress-strain curves for nickel alloy 800 tested at 450 and 600°C (840 and 1100°F) in helium and in oxidizing/sulfidizing and oxidizing/sulfidizing/carburizing coal gasification environments at a strain rate of 10^{-6} /s.

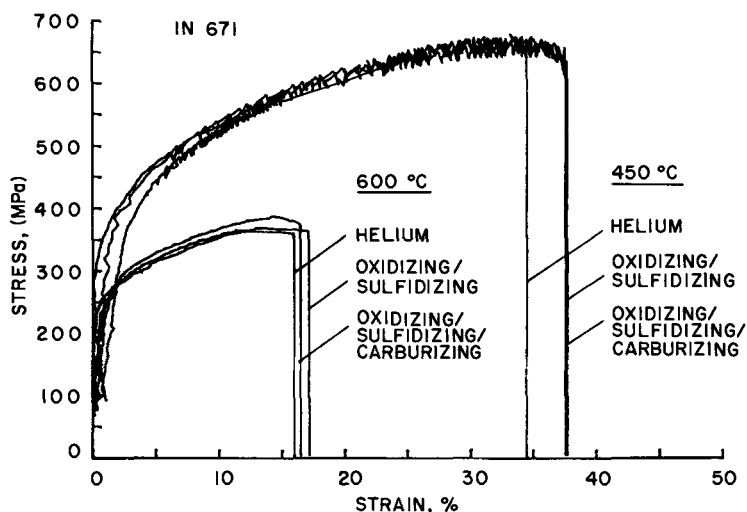


FIG. 9—Stress-strain curves for nickel alloy 671 tested at 450 and 600°C (840 and 1100°F) in helium and in oxidizing/sulfidizing and oxidizing/sulfidizing/carburizing coal gasification environments at a strain rate of 10^{-6} /s.

steel specimens in the stimulated coal gasification environments and helium at 600°C, although at 600°C surface cracking was apparent in the Type 310S stainless steel specimens tested in all three gaseous environments—the increase in test temperature from 540 to 600°C resulted in cracking of the Type 310S stainless steel. Neither alloy was susceptible to cracking at 450°C in the coal gasification environments or helium. When comparing Figs. 4 and 5, it is obvious that at 600°C the strain at failure (elongation) was considerably higher for the Type 310S stainless steel (Fig. 5) than for the Type 310 stainless steel (Fig. 4). Type 347 stainless steel, which was tested because it is stabilized with niobium and tantalum to resist sensitization, showed slightly lower strength and ductility at 600°C when compared to 450°C in all of the test environments (Fig. 6). Some small surface cracks were detected in the necked down region next to the fracture surface in Type 347 stainless steel tested in the oxidizing/sulfidizing/carburizing environment at 600°C with little, if any, difference in ductility compared to Type 347 stainless steel tested in helium or oxidizing/sulfidizing environments at 600°C. The fact that the sensitization resistant alloys, Type 347 stainless steel as well as the Type 310S stainless steel, showed less difference in ductility between the 600 and 450°C specimens than the Type 310 stainless steel showed when tested under the same conditions further supports the previously mentioned rationale that the cracking is caused by strain rate induced sensitization and the environmental interaction with the chromium depleted grain boundary regions. The Type 310S

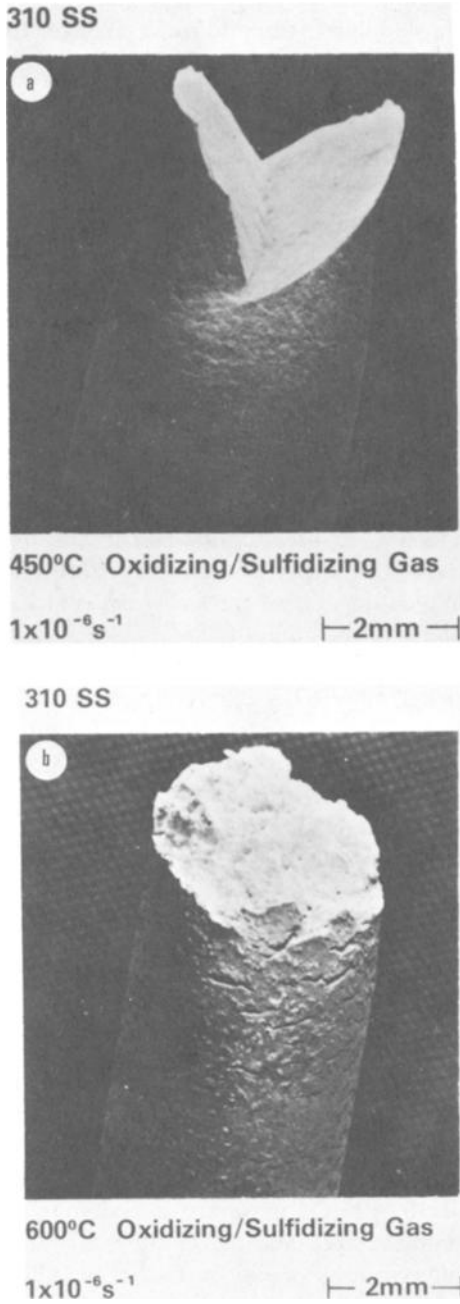


FIG. 10—Scanning electron micrographs of Type 310 stainless steel specimens tested in the oxidizing/sulfidizing coal gasification environment at 10^{-6} /s at 450°C (a) and at 600°C (b).

stainless steel, with the lower carbon content than Type 310 stainless steel, has to be subjected to a higher temperature or a longer time at temperature for sensitization and for cracking to occur.

Of the alloys tested, the Type 446 stainless steel was the only one tested above its useful temperature range (see the 600°C data in Fig. 7). As can be seen in Fig. 7, the Type 446 stainless steel specimens tested at 600°C were strained almost entirely in the plastic region. No cracking was observed at either 450 or 600°C in any of the test environments.

The oxidizing/sulfidizing and the oxidizing/sulfidizing/carburizing (but not helium) environments both caused cracking of the nickel alloy 800 when tested at 600°C but not at 450°C. When tested at 600°C in the oxidizing/sulfidizing and in the oxidizing/sulfidizing/carburizing gases, the nickel alloy 800 had considerably lower strength and marginally lower ductility than when tested in helium (Fig. 8). Although susceptibility to cracking is not obvious from the curves of Fig. 8, examination of the specimens revealed the cracking mentioned above. Figure 11 shows the ductile fracture at 450°C and the intergranular fracture (with many surface cracks) at 600°C of nickel alloy 800 in the oxidizing/sulfidizing environment. As with the Type 310 stainless steel, the cracking of the nickel alloy 800 is also dependent on environmental interaction with the grain boundary regions of the alloy.

The one alloy which cracked apparently independent of environmental effects was the nickel alloy 671. Figure 9 shows the almost coincident stress-strain curves at 450°C and also at 600°C for all environments. The considerably lower strength and ductility at 600°C (compared to 450°C) are accurate indications of the brittle failure observed at 600°C but not at 450°C in each test environment. However, the cracking unlike that of the Types 310 stainless steel and 310S stainless steel and the nickel alloy 800 was not initiated at the specimen/gas interface, Fig. 12. The cracks initiated internally at α -chromium grain boundaries. The brittle α -chromium phase underwent considerable growth only at the test temperature of 600°C.

Conclusion

A total of six different alloys—stainless steel Types 310, 310S, 347, and 446, and nickel alloys 800 and 671—were tested in helium (and other inert environments), in an oxidizing/sulfidizing and in an oxidizing/sulfidizing/carburizing simulated coal gasification environment at both 450 and 600°C at a strain rate of 10^{-6} /s. Of these six alloys, four (Type 310 stainless steel, Type 310S stainless steel, and nickel alloys 800 and 671) were seen to be susceptible to intergranular cracking. Two of the alloys (Type 310 stainless steel and nickel alloy 671) failed with relatively low ductility compared to the other two alloys (Type 310S stainless steel and nickel alloy 800) when tested at 600°C. These failures were possibly due to different mecha-

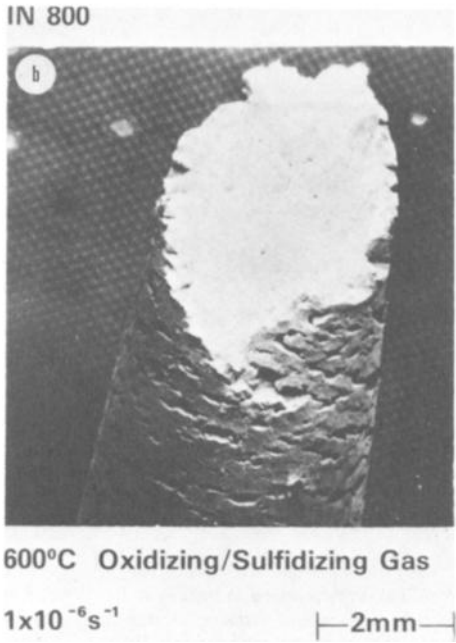
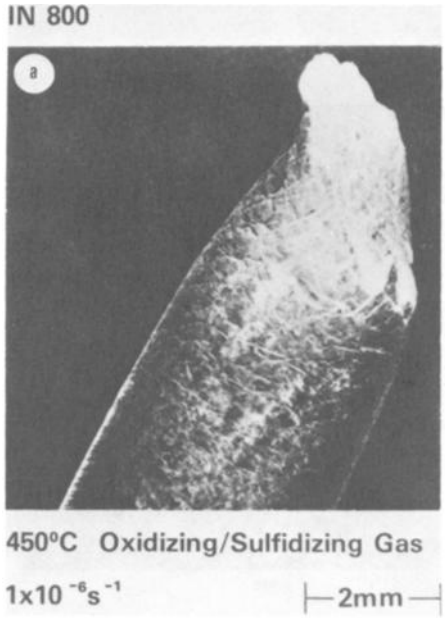


FIG. 11—Scanning electron micrographs of nickel alloy 800 specimens tested in the oxidizing/sulfidizing coal gasification environment at 10^{-6} /s at 450°C (a) and at 600°C (b).

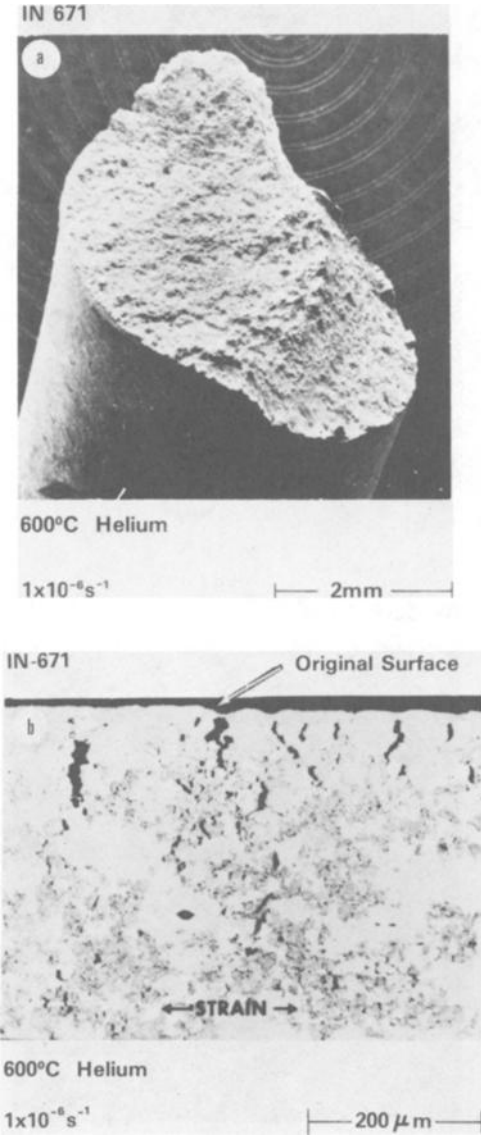


FIG. 12—Nickel alloy 671 specimen tested in helium at $10^{-6}/\text{s}$ and at 600°C. Scanning electron micrograph of fracture surface and reduced section of specimen (a) shows few surface cracks. Optical micrograph of section through specimen (b) shows internal cracking.

TABLE 3—Alloys and conditions for cracking.

Alloy	Nickel Alloy 671	Types 310 and 310S Stainless Steels	Nickel Alloy 800
Environment needed for cracking at 600°C	No reactive environment needed. Internal cracking in helium and all other environments.	Very little reactive environment needed. Surface cracking in coal gasification gases and in low vapor pressure O ₂ and/or H ₂ O environment (for example, helium)	Reactive environment needed. Surface cracking in coal gasification gases but not in low vapor pressure O ₂ and/or H ₂ O environment (for example, helium)

nisms, however, all were detected by the slow strain-rate technique. The specific environmental conditions needed for cracking of the above mentioned four alloys are summarized in Table 3. The detection of the failure of nickel alloy 671 shows that the use of the slow strain-rate technique need not be limited to use for testing for susceptibility to cracking by SCC. In summary, the slow strain-rate technique has proven to be a viable testing method for detecting an alloy's propensity to premature failure in simulated coal gasification environments. Since the environmental conditions in actual coal gasification systems are so diverse, the specific test conditions used in this study may or may not bear any resemblance to actual coal gasification plant conditions.

Acknowledgments

The support of this work under the project "Materials Research for the Clean Utilization of Coal" for the U.S. Department of Energy (Contract No. EA-77-A-01-6010) is gratefully acknowledged. We thank J. Kruger for the many helpful discussions and I. G. Wright of Battelle Columbus Laboratories for information on the gas equilibrium compositions and phase equilibria.

References

- [1] Parkins, R. N., "The Development of Slow Strain Rate Testing and its Implications," *Stress Corrosion Cracking—The Slow Strain Rate Technique*, ASTM STP 665, this volume.
- [2] Logan, H. L., *The Stress Corrosion of Metals*, Wiley, New York, 1967, p. 1.
- [3] Fontana, M. G. and Greene, N. D., *Corrosion Engineering*, McGraw-Hill, New York, 1967, p. 2.
- [4] Takano, M., *Corrosion Science*, Vol. 11, No. 11, Nov. 1971, pp. 813-820.
- [5] Ugiansky, G. M. and Johnson, C. E., "Materials Research for Clean Utilization of Coal," Fourth Quarterly Report to Office of Coal Research, U. S. Dept. of Interior, National Bureau of Standards, Washington, D. C., June 1975, pp. 2-24.
- [6] Ugiansky, G. M. and Johnson, C. E., "Materials Research for Clean Utilization of Coal," Metal Corrosion, Constant Strain-Rate Test, Quarterly Progress Report to the U. S. Energy Research and Development Administration, National Bureau of Standards, Washington, D. C., September 1975, pp. 3-19.
- [7] Wright, I. G., Battelle Columbus Laboratories, private communication.

DISCUSSION

*R. B. Diegle*¹—Some of your results indicate that SCC can occur in the presence of H₂O and O₂, without H₂S. What do you propose is the role of H₂S in the overall cracking process, and is it necessary in actual plant components to cause SCC failure?

¹ Battelle's Columbus Laboratories, Columbus, Ohio.

Also, did you attempt to characterize the nature of the corrosion films formed on these alloys by qualitative or quantitative techniques, and if so, what did you find?

G. M. Ugiansky and C. E. Johnson (authors' closure)—Cracking did occur with Type 310 stainless steel in the presence of gaseous H_2O or O_2 , or both, without H_2S . At this point in our work, we do not propose any specific role for H_2S in the overall cracking process for any of the alloys tested. Our experiments indicate that H_2S would not be necessary for the cracking of Type 310 stainless steel but could be necessary for the cracking of nickel alloy 800. However, without studying the effects of the individual gas components on the cracking processes for the various alloys, no answer can be given as to the necessity of the presence of any one gas component for cracking of actual plant components.

Qualitative microprobe analysis of the cracks on the profile of the Type 310 stainless steel specimen and on the exterior surface of the specimen revealed the presence of a duplex corrosion film. The initial layer next to the substrate was found to be oxygen rich, indicating a mixed oxide of chromium, manganese, iron, and nickel. The second layer was found to be sulfur rich, indicating a mixed sulfide of chromium, manganese, iron, and nickel. This specimen was tested in a gaseous mixture of H_2S/H_2O at $540^\circ C$ ($1000^\circ F$). Corrosion films on other alloys were not characterized but the duplex film was observed.

H. D. Solomon,¹ M. J. Povich,² and T. M. Devine¹

Slow Strain-Rate Testing in High Temperature Water

REFERENCE: Solomon, H. D., Povich, M. J., and Devine, T. M., "Slow Strain-Rate Testing in High Temperature Water," *Stress Corrosion Cracking—The Slow Strain-Rate Technique*, ASTM STP 665, G. M. Ugiansky and J. H. Payer, Eds., American Society for Testing and Materials, 1979, pp. 132-148.

ABSTRACT: The apparatus and technique employed in slow strain-rate testing of stainless steels in high temperature high purity water are described and discussed. Typical results from work in progress on the influence of heat treatment and surface treatment on the intergranular stress corrosion cracking of Types 304 and 308 stainless steel and Alloy XM-19 are described. The correspondence between strain-rate tests varies from alloy to alloy. The minimum strain rate required to cause intergranular cracking varied significantly with the alloy and with the surface treatment. It is suggested that reduction of area and observation of the fracture mode provide better measures of environmental interactions than measures of tensile parameters obtained from the test records.

KEY WORDS: stress corrosion cracking, slow-strain rate technique, stainless steels, Alloy XM-19, intergranular corrosion, sensitization

Exposing austenitic stainless steels to temperatures in the range of 500 to 850 °C can sensitize the steel, depending upon the composition of the alloy and the exact thermal treatment. Sensitized stainless steels will undergo intergranular attack in a variety of media. In addition, they can also undergo intergranular stress corrosion cracking (IGSCC) in high temperature water [1-5].³ We are interested in this problem because we have encountered IGSCC in weld sensitized Type 304 stainless steel in the high temperature (288 °C) water, containing 0.2-ppm oxygen (O₂), that is present in boiling water reactors (BWR). The phenomenon of IGSCC has been studied extensively by means of constant load tests [1-5]. These tests have shown that

¹Metallurgists, General Electric Company, Research and Development Center, Schenectady, N.Y. 12301.

²Project manager, Electric Power Research Institute, Palo Alto, Calif. 94303.

³The italic numbers in brackets refer to the list of references appended to this paper.

the occurrence of stress corrosion is a strong function of the alloy being tested, its heat treatment, the water chemistry, and stress level employed. Variations in any of these variables can alter the behavior from failure in less than 100 h to lives greater than 10 000 h. The potential for very long lives has necessitated the use of many test stations with multiple specimens. An alternate approach is to use the slow strain-rate test (SSRT),⁴ which enables tests to failure to be run in, at most, hundreds of hours as opposed to thousands of hours for the constant load test. The SSRT is being used to screen alloys for possible use in high temperature water and to learn about IGSCC. This paper will describe the SSRT procedures being employed and results on primarily austenitic alloys in high temperature water. The emphasis will be on the high temperature water SSRT, its use and interpretation, rather than on the results of experiments on any one alloy.

Experimental Procedures

SSRT Procedures in High Temperature Water

Basically, SSRT are nothing more than slow tension tests, in our case, run in high temperature water. A schematic layout of one of the high temperature water loops used for these tests is shown in Fig. 1. Distilled and deionized water is held in a 378.5-litre (100-gal) tank. The exact water chemistry desired is created by mixing gases or chemical additives into the room temperature holding tank reservoir. The oxygen content of the water is controlled by bubbling gas into the holding tank. Saturating with pure oxygen yields 36-ppm O₂ in the water, saturating with air yields 8-ppm O₂, and deaeration with argon yields undetectable O₂ levels. The measurements are performed at room temperature but since no O₂ is lost at 288°C, they are valid for this temperature. By using mixed gases, it is possible to vary the oxygen content between 0 and 36 ppm. For instance, 0.5 mol percent O₂ in argon is used to achieve an oxygen level of 0.2 ppm. To achieve higher oxygen contents, than 36 ppm requires pressurization with O₂. All of the tests reported here have been run with air saturated (8-ppm) 288°C water, as it has been shown [2-4] that this oxygen level accelerates IGSCC, compared to lower oxygen levels, such as the 0.2 ppm commonly present in BWRs at steady state operation. This oxygen content, pH, and conductivity of the water are monitored continuously as the water leaves the holding tank on its way to a pressurizing pump. A back pressure regulator maintains a constant output pressure of 10.3 mPa (1500 psi). The water loop supplies several parallel testing facilities (as many as five for one of

⁴In previous papers the authors have used the term Constant Extension Rate Technique (CERT) to describe exactly the same experimental technique.

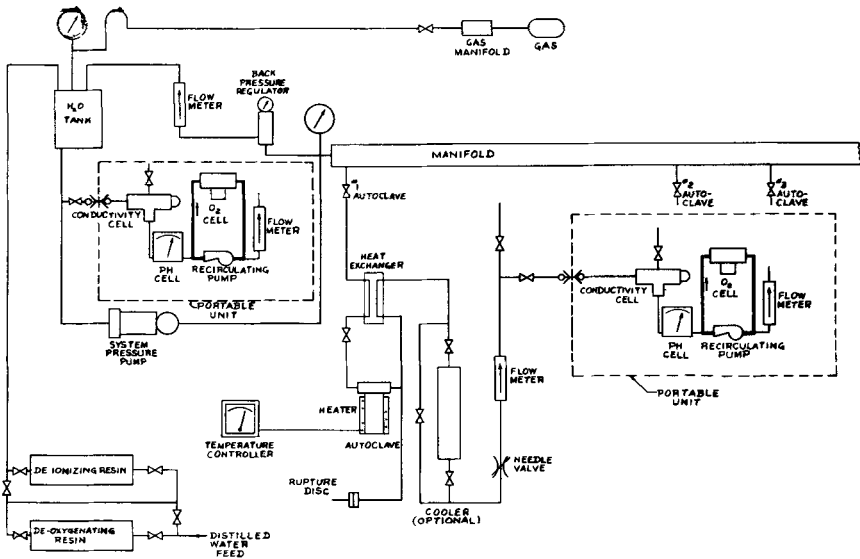


FIG. 1—Schematic layout of a high pressure water system with parallel autoclaves.

our loops) which can be valved off when changing specimens so that the operation of the other branches is unaffected.

The testing is done inside a 1-litre autoclave which is shown schematically in Fig. 2. A resistance furnace surrounds each autoclave and is used to heat the water in the autoclave to 288°C. The specimen is mounted within a compression tube which provides the support between the bottom of the specimen and the autoclave cover. The incoming water passes through a concentric shell and tube counter current flow heat exchanger and is preheated by hot outlet water. To ensure good mixing in the autoclave, the preheated water is injected at the bottom of the autoclave, inside the compression tube, and exits from the top.

The load is applied using an Instron testing machine modified by the manufacturer with ball screws so that very small uniform displacements can be achieved, without sticking friction producing a series of high strain-rate steps separated by a region of no displacement. Smooth extension rates as low as 2.1×10^{-7} mm/s (5×10^{-7} in./min) have been achieved. A strip chart recorder monitors the load time record which is the source of the mechanical data used to analyze the test. These machines have a 3400-kg (7500-lb) capacity and this limits the size of specimen that can be tested. A variety of different cylindrical geometries have been used. The largest size specimen has a 6.4 mm (0.25 in.) diameter with a 63.5 mm (2.5 in.) long gage section. The smallest specimen size used is 0.89 mm (0.035 in.) in diameter and the gage is 12.7 mm (0.5 in.) long. The large

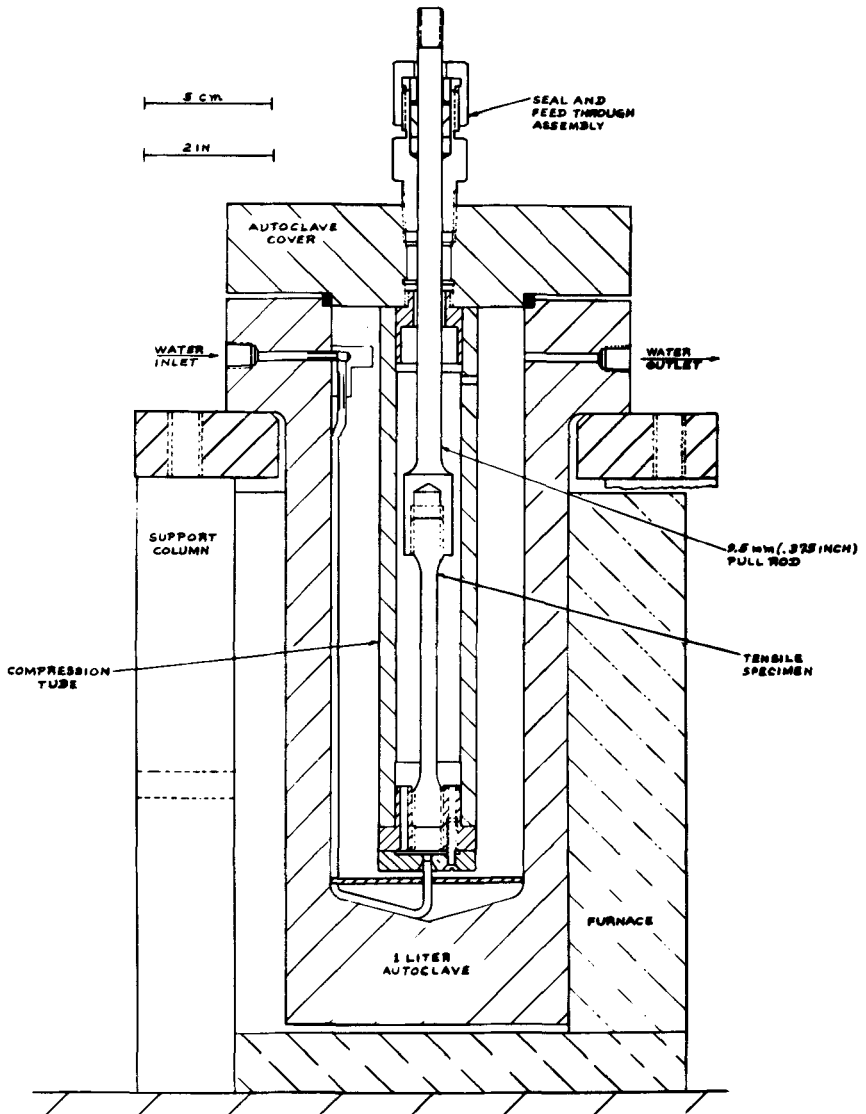


FIG. 2—Autoclave, compression tube, and specimens.

specimens are threaded into the pull rod and autoclave attachments. The smaller specimens are attached by means of screw tightened pressure grips.

Different materials with different geometries (including notches) have been tested, with the strain rate and water chemistry being the chief test system variables. Since each testing machine is independent, each can be run at any desired extension rate. Bulk water chemistry variations, however, affect all the branches in the loop.

Operating SSRT in High Temperature Water

High temperature, high pressure water is too aggressive for most standard extensometers and the presence of the autoclave is an impediment to remote strain measurements via extension rods attached to the gage sections. Hence, the crosshead displacement is used to determine the strains and strain rates imposed on the specimen. The relation between the crosshead displacement and the strain has been estimated from room temperature tests employing an extensometer. The resulting empirical machine deflection versus specimen strain relationship was used to determine the specimen strain and strain rate [6]. At any load, the specimen displacement is only a fraction of the crosshead displacement with the remainder being the displacement of the load train and testing apparatus. The proportion of specimen and machine deflection continually changes as the relative compliance of the specimen and the machine changes. During the elastic loading of the specimen, the strain rate is constant. As yielding occurs, more of the displacement occurs in the specimen, resulting in higher specimen strain rates. At the necking strain, the load drops and thus the elastic strains of the specimen and the machine decrease. Because the crosshead displacement is held constant, the plastic strain rate in the neck must increase rapidly to compensate for the decrease in the elastic strain rate. An example of the calculated strain rate versus strain is shown in Fig. 3 [6]. When the load is constant the machine deflection is constant, and all of the crosshead displacement must be taken up by plastic straining of the specimen. A constant extension rate test will yield a constant strain rate only when the work hardening behavior exactly balances the reduction in specimen area and a constant load is maintained. Thus a constant extension rate test is almost never a constant strain-rate test. The strain rate is established by the extension rate but is variable and is a function of the compliance of the testing system.

Several variables can be monitored during a test which can be used to study the influence of material, environment, or surface treatments on environmentally assisted cracking. These variables can be characterized from the load-time record as tensile parameters such as the ultimate tensile strength and elongation to failure, or by specimen parameters determined from the fractured specimen such as reduction of area and fracture mode.

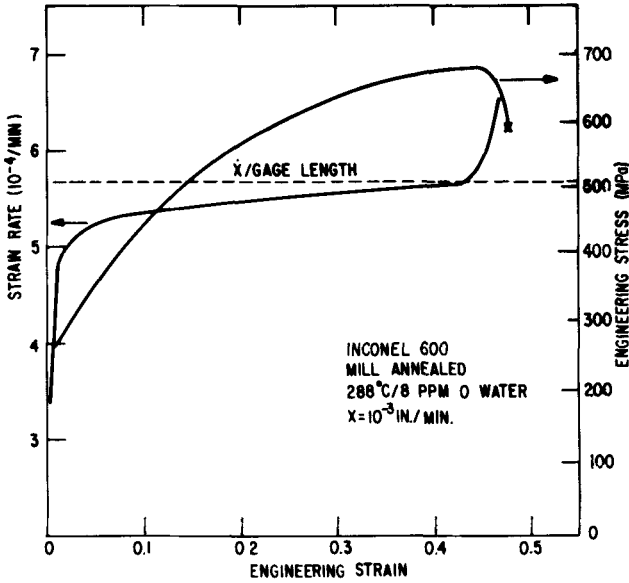


FIG. 3—Stress and strain rate versus engineering strain.

Work to date suggests that the fracture mode and reduction of area give a better indication of sensitivity to the environment than parameters from the test record. For instance, relatively simple annealing treatments on Inconel 600 resulted in significant changes in strength level [6]. These changes altered the 288°C air saturated water SSRT stress-strain curve, with elongations being different by 40 percent. In these conditions, however, no IGSCC was observed and the reductions in area for all tests were 79.6 percent with a standard deviation of 1.5 percent. Tests in 288°C laboratory air showed that the difference in the stress-strain curve resulted from alterations in the work hardening characteristics and not IGSCC. Tensile properties can show environmental influences *but must* be supplemented by observations of the specimen and duplicate tests must be run in an inert environment.

Results and Discussion

In keeping with the theme of this conference, the following results and discussion are directed towards aspects of SSRT. We are using the SSRT to screen alloys for high temperature water service and to learn more about IGSCC in this environment. Therefore, our testing has concentrated on comparing the SSRT with other screening tests, integrating the SSRT into

a general screening procedure, and investigating such factors as the influence of surface work on the screening tests and operation in high temperature water. This paper will consider the correlation of the SSRT with the A262E [12] test for intergranular attack, the influence of the extension rate of the SSRT on this correlation, and the influence of surface cold work. Several alloys are being studied in our programs. Rather than concentrating on a single alloy, results obtained with several alloys will be discussed, because the relative behavior in the SSRT and A262E varies to some extent from alloy to alloy.

Comparison of SSRT with A262E Results and Interrelation of Extension Rate for Three Alloys

Almost all of the intergranular stress corrosion failures that have occurred in high temperature water have occurred in stainless steels which have received sensitizing heat treatments. Chemical tests for sensitization therefore, have been used to screen material for susceptibility to failure. One of the tests that has been used is the modified Strauss test as described in ASTM Recommended Practices for Detecting Susceptibility to Intergranular Attack in Stainless Steels (A 262, Practice E). This test has been quantified by performing a room temperature tension test on specimens which have been exposed for 72 h in the A262E solution. After this tension test, the degree of attack can be characterized by the intergranular penetration measured on the fracture surface and by the ultimate tensile strength (σ_{UTS}).

The A262E test conditions are fixed whereas the SSRT conditions are not. The variables in the SSRT are the extension rate and the environment. We are presently evaluating both sets of variables but, for this paper, we will confine ourselves to discussing tests run at 288 °C in air saturated water containing 8-ppm O₂, which is a highly accelerated condition for IGSCC relative to operating conditions. The extension rate is the chief SSRT variable and must be considered when comparisons are made. The results obtained on three alloys are discussed because they represent three different degrees of correlation between SSRT and A262E.

For Type 304 stainless steel, the A262E test is not as severe a screening test as the SSRT. This is illustrated in Fig. 4. Sensitization of the Type 304 stainless steel was achieved by heating the specimen to 1000 °C and cooling at a controlled rate; the lower the cooling rate, the greater the degree of sensitization. Tests have shown [7] that cooling from 1000 °C at less than 0.3 °C/s will sensitize an annealed 0.08 C Type 304 stainless steel to the extent that intergranular attack is noted in the A262E test. Cooling at faster rates does not result in intergranular failure in a subsequent A262E test, but can if a SSRT is used. This is illustrated in the two right-hand micrographs of Fig. 4. A clear intergranular region can be seen in the

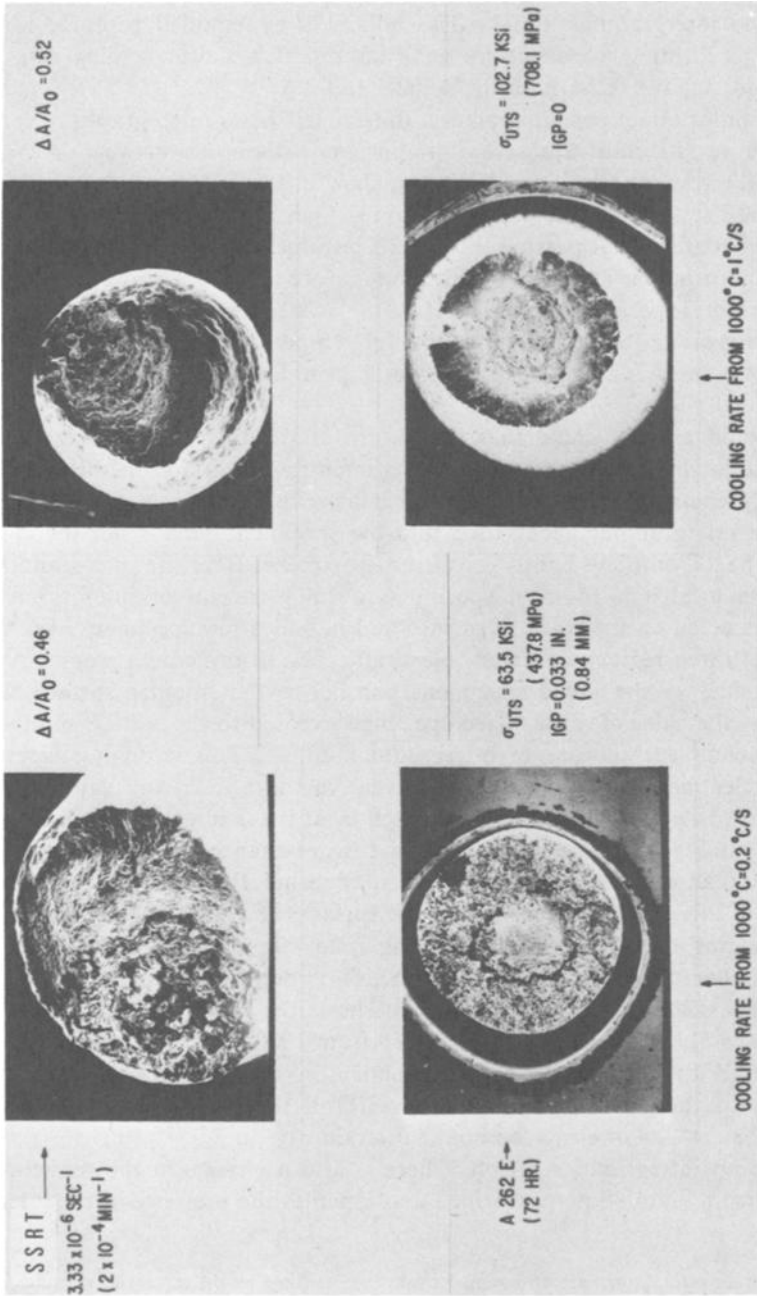


FIG. 4.—Comparison of the fracture surfaces of Type 304 stainless steel specimens tested in A262E and SSRT for specimens cooled from 1000°C at 0.2°C/s and 1°C/s . All specimens are 3.175 mm (0.125 in.) in diameter.

specimen tested at $3.33 \times 10^{-6} \text{ s}^{-1}$ in 288°C saturated water.⁵ A companion specimen, exposed to the same thermal cycle and tested in A262E, shows no intergranular attack. The failure is by dimpled rupture, with shear lips forming a classic cup cone failure. If a slower cooling rate is employed, say 0.2°C/s , both the A262E and $3.33 \times 10^{-6} \text{ s}^{-1}$ SSRT show intergranular attack, as illustrated in the two left-hand micrographs.

These results illustrate several important differences between A262E and SSRT results. First, the SSRT can show intergranular cracking where the A262E tests show none. A variety of tests performed on Type 304 stainless steel confirm that passing the A262E test does not guarantee there will be no intergranular attack in a high temperature air saturated water SSRT. A failure of Type 304 stainless steel in the A262E test, however, will predict intergranular SCC in high purity, high temperature air saturated water. Therefore, the A262E test can be used as a preliminary screening test for this alloy.

It should also be noted that the nature of the intergranular attack is different in the A262E and SSRT experiments. The attack in the A262E is purely chemical. The outer surface is attacked uniformly and there is uniform intergranular penetration into the specimen. This is not the case for the SSRT on these lightly sensitized specimens. Here the intergranular attack is localized. In most specimens a single region of intergranular attack is noted on the fracture surface and in only a few specimens were as many as three regions observed. Generally, few if any cracks were noted on the sides of the failed specimens parallel to the fracture surface. In contrast, the sides of a sensitized specimen exposed to the A262E solution show a complete network of intergranular attack. This strongly suggests that nucleation is a highly localized event in the SSRT, and subsequent crack growth continues at regions of high local stress intensity. Such crack growth into the specimen appears to be faster than on the surface. The intergranular regions appear more circular rather than semicircular. Examples of this are shown on the fracture surfaces of Figs. 4 and 5.

In judging the SSRT and comparing it to other tests, it is important to remember that the severity of the SSRT is dependent upon the strain rate. This is illustrated in Fig. 5 which shows the fracture surface of two Type 304 stainless steel specimens cooled from 1000°C at 2°C/s and tested in SSRT. With this cooling rate, there is no intergranular attack in an A262E test, nor is there IGSCC attack in a SSRT if the nominal strain rate is $3.3 \times 10^{-6} \text{ s}^{-1}$. Lowering the nominal strain rate to $8.3 \times 10^{-7} \text{ s}^{-1}$ does produce an intergranular region. There is also a change in the reduction of area from 72 to 48 percent which accompanies the presence of the inter-

⁵The strain rates quoted are all nominal strain rates defined by the crosshead rate divided by the initial gage section. As discussed previously, the actual strain rate is variable and approaches the nominal strain rate as the maximum load is approached.

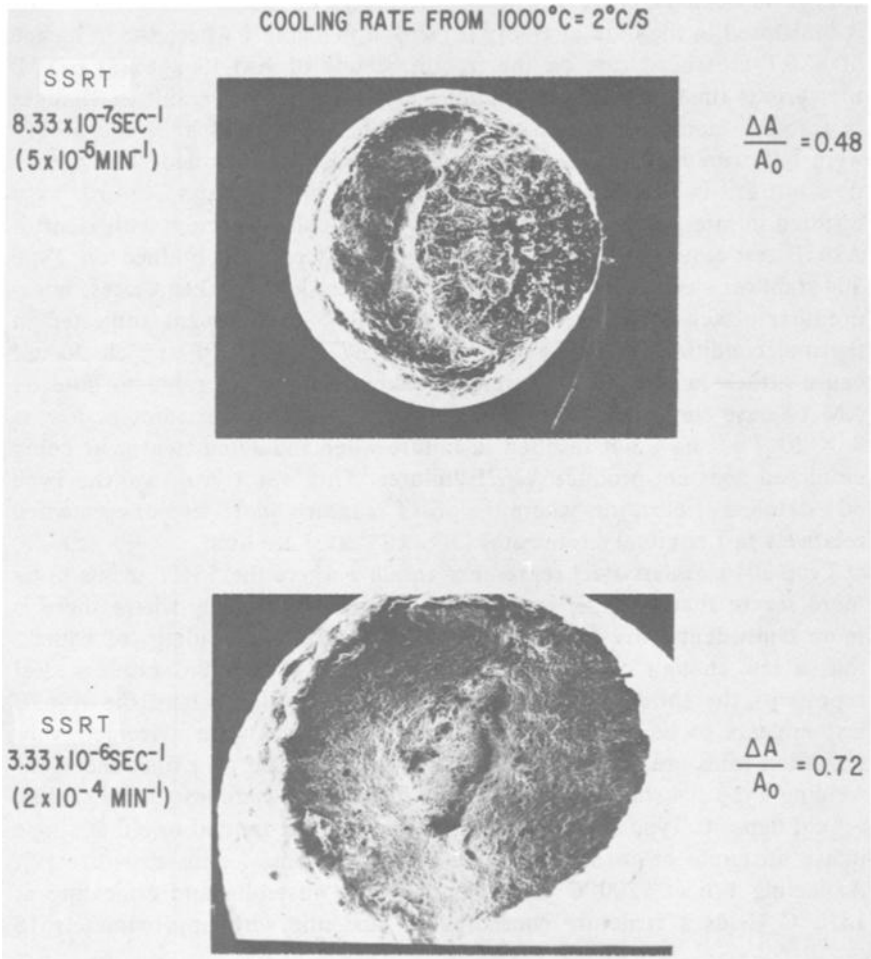


FIG. 5—Comparison of the fracture surfaces of Type 304 stainless steel specimens (SSRT at $8.33 \times 10^{-7} \text{ s}^{-1}$ and $3.33 \times 10^{-6} \text{ s}^{-1}$). The specimens are 3.175 mm (0.125 in.) in diameter.

granular attack. These experiments performed on Type 304 stainless steel show that intergranular cracking can be observed in $8.3 \times 10^{-6} \text{ s}^{-1}$ SSRT and that such a test is more severe than an A262E test. Decreasing the strain rate further makes the SSRT still more severe in terms of identifying IGSCC susceptibility.

Tests [8] run on XM-19 (a high chromium, nitrogen strengthened stainless steel) show a somewhat different behavior than that observed in Type 304 stainless steel. The transition from transgranular to intergranular cracking with decreasing strain rate occurs quite precipitously with little

change in behavior with still further decreases in the extension rate. This is illustrated in the data of Henry [8] shown in Table 1 where the influence of SSRT crosshead rate on the fracture mode of XM-19 aged at 675°C for various times is listed. Variations in crosshead rate result in changes in fracture modes for specimens aged for 5, 10, and 24 h. If the SSRTs were only run at $6 \times 10^{-6} \text{ s}^{-1}$, one would have concluded that XM-19 does *not* fail in SSRT. Reducing the nominal strain rate to $3 \times 10^{-6} \text{ s}^{-1}$ resulted in intergranular attack and this is in good agreement with Henry's A262E test results. Judging from previous test results obtained on Type 304 stainless steel, one would expect that at very low crosshead rates, intergranular attack could be observed in a SSRT, in specimens subjected to thermal conditions (such as aging 1 h at 677°C (1250°F) which do not cause attack in A262E. However, the experiments performed to date on XM-19 have shown this not to be so. The SSRTs run at rates as low as $3 \times 10^{-7} \text{ s}^{-1}$ have not resulted in failure when the aging treatment being employed does not produce A262E failures. This is in contrast to the Type 304 stainless steel results where the SSRT is clearly more severe, even when relatively fast nominal strain rates ($3 \times 10^{-6} \text{ s}^{-1}$) are used.

Type 304 stainless steel represents an alloy where the SSRT seems to be more severe than A262E, and XM-19 represents an alloy where there is more equivalent correspondence of SSRT behavior providing, of course, that a low enough crosshead rate is employed. Type 308 stainless steel represents the third possibility. Namely, it is an alloy where the A262E test appears to be more severe than a SSRT even when extremely slow extension rates are employed. This latter alloy is used as a filler metal for welding Type 304 stainless steel. Wrought filler rods were tested rather than a weld deposit. Type 308 stainless steel can be heat treated to either single phase austenite or to have a duplex austenite plus ferrite structure [9]. Annealing 1 h at 1200°C yields single phase austenite and annealing at 1350°C yields a structure consisting of austenite with approximately 15

TABLE 1—Summary of fracture modes for XM-19 SSRT tested in air saturated 288°C water as a function of prior aging time at 675°C and test strain rate.

Time at 675°C, h	Strain Rate (10^{-6} min^{-1}), assuming $l_0 = 0.22 \text{ cm (0.55 in.)}$				
	0.30	0.60	3.00	6.00	15.2
1	ductile	ductile	ductile
5	inter	ductile	ductile
10	inter	ductile	ductile
24	inter	ductile	ductile
96	ductile	ductile	ductile
336	ductile	ductile	ductile

NOTE—

ductile = dimpled rupture, and
inter = intergranular cracking noted.

volume percent ferrite. To date the results obtained on the 1200 °C annealed material where the structure is austenitic are in general agreement with the Type 304 stainless steel and XM-19 results, that is, failures in both A262E and SSRT at an appropriate strain rate are noted. This is not the case for the duplex structure established at 1350 °C. The SSRT run at $2.2 \times 10^{-6} \text{ s}^{-1}$ for the duplex alloys are compared to A262E results in Fig. 6. Here a slight degree of intergranular attack was noted in the A262E test but none was noted in the SSRT even though extremely low rates of $8.3 \times 10^{-8} \text{ s}^{-1}$ were employed in several tests. It is not yet clear if the resistance to IGSCC in the SSRT is a manifestation of a strain-rate effect (that is, the strain rate used was too high for SCC initiation) or if intergranular SCC will not occur by SSRT in a sensitized but initially unflawed condition in air saturated high temperature water regardless of the strain rate.

It is clear from the preceding examples that the correlation of the SSRT and the A262E test varies from material to material and is a function of the crosshead rate being employed. All three possible correlations have been observed. More will be said about the use of the A262E and SSRT in the section on General Comments.

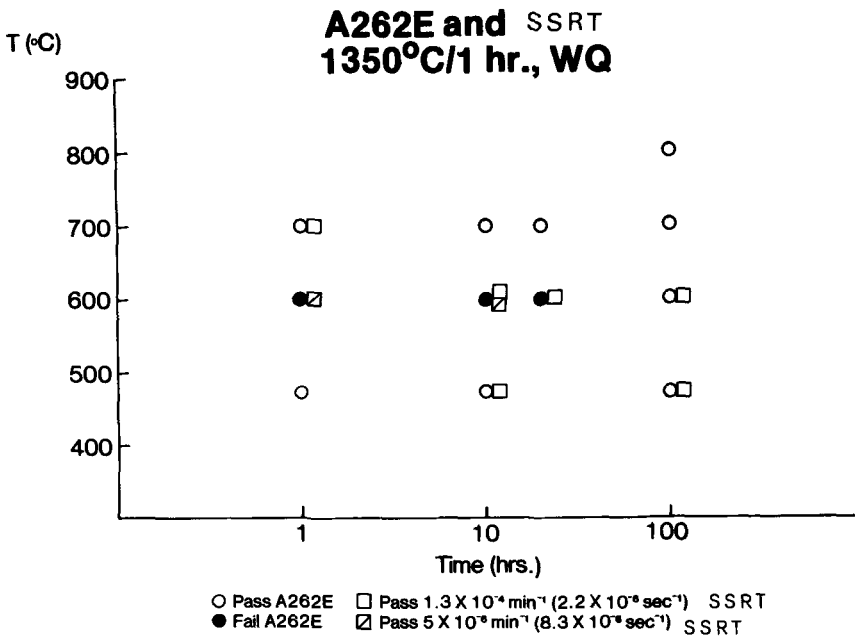


FIG. 6—Effect of heat treatment on the corrosion in A262E of Type 308 stainless steel, Heat L-B7, annealed at 1350°C/1 h.

Influence of Surface Working

The SSRT is also being used to screen various surface treatments in various alloys. It has been found that the SSRT gives dramatically different results than purely chemical intergranular attack tests when treatments such as grinding or shot peening are imposed on the surface prior to testing.

It has been generally believed that shot peening enhances the SCC resistance of Type 304 stainless steels. For example, Fiske [10] reported that shot peening could prevent intergranular attack of sensitized stainless steel, provided that the shot peening was performed before the sensitizing heat treatment.

An example of the shot-peening effect on intergranular attack is presented in Fig. 7. The specimen of Type 304 stainless steel was shot peened on one side prior to a sensitizing heat treatment (600°C for 24 h) and then exposed to the A262E test. The effect of shot peening is dramatically beneficial under these conditions [11].

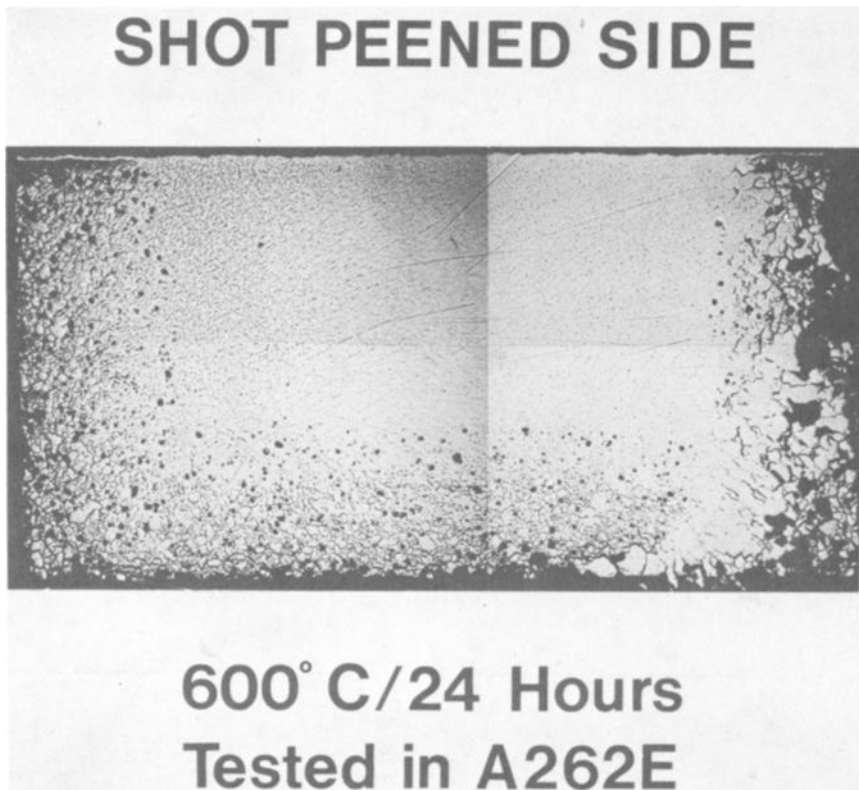


FIG.7—Partially shot peened, sensitized Type 304 stainless steel, specimens after exposure to A262E. The test coupon is 120 mm wide by 240 mm long.

Shot peening is not beneficial when a SSRT is used because the shot-peened layer cracks mechanically at low strains, even if the test is run in an inert environment [11]. This is illustrated in Fig. 8. The fracture surface (Fig. 8(a), (b)) and sides (Fig. 8 (c), (d)) of a mill-annealed, shot-peened Type 304 stainless steel specimen tested at $2.2 \times 10^{-6} \text{ s}^{-1}$ in argon are shown in this figure. Cracks are observed on the sides of the specimen in the surface deformed layer, but these cracks did not alter the ductile

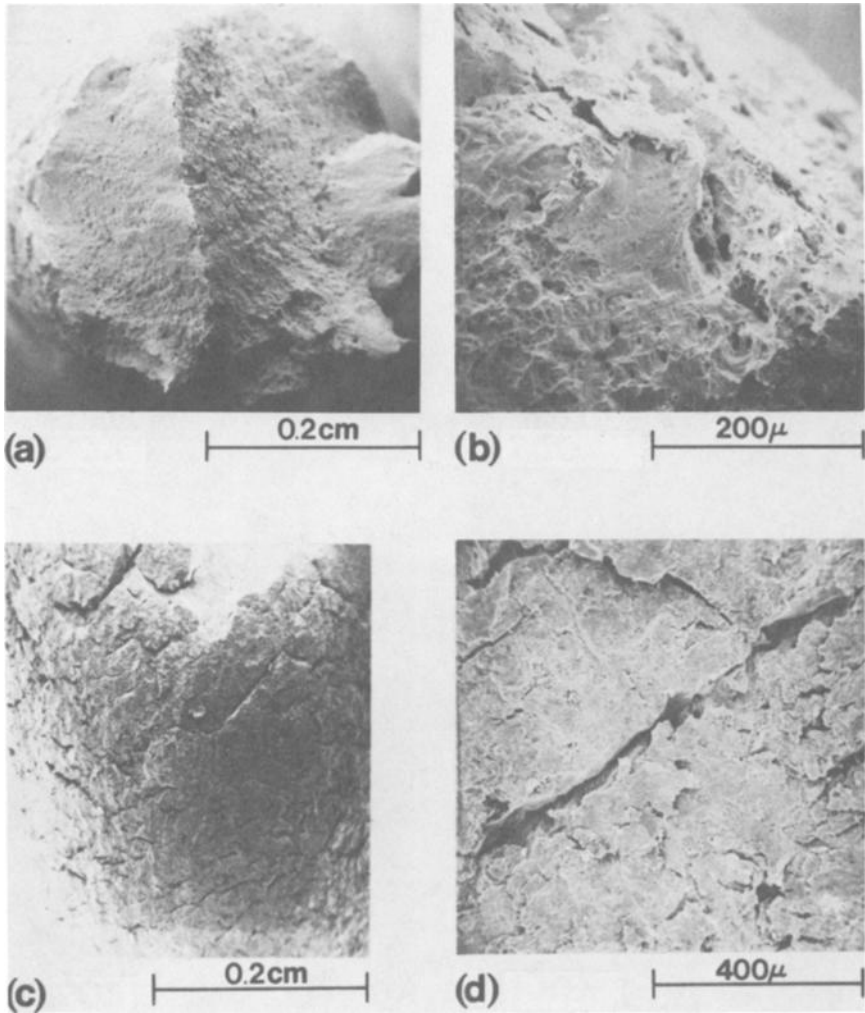


FIG. 8—Fracture surface (a, b) and side (c, d) of a Type 304 stainless steel specimen after $3.33 \times 10^{-6} \text{ s}^{-1}$, argon, SSRT. The specimen was tested in a furnace sensitized and shot-peened condition.

fracture mode. Interrupted tests have shown that the surface cracking is readily observed with as little as 3 percent strain. If the specimen is sensitized and shot peened, the cracked surface layer *promotes rather than retards* the intergranular cracking in air saturated water. This is shown in Fig. 9. This enhancement is presumably by local stress concentration or crevice chemistry effects. The cracked shot-peened layer promotes intergranular attack all around the circumference of the specimen rather than at localized

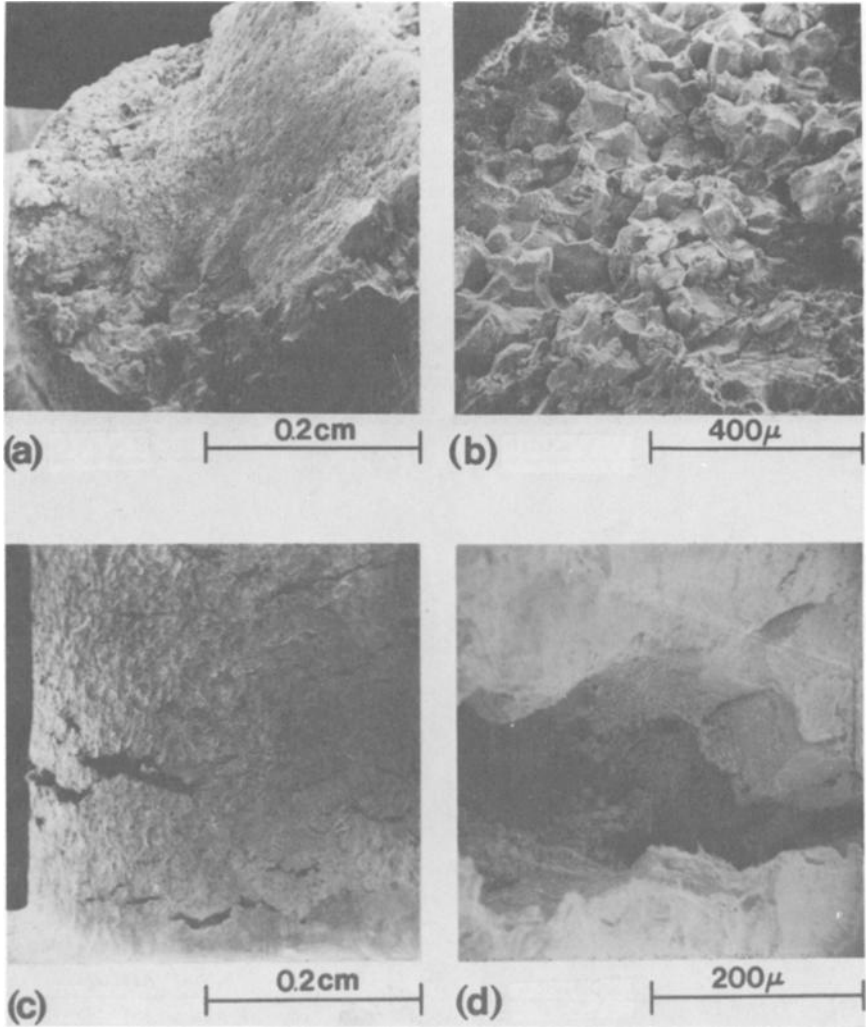


FIG. 9—Fracture surface (a, b) and side (c, d) of a Type 304 stainless steel specimen after a $3.33 \times 10^{-6} \text{ s}^{-1}$, oxygenated 288°C water, SSRT. The specimen was tested in furnace sensitized and shot-peened condition.

spots as in the sensitized, nonshot-peened specimens (see Figs. 4 and 5). The shot-peened layer prevented intergranular attack when a furnace sensitized specimen was exposed to A262E but when this layer cracks in a SSRT, it is no longer protective and, in fact, can be harmful.

The SSRT results suggest that shot peening or other severe surface treatments such as grinding are not a beneficial surface treatment in components subjected to plastic straining during service.

General Comments

The results presented here are the results of work in progress. Although many of the investigations are incomplete, they do point up several important features of the SSRT in high temperature water. A SSRT run in air saturated water is an accelerated test for out service applications. The oxygen level is much higher and the stress-strain levels reached are also much higher. However, the SSRT is much closer to the service conditions than a chemical test such as A262E and, therefore, is considered to be a more reliable measure of the probable in-service behavior. Our results thus far have shown that extreme care should be used in drawing conclusions about IGSCC susceptibility of a material solely from chemical tests such as A262E. For some alloys such as Type 304 stainless steel or XM-19 failure in A262E will predict failure in SSRT, providing a low enough crosshead rate is used. In duplex Type 308 stainless steel, this does not seem to be so.

A262E is being used to define the test matrix for the more time consuming SSRT for those alloys such as Type 304 stainless steel or XM-19 where it has been shown that SSRT is at least as severe a test as A262E. If failure is noted in A262E, then the companion SSRT does not have to be run.

The chief drawback of the SSRT is that the results are a function of the crosshead rate used and a rather precipitous change to intergranular cracking is possible with as small as a factor of 2 change in the crosshead rate. If no intergranular cracking is observed at the lowest strain rate tested, one can always argue that it might occur at a lower strain rate. For screening purposes, however, this is not a serious obstacle. The tests are run at decreasing crosshead rates with lower crosshead rates being chosen so long as there is no failure. This is done to a limit of about 10^{-7} s⁻¹. If still no intergranular attack is noted, the material or condition is deemed to have passed the screening test and is a good candidate for more extensive testing.

The SSRT performed on smooth specimens is a reasonably good screening test, but it is not a quantitative test to use to gather fundamental information on IGSCC or to generate engineering design data. The SSRT provides useful information and is helpful in scoping out test matrices for more extensive testing.

Acknowledgments

The authors would like to thank R. F. Berning and J. H. Steadwell of the Mechanical Testing Unit of our laboratory for the design, construction, and set up of the SSRT water loops and testing machines. The tests have been conducted with the assistance of P. T. Hill and D. E. Broecker. Technical discussions with M. F. Henry, R. H. Van Stone, R. P. Gangloff, and L. F. Coffin, Jr. were greatly appreciated. The authors are in gratitude to M. F. Henry and R. H. Van Stone for the use of their unpublished data.

References

- [1] Wilde, B. E. and Weber, J. E., *British Corrosion Journal*, Vol. 4, 1967, pp. 42-46.
- [2] Clarke, W. L. and Gordon, G. M., *Corrosion*, Vol. 29, 1973, pp. 1-12.
- [3] Berry, W. E., White, E. L., and Boyde, W. K., *Corrosion*, Vol. 29, 1973, pp. 451-469.
- [4] Cowan, R. L., II and Gordon, G. M., "Intergranular Stress Corrosion Cracking and Grain Boundary Composition in Fe-Ni-Cr Alloys," International Conference on Stress Corrosion Cracking and Hydrogen Embrittlement of Iron Base Alloys, Unieux-Firmin France June 1973, General Electric Report No. NEDO-12399, 73 NED106.
- [5] Clarke, W. L., Danko, J. C., and Gordon, G. M., "Stress Corrosion Cracking Behavior of Newer Iron-Chromium-Nickel Alloys at 550°F in High Purity Water, in Corrosion Problems in Energy Conversion and Generation," The Electrochemical Society, 1974, pp. 410-423; also General Electric Report NEDO 12513, 74 NED57.
- [6] Van Stone, R. H., General Electric Co., to be published.
- [7] Solomon, H. D., "Continuous Cooling Sensitization," *Corrosion*, Vol. 34, 1978, pp. 183-193.
- [8] Henry, M. F., General Electric Co., to be published.
- [9] Devine, T. M., General Electric Co., to be published.
- [10] Fiske, W. H., "Shot Peening to Prevent Corrosion of Austenitic Stainless Steels," presented at an ASTM symposium, Wryllsville Beach, N.C., Aug. 1970.
- [11] Povich, M. J., *Corrosion* 77, San Francisco, March 1977.

W. L. Clarke,¹ R. L. Cowan,¹ and J. C. Danko¹

Dynamic Straining Stress Corrosion Test for Predicting Boiling Water Reactor Materials Performance

REFERENCE: Clarke, W. L., Cowan, R. L., and Danko, J. C., "Dynamic Straining Stress Corrosion Test for Predicting Boiling Water Reactor Materials Performance," *Stress Corrosion Cracking—The Slow Strain-Rate Technique*, ASTM STP 665, G. M. Ugiasky and J. H. Payer, Eds., American Society for Testing and Materials, 1979, pp. 149-169.

ABSTRACT: A dynamic straining test has been developed for rapid screening of materials relative to stress corrosion cracking (SCC) in an accelerated high-temperature aqueous environment. The technique consists of conducting slow tension tests in an environment of 289°C high-purity water with 8 ppm dissolved oxygen. This extremely aggressive environment was used in this investigation to maximize the potential for intergranular SCC. Future correlations in environments of industrial concern are required before full industrial utilization of this technique can be realized. Because of the nature of the environment, the test is conducted in an autoclave assembly using a unique sliding seal arrangement. In turn, the autoclave is connected to a recirculating, water-chemistry controlled loop system. Several applications are discussed to illustrate the use of the test method. In addition, a summary of the various qualification data correlating the dynamic straining test results with longer term constant load test results are presented.

KEY WORDS: dynamic strain, stress corrosion cracking, intergranular stress corrosion cracking, sensitivity, Type 304 stainless steel, 17-4PH (H1100) stainless steel, Type 308L stainless steel, Nitronic 50, ICL 473, ICL 167, weldments, nitriding, constant load, constant extension rate

Austenitic stainless steel components of commercial boiling water reactors (BWR) have occasionally suffered intergranular stress corrosion cracking (IGSCC) in service [1-4]. The frequency of this cracking is quite low (for example, approximately 85 cases of IGSCC out of over 17 000 pipe weldment heat-affected zones), and the times for crack initiation are long (approx-

¹Principal metallurgical engineer, manager, Plant Component Behavior Analysis, and manager, Plant Materials and Process Development, respectively, General Electric Company, San Jose, Calif. 95125.

²The italic numbers in brackets refer to the list of references appended to this paper.

imately 2 to 5 years). Laboratory tests can reproduce the phenomenon and show austenitic stainless steels are susceptible to IGSCC only when they have been subjected to a thermal treatment which produces grain boundary sensitization and are subsequently subjected to a sustained load above the yield stress in high temperature (for example, 289°C) oxygenated water [5]. The BWR utilizes high purity water (approximately 10^{-6} s) which has a steady-state oxygen content of 0.1 to 0.2 ppm in the piping system due to radiolysis. The failure times of sensitized austenitic stainless steels in laboratory tests can be accelerated by increasing the oxygen content (8 to 100 ppm) of the water [5], and by testing with sustained loads of 140 to 160 percent of the 289°C yield strength. However, even with these gross accelerants, failure times are still quite long and the reproducibility of results can be a problem with marginally susceptible material. A more rapid test was needed, and a successful technique has been developed to subject specimens to dynamic straining in the accelerated environment to screen variables quickly and to determine susceptibility to IGSCC. The technique can be used for both laboratory and production testing applications when correlations are determined for environments of industrial concern. The potential use of the technique is being studied at General Electric; several examples of the studies to date are presented.

Testing Technique

The technique consists of conducting relatively slow [0.0008 mm/min (0.032 mil/min) "crosshead speed"] tension tests in environments of industrial concern. In this investigation an extremely aggressive environment of high-purity oxygenated (8 ppm) water at 289°C was used to maximize the potential for IGSCC. Because of the high saturation pressure of water at this temperature, the specimens and solution are contained in an autoclave system. As shown in Fig. 1, the specimen is connected to a pull rod which passes through a trifluoroethylene resin sealing gland which allows a low-friction, pressure-tight seal to the crosshead system. To maintain the high-purity water with the desired oxygen content, the autoclave is connected to a recirculating loop that constantly supplies high-pressure, high-purity makeup water containing 8 ppm dissolved O_2 at a flow rate of 60 cm³/min. The influent conductivity is approximately 0.1 μs and the effluent is approximately 1 μs . During the test, the load-elongation curve is measured by a load cell in series with the pull rod. The specimen is strained until the load cell indicates failure, after which the test is terminated and the specimen is evaluated. The specimens used for dynamic strain testing from bar and plate are 0.318-cm (0.125-in.) diameter gage, cylindrical, uniaxial, tension specimens 5.72 cm (2.25 in.) long with a 1.91-cm (0.750-in.) long gage section. The pipe specimens were flat, semicurvilinear (inside surface intact), uniaxial, tensile-types, nominally 2.72 cm (2.25 in.) long, with a 1.91 cm

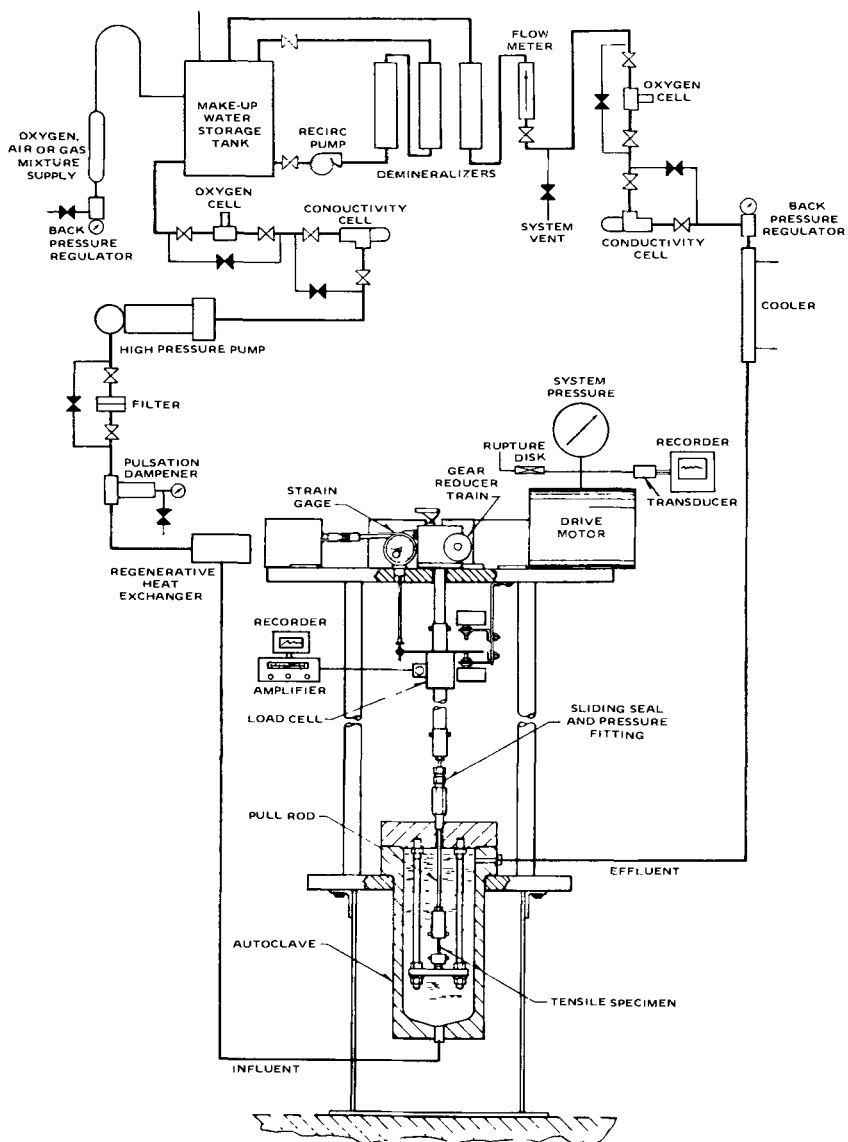


FIG. 1—Dynamic straining stress corrosion test facility.

(0.750 in.) long gage section. The gage section dimensions were 0.254 cm (0.100 in.) thick and 0.318 cm (0.125 in.) wide. Specimens from the welded pipes contained the root side of the weld in the center of the gage section (Fig. 2).

The gear-driven dynamic strain machines used are capable of extension rates of 4.2×10^{-7} to 2.1×10^{-4} m/s (strain rates of 3.3×10^{-7} and 1.7×10^{-4} /s, respectively), at 343°C (650°F) and 151 MPa (2200 psi).

Although the reduction of mechanical properties in the environment compared to those of control specimens in air or argon usually indicate if an environmental effect has occurred (such as IGSCC), all specimen fracture surfaces from the environmental test are examined by scanning electron microscopy (SEM) and/or conventional metallography to determine if the fracture has initiated by an intergranular or other nonductile mode. If not, the specimen is judged to be nonsusceptible. The failure stress (σ), percent reduction of area (RA), percent elongation (E), and time to fracture (T_F) are used to assign the *degree* of susceptibility. Two of these parameters, failure

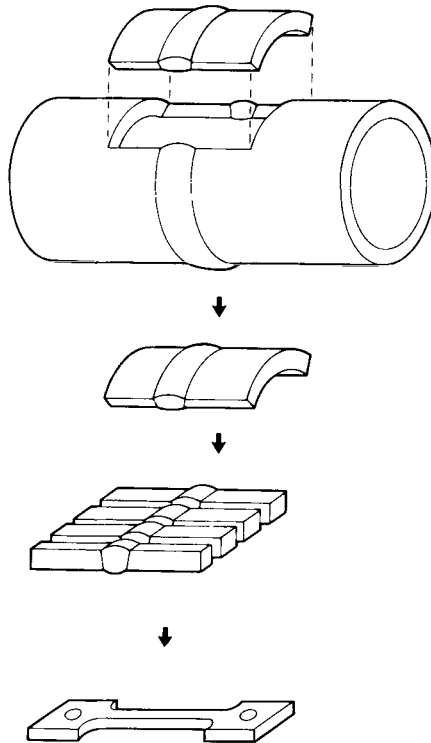


FIG. 2—Schematic of sectioning procedures to prepare corrosion specimens from welded pipes.

stress and elongation, can be combined to obtain an IGSCC susceptibility index $[6]$, I_{DS} , using the expression

$$I_{DS} = 1 - \frac{\sigma_w(1 + E_w)}{\sigma_A(1 + E_A)}$$

where

σ_w = failure stress in water environment,

E_w = elongation in water environment,

σ_A = failure stress in air or argon, and

E_A = elongation in air or argon.

The susceptibility to IGSCC increases as the I_{DS} value approaches unity.

In addition to the dynamic straining tests, numerous longer term constant load tests were conducted for comparison using companion specimens. The constant load tests were also performed in the extremely aggressive environment of 289°C water with 8 or 36 ppm dissolved oxygen at applied stresses normalized to 60 percent ultimate tensile strengths at 289°C for each material. The details of the constant load test technique have been described [5, 7].

Results and Discussion

The Boiling Water Reactor Systems Department of the General Electric Company is experimenting with the use of the high-temperature aqueous dynamic straining test in several different, but related, applications. These applications will be discussed separately in the succeeding paragraphs. For brevity, the control data obtained in argon have been eliminated, however, these data are included in the susceptibility indices (I_{DS}) calculations. The chemical compositions of all alloys used in these studies are given in Table 1.

Reference Tests for Qualifying Low Temperature Chemical and Electrochemical Tests as Acceptance Methods for Incoming Materials

A study [9] on the comparison of the chemical (ASTM Recommended Practices for Detecting Susceptibility to Intergranular Attack in Stainless Steels A 262, Practices A and E) and recently developed [10] electrochemical reactivation methods for measuring the degree of sensitization in Types 304 and 316 stainless steels is nearing completion. These methods are used as a quality control method for determining the adequacy of production solution heat treatments. In this study, 12 heats of Type 304 stainless steel representing a range of product forms are being tested for IGSCC susceptibility in the as-received condition (mill annealed), and a mildly sensitized condition (20 h at 500°C). The IGSCC results in the air-saturated water en-

TABLE 1—Chemical composition of alloys tested by dynamic strain.

Alloy	Heat	C	Cr	Ni	Mn	Si	Mo	Cu	S	P	Other
304	2P1486	0.050	18.30	10.95	1.65	0.60	0.20	0.07	0.008	0.022	...
	27388	0.046	18.75	8.84	1.59	0.60	nd	0.49	0.005	0.023	0.44Se
	M7616	0.060	18.68	10.16	1.69	0.50	0.08	0.08	0.012	0.022	...
	2P6424	0.040	18.37	9.61	1.65	0.46	0.25	0.08	0.013	0.021	...
	834264	0.060	18.30	9.12	1.58	0.62	0.30	0.09	0.028	0.030	...
	2P6396	0.040	18.66	10.30	1.65	0.53	0.20	0.12	0.016	0.022	...
	TH6656	0.060	18.31	9.30	1.72	0.47	0.24	0.25	0.006	0.024	...
	M7772	0.050	18.81	10.15	1.80	0.38	0.11	0.15	0.015	0.026	...
304	4S4659	0.045	18.40	9.76	1.25	0.57	0.23	0.07	0.015	0.018	...
304L	482038	0.026	18.50	10.30	1.19	0.51	nd	nd	0.010	0.016	...
304L	482135	0.025	18.00	10.50	1.24	0.51	nd	nd	0.010	0.018	...
304L	00575	0.024	18.18	9.38	1.79	0.35	0.30	0.23	0.004	0.019	...
304	X14902	0.065	18.68	9.20	1.75	0.48	nd	nd	0.028	0.029	...
IC1473	T6842	0.017	19.66	9.99	1.92	0.42	0.37	0.18	0.015	0.033	...
IC1473	E6881	0.030	19.23	9.26	1.96	0.47	0.19	0.12	0.007	0.027	...
IC1167	T6689	0.036	17.37	12.20	1.88	0.42	2.50	0.18	0.020	0.035	...
Nitronic 50	302556	0.042	22.04	12.20	4.97	0.54	2.20	nd	0.008	0.021	0.2Cb + Ta
308L	05518	0.030	19.93	9.96	1.58	0.61	0.06	0.05	nd	0.014	...
308L	26202	0.020	20.59	9.83	1.57	0.39	0.22	0.09	nd	0.016	...
17-4 PH	546344	0.040	15.77	4.34	0.37	0.48	0.19	3.36	0.024	0.016	0.37Cb
17-4 PH	29458	0.045	16.03	4.76	0.44	0.62	0.36	3.67	0.018	0.017	0.38Cb

NOTE—Element, %; nd = not determined.

vironment referenced were then compared to degree of sensitization values obtained using the three methods above, so that the most discerning method for accepting material utilizing a sensitization criteria can be established. The dynamic straining test was used as the referee test for this study, since many thousands of hours would be required to obtain IGSCC failures in susceptible materials using the constant load techniques previously described.

The results of this study [9] indicate the electrochemical reactivation technique (EPR) is the best method for predicting IGSCC behavior, especially at the lower levels of sensitization where IGSCC susceptibility is marginal. For example, a good correlation (correlation coefficient, $r = 0.70$) was obtained between the degree of sensitization measured by EPR, and I_{DS} for 11 heats of Type 304 stainless steel sensitized at 500°C. An even better correlation ($r = 0.89$) can be obtained by performing similar correlations between electrochemical reactivation results and dynamic straining in this environment on Type 304 stainless steel weldments; the testing of weldments is presented in a later section of this paper. For industrial use this same type of correlation will have to be performed for environments of industrial significance.

Screening Various Alloys and Metallurgical Variables for Suitability to BWR Service

The dynamic straining test can be used to screen commercial alloys relative to IGSCC resistance, and to identify those alloys which are immune to IGSCC in BWR service. Those alloys which appear promising are then qualified further in longer term, more extensive tests such as constant load coupon and full-scale component tests.

Using this method, a relatively new alloy, Nitronic 50, was selected for control rod drive application in the nitrided condition (Table 2). The alloy was resistant to IGSCC in the mill-annealed and welded condition after dynamic straining, and was even resistant after severe furnace sensitizing or nitriding cycles in the longer term, constant load tests.

In the above case, nitrided Nitronic 50 was selected over 17-4 PH H1100, because one of two 17-4 PH heats failed by stress corrosion cracking (SCC) during the dynamic straining test. As a reference, nitrided Type 304 stainless steel would undergo extensive IGSCC in this test; Nitronic 50 is superior because it is a partially stabilized lower carbon alloy and does not sensitize during a nitriding treatment of approximately 590°C/20 h.

Earlier studies [7] employing constant load testing indicated a Creusot-Loire ICL-473 (Type 304) alloy was very resistant to IGSCC after welding or furnace sensitizing at 620°C. One heat was tested under constant load for times to 5000 h with no failures. The ICL alloys were developed by

TABLE 2—IGSCC resistance of four alloys tested by constant extension rate in 289°C water with 8-ppm dissolved oxygen.

Alloy	Heat	Condition	Constant Extension Rate Test ^a					Constant Load Tests			
			Breaking Stress, mPa	Failure Time, h	RA, %	I _{D5}	IGSCC ^b	Applied Stress, mPa	Applied Stress, ksi	Exposure Time, h	IGSCC
Nitronic 50	302556	1121°C solution anneal	673 (97.6)	227	53.9	0.00	no	517 (75.0)	5000	no	
Nitronic 50	302556	as-welded	662 (96.0)	123	32.7	0.00	no	517 (75.0)	5000	no	
Nitronic 50	302556	620°C/40 h	517 (75.0)	6400	no	
Nitronic 50	302556	nitrided	517 (75.0)	5000	no	
17-4PH	546344	H1100/nitrided ⁱ	779 (113.0)	49	1.8	0.68	yes ^g	
17-4PH	29458	H1100/nitrided ⁱ	770 (111.6)	46	5.0	0.35	no	
ICL473 ^d	T6842	620°C/40 h	441 (63.9)	116	30.0	0.55	yes	261 (37.9)	3800	no	
ICL473 ^d	E6881	620°C/40 h	301 (43.6)	45	12.1	0.79	yes	272 (39.4)	121	yes	
ICL167 ^e	T6689	620°C/40 h	379 (54.9)	126	22.5	0.59	yes	289 (41.9)	1432	yes	
308L ^f	05518	620°C/40 h	295 (42.8)	44	11.3	0.86	yes ^g	
308L ^h	26202	620°C/40 h	407 (59.0)	101	39.3	0.23	no	

^aExtension rate = 0.0008 mm/min (0.032 mil/min).

^bSEM examination of fracture surfaces.

^cNormalized to 60 percent ultimate tensile strength at 289°C.

^dCreusot-Loire Type-304 (T6942 = 0.017C; E6881 = 0.030C).

^eCreusot-Loire Type-316 (0.036C).

^fWeld metal with 0.2 percent ferrite.

^gFailed by SCC intercolumnar.

^hWeld metal with 3.3 percent ferrite.

ⁱ7-mil-thick nitride case.

Creusot-Loire [8] to optimize resistance to sensitization while maintaining strength and chemical composition within the ASTM specifications for Type 304 stainless steel. By carefully controlling the carbon, chromium, and nickel content, these alloys are very resistant to intergranular corrosion after thermal treatments which would normally produce severe sensitization in Type 304 stainless steel. Because of the promising results of the first heat investigated, two additional heats of ICL-473 and one heat of ICL-167 (Type 316) were subsequently investigated in the furnace sensitized condition. All three heats were susceptible to IGSCC in the air-saturated 289°C water environment, although the level of susceptibility was different (Table 2). In this study, the low carbon Heat T6842 is susceptible when dynamically tested, but not to the extent of the higher carbon grade (Heat E6881), and certainly not so susceptible as regular grades of Type 304 stainless steel [5] tested after the same furnace sensitizing treatment.

The furnace sensitized ICL-167 (Type 316) stainless steel also revealed IGSCC, although initiation in the dynamic test was only about 3 grains deep, and the bulk of the fracture occurred by a ductile mode. Corresponding data were obtained by constant load testing in the above environment, where a companion specimen failed by IGSCC after 1432 h. However, this time is considerably longer than the ICL-473 material (Heat E6881) with comparable carbon content. The results of these preliminary screening tests on the ICL alloys using dynamic straining indicate the alloys are not immune to IGSCC after severe furnace sensitizing thermal treatments in an extremely severe environment which is not representative of industrial applications, but do seem to offer considerable improvement over the normal Types 304 and 316 stainless steel grades heat treated similarly.

The dynamic straining test in this extremely severe environment was also used to evaluate the effects of different ferrite levels in Type 308L stainless steel weld metal subjected to a sensitizing heat treatment. The low ferrite-containing (0.2 percent) material (Heat 05518) failed by intercolumnar SCC (Table 2), while the higher ferrite (3.3 percent) material (Heat 29458) was resistant. This difference in stress corrosion susceptibility is illustrated in Fig. 3, where the load versus time curves for the two materials are shown after the dynamic tests. Further tests of this type are planned to study the role of ferrite level in both welding and casting grades of austenoferritic stainless steels.

Fabrication Method Studies

The dynamic straining test is very useful in quickly studying how fabrication methods and histories affect IGSCC susceptibility. For example, the range in IGSCC susceptibilities between several welded seamless Type 304 stainless steel pipes was rapidly developed by dynamic straining in this extremely severe environment (Table 3), and these data are being sup-

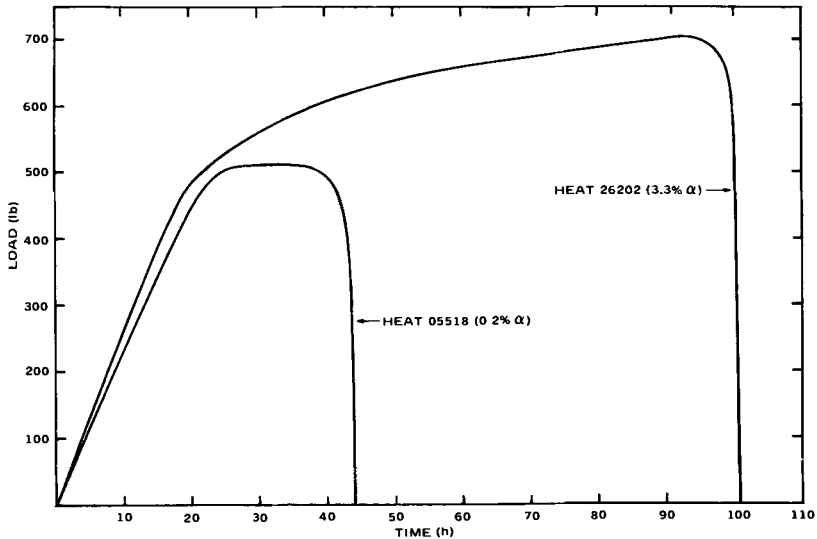


FIG. 3—Load/time curves developed during dynamic strain testing of Type 308L weld pad specimens in 289°C water with 8-ppm O_2 at an extension rate of 0.0008 mm/min.

plemented by longer term, constant load testing. It is apparent from Table 3 that the welded low carbon stainless steel which were tested are fully resistant to IGSCC, even in the extremely severe dynamic straining tests. Also evident is the large amount of heat-to-heat variability in IGSCC susceptibilities after welding. It is because of this variability that accurate ranking of material is difficult. However, those materials exhibiting low I_{DS} values after dynamic straining generally reveal the longer failure times when tested under constant load. Similarly, the more susceptible heats, such as M7616, are identifiable in both tests. In the intermediate susceptibility ranges ($I_{DS} = 0.61$ to 0.35), there is an overlap in failure times after constant load testing. This overlap is attributed to the usual scatter observed in times-to-failure with constant load testing or from welding variability; the welding variability is influenced by variable degrees of sensitization which are under investigation in a combined U.S. Nuclear Regulatory Commission and Electric Power Research Institute-sponsored program [10].

The effect of different weld heat inputs was investigated using a single heat (X14902) of Type 304 stainless steel plate (2.86 cm (1¼ in. thick)). The heat inputs used were 14.2, 25.1, and 40.9 kg/cm (104 kJ/in.) and the welds were produced using the tungsten-inert gas shielded method with added Type 308 stainless steel filler metal (GTAW). All three heat inputs used produced IGSCC susceptible welds for this particular heat in both the dynamic straining and the constant load tests as shown in Table 4. The dynamic test indicated a slight improvement in IGSCC resistance for the low heat input weld ($I_{DS} =$

TABLE 3—Relative IGSCC susceptibilities for ten heats of welded stainless steel pipe in 289°C water with 8-ppm dissolved oxygen.

Alloy	Heat ^b	Carbon Content, %	Constant Extension Rate Tests ^a					Constant Load Tests			
			Breaking Stress, mPa (ksi)	Failure Time, h	RA, %	I _{DS}	IGSCC ^c	Applied ^d Stress, mPa (ksi)	Exposure Time, h	IGSCC ^c	
304	M7616	0.060	373 (54.2)	38	9.5	0.74	yes	287 (41.6)	550	yes	
	M7616	0.060	287 (41.6)	481	yes	
	2P6424	0.040	399 (57.9)	47	30.1	0.61	yes	273 (39.6)	3602	yes	
	2P6424	0.040	273 (39.6)	696	yes	
	834264	0.060	455 (66.1)	88	23.5	0.48	yes	274 (39.7)	464	yes	
	834264	0.060	274 (39.7)	2547	yes	
	2P6396	0.040	449 (65.2)	78	18.8	0.37	yes	270 (39.2)	5200	no	
	2P6396	0.040	270 (39.2)	1500	no	
	TH6656	0.060	474 (68.8)	94	40.6	0.35	yes	274 (39.7)	9500	no	
	TH6656	0.060	274 (39.7)	6628	yes	
	M7772	0.050	462 (67.0)	95	21.2	0.24	yes	288 (41.8)	7000	no	
	M7772	0.050	288 (41.8)	7000	no	
	454659	0.045	474 (68.8)	165	36.5	0.00	no	276 (40.0)	7200	no	
	454659	0.045	276 (40.0)	7000	no	
	304L	482038	0.026	391 (56.8)	72	45.6	0.00	no	243 (35.2)	5200	no
304L	482135	0.025	492 (71.4)	145	44.0	0.00	no	261 (37.8)	7200	no	
304L	00575	0.024	507 (73.6)	100	44.5	0.00	no	279 (40.4)	5200	no	

^aExtension rate = 0.0008 mm/min (0.032 mil/min).

^bAll 10.16-cm (4-in.), Schedule 80 seamless pipe except TH6656 (25.4-cm (10-in.), Schedule 80 seamless) and 834264 (66-cm (26-in.), Schedule 80, rolled and welded).

^cDetermined by SEM of specimen fracture surfaces.

^dNormalized to 60 percent ultimate tensile strength at 289°C.

TABLE 4—IGSCC Results for welded Type 304 stainless steel (Heat X14902) plate in 289°C water with 8-ppm dissolved oxygen.

Weldment ^b	Constant Extension Rate Tests ^a						Constant Load Tests		
	Heat Input, kJ/cm	Breaking Stress, mPa (ksi)	Failure Time, h	RA, %	I_{DS}	IGSCC ^c	Applied Stress, mPa (ksi)	Failure Time, h	IGSCC
Low heat input	14	379 (55.0)	88	21.3	0.76	yes	288 (41.8)	3986	yes
Medium heat input	25	355 (51.5)	96	15.4	0.84	yes	288 (41.8)	1931	yes
High heat input	41	326 (47.3)	76	14.8	0.86	yes	288 (41.8)	435	yes

^aExtension rate = 0.0008 mm/min (0.032 mil/min).

^bTungsten-inert gas shielded method with added 308 filler metal (GTAW).

^cSEM examination of fracture surfaces.

^d60 percent ultimate tensile strength at 289°C.

0.76) compared to the medium and high heat inputs ($I_{DS} = 0.84$ and 0.86). The constant load tests predictably revealed the superior resistance of lower heat inputs on the IGSCC of welded Type 304 stainless steel. In this study, the dynamic strain test is useful in revealing the IGSCC susceptibility of the welded material, but is not the optimum test for differentiating between second order levels of susceptibility for a given heat of material.

Mechanistic Studies of Stress Corrosion Processes

The necessity for sensitization as a precursor to IGSCC of Type 304 stainless steel was studied in one heat of material and is presented in Table 5 and Fig. 4. Here, mill-annealed and very lightly sensitized (620°C/15 min) materials do not undergo IGSCC after dynamic strain testing in high oxygenated water (36 ppm), but those specimens sensitized at 620°C for 1 h or greater are very susceptible. It is of interest that the 1- and 4-h sensitization treatments appear more severe, in terms of IGSCC resistance, than the 40-h sensitization. Presumably, rediffusion of chromium begins to occur after 40 h, such that the chromium depleted regions around the grain boundary chromium carbides ($Cr_{23}C_6$) are replenished, with concomitant improvement of IGSCC resistance.

Another mechanistic finding which confirms earlier observations [5] is that even severely sensitized (620°C/40 h) Type 304 stainless steel does not undergo IGSCC in 289°C high-purity water without oxygen being present. The cracking kinetics is a very strong function of the dissolved oxygen content of the water. For example, there is an order of magnitude increase in the minimum failure times (constant load test) in going from 10 ppm dissolved O_2 to the 0.2 ppm level. The 0.2 ppm corresponds to the nominal value of dissolved oxygen at rated operating conditions during boiling water reactor operation. This oxygen occurs during dynamic equilibrium in the reactor vessel water phase and results from the steam-gas stripping and the radiolytic decomposition (principally) of the water. This finding emphasizes that these types of tests must be performed in the environment of interest for the industrial application to be meaningful with respect to designing for IGSCC protection. In the present study, however, air-saturated water (8-ppm O_2) was used to accelerate the corrosion process, so that variables causing IGSCC could be studied on a timely basis.

The dynamic straining method was also used to evaluate the effect on IGSCC of test temperature for Type 304 stainless steel given a simulated nitride process heat treatment (590°C/20 h). These results are also given in Table 5, where IGSCC was the failure mode at test temperatures down to 121°C in the air-saturated 289°C water environment. The I_{DS} values for these specimens indicate that the 177°C test was more severe, and this finding is apparent by evaluating the load versus time curves shown in Fig. 5. Although

TABLE 5—Constant extension rate [0.0008 mm/min (0.032 mil/min)] IGSCC susceptibility of Type 304 stainless steel (Heat 27388) in oxygenated water as function of sensitization treatment and test temperature.

Heat Treatment	Test		Dissolved O ₂ , ppm	Maximum Stress,		Failure Time, h	RA, %	I _{DS}	IGSCC ^a
	Temperature, °C	(°F)		mPa	(ksi)				
MA ^b	289	(550)	36	481	(69.8)	129	67.0	0.00	no
MA + 620°C/40 h	289	(550)	0 ^c	476	(69.0)	111	72.0	0.00	no
MA + 620°C/15 min	289	(550)	36	500	(72.5)	119	74.6	0.00	no
MA + 620°C/1 h	289	(550)	36	302	(43.8)	28	10.0	0.90	yes
MA + 620°C/4 h	289	(550)	36	247	(35.8)	30	11.9	0.91	yes
MA + 620°C/40 h	289	(550)	36	272	(39.5)	74	27.1	0.78	yes
MA + 590°C/20 h ^d	177	(350)	8	469	(68.0)	79	27.8	0.61	yes
MA + 590°C/20 h	149	(300)	8	476	(69.0)	118	53.4	0.25	yes
MA + 590°C/20 h	121	(250)	8	492	(71.4)	116	53.4	0.23	yes
MA + 590°C/20 h	107	(225)	8	503	(73.0)	120	73.0	0.00	no
MA + 590°C/20 h	93	(220)	8	528	(76.5)	150	76.5	0.00	no

^aDetermined by SEM examination.

^bMill annealed.

^cDegassed water.

^dSimulated nitride process heat treatment.

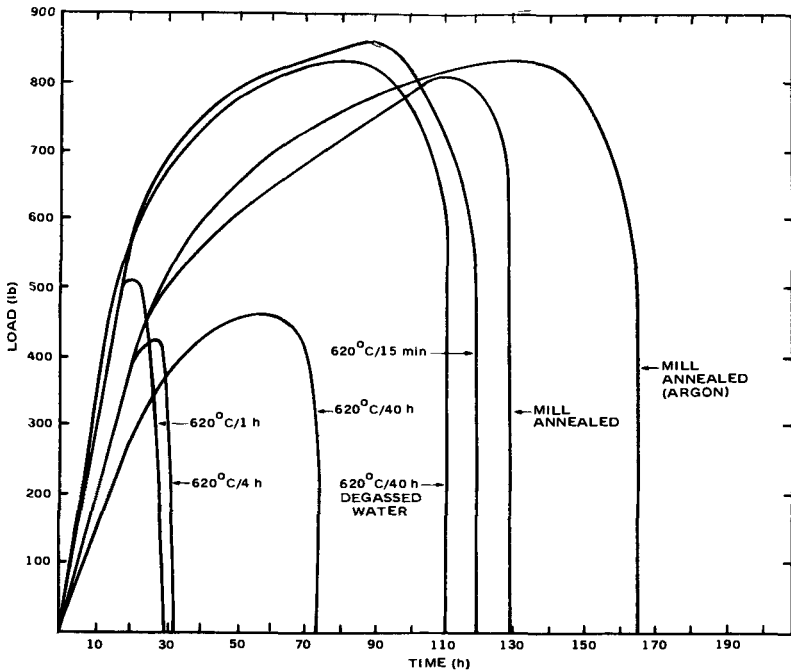


FIG. 4—Load/time curves developed during dynamic strain testing of Type 304 stainless steel (Heat 27388) in 289°C water with 36-ppm O₂ at an extension rate of 0.0008 mm/min.

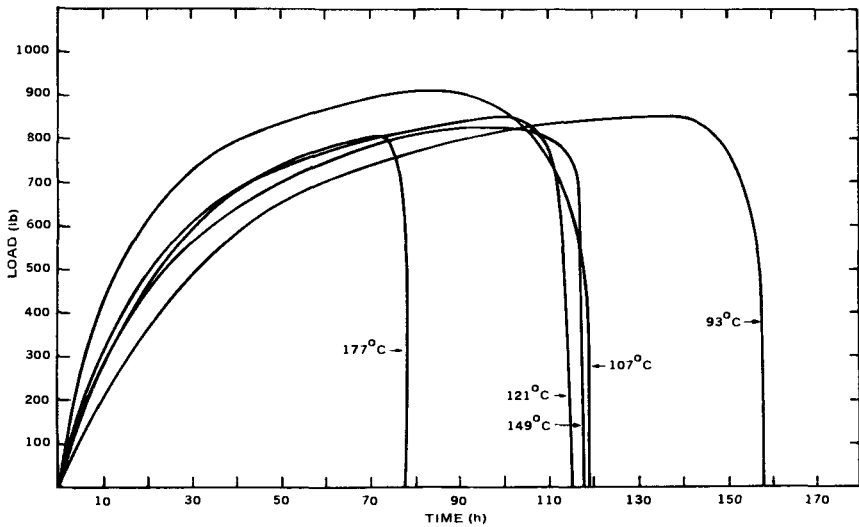


FIG. 5—Load/time curves developed as a function of test temperature during dynamic strain testing in water with 8-ppm O₂ for Type 304 stainless steel (Heat 27388) at an extension rate of 0.0008 mm/min.

specimens tested at 149 and 121°C failed by IGSCC, the level of susceptibility is considerably lower than at temperatures of 177°C and greater. The fractures obtained at 149 and 121°C are intergranular, but a substantial amount of grain elongation was evident, especially at 121°C, which indicates some ductility is present at these lower temperatures. No effects of the environment were evident at test temperatures below 121°C in this study.

Operating Reactor Component Study

One example can be used to illustrate the use of the dynamic straining test for evaluating the IGSCC susceptibility of components from operating reactors. Archive (never used in service) pieces of a Type 304 stainless steel seamless pipe (10.16-cm (4-in., Schedule 80)) which accounted for the bulk of the IGSCC failures in the recent pipe cracking investigation [4] were acquired for evaluation. Segments of the pipe (Heat 2P1486) were welded using specified field procedures, and tensile-bar specimens fabricated such that the weld was in the center of each specimen (1.9 cm (0.75-in. gage)), and the pipe inside surface was preserved as one side of the specimen. One welded specimen was machined on the inside to remove the weld bead; the other weldment was left intact to preserve the original service. The dynamic tests in the 289°C air-saturated water environment revealed (Table 6) this heat was extremely susceptible to IGSCC in the welded condition, and even more susceptible than the worst (Heat M7616) of the ten piping heats evaluated in a separate study (Table 3). The specimen with the original surface preserved after welding was slightly more susceptible in both the dynamic test and the longer term constant load test. This specimen more closely simulates the welded surface of the reactor bypass pipes where IGSCC was noted in the weld heat affected zones. The fracture in the dynamically strain tested specimens occurred about 0.457 cm (0.180 in.) from the weld fusion line, which is comparable to the field failure locations [0.5 cm (0.2 in.)]. The fracture surface is shown in Fig. 6 for the dynamic strain tested specimen. While these tests are encouraging to provide correlation with service experience, this same material now needs to be tested in 0.2 ppm O₂ containing water, which is the actual coolant environment during BWR operation.

Acceptance of Heats of Material for Specific Applications

The General Electric Company has developed two processing procedures that can immunize welded austenitic stainless steels to IGSCC in the BWR environment [11]. These procedures are:

1. *Solution Heat Treatment after Welding*—Fully solution heat-treated material is immune to IGSCC in laboratory and in-reactor tests. Therefore, solution heat treatment of components after welding eliminates IGSCC susceptibility caused by welding. This procedure is applicable to shop welds but is impractical for field welds.

TABLE 6—Laboratory confirmation of the IGSCC susceptibility of a Type 304 stainless steel (Heat 2P1486) BWR bypass pipe which failed in the field. Tests conducted in 289°C water with 8-ppm dissolved oxygen.

Condition	Constant Extension Rate Tests ^a					Constant Load Tests			
	Breaking Stress, mPa (ksi)	Failure Time, h	RA, %	I_{DS}	IGSCC	Applied Stress, mPa (ksi)	Exposure Time, h	IGSCC	IGSCC
Welded/original surface removed	240 (34.9)	27	10.4	0.81	yes	279 (40.4)	401	yes	yes
Welded/original surface not removed	319 (46.3)	31	1.0	0.96	yes	276 (40.0)	740	yes	yes

^aExtension rate = 0.0008 mm/min (0.032 mil./min).

^bNormalized to 60 percent ultimate tensile strength at 289°C.

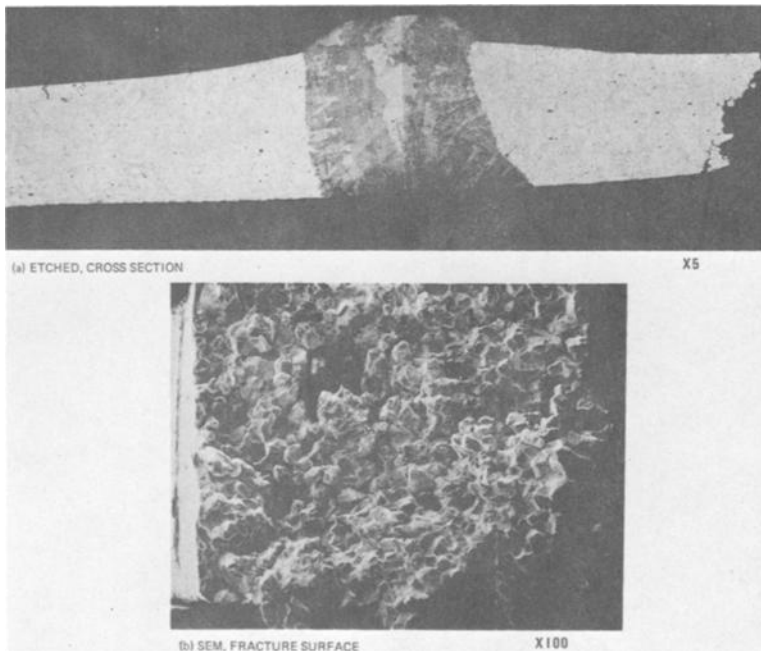


FIG. 6—Welded Type 304 stainless steel (2P1486) BWR by-pass pipe specimen dynamically tested (0.0008 mm/min) in 289°C water with 8-ppm O_2 .

2. **Corrosion Resistant Cladding**—Stainless weld metal containing over 5 percent ferrite is immune to intergranular cracking in the BWR environment. Thus, this corrosion-resistant cladding is applied to the area near a weld preparation before the groove weld is made. The weld heat-affected zone is then present in the material that is immune to stress corrosion cracking. The corrosion-resistant cladding can be applied in the shop and the component welded in the field by this technique providing immunity to stress corrosion cracking of weld heat-affected zone areas. A detailed discussion of this procedure was given by Gordon et al [11].

While these two methods have shown to provide immunity to SCC in areas that have been shown by experience or duty cycle calculations to have some risk for IGSCC in BWR service, there are occasions where utilization of these two methods are impractical. For these cases, the dynamic straining test has been used to qualify Type 316L stainless steel material on a heat-by-heat basis for the specific application. The heat of material to be qualified is welded in the same configuration using the same welding procedure that will be utilized in the field. Uniaxial tension specimens are then machined from the weld mockups such that the specimen contains the surface area that

would be wet by reactor water. Duplicate specimens are then tested in the dynamic straining test system in 289°C high-purity water containing 8-ppm O₂ at an extension rate of 0.0008 mm/min. This severe environment is used for acceptance at this time because of the lack of qualification data in the environment of interest. The heat of material in question is accepted for commercial use if the posttest SEM of the fracture surface shows no evidence of intergranular cracking. It should be noted that control specimens of a sensitized susceptible heat of Type 304 stainless steel are tested periodically to ensure that the test system is operating correctly.

The dynamic straining test is also used to accept heats of Nitronic 50 (XM-19) for a specific nitriding operation. The nitriding cycle operates at a time and temperature regime that will cause the 300 series stainless steels to be susceptible to IGSCC. Laboratory tests show that Nitronic 50, when properly processed and annealed, is immune to IGSCC after the nitriding cycle. The dynamic straining test is used as a quality control tool to check all heat treat lots after a simulated nitride treatment.

Conclusions

It has been our objective to demonstrate that the dynamic straining test is a very versatile technique for investigating SCC in high-temperature aqueous environments, with applications ranging from use as a research tool, to use as a quality control method for a production operation. The rapidity of the dynamic straining method for developing data relative to the evaluation of component fabrication variables is invaluable. Because of the good correlation between dynamic strain and longer term constant load tests, however, dynamic strain also has proved to be a valuable tool as a reference test for a variety of qualification programs. However, for industrial use, the method should be qualified for the environment of interest and utilized accordingly. The mechanistic study of SCC in the 300 series stainless steels has also been enhanced by quickly providing data which would otherwise require long periods of time to develop.

The dynamic straining test can be used to screen new alloys for stress corrosion resistance in a given environment to eliminate susceptible materials quickly and to identify promising materials that may warrant further evaluation. However, long-term constant load testing or special component qualification testing must follow these critical screening tests to confirm resistance. In those cases where an alloy system has been well characterized and shows one-to-one correlation between dynamic straining and constant load test or component qualification results, the dynamic straining technique can be used to study both environmental and materials variables, such as heat treatment and minor alloying affects. When sufficient data exist to provide full confidence in the results of the dynamic straining tests in the appropriate environment, it can then be used as a quality control tool.

Acknowledgments

The authors are indebted to the Electric Power Research Institute and the U.S. Nuclear Regulatory Commission for sponsoring much of the work reported here. The authors also acknowledge M. E. Indig, who was largely responsible for the development of the dynamic strain machine. All the dynamic strain and constant load tests and results given were conducted by G. L. Smith, and the scanning electron microscopic work performed by E. Plaza-Meyer and R. W. Warner. Also, the authors express their appreciation to J. N. Kass and G. M. Gordon for their helpful discussions.

References

- [1] Higgins, J. P., *Nuclear News*, Vol. 11, The General Electric Report, Nov. 1968, p. 37.
- [2] Walker, W. L. and Higgins, J. P., "Performance of 304 Stainless Steel Structural Components in General Electric Company Boiling Water Reactor," Paper No. 103, NACE Corrosion Conference, Anaheim, CA, 1973.
- [3] Cheng, C. F., *Reactor Technology*, Vol. 13, No. 3, 1970, pp. 310-319.
- [4] Klepfer, H. H. et al, "Investigation of Cause of Cracking in Austenitic Stainless Steel Piping," General Electric Report NEDO-21,000, July 1975.
- [5] Clarke, W. L. and Gordon, G. M., *Corrosion*, Vol. 29, No. 1, Jan. 1973, pp. 1-12.
- [6] Hishida, Mamoru and Nakada, Hiroshi, *Corrosion*, Vol. 33, No. 9, Sept. 1977.
- [7] Clarke, W. L., Danko, J. C., and Gordon, G. M. in *Corrosion Problems in Energy Conversion and Generation*, The Electrochemical Society, Inc., Princeton, N. J., 1974.
- [8] Combrade, P. et al, "Aciers Inoxydables Dans Les Reacteurs A Eau Bouillante Problemes De Corrosion Solutions Possibles," Presented at Colloque SPAS, Les Aciers Speciaux Dans L'Industrie Nucleaire, Dec. 1976, Paris, France.
- [9] Clarke, W. L., Cowan, R. L., and Walker, W. L., in *Intergranular Corrosion of Stainless Steel Alloys*, ASTM STP 656, American Society for Testing and Materials, 1978, pp. 99-132.
- [10] Clarke, W. L., Romero, V. M., and Danko, J. C., "Detection of Sensitization in Stainless Steels Using Electrochemical Techniques," Paper No. 180, NACE Corrosion Conference, 14-18 March 1977, San Francisco, Calif.
- [11] Gordon, G. M., Hayes, T. R., and Ferrari, G., "Design Criteria for Stress Corrosion Cracking Prevention in Water Reactors," XXII Nuclear Congress of Rome, The Behavior of Nuclear Water Cooled Reactor Materials, 24-25 March 1977.

DISCUSSION

*W. I. Pollock*¹—Are you using this test as an acceptance test with a specific criteria for purchase and use of heats of material? If so, please detail.

W. L. Clarke, R. L. Cowan, and J. C. Danko (authors' closure)—Yes, we use the constant extension rate test as an acceptance test for all heat treatment lots of XM-19 (Nitronic 50), but after these materials are purchased. We do not purchase material based on a previous constant extension rate test

¹Du Pont Company, Engineering Department, Wilmington, Del. 19898.

response. The acceptance tests are conducted in 289°C (550°F) high purity water containing 8-ppm dissolved oxygen at an extension rate $< 1 \times 10^{-4}$ in./min. (2.54×10^{-4} cm/min). The acceptance criteria are based on no IGSCC either on the specimen fracture surface or secondary cracks along the gage length.

*I. L. W. Wilson*²—Your data appear to segregate into 3 groups: (a) index = 0, no cracking in constant load, (b) index $I_{DS} 0 < I_{DS} < 0.48$, no cracking in constant load, and (c) index > 0.48 , cracking in constant load.

Do you use this type of ranking: (a) group (i) acceptable, (b) group (ii) use judgment, and (c) group (iii) not acceptable.

Would you comment on this and are the data consistently like this?

W. L. Clarke, R. L. Cowan, and J. C. Danko (authors' closure)—No, we do not use that type of ranking. The I_{DS} index is a useful value for evaluating data, however, there is presently too much inconsistency for accurate ranking analysis. This inconsistency derives from difficulty in accurate elongation measurements after constant extension rate testing. The specimens often break in irregular shapes, and the presence of secondary side cracks disrupts the accuracy of the elongation measurements. Other indexes are currently under investigation (extent of IGSCC on fracture surface, etc.).

²Westinghouse Research and Development Center, Pittsburgh, Pa. 15235.

M. E. Indig¹

Slow Strain-Rate Stress Corrosion Testing for Liquid Metal Fast Breeder Reactor Steam Generator Applications

REFERENCE: Indig, M. E., "Slow Strain-Rate Stress Corrosion Testing for Liquid Metal Fast Breeder Reactor Steam Generator Applications," *Stress Corrosion Cracking—The Slow Strain-Rate Technique*, ASTM STP 665, G. M. Ugiansky and J. H. Payer, Eds., American Society for Testing and Materials, 1979, pp. 170-202.

ABSTRACT: A high-temperature slow strain-rate facility was developed to evaluate the stress corrosion resistance of alloys considered for the construction of liquid metal fast breeder reactor (LMFBR) steam generators. The primary concern was stress corrosion that might occur on the water side during steam generator operation in locally faulted caustic environments. Most of the studies were performed at 316°C in 5 or 10 percent sodium hydroxide (NaOH) solutions with 2¼Cr-1Mo steel and Incoloy-800.

With minor modification, the slow strain-rate test was converted to a straining electrode test. Experiments conducted by the straining electrode test permitted the study of stress corrosion behavior in the high temperature caustic solutions over a range of oxidizing potentials.

It was found that 2¼Cr-1Mo steel was extremely resistant to caustic cracking at 316°C in all metallurgical conditions tested by the slow strain-rate test and the straining electrode test. A few slow strain-rate tests performed at 232°C in 5 to 10 percent NaOH resulted in intergranular and transgranular stress corrosion failures of 2¼Cr-1Mo steel.

Unlike 2¼Cr-1Mo, Incoloy-800 was susceptible to caustic cracking at 316°C. The susceptibility depended on the metallurgical condition and to some extent, the oxidizing potential. The cold-worked and Grade 1 conditions exhibited excellent resistance to caustic cracking in the slow strain-rate test. However, limited studies in the straining electrode test showed the Grade 1 condition could be readily cracked at anodic oxidizing potentials.

KEY WORDS: stress corrosion cracking, slow strain-rate test, straining electrode test, caustic cracking, high temperature, high pressure, liquid metal fast breeder reactor, boilers, 2¼Cr-1Mo steel, Incoloy-800, metallurgical condition, alloys

One of the major concerns in the development of steam generators for liquid metal fast breeder reactors (LMFBR) is the possibility of caustic stress corrosion cracking (SCC). The operational histories of nuclear-

¹ Principal engineer, General Electric Company, San Jose, Calif. 95125.

powered steam generators have included many cases of SCC [1,2]² which were related to high concentrations of a caustic that had developed in specific regions as a result of design and operating characteristics [3]. In the LMFBR steam generator, a caustic could accumulate in the water side as a result of direct liquid sodium in-leakage from the shell side or from sodium ion in-leakage through the feed-water system. For this reason it was necessary to determine the SCC resistance of materials considered for the LMFBR steam generator construction. As a result, the slow strain-rate test was employed for rapidly determining the relative stress cracking resistance of structural alloys in high temperature aqueous environments. The slow strain constant extension rate test (SSRT) continuously strains a specimen at a constant extension rate while the specimen is exposed to the specific environment of interest. The results of the SSRTs were compared with those obtained with longer term constant load tests.

Humphries and Parkins [4] and Parkins [5,6] first developed and applied the SSRT for the study of caustic cracking of mild steel. For the earliest study, experiments were conducted in 35 percent sodium hydroxide (NaOH) solutions at 1 atm over a range of controlled electrochemical potentials. It was found that caustic cracking occurred in a rather narrow potential range around the active-to-passive transition region and was associated with the formation of iron oxide (Fe_3O_4) films [4]. The strain rate significantly affected the failure mode. For example, at a strain rate of $1.6 \times 10^{-6}/\text{s}$ stress corrosion occurred, while at strain rates $\geq 4.2 \times 10^{-5}/\text{s}$ specimens failed mechanically with no sign of caustic cracking.

In the present experimental program we were primarily concerned with LMFBR steam generator operation. Thus, most of the experiments were performed at an approximate evaporator temperature, 316°C (600°F), in what was considered an environment badly faulted by caustic. For this reason a facility was developed that could study caustic cracking at elevated temperatures and pressures. The materials of interest in these studies were limited to $2\frac{1}{4}\text{Cr-1Mo}$ steel and Incoloy-800. However, the fundamental and practical applications of the SSRT technique includes the development of data in support of (a) screening of materials for environmental capability; (b) qualification of materials of construction for specific applications; (c) fabrication procedures, such as welding, machining, and heat treatments; (d) the role of environmental variables on stress corrosion material response; and (e) understanding the mechanism of SCC.

Experimental Procedures

Materials and Specimen Description

The chemical compositions of the $2\frac{1}{4}\text{Cr-1Mo}$ steel and the Incoloy-800

²The italic numbers in brackets refer to the list of references appended to this paper.

alloys used in the stress corrosion studies are given in Table 1. The metallurgical treatments for the alloys are given in Table 2.

The stress corrosion tests were conducted with dog-bone tension specimens (Fig. 1). A few of the tension specimens of 2¼Cr-1Mo were prepared from weldments. The weldments simulated the tube-to-tube sheet welds in steam generators. These weldments were prepared from 2.54-cm (1-in.) annealed plate and split and flattened tubing. The tubing had an outside diameter of 1.27 cm (0.5 in.) and a wall thickness of 47.8 mm (0.188 in.). The tubing was split axially, flattened, annealed, and then welded to the plate with an automatic tungsten arc welder using 2¼Cr-1Mo weld filler material. After welding, the thick-to-thin weldments were machined into the dog-bone tension specimens and given a postweld heat treatment of 732°C (1350°F) for 1 h. In final form, the tension specimens had one end from the plate (simulated tube sheet) and the other end from the split and flattened tubing (simulated tube portion). At the center of the gage section was the weld which joined the two ends.

To determine the effect of stress intensity on possible caustic cracking, a few specimens were notched in the center of one face of the gage section by electrical discharge machining. The notches had a radius of 0.1 mm (0.004 in.) and a depth about 1 mm (0.04 in.). The theoretical stress concentration, K_t , at the base of the notch was about 4.

The SSRT Facility

The SSRT facility can be operated as a static or refreshed system. The experiments reported here were conducted in a static system with 5 and 10 percent caustic solutions at 316°C (600°F). A few experiments were also conducted at 232°C (450°F) with 2¼Cr-1Mo steel. A schematic of the slow strain-rate facility is shown in Fig. 2. The system essentially consists of a tension specimen within a high pressure, high temperature autoclave. Although not indicated in Fig. 2, the autoclave cover is bolted to the autoclave body and the body is bolted to the main frame. The specimen is coupled to a drive system located above the autoclave in the ambient environment. The facility elongates a tension specimen while the specimen is exposed to the hot caustic solution within the autoclave. The specimen is held to the upper and lower grips by high strength pins which pass through the holes in the grips and the specimen tab section. The lower grip is screwed into the bottom retaining plate. Three support columns are bolted in the retaining plate and the upper ends of the support columns are screwed into tapped holes on the inner surface of the autoclave cover. The arrangement of the lower grip, retaining plate, support columns, and autoclave cover form a rigid frame which prevents the lower tab section from moving axially.

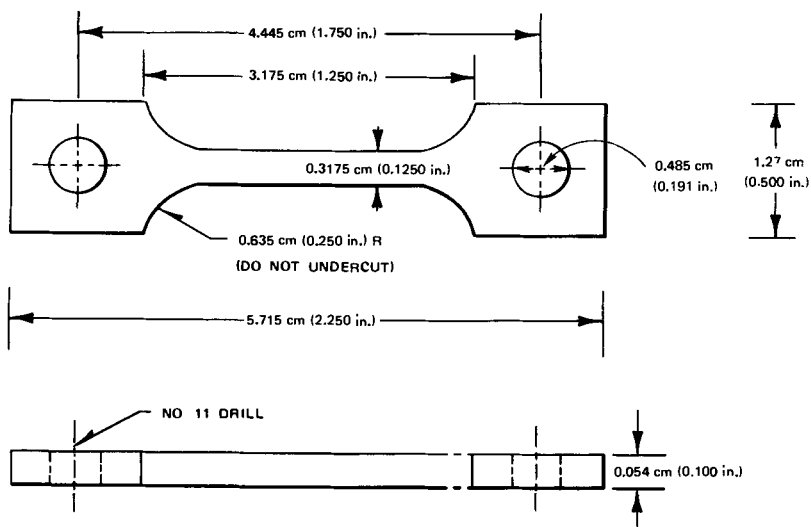
The upper tab section is coupled to the pull rod by the upper grip. The

TABLE 1—Alloy compositions.

1.2½Cr-1Mo Product Form	Application	C	Mn	Fe	P	S	Si	Ni	Cr	Cu	Mo
Bar	tension specimens	0.12	0.47	+	0.017	0.025	0.39	0.12	2.25	0.14	0.97
Plate	simulated tubesheet	0.11	0.55	+	0.011	0.012	0.29	...	2.13	...	0.96
Filler rod	weld for above	0.10	0.74	+	0.017	0.017	0.14	...	2.62	...	0.96
Split tubing	simulated tube	0.11	0.48	+	0.015	0.015	0.21	...	2.22	...	0.96
2. Incoloy-800 Product Form	Application	C	Mn	Fe	S	Si	Ni	Cr	Cu	Ti	
Bar	tension specimens	0.04	0.81	43.5	0.007	0.25	35.5	20.5	...	0.43	

TABLE 2—*Metallurgical treatments.*

Alloy	Treatment
2¼Cr-1Mo	<ol style="list-style-type: none"> 1. Annealed—924°C (1695°F) for 20 min, furnace cool to 732°C (1350°F) and hold for 45 min; air cool 2. Normalized and tempered—924°C (1695°F) for 30 min, air cool, temper at 677°C (1250°F) for 1 h; air cool 3. Cold-worked—annealed; cold-rolled 25% 4. Cold-worked—normalized and tempered; cold-rolled 25% 5. Welded tension specimens. After welding, given postweld heat treatment, 732°C (1350°F) for 1 h
Incoloy-800	<ol style="list-style-type: none"> 1. Annealed (Grade 2)—15 min at 1149°C (2100°F); water quench 2. Cold-worked—annealed; cold-rolled 25% 3. Annealed (Grade 1)—927°C (1700°F) for 1 h; water quench

FIG. 1—*Stress corrosion tension specimen.*

pull rod passes out of the autoclave through the polyfluoroethylene resin packing of a pressure sealing gland. As the rod is withdrawn from the autoclave, the specimen gage section strains.

Above the autoclave, the pull rod is coupled to the drive system. The drive system consists of a motor coupled to three variable speed gear heads, a fixed gear reducer, and a worm gear. The worm gear transforms the rotary motion of the motor to a vertical movement on the pull rod. By adjustment of the gearheads, the pull rod movement or specimen extension rate can be varied from 7.1×10^{-7} to 5.5×10^{-4} cm/s which approximates strain rates of 3.7×10^{-7} to 1.9×10^{-4} /s for a gage length of 1.91 cm (0.75 in.).

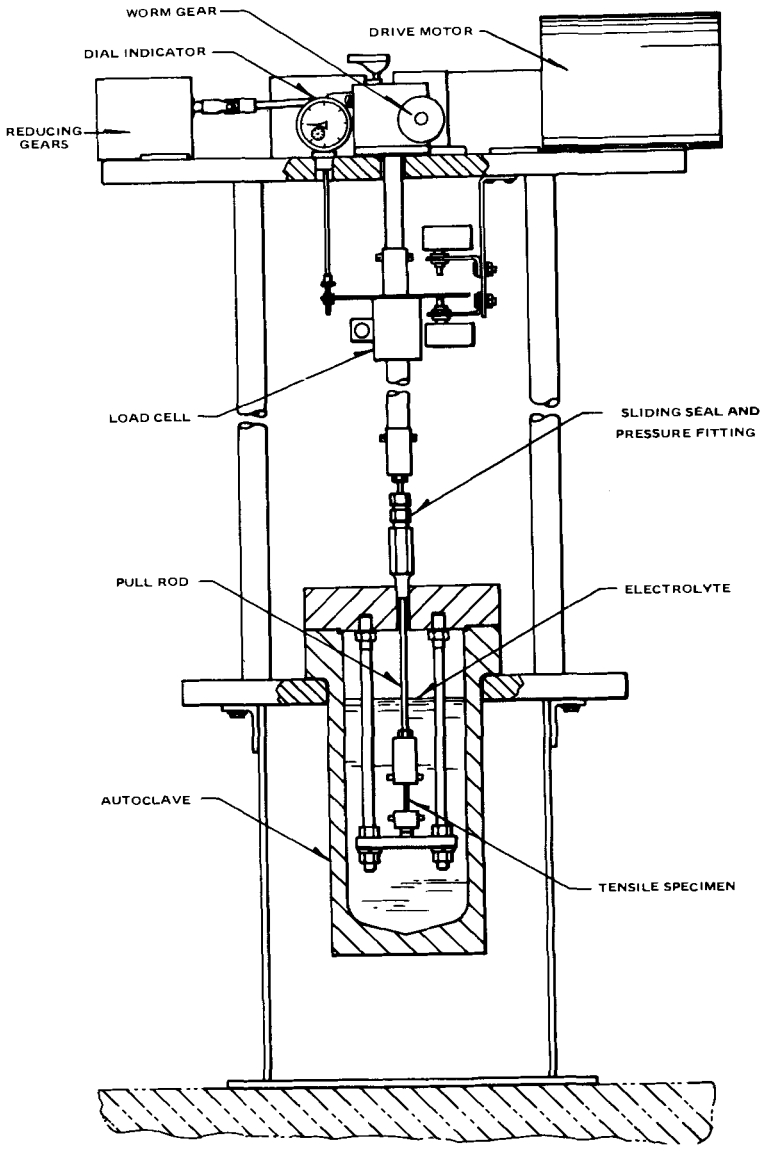


FIG. 2—SSRT facility.

A load cell was permanently attached to a section of the pull rod outside the autoclave and during operation, the load-deformation curve of the specimen in caustic is determined. The curve is compared to a standard, determined for the same alloy pulled to failure in either pure water or air at 316°C. Of particular interest is the percent strain and the ultimate tensile strength. A significant decrease in these values compared to the standard is an indication of possible SCC. After the test, the specimen is removed from the facility, the reduction in area is measured, and the failure mode is determined by optical scanning electron microscopy.

In the SSRT experiments, the autoclave was fabricated from Type 316 stainless steel and the pull rod and retaining pins were made from high strength Inconel-X750. To protect the stainless steel autoclave from caustic cracking, a loose-fitting nickel liner, which held the caustic solutions, was installed in the autoclave. A small amount of distilled water was injected between the liner and the autoclave to improve heat transfer and prevent the formation of a concentrated caustic solution in this crevice. After sealing, the system (with all fixtures and the specimen in place in the autoclave) was overpressured with 0.689 MPa (100 psi) argon. The overpressure prevented boiling and minimized the transfer of caustic solution from inside the nickel liner to the austenitic stainless components, especially to the crevice between the liner and the autoclave.

Straining Electrode Experiments

In the SSRT, the tension specimen is maintained at the natural corrosion potential determined by specimen interaction with the test environment and any galvanic coupling to the support system. The corrosion potential also can be controlled to some predetermined value by the use of an external potentiostat. The SSRT under potential control will be referred to as the straining electrode test in the paper. Hoar and Hines [7] initially suggested the term "straining electrode" when describing a crack tip advancing under the combined influence of mechanical strain on corrosion.

With a few modifications, the SSRT facility was converted to a straining electrode facility. The most important modifications were the electrical insulation of the straining electrode (tension specimen) from the retaining fixtures, autoclave and drive system, the electrical connection of the straining electrode to an external potentiostat, and the installing of a reference electrode within the autoclave.

In the SSRT, the tension specimens were attached to the upper and lower grips with Inconel-X750 high strength pins. For the straining electrode experiments, preoxidized Zr_{2.5}Nb pins were used. The zirconium alloy was preoxidized by heating in air at 500°C for 24 h which formed an electrically insulating oxide. In addition, the tab faces of the tension specimens were lined with strips of polyfluoroethylene resin to insulate

further the tension specimen from the grips. A stainless steel, polyfluoroethylene resin coated wire was connected to the specimen and the wire was passed out of the autoclave through an insulated sealing gland. Outside the autoclave, the wire was connected to the working electrode post of a potentiostat. During a straining electrode experiment, the potential between the tension specimen and a reference electrode was controlled with a potentiostat. The reference, a cylindrical platinum electrode, was positioned adjacent to the working electrode within the autoclave. As shown in Fig. 3, the lower end of the stainless steel conductor was screwed into a tapped hole in the platinum reference electrode and the upper end passed out of the autoclave through an insulated pressure sealing gland. The upper end of the stainless steel conductor rod was connected to the reference electrode terminal to the potentiostat. The autoclave was grounded and used as the auxiliary electrode. To prevent ground loops, the potentiostat was connected to an isolation transformer.

Straining electrode experiments were performed with 2¼Cr-1Mo steel and Incoloy-800. Most of the potentials chosen for straining electrode experiments were anodic to the rest potential. A single experiment with 2¼Cr-1Mo steel was conducted at a potential cathodic to the rest potential. All the straining electrode tests experiments were performed at a strain rate of about $3.7 \times 10^{-7}/s$.

Polarization Curves

The applied potentials for the straining electrode tests were predetermined based on the anodic polarization curves. The polarization curves were determined for both 2¼Cr-1Mo steel and Incoloy-800 with cylindrical electrodes. The electrodes were similar in design to the reference electrode shown in Fig. 3. The autoclave was used as the counter electrode. The electrolytes (degassed 1, 5, and 10 percent NaOH) were contained in the nickel liner as described previously. The curves were determined with the potentiostat. In the active region, 10-mV potential steps were used. In the passive and transpassive region, 50 or 100-mV steps were used. The current readings were taken after a two-minute hold period at a constant potential. The curves were determined from the rest potential to oxygen evolution.

Results

Slow Strain-Rate Tests

A summary of the results obtained for 2¼Cr-1Mo at 316°C in the slow strain-rate tests is given in Table 3. In 5 percent NaOH, no caustic cracking occurred for any metallurgical condition and over a range of strain

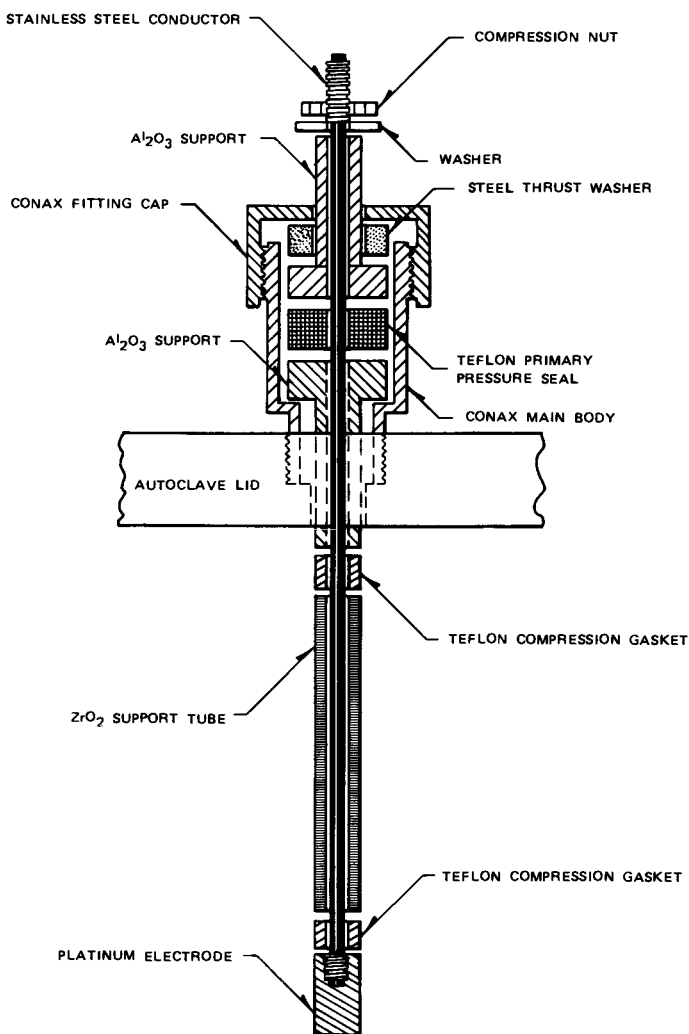


FIG. 3—Platinum reference assembly.

rates. In 10 percent NaOH, a single marginal case of cracking did occur. The cracks shown in Fig. 4 propagated to a maximum length of about $75\ \mu\text{m}$ before blunting.

In general, examination of the specimens after test showed a fairly thick cracked oxide had formed on the specimen surface in the caustic environment. The cracks in the oxide extended both in length and width forming finger-like extensions which propagated 50 to $75\ \mu\text{m}$. Typical penetrations are shown in Fig. 5. At slow strain rates, approximately

TABLE 3—Slow strain-rate testing for 2½Cr-1Mo at 316°C (600°F).

Metallurgical Treatment	Environment	Extension Rate, cm/s × 10 ⁷	Tensile Strength		Elongation, %	Reduction of Area, %	Observation
			MPa	(ksi)			
Annealed	pure water	28	491.2	(71.3)	22	53	no SCC ^a
	5% NaOH	28	473.3	(68.7)	16	25	
	5% NaOH	7.1	490.6	(71.2)	18	31	
	5% NaOH + O ₂	7.1	468.5	(68.0)	23	41	no SCC ^b
Annealed and notched Normalized and tempered	10% NaOH	7.1	461.6	(67.0)	13	26	minor cracks 75 μm depth
	10% NaOH	7.1	527.0	(76.5)	14	25	no SCC
	5% NaOH	7.1	479.5	(69.6)	
	pure water	7.1	601.5	(87.3)	18	50	
Cold-worked 25%	5% NaOH	7.1	553.9	(80.4)	14	50	
	10% NaOH	7.1	655.9	(95.2)	12	28	
	air	...	635.9	(92.3)	...	39.1	
	10% NaOH	7.1	654.5	(95.0)	4.6	12.7 ^d	^e
Welded and stress relieved	pure water	7.1	527.0	(76.5)	15.7	64.7	
	5% NaOH	7.1	516.1	(74.9)	14.9	60.6	^d
	10% NaOH	7.1	437.5	(63.5)	...	56.4	
	10% NaOH	239	488.5	(70.9)	14.9	49.4	

^a SCC.

^b SCC of 17-4 PH stainless steel retaining pins.

^c 2.1 × 10⁻³ cm/s.

^d Metal cross section reduced by general corrosion as well as strain.

^e Severe general corrosion.

^f Severe general corrosion, gage marks obliterated.

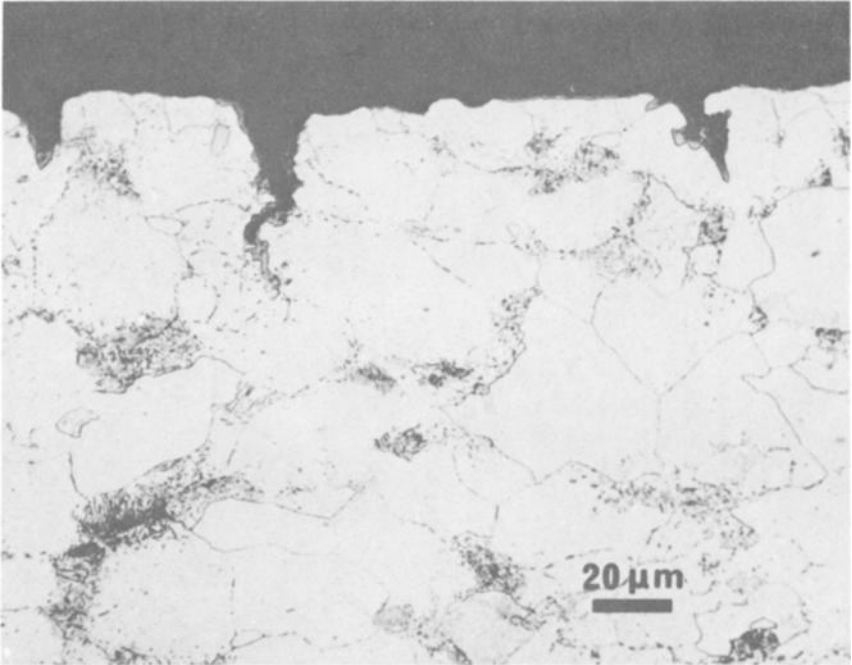


FIG. 4—Marginal cracks on 2¼Cr-1Mo in 10 percent NaOH, 316°C, 3.7×10^{-7} /s strain rate.

10^{-7} /s, the penetrations were surrounded with a thick reaction product which appeared similar to the surface oxide. Faster strain rates, approximately 10^{-4} /s, produced penetrations that were somewhat sharper and had thinner oxides associated with them. Posttest examination of the notched specimens, where the stress concentration at the base of the notch was about 4, showed that the failures were ductile.

The simulated tube-to-tube sheet weld specimens also failed mechanically. The failures were always away from the weld since the weld region was mechanically stronger (similar to quenched and tempered material) than the annealed regions.

The mechanical properties of the 2¼Cr-1Mo tension specimens were in general only slightly affected by the exposure to the caustic solutions. When compared to standards strained to failure in pure water or air (Table 3), a slight decrease in ultimate tensile strength and elongation was noted. The changes in reduction of area depended on the general corrosion rate. Where the corrosion was not severe, for example for annealed specimens in 5 or 10 percent caustic solution, the reduction of area decreased to about one-half the value measured in pure water. However, where metal corrosion was severe, as with the welded specimens

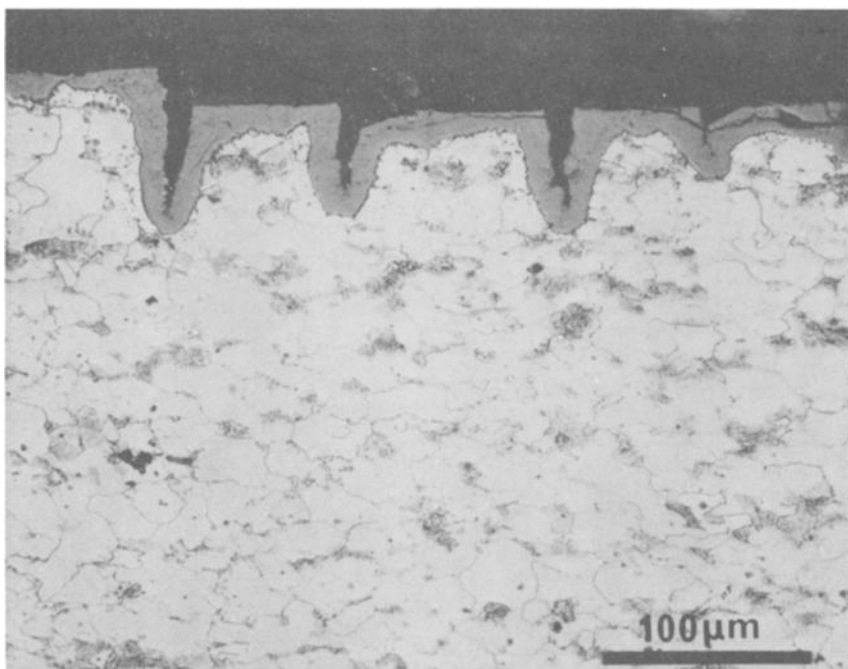


FIG. 5—Fingers of oxides, on 2¼Cr-1Mo 5 percent NaOH, 316°C, 3.7×10^{-7} /s strain rate.

strained to failure in 10 percent NaOH at the slowest strain rate, the gage section was reduced by general corrosion as well as strain. The combined effect resulted in higher apparent reductions of area compared to the standard but lower ultimate tensile strengths.

Although it was found that 2¼Cr-1Mo steel exhibited excellent resistance to caustic cracking at 316°C, at lower temperatures, others had cracked this and related alloys [5]. Dahl et al [8] found 3Cr-0.5Mo steel cracked at 225°C (437°F) in 20 percent caustic. For this reason a few slow strain-rate tests were conducted at 232°C (450°F) in 5 and 10 percent caustic, although this temperature was not prototypical of steam generator operation. As expected, both transgranular and intergranular caustic cracking occurred for annealed and welded specimens. Figure 6 shows some of the cracks in a welded specimen at some distance from the weld. Only minor cracks were detected in the weld region.

The results for Incoloy-800 obtained in the SSRT are given in Table 4. Data are presented for the Grade 2, Grade 1, and cold-worked conditions. While only a single specimen of the Grade 1 condition was tested by SSRT and the test was stopped at the onset of necking, it was clear from the mechanical properties (tensile strength, elongation, and reduction of area)

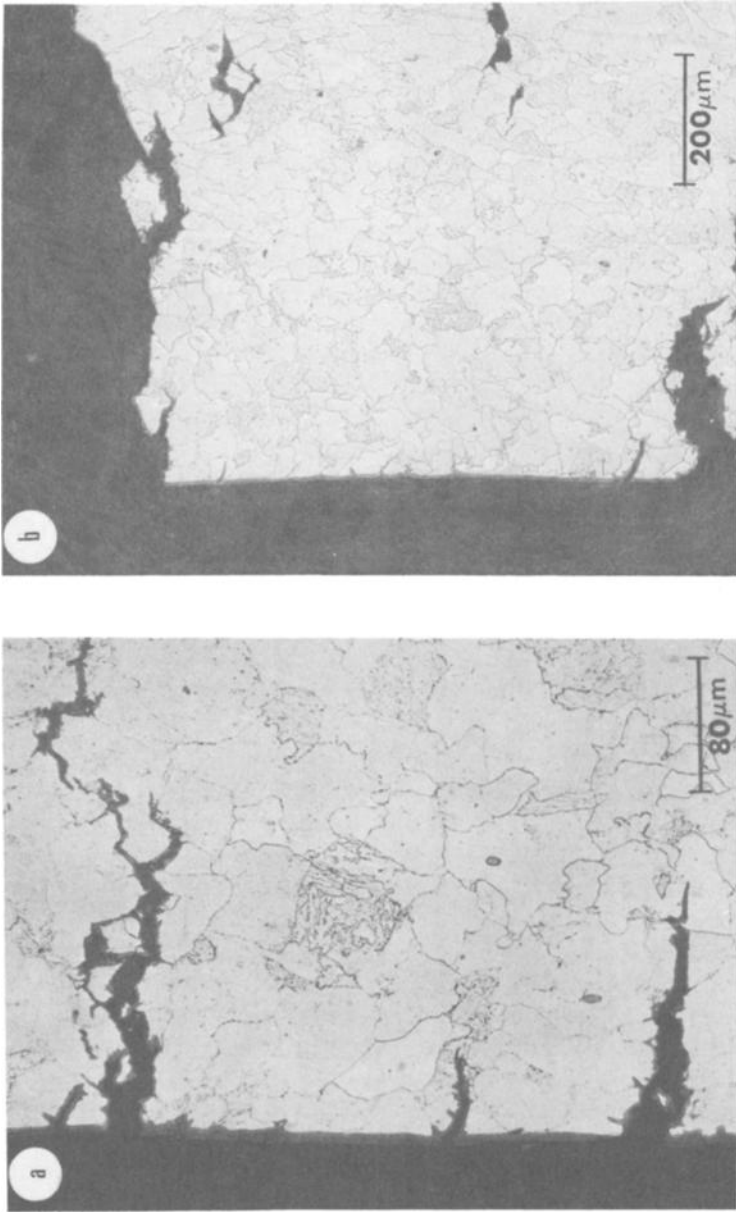


FIG. 6—Caustic cracking in $2\frac{1}{2}\text{Cr-1Mo}$, 10 percent NaOH, 232°C , $3.7 \times 10^{-7}/\text{s}$ strain rate.

TABLE 4—Slow strain rate testing, 316°C (600°F), IncoLOY-800.

Condition	Environment	Extension Rate, cm/s × 10 ⁷	Tensile Strength		Elongation, %	Reduction of Area, %	Observation
			MPa	(ksi)			
Annealed, Grade 2	calibration in water 5% NaOH 5% NaOH	7.1	457.5	(66.4)	61	54	ductile failure
		7.1	301.8	(43.8)	38	15	intergranular SCC
		508	435.4	(63.2)	57.3	57	surface cracks, ductile rupture
Annealed, Grade 1	10% NaOH 5% NaOH	7.1	320.4	(46.5)	26.9	16	transgranular SCC
		7.1	505.7	(73.4)	44.7	38.2	test stopped just prior to mechanical failure; minor cracks found only in neck
Cold-worked 25%	calibration in air 5% NaOH 10% NaOH	...	655.2	(95.1)	6.9	32.0	ductile failure
		7.1	744.1	(108)	6	34.0	ductile failure, minor SCC at neck
		7.1	673.8	(97.8)	6.7	18.4	mostly ductile failure, minor SCC at neck

^a2.1 × 10⁻³ cm/s.

and the presence of minor cracks only at the neck that this metallurgical condition was quite resistant to caustic cracking. Incoloy-800 in the Grade 1 condition was the choice for the steam generators of the Super Phoenix in France.

Of those metallurgical conditions tested in the SSRT, the most susceptible to caustic cracking was the Grade 2 state. At the slowest strain rates in 5 percent NaOH, cracking was severe and propagated by an intergranular mode as shown in Figs. 7 and 8. Figure 9 shows striations on the crystal facets which may be the record of crack arrest sites for a discontinuous cracking process. If the strain rate was too fast, the failure was mostly ductile with only minor surface stress cracks. In 10 percent NaOH, the mode of failure was transgranular stress corrosion. It should be noted when stress corrosion was severe, there was a significant reduction in the failure stress, elongation, and reduction of area.

Figure 10 shows the single specimen of the Grade 1 condition after the SSRT. The considerable amount of plastic strain is clearly evident. However, the minor cracks at the neck cannot be seen in this macrograph.

The cold-worked condition exhibited excellent stress corrosion resistance. No cracking occurred in the 5 percent caustic environment, and in the 10 percent caustic environment only minor cracking occurred. The minor cracks were located at the neck of the tension specimen and thus must have occurred at the onset of plastic instability.

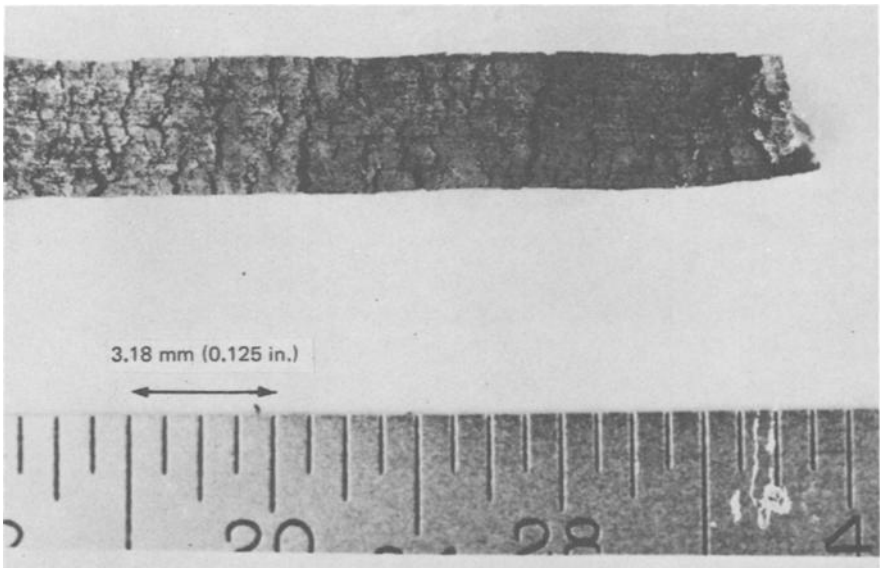


FIG. 7—Caustic cracking, Incoloy-800, Grade 2 in 5 percent NaOH, 316°C, 3.7×10^{-7} /s strain rate.

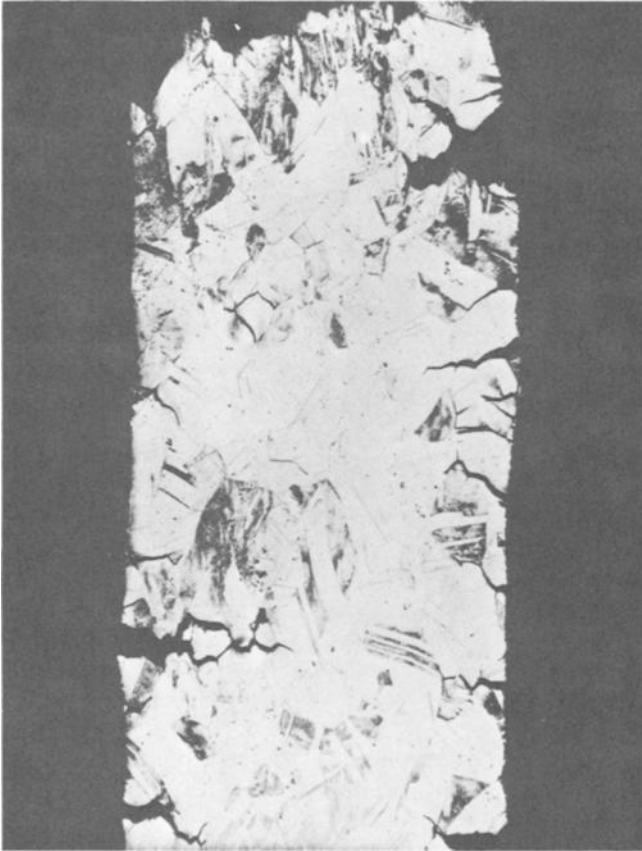


FIG. 8—Microstructure of Fig. 7.

High Temperature Anodic Electrochemical Studies

The anodic polarization curves for $2\frac{1}{4}$ Cr-1Mo and Incoloy-800 in several metallurgical conditions and in several caustic solutions at 316°C (600°F) are shown in Figs. 11 through 16.

The main feature of the $2\frac{1}{4}$ Cr-1Mo curve is the increasing presence and sharpness of the active region with increasing NaOH concentration. Sharp transitions between the active and passive regions often indicate regions of film instability and susceptibility to stress corrosion. The presence of the transition may account for the marginal stress cracking in 10 percent NaOH.

The Incoloy-800 curves show an increased active region with increased NaOH concentration. At high potentials, transpassivity and secondary passivation are observed. The most probable reaction in the transpassive

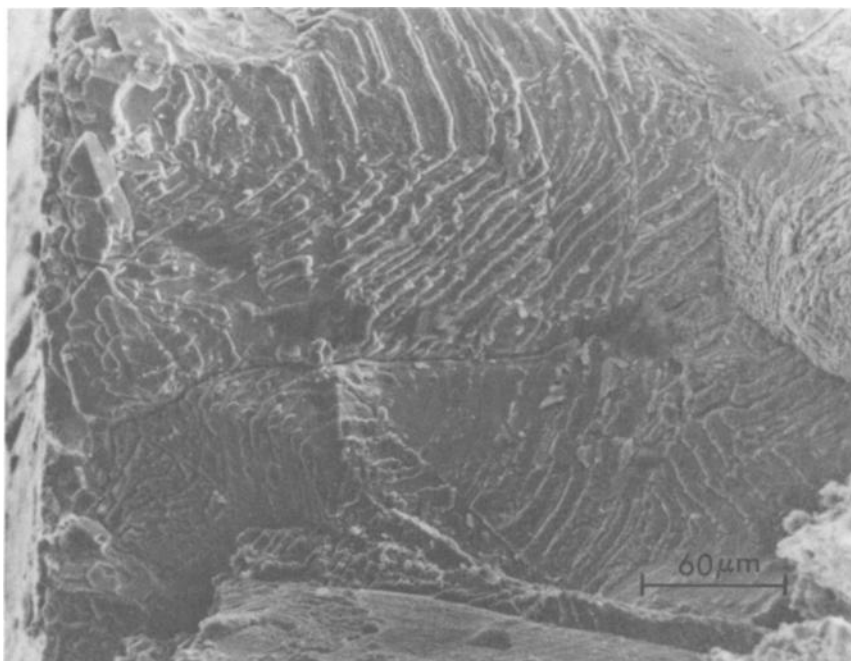
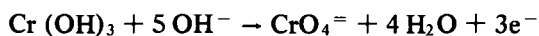


FIG. 9—*Striations on fracture surface Incoloy-800.*

region is the oxidation of chromium in the reaction film from the +3 to the +6 state according to the reaction



The final upturn in current for both alloys is caused by oxygen evolution



Straining Electrode Experiments

A summary of the results of the straining electrode experiments for 2¼Cr-1Mo at 316°C (600°F) in 5 and 10 percent NaOH is given in Table 5. For comparison, results obtained from experiments without the application of potential (in SSRT) are also presented for 2¼Cr-1Mo in pure water, 5 percent NaOH, and 10 percent NaOH.

The application of anodic (oxidizing) potentials during straining did not result in stress corrosion. Metallographic examination indicated the oxidizing potentials resulted in some increase in oxide formation and minor localized attack. The attack was manifested in the formation of fingers of

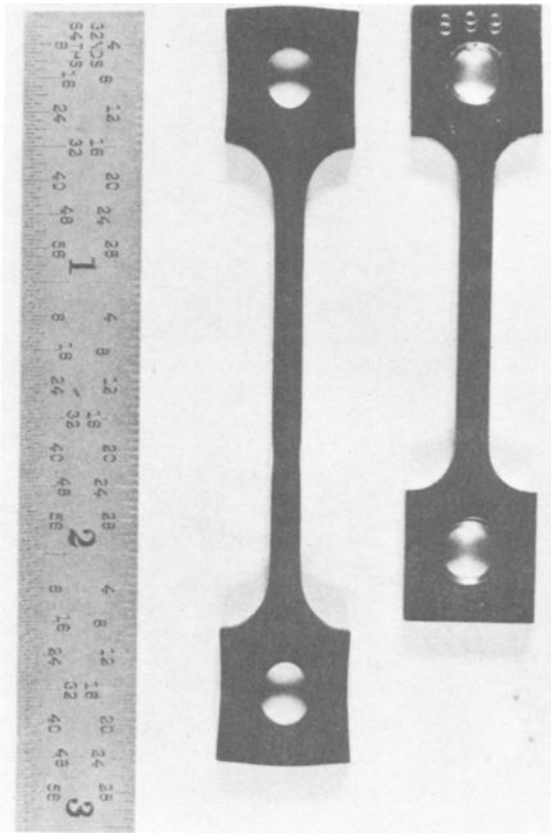


FIG. 10—Incoloy-800, Grade 1, before and after SSRT, 316°C, 5 percent NaOH, 3×10^{-7} /s strain rate.

oxide, which penetrated several grains into the metal before terminating, and a slight decrease in elongation. Figure 17 is an example of the thick reaction product and minor localized attack. In 10 percent NaOH, the applied anodic potentials greatly increased the general dissolution which significantly thinned the specimens.

A straining electrode experiment was also performed at a reducing (cathodic) potential. The cathodic potential was used to determine whether a forced decrease in the general corrosion could result in stress corrosion of 2¼Cr-1Mo. As indicated in Table 5, only minor cracking occurred. Figure 18 shows the microstructure of the specimen strained to failure under cathodic control. The penetrations were slightly deeper, about 0.1 mm (0.004 in.), and somewhat sharper than those formed under anodic

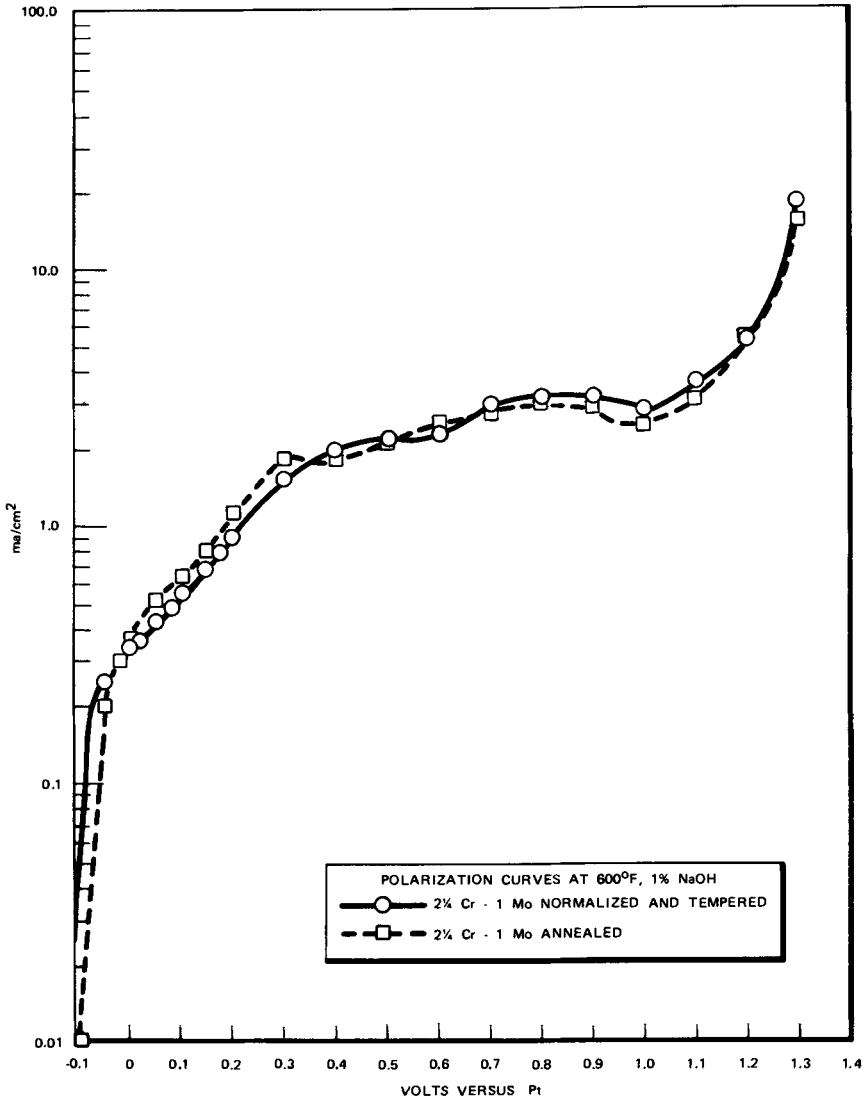


FIG. 11—Polarization curves, 2%Cr-1Mo, 1 percent NaOH, 316°C.

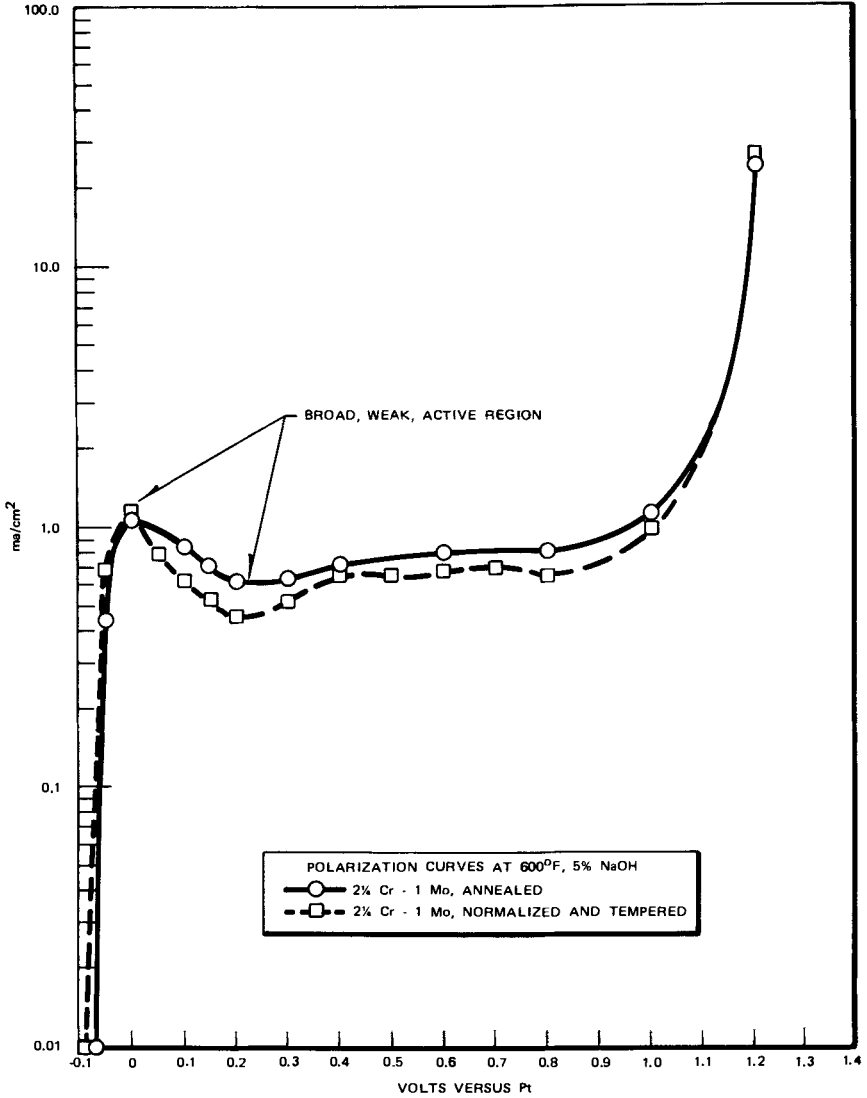


FIG. 12—Polarization curves, 2%Cr-1Mo, 5 percent NaOH, 316°C.

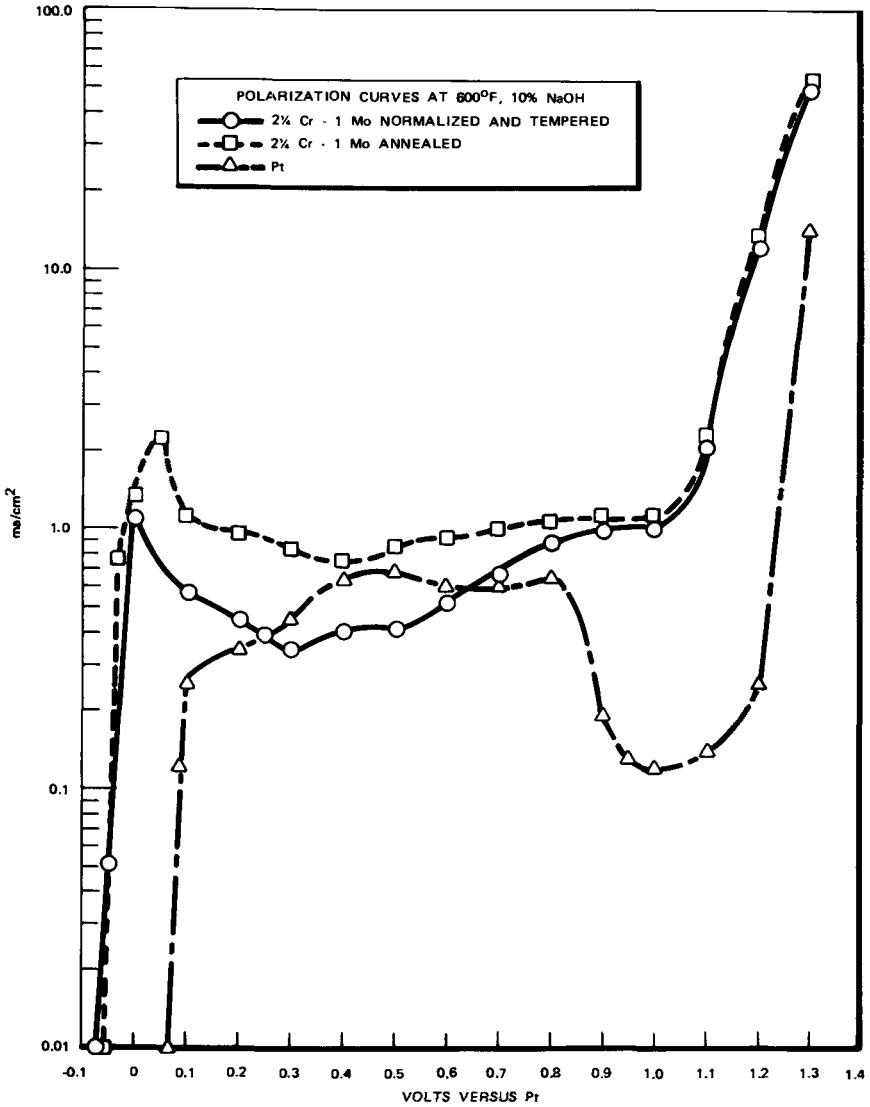


FIG. 13—Polarization curves, 2 1/4Cr-1Mo, 10 percent NaOH, 316°C.

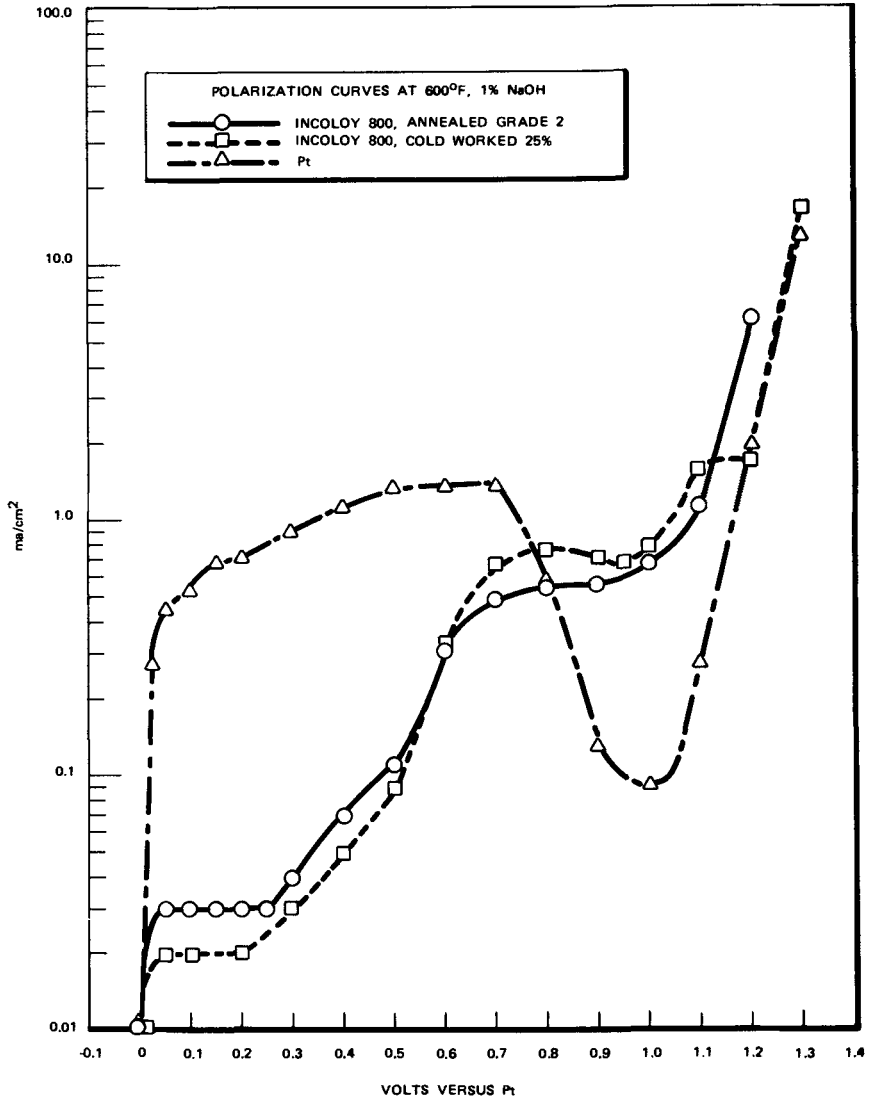


FIG. 14—Polarization curves, Incoloy-800, 1 percent NaOH, 316°C.

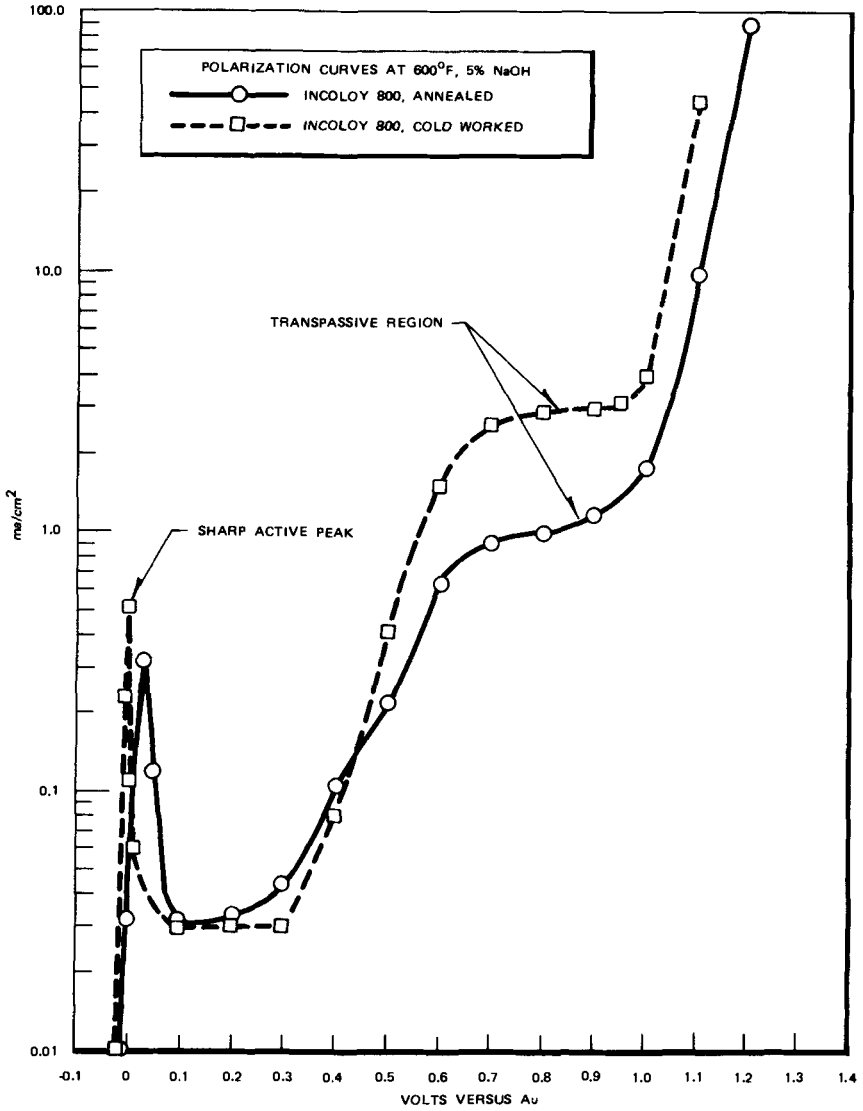


FIG. 15—Polarization curves, Incoloy-800, 5 percent NaOH, 316°C.

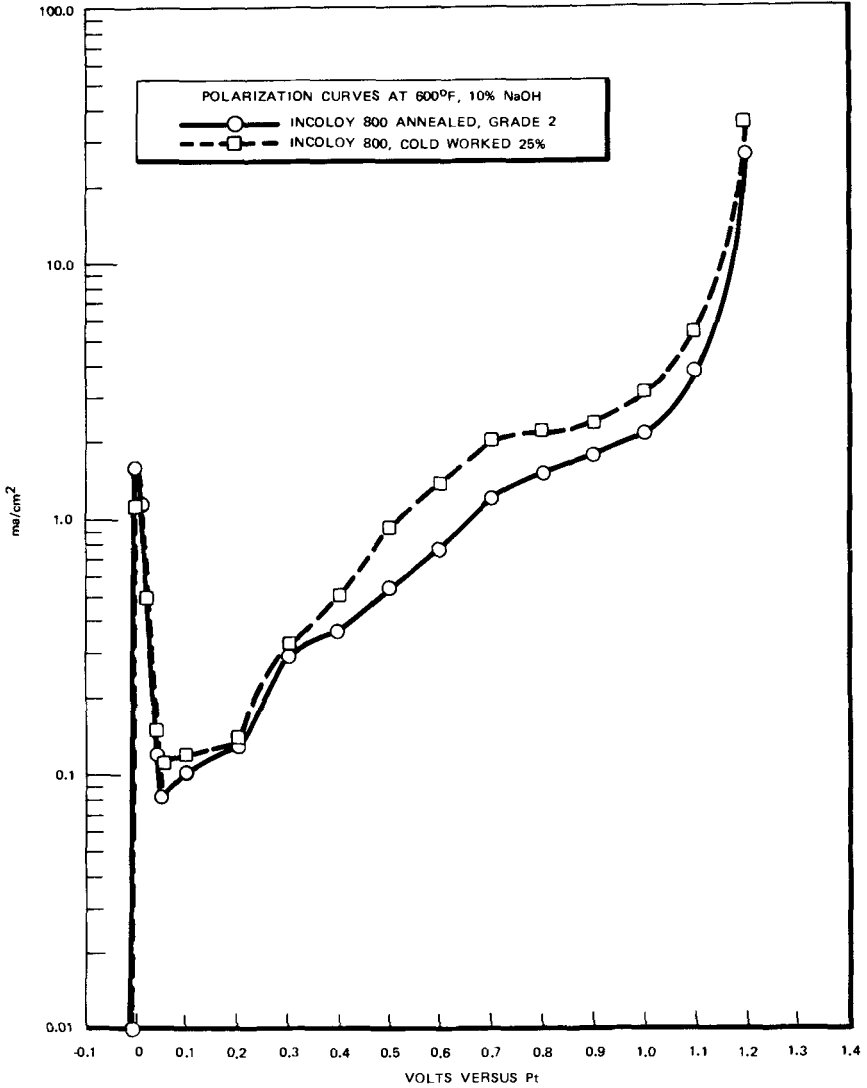


FIG. 16—Polarization curves, Incoloy-800, 10 percent NaOH, 316°C.

TABLE 5—Summary of straining electrode results, annealed 2¼Cr-1Mo steel, 316°C (600°F), 3.7×10^{-7} /s.

NaOH, weight %	Applied Potential versus Pt, V	Tensile Strength		Elongation, %	Reduction of Area, %	Observation
		MPa	(ksi)			
0	0	491.6	(71.3)	22.0	53	no SCC ^a
5	0	490.9	(71.2)	18.0	31	no SCC
10	0	462.0	(67.0)	13.3	26	minor cracks, maximum depth ~75 μm
5	0.050	> 434.4	(> 63) ^b	11.6	27.4	no SCC
5	0.100	510.2	(74.0)	11.4	31.0	no SCC
5	0.150	504.0	(73.1)	12.5	33.0	no SCC
5	0.400	487.5	(70.7)	14.2	39.6	no SCC
5	-0.150	482.6	(70.0)	10.1	10.5	minor cracks, maximum depth ^c ~100 μm
10	0.080	398.5	(57.8)	11.9	74.7 ^d	no SCC
10 ^e	0.080	440.6	(63.9)	.. ^f	72.9 ^d	no SCC
10	0.300	471.6	(68.4)	14.2	67.2 ^f	no SCC

^a SCC.

^b Electronic malfunction in load cell, after load of 434.4 MPa (63 ksi); test continued to specimen failure.

^c See Fig. 18.

^d High apparent reduction in area values due to specimen thinning from high corrosion rate rather than strain.

^e Electroslag remelt (ESR) alloy used.

^f Gage marks not visible due to general corrosion.

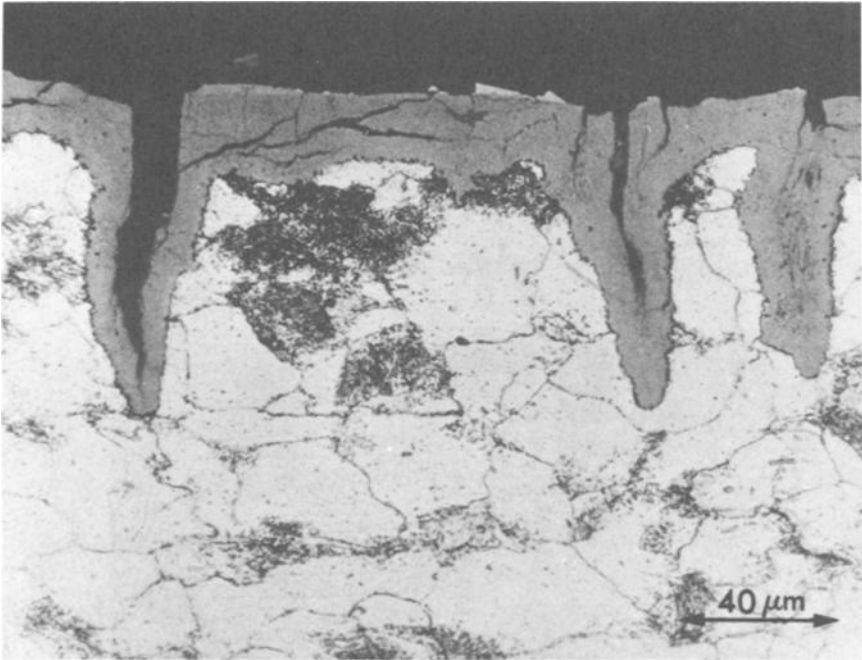


FIG. 17— $2\frac{1}{4}\text{Cr-1Mo}$ annealed, 5 percent NaOH, 316°C , $3 \times 10^{-7}/\text{s}$ strain rate, 0.100 V versus platinum.

potentials. In addition, the oxide formed under cathodic control was reduced in thickness.

The results of the straining electrode experiments run with Incoloy-800 are given in Table 6. For comparison, results obtained with no applied potential are also presented.

Discussion

$2\frac{1}{4}\text{Cr-1Mo}$

In the SSRT and the straining electrode experiments, $2\frac{1}{4}\text{Cr-1Mo}$ has shown excellent resistance to caustic cracking at 316°C . Similar results were also obtained in constant load tests conducted in 3 and 10 percent NaOH solutions at 316°C [9]. The 3 percent NaOH tests, reported earlier [9], were conducted in a continuously refreshed system and no cracks occurred in specimens of $2\frac{1}{4}\text{Cr-1Mo}$ in any of the metallurgical conditions tested. Exposure times for some specimens were greater than 3000 h, and stresses were maintained considerably above the 316°C , 0.2 percent offset yield strength. The 10 percent tests were conducted in a static system, and

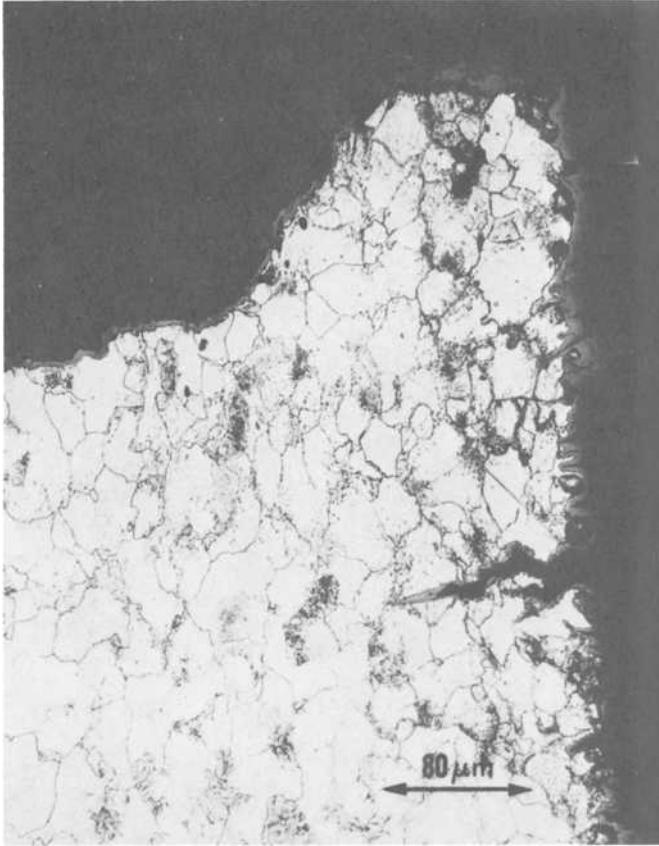


FIG. 18— $18\text{--}2\frac{1}{4}\text{Cr-1Mo}$ annealed, 5 percent NaOH, 316°C , $3.7 \times 10^{-7}/\text{s}$ strain rate, cathodic control.

a summary of these results [10] is given in Table 7. Failures of some of the welded specimens occurred, but the failures were due to severe corrosion which thinned these specimens until mechanical overload occurred.

As temperature is reduced, the rate of general corrosion is reduced. Thus after a film rupture event, the localized strain enhanced corrosion may be considerably greater than the general corrosion. It is the difference between the general corrosion and strain enhanced corrosion that allows a sharp crack to propagate. At lower temperatures, 232°C , stress corrosion occurred while at 316°C ; generally crack blunting was observed.

At 316°C , cathodic polarization was partially effective in reducing the general corrosion rate. A specimen tested under a reducing potential had a thin surface oxide. Penetrations formed that appeared to have more of

TABLE 6—Summary of straining electrode experiments for Incoloy-800, 3.7×10^{-7} /s strain rate, 316 °C, (600 °F).

Metallurgical Condition	Environment	Applied Potential versus Pt, V	Tensile Strength		Elongation, %	Reduction of Area, %	Observation
			MPa	(ksi)			
Grade 2	Calibration in pure water	...	457.4	(66.4)	61	54	ductile failure
Grade 2	5% NaOH ^a	0	301.8	(43.8)	38	15	intergranular SCC ^b
Grade 2	10% NaOH ^a	0	320.4	(46.5)	27	16	transgranular SCC ^b
Grade 2	10% NaOH ^c	+0.030	457.5	(66.4)	43	49	ductile failure
Grade 1	5% NaOH ^a	0	506.4	(73.5)	45	38	no failure ^d
Grade 1	10% NaOH ^c	+0.030	490.6	(71.2)	47	42	ductile failure
Grade 1	10% NaOH ^c	+0.200	356.9	(51.8)	15.5	11.5	many cracks initiated along gage section ^e

^a Argon cover gas.

^b SCC.

^c 90Ar-10H₂ cover gas.

^d Test stopped prior to mechanical failure (see Fig. 10).

^e Test interrupted due to electronic malfunction.

TABLE 7—Typical results from constant load experiment, 316°C (600°F) 10% NaOH (no SCC) [10].

Metallurgical Conditions	Applied Stress		Exposure Time under Stress, h
	MPa	(ksi)	
Welded and stress relieved	379.2	(55)	948 ^a
	379.2	(55)	836
	413.7	(60)	861 ^a
	413.7	(60)	298
Temper embrittled ^b	448.1	(65)	1347
	448.1	(65)	1626
Annealed	241.3	(35)	2033
	241.3	(35)	2033
	344.7	(50)	1822
	344.7	(50)	1324
Electroslag remelt, ^c annealed	344.7	(50)	1115
	344.7	(50)	1115
	344.7	(50)	1895
	344.7	(50)	1895
Normalized and tempered	448.1	(65)	1324
	448.1	(65)	1324

^a Specimen fractured due to severe general attack and mechanical overload.

^b 1000 h at 513°C.

^c Electroslag remelt.

the characteristics of stress cracks than the usual blunt oxide fingers that formed under anodic potentials or at the corrosion potential.

In addition to the local strain enhanced corrosion following film rupture, electrochemical factors may have a specific effect on stress corrosion. According to electrochemical theory, over the potential region of active-to-passive transitions the surface reaction product may not be stable and under strain, the alloy may be susceptible to stress corrosion. Usually the current between the active peak and the steady state passive region will vary by several orders of magnitude. In the present studies, the polarization curves showed increased and sharper current peaks over the active-to-passive transitions with increasing caustic concentrations. However, these current peaks were either absent in the 1 percent NaOH solution or slight in the 5 and 10 percent NaOH solutions. Thus we might expect either the absence or perhaps a marginal stress corrosion behavior. In 10 percent NaOH, where the current peak was the greatest, a single marginal case of cracking was found.

At lower temperatures, 120°C, Bohnenkamp [11] reported sharp active-to-passive current peaks for carbon steel in 33 percent NaOH. In addition, Bohnenkamp [11] reported stress corrosion susceptibility at a potential just above the active peak. Humphries and Parkins [4] reported similar results. In the potential region of film instability, Diegle and Vermilyea

[12] reported a significant decrease in the film ductility which covered an iron oxide electrode. Thus, the electrochemical potential can affect the anodic dissolution kinetics, film stability, mechanical properties of the oxide, and the susceptibility to stress corrosion.

Incoloy-800

In contrast to 2¼Cr-1Mo steel, Incoloy-800 in the Grade 2 condition was susceptible to caustic cracking at 316°C in the SSRT. Cracking was intergranular in 5 percent NaOH and transgranular in 10 percent NaOH. The same alloy stressed under constant load in a continuously refreshed system also resulted in intergranular caustic cracking, but much longer times were necessary to obtain failures [9]. These experiments were conducted in 3 percent NaOH at 316°C, and the failure times were determined as a function of applied stress. It was found that extremely high stresses were necessary to obtain caustic cracking in reasonable times. In the SSRT, severe SCC failures occurred in about 10 days. Apparently the continuous strain results in accelerated stress corrosion; although it should be mentioned if the strain rates are high, approximately $2 \times 10^{-4}/s$, failures will be mostly mechanical.

The anodic polarization curves give some hint to the stress corrosion susceptibility. In 5 and 10 percent NaOH (Figs. 15 and 16), sharp active-to-passive current transitions were observed where the current varied at least 1 order of magnitude. At higher potentials, transpassive regions are also observed. Thus stress corrosion susceptibility may exist over the potentials of the transitions. Stress corrosion susceptibility in the transpassive region is only of academic interest in the present studies, because the transpassive potentials represent a powerful oxidizing environment and one that would be difficult to obtain in an operating steam generator.

In general, the presence of the transition means that following rupture of a protective oxide in the passive region, a large current transient occurs as the metal repassivates to heal the break. In 1 percent NaOH, the active-to-passive transition was not observed, probably because the alloy is already passive at the natural corrosion potential. Thus in 1 percent NaOH, rupture of the passive film as a result of strain might not be followed by a large anodic dissolution current transient and the alloy might not stress crack. Experimentally, Incoloy-800 was not found susceptible to caustic cracking in ≤ 1 percent NaOH at 316°C [6].

Recent tests conducted by stressing Incoloy-800 by the constant load technique in an environment of 10 percent NaOH in a static autoclave did not result in any sign of caustic cracking. Specimens were stressed for about 1700 h at 345 MPa (50 ksi). The lack of failures in the 10 percent NaOH static environment can be explained by either of two hypotheses.

1. In the slow strain-rate tests the fracture strength of Incoloy-800, Grade 2, was about the same in 5 and 10 percent NaOH. Thus we might expect that cracking times at constant load would be about the same in the two environments. Previously, the cracking time at 345 MPa (50 ksi) in 3 percent NaOH was about 2200 h [9]. In the 10 percent NaOH static tests, the stress and exposure time for duplicate specimens were 345 MPa (50 ksi) and 1738 h, respectively. It may be that either a longer exposure time or higher stress was required to initiate cracking.

2. Perhaps a more plausible explanation of the lack of cracking can be obtained from electrochemical principles. The constant load tests in 3 percent NaOH were conducted in a circulating system. The source of the electrolyte was a low pressure 113-litre stainless steel tank which was purged continuously with argon. Thus the concentration of dissolved oxygen and hydrogen in the solution that was pumped into the autoclave was very low. We know by chemical analyses of the feed water that the oxygen content was less than 5 ppb. The constant load tests in 10 percent NaOH were conducted in a static autoclave. In the 10 percent NaOH static tests, most of the stressed specimens tested were 2¼Cr-1Mo. The general corrosion of 2¼Cr-1Mo would generate an increasing concentration of hydrogen. Hydrogen in sufficient concentrations can lower the corrosion potential of Incoloy-800. At the lower corrosion potential, Incoloy-800 may be immune to caustic cracking. Evidence of this electrochemical effect was obtained in the study and by Theus and Cels [13,14]. It was demonstrated in this study that Incoloy-800 cracked transgranularly in 10 percent NaOH when tested in the SSRT facility. The cracking occurred when the electrolyte and the gas space in the autoclave were purged with argon. In straining electrode experiments in 10 percent NaOH, a 90Ar-10H gas mixture was used. At a potential of +0.030 V versus the platinum electrode, no stress corrosion occurred for either the Grade 2 or Grade 1 condition. Apparently the hydrogen in the cover gas lowers the corrosion potential to a region of immunity for both heat-treated conditions. We can compensate the environmental effect by raising the potential with a potentiostat and in the last straining electrode experiment, the potential was increased to 0.200 V versus the platinum electrode. Incoloy-800 was used in the most crack-resistant heat treatment (the Grade 1 condition). This experiment was terminated before failure because of an electronic malfunction. However, examination of the specimen by optical microscopy showed numerous stress corrosion cracks had nucleated and had begun to propagate. Thus for Incoloy-800, unlike 2¼Cr-1Mo, at 316°C (600°F) in caustic solutions, there appears to be a strong electrochemical potential dependency on stress corrosion.

Theus and Cels [13,14] found that mill annealed Incoloy-800 would crack in 10 percent NaOH at 289°C with a cover gas of pure nitrogen, but cracking would not occur if cover gas of 95N₂-5H₂ was used. However

even with the cover gas containing H_2 , transgranular cracking would occur at applied anodic potentials 60 to 100 mV from the corrosion potential. In addition, Cels noted that the severity of cracking increased if the potential was cycled 40 to 80 mV anodic to the corrosion potential rather than held a constant value [14].

The metallurgical condition of Incoloy-800 appears to be a major factor in the susceptibility of the alloy to caustic cracking. It had been shown [6] that heat treating the mill-annealed alloy to produce the Grade 2 condition or cold-working resulted in a significant increase in stress corrosion resistance. In the present studies, it was found that the alloy heat treated to produce the Grade 1 condition was far more resistant to caustic cracking than the alloy in Grade 2 condition. Figure 10 shows the appearance of the Grade 1 specimen after test, compared to a similar untested specimen. An argon overpressure and a 5 percent NaOH solution was used in the experiment. Straining electrode experiments indicated that the Grade 1 condition could be cracked in 10 percent NaOH. However, a high stress greater than 356 MPa (51 ksi) and a high potential (0.200 V from the rest potential) were required before cracking became obvious. In comparison, the Grade 2 condition failed completely by transgranular stress corrosion in 10 percent NaOH at 317 MPa (46 ksi).

By a combination of SSRT and straining electrode tests, we have seen major variations of the stress corrosion behavior of Incoloy-800 in different metallurgical conditions. In addition, the variations were determined rapidly compared to the constant load technique.

We may postulate that dislocation structure, grain size effects, types of grain boundaries, or the presence or absence of solute segregates may account for the difference in stress corrosion behavior. However, once the behavior is established by SSRT and straining electrode tests, other fundamental microstructural studies must be performed to determine the subtle differences that cause the variation of response.

Summary

The slow strain-rate and the straining electrode techniques were shown to be valuable tools in rapidly evaluating alloys of construction for LMFBR steam generator applications in environments that simulate a badly faulted local chemistry.

In the case of $2\frac{1}{4}Cr-1Mo$ steel, the alloy in different metallurgical conditions which may arise from mechanical fabrication procedures, heat treatments, or welding operations was found to be immune to stress corrosion in caustic solutions at 316°C. At a lower temperature (232°C), testing by SSRT resulted in failure by intergranular and transgranular SCC.

Incoloy-800 tested by SSRT and the straining electrode technique was shown to crack in caustic solutions at 316°C. The susceptibility of the

alloy was a function of the metallurgical condition. The cold-worked and Grade 1 conditions were more resistant to caustic cracking than the Grade 2 condition. For Incoloy-800, the oxidizing potential can have a significant effect on the material response to caustic cracking. For example, while the Grade 1 condition did not suffer stress corrosion when tested by SSRT at the natural corrosion potential and by the straining electrode techniques at a slight oxidizing potential, a straining electrode test at 0.200 V from the corrosion potential resulted in the formation of numerous stress corrosion cracks.

Acknowledgments

The author wishes to acknowledge J. E. Weber and A. N. Bornstein for their assistance in the experiments. Appreciation is also extended to K. D. Challenger and C. N. Spalaris for their advice and support. These studies were funded by the Energy Research and Development Administration under Contract E(04-3)-893 Task 18.

References

- [1] Indig, M. E., "Review of Stress Corrosion Cracking Incident in Nuclear and Fossil-Fired Power Plants," GE-FBRD, General Electric Company, June 1972 (NEDG-13854).
- [2] Bush, S. H. and Dillon, R. L., "Stress Corrosion in Nuclear Systems," *Proceedings*, International Conference on Stress Corrosion Cracking and Hydrogen Embrittlement of Iron Base Alloys, Firminy, France, June 1973.
- [3] Weeks, J. R., "Corrosion of Steam Generator Tubing in Operating Pressurized Water Reactors," *Corrosion Problems in Energy Conversion and Generation*, The Electrochemical Society, Princeton, N. J., 1974.
- [4] Humphries, M. J. and Parkins, R. N., *Corrosion Science*, Vol. 7, 1967, p. 747.
- [5] Parkins, R. N., *Proceedings*, Conference on Fundamental Aspects of Stress Corrosion Cracking, National Association of Corrosion Engineers, Houston, Tex., 1969, p. 361.
- [6] Parkins, R. N., *The Theory of Stress Corrosion Cracking in Alloys*, J. C. Scully, Ed., North Atlantic Treaty Organization, Scientific Affairs Division, Brussels, 1971, p. 499.
- [7] Hoar, T. P. and Hines, T. G., *Journal of the Iron and Steel Institute*, Vol. 182, 1956, p. 124.
- [8] Dahl, L., Dahlgren, T., and Lagmyr, N., *Proceedings*, International Conference on High Temperature High Pressure Electrochemistry in Aqueous Solutions, NACE-3, National Association of Corrosion Engineers, University of Surrey, England, Jan. 1973.
- [9] Indig, M. E., "Caustic Cracking in Hot Aqueous and Superheated Steam Environments," *Corrosion Problems in Energy Conversion and Generation*, The Electrochemical Society, Princeton, N. J., 1974.
- [10] Indig, M. E., "Stress Corrosion Studies for 2¼Cr-1Mo Steel," Conference on Ferritic Steels for Fast Reactor Steam Generators, British Nuclear Energy Society, June 1977.
- [11] Bohnenkamp, K., "Caustic Cracking of Mild Steel," *Proceedings*, Conference on Fundamental Aspects of Stress Corrosion Cracking, NACE-1, National Association of Corrosion Engineers, Ohio State University, September 1967.
- [12] Diegle, R. B. and Vermilyea, D. A., *Corrosion*, Vol. 32, 1976, p. 411.
- [13] Theus, G. J., *Nuclear Technology*, Vol. 28, 1976, p. 388.
- [14] Cels, J. R., *Journal of the Electrochemical Society*, Vol. 123, 1976, p. 152.

R. S. Ondrejcin¹

Stress Corrosion Cracking Test with Slow Strain Rate and Constant Current

REFERENCE: Ondrejcin, R. S., "Stress Corrosion Cracking Test with Slow Strain Rate and Constant Current," *Stress Corrosion Cracking—The Slow Strain-Rate Technique, ASTM STP 665*, G. M. Ugiansky and J. H. Payer, Eds., American Society for Testing and Materials, 1979, pp. 203-221.

ABSTRACT: A rapid electrochemical tension test was developed for evaluating stress corrosion crack initiation in carbon steel. Constant anodic current was imposed on smooth-bar tension specimens as the specimens were slowly strained to fracture at 1.3×10^{-6} /s. Equivalent results were obtained for the following ductility properties measured: uniform elongation, total elongation, and reduction of area. Total elongation was chosen as the index for stress corrosion crack initiation. An equation was developed that allowed calculation of total elongation of specimens in electrolytes (test solutions) with composition ranges of 1.5 to 5.5 *M* nitrate, 0 to 3.5 *M* nitrite, and 0 to 5.0 *M* hydroxide, and a temperature range of 50 to 100°C. A minimum of 13 percent total elongation was selected to indicate the possible initiation of cracking in A 285-B steel alloy.

The test was used to evaluate relative aggressiveness of synthetic nuclear wastes on A 285-B carbon steel and the relative resistances of several steels to given solution compositions. Test results formed one of the bases for setting temperature and concentration limits for several ions in nuclear wastes that are stored in carbon steel tanks at the Savannah River Plant.

KEY WORDS: stress corrosion cracking, nitrate stress corrosion, stress corrosion cracking tests, strain rate, constant current, mechanical tests, carbon steels, waste disposal, radioactive wastes, application of mathematics

Introduction

Background

The carbon steel that is the main structural material in tanks used for

¹Staff chemist, Savannah River Laboratory, E. I. du Pont de Nemours and Company, Aiken, S.C. 29801.

storing wastes from nuclear fuel reprocessing at the Savannah River Plant (SRP) is susceptible to stress corrosion cracking (SCC) in nitrate or hydroxide solutions. The primary carbon steel shells of 9 of 16 older, nonstress relieved, double-shell tanks at SRP have leaked. Stress corrosion cracking was identified [1]² as the cause of leaks in 5 tanks and is assumed to be the cause of leaks in the other 4. Cracks normally have sealed themselves when the leaking liquid, an alkaline nitrate solution, dried on the exterior wall of the primary container. The 7 newest waste tanks constructed at SRP were heat treated to relieve stresses accumulated during construction, thereby minimizing potential for SCC, and no leaks have occurred in these 7 stress-relieved, double-shell tanks.

Standard stress corrosion specimens, such as welded or notched, three-point loaded, or U-bend, have not cracked in the actual alkaline nitrate wastes, although waste tanks containing apparently equivalent solutions cracked after 0.5 to 15 years. The absence of specimen cracking was assumed to mean that standard specimens were not sufficiently susceptible to cracking in a reasonable period of time. Therefore, a test was required to evaluate the effects of a large number of variables, including temperature and the concentrations of many ions in the waste solutions, on initiation of SCC. These test results helped to define operating limits of temperature and composition of waste solution so as to avoid further SCC of waste tanks.

Corrosion of Specimens Undergoing Strain

Tests of specimens undergoing strain, either with or without electrochemical control, have been used by a number of investigators to study the mechanism of stress corrosion, often for carbon steel. Early stress corrosion experiments showed the importance of plastic flow and the more rapid attack at grain boundaries in the presence of stress [2]. Susceptibility of carbon steel to stress corrosion by migration of impurities to and from grain boundaries also has been tested by the slow strain-rate techniques [3]. Grain boundaries that were pure underwent attack because of high free energy, but commercial steels with high-impurity grain boundaries were attacked more rapidly because the impurities made the grain boundaries anodic. Slow strain-rate stress corrosion tests verified the prediction of polarization measurements that the carbonate ion would attack carbon steel intergranularly, and the potential and concentration ranges where cracking occurred were determined [4].

Strain rate appears to have a direct influence on crack velocity in iron alloys [5]. In titanium alloy systems, the effect of low strain rate on cracking susceptibility has been shown to depend on repassivation kinetics [6].

²The italic numbers in brackets refer to the list of references appended to this paper.

Experiments with high constant strain rates have been used to study the anodic behavior of mild steel in nitrate solutions [7]. High anodic current densities were observed when the oxide film fractured under controlled potential. At low strain rates, stress corrosion "cracks" were observed.

Stress Corrosion in the Presence of Slow Strain Rate and Constant Current

The slow strain-rate test described in this paper was devised to study the corrosive effect of complex nuclear waste solutions on carbon steel. Electrochemical control was used to accelerate the attack. Current was controlled, rather than potential, because corrosion requires current flow rather than potential difference. Arguments have been already advanced to the effect that SCC is caused by a current flow over a given period of time, that is, by a given quantity of current, and that stress corrosion is also related to the time required for passivation [8].

Test Procedures and Equipment

Polarization curves were determined with a potentiostat combined with a *x-y* recorder. Data points for the curves were normally determined at 100°C, and occasionally at 50 or 75°C. A standard polarization cell prepared in accordance with ASTM Standard Reference Method For Making Potentiostatic and Potentiodynamic Anodic Polarization Measurements was used for nonradioactive solutions. A smaller cell, similar in design and cross checked against the standard cell, was used for radioactive solutions.

The special electrochemical tension test cell was machined from trifluoroethylene resin as shown in Fig. 1. The cell contains a standard tension specimen with a 31.7-mm gage length immersed in the test solution (electrolyte). The load is applied with a hard beam machine at an initial strain rate of 1.3×10^{-6} /s. A platinum counter electrode surrounds the specimen. The cell is connected to a saturated calomel reference electrode by a string salt bridge which enters the top of the cell and is positioned within 2 mm of the specimen. The other end of the bridge is immersed in a beaker containing the test solution and the reference electrode at room temperature. The reference electrode lead is the second connection to the potentiostat, and the lead from the threaded portion of the specimen is the third. An environmental chamber controls the temperature of the specimen, cell, and solution to within $\pm 1^\circ\text{C}$. Change in solution concentration by evaporation during testing is prevented by a total-reflux condenser connected to the cell.

Current flow between the counter electrode (platinum sheet) and working electrode (tension specimen) is controlled by the potentiostat to within about 1 percent of the preset value. Values either 0.20 or 0.5 mA/cm² were selected because they represent currents produced by small potential

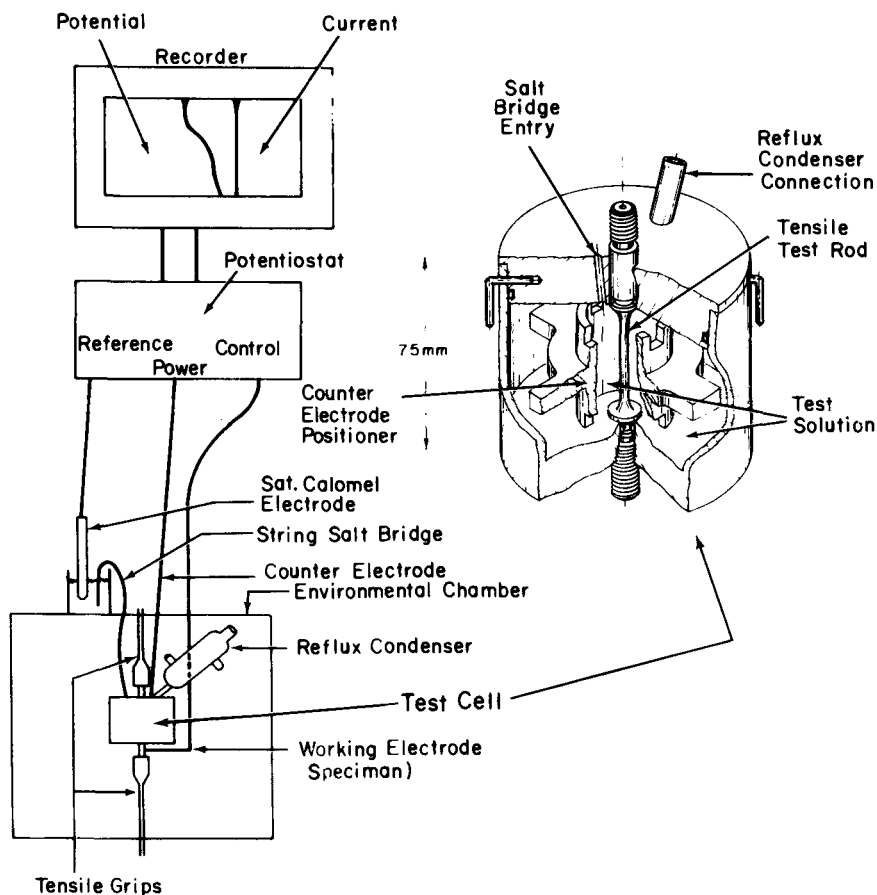


FIG. 1—Electrochemical tension test equipment (cell material is trifluoroethylene resin).

differences as shown by polarization curves such as those in Fig. 2. A current value was chosen that represented <50 percent of the active portion of the polarization curve. Curves were run at 10-mV/min scan rates. Current, rather than potential, was chosen for these tests for the reason given in the section "Stress Corrosion in the Presence of Slow Strain Rate and Constant Current." These currents were based on polarization curves which were developed for the steel in various actual waste supernates.

The SCC tests were performed on specimens machined from a single plate of ASTM A 285-B steel originally used in the fabrication of one of the SRP nuclear waste tanks. This grade is a hot-rolled, plain carbon steel of pressure vessel quality. The microstructure of the steel was primarily ferrite with small amounts of pearlite. Grain size was about 50 μm di-

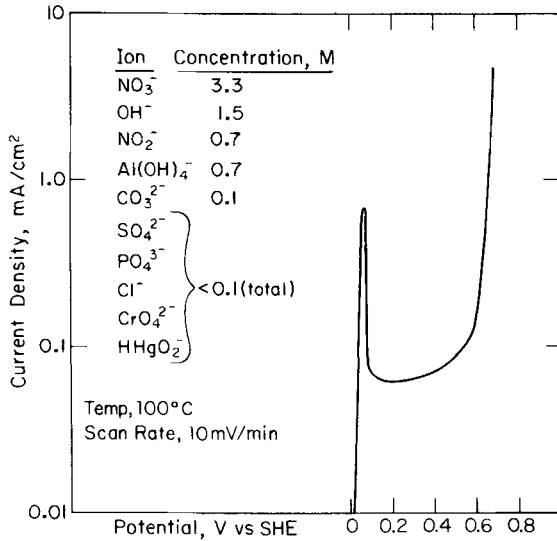


FIG. 2—Anodic potentiodynamic polarization of A 285-B carbon steel in HLW tank 32H.

ameter. The composition of the steel is given in Table 1. Longitudinal tension specimens, as shown in Fig. 3, were machined from this steel to a 63-rms surface finish. Prior to testing, specimens were vapor degreased in benzene, rinsed in acetone, and dried in air.

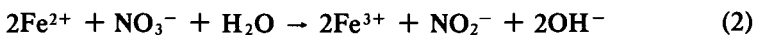
Experimental Work

Corrosion Reactions and Effects of Potential

Corrosion reactions that occur during cracking of carbon steel in nitrate solutions are not agreed upon [7,9,10]. Steel is proposed to react according to



by Engell and Baumel [9] or, after oxidation of the iron to ferrous ion, by the reaction



as proposed by Smialowski et al [10], or anodically by the reaction

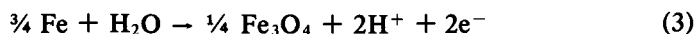


TABLE 1—ASTM A 285-B carbon steel.

	Weight %				Ultimate Tensile Strength, kpsi (MPa)	Elongation, %
	Mn	C	P	S		
Specification	0.90 ^a	0.22 ^a	0.025 ^a	0.045 ^a	50 to 60 (434 to 521)	25 ^b
Actual analysis	0.49	0.12	0.010	0.015	55.4 (481)	31

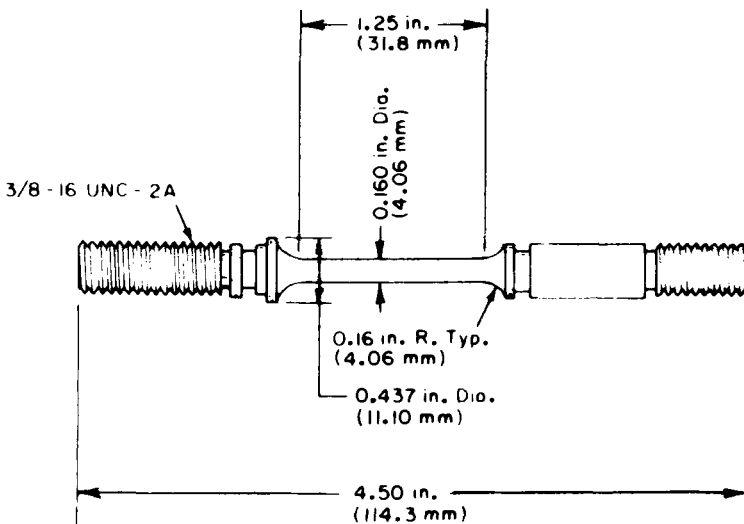
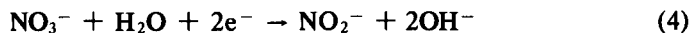
^a Maximum.^b Minimum.

FIG. 3—Tension specimen.

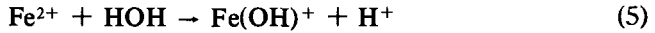
According to Hoar and Galvele [7], at least two cathodic reactions probably take place, with the result being



On the basis of Reactions 3 and 4, the H^+ produced in the anodic reaction and the OH^- produced in the cathodic reaction may react, depending on the distances between the anode and cathode. If the electrode surfaces are separated, for example, if the anode is the tip of a crack or the bottom of a pit, and the cathode is the wall of the crack or pit, the anode becomes more acidic and the cathode more basic.

Stress corrosion work at the Naval Research Laboratory (NRL) has shown that during cracking of a number of high-strength steels, the tip of

the crack becomes acidic [11], as inferred from Reaction 3. Measurements showed the solutions at the crack tip consistently to have a pH of ~ 3 . Sandoz et al [11] concluded that the pH was controlled by the hydrolysis of the ferrous ion, that is, that the reaction



was controlling.

Parkins and Usher [12] showed that in nitrate solutions the severity of cracking increases according to the cation series $\text{Na}^+ < \text{Ca}^{2+} < \text{NH}_4^+$ [12]. In addition to causing greater cracking, this series is also one of increasing acidity due to cation hydrolysis which causes the open-circuit potential of the steel to become more and more anodic [7]. Increasing anodic potential in the active portion of the polarization curve either increases anodic current density or stimulates cathodic reactions.

Corrosion, the precursor to SCC, is normally under the control of cathodic reactions in aqueous solutions [13] and is relatively unaffected by minor changes in steel composition. The rate is influenced by the reduction kinetics and diffusion of reactants to cathodic sites. Nitrate, which takes part in the cathodic reaction, is reduced more easily as the solution becomes more acidic.

To reduce nitrate SCC, the best theoretical approach, on the basis of Reactions 1 through 4 and information in the previous two paragraphs, is to reduce the cathodic reaction. The cathodic reaction can be reduced either by increasing the concentration of OH^- alone or by increasing the OH^- and NO_2^- concentrations together depending on whose reaction you accept.

Investigation of Corrosion of SRP Waste Tanks

To determine whether cracking of SRP waste tanks was actually caused by nitrate corrosion, the open-circuit potentials of 4 SRP waste tanks containing alkaline nitrate radioactive wastes were measured against saturated calomel electrodes (SCE). The potentials were -0.44 , -0.12 , -0.085 , and -0.064 V. These potentials fall generally in the range for cracking in pure 4 M sodium nitrate (-0.30 to $+1.10$ V) [14] rather than for cracking in hydroxide, which would be expected to occur in the range -0.90 to -1.04 V [15].

Waste Solution Compositions—A large number of supernate solutions were taken from 14 SRP waste tanks and analyzed to determine general compositions and specifically the nitrate concentration. The solutions represented about 42 million litres (11 million gallons) of radioactive waste. Measured concentration ranges are shown in Table 2 and the actual compositions of test solutions are given in Table 3.

TABLE 2—Ionic concentrations of SRP waste supernates.

Ion	Concentration Range, <i>M</i>
NO ₃ ⁻	1.6 to 4.5
NO ₂ ⁻	0.5 to 3.2
OH ⁻	0.8 to 6.3
Al(OH) ₄ ⁻	0.4 to 1.6
CO ₃ ²⁻	<0.1 to 0.3
SO ₄ ²⁻	0.02 to 0.20
PO ₄ ³⁻	0.01 to 0.08
Cl ⁻	0.005 to 0.11
CrO ₄ ²⁻	0.001 to 0.009
F ⁻	0.001 to 0.004

Polarization Curves—The effects causing stress corrosion in SRP waste supernates are expected to be maximized in a tension test under electrochemical control. Stress is high and continuously increasing because the specimen is being strained continuously. Electrochemical control is expected to cause crack initiation at locations where it would occur without control and also to accelerate the process. Initiation of mild steel cracking by nitrate solutions is believed to involve carbon in the steel [16]. Carbon, when present either in solid solution or as iron carbide (Fe₃C), acts as an efficient cathode. This cathodic action stimulates anodic dissolution very close to the cathode, forming a micropit or trench, the precursor of a crack. Anodic dissolution of the grain boundaries also can be stimulated by electrochemical control if an anodic current flows through a specimen.

Current flows that can be expected from metals in solution are defined by anodic polarization curves. In certain solutions where the metal shows an active-passive transition, such as mild steel in some SRP wastes, small potential differences can cause relatively high current flows, as seen in Fig. 2.

Polarization curves run in actual alkaline nitrate wastes in shielded facilities showed that carbon steel normally acted as an active-passive metal. These curves and curves subsequently obtained with synthetic wastes are shown in Fig. 4. The curves for synthetic and actual wastes were so close together that the two solutions would be expected to cause equivalent corrosion. Therefore, synthetic solutions were used in further testing. The use of synthetic wastes provided a less difficult, faster, and less expensive approach in testing.

Electrochemical Tension Test

Plackett-Burman Series [17]—To determine which independent variables were most effective in causing nitrate SCC, a statistically designed series of

TABLE 3—Analyses of synthetic waste supernates.

Solution, Designation	Ionic Concentration, M											Hg, µg/ml
	NO ₃ ⁻	NO ₂ ⁻	OH ⁻	Al(OH) ₄ ⁻	CO ₃ ²⁻	SO ₄ ²⁻	PO ₄ ³⁻	Cl ⁻	CrO ₄ ²⁻			
H9 Salt	1.9	3.2	2.8	1.6	0.10	0.02	0.05	0.03	0.003			130
221-F Purex	2.9	0.0	0.8	0.5	0.0	0.40	0.0	ND ^a	0.01			ND
221-H HM	4.8	0.0	0.3	1.5	0.0	0.04	0.0	ND	0.00			ND
H Purex ^b	7.4	0.0	0.5	0.0	0.0	0.28	0.0	0.0	0.0			0.0
H11, not evaporated	3.6	1.2	1.5	0.6	0.01	0.03	0.0	ND	0.004			500
H12, not evaporated	3.0	1.2	1.4	0.4	0.07	0.04	0.0	ND	0.002			200
H13, not evaporated	3.7	0.25	1.4	0.16	0.06	0.10	0.0	ND	0.001			ND
H32, not evaporated	3.3	0.7	1.5	0.7	0.10	0.07	0.0	ND	0.002			260

^a Not determined.

^b A hypothetical composition calculated from the process flow sheet. All other compositions based on chemical analyses of actual solutions.

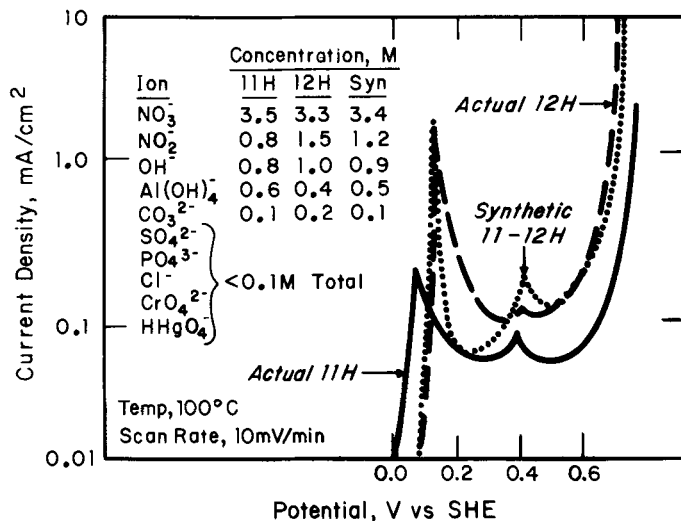


FIG. 4—Anodic potentiodynamic polarization of A 285-B carbon steel in SRP water supernate.

experiments, known as the Plackett-Burman series, was performed using the electrochemical tension test described above. This experimental design is generally used for screening a variable space in selected portions of a 2^n factorial design where one variable is changed at a time with a high and a low value for each. As a screening design, the Plackett-Burman series has the advantage that a small number of experiments are required to investigate a large number of independent variables; it has the disadvantage of eliminating interaction effects. Thus, the possible combined effect of nitrite or hydroxide ions to reduce SCC predicted by Reactions 1 through 4 would not be seen.

Because many independent variables can affect the cracking, the Plackett-Burman test series included seven independent variables: temperature and six anionic concentrations. This approach required only 12 experiments rather than 128 for a two-level 2^n factorial design. The variables are shown in Table 4.

Four dependent variables, ultimate tensile strength (UTS) and three measures of ductility, were chosen as values that might be affected by the independent variables based on a stress-strain curve.

Plackett-Burman Results—Analyses of the Plackett-Burman data showed that temperature and NO₃⁻ concentration stood out above interactions and experimental error in affecting ductility parameters (Table 5). Calculated minimum factor effects had to be exceeded by each independent variable to be correlated at the 90 percent confidence level with the de-

TABLE 4—Plackett-Burman variables and constants.

Independent Variables	Values ^a		Dependent Variables ^b	Constants ^{a,c}	
	Low	High			
Temperature, °C	50	100	UTS	CO ₃ ²⁻	0.1
NO ₃ ⁻	1.5	5.5	TE	SO ₄ ²⁻	0.1
NO ₂ ⁻	0	3.5	UE	PO ₄ ³⁻	0.05
Al(OH) ₄ ⁻	0	1.6	RA	CrO ₄ ²⁻	0.005
OH ⁻	0	6.0			
Cl ⁻	0.005	0.15			
HHgO ₂ ⁻	0	0.002			

^a All ionic values are molar concentrations.

^b UTS = ultimate tensile strength, T = total, E = elongation, U = uniform, and RA = reduction of area.

^c Added to simulate actual waste.

TABLE 5—Plackett-Burman factor effects.

Independent Variables	Dependent Variable Effects			
	Total Elongation	Uniform Elongation	Reduction in Area	Ultimate Tensile Strength
Temperature	6.2	4.6	28.7	5.4
[NO ₃ ⁻]	5.9	4.3	28.0	6.2
[NO ₂ ⁻]	1.3	1.7	5.3	3.3
[Al(OH) ₄ ⁻]	2.5	1.4	9.7	7.6
[OH ⁻]	2.7	2.2	9.7	5.6
[Cl ⁻]	1.0	1.6	3.7	6.4
[HHgO ₂ ⁻]	0.9	0.3	7.0	4.0
Minimum factor effect	3.6	3.2	20.2	11.9

pendent variable. All three ductility (dependent) variables correlated with temperature and NO₃⁻ concentration. However, no statistically significant correlation was found between UTS and any of the independent variables. The large minimum factor effect (12) required for correlation of UTS with any independent variable versus the small minimum factor effect (3 for elongation) required for correlation indicate that an apparently inflated experimental error in UTS and reduction in area was caused by ion interactions. The minimum factor effect required for correlation would be about 4 for both strength and ductility correlations, if its value were due only to experimental error.

Hydroxide concentration was believed to be the most likely ion to inflate the minimum factor effect required for correlation of strength with independent variables. To evaluate the hydroxide effect, a known inhibitor for nitrate stress corrosion, UTS, was measured in a series of electrochemical tension tests. These strength data are plotted in Fig. 5 against OH⁻ concentration. Obviously there is a hydroxide effect; as hydroxide concen-

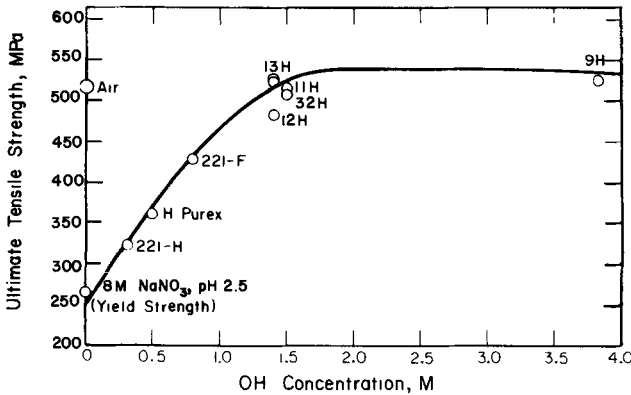


FIG. 5—Electrochemical tension test: variation of strength of 285-B carbon steel with hydroxide concentration, 100°C, 0.2 mA/cm² (see Table 3).

tration increases, so does UTS. The lowest value observed was for high nitrate that was acidified with nitric acid. The next three were synthetic solutions representing fresh wastes from fuel reprocessing facilities and a hypothetical waste composition (H Purex) based on flow sheet calculations. The others were representative of wastes from actual waste tanks.

Metallographic examination of the cracked specimens showed that the failures were intergranular stress corrosion cracks that would be typical of nitrate stress corrosion (Fig. 6). The cracks contained some loose grains and corrosion products.

Fractographs showed that greatest damage occurred when the nitrate solutions contained the lowest concentrations of NO₂⁻ and OH⁻. (Nitrite is a radiolysis product of nitrate.) Figure 7 shows that the specimen in 221-F Purex (total NO₂⁻ and OH⁻ of 0.8 M) cracked along the gage length and failed with almost no reduction of area. The other two specimens (total NO₂⁻ and OH⁻ ≥ 1.6 M) did not crack and showed more ductility with a shear fracture profile. All fracture surfaces were severely corroded; in the 221-F Purex specimen, intergranular separations were also prevalent and fracture surface characteristics showed less ductility than other specimens. The other two specimens showed dimples resulting from micovoid formation typically of ductile fracture.

Box-Behnkin Series—The simultaneous effects of temperature, nitrate, nitrite, and hydroxide on strength and ductility were systematically evaluated using a Box-Behnkin series of experiments [18]. The final result of this series of experiments is a response surface equation that correlates a dependent variable, such as ductility, to a series of independent variables, such as ionic concentrations. With independent variables specified, the dependent variable can be calculated once the equation is established.

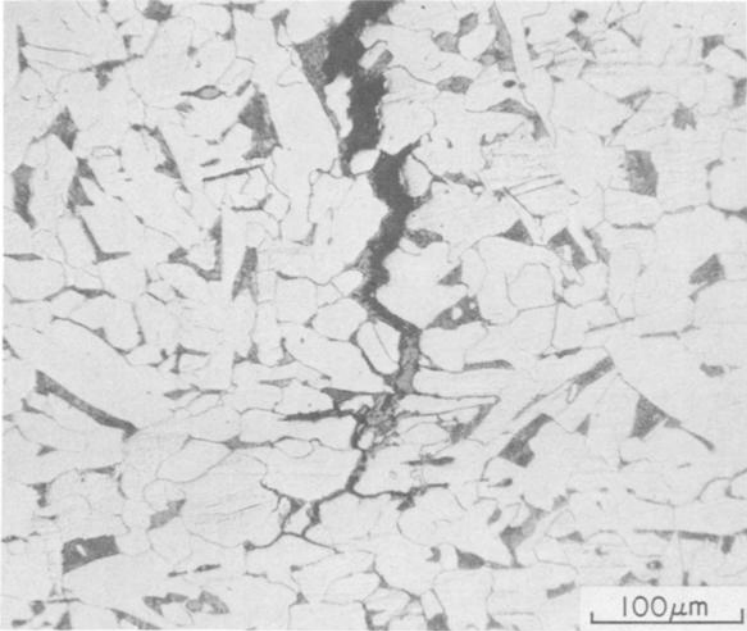


FIG. 6—Intergranular cracking of A 285-B steel in constant-current tension test.

The usual method of varying each variable individually (factorial design) to obtain an equation would have required prohibitively extensive testing as seen in Table 6. The conditions selected for the experimental series are shown in Table 7.

Temperature and nitrite were chosen on the basis of the Plackett-Burman series of experiments, and hydroxide and nitrite were chosen from actual test data (Fig. 5) and previous work. Tests in appropriate combinations of the low, mean, and high values of the independent variables were run. The combinations were assigned to each test according to the standard four-variable Box-Behnkin design; the corresponding tension tests were performed in random order.

In the tests, concentrations of constituents other than NO_3^- , NO_2^- , and OH^- were held constant. One of the others, aluminate, is a major waste solution constituent and is known to have a significant effect on caustic cracking, probably because of the high hydroxide concentration required to keep the aluminate in solution [19]. However, aluminate ion apparently has at most a minor effect in nitrate stress corrosion cracking. Of the minor constituents, SO_4^{2-} and Cl^- are often corroding agents and, therefore, could initiate the SCC sequence. Mercury changes the open-circuit potential of steel by 0.4 to 0.5 V in the positive direction and could

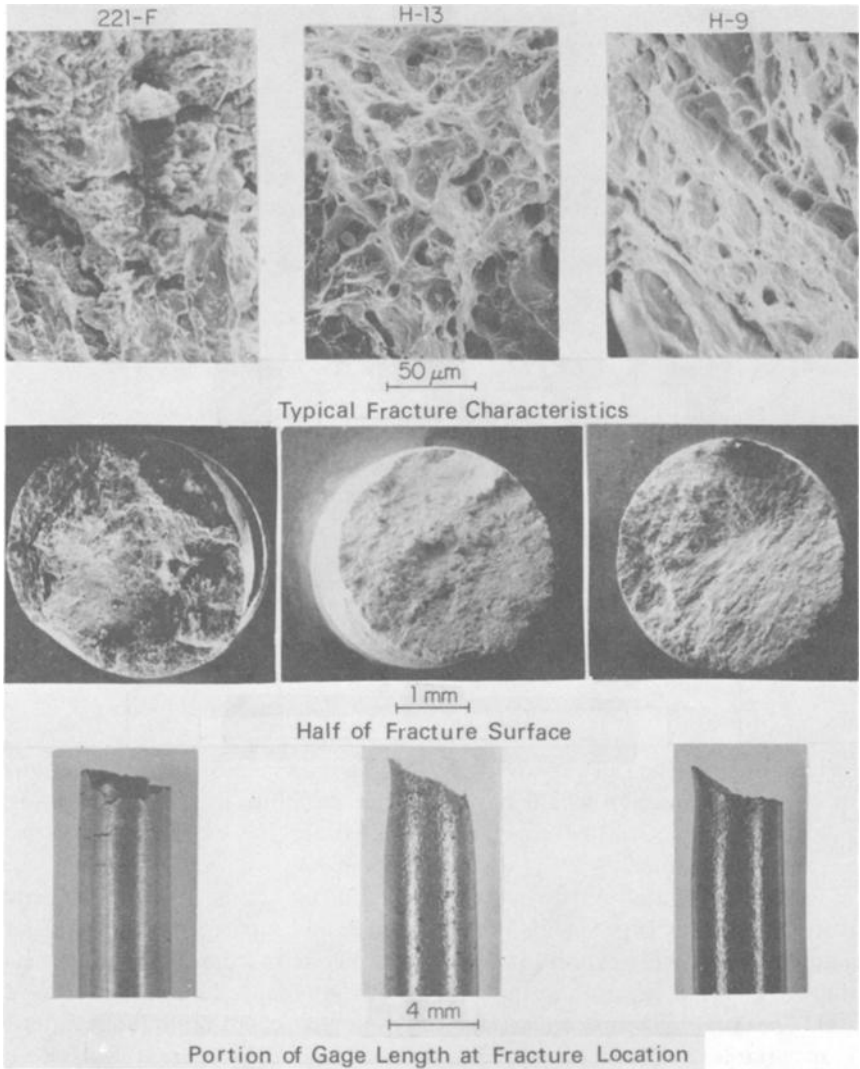


FIG. 7—Fracture characteristics of A 285-B steel in 0.2-mA/cm² tension test.

TABLE 6—Factorial and Box-Behnkin designs.

Independent Variables	Number of Experiments	
	Three-Level Factorial	Box-Behnkin Design
3	27	15
4	81	27
5	243	46

TABLE 7—Box-Behnkin conditions.

Independent Variables	Range	Dependent Variables	Constants ^a	
			Ion	Concentration, <i>M</i>
Temperature, °C	50 to 100	ultimate strength	Al(OH) ₄ ⁻	Saturated 0 to 1.5
NO ₃ ⁻ , <i>M</i>	1.5 to 5.5	total elongation	CO ₃ ²⁻	0.1
NO ₂ ⁻ , <i>N</i>	0 to 3.5	uniform elongation	SO ₄ ²⁻	0.1
OH ⁻ , <i>M</i>	0 to 5.0	reduction of area	PO ₄ ³⁻	0.05
			CrO ₄ ²⁻	0.005
			HHgO ₂ ⁻	0.002

^a Added to simulate actual wastes.

put the steel in the potential range for nitrate cracking. The wastes also contain inhibitors such as PO₄³⁻ and CrO₄²⁻, some at high enough concentrations to inhibit corrosion in water. Therefore, these ions were included in the test solutions at a constant level which simulates the concentrations routinely found in waste solutions.

For the data reduction, a multiple regression, least squares program with the following features was used: (1) a full quadratic model, (2) an augmented correlation matrix to show correlation among all independent and dependent variables, and (3) analyses of residuals to reject results with large errors. The program also could plot dependent variables against each other to test whether the dependent variables measured the same or different effects. Other output data included equations representing the dependent variables and contour maps of the fitted dependent variables.

To improve the precision of the equations describing the response surfaces, especially in certain sections of the variable space, the Box-Behnkin data (27 tests) were combined with the Plackett-Burman data (12 tests) and five additional experiments were completed. Only one result of the 44 was rejected on the basis of the computer analysis of residuals; the remaining were used to establish the equations for the response surface. The 43 data points were significant at the 95 percent confidence level based on the "t"-test.

Cross plots of the four dependent variables showed that only two responses were present, one for UTS and one for ductility (total elongation, uniform elongation, or reduction of area). Thus, the same information would be obtained regardless of which ductility measurement was used. The correlations are shown in Table 8.

The first response surface equation correlated UTS with changes in NO₃⁻ and OH⁻ concentration. The second equation for ductility was similar to the first, but more complex. Ductility correlated with tempera-

TABLE 8—*Dependent variable correlations.*

Plot ^a	Correlation Coefficient
UE versus TE	0.9
RA versus TE	0.8
UE versus RA	0.7
UE versus UTS	0.5
TE versus UTS	0.5
RA versus UTS	0.4

^a U = uniform, T = total, E = elongation, RA = reduction of area, and UTS = ultimate tensile strength.

ture, nitrate, nitrite, and hydroxide; the effect of the nitrate ion concentration depended on temperature as well as on nitrite concentration.

The ductility response was chosen as the more important one because stress corrosion is a phenomenon in which normally ductile material behaves in a brittle (less ductile) manner. The equation was developed specifically for total elongation because this is the simplest ductility property to measure in a tension test. The equation is a Taylor series restricted to second order. It is long (33 coefficients), but relatively simple to solve in that it only has linear, cross product, and quadratic terms of the four independent variables.

Correlation of Elongation to SCC

An elongation of 13 percent or less was selected to indicate the possible initiation of cracking for three separate, but related, reasons: (1) at <13 percent total elongation, the specimens were always intergranularly cracked at failure. Above this value, cracking was unusual and, if observed, always minor. (2) Evaluation of tensile data in air showed that 13 percent elongation was the limit of uniform elongation at elevated temperatures. (3) The 13 percent limit agreed with tests made by Donovan [20] on wedge-opening-loaded (WOL) specimens over a limited range of variables. The WOL specimens were tested at 97°C in 5.0 M NO₃⁻ solutions with 0 to 1.5 M NO₂⁻ and 0 to 1.5 M OH⁻; none of the minor constituents were added. This agreement is shown in Fig. 8. The WOL test differs from the electrochemical tension test in that it measures crack growth rather than crack initiation. There is disagreement as to the effect of nitrite at low hydroxide levels, which may be due to the minor ions added in the electrochemical tests. However, this portion of the data is not pertinent to waste tank operation, since hydroxide in waste solutions is >0.3 M.

The surface response relationship for elongation permits a rapid evaluation of whether SRP nuclear wastes might be expected to cause stress corrosion of carbon steels. The response equation is applicable in the four-

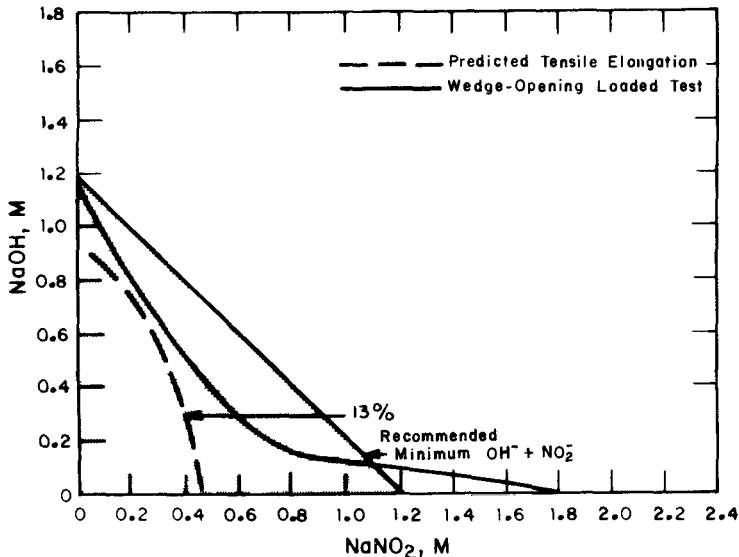


FIG. 8—Effect of NaNO_2 and NaOH on SCC of A 285-B steel in 5 M NaNO_3 at 97°C .

dimensional space enclosed by the variables including temperature (50 to 100°C), nitrate (1.5 to 5 M), nitrite (0 to 3.5 M), and hydroxide (0 to 5.0 M). The 13 percent elongation limit for the initiation of cracking defines a value below which cracks may initiate.

Applications

The test described in this paper was used to establish compositional and temperature limits for waste tanks that presently store alkaline nitrate nuclear wastes at SRP. It was also used to evaluate several varieties of carbon steel for tank construction. So far, four grades of mild steel have been examined and found to have increasing resistance to cracking in the order A 285-B, A-516-70, and A-537 Class I, as shown in Table 9. Little or no effect is seen due to normalization of the steel. The last two grades in the table also have improved fracture toughness and were specified for new tank construction beginning in 1976.

Conclusion

A slow strain-rate tension test with constant current control was developed. This test is intended to evaluate the initiation phase of nitrate SCC of carbon steel. Experiments performed with this test in statistical formats identified the four most important factors involved in nitrate stress corro-

TABLE 9—Mild steel elongation-electrochemical tension test.

Steel	Figure of Merit ^a
A 285-B	50
A 516-70	60
A 516-70N	57
A 537 Class I	65

^a Elongation in synthetic (F-8) solution at 0.2 mA/cm² and 100°C divided by elongation in air at room temperature expressed as a percent.

sion cracking of carbon steels. These factors are: temperature and the concentrations of nitrate, nitrite, and hydroxide ions. An equation for predicting total elongation of a steel from the four factors was developed. The total elongation of 13 percent or less was correlated to intergranular crack initiation. Predicted data at 13 percent elongation generally agreed with results of WOL tests performed in a portion of one plane of the tension test data limited by 5 M NaNO₃ and 97°C.

References

- [1] Holzworth, M. L. et al, *Materials Protection*, Vol. 7, 1968, pp. 36-38.
- [2] Henthorne, M. and Parkins, R. N., *Corrosion Science*, Vol. 6, 1966, p. 357.
- [3] Flis, J. and Scully, J. C., *Corrosion*, Vol. 24, 1968, p. 326.
- [4] Sutcliffe, J. M. et al, *Corrosion*, Vol. 28, 1972, p. 313.
- [5] Parkins, R. N. in *Stress Corrosion Cracking and Hydrogen Embrittlement of Iron Base Alloys*, R. D. McCright, J. E. Slater, and R. W. Staehle, Eds., National Association of Corrosion Engineers, Houston, Tex., to be published.
- [6] Scully, J. C. and Powell, D. T., *Corrosion Science*, Vol. 10, 1970, p. 719.
- [7] Hoar, T. P. and Galvele, J. R., *Corrosion Science*, Vol. 10, 1970, p. 211.
- [8] Scully, J. C., *Corrosion Science*, Vol. 15, 1975, p. 207.
- [9] Engell, H. J. and Bamel, A. in *Physical Metallurgy of Stress Corrosion Fracture*, T. N. Rhodin, Ed., Interscience Publishers, New York, 1959, p. 341.
- [10] Smialowski, M. and Szklarska-Smialowski, Z., *Corrosion*, Vol. 18, 1962, p. 1t.
- [11] Sandoz, G., Fujii, C. T., and Brown, B. F., *Corrosion Science*, Vol. 10, 1970, p. 839.
- [12] Parkins, R. N. and Usher, R. in *First International Congress on Metallic Corrosion*, Butterworth, London, 1969, p. 289.
- [13] Legault, R. A., Mori, S., and Leckie, H. P., *Corrosion*, Vol. 6, 1970, p. 121.
- [14] Humphries, M. J. and Parkins, R. N. in *Proceedings of Symposium—Fundamental Aspects of Stress Corrosion Cracking*, National Association of Corrosion Engineers, Houston, Tex., 1969, p. 389.
- [15] Reinoehl, J. E. and Berry, W. E., *Corrosion*, Vol. 28, 1972, p. 151.
- [16] Parkins, R. N. in *Proceedings of Symposium—Fundamental Aspects of Stress Corrosion Cracking*, National Association of Corrosion Engineers, Houston, Tex., 1969, p. 361.
- [17] Plackett, R. L. and Burman, J. P., *Biometrika*, Vol. 33, 1946, p. 505.
- [18] Box, G. E. P. and Behnkin, D. W., *Technometrics*, Vol. 2, 1960, p. 455-745.
- [19] *Encyclopedia of Chemical Technology*, R. E. Kirk and D. L. Othmer, Eds., Vol. 2, Wiley, New York, 1963, p. 6.
- [20] Donovan, J. A., *Transactions*, American Nuclear Society, Vol. 21, 1975, p. 266.

DISCUSSION

*R. B. Diegle*¹—Due to the presence of a layer of sludge of precipitated chemicals on the tank bottoms which may cause local variability in temperature and electrode potential, is it possible that your experiments did not closely simulate the electrochemical conditions at the bottom of the tanks?

Also, in light of the fact that SCC in nitrate and hydroxide solutions is potential dependent, why wasn't potentiostatic rather than galvanostatic control used on the specimens?

R. S. Ondrejcin (author's closure)—The author believes the electrochemical conditions in the sludge were simulated reasonably well. Analyses of dried sludge showed that its composition was about 70 weight percent salt and 30 weight percent insolubles. Therefore the sludge is primarily interstitial liquid rather than insoluble solids. Analyses of both the interstitial liquid and the dried soluble salt showed relatively high nitrite and low nitrate compositions compared to those of the bulk solution in the tanks. The precipitated fission products had radiolytically reduced some of the nitrate to nitrite in the liquid phase. The experimental matrix covered the ranges of nitrite and nitrate concentrations that were found. Since experimental results indicated that high nitrite was beneficial in preventing nitrate SCC, evaluation of the effects of insoluble solids was not added to the experimental program.

Concerning the second question, although most work on stress corrosion in hydroxide and nitrate is done potentiostatically, this work was done galvanostatically because oxidation-reduction requires a current flow. This is shown by the electron symbol used in any half-cell reaction. Usually most experimenters use a potential difference to produce this flow, but a potential difference does not guarantee current flow. Arguments already have been advanced to the effect that SCC is caused by a current flow over a given period of time, that is, by a given quantity of current. The possibility of stress corrosion is also related to the length of time the current can flow because of repassivation kinetics. For further information on this question, please refer to Scully, J. C., *Corrosion Science*, Vol. 15, 1975, p. 207.

¹Battelle's Columbus Laboratories, Columbus, Ohio.

J. H. Payer,¹ W. E. Berry,¹ and R. N. Parkins²

Application of Slow Strain-Rate Technique to Stress Corrosion Cracking of Pipeline Steel

REFERENCE: Payer, J. H., Berry, W. E., and Parkins, R. N., "Application of Slow Strain-Rate Technique to Stress Corrosion Cracking of Pipeline Steel," *Stress Corrosion Cracking—The Slow Strain-Rate Technique*, ASTM STP 665, G. M. Ugiansky and J. H. Payer, Eds., American Society for Testing and Materials, 1979, pp. 222-234.

ABSTRACT: Slow strain-rate technique has been used extensively in the study of stress corrosion cracking (SCC) of pipeline steel. Results were obtained to guide development and evaluation of SCC control methods and to study the SCC process. Application of the slow strain-rate technique led to determination of the specific environment of practical importance, identification of effective SCC inhibitors, determination of critical potential range for SCC, increased awareness of the major role of strain rate in the SCC process, and development of coatings incorporating SCC inhibitors.

KEY WORDS: stress corrosion cracking, carbonates, hydroxides, nitrates, carbon dioxide, carbon monoxide, inhibitors, potential, coatings, gas transmission, underground, cathodic protection, pipeline steel

Over the past decade, the slow strain rate technique has been used extensively to investigate stress corrosion cracking (SCC) of pipeline steel. Pipelines of interest are large diameter transmission pipelines for transport of natural gas. Research sponsored by the Pipeline Research Committee of the American Gas Association (AGA) (Project NG-18) was directed toward: (a) determination of controlling parameters of SCC, and (b) development and evaluation of methods for prevention and control of SCC of buried pipelines. Work reported here was done at Battelle's Columbus Laboratories and University of Newcastle Upon Tyne, and details of the overall SCC study were presented in proceedings of an AGA Symposium [1-4].³ The objective

¹Associate manager and manager, respectively, Battelle's Columbus Laboratories, Columbus, Ohio 43201.

²Head, Metallurgy Department, University of Newcastle Upon Tyne, England.

³The italic numbers in brackets refer to the list of references appended to this paper.

of this paper is to document the essential role of the slow strain-rate technique in accomplishing the program goals and to illustrate a variety of procedures having general applicability to the study of SCC.

Stress corrosion cracking of buried pipelines from external surfaces has been recognized as a possible cause of failure since 1965. Stress corrosion of pipeline steel is characterized by multiple, branched, intergranular cracks. Orientation of cracks, typically parallel to the pipe axis, is perpendicular to maximum tensile stress, and black deposit, primarily magnetite (Fe_3O_4), covers the crack surface. Stress corrosion occurs in pipeline steel meeting both mechanical and chemical specifications and is not related to minor changes within typical pipeline steel compositions.

A series of conditions must prevail simultaneously for SCC to occur, which include critical ranges of chemical environment, oxidizing condition, coating quality, stress, steel, and temperature [5]. If any of these conditions is outside of the critical range, SCC will not occur; this accounts for the limited occurrence of SCC on pipelines. A major accomplishment of the study on SCC of pipeline steel was identification of the chemical environment that promotes SCC. Slightly alkaline solutions of sodium carbonate and sodium bicarbonate, pH 8 to 10.5, promote SCC. These solutions are generated from dissolution of carbon dioxide from the soil in alkaline solutions at the pipeline surface resulting from cathodic protection currents.

Oxidizing condition is influenced by soil composition, cathodic protection current, steel surface, and coating quality. Laboratory results indicate that cathodic protection current and either corrosion products or hot-rolled mill scale on the pipe surface contribute to maintaining oxidizing condition within the critical potential range for SCC. Coating quality is relevant, as defects in the coating allow contact of ground waters with pipeline steel. It follows that failures are observed almost exclusively on the bottom of pipelines where coating defects are most prevalent and time of wetness is greatest.

The principal source of tensile stress in gas transmission pipelines is operating, internal gas pressure. Residual stresses can also contribute to total stress; however, the latter have not been found to make a major contribution. Failures have occurred for pipelines with operating pressures of 46 to 76 percent of specified minimum yield strength of the pipe. In addition to absolute value of stress, stress or pressure fluctuations can play an important role by promoting SCC more readily than static stress.⁴

While chemical composition within the normal range for pipeline steel does not have a major effect, minor alloy addition can affect SCC. In addition, SCC susceptibility is influenced by thermal-mechanical history. Other contributions of steel are associated with surface condition, that is, mill scale and decarburization.

⁴Unpublished results.

Increasing temperature increases SCC susceptibility by increasing crack growth rate, increasing the critical potential range for SCC, and favoring stability of potential in the cracking range.

The preceding description of SCC of pipelines is based upon a combination of results of field studies and laboratory experiments. The applications of slow strain-rate technique in determining the effects of environment, oxidizing condition, temperature, and strain rate on SCC are described here.

Equipment

The majority of constant strain-rate experiments were run with smooth, round tension specimens having a reduced test section 1.3 cm long by 2.5 mm diameter. Specimens were machined from sections of pipeline in which stress corrosion was observed in the field. Data are reported for various steel specimens, and all specimens met the specifications of American Petroleum Institute (API) Grade X-52 steel. The specimens were oriented with their length in the longitudinal direction of the pipe. A strain rate of $2.5 \times 10^{-6}/s$ was used for all experiments except those series where effect of strain rate was investigated. Experimental procedures were described in detail previously [6].

Cells to contain the environments were glass or polymerized tetrafluoroethylene for nitrate and carbonate-bicarbonate solutions and polymerized tetrafluoroethylene for hydroxide solutions. A stainless steel cell capable of maintaining pressure to 2050 kg/mm² (700 psig) was used for carbon dioxide, carbon monoxide experiments. Potential was controlled with a platinum counter electrode and string bridge to an external reference saturated calomel electrode (SCE). Load was measured and recorded throughout each test.

In addition to uniaxial tensile experiments, fatigue precracked cantilever beam specimens were used. For these tests, the cantilever beam was pulled down at a constant rate after applying an initial load.

Metallography was used in all cases to determine whether SCC had occurred. A variety of parameters were used to express severity of SCC: time-to-failure, percent reduction of area, stress corrosion crack length, and crack velocity. All were found to be useful expressions. Crack velocity, while requiring some additional effort, was the most sensitive parameter in several instances.

Application of Slow Strain-Rate Technique

Effect of Environment

When SCC was first determined to be a cause of failure in gas transmission pipelines, the chemical solution promoting SCC was not known. The slow

strain-rate technique played a major role in identification of carbonate-bicarbonate solutions as the SCC environment [7]. Based upon analysis of solutions at the pipe surface in areas where SCC was observed, laboratory SCC experiments were carried out with pipeline steel in carbonate-bicarbonate solutions. Slow strain-rate tests readily provided SCC in short periods of time in these solutions, while constant load and constant strain tests resulted in SCC only after long periods of time and with considerable scatter in results.

The results of a study of carbonate-bicarbonate solutions over the range of pH 8 to 10.5 are shown in Fig. 1. Stress corrosion was observed for potential-pH combinations bounded by the two straight lines [2]. No SCC was observed outside of the cross-hatched area. As pH increased, the potential range over which SCC was observed decreased from over 200 mV (-0.4 to -0.6 V, SCE) in 2 N sodium bicarbonate (NaHCO_3), approximately pH 8, to 0 mV in 1 N sodium carbonate (Na_2CO_3), approximately pH 10.5. At potentials more active (negative) than those in the SCC range, pitting or no corrosion because of cathodic protection was observed. At potentials more noble (positive) than those in the SCC range, steel was protected by a stable passive film. The SCC region was determined by running a series of tests at constant potentials in each solution. Metallographic examination confirmed the occurrence or absence of SCC.

Having established carbonate-bicarbonate solutions to be the environments of interest, many chemicals were screened as SCC inhibitors for

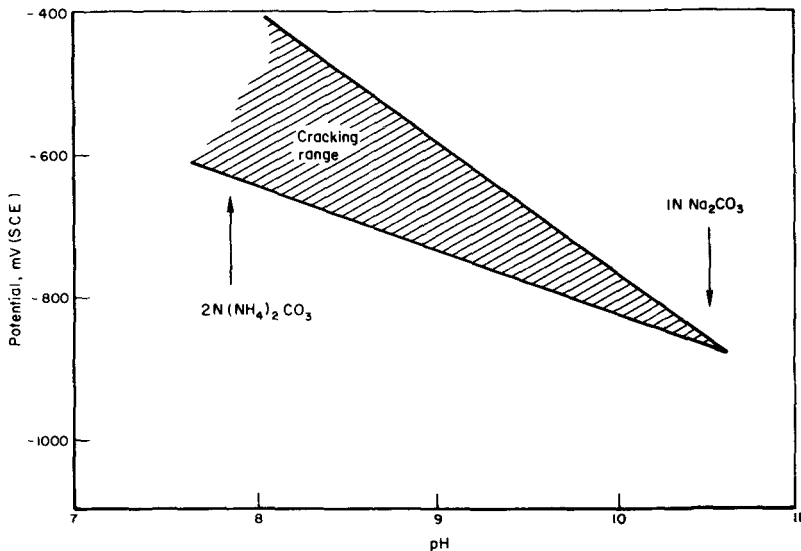


FIG. 1—Intergranular SCC range for pipeline steel in carbonate-bicarbonate solutions as a function of pH at 75°C.

steel using the slow strain-rate technique. Each chemical was added at a concentration of 1 weight percent to a $1\text{ N Na}_2\text{CO}_3 + 1\text{ N NaHCO}_3$ solution, and the effect on SCC severity was determined. Initial tests were run at the potential of most severe SCC in the base solution. Those chemicals found to be effective were tested over a wide potential range to determine if they were true inhibitors or acted by simply shifting the critical potential range for SCC. Those determined to be in the latter group were not considered further.

Several chromates, potassium silicate, and several phosphates were effective SCC inhibitors for steel in carbonate-bicarbonate [3]. The results for potassium dichromate ($\text{K}_2\text{Cr}_2\text{O}_7$) are shown in Fig. 2. The two solid curved lines bound results for the base solution. A loss of ductility reflected as lower percent reduction of area (ROA) indicates SCC. Stress corrosion was observed over the potential range of approximately -0.61 to -0.68 V (SCE) and was most severe at -0.65 V (SCE) . Solid points bounded by dashed lines are results for slow strain-rate tests with $\text{K}_2\text{Cr}_2\text{O}_7$ added. As indicated by increased ROAs and confirmed by metallography, SCC was inhibited and in this case completely prevented.

Chromates are in a category of "unsafe" corrosion inhibitors in that insufficient amounts to achieve inhibition in fact can accelerate corrosion. The series of experiments presented in Fig. 3 was run to determine whether chromates are unsafe SCC inhibitors. Beginning at 1 weight percent, concentration was reduced by factors of 10 down to 0.0001 weight percent (1 ppm). In no case was SCC severity increased by chromate additions and effective inhibition was observed at decreasing levels to 0.01 weight percent.

A further aspect of the use of inhibitors to control SCC of pipelines involved a study of the feasibility of incorporating SCC inhibitors in pipeline coating systems. Two types of slow strain-rate tests were used: leachant experiments and *in-situ* coating experiments. In the former, panels coated with

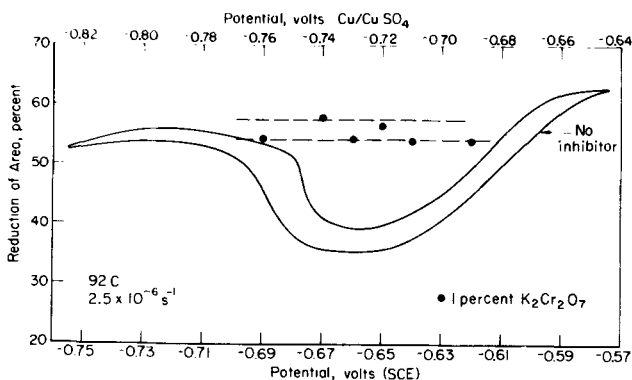


FIG. 2—Inhibiting effect of 1 weight percent potassium dichromate on SCC of pipeline steel in $1\text{ N Na}_2\text{CO}_3$ - 1 N NaHCO_3 .

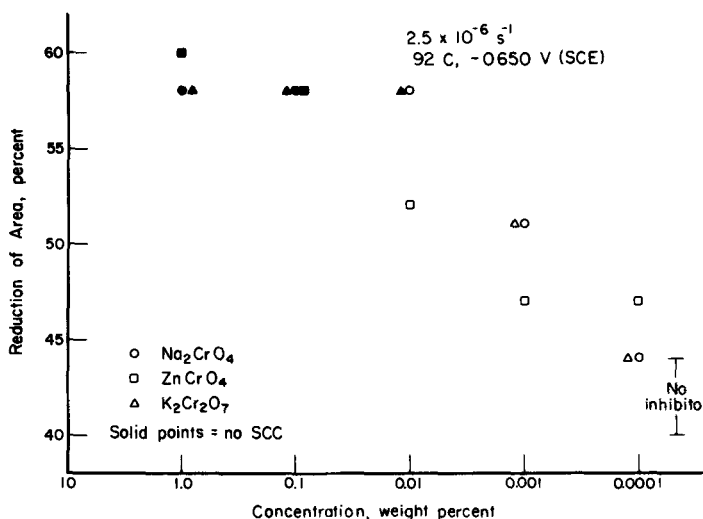


FIG. 3—Effect of chromate concentration on SCC severity for pipeline steel in 1 N Na_2CO_3 -1 N NaHCO_3 .

inhibitor-containing coatings were leached in carbonate-bicarbonate solution and the resulting leachant solution used in a conventional slow strain-rate test. The procedure indicated whether the inhibitor could be leached from coatings at concentrations sufficient to inhibit SCC. The latter technique used coated steel specimens with scribe marks in the inhibitor-containing coating to expose steel to carbonate-bicarbonate solution. As shown schematically in Fig. 4, a polymerized tetrafluoroethylene cell was adapted to decrease the volume of solution in contact with the coated steel and to increase the ratio of coating area to solution volume. This cell is similar to that used in other tests but with the addition of a small polymerized tetrafluoroethylene cylinder (volume = 0.75 ml) around the specimen. Results of these tests indicate whether an SCC inhibitor can be leached effectively from an *in-situ* coating.

The feasibility of incorporating inhibitors in coatings for control of SCC was demonstrated by results from both procedures which showed reduced SCC severity with a variety of pipeline coatings that contained inhibitor. Not all formulations evaluated successfully inhibited SCC. For leachant experiments, ROA was useful to express inhibitor effectiveness, whereas crack velocity was selected for the *in-situ* coating experiments.

Carbon steel is susceptible to transgranular SCC in carbon dioxide-carbon monoxide aqueous solution. To determine the effect of gas composition on SCC severity, an investigation of CO_2 - CO - CH_4 mixtures at a total system pressure of 1460 kg/mm² (500 psig) was undertaken using the slow strain-rate technique with pipeline steel. A broad range of corrosive deterioration

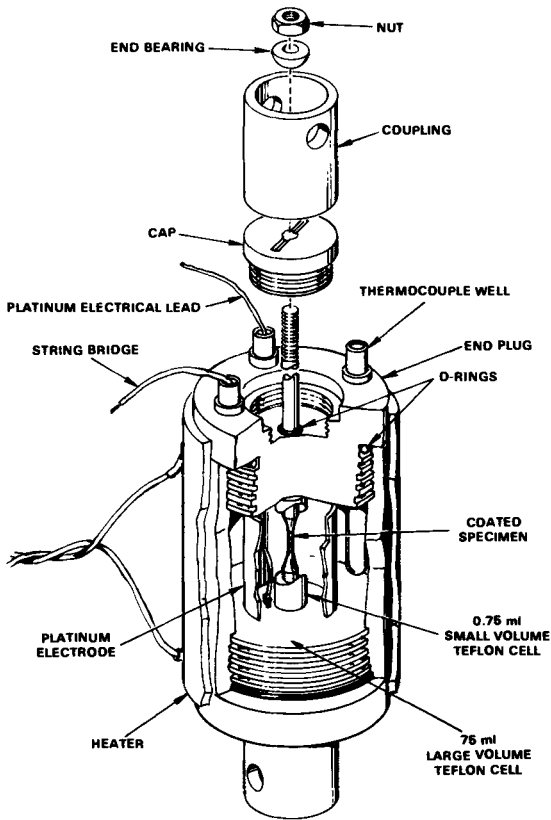


FIG. 4—Slow strain-rate cell for coated steel specimens.

was found as shown schematically in Fig. 5. Results determined by metallographic examination ranged from little or no corrosion to severe general corrosion with intermediate stages of shallow SCC, moderate SCC, severe SCC, and severe SCC with general corrosion.

Increased corrosivity was observed with increased carbon dioxide and oxygen pressure, decreased carbon monoxide pressure, and increased oxidizing potential. Carbon monoxide was necessary for SCC, that is, without carbon monoxide, steel corrosion became more severe as shown in Fig. 5, but no SCC was observed.

Effect of Oxidizing Condition

Steel exhibits SCC in a solution only within a critical range of oxidizing conditions. The slow strain-rate technique provides a means to determine the SCC potential range for a metal/solution combination. Results presented in

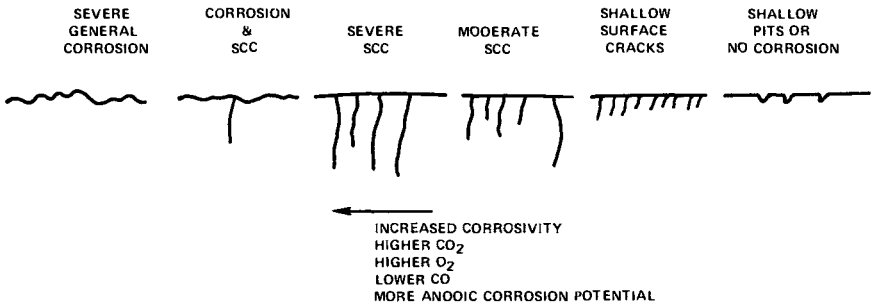


FIG. 5—Schematic diagram of steel corrosion behavior in carbon dioxide-carbon monoxide aqueous solutions.

Fig. 2 for steel in carbonate-bicarbonate solution indicate a critical potential range for SCC from approximately -0.61 to -0.68 V (SCE) with most severe SCC at -0.65 V (SCE). In this system SCC is observed at potentials more positive (noble) than the free corrosion potential of steel. At potentials slightly more negative than the SCC potential range, pitting is observed and at still more negative potentials, cathodic protection with no corrosion is observed. More positive potentials than those in the SCC range result in stable passivation and no SCC.

The extent and location of a SCC potential range is a function of solution composition. Figure 6 is a composite of slow strain-rate results in three solu-

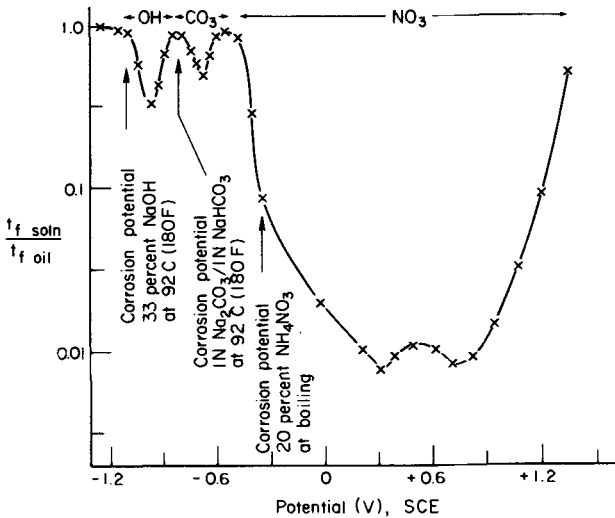


FIG. 6—SCC potential ranges of pipeline steel in hydroxide, carbonate-bicarbonate, and nitrate solutions in slow strain-rate tests at 2.5×10^{-6} s⁻¹.

tions: hydroxide, carbonate-bicarbonate, and nitrate [3]. Each solution has a distinct range within which steel exhibited SCC. Caustic cracking occurred over a range of approximately 200 mV with most severe SCC at -1.1 V (SCE). Carbonate-bicarbonate SCC occurred over a 150-mV range with most severe SCC at -0.68 V (SCE), and nitrate cracking occurred over a broad range from -0.3 V (SCE) to approximately $+1.2$ V (SCE). Increased SCC severity is indicated by lower values of the ratio of times-to-failure in solution and in oil. A value of unity is determined in the absence of SCC. Other parameters which affect SCC potential range are temperature, pH, steel composition, and strain rate.

In practice the corrosion potential of steel can vary considerably. Thus, it is important to determine SCC susceptibility over the entire range of oxidizing conditions that may pertain in service. For buried pipelines, the presence of mill scale or corrosion products and the application of cathodic protection currents shift the potential of steel from that for a freely corroding clean steel surface.

Effect of Steel Composition

Steel composition and microstructure can influence stress corrosion susceptibility. Many of these effects can be investigated by the slow strain-rate technique, while some effects associated with strain response to loading are investigated more readily by other SCC tests. As discussed in the preceding section, it is important to measure the effect of alloying addition on SCC susceptibility over a potential range. A particular alloying element could cause the free corrosion potential to move outside the SCC range in one solution and into the SCC range in another solution, from which it may be deduced that alloying was beneficial in the former and detrimental in the latter. However, since actual potential in service can vary widely from freely corroding conditions, neither deduction may be correct. The most effective way to determine alloying effects is to conduct experiments over a range of potentials in all solutions of interest.

Slow strain-rate test results for alloying additions to carbon steel in carbonate-bicarbonate solution are shown in Fig. 7. All alloying elements were beneficial through reducing the SCC potential range and reducing SCC severity at the most susceptible potential [2]. Similar results were obtained in nitrate and hydroxide solutions. It is important to note that the effect of an alloy can vary from solution to solution. For example, molybdenum, while beneficial in carbonate-bicarbonate solution, increased susceptibility to SCC in hydroxide solutions by extending the SCC potential range by several hundred millivolts.

In general, different alloying additions to steel produce different responses for SCC susceptibility, and the magnitude and extent of effects can vary with the solution. Results of slow strain-rate tests were used to assess the effects of

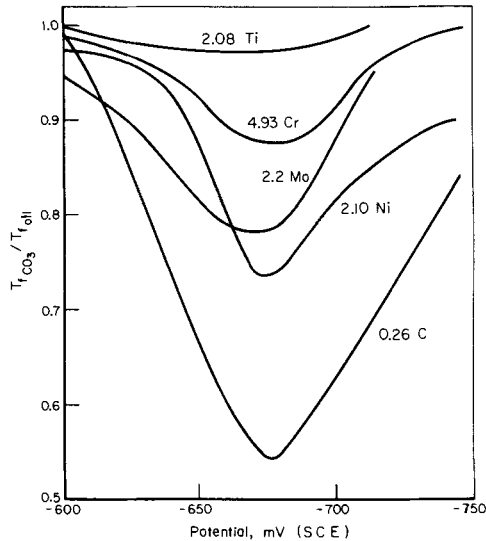


FIG. 7—Alloying additions effect on SCC susceptibility of carbon steel in carbonate-bicarbonate solution at 75°C (strain rate: $2.5 \times 10^{-6} \text{ s}^{-1}$).

alloy additions in nitrate, carbonate-bicarbonate, and hydroxide solutions.

Steel composition and microstructure affect both electrochemical and mechanical behaviors. While well suited for the former, the slow strain-rate technique is not applicable for investigating some mechanical effects. Recent results have shown that thermal-mechanical treatments over the range of 149 to 371°C (300 to 700°F) and 1 to 11 percent strain can significantly affect the SCC susceptibility of steel in carbonate-bicarbonate solution (see footnote 3). This effect appears to be related to a change in strain response of the steel. In slow strain-rate experiments, this effect is overridden and constant load SCC tests are more appropriate.

Effect of Temperature

Temperature dependency of pipeline steel SCC was investigated in nitrate, carbonate-bicarbonate, and hydroxide solutions by the slow strain-rate technique [3]. Decreasing temperature resulted in decreasing SCC susceptibility as indicated by reduced SCC potential range, reduced SCC severity at the most susceptible potential, and reduced SCC crack velocity.

The effect of temperature on SCC susceptibility of steel in 33 percent sodium hydroxide (NaOH) is shown in Fig. 8 for strain rates of 2.6×10^{-6} , 2.5×10^{-7} , and $9.9 \times 10^{-8} \text{ s}^{-1}$. A break in the $2.5 \times 10^{-6} \text{ s}^{-1}$ curve at approximately 72°C (160°F) is at the transition between SCC and no SCC. At temperatures below approximately 72°C (160°F), no SCC was observed by

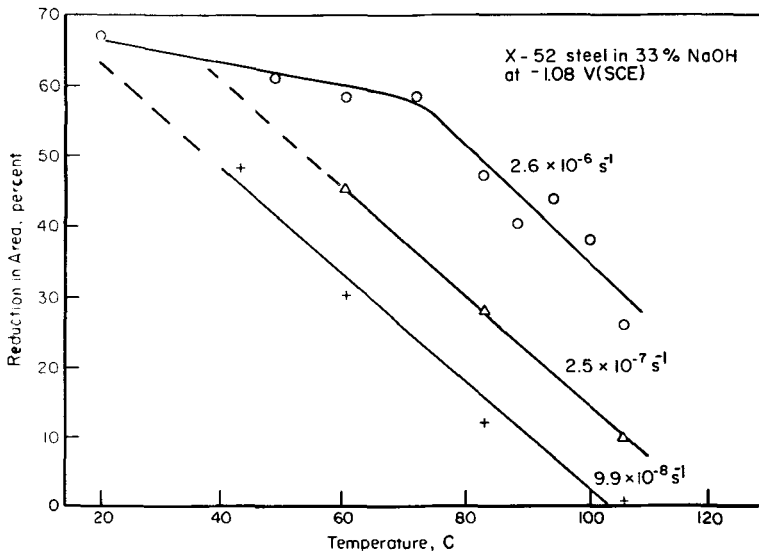


FIG. 8—Effect of temperature and strain rate on SCC susceptibility of pipeline steel in caustic solution.

metallographic examination. Stress corrosion was observed at as low as 32°C (90°F) for a strain rate of $9.9 \times 10^{-8} \text{ s}^{-1}$. All tests were run at the potential for the most severe SCC in hydroxide solution.

Effect of Strain Rate

The strain rate selected for experiments affects SCC severity. From Fig. 8 it is apparent that for a given temperature, SCC is more severe as strain rate decreased from 2.6×10^{-6} to $9.9 \times 10^{-8} \text{ s}^{-1}$ in hydroxide solution. Further results on the effect of strain rate are presented in Fig. 9. Average crack velocity is plotted as a function of strain rate in 33 percent NaOH at 92°C (197°F) [3]. Crack velocities were determined by measuring depth of cracks and dividing by time of exposure in the slow strain-rate experiment. At faster strain rates, no SCC was observed because mechanical failure occurred prior to the onset of SCC. At slower strain rates, SCC was observed with no apparent crack velocity dependence upon strain rate being found. No decrease in SCC severity was observed at slower strain rates down to $9.9 \times 10^{-8} \text{ s}^{-1}$.

While slow strain-rate results can provide a conservative measure of SCC susceptibility, for some applications it should be recognized that plastic deformation at rates of interest (creep rates) can occur in service on structures designed and operated at stresses below the nominal yield stress. Small stress fluctuations superimposed on a constant stress level well below the

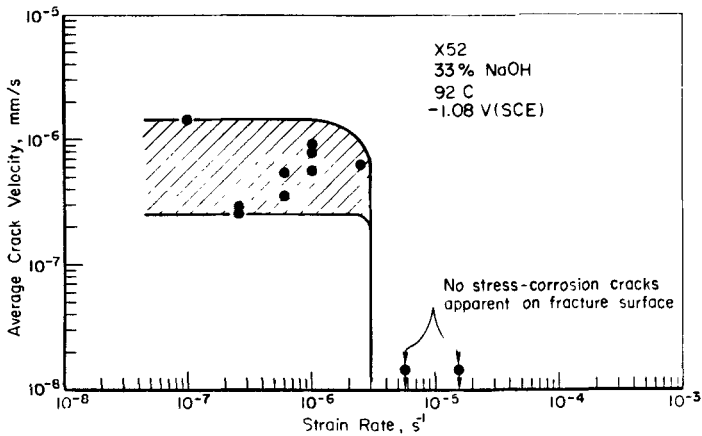


FIG. 9—Effect of strain rate on SCC susceptibility of pipeline steel in caustic solution.

yield stress are sufficient to induce plastic deformation and promote SCC. Frequency of stress fluctuations as low as a cycle per day can promote SCC. This effect was demonstrated for pipeline steel in carbonate-bicarbonate solution where threshold stress was significantly reduced by application of low frequency, low magnitude stress fluctuation (see footnote 3).

Summary

The slow strain-rate technique was an essential tool in the study of SCC of pipeline steel. The technique was applied successfully to determine controlling parameters of the SCC process and to develop and evaluate methods to prevent SCC. Other procedures were used in conjunction with slow strain rate throughout the study, for example, electrochemical techniques, other SCC tests, and metallographic and chemical analysis. Application of slow strain rate to determine the effects of solution composition, oxidizing condition, steel composition, temperature, and strain rate on SCC susceptibility of pipeline steels were presented.

Acknowledgments

Appreciation is expressed to the Pipeline Research Committee of the American Gas Association for supporting the work described here and to the NG-18 Committee of AGA for offering encouragement and advice regarding the work. Important contributions were made by T. J. Barlo, W. K. Boyd, A. R. Eisea, and R. R. Fessler of Battelle's Columbus Laboratories.

References

- [1] Wenk, R. L., "Field Investigation of Stress Corrosion Cracking," Fifth Symposium on Line Pipe Research, Houston, Tex., T-1—T-22, American Gas Association, Arlington, Va., Nov. 1974.
- [2] Parkins, R. N., "The Controlling Parameters in Stress-Corrosion Cracking," Fifth Symposium on Line Pipe Research, Houston, Tex., U-1—U-40, American Gas Association, Arlington, Va., Nov. 1974.
- [3] Berry, W. E., "Stress Corrosion Cracking Laboratory Experiments," Fifth Symposium on Line Pipe Research, Houston, Tex., V-1—V-43, American Gas Association, Arlington, Va., Nov. 1974.
- [4] Fessler, R. R., "Applications of Stress Corrosion Cracking Research to the Pipeline Problem," Fifth Symposium on Line Pipe Research, Houston, Tex., W-1 to W-22, American Gas Association, Arlington, Va., Nov. 1974.
- [5] Fessler, R. R., "Present Understanding of the Causes of Stress Corrosion Cracking in Buried Pipelines," *Proceedings, Interpipe 76*, Houston, Tex., Jan. 1976.
- [6] Payer, J. H., Berry, W. E., Boyd, W. K. in *Stress Corrosion—New Approaches, ASTM STP 610*, American Society for Testing and Materials, 1976, p. 82.
- [7] Sutcliffe, J. M., Fessler, R. R., Boyd, W. K., and Parkins, R. N., *Corrosion*, Vol. 18, 1972, p. 313.

Slow Strain-Rate Test Technique for Specific Metals and Alloys

Propagation of Stress Corrosion Cracks under Constant Strain-Rate Conditions

REFERENCE: Scully, J. C., "Propagation of Stress Corrosion Cracks under Constant Strain-Rate Conditions," *Stress Corrosion Cracking—The Slow Strain-Rate Technique*, ASTM STP 665, G. M. Ugiansky and J. H. Payer, Eds., American Society for Testing and Materials, 1979, pp. 237–253.

ABSTRACT: Stress corrosion crack velocities have been measured in α and β titanium alloys, Zircaloy-2, and in 70Cu-30Zn brass at room temperature as a function of crosshead speed. Constant crack velocities have been observed in constant crosshead speed tests. In α titanium alloys in aqueous sodium chloride (NaCl) solutions cracking occurs only at crosshead speeds $\geq 8.3 \mu\text{m/s}^{-1}$ because crack-tip repassivation occurs at lower crosshead speeds. In brass, the velocity and type of fracture are dependent upon the potential and the metallurgical condition of the specimen. The use of double crosshead speed tests and work on β titanium alloy and on brass shows that the work-hardening capacity of an alloy is important in determining crack velocity. Limitations of the technique are indicated.

KEY WORDS: stress corrosion cracking, strain rate, crosshead speed, repassivation, work-hardening capacity, crack propagation

The application of constant strain-rate conditions to the study of stress corrosion crack propagation is a logical development in the study of stress corrosion mechanisms. It focuses attention upon the role of plastic deformation occurring at the tip of the propagating crack which has been discussed widely in the literature. Many specific functions have been ascribed to plastic deformation although direct evidence has not been easy to obtain. Phase precipitation, the creation of active dislocations, and the fracture of surface films are very general functions that have been commonly proposed. Even if a specific function has not been discerned, the important role of plastic deformation is not in dispute. The rate at which it occurs constitutes

¹Reader in corrosion science, Department of Metallurgy, University of Leeds, Leeds LS2 9JT, England.

the principle mechanical factor in crack propagation. It has been shown, for example, that in austenitic stainless steels the stress corrosion crack velocity is constant under conditions of constant stress [1],² and that in copper-beryllium alloys the crack velocity and associated fractography depend upon the rate of change of the stress intensity factor, \dot{K} , rather than upon the absolute instantaneous value of K [2]. There has been the widely reported [3] observation that stress corrosion crack velocity depends upon the value of K in constant K tests in the K -dependent range of velocity values called Region 1. These are not the only examples from the literature that the rate of plastic deformation (or crack-tip strain rate) is the mechanical factor that determines the crack velocity.

In the consideration of stress corrosion mechanisms, much attention has been focused upon the competitive nature of two kinetic events at the tip of a propagating crack. These are depicted schematically in Fig. 1. The function of plastic deformation is to produce a tensile strain which creates fresh unfilmed metal at the crack tip surface. The important electrochemical mechanism is the filming or repassivation process since this will impede the essential reaction between the metal and solution, which will include dissolution and (possibly) hydrogen absorption processes. The necessary initial imbalance between fresh metal creation rate and repassivation rate has been discussed in detail elsewhere [4]. If repassivation occurs too rapidly, insufficient corrosion will have occurred to cause a further increment of crack growth. If repassivation is too slow, then the corrosion attack will occur on too broad a front and pitting rather than cracking will take place. The

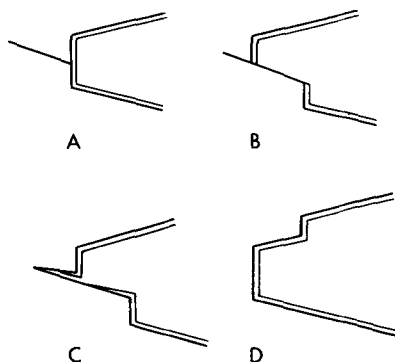


FIG. 1—Schematic diagram of the sequence of events occurring at the tip of a propagating crack. Under the action of the tensile stress the slip plane in A operates to produce a step of unfilmed new metal surface (B). The overall effect is to produce a filmed surface after an increment of crack growth (C and D) and the whole sequence is then repeated.

²The italic numbers in brackets refer to the list of references appended to this paper.

kinetic relationship between the fresh surface creation rate and the repassivation rate is of critical importance.

In examining stress corrosion crack propagation processes by using a constant strain-rate technique, the mechanical factor is controlled exactly. Maintaining the strain rate at a constant value, for example, might be likened by analogy to controlling the electrochemical potential of a specimen. In constant strain-rate tests, the metallurgical and electrochemical factors of the cracking process then can be easily examined. Factors that might be difficult to examine in constant stress tests, which are difficult to perform, and constant K tests, which are expensive, are more clearly discerned in a constant strain-rate test. The role of the work-hardening rate is an example, as will be described later. The constant strain-rate technique is much simpler to apply than the other techniques. In the work described next, for example, most of the experiments were performed on notched-strip specimens 0.5 mm thick.

During the course of a series of detailed studies of stress corrosion mechanisms in titanium, zirconium and copper-zinc alloys, crack velocities have been measured as a function of tensile strain rate under a wide variety of electrochemical and chemical conditions. Some of the principle observations are shown next. Experiments have been done on two machines. An Instron tension testing machine (ITTM) was used with crosshead speeds down to $0.33 \mu\text{m/s}^{-1}$. In stress corrosion tests the value of the crosshead speed required is very dependent upon the maximum crack velocity. For titanium alloys in which crack velocities can be $>0.16 \text{ mm/s}^{-1}$ the ITTM is a suitable machine. In 70Cu-30Zn alloy, however, where velocities are $<8.3 \mu\text{m/s}^{-1}$, a lower range of crosshead speeds was required. This was obtained by employing a simple tensile straining machine based upon a design by Parkins [5]. This had a crosshead speed range spanning from the lower end of the ITTM to 3 nm/s^{-1} . Crack velocities were measured optically by observing the propagation of a simple crack initiated in a simple edge notch (SEN) specimen 17 mm wide across the notched region. The surface in this region was marked in 2 and 3-mm intervals which were measured accurately. All measurements were made on specimens that were examined by scanning electron microscopy (SEM) after fracture. This was necessary in order to ensure that the measured surface velocity was accurately representative of crack propagation through the whole thickness. Generally this was found to be so. In all examples described, single cracks were initiated. Multiple crack initiation was promoted by residual cold work in sheared edges, by highly corrosive environments, and by anodic polarization. In addition to the competition described in Fig. 1 between fresh metal generation and repassivation, in dynamic straining tests there is competition between two fracture processes, one causing stress corrosion cracking, the other ductile failure. The kinetics of the stress corrosion cracking process determine the

maximum crosshead speed that will give cracking, and the ratio of the two in a given fracture will vary according to the employed crosshead speed.

In notched specimens, the initial strain rate is not known. The constant strain-rate test applies to specimens with a uniform measurable gage length extending as a result of crosshead movement. In notched specimens the straining is concentrated at the notch root. In titanium alloy and 70Cu-30Zn specimens, for example, the measured crack velocities were independent of specimen length between the values 100 to 400 mm. Furthermore, at all values of crosshead speed over which stress corrosion crack propagation occurred, the velocity was observed to be constant across the middle width of a specimen. Typical values are shown in Table 1 for a

TABLE 1—*Variation in crack velocity across specimen width of a titanium-oxygen alloy in CH₃OH/HCl solutions in dynamic straining experiments [7].*

Crosshead Speed, $\mu\text{m/s}^{-1}$	Successive Intervals from Notch, mm	Crack Velocity, mm/s^{-1}
0.83	0 to 2	0.011
	2 to 5	0.010
	5 to 8	0.011
	8 to 11	0.013
	11 to 13	0.204
1.66	0 to 2	0.201
	2 to 5	0.015
	5 to 8	0.015
	8 to 11	0.015
	11 to 13	0.025
3.3	0 to 2	0.026
	2 to 5	0.027
	5 to 8	0.028
	8 to 11	0.028
	11 to 13	0.041
8.3	0 to 2	0.083
	2 to 5	0.091
	5 to 8	0.083
	8 to 11	0.094
	11 to 13	0.14
16.6	0 to 2	0.0166
	2 to 5	0.0167
	5 to 8	0.0170
	8 to 11	0.0169
	11 to 13	0.23
33.3	0 to 2	0.265
	2 to 5	0.25
	5 to 8	0.25
	8 to 11	0.29
	11 to 13	0.34
83.3	0 to 2	0.45
	2 to 5	0.47
	5 to 8	0.49
	8 to 11	0.53
	11 to 13	0.56

titanium-oxygen alloy and in Table 2 for a 70Cu-30Zn alloy for which standard deviations were determined. The constant velocity measurements emphasize the critical importance of the crosshead speed in determining crack velocity. Considered with observations already described [1-3] the measurements indicate that the crosshead speed causes a constant strain rate at the crack tip.

The results are presented and discussed for different alloys, and a general summary is presented at the end.

Titanium Alloys

The role of strain rate upon the propagation of stress corrosion cracks in a titanium-oxygen alloy is shown in Figs. 2 and 3, representing two different solutions, aqueous sodium chloride (NaCl) in which titanium does not corrode and a methanol/hydrochloric acid (CH₃OH/HCl) mixture in which titanium does corrode [6]. In the aqueous solution, there was a crosshead speed below which cracking was not observed ($8.3 \mu\text{m/s}^{-1}$). This can be interpreted with direct reference to K_{Isc} which is observed in this alloy/environment system. There is a strain rate at the crack tip at which repassivation can occur. This has been designated [4] $\dot{\epsilon}_r$ and will occur at a crosshead speed between $3.3 \mu\text{m/s}^{-1}$ where cracking does not occur and $8.3 \mu\text{m/s}^{-1}$ where cracking does occur, as shown in Fig. 2. Stress relaxation experiments have indicated [7] that repassivation would occur at a crosshead speed of approximately $3.8 \mu\text{m/s}^{-1}$ if this were available on the ITTM. In stress intensity tests, K_{Isc} corresponds to the value of K which produces a crack-tip strain-rate of $\dot{\epsilon}_r$. When the pH of the aqueous solution was lowered

TABLE 2—Variation in crack velocity across specimen width for a 70Cu-30Zn alloy in a solution of 1.5 M total ammonia and 0.04 M total copper at different crosshead speeds [11]. Crack velocity ($\mu\text{m/s}^{-1}$) over a range of crack length.

Crosshead Speed $\mu\text{m/s}^{-1}$	2 to 4 mm	4 to 6 mm	6 to 8 mm	8 to 10 mm	10 to 12 mm	Average of 2 to 12 mm
0.33	2.9 (0.3)	3.4 (0.3)	4.5 (0.4)	4.1 (0.3)	4.3 (0.4)	3.9 (0.4)
0.83	5.1 (0.7)	5.3 (0.4)	5.1 (0.5)	5.9 (0.7)	6.1 (0.5)	5.4 (0.5)
1.6	8.1 (0.8)	7.8 (0.7)	8.7 (0.9)	9.2 (1.1)	9.5 (0.7)	9.2 (1.3)
3.3	11.1 (1.0)	12.2 (1.1)	13.7 (1.4)	13.4 (1.2)	14.3 (1.4)	13.1 (1.5)
8.3	26 (2.5)	24.1 (2.1)	32.6 (3.6)	35 (3.2)	34 (3.2)	3.2 (2.7)
16.6	40 (1.3)	42 (1.6)	58.7 (4.0)	59 (6.0)	67 (5.9)	57 (5.1)

NOTE—The figures in parentheses are standard deviations.

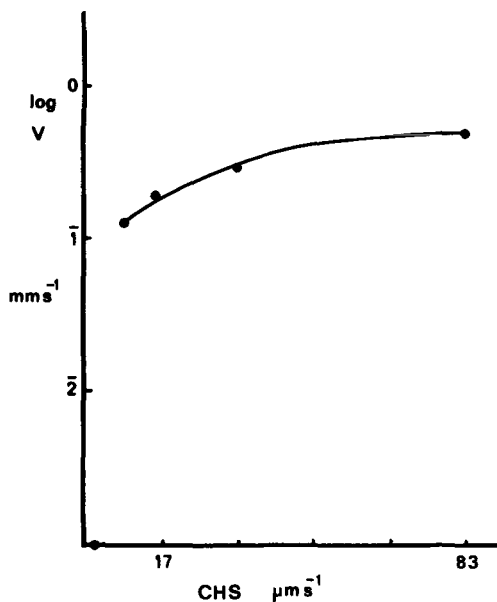


FIG. 2.—The relationship between stress corrosion crack velocity and crosshead speed for a titanium-oxygen alloy in an aqueous 3 percent NaCl solution. Cracking does not occur at a crosshead speed $< 8.3 \mu\text{m/s}^{-1}$ [7].

to 1.5 cracking was observed at the crosshead of $3.3 \mu\text{m/s}^{-1}$. Since repassivation would be slower in the acidified solution, the strain rate at which it could occur rapidly enough to prevent crack propagation would be lower. In the corrosive $\text{CH}_3\text{OH}/\text{HCl}$ solution, cracking occurred at all the crosshead speeds employed as is shown in Fig. 3. In the aqueous and methanolic solutions, the fracture exhibited the characteristic cleavage and fluted fracture [8].

The necessity of maintaining the crack-tip strain rate $> \dot{\epsilon}_c$ was demonstrated by employing a double crosshead speed test [7]. If during a test in aqueous neutral NaCl the crosshead speed were lowered to a value $< 8.3 \mu\text{m/s}^{-1}$ or the crosshead movement were stopped, crack arrest would occur provided that the operative stress at the moment of crosshead speed alteration were not too high. Such a result indicated that the absence of cracking in single crosshead speed tests applied not only to crack initiation but also to crack propagation. In $\text{CH}_3\text{OH}/\text{HCl}$ solutions, lowering the crosshead speed produced a fall in velocity corresponding to the velocity in single crosshead speed tests at the lower value, provided that the stress at the change down was not too high in which case the fall in velocity was less. Typical values after change down are shown in Table 3. The differences in the two velocities depend upon the work-hardening rate of the alloy which

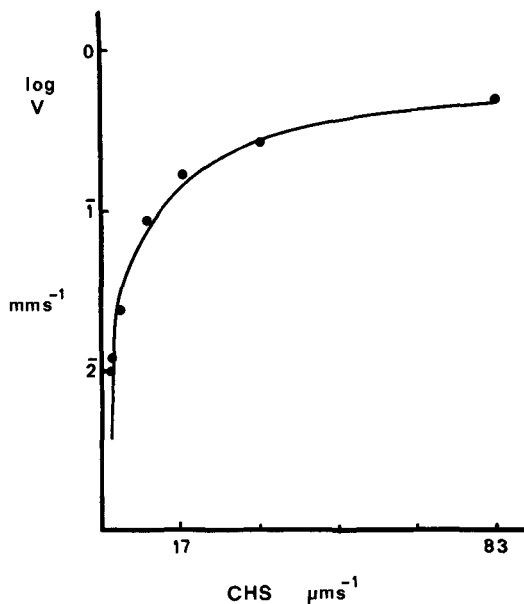


FIG. 3—The relationship between stress corrosion crack velocity and crosshead speed for a titanium-oxygen alloy in a $\text{CH}_3\text{OH}/\text{CHI}$ solution [7].

falls as the acting stress is increased. At any time the effective strain rate at a crack tip is caused by two factors: (a) the applied crosshead speed, and (b) the stress acting on the specimen at any moment. At low values of stress, the strain rate caused by the stress will be negligible and will disappear rapidly so that the crack-tip strain rate will be entirely dependent upon the external crosshead speed which therefore will control the crack velocity. At high values of stress the strain rate caused by the stress will make a significant contribution to the effective crack-tip strain rate. Lowering the crosshead speed will have less effect upon changes in crack velocity than for changes at low stress values. These differences are consistent with the results shown in Table 3.

The essence of the two pairs of competing processes of new surface creation and repassivation and of the stress corrosion cracking and ductile tearing is demonstrated clearly by the effect of inhibitor additions. An example is provided in Table 4 which shows the influence of a single sodium nitrate (NaNO_3) concentration addition on crack velocity in aqueous solutions. The slowing down can be attributed to a more rapid repassivation process. The results indicate that the effect of these additions is less marked at the higher values of crosshead speeds. This can be attributed to the increased tearing component of the fracture process at the higher values as compared with the lower values.

TABLE 3—The influence of stress upon crack velocity in a titanium-oxygen alloy in a $\text{CH}_3\text{OH}/\text{HCl}$ solution in double crosshead speed tests [7]. Initial crosshead speed $8.3 \mu\text{m/s}$. Final crosshead speed $8.3 \mu\text{m/s}$.

Stress at Changing, N/mm^2	Velocity under Initial Crosshead Speed, mm/s^{-1}	Velocity under Final Crosshead Speed, mm/s^{-1}
393	0.46	0.102
437	0.46	0.105
485	0.45	0.103
600	0.46	0.29

TABLE 4—The effect of sodium nitrate (NaNO_3) addition upon crack velocity in MeOH/HCl solution for a titanium-oxygen alloy in a $\text{CH}_3\text{OH}/\text{HCl}$ solution [7].

Crosshead Speed, $\mu\text{m/s}^{-1}$	Crack Velocity, mm/s^{-1} , 2 weight percent of NaNO_3 Addition	
	No Addition	
8.3	0.130	0.062
16.6	0.27	0.11
33.3	0.4	0.27

Similar work on a β alloy (Ti-13Cr-11V-3Al) has given the results [9] shown in Fig. 4 which shows the measured velocities in the same $\text{CH}_3\text{OH}/\text{HCl}$ solution and with an addition of mercuric chloride (HgCl_2). The alloy exhibits (100) cleavage under such conditions. The addition of HgCl_2 increases the amount of cleavage in the fracture considerably, an effect that may be caused by the additional uptake of hydrogen that is promoted by the Hg^{2+} ion and by the adsorption of mercury at the crack tip which could give an effect of a liquid metal embrittlement type. What is apparent is that the additional embrittlement results in a lower velocity at low crosshead speeds and a higher velocity at high speeds relative to the mercury-free solution. This result underlines the point that crack velocity by itself may not always be the only criterion for comparing environments. The stress values at which cracking occurs must also be considered. In this case the additional embrittlement at low crosshead speeds initiates cleavage at a lower stress but the associated tearing processes take longer to occur. In much of the fracture tearing is reduced as a result of the HgCl_2 addition because cleavage is being initiated at low stresses. The additional embrittlement at high crosshead speeds arises from cleavage occurring at lower stresses but this type of fracture is in competition with the tearing process. More embrittlement gives a higher velocity because at high crosshead speeds the tensile fracture stress is rapidly approached. This alloy has little ductility and work-hardening capacity and crack velocity is therefore en-

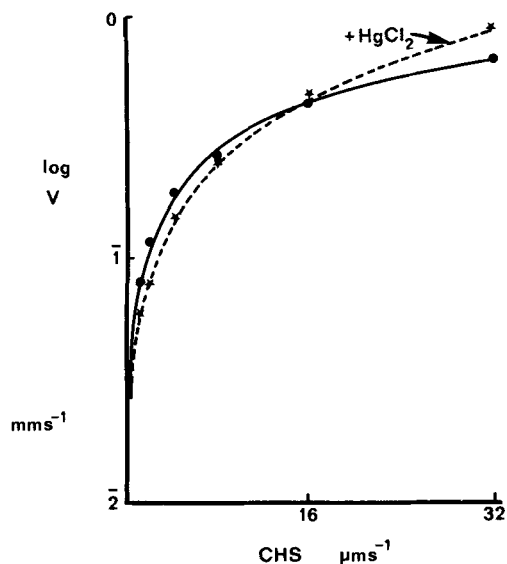


FIG. 4—The relationship between stress corrosion crack velocity and crosshead speed for the Ti-13Cr-11V-3Al alloy in a $\text{CH}_3\text{OH}/\text{HCl}$ solution with and without additions of HgCl_2 [9].

tirely dependent upon the stress at any time rather than the external cross-head speed. This alloy is therefore quite different from the α alloy described previously with reference to Table 3. Double crosshead speed tests of the same kind showed that in this β alloy the velocity was dependent only upon the stress at change down and not the initial nor final crosshead speeds.

Zircaloy-2

Identical experiments to those described for titanium alloys have been performed on Zircaloy-2 specimens in a $\text{CH}_3\text{OH}/\text{HCl}$ solution containing 0.4 volume percent of hydrochloric acid (HCl) [10]. Intergranular corrosion occurs in unstressed specimens. It appears, therefore, in tests at low cross-head speeds in which the specimen is in contact with the solution for a long time. At some point in the fracture, however, transgranular cleavage is observed and finally ductile overload failure. The range of crosshead speeds over which cracking occurs is lower than for the titanium-oxygen alloy. Tests on the ITTM, for example, give air fracture except at the lowest end of the speed range. Typical values of crack velocity were $3 \mu\text{m}/\text{s}^{-1}$ at $8.3 \mu\text{m}/\text{s}^{-1}$ crosshead speed to $0.05 \mu\text{m}/\text{s}^{-1}$ at $0.16 \mu\text{m}/\text{s}^{-1}$ crosshead speed.

70-30 Brass

In SEN sheet specimens immersed in ammoniacal cupric sulfate (CuSO_4) solutions of pH 6.8 cracking was observed [11] over a wide range of crosshead speeds as is shown in Fig. 5 in which both coordinates are plotted on a logarithmic scale. At very low crosshead speeds, a region of constant velocity was observed. This had been observed also in cantilever beam specimens of brass in a 15 N ammoniacal solution where the upper limit of the constant velocity corresponded to the onset of general yield in the specimens. This was not confirmed for the sheet SEN specimens but the constant velocity region was in the same range and showed the same upper limit. It can be hypothesized that below general yielding the plastic zone spreads as the crack propagates, but the average size of the zone goes up with increasing crosshead speed until it spreads throughout the specimen. Until this happens the strain rate acting at the crack tip does not change. In an alloy like brass the high work-hardening rate ensures that the plastic zone spreads in preference to an increase in the crack-tip strain rate with in-

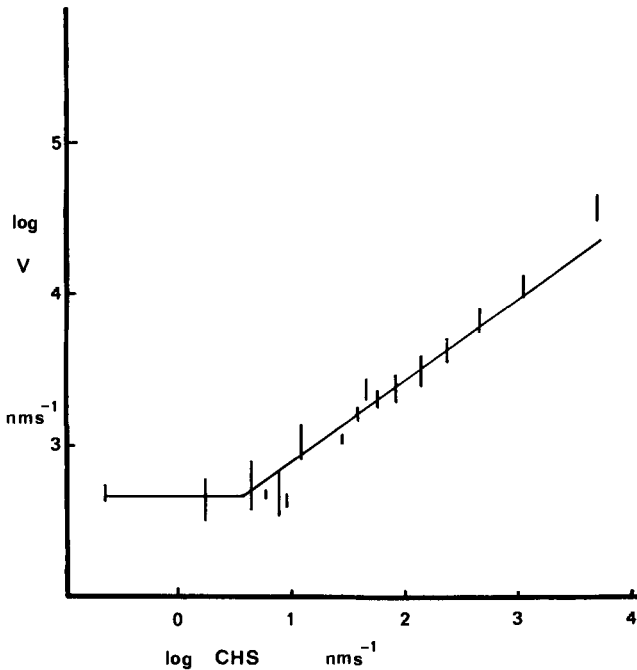


FIG. 5—The relationship between stress corrosion crack velocity and crosshead speed for 70Cu-30Zn in a solution containing 1.5 M total ammonia and 0.04 M total copper and pH 6.8 [11].

creasing crosshead speed. Once general yielding has occurred, increasing crosshead speed causes an effective increase in crack velocity.

Cracking in pH 6.8 solutions is intergranular and examination of the specimen provides a simple indication of the point at which ductile fracture contributes to the propagation process. Typical results are shown in Fig. 6 which shows the relative amounts of the two types of fracture as a function of crosshead speed. The elongation to fracture and ultimate tensile strength of specimens broken in solution and in air are also shown. Completely intergranular fracture was observed at crosshead speeds as high as $1.66 \mu\text{m/s}^{-1}$ corresponding to a crack velocity of $8.3 \mu\text{m/s}^{-1}$. This is rather high when compared to values obtained by other workers using different loading techniques. In tests employing stress and stress intensity the range of crack-tip strain rates may be large and whether the strain-rate increases or decreases will depend upon the experimental arrangement. In the as-received condition the crack velocity at any crosshead speed was considerably higher, as is shown in Fig. 7.

It has been emphasized that controlling the crack-tip strain rate is an important part of a test which is omitted in many types of tests involving a

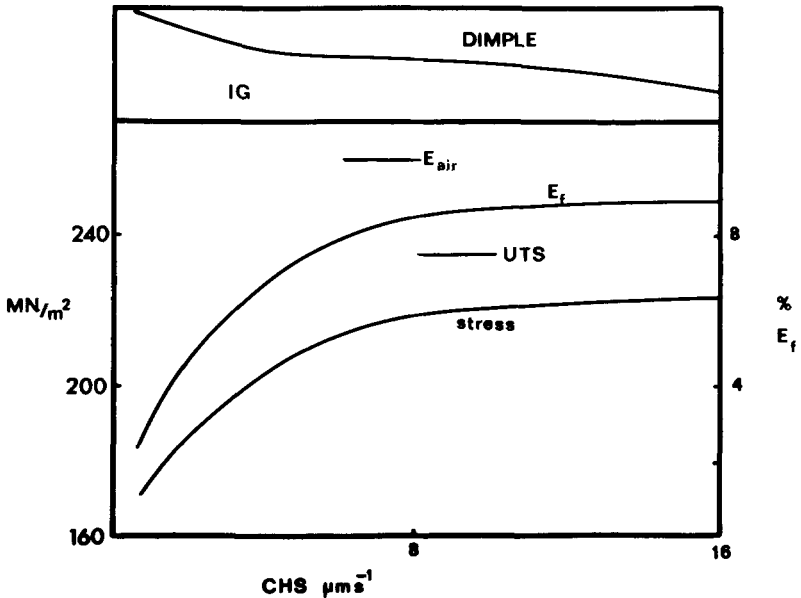


FIG. 6—The relationship between type of fracture, elongation to failure, and tensile stress at failure for a specimen of 70Cu-30Zn exposed to pH 6.8 solution described in Fig. 5 as a function of the range of crosshead speed where the fracture ceases to be 100 percent intergranular [11].

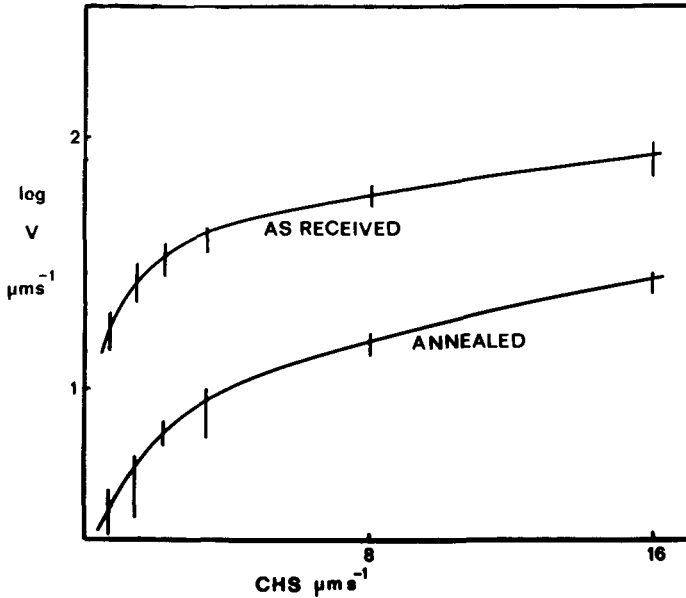


FIG. 7—The variation in stress corrosion crack velocity for a 70Cu-30Zn alloy in the annealed and as-received condition in pH 6.8 solution described in Fig. 5 as a function of crosshead speed. The as-received material had a VHN hardness of 115, 0.1 percent proof stress of 275 MN/m^{-2} and ultimate tensile strength of 373 MN/m^{-2} . The annealed material properties were: hardness 86, 0.1 percent proof stress 205 MN/m^{-2} and ultimate tensile strength of 298 MN/m^{-2} [11].

constant load or increasing stress intensity factor. Equally, controlling the value of the electrochemical potential is another important part of a test since the value of the potential determines the rate of an electrode reaction, including, where applicable, the repassivation rate.

The effect of potential upon crack velocity has been demonstrated for a number of alloys [3] in stress intensity tests. For brass, where such effects have not been demonstrated, controlling the potential indicates at what values of potential the slower transgranular stress corrosion crack propagation process occurs in pH 6.8 solutions. A typical result is shown in Fig. 8. Under open circuit conditions the fracture is intergranular as has been indicated in Fig. 6. In this particular case the open circuit potential is in the potential range where the maximum crack velocity is observed. Either anodic or cathodic polarization cause a diminution in velocity outside the range $+20$ to $60 \text{ mV } E_{\text{sc}}$.

In 15 N ammoniacal solutions the specimen surface could not be seen

because of the deep blue coloration of the solution. The velocity was calculated according to the formula

$$v = \frac{A_{\text{sc}}}{x (t_{\text{max}} - t_i)}$$

where

- v = stress corrosion crack velocity,
- A_{sc} = area of the stress corrosion fracture which could be estimated by SEM and calculated as indicated below; both values so obtained were very similar,
- t_{max} = time taken to attain a maximum load in a stress corrosion test at each crosshead speed,
- t_i = time taken to attain the crack initiation load, L_i , and
- x = specimen thickness.

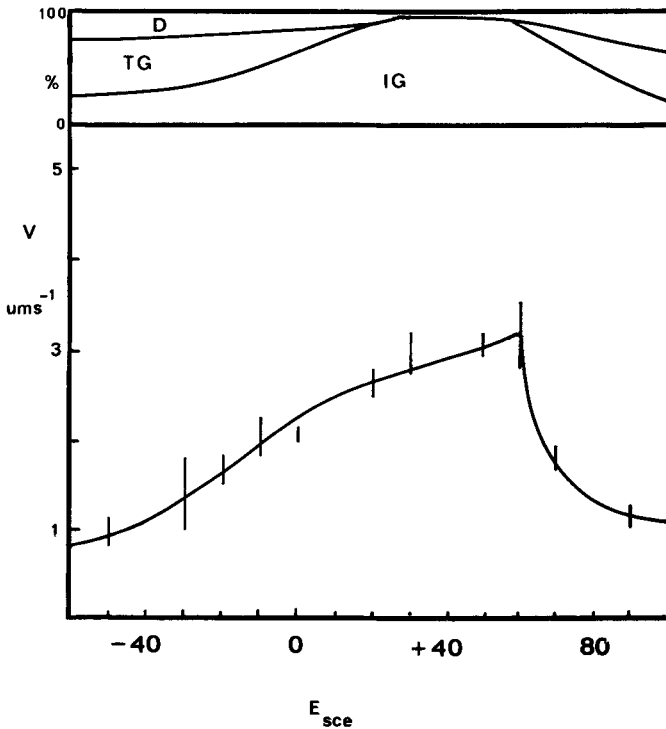


FIG. 8—The effect of potential upon stress corrosion crack velocity in a 70Cu-30Zn alloy in pH 6.8 solution described in Fig. 5 and upon the type of fracture observed at a crosshead speed of $0.33 \mu\text{m/s}^{-1}$ [11].

A_{sc} was calculated by considering that the total area, A_{total} , consisting of two parts

$$A_{\text{total}} = A_{\text{sc}} + A_{\text{mech}}$$

where A_{mech} is the calculated ductile proportion of the fracture.

In the pH 6.8 tests, velocities could be both measured and calculated. It was found that the two values correspond well provided that the stress corrosion proportion part of the fracture was >70 percent of the total fracture. Typical results are shown in Table 5.

Discussion

The use of the constant strain-rate technique for crack propagation studies provides a valuable, rapid, and economical method for studying crack propagation. The results described above indicate the range of electrochemical and metallurgical variables that can be examined in this way and also some of the mechanistic points that have been investigated. Comparison between alloys, which was not described, also can be undertaken with this technique but care needs to be exercised in comparisons of velocity. The effective strain rate at the crack tip depends upon not only the straining machine but also the work-hardening capacity of the alloy.

TABLE 5—A comparison between measured and calculated values of crack velocity at different crosshead speeds in a 70Cu-30Zn brass exposed to a solution containing 1.5 M total ammonia and 0.04 M total copper at pH 6.8 [11].

Crosshead Speed, $\mu\text{m/s}^{-1}$	Velocity $\mu\text{m/s}^{-1}$		
	Calculated	Measured	
		Over 2 to 4 mm	Average over 2 to 12 mm
0.33	3.7 (0.3)	2.9 (0.3)	3.9 (0.4)
0.83	5.7 (0.32)	5.1 (0.7)	5.4 (0.4)
1.66	7.6 (0.7)	8.1 (0.85)	9.1 (1.3)
3.33	9.5 (0.8)	11.1 (1.0)	13.1 (1.5)
8.3	13.5 (1.6)	26.0 (2.5)	32.4 (2.8)

NOTE—Figures in parentheses are standard deviations.

The conclusion can be drawn that while the emphasis in this paper has been on velocity measurements, care must be taken to look at values of fracture loads (and stresses) as well. In this way the distinction between effects on crack initiation and crack propagation can be made, and it can be an important one. In the simplest case, for example, if a cathodic poison lowers the corrosion rate of a titanium alloy the rate of hydrogen ion discharge will be lowered and even if the proportion of hydrogen entering the metal is increased by the presence of the poison, the amount may be diminished from the amount entering in the absence of inhibitor. The time required to initiate an increment of cleaved crack will be extended if the amount of hydrogen entering the lattice is reduced in this way. A higher load for fracture initiation therefore will be observed in a constant strain-rate test. Once cleavage occurs, however, since it is initiated at a higher stress than in the absence of inhibitor, the ensuing fluting may extend over larger distances and the velocity therefore may increase. Where the corrosion rate is either not diminished, or not diminished by a significant amount, the embrittlement and cleavage initiation may occur more rapidly than in the absence of inhibitor. The result will be the occurrence of cleavage at a lower applied stress. Whether the velocity is lower or higher will depend upon the work-hardening characteristics of the alloy and the tolerance of the alloy lattice for hydrogen. This is a very simple picture and it is not difficult to envisage more complex situations. Such considerations are intended to emphasize that the measurements of crack propagation in a constant strain-rate test is a very valuable technique but the results need to be interpreted with care and with a careful scrutiny of the processes that are operating together to produce a stress corrosion crack.

References

- [1] Robinson, M. J. and Scully, J. C., "Stress Corrosion Crack Propagation in Austenitic Stainless Steels," *Stress Corrosion Cracking and Hydrogen Embrittlement of Iron Base Alloys*, R. W. Staehle, J. Hochmann, R. D. McCright and J. E. Slater, Eds., National Association of Corrosion Engineers, Houston, Tex., 1978, p. 1095.
- [2] Sparkes, G. M. and Scully, J. C., *Corrosion Science*, Vol. 11, 1971, pp. 641-659.
- [3] Scully, J. C., Ed., *The Theory of Stress Corrosion Cracking in Alloys*, North Atlantic Treaty Organization, Brussels, 1971.
- [4] Scully, J. C., *Corrosion Science*, Vol. 7, 1967, pp. 197-208.
- [5] Parkins, R. N., private communication, 1975.
- [6] Sanderson, G. and Scully, J. C., *Corrosion Science*, Vol. 8, 1968, pp. 541-548.
- [7] Scully, J. C. and Adepoju, T. A., *Corrosion Science*, Vol. 17, 1977, pp. 789-812.
- [8] Aitchison, I. and Cox, B., *Corrosion*, Vol. 28, 1972, pp. 83-88.
- [9] Lycett, R. W. and Scully, J. C., University of Leeds, to be published.
- [10] Mujumdar, P. M. and Scully, J. C., University of Leeds, in press.
- [11] Kermani, M. and Scully, J. C., *Corrosion Science*, in press.

DISCUSSION

*G. Cragnolino*¹—I would like to point out that the same type of dependence between the crack propagation rate and the crosshead speed, in titanium alloys as shown by the author, was found in NaCl solutions with Zircaloy-4 at potentials higher than the pitting potential.² The mean intergranular crack length was measured on the fracture surfaces through SEM pictures, and the propagation time was the time to failure minus the time elapsed during the elastic strain. The experiments were performed at controlled potential with initial strain rates from 10^{-4} to 10^{-1} min⁻¹ and the crack propagation rate increased, following the same pattern described by the author, from 3×10^{-5} to 7×10^{-4} mm/s. At higher strain rates ductile fracture was observed.

J. C. Scully (author's closure)—I look forward to reading the paper referred to when it becomes available. In Leeds we have done some stress corrosion cracking on Zircaloy-2 in aqueous NaCl and have observed also that cracking occurs at or above the pitting potential. Cracking was both intergranular and transgranular. The velocities observed were somewhat higher than those observed by the questioner.

*W. J. Baxter*³—You report that the crack velocity in brass is independent of strain rate at low strain rate, but increases with strain rate at higher values of strain rate. You suggest that this transition occurs when the plastic zone size approximates the specimen dimensions. If this is the case, then this transition will depend upon specimen size. As such the reported values of crack velocity at high strain rate are not fundamental, but apply only to your particular experimental conditions.

J. C. Scully (author's closure)—The brevity of my description in the paper has caused a lack of understanding. At low crosshead speeds in α brass (and austenitic stainless steels also) the effective strain rate on tension specimens declines after yielding because the creep rate is faster. The measured load on specimens, for example, falls. At some value of the crosshead speed, which will depend upon the condition of the specimen material, this is not the case. At and above this crosshead speed, the velocity increases with increasing crosshead speed. The velocity values are applicable to any type of specimen and yield 100 percent intergranular fractures up to certain values. The transition point arises from the onset of general yielding across the whole width of the specimen. Below that crosshead speed, the plastic

¹Department of Metallurgical Engineering, The Ohio State University, Columbus, Ohio 43202.

²Cragnolino, G. and Galvele, J. R., Fourth National Meeting on Electrochemistry and Corrosion, La Plata, Argentina, Nov. 1975, to be published.

³General Motors Research Laboratories, Warren, Mich. 48090.

zone is confined to less than the full width of the specimen. It would be wrong to suppose that specimen size is important. What is important is the stress generated by the moving crosshead and its relief by the ensuing creep process. Below the yield point, the latter prevails over the former. The important point is that the constant velocity region is dependent upon the testing system and is not to be explained with reference to mechanistic aspects of stress corrosion cracking.

G. M. Ugiansky,¹ C. E. Johnson,¹ D. S. Thompson,² and E. H. Gillespie²

Slow Strain-Rate Stress Corrosion Testing of Aluminum Alloys

REFERENCE: Ugiansky, G. M., Johnson, C. E., Thompson, D. S., and Gillespie, E. H., "Slow Strain-Rate Stress Corrosion Testing of Aluminum Alloys," *Stress Corrosion Cracking—The Slow Strain-Rate Technique*, ASTM STP 665, G. M. Ugiansky and J. H. Payer, Eds., American Society for Testing and Materials, 1979, pp. 254–265.

ABSTRACT: The use of the slow strain-rate stress corrosion technique for testing aluminum alloys is discussed. This technique is compared to the more frequently used statically loaded, alternate immersion test technique used for evaluating the susceptibility of aluminum alloys to stress corrosion cracking (SCC). Aluminum alloys (2124 and 7075), each in three conditions with differing susceptibilities to SCC, were tested by both the statically loaded alternate immersion test and the slow strain-rate technique. The results of these tests are compared and the slow strain-rate test is shown to be a viable, rapid technique for determining the SCC susceptibility of aluminum alloys.

KEY WORDS: air, alternate immersion test, aluminum alloys, ductility, elongation, heat treatment, sodium chloride, plate gage, reduction of area, slow strain-rate technique, strain rate, stress corrosion cracking, 2124-T851, 7075, 7075-T6, 7075-T7351 alloys

For the high strength aluminum alloys where slight changes in chemistry or heat treatment from one lot to another can cause large differences in the susceptibility to stress corrosion cracking (SCC), there is a need for a rapid reproducible test for differentiating between materials of varying susceptibility to SCC. For many years this need has not been filled very adequately by the use of an alternate immersion test, where aluminum alloy specimens are alternately immersed in sodium chloride (NaCl) solution (generally 3.5 percent) and dried in air. For example, the specimens are immersed for 10 min and then exposed to air for the remaining 50 min of each hour. A

¹Metallurgist and physical science technician, respectively, National Measurement Laboratory, National Bureau of Standards, Washington, D.C. 20234.

²Director of alloy development and metallurgical engineer, respectively, Metallurgical Research Division, Reynolds Metals Company, Richmond, Va. 23219.

specific alternate immersion test for testing the susceptibility to SCC of high strength aluminum alloys has been evaluated recently and compared to the results of atmospheric SCC tests of the same alloys at various locations in the United States [1].³ Although the results from this alternate immersion test indicate differences in susceptibility to SCC for the different heat treatments and the same general trend as is seen in atmospheric testing, there is significant scatter in the data, and the tests are considerably time consuming. There is clearly a need for a faster, more reproducible technique to separate changes in alloy chemistry or heat treatments of varying susceptibility to SCC. The purpose of this investigation is to examine the relative merits of the slow strain-rate test technique as compared to the alternate immersion test for differentiating the susceptibility to SCC of the various heat treatments or slight changes in chemistry of high strength aluminum alloys.

The slow strain-rate test has been used to examine mechanistic aspects of SCC in aluminum alloys by Watkinson and Scully [2] and Scamans et al [3] and to examine the differences in susceptibility to SCC of different aluminum alloys by Brown and Gray [4] and Buhl [5]. However, in this study, the slow strain-rate technique was used to test two high strength aluminum alloys (2124 and 7075), each with three different degrees of resistance to SCC: susceptible to SCC, resistant to SCC, and of intermediate resistance to SCC. The results of these tests were then compared with results from alternate immersion tests for 2124 and the expected performance of 7075 in the various conditions. The advantages and disadvantages of the slow strain-rate technique are also discussed.

Experimental Procedures

Materials and Specimen Description

Two high strength aluminum alloys were used for the present study: 7075 (Al-5.6Zn-2.5Mg-1.6Cu-0.26Cr) and 2124 (Al-4.4Cu-1.5Mg-0.6Mn). Three lots of 2124 alloy with differing levels of resistance to SCC were selected (Table 1). From these three lots ("Series A" with a plate gage of 10 cm, "Series B" with a plate gage of 7.5 cm, and "Series C" with a plate gage of 6.35 cm), short transverse tension specimens of 6.35 mm diameter by 6.0 cm long with a 2.5 cm long gage length of 3.18 mm diameter were machined. The properties of the 2124 alloy are given in Table 2.

The 7075 aluminum alloy was tested in three tempers: "T7351" condition (resistant to SCC), in the "T6" condition (very susceptible to SCC), and in an intermediate heat treatment (of intermediate susceptibility to SCC). The heat treatments for the 7075 alloy are contained in Table 3. The specimens were

³The italic numbers in brackets refer to the list of references appended to this paper.

TABLE 1—*Alternate immersion stress corrosion tests of 2124-T851 subsize smooth tension specimens.*

Specimen Description	Test Results
2124-T851: Solution heat treated 4 h at 493°C (920°F); cold water quenched; stress relieved; aged 12 h at 240°C (375°F)	
Series A: plate gage of 10.2 cm (4 in.)	no failures after 30 day exposure at 50% of yield strength (172 MPa (25 ksi))
Series B: plate gage of 7.6 cm (3 in.)	no failures after 30 day exposure at 50% of yield strength (172 MPa (25 ksi)); 2/3 failures at a stress level of 207 MPa (30 ksi) after 90 day exposure; actual time to failure not known; 1/3 failures at a stress level of 242 MPa (35 ksi) after 90 day exposure; actual time to failure not known
Series C: plate gage of 6.35 cm (2.5 in.)	2/3 failures (8 days, 21 days) at 50% of yield strength (172 MPa (25 ksi))

machined from the short transverse direction and were of the same size as the 2124 specimens. The properties of the 7075 alloy are given in Table 4.

Test Facility

The slow strain-rate test facility was described previously in a paper by Ugiansky and Johnson [6]. However, in the present study, the test cells consisted of 25 cm³ polyethylene cups that surrounded the reduced section of the specimens and were sealed at the bottom. The cup had an inlet port at the bottom and outlet port at the top through which the solution flowed at the rate of 25 cm³/h. The corrosive solution consisted of 3.5 percent (by weight) NaCl (certified American Chemical Society) in distilled water. The reduced section of the specimens were totally immersed for the duration of the slow strain-rate tests. The specimens were pulled in tension to fracture at strain rates of from 6.0×10^{-8} /s to 1.0×10^{-4} /s. Comparative tests also were carried out in air. The data from these tests were collected, stored, and analyzed mathematically as described previously (see footnote 5).

For the alternate immersion tests, the technique used was similar to that described in the ASTM Recommended Practice for Alternate Immersion Stress Corrosion Testing in 3.5% Sodium Chloride Solution (G 44) using tension specimens.

Results and Discussion

The results of the alternate immersion tests of the 2124-T851 and the 7075 alloys are given in Tables 1 and 3, respectively. Table 1 shows that the

TABLE 2—Properties of the 2124-T851 alloy from the slow strain-rate test.

Plate Gage	Test Direction	Strain Rate, 1/s	Test Environment	Tensile Strength MPa	Tensile Strength (ksi)	Elongation % in 1 in.	Reduction of Area, %	Electrical Conductivity % IACS ^a
Series A 10.2 cm (4 in.)	short transverse	1.3 × 10 ⁻⁴	air	451	(65.3)	1.87	5.1	40.0 ^b
		1.3 × 10 ⁻⁴	3.5% NaCl	455	(65.9)	1.96	5.6	
		1.2 × 10 ⁻⁵	air	437	(63.3)	1.87	4.5	
		1.2 × 10 ⁻⁵	3.5% NaCl	441	(63.9)	1.71	4.7	
		1.1 × 10 ⁻⁷	air	444	(64.4)	1.69	6.4	
Series B 7.6 cm (3 in.)	short transverse	1.1 × 10 ⁻⁷	3.5% NaCl	443	(64.2)	1.51	5.2	
		1.3 × 10 ⁻⁴	air	458	(66.4)	2.60	8.2	
		1.3 × 10 ⁻⁴	3.5% NaCl	455	(66.0)	3.10	8.2	
		1.2 × 10 ⁻⁵	air	446	(64.6)	3.61	7.3	
		1.2 × 10 ⁻⁵	3.5% NaCl	444	(64.4)	2.85	6.5	
Series C 6.35 cm (2.5 in.)	short transverse	1.1 × 10 ⁻⁶	air	438	(63.5)	2.85	7.8	
		1.1 × 10 ⁻⁶	3.5% NaCl	442	(64.0)	3.53	8.0	
		5.1 × 10 ⁻⁷	3.5% NaCl	443	(64.2)	2.84	6.3	
		1.1 × 10 ⁻⁷	3.5% NaCl	436	(63.2)	2.94	7.5	
		1.3 × 10 ⁻⁴	air	458	(66.4)	2.28	6.0	
		1.3 × 10 ⁻⁴	3.5% NaCl	459	(66.5)	2.23	5.4	
		1.2 × 10 ⁻⁵	air	442	(64.1)	2.01	6.7	
		1.2 × 10 ⁻⁵	3.5% NaCl	442	(64.1)	1.97	4.6	
		1.1 × 10 ⁻⁶	3.5% NaCl	453	(65.7)	1.44	3.6	
		5.1 × 10 ⁻⁷	3.5% NaCl	420	(60.3)	0.96	2.2	
		1.1 × 10 ⁻⁷	3.5% NaCl	451	(65.4)	1.93	6.2	
		8.8 × 10 ⁻⁸	air	445	(64.5)	1.91	7.6	
		6.0 × 10 ⁻⁸	3.5% NaCl	440	(63.8)	2.40	7.9	

^aConversion factor—1 in. = 25.4 mm.

^bIACS = International Annealed Copper Standard.

^cShould be the same for Series B and C.

TABLE 3—Alternate immersion stress corrosion resistance of 7075 subsized smooth tension specimens.^a

Specimen Description	Typical Test Results
T7351: solution heat treated 4 h at 482°C (900°F); cold water quenched; stress relieved aged 6 to 8 h at 107°C (220°F) plus 24 to 30 h at 163°C (325°F)	no failures after 30 day exposure at 75% of yield strength (269 MPa (39 ksi))
Intermediate: solution heat treated as T6 but aged 4 h at 121°C (250°F) plus 4 h at 163°C (325°F); used 19°C (35°F)/h heat-up rate from 24°C (75°F)	specimens fail within 3 to 10 days of exposure at 75% of yield strength (304 MPa (44 ksi))
T6: solution heat treated 1 h at 471°C (880°F) plus 1 h at 496°C (925°F), quenched in cold 50% H ₂ O and 50% Quenchant "A" (a quenching oil), aged 24 h at 121°C (250°F)	specimens fail within 1 day of exposure at 75% of yield strength (321 MPa (48 ksi))

^aNo actual alternate immersion testing was conducted on these particular 7075 specimens. The time to failure ranges given are based on a very extensive experience of stress corrosion testing 7075. The performance of 7075 is quite predictable, thus we feel quite confident in the ranges given.

susceptibility to SCC of the three series of 2124-T851 specimens increases in the order: Series A < Series B < Series C. We also note that Series A and B have identical results when stressed at 50 percent of yield strength (172 MPa (25 ksi))—no failures after 30 days—whereas, the Series C tests resulted in 2 out of 3 failures in less than 30 days when stressed at 50 percent of yield strength (172 MPa (25 ksi)). Therefore, Series C is definitely more susceptible than either Series A or B. The alternate immersion test results for Series B indicate a possible intermediate susceptibility to SCC since 3 of 6 specimens failed at stresses greater than 50 percent of yield strength in less than 90 days. Two of three specimens failed at a stress level of 207 MPa (30 ksi) and one of three specimens failed at a stress level of 242 MPa (35 ksi).

For the same 2124-T851 alloy and series, the slow strain-rate SCC tests results are given in Figs. 1, 2, and 3 for Series A, B, and C, respectively. These figures compare two measures of ductility—reduction of area (ROA) and elongation—versus strain rate. Series A (Fig. 1) in NaCl and in air are very similar and the elongation results in NaCl and in air are practically coincident. Also, both sets of data vary little with strain rate. For Series B (Fig. 2), the results of the tests in NaCl and in air differ by more than for Series A indicating a possibly greater susceptibility to SCC for Series B than for Series A. However, since the absolute values of the ROA (~7 percent) and of the elongation (~3 percent) are so low, the error in the measurement of these data could be significant and could account for the variations in ductility. On the other hand, the largest reduction in ductility seen in the data of Fig. 2 occurs at a strain rate of $5.1 \times 10^{-7}/s$. This is at exactly the same strain rate where the minima in both the ROA and in the elongation versus strain rate curves occurs for Series C (Fig. 3). Therefore, it appears that the

TABLE 4—Properties of the 7075 alloy from the slow strain-rate test.

Temper	Test Direction	Strain Rate, 1/s	Test Environment	Tensile Strength MPa	Tensile Strength (ksi)	Elongation % in 1 in.	Reduction of Area, %	Electrical Conductivity % IACS ^a
T7351	short transverse	1.4×10^{-5}	air	463	(67.1)	4.7	17.7	42.0
		1.3×10^{-5}	3.5% NaCl	464	(67.2)	4.5	18.6	
		2.5×10^{-6}	3.5% NaCl	460	(66.7)	4.9	15.6	
		7.0×10^{-7}	air	465	(67.4)	5.6	16.7	
		7.0×10^{-7}	3.5% NaCl	466	(67.6)	4.5	16.1	
		1.4×10^{-7}	3.5% NaCl	442	(64.0)	5.3	19.8	
		1.4×10^{-5}	air	518	(75.0)	5.0	14.2	
Intermediate	short transverse	1.2×10^{-5}	3.5% NaCl	515	(74.7)	4.0	14.8	35.0
		2.5×10^{-6}	3.5% NaCl	524	(76.0)	4.2	15.0	
		7.0×10^{-7}	air	526	(76.2)	4.6	15.9	
		7.0×10^{-7}	3.5% NaCl	507	(73.5)	2.4	8.3	
		1.8×10^{-7}	3.5% NaCl	501	(72.6)	1.7	4.6	
		5.0×10^{-8}	3.5% NaCl	468	(67.3)	1.1	1.1	
		1.0×10^{-4}	air	506	(73.3)	4.5	17.5	
T6	short transverse	1.3×10^{-4}	3.5% NaCl	500	(72.5)	4.3	13.1	33.0
		1.2×10^{-5}	air	499	(72.3)	4.3	14.3	
		1.2×10^{-5}	3.5% NaCl	477	(69.2)	4.0	12.5	
		1.9×10^{-6}	3.5% NaCl	476	(69.0)	1.9	9.5	
		1.2×10^{-7}	air	500	(72.5)	4.2	13.9	
		1.1×10^{-7}	3.5% NaCl	442	(64.1)	0.8	3.0	
		5.3×10^{-8}	3.5% NaCl	413	(59.9)	1.1	5.7	

Conversion factor—1 in. = 25.4 mm.
^aIACS = International Annealed Copper Standard.

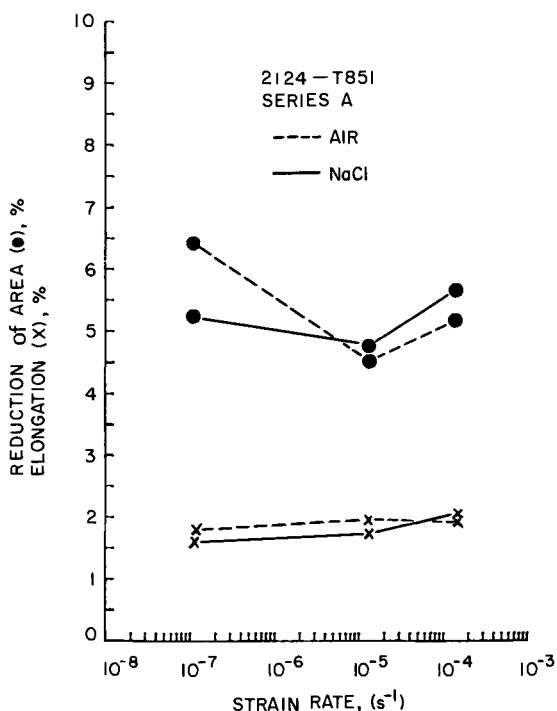


FIG. 1— Slow strain-rate SCC test results for 2124-T851 Series A.

low value for the ROA at $5.1 \times 10^{-7}/s$ for Series B in NaCl is indicative of marginal susceptibility to SCC. For Series C, the great differences between the air and NaCl values of both ROA and elongation, with minima at $5.1 \times 10^{-7}/s$, indicate a strong susceptibility to SCC for Series C 2124-T851 in 3.5 percent NaCl solution.

These slow strain-rate test results are in good agreement with the alternate immersion test results. By the slow strain-rate test (especially at $\sim 5 \times 10^{-7}/s$), Series A has little susceptibility to SCC, Series B results has a possible, slight, susceptibility to SCC, and Series C results reveal a very definite susceptibility to SCC.

The susceptibility to SCC of the three different heat treatments of 7075 are given as alternate immersion test results in Table 3 and as slow strain-rate test results in Figs. 4 to 6. Table 3 shows the susceptibilities to SCC to increase in the order T7351 < intermediate < T6. The slow strain-rate SCC test results in Fig. 4 (T7351) reveal a variation in ductility with strain rate. This variation in ductility is practically the same for the air tested and the NaCl tested specimens, indicating no loss in ductility (no susceptibility to SCC) in NaCl. However, the results for the slow strain-rate SCC tests of the

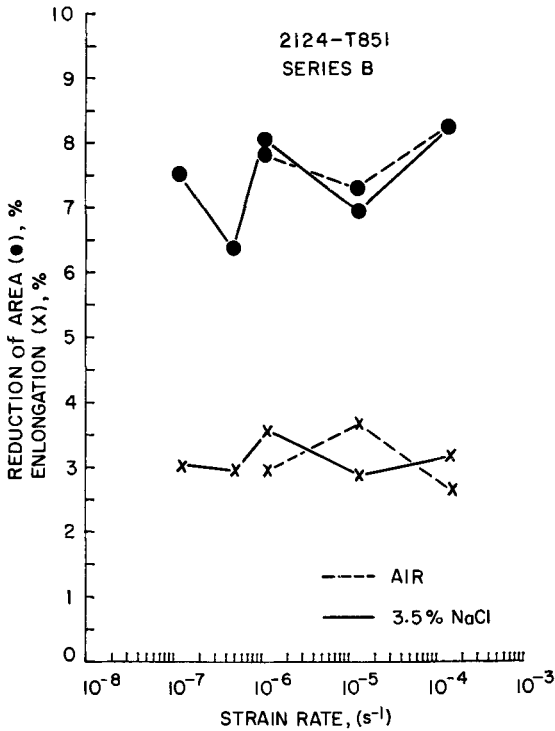


FIG. 2—Slow strain-rate SCC test results for 2124-T851 Series B.

7075-intermediate and the 7075-T6 indicate strong susceptibility to SCC in NaCl for both heat treatments, Figs. 5 and 6. In Fig. 5, it is seen that the 7075-intermediate exhibits minimum ductility at a strain rate of $5 \times 10^{-8}/s$. The ductility (both ROA and elongation) in NaCl differs significantly from the air values at strain rates of less than $2.5 \times 10^{-6}/s$. Comparing the results for the 7075-intermediate in Fig. 5 with those for the 7075-T6 in Fig. 6, we see that the ductility of 7075-T6 in NaCl deviates from the air values at strain rates of less than $1.2 \times 10^{-5}/s$ with a minimum at a strain rate of $1.1 \times 10^{-7}/s$. Since one of the prominent theories for the mechanism of SCC involves the relative rates of repassivation and dissolution when the oxide film at the surface of the metal is ruptured, this theory is used to judge the differences in susceptibility between the 7075-intermediate and 7075-T6. Because in NaCl both the strain rate at which the minimum ductility occurs and the strain rate at which deviation from the values determined in air are higher for 7075-T6 than for 7075-intermediate, it seems reasonable to assume that this is good evidence for the greater susceptibility to SCC of 7075-T6 than for 7075-intermediate; 7075-T6 seems to exhibit a higher crack velocity.

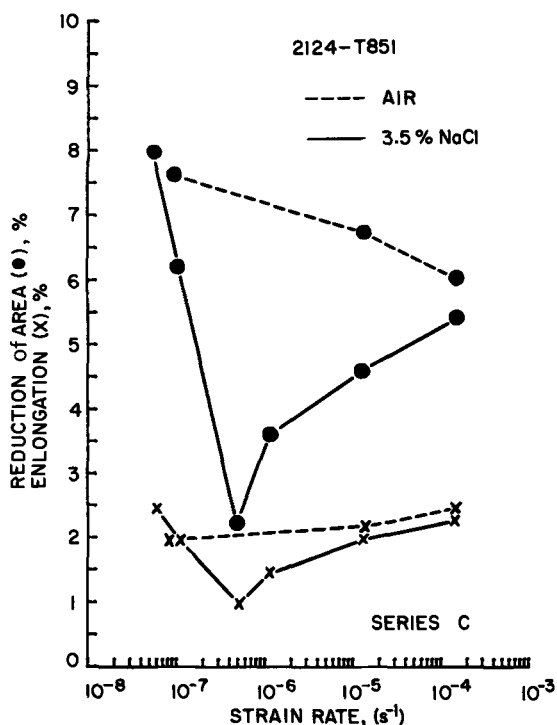


FIG. 3—Slow strain-rate SCC test results for 2124-T851 Series C.

Summary

High strength aluminum alloys 2124 and 7075 (each in three different conditions with respect to susceptibility to SCC) were tested in 3.5 percent NaCl solutions by both the alternate immersion technique and the slow strain-rate technique. Both test techniques for the two alloys indicated the same changes in the degree of susceptibility to SCC with respect to heat treatment for alloy 7075 and plate gage thickness for alloy 2124. The results of the slow strain-rate technique indicate that the minimum in the ductility versus strain-rate curves shifts to higher strain rates for the more susceptible 7075 alloy heat treatments and, also, that the results for the tests in the NaCl solution deviate from the results of the tests in air at higher strain rates for more susceptible alloys. Although more work is needed to validate the usefulness of the slow strain-rate SCC test technique for other aluminum alloys, the results of this study indicate that this technique could be a viable, rapid technique for determining the SCC susceptibility of aluminum alloys.

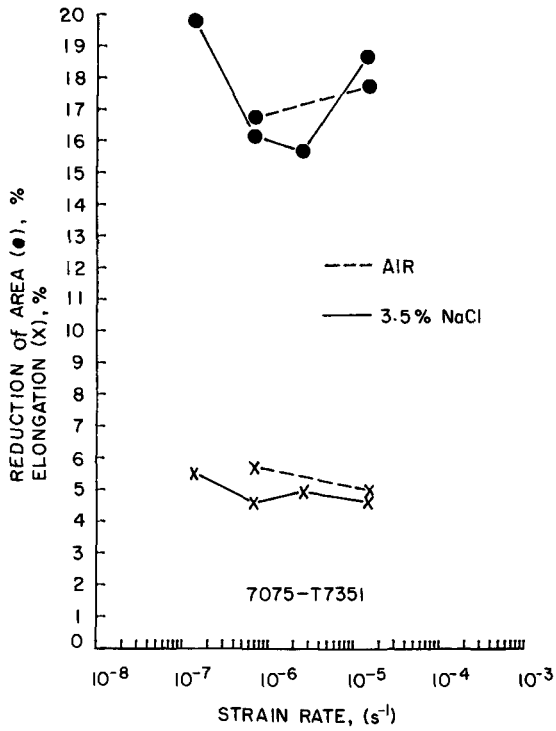


FIG. 4—Slow strain-rate SCC test results for 7075-T7351.

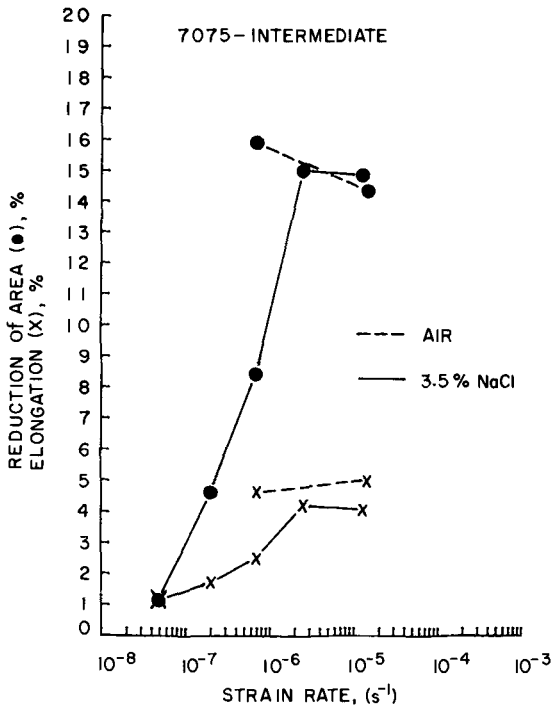


FIG. 5—Slow strain-rate SCC test results for 7075-intermediate.

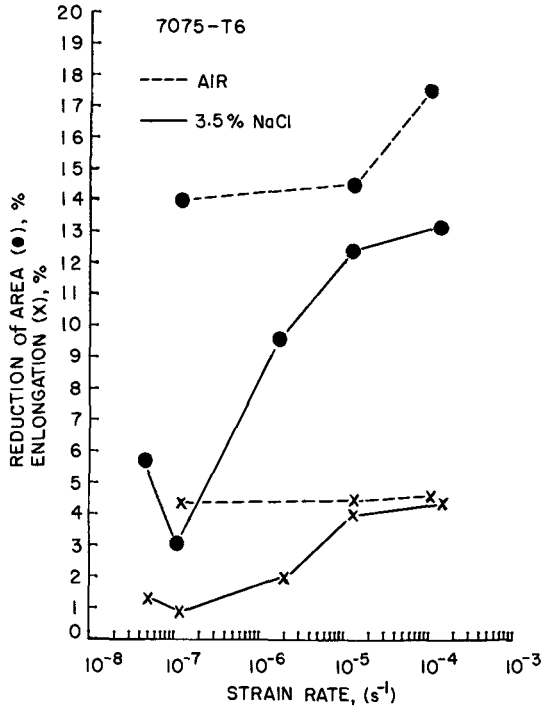


FIG. 6—Slow strain-rate SCC test results for 7075-T6.

References

- [1] Sprowls, D. O., Summerson, T. J., Ugiansky, G. M., Epstein, S. G., and Craig, H. L., Jr. in *Stress Corrosion—New Approaches*. ASTM STP 610, American Society for Testing and Materials, 1976, pp. 3-31.
- [2] Watkinson, F. E. and Scully, J. C., *Corrosion Science*, Vol. 12, 1972, pp. 905-924.
- [3] Scamans, G. M., Alani, R., and Swann, P. R., *Corrosion Science*, Vol. 16, 1976, pp. 443-459.
- [4] Brown, A. R. G. and Gray, J. A., "A Comparison of RAE Stress Corrosion Test Data on Aluminum Alloys Including the Merits of the Testing Techniques," Technical Report 74153, Royal Aircraft Establishment.
- [5] Buhl, H., this publication, pp. 333-346.
- [6] Ugiansky, G. M. and Johnson, C. E., this publication, pp. 113-131.

Effect of Oxyanions and Chloride Ion on the Stress Corrosion Cracking Susceptibility of Admiralty Brass in Nonammoniacal Aqueous Solutions

REFERENCE: Kawashima, A., Agrawal, A. K., and Staehle, R. W., "Effect of Oxyanions and Chloride Ion on the Stress Corrosion Cracking Susceptibility of Admiralty Brass in Nonammoniacal Aqueous Solutions," *Stress Corrosion Cracking—The Slow Strain-Rate Technique*, ASTM STP 665, G. M. Ugiansky and J. H. Payer, Eds., American Society for Testing and Materials, 1979, pp. 266-278.

ABSTRACT: The stress corrosion cracking (SCC) susceptibility of admiralty brass in several nonammoniacal solutions of pH ~8 has been investigated at 25°C using the slow strain-rate technique. The SCC tests were made at a controlled potential of 300 mV_H. This potential is close to the cupric oxide/cuprous oxide (CuO/Cu₂O) equilibria, in near neutral solutions (6 < pH < 8), on the potential-pH diagram of copper. In the present study, cracking occurred in several solutions; the severity of the cracking depended upon the type of anion present in the test solution. The order of anions in decreasing tendency to promote SCC in admiralty brass was: NO₂⁻ > NO₃⁻ > ClO₃⁻ > SO₄⁼ > MoO₄⁼ > Cl⁻ > WO₄⁼ > HCO₃⁻ > B₄O₇⁼ > CrO₄⁼. The estimated crack velocity ranged from high values of the order of 10⁻⁷ m/s in the nitrite solution to no cracking in the phosphate and the solutions following it in the above series. The cracking was always transgranular with considerable branching in some cases.

KEY WORDS: admiralty metal, stress corrosion cracking, oxyanions, slow strain rate

Admiralty brass is widely used for tubing in condensers of fossil fuel and nuclear power plants, as well as for other industrial applications [1].² Service failures of admiralty brass due to stress corrosion cracking (SCC) have been summarized by Papamarcos [1] and Reynolds and Pement [2]. The susceptibility of brasses to SCC in ammoniacal environments is well known, and extensive efforts in the past have been directed towards elucidating its mechanisms [3-6]. However, several species other than ammonia derivatives

¹ Visiting research associate, adjunct assistant professor, and professor, respectively, Department of Metallurgical Engineering, The Ohio State University, Columbus, Ohio 43210.

² The italic numbers in brackets refer to the list of references appended to this paper.

have been reported to cause SCC in brasses. Bobylev [7] has reported, but without giving any references or experimental evidence, that brasses can undergo SCC in solutions containing nitrites, carbonates, pyrophosphates, and alkalis. Johnson and Leja [8], and Uhlig et al [6] have shown that α -brasses crack in alkaline solutions of citrate and tartrate; these can complex with copper like ammonia derivatives. Stress corrosion cracking occurs in ammonia-free nitrate solutions as shown by Graf [9] for 80, 70, and 63 percent copper brasses, and this has been confirmed by Reynolds and Pement [2] for admiralty brass. Graf has also reported SCC of 70 and 63 percent copper brasses, but not of 80 percent copper brass, in a ferric chloride (FeCl_3) solution. Copper sulfate solutions as well as acid sodium sulfate solutions have been shown to cause cracking in admiralty and 70/30 brasses, respectively, by Pinchback et al [10] and by Pickering and Byrne [11]. On the other hand, Lynes [12] has found no SCC in admiralty brass in acid sulfate solutions of ferric sulfate ($\text{Fe}_2(\text{SO}_4)_3$), cerium sulfate ($\text{Ce}(\text{SO}_4)_2$), sodium metaborate (NaBO_3) and sodium molybdate (Na_2MoO_4), and also no cracking in 70/30 brass in acid solutions of Na_2MoO_4 and bismuth trichloride (BiCl_3).

Uhlig [6,13] suggested that SCC in α -brasses and admiralty brass does not occur in sulfate solutions without ammonia or its derivative. However, Kawashima et al [14] have shown recently that SCC of admiralty brass occurs in nonammoniacal sulfate solutions over a wide pH and potential range. Specimens were tested in 0.5 M sodium sulfate (Na_2SO_4) solutions whose pH was adjusted with either sulfuric acid (H_2SO_4) or sodium hydroxide (NaOH) to the desired value. These tests were conducted at room temperature in a naturally aerated condition, using a slow strain-rate technique.

The boundary between cracking and no cracking of admiralty brass in 0.5 M Na_2SO_4 solutions is shown on the potential-pH diagram of a copper-water ($\text{Cu-H}_2\text{O}$) system in Fig. 1. The cracking was always transgranular with considerable branching and occurred only at potentials more noble to, but never below, the corrosion potential. The minimum potential for SCC is about 200 mV_H. The over potential required for cracking to take place varied with pH; it was about 20 mV in the pH range 4 to 9, but increased to ~150 mV at either end of the forementioned pH range. In very acidic (pH < 2) and very basic (pH > 12) solutions only general corrosion and no SCC was observed.

The purpose of the present investigation was to find the effect of other oxyanions and chloride ion on the SCC susceptibility of the admiralty brass in nonammoniacal solutions. All the SCC tests in the present study were conducted in nearly neutral solutions of various anions at the controlled potential of 300 mV_H. This potential falls close to the cupric oxide/cuprous oxide ($\text{CuO/Cu}_2\text{O}$) equilibria in the neutral solutions ($6 < \text{pH} < 8$) on the Pourbaix diagram. Also, several investigators [3,4] have shown that suscep-

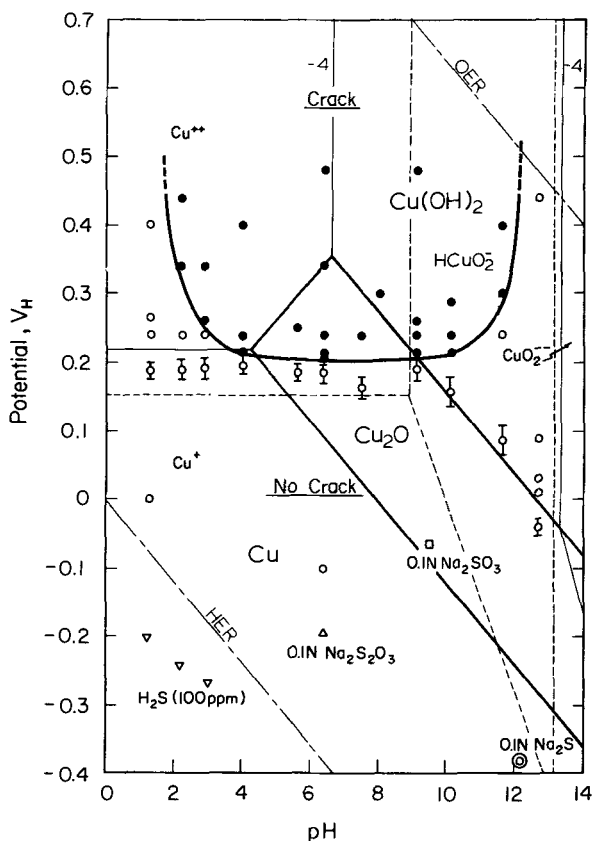


FIG. 1—The SCC boundary of admiralty brass in sulfate solutions on potential—pH diagram of copper [14]. Solid points represent cracking and the open points no cracking.

tibility of α -brasses is at a maximum in the 200 to 300 mV_H range in neutral ammoniacal sulfate solutions.

Experimental

Admiralty brass was tested using a slow strain-rate technique at a strain rate of $1.5 \times 10^{-5} s^{-1}$. This strain rate was chosen because it was found to be an optimum rate for admiralty brass in sulfate solutions [14]. All the tests were conducted at room temperature, $25 \pm 2^\circ C$, in naturally aerated solutions, and a reference test was conducted in air. The test cell was of glass, 200 ml in volume, the lower end of which was plugged with a neoprene stopper and the upper end was open to the atmosphere. The potential of the specimens was controlled at 300 mV_H with a potentiostat, and the current was recorded on a strip-chart recorder. The reference electrode

used was mercury-mercurous sulfate. The straining was started a few minutes after applying the potential. The load during straining was monitored with a load cell on another strip-chart recorder. Fractured specimens were examined metallographically.

In a separate set of experiments, anodic polarization curves of unstressed admiralty brass were taken in various solutions using a potential stepping method. The potential was raised in steps of 25 mV at 2-min intervals, and the current at the end of an interval was recorded. The stepping was started at the steady state corrosion potential of the specimen and stopped below the oxygen evolution region.

Material used was commercial CDA 443 admiralty brass with a nominal composition of 71Cu-28Zn-1Sn-0.06As. The alloy was received as extruded tube blanks of about 7.6 cm diameter and 0.76 cm wall thickness. The blanks were longitudinally cut and cold rolled into 0.25 cm thick plates. Tension specimens, 22.9 cm by 0.125 cm, with a gage length of 1.25 cm and width of 0.51 cm were machined from the plates. The specimens were annealed for 1 h at 550°C under a blanket of argon and furnace cooled, which gave a final average grain diameter of 0.05 mm. Prior to testing, these were longitudinally abraded with 600 grade silicon carbide (SiC) paper, rinsed with acetone and distilled water, and air dried.

All solutions used in this study were prepared from reagent grade chemicals and double distilled water. To obtain the test anion, its sodium salt was used; the salts were sodium nitrite (NaNO_2), sodium nitrate (NaNO_3), sodium chlorate (NaClO_3), sodium sulfate (Na_2SO_4), sodium molybdate (Na_2MoO_4), sodium chloride (NaCl), sodium tungstate (Na_2WO_4), sodium phosphate (Na_2HPO_4), sodium bicarbonate (NaHCO_3), sodium tetraborate ($\text{Na}_2\text{B}_4\text{O}_7$), and sodium chromate (Na_2CrO_4). The normality of all the solutions was unity, except for Na_2MoO_4 , Na_2HPO_4 , $\text{Na}_2\text{B}_4\text{O}_7$, and Na_2CrO_4 solutions whose normality was 0.1, because of either solubility or pH limitations. The pH of solutions in a few cases was adjusted with dilute NaOH to bring it up to 8. In the case of $\text{Na}_2\text{B}_4\text{O}_7$ and Na_2HPO_4 solutions, pH had to be lowered with boric acid and phosphoric acid, respectively, in order to bring solutions closer to pH 8. The pHs of various solutions used are listed in Table 1.

Results

The results of slow strain-rate tests are summarized in Table 1, where the quasisteady state corrosion potential of the unstrained specimen, ratio of the fracture stress in solution to that in air ($\sigma_{\text{soln}}/\sigma_{\text{air}}$), estimated crack velocity, surface appearance after exposure, and the cracking mode of the admiralty brass in different solutions are listed. Data in the table are arranged in the order of decreasing SCC susceptibility, that is, increasing fracture stress ratio. Thus the lowest fracture ratio, 0.09, indicating the maximum SCC susceptibility in the nitrite solution, is at the top; and the

TABLE 1—The corrosion potential, ratio of fracture stress in solution to that in air, average crack velocity, surface appearance of the fractured specimen, and the cracking mode of admiralty brass in various solutions at 25°C.

Anion	pH	E_{cor} , mV _H	$\sigma_{soln}/\sigma_{air}$	V_{avg} , m/s	Surface Appearance	Cracking Mode ^a
NO ₂ ⁻	8.1	80	0.09	2×10^{-7}	black film	TC
NO ₃ ⁻	8.0	150	0.34	1×10^{-8}	reddish brown	TC
ClO ₃ ⁻	8.0	210	0.51	6×10^{-9}	reddish brown	TC
SO ₄ ⁼	8.0	180	0.55	6×10^{-9}	reddish brown	TC
MoO ₄ ⁼	10.2	100	0.68	4×10^{-9}	bright yellow	TC, mild
Cl ⁻	8.4	20	0.84	4×10^{-10}	black film	TC, mild
WO ₄ ⁼	9.4	80	0.89	2×10^{-9}	bright yellow	TC, mild
HPO ₄ ⁼	8.1	120	0.93		bright yellow	NC
HCO ₃ ⁻	8.0	80	0.95		bright yellow	NC
B ₄ O ₇ ⁼	8.0	150	0.96		bright yellow	NC
CrO ₄ ⁼	8.7	40	0.97		bright yellow	NC

^aTC = transgranular cracking, and

NC = no cracking.

highest ratio, 0.97, for the chromate solution in which no cracking was observed, is at the bottom of the table. The fracture ratio in each case was calculated from the load recorded at fracture during straining in the test solution and the fracture load observed in air. Photomicrographs of the specimens are shown in Fig. 2 along with the corresponding fracture ratio which is indicated by a bar of the appropriate length.

The crack velocity was calculated from the average crack penetration in the gage section of the specimen and the time for attaining the maximum load during straining. The time for crack initiation in these calculations was assumed to be the yield point of the brass. There was little difference (<10 percent) in value of the crack velocity when time to fracture, instead of time to maximum load, was used in the calculation. The calculated values are only to give an idea of the magnitude of the crack propagation rate, and the values should not be considered as absolute rates. In the case of Na₂HPO₄, NaHCO₃, Na₂B₄O₇, and Na₂CrO₄ solutions, no cracks were detected in the fractured specimens.

The decreasing crack velocity values, from NO₂⁻ to Cl⁻, correlate the rising fracture ratios or the decreasing SCC susceptibility of admiralty brass in these solutions. However, in WO₄⁼ solution the crack velocity calculated is one order of magnitude higher than expected for the $\sigma_{soln}/\sigma_{air}$ ratio. The secondary cracks in this case were very few in comparison to the Cl⁻ or other solutions where SCC occurred, and the measured crack lengths may have included notches from the dropping off of a few surface grains or abrasion marks with crack-like appearance, thus giving a higher average crack velocity than warranted.

The appearance of the exposed specimens varied with the test solution. A black or brown film was observed on the surface with severe SCC. In all

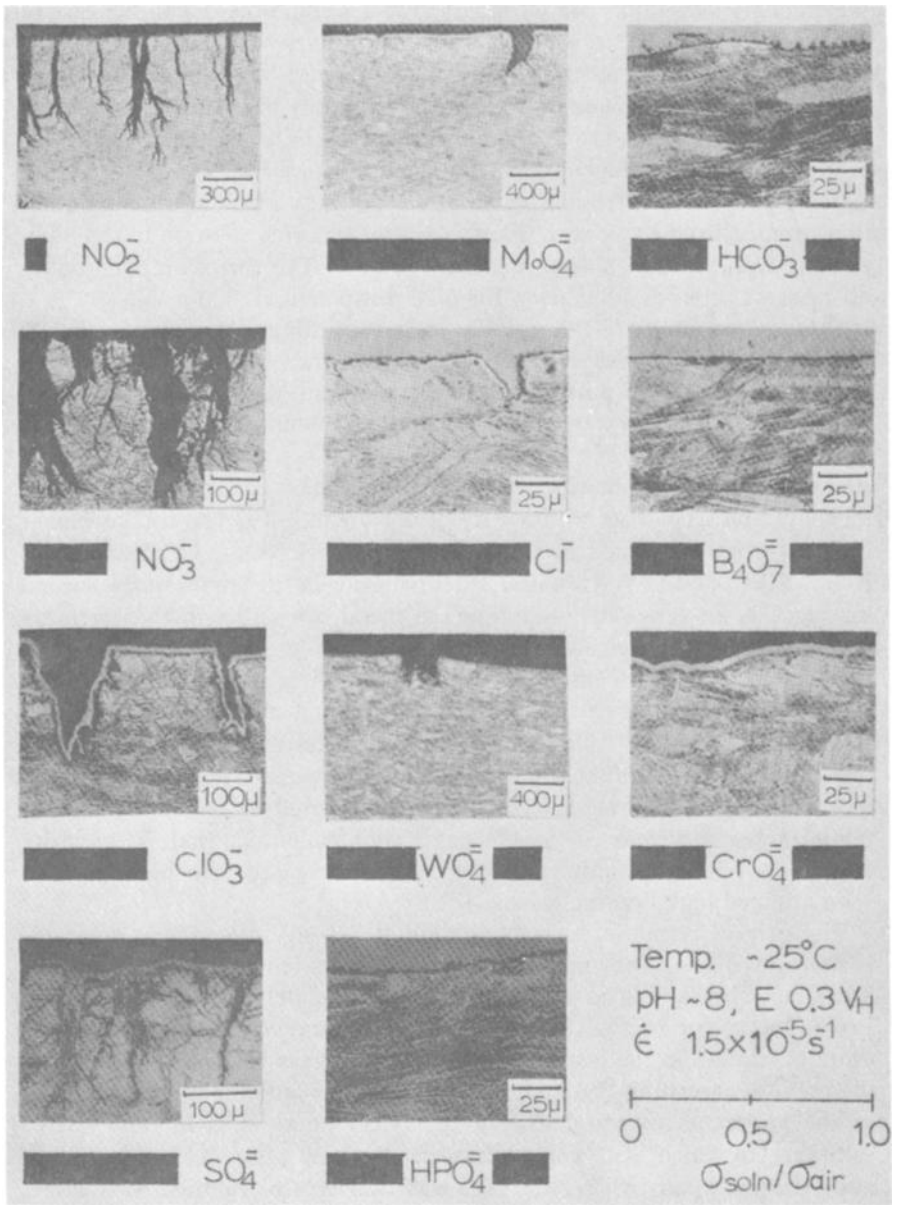


FIG. 2—Photomicrographs of fractured specimens and the corresponding fracture stress ratios of admiralty brass in various solutions.

other cases, except Cl^- solution, the surface had a bright yellow luster. In the Cl^- solution, the surface was covered with a black film, even though the cracking was mild. The secondary cracks were numerous in the case of $\text{SO}_4^{=}$, NO_3^- , and NO_2^- solutions, but relatively few in ClO_3^- , Cl^- , and $\text{MoO}_4^{=}$ solutions. As mentioned before, there were very few cracks in the $\text{WO}_4^{=}$ solution. The mode of cracking of admiralty brass in every case was transgranular, with considerable branching in $\text{SO}_4^{=}$, NO_3^- , and NO_2^- solutions, and little branching in ClO_3^- solution (see Fig. 2).

The steady state corrosion potential of admiralty brass in different solutions ranged from the lowest, 20 mV_H, in the chloride solution to the highest, 210 mV_H, in the chlorate solution, Table 1. The corrosion potential in all cases was considerably below the SCC test potential, 300 mV_H.

Polarization curves of the metal in various solutions are shown in Fig. 3. The polarization curves can be grouped into two sets according to the current density at the potential of interest, 300 mV_H. Thus the first set of solutions in which the current density was less than 10^{-4} A/cm² includes, in decreasing order, $\text{HPO}_4^{=}$, $\text{B}_4\text{O}_7^{=}$, $\text{MoO}_4^{=}$, $\text{CrO}_4^{=}$, and $\text{WO}_4^{=}$. The metal showed only passive behavior in this set of solutions, particularly in the latter four. The second set with a current density of $\sim 10^{-4}$ A/cm² or higher includes solutions, listed in the increasing order, NO_2^- , HCO_3^- , ClO_3^- , NO_3^- , $\text{SO}_4^{=}$, and Cl^- . An initial Tafel behavior in the curves of the second set suggests an active dissolution of the metal, even though the corrosion potentials in this set are not necessarily lower than in the first set. The Tafel region was followed by either a brief passivation as in NO_2^- , ClO_3^- , and Cl^- , or high limiting current with no passivation as in $\text{SO}_4^{=}$ and NO_3^- solutions. The HCO_3^- solution with a short Tafel region was a boundary line case between the first and second sets. The passivity in NO_2^- , ClO_3^- , and Cl^- solutions is only marginal; it was destroyed by increasing the potential a few millivolts above the passivation potential, that is, passivity existed for only a few millivolts, the current increased with potential and soon attained high limiting values, $\sim 10^{-1}$ A/cm².

The current response during straining at 300 mV_H in various solutions is shown in Fig. 4. The apparent current densities (current/original surface area) during straining in all cases are approximately half to one decade lower, except for HCO_3^- solution where it is practically the same, than that at 300 mV_H in the respective polarization curves in Fig. 3. An interesting point to observe in Fig. 4 is the more than one order of magnitude jump in the apparent current density at the yield point in NO_2^- and ClO_3^- solutions, in which SCC was very severe. No such jump is seen for NO_3^- and $\text{SO}_4^{=}$ solutions where the SCC was also severe. In these two cases, however, the apparent current density was considerably higher at all times than the highest in NO_2^- and ClO_3^- solutions.

The highest apparent current density in Fig 4 is for Cl^- solution in which the cracking was only nominal. Similarly, for HCO_3^- in which no

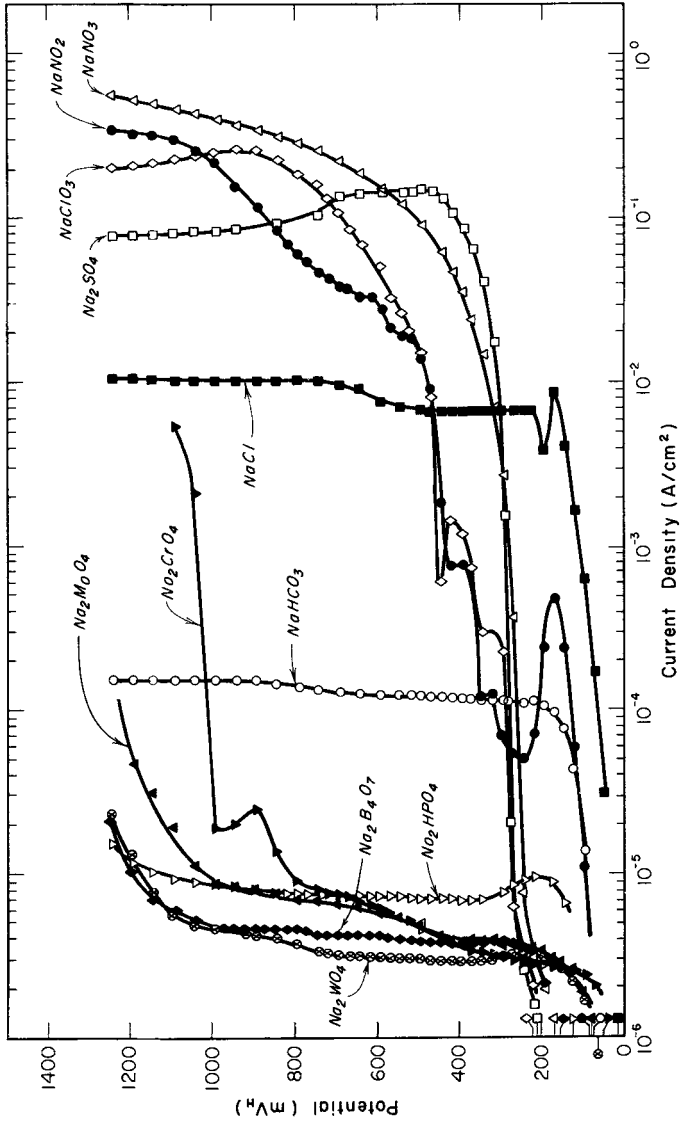


FIG. 3—Anodic polarization behavior of admiralty brass in various solutions.

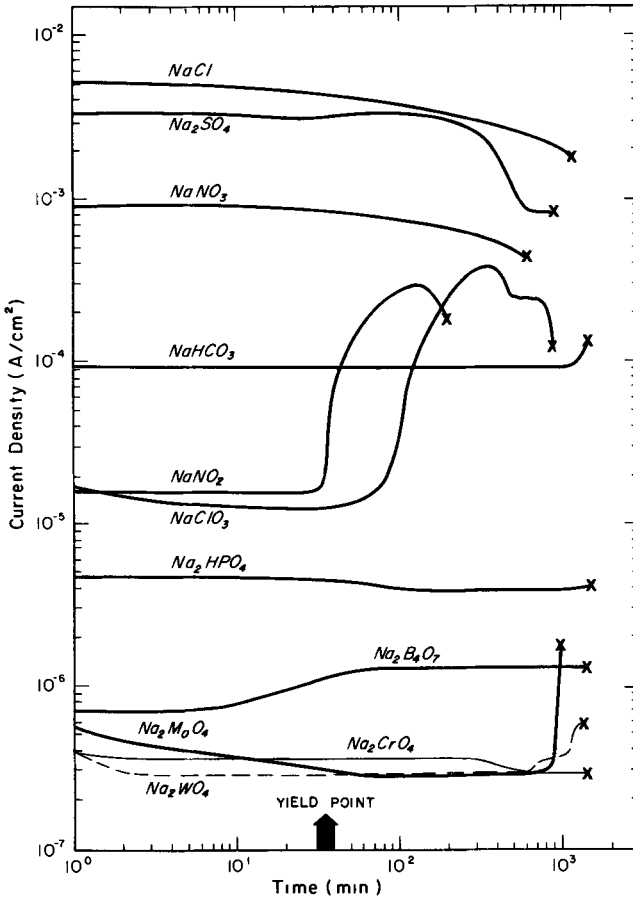


FIG. 4—The current response of admiralty brass at 300 mV_H during straining in various solutions.

SCC was observed the apparent current density is of the same order of magnitude as with NO_2^- and ClO_3^- . In other solutions where the SCC was either nominal or absent, the apparent current density is indeed one to two orders of magnitude lower than that in NO_2^- or ClO_3^- solution.

Discussion

The results in Table 1 and Fig. 2 clearly show that admiralty brass undergoes SCC in nonammoniacal solutions. The SCC condition for an alloy is largely determined by its potential, temperature, pH, and the ionic species in the test environment. In the present study the potential, pH, and temperature were arbitrarily fixed at 300 mV_H , pH ~ 8 , and 25°C. The

only variable in the experiments was the anionic species. The objective of this discussion is to identify the properties of ions responsible for the SCC in admiralty brass and to correlate these properties with the SCC intensity.

Tracy [15] has reported that in general the corrosion resistance of copper alloys is akin to that of pure copper in an acid environment. The corrosion rate increases with the acidity and oxidizing power of the solution. Strong oxidizing agents, such as dissolved oxygen and cupric and ferric salts, when present in a solution greatly accelerate the corrosion rate even in neutral solutions. Tracy also has pointed out that the low-solubility corrosion products tend to reduce the corrosion rate, presumably because they form a protective coating on the metal surface.

One generally accepted mechanism of SCC is the anodic dissolution of the bare metal, at the dislocation slip steps forming at the surface of the stressed specimen, at a dissolution rate which is faster than the repassivation rate in the solution [16]. Usually the solution chemistry at the crack site changes from the bulk because of the hydrolysis of the metal ions and quickly produces an acidic condition which promotes dissolution and cracking. The presence of anions of a weak acid near the crack site may buffer the solution and prevent the development of acidity and thereby retard SCC.

In view of the foregoing, the chemical properties of an anion that must be considered are its oxidizing power, ionization constant of the oxyacid, and the solubility of its copper salt.

From Fig. 2 and Table 1, it is clear that the most severe cracking in admiralty brass occurred in solutions of strong oxidizing anions, namely, NO_2^- , NO_3^- , and ClO_3^- and no cracking occurred in solutions of non-oxidizing anions $\text{B}_4\text{O}_7^{=}$, $\text{HPO}_4^{=}$, and HCO_3^- . Whereas amongst the mild oxidizing anions, namely, $\text{SO}_4^{=}$, $\text{WO}_4^{=}$, $\text{MoO}_4^{=}$, and $\text{CrO}_4^{=}$, the cracking was severe in the $\text{SO}_4^{=}$ solution, mild in the $\text{WO}_4^{=}$ and the $\text{MoO}_4^{=}$ solutions, and none in the $\text{CrO}_4^{=}$ solution. The anions which caused severe cracking also form strong oxyacids, for example, HNO_3 , HClO_3 , and H_2SO_4 . The other anions which caused mild or no cracking form only weak oxyacids, for example, H_2WO_4 , H_2MoO_4 , and H_2CO_3 . This suggests that the oxyanions which are strongly oxidizing and also form strong acids are likely to cause most severe cracking in admiralty brass, whereas those with weak oxidizing property and acid forming character will cause only mild or no SCC.

The chloride ion behaved differently from the other anions, as should be expected, since it is not an oxyanion. The cracking was mild in the chloride solution in spite of the fact that Cl^- forms a strong acid, hydrochloric.

The size of an anion affects its mobility, hydration number, and absorbability, all of which in turn affect the reaction rate at the electrode surface. In order to determine whether the size has an affect on the SCC propensity

of admiralty brass, the fracture stress ratio was plotted against the radius, R , of the anions (see Fig. 5). The R values in Fig. 5 are the thermochemical Yatsimirskii radii [17] which semiquantitatively represent the ion sizes. A very good relationship is seen between the R and $\sigma_{\text{soln}}/\sigma_{\text{air}}$ for solutions in which cracking occurred. The bigger the anion the less severe was cracking and vice-versa. The radius of the WO_4^- ion was not listed in reference [17] and therefore could not be shown in Fig. 5. The manner in which anion size plays a part in SCC process is not obvious. Certainly, further consideration is required to discern the significance of size effects.

The solubility of many of the copper salts of interest are not readily available in a form which could be quantitatively related with the SCC susceptibility of admiralty brass. However, some general observations can be made from the data available. The anions, for example, NO_2^- , NO_3^- , ClO_3^- , and SO_4^- , which form soluble copper salts, produced most severe cracking, with one exception of Cl^- which is discussed later. The rest whose salts are sparingly soluble or insoluble produced only mild or no cracking. The current densities in Figs. 3 and 4 nearly follow the solubility and therefore also the SCC trend. The brief passivity in NO_2^- and ClO_3^- solutions, in Fig. 3, may be due to their basic copper salts, that is, $\text{Cu}(\text{NO}_2)_2 \cdot 3\text{Cu}(\text{OH})_2$ and $\text{Cu}(\text{ClO}_3)_2 \cdot 3\text{Cu}(\text{OH})_2$ respectively, which are insoluble. The insoluble salt films were probably also responsible for the low currents below the yield point during straining, shown in Fig. 4. Once

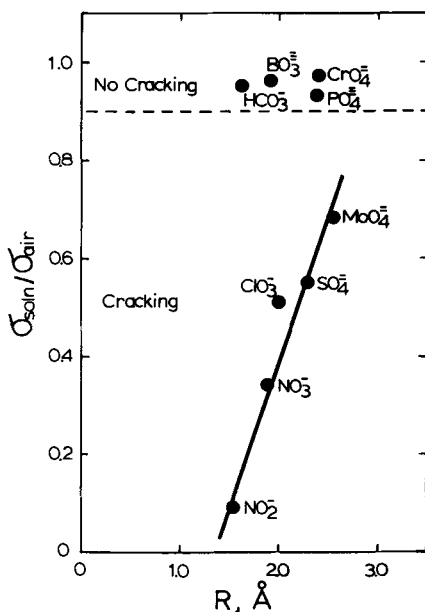


FIG. 5—The fracture stress ratio of admiralty brass versus Yatsimirskii radii of oxyanions.

the plastic deformation perforated the film and exposed the bare metal, the current jumped approximately ten fold.

The reason for high current and little SCC in chloride solution is not entirely clear. The cupric salt (CuCl_2) is extremely soluble, but the basic salt $\text{CuCl}_2 \cdot 3\text{Cu}(\text{OH})_2$ and the cuprous salt (CuCl) are insoluble in aqueous solutions. Flatt and Brook [18] have reported the presence of cuprous chloride film on the surface of 70/30 brass at all potentials above the corrosion potential in sodium chloride solutions. It is possible that CuCl only was formed at the slip steps, the insoluble CuCl hindered further dissolution and therefore SCC.

Conclusions

The ammonium ion or its derivative is not necessary for causing transgranular SCC in admiralty brass. The SCC propensity in nonammoniacal environments is effected by the oxidizing power of the oxyanion in the solution, pK_a of the oxyacid, size of the anion, and the solubility of its copper salt. The order of anions in decreasing tendency to promote SCC in admiralty brass at a controlled potential of 300 mV_H was: $\text{NO}_2^- > \text{NO}_3^- > \text{ClO}_3^- > \text{SO}_4^{=} > \text{MoO}_4^{=} > \text{Cl}^- > \text{WO}_4^{=} > \text{HPO}_4^{=} > \text{HCO}_3^- > \text{B}_4\text{O}_7^{=} > \text{CrO}_4^{=}$. The estimated crack velocity ranged from high values of the order of 10^{-7} m/s in nitrite solution to no cracking in phosphate and the solutions following it in the above series. The cracking was always transgranular with considerable branching in some cases.

Acknowledgments

This work was sponsored by the Electric Power Research Institute of Palo Alto, Calif. under contract number RP311-1. The encouragement and support of E. L. Zebroski, L. J. Martel, and T. O. Passell of EPRI are greatly appreciated.

References

- [1] Papamarcos, J., *Power Engineering*, July 1973, p. 24.
- [2] Reynolds, S. D., Jr. and Pement, F. W., *Materials Performance*, Vol. 13, 1974, p. 21.
- [3] Mattsson, E., *Electrochimica Acta*, Vol. 3, 1961, p. 279.
- [4] Hoar, T. P. and Booker, C. J. L., *Corrosion Science*, Vol. 5, 1965, p. 821.
- [5] Pugh, E. N. in *The Theory of Stress Corrosion Cracking in Alloys*, J. Scully, Ed., North Atlantic Treaty Organization, Brussels, 1971.
- [6] Uhlig, H., Gupta, K., and Liang, W., *Journal of the Electrochemical Society*, Vol. 122, 1975, p. 343.
- [7] Bobylev, A. V. in *Intercrystalline Corrosion and Corrosion of Metals Under Stress*, I. A. Levin, Ed., Consultants Bureau, New York, 1962.
- [8] Johnson, H. E. and Leja, J., *Corrosion*, Vol. 22, 1966, p. 178.
- [9] Graf, L. in *Fundamental Aspects of Stress Corrosion Cracking*, R. W. Staehle, A. J.

- Forty, and D. van Rooyen, Eds., National Association of Corrosion Engineers, Houston, 1969.
- [10] Pinchback, T. R., Clough, S. P., and Heldt, L. A., *Corrosion*, Vol. 32, 1976, p. 469.
- [11] Pickering, H. W. and Byrne, P. J., *Corrosion*, Vol. 29, 1973, p. 325.
- [12] Lynes, W., *Corrosion*, Vol. 21, 1965, p. 125.
- [13] Uhlig, H., *Corrosion*, Vol. 33, 1977, p. 189.
- [14] Kawashima, A., Agrawal, A. K., and Staehle, R. W., *Journal of the Electrochemical Society*, Vol. 124, 1977, p. 1822; also, EPRI Project RP311-1, Reports 30 June 1976 and 31 Dec. 1976, Ohio State University.
- [15] Tracy, A. W. in *Corrosion Resistance of Metals and Alloys*, F. L. LaQue and H. R. Copson, Eds., 2nd ed., Reinhold, New York, 1963.
- [16] Staehle, R. W. in *The Theory of Stress Corrosion Cracking in Alloys*, J. C. Scully, Ed., North Atlantic Treaty Organization, Brussels, 1971.
- [17] Huhey, J. E. in *Inorganic Chemistry: Principles of Structure and Reactivity*, Harper and Rowe, New York, 1972, p. 77.
- [18] Flatt, R. K. and Brook, P. A., *Corrosion Science*, Vol. 11, 1971, p. 185.

A. I. Asphahani¹

Slow Strain-Rate Technique and Its Applications to the Environmental Stress Cracking of Nickel-Base and Cobalt-Base Alloys

REFERENCE: Asphahani, A. I., "Slow Strain-Rate Technique and Its Applications to the Environmental Stress Cracking of Nickel-Base and Cobalt-Base Alloys," *Stress Corrosion Cracking—The Slow Strain-Rate Technique*, ASTM STP 665. G. M. Ugiansky and J. H. Payer, Eds., American Society for Testing and Materials, 1979, pp. 279–293.

ABSTRACT: The slow strain-rate technique (SSRT) was used to investigate the susceptibility of several nickel-base and cobalt-base alloys to environmental stress cracking. This technique was successful in revealing the stress corrosion cracking (SCC) tendency of a given alloy in a specific environment. Yet, the measurable quantities (percent elongation, percent reduction in area, load at failure, and the total time to failure) were not always consistent indicators of the SCC phenomenon nor of its severity. Metallographic examination allowed to quantify the susceptibility to SCC through the measurement of the average "secondary stress corrosion crack" depth. The effects of strain rate, solution temperature, and solution concentration were clearly established using the SSRT. However, the effect of cold work on the susceptibility to hydroxide stress cracking was inconclusive. Also, the SSRT was not able to distinguish the SCC phenomenon from that of a "stress assisted intergranular corrosion" occurring on sensitized material.

KEY WORDS: stress corrosion cracking, strain rate, nickel-base alloys, cobalt-base alloys, hydroxide stress cracking, chloride stress cracking, stress assisted intergranular corrosion

Several techniques are used to investigate the susceptibility of various alloys to environmental stress cracking [1–4].² These techniques are based on accelerated laboratory tests designed to generate data that can be properly translated to practical applications and directly correlated with service performances.

¹Group leader, Corrosion, Stellite Division, Cabot Corporation, Kokomo, Ind. 46901.

²The italic numbers in brackets refer to the list of references appended to this paper.

From these different accelerated test methods, the slow strain-rate technique (SSRT) is receiving considerable attention. The validity of this technique was first established by Parkins and his co-workers in their studies of the stress corrosion cracking (SCC) phenomenon [5,6]. Also, through their evaluations of the performances of carbon steel in carbonate solutions [7], they confirmed the advantages of this technique as a reproducible, accelerated "sorting test," capable of revealing the SCC tendencies of materials in "potent" environments.

When used to test high performance alloys, the SSRT was successful in evaluating the susceptibility of a variety of cobalt-base alloys to hydroxide stress cracking [1]. With this technique, relevant and reproducible SCC data were generated within a few days, while it had taken several months to induce cracking in U-bend specimens exposed to the same hydroxide environment.³ However, for some sensitized nickel-base alloys, the SSRT had a tendency to confuse the stress assisted intergranular corrosion with the SCC phenomenon.⁴

This paper presents data which demonstrate the applicability of the SSRT in studying the environmental stress cracking of various nickel-base and cobalt-base alloys. The response of this accelerated testing method to the environmental, mechanical, metallurgical, and electrochemical factors that alter the SCC susceptibility of these alloys are described.

Experimental Procedure

Materials

Although several nickel-base and cobalt-base alloys were tested using the SSRT, the pertinent data are limited to those generated on Incoloy^{®5} alloy 825, Haynes Stellite^{®6} Alloy No. 6B, Hastelloy^{®6} Alloy C-276, and Hastelloy[®] Alloy B. The nominal chemical compositions of these alloys are given in Table 1.

Specimens

Tension specimens were used, measuring 1.8 cm (0.70 in.) average gage length and 0.18 cm (0.07 in.) average reduced section diameter. The overall length of the specimen varied from 23 cm (\approx 9 in.) to 3 cm (\approx 1.25 in.); the small specimens were very practical in that they allowed versatile test-

³Silence, W. L., Corrosion Laboratory, Stellite Division, Cabot Corporation, private communication.

⁴Asphahani, A. I., Corrosion Laboratory, Stellite Division, Cabot Corporation, 1976, unpublished research.

⁵Registered trademark, The International Nickel Company, Inc.

⁶Registered trademark, Cabot Corporation.

TABLE 1—Alloys nominal chemical composition (weight percent).

Alloy	Ni	Co	Fe	Cr	Mo	W	Mn	Si	C	Others
Alloy 825	42	...	30	21	3	...	1 ^a	0.5 ^a	0.05 ^a	Cu + Ti-2.5
Alloy 6B	3 ^a	53	3 ^a	30	1.5 ^a	4.5	2 ^a	2 ^a	1	
Alloy C-276	55	2.5 ^a	5	16	16	4	1 ^a	0.08 ^a	0.02 ^a	V-0.35 ^a
Alloy B	61	2.5 ^a	5	1 ^a	28	...	1 ^a	1 ^a	0.05 ^a	V-0.30

^aMaximum.

ing of fabricated products, as illustrated in Fig. 1. When comparative data were needed, small flat specimens measuring 4.5 by 0.5 by 0.1 cm ($1\frac{3}{4}$ by $\frac{3}{16}$ by 0.04 in.) were used. These were tested as plastically deformed C-shape specimens ($\epsilon \approx 7$ percent). This type of specimen was used extensively by Uhlig and his co-workers in SCC testing of stainless steels [8,9], mild steels [10,11], high strength steels [12], and brass [13].

Equipment

The slow strain-rate testing unit used in this work was similar to the one used by Deegan and Wilde in their study of the SCC behavior of steel in liquid ammonia [14]. A detailed description of the apparatus is given by Payer et al [15]. For tests in aqueous environments, 1-litre containers were used (glass container for tests in magnesium chloride (MgCl_2) solu-

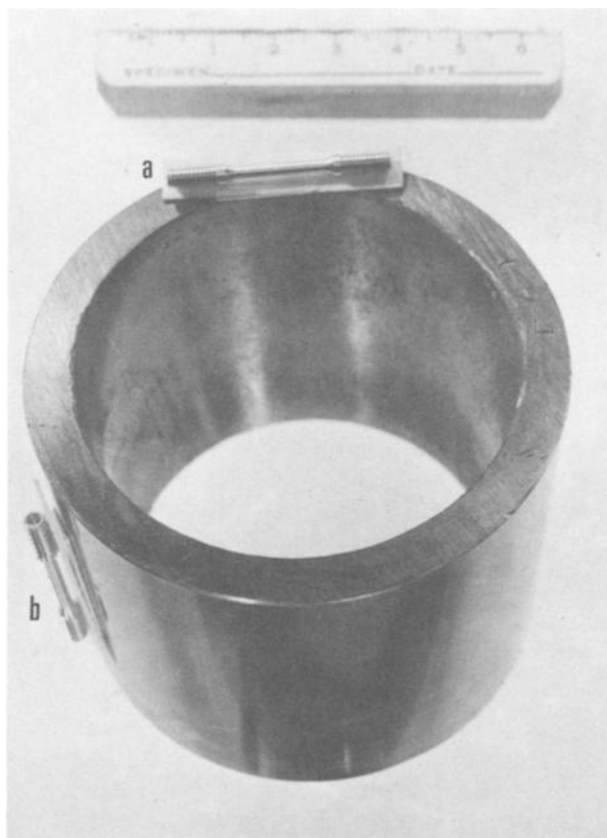


FIG. 1—Small tension specimen as prepared from fabricated products: (a) tangential and (b) longitudinal.

tions and an Alloy C-276 container for tests in sodium hydroxide (NaOH) solutions). The containers were surrounded by resistance heating elements, which allowed for testing at elevated temperatures. A thermocontroller helped to maintain a constant solution temperature ($\pm 3^\circ\text{C}$). Appropriate electrical connections allowed tests to be conducted on specimens maintained at a constant applied potential using a potentiostat, two platinum sheets (3.5 by 2 by .02 cm) as counter electrodes, and a saturated calomel electrode (SCE) as the reference electrode. The crosshead displacement, the applied load, and the elapsed time were recorded. All testing solutions were prepared from single distilled water and reagent grade chemicals.

Evaluation and Reporting of Data

To assess the susceptibility of the alloys to stress cracking, a tension specimen is tested in the desired environment using the slow strain-rate testing method. The values of the percent reduction in elongation ($\Delta l/l$), the percent reduction in area ($\Delta A/A$), the maximum load (expressed as an ultimate tensile strength), or the time to failure are each compared directly to the corresponding values of a similar specimen tested in inert environment, for example, air. In general, these comparisons reveal the occurrences of stress cracking and provide a quantitative assessment of the SCC phenomenon [4]. None of the above comparisons is universally valid, and only metallographic examinations of the specimen determine the presence or absence of SCC [5]. The results in Table 2 reaffirmed this point. The lower values of $\Delta l/l$, $\Delta A/A$, ultimate tensile strength, and time to failure confirmed the susceptibility of Alloy 825 to SCC in 42 percent MgCl_2 at 147°C . However, the susceptibility of this alloy to stress cracking in 50 percent NaOH at 190°C was not revealed in the same way. The measured

TABLE 2—Results of slow strain-rate tests, $\dot{\epsilon} \approx 3.4 \times 10^{-6} \text{ s}^{-1}$.

	$\Delta l/l$, %	$\Delta A/A$, %	UTS, MPa	Time, h	Observations
Alloy 825, air, 25°C	32	65	710	35	ductile material
Alloy 825, 50% NaOH, 190°C	30	61	703	33	few secondary stress corrosion cracks in the necked region
Alloy 825, MgCl_2 , 147°C	20	47	407	26	secondary stress corrosion cracks over the full gage length
Alloy 6B, air, 25°C	15	21	1572	27	low ductility material
Alloy 6B, 28% NaOH, 147°C	13	18	1572	29	secondary stress corrosion cracks over the full gage length

values of $\Delta l/l$, $\Delta A/A$, ultimate tensile strength, and time to failure in the hydroxide environment were close to those obtained in air, even though optical examination showed the presence of several secondary stress corrosion cracks in the necked region. Similar behavior was also observed in a "low-ductility" material, Alloy 6B. The tensile data ($\Delta l/l$, $\Delta A/A$, ultimate tensile strength, and time to failure, as measured from tests in 28 percent NaOH at 147°C (Table 2), did not unequivocally indicate the occurrences of SCC; however, stress corrosion was easily confirmed by the presence of multiple secondary cracks along the reduced section.

The inconsistency of the measurable properties $\Delta l/l$, $\Delta A/A$, ultimate tensile strength and time to failure in revealing SCC severity led to a systematic metallographic examination of a longitudinal cross section of the tensile gage region. Any environmental stress cracking occurrences were confirmed by the presence of secondary stress corrosion cracks, as shown in Fig. 2. The average secondary stress corrosion crack length, \bar{l} , was used to quantify the susceptibility of an alloy to stress cracking.

Results

Environmental Factors—Solution Temperature and Concentration

For all tested materials, increasing the solution temperature induced susceptibility to SCC and increased the cracking severity. Typical results generated on Alloy 6B indicated that at low temperatures of 25 and 65°C, this alloy was highly resistant to SCC in the 28 percent NaOH solution. However, at elevated temperatures of 107°C and greater, secondary stress corrosion cracks were observed. The number and depth of cracks increased with increasing temperature.

At 147°C, dilution of the solution concentration helped to eliminate the secondary stress corrosion cracks that were observed on Alloy 825 tested in concentrated hydroxide solution. The average stress corrosion crack length decreased from $\bar{l} \approx 3.6 \times 10^{-5}$ m (1.4×10^{-3} in.) in 50 percent NaOH solution to $\bar{l} < 10^{-5}$ m ($< 0.1 \times 10^{-3}$ in.) in 10 percent NaOH solution. Similar behavior was also observed on several austenitic nickel-base alloys.

As the time of exposure to the damaging environment depended on the crosshead speed (or strain rate), its effects on the stress cracking tendencies are treated next.

Mechanical Factors—Strain Rate, Stress Level, and Stressing Direction

Within the appropriate strain-rate leading to stress cracking (10^{-5} to 10^{-7} s⁻¹), the severity of the SCC phenomenon was increased with decreasing values of the strain rate for all tested materials. Representative

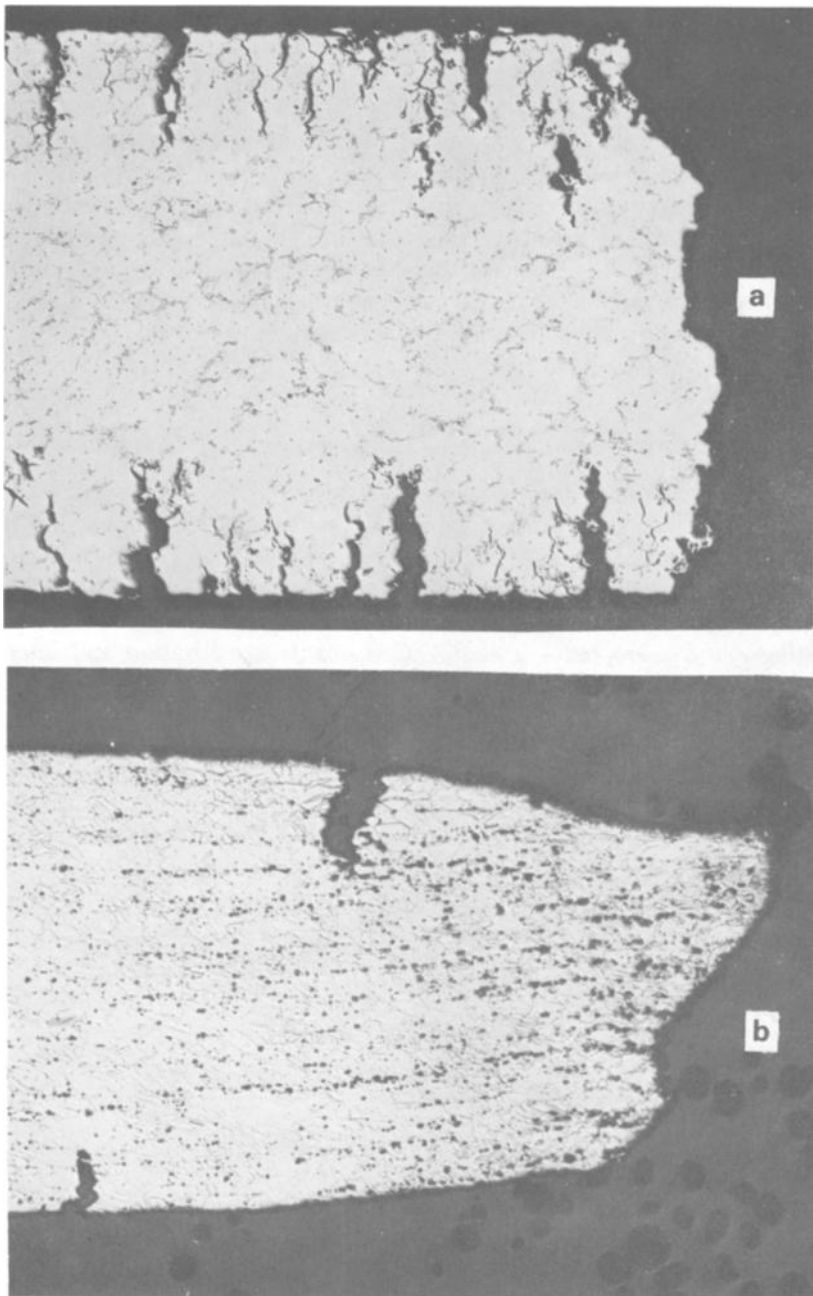


FIG. 2—Longitudinal cross section of tensile gage region showing secondary stress corrosion cracks; $\dot{\epsilon} \approx 3.4 \times 10^{-6} \text{ s}^{-1}$; $\times 40$. (a) Low ductility material (Alloy 6B) and (b) ductile material (Alloy B).

results were obtained on Alloy 825. They indicated that the hydroxide stress cracking of this alloy became more severe when the strain rate was decreased from $3.4 \times 10^{-6} \text{ s}^{-1}$ to $2.4 \times 10^{-6} \text{ s}^{-1}$, crack lengths of $1.8 \times 10^{-5} \text{ m}$ and $3.6 \times 10^{-5} \text{ m}$, respectively.

In addition to its flexibility for testing at various slow crosshead speeds, the slow strain-rate unit allowed static testing at constant load. This mode of testing was used to investigate the effects of stress level and orientation of the applied tensile stress on the resistance of Alloy C-276 tubing to hydrogen cracking. The data are presented in Table 3. No failure, within 300 h, occurred in longitudinally oriented specimens, tensile loaded to various stress levels. However, the specimen stressed transverse to the cold work direction, failed in 23 h at stress levels above the yield strength.

Metallurgical Factors—Composition, Heat Treatment, and Cold Work

The slow strain-rate technique was sensitive to the effects of alloying elements on the cracking mode in nickel-base alloys. As summarized in Table 4 and illustrated in Fig. 3, annealed Alloy C-276 (Ni-16Cr-16Mo) showed transgranular stress cracking, while annealed Alloy B (Ni-28Mo) failed intergranularly in the 50 percent NaOH solution at 147°C . Heat treating Alloy C-276 for 1 h at 871°C (to cause sensitization and intergranular corrosion due to secondary M_6C carbides and Mu -phase precipitations [16,17]) did not affect its transgranular mode of cracking. However, sensitization of Alloy B for 1 h at 800°C (secondary M_6C carbide

TABLE 3—Effects of stress level and of stressing direction. Alloy C-276, 37 percent cold work + 100 h at 500°C , cathodic charging $i_c = 40 \text{ mA/cm}^2$, 5 volume percent H_2SO_4 , 25°C .

Stress Level	Time to Failure, h	
	Longitudinal, $Y = 1076 \text{ MPa}$	Tangential, $Y = 924 \text{ MPa}$
95% Y	> 300	> 300
100% Y	> 300	> 300
110% Y	> 300	23

TABLE 4—Effects of heat treatment, Alloys C-276 and B. 50 percent NaOH at 147°C , $\dot{\epsilon} = 3.4 \times 10^{-6} \text{ s}^{-1}$.

Alloys	Average Length of Secondary Stress Corrosion Cracks
C-276, annealed	transgranular SCC: $13 \times 10^{-5} \text{ m}$ ($5 \times 10^{-3} \text{ in.}$)
C-276, 1 h at 871°C	transgranular SCC: $13 \times 10^{-5} \text{ m}$ ($5 \times 10^{-3} \text{ in.}$)
B, annealed	intergranular SCC: $30 \times 10^{-5} \text{ m}$ ($12 \times 10^{-3} \text{ in.}$)
B, 1 h at 800°C	no SCC: 0

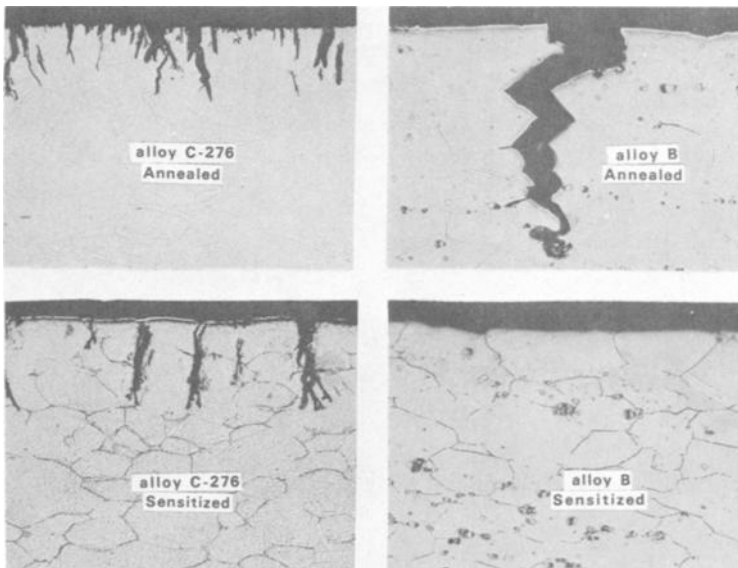


FIG. 3—Effects of heat treatment on the hydroxide stress cracking of Alloys C-276 and B; $\dot{\epsilon} \approx 3.4 \times 10^{-6} \text{ s}^{-1}$; $\times 100$.

precipitation) eliminated the intergranular cracking and suppressed the SCC phenomenon observed in annealed material (Table 4 and Fig. 3).

For erosion shield application hydroxide stress cracking is a major problem. In this instance involving the evaluation of cobalt-base alloys, the SSRT was able to define within short times of testing the proper chemical composition and processing procedure necessary to raise the resistance of these alloys to SCC (see footnote 4).

For cold worked material, typical results generated by the SSRT are presented in Table 5. They show that at the same slow strain rate ($\dot{\epsilon} \approx 3.4 \times 10^{-6} \text{ s}^{-1}$) the 50 percent cold swaged Alloy C-276 exhibited good resistance to hydroxide stress cracking compared to the annealed material. This apparent resistance to stress cracking of cold worked specimens was not observed at slower strain rates of 9 and $5.3 \times 10^{-7} \text{ s}^{-1}$; however, the cold swaged specimens still exhibited fewer and smaller secondary stress corrosion cracks than did the annealed specimens. These observations were contradictory to results from constant total strain tests using the C-shape specimens ($\epsilon \approx 7$ percent). Upon exposure to the 50 percent NaOH at 147°C , several deep cracks were observed on the cold worked specimens, while the annealed specimens exhibited shallower attacks, as shown in Fig. 4 for Alloy C-276 and Alloy MP 35 N Multiphase^{®7} (35Ni, 35Co, 20Cr, 10Mo).

⁷Registered trademark, Standard Pressed Steel Company.

TABLE 5—Effects of cold work, alloy C-276.

Alloy Condition	Strain Rate, s^{-1}	Environment	$\Delta A/A$, %	UTS, MPa	Time to Failure, h	Average Length of Secondary Stress Corrosion Cracks
Mill annealed	3.4×10^{-6}	air	71	745	60	0
Mill annealed	3.4×10^{-6}	50% NaOH, 147°C	61	593	52	13×10^{-5} (5 mils) SCC
50% cold swagged	3.4×10^{-6}	air	49	1524	17	0
50% cold swagged	3.4×10^{-6}	50% NaOH, 147°C	51	1503	18	$<1 \times 10^{-5}$ m (<0.1 mils) no obvious SCC
50% cold swagged	9×10^{-7}	air	53	1558	29	0
50% cold swagged	9×10^{-7}	50% NaOH, 147°C	47	1524	30	2.5×10^{-5} m (1 mil) SCC
50% cold swagged	5.3×10^{-7}	air	51	1593	51	0
50% cold swagged	5.3×10^{-7}	50% NaOH, 147°C	47	1565	60	4.8×10^{-5} m (1.9 mils) SCC

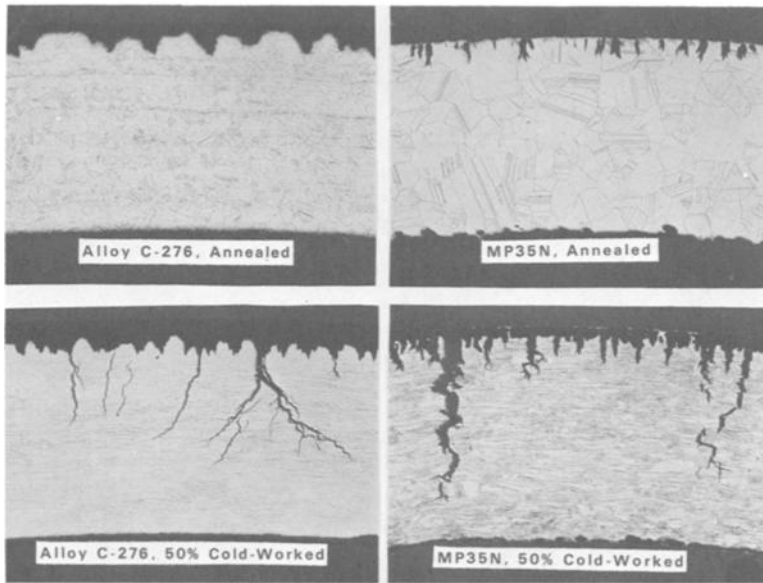


FIG. 4—C-shape specimens tested in 50 percent NaOH, 147°C; $\times 25$. Alloy C-276, 200-h exposure; Alloy MP35N, 75-h exposure.

Electrochemical Factors—Applied Current and Potential

The concept of cathodic protection was checked for its compatibility with the slow strain-rate testing of nickel-base alloys. Stress corrosion cracking was prevented upon applying a constant cathodic current density of $\approx 20 \mu\text{A}/\text{cm}^2$ on Alloy C-276 specimens tested in 50 percent NaOH at 147°C (Fig. 5). Higher current density suppressed SCC completely, and the cathodically protected specimens exhibited the ductile behavior observed in air. Yet, upon cathodically charging the material with 40 mA/cm² in the same solution at room temperature, brittle intergranular failure occurred as shown in Fig. 5, indicating the case of a hydrogen cracking phenomenon [18].

Slow strain-rate tests also were conducted on specimens polarized to constant applied potentials. The effects of applied anodic potential on the performances of Alloy C-276 in chloride environment were investigated. At all anodic potentials, no secondary cracks were observed on annealed material, and accelerated uniform corrosion occurred. Thinning of the specimens took place at more noble potential value of $-100 \text{ mV}(\text{SCE})$, due to the increase in the dissolution rate; however, upon sensitizing the alloy (1 h at 871°C), several secondary cracks appeared in the reduced section when the specimens were anodically polarized in the range of -150 to -75 mV , SCE. The brittle fracture and secondary cracks resembled

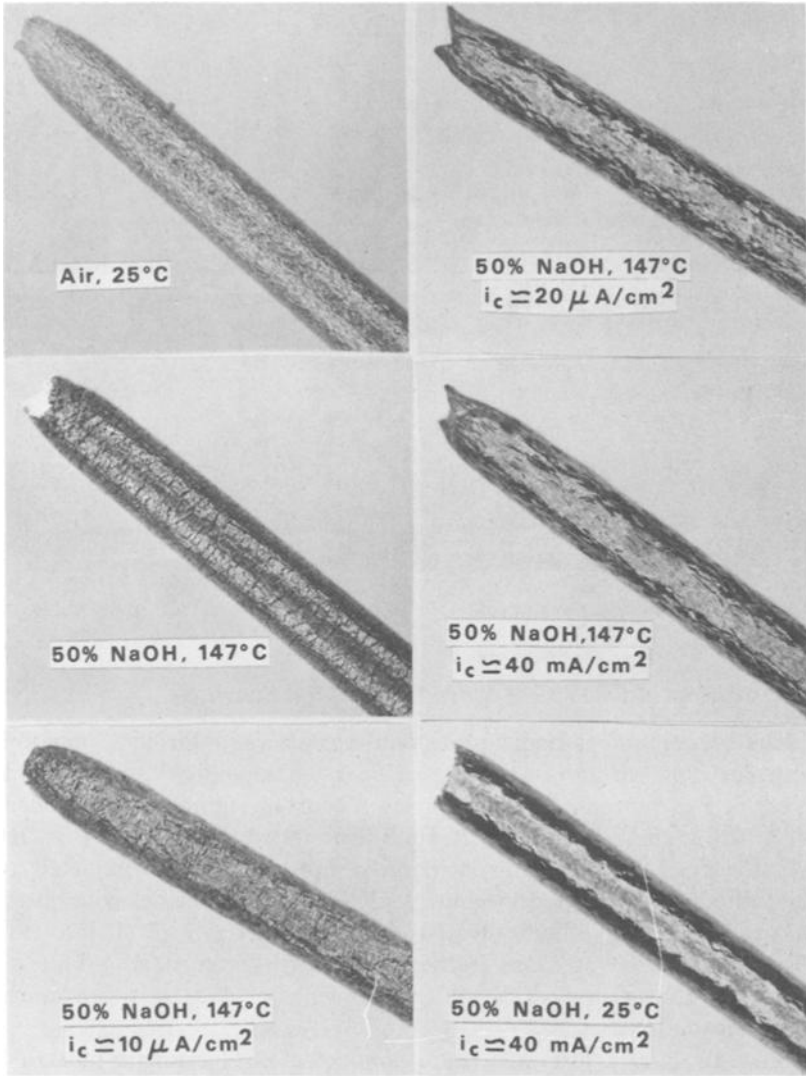


FIG. 5—Effects of cathodic current density on the hydroxide stress cracking of Alloy C-276; $\dot{\epsilon} = 3.4 \times 10^{-6} s^{-1}$; $\times 7$.

those of a material susceptible to SCC; however, similar tests on C-shape specimens (constant total strain tests, $\epsilon = 7$ percent) revealed the occurrences of localized intergranular dissolution on both the tension and the compression sides of the sensitized material. This behavior was also observed on sensitized material tested at their freely corroding potential in an acidic oxidizing environment that promotes localized corrosion (see footnote 4).

Discussion

The present observations, which concern the applicability of the slow strain-rate testing methods for investigating the environmental stress cracking of high performance nickel-base and cobalt-base alloys, are in general agreement with most of the published information on SCC.

The SSRT successfully responded to the variations in testing temperature and in solution concentration. Similar to the behavior of steels in 35 percent NaOH [10,15], the hydroxide stress cracking phenomenon in cobalt-base alloys was accelerated with increasing solution temperature. Also, the effectiveness that the concentrated 50 percent NaOH solution had on inducing stress cracking of the Alloy 825 (as compared to the ineffectiveness of the 10 percent NaOH solution) was in agreement with results on mild steel, indicating higher susceptibility to SCC in more concentrated solution [5].

Furthermore, when testing the high performance alloys with the SSRT, the severity of the environmental stress cracking depended on the cross-head speed, that is, the average strain rate (the strain rate was not necessarily constant during the test; in general, it was slow at the beginning and increased rapidly after reaching the ultimate tensile strength). Similar to results reported for mild steel [5], the average length of the secondary stress corrosion cracks in nickel-base alloys increased with decreasing cross-head speed. No suppression of the hydroxide stress cracking phenomenon in the high performance alloys was observed upon further decrease of the average strain rate in the range of 10^{-5} to 10^{-7} s⁻¹. This behavior was similar to that reported for steel in carbonate-bicarbonate solution [15], but it was contrary to that observed for titanium in chloride environment [19] and for hydrogen-precharged nickel-base alloys [18]. The increase in SCC severity with decreasing strain rate was presumably caused by the longer test durations of the stressed specimens tested at slower crosshead speeds. On the other hand, upon testing at higher strain rates, that is, shorter test duration, the specimen was broken mechanically before major stress corrosion cracks would nucleate and propagate.

When considering specimen orientation and stress level (mechanical factors), the slow strain-rate unit (used in the constant load testing mode) was in agreement with the constant total strain method of testing using C-shape specimens [18]. Both techniques confirmed the extreme susceptibility to hydrogen cracking of cold worked specimens stressed in the transverse direction. Furthermore, with an appropriate specimen design, this slow strain-rate testing unit provided a versatile and precise way of investigating the effects of specimen orientation and stress level on the environmental stress cracking phenomenon of fabricated products.

The effects of metallurgical structure and composition of the alloys were clearly illustrated with the SSRT. It was interesting to observe the change

in the fracture mode from intergranular to transgranular upon changing the alloy chemistry (Alloy B and Alloy C-276). Also similar to data reported by Theus et al [20,21] on the cracking of Alloy 600, grain boundary precipitation suppressed the intergranular hydroxide stress cracking of Alloy B. However, such grain boundary precipitation did not alter the cracking mode of Alloy C-276, which failed transgranularly in both the annealed and the sensitized condition.

The SSRT was recognized already to have the ability to disclose the effects of cold work on the susceptibility of nickel-base alloys to hydrogen cracking [18]. Yet, in the case of hydroxide stress cracking, the results from the SSRT suggested increased resistance to SCC upon cold working the alloy while the results generated by the constant total strain mode of testing using C-shape specimens indicated higher susceptibility of the cold worked material. The strain rate cannot be the major reason for this discrepancy, as the cold worked specimens tested at slower crosshead speeds (to attain the same test duration as the annealed specimens) showed shallower secondary stress corrosion cracks than did the annealed material. However, in the constant total strain test ($\epsilon \approx 7$ percent), the cold worked specimen was subjected to a much higher stress ($\sigma \approx 1380$ MPa, or 200 ksi) than was the annealed specimen ($\sigma \approx 483$ MPa, or 70 ksi). At such high stress values, crack nucleation and propagation occurred more readily, thus leading to the observed rapid failure of the cold worked material.

Another distinction appeared between the SSRT and the constant total strain method when studying the effects of some electrochemical factors. While the cathodic protection of high performance alloys from hydroxide stress cracking was properly depicted by the SSRT, the effects of applied anodic potentials (or currents) were somewhat misleading. They suggested the occurrences of intergranular chloride stress cracking in sensitized Alloy C-276. Yet, the C-shape specimens indicated intergranular localized attacks on both the tension and the compression sides. Thus, the secondary cracks revealed by the SSRT on sensitized Alloy C-276 tested at anodic potentials were nothing else but intergranular penetrations caused by anodic dissolution. Their appearance as secondary stress corrosion cracks was presumably the result of widening due to the tensile deformation [13,22]. It is anticipated that any environment which causes localized intergranular corrosion will lead to the formation of the intergranular secondary cracks by the SSRT. Therefore, when using the SSRT, one should be careful not to confuse the stress assisted localized corrosion with the SCC. However, from an engineering point of view, both phenomena could lead to catastrophic service failures, and the SSRT remains capable of revealing each. Indeed, the SSRT was used to evaluate various welding procedures for their localized corrosion and pitting resistance. This was accomplished by using properly designed specimens with reduced gage region containing the weld itself or the heat-affected zone, or both (see footnote 4).

Conclusions

From the various parameters that can be measured when testing high performance alloys with the SSRT, the average length of the secondary stress corrosion cracks (as determined by metallographic examination) appears to be the proper parameter to use in quantifying the severity of the SCC phenomenon in most "material environment" systems.

Except for some apparent discrepancy when testing cold worked material, the slow strain-rate method of evaluating the SCC susceptibility of high performance alloys can be used suitably to reveal the various environmental, mechanical, and metallurgical factors.

Despite its tendencies (in some specific instances) to confuse SCC with stress assisted intergranular corrosion, the SSRT remains an excellent, reliable, and reproducible, accelerated laboratory test for revealing the environmental stress cracking of high performance alloys.

References

- [1] Champion, F. A. in *Corrosion Testing Procedures*, Chapman and Hall, London, 1952, p. 137.
- [2] Logan, H. L. in *The Stress Corrosion of Metals*, Wiley, New York, 1966, p. 273.
- [3] *Stress Corrosion Testing, STP 425*, American Society for Testing and Materials, 1967, p. 3.
- [4] Parkins, R. N., *The Theory of Stress Corrosion Cracking in Alloys*, J. C. Scully, Ed., North Atlantic Treaty Organization, Brussels, 1971, p. 449.
- [5] Humphries, M. J. and Parkins, R. N., *Corrosion Science*, Vol. 7, 1967, p. 747.
- [6] Middleton, W. R. and Parkins, R. N., *Corrosion*, Vol. 28, 1972, p. 88.
- [7] Stutcliffe, J. M., Fessler, R. R., Boyd, W. K. and Parkins, R. N., *Corrosion*, Vol. 28, 1972, p. 313.
- [8] Lee, H. H. and Uhlig, H. H., *Journal of the Electrochemical Society*, Vol. 117, 1970, p. 18.
- [9] Newberg, R. T. and Uhlig, H. H., *Journal of the Electrochemical Society*, Vol. 119, 1972, p. 981.
- [10] Mazille, H. and Uhlig, H. H., *Corrosion*, Vol. 28, 1972, p. 427.
- [11] Hixson, D. and Uhlig, H. H., *Corrosion*, Vol. 32, 1976, p. 56.
- [12] Asphahani, A. I. and Uhlig, H. H., *Journal of the Electrochemical Society*, Vol. 122, 1975, p. 174.
- [13] Uhlig, H. H., Gupta, K., and Liang, W., *Journal of the Electrochemical Society*, Vol. 122, 1975, p. 343.
- [14] Deegan, D. C. and Wilde, B. E., *Corrosion*, Vol. 29, 1973, p. 310.
- [15] Payer, H. J., Berry, W. E., and Boyd, W. K. in *Stress Corrosion—New Approaches, ASTM STP 610*, H. L. Craig, Jr., Ed., American Society for Testing and Materials, 1976, p. 82.
- [16] Hodge, F. G., *Corrosion*, Vol. 29, 1973, p. 375.
- [17] Kirchner, R. W. and Silence, W. L., *Materials Protection and Performance*, Vol. 10, 1971, p. 11.
- [18] Asphahani, A. I., Second International Congress on Hydrogen in Metals, Paris, June 1977, Paper No. 3C2.
- [19] Powell, D. T. and Scully, J. C., *Corrosion*, Vol. 24, 1968, p. 151.
- [20] Theus, G. J., National Association of Corrosion Engineers Meeting, Houston, March 1976, Paper No. 101.
- [21] Domian, H. A., Emanuelson, R. H., Katz, L., Sarver, L. W., and Theus, G. J., National Association of Corrosion Engineers Meeting, Houston, March 1976, Paper No. 99.
- [22] Spaehn, H., Wagner, G. H., and Steinhoff, U., Conference on Stress Corrosion Cracking and Hydrogen Embrittlement of Iron-Base Alloys, Firminy, June 1973, Paper No. A-2.

Stress Corrosion Cracking Susceptibility Index, I_{SCC} , of Austenitic Stainless Steels in Constant Strain-Rate Test

REFERENCE: Abe, Seizaburo, Kohima, Masao, and Hosoi, Yuzo, "Stress Corrosion Cracking Susceptibility Index, I_{SCC} , of Austenitic Stainless Steels in Constant Strain-Rate Test," *Stress Corrosion Cracking—The Slow Strain-Rate Technique*, ASTM STP 665, G. M. Ugiansky and J. H. Payer, Eds., American Society for Testing and Materials, 1979, pp. 294–304.

ABSTRACT: A new stress corrosion cracking (SCC) susceptibility index, I_{SCC} , is proposed in constant strain rate SCC test both for transgranular (TG)SCC and for intergranular (IG)SCC. I_{SCC} is best defined by the equation

$$I_{SCC} = A_{SCC}/A_{mech}$$

where A_{SCC} and A_{mech} are the area of SCC fractured surface and that of mechanically fractured surface, respectively. It is found that there is a good correlation between I_{SCC} in constant strain-rate test and the time to fracture in constant load test.

KEY WORDS: stress corrosion cracking, transgranular corrosion, intergranular corrosion, constant strain rate test, constant load test, susceptibility, time to fracture, susceptibility index, chlorides, high temperature water, austenitic stainless steels, sensitization

It has been recognized that the role of stress in stress corrosion cracking (SCC) of austenitic stainless steels is to break protective surface films exposing the fresh metal surface to corrosive environments as illustrated schematically in Fig. 1.

Therefore, constant strain-rate or slow extension rate tests seem to be the most promising among others in making a quantitative estimation of SCC

¹Senior research metallurgist, assistant research chemist, and head, respectively, Corrosion and Heat Resistant Steels Laboratory, Fundamental Research Laboratories, Nippon Steel Corporation, Kawasaki 211 Japan.

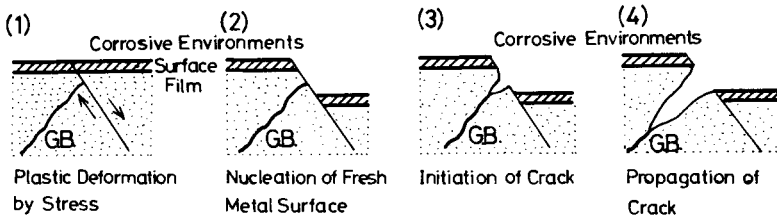


FIG. 1—Schematic illustration of the initiation and propagation process of SCC.

susceptibility of materials. The straining rate observed during propagation of SCC in constant load test shown in Fig. 2 demonstrates clearly the validity of constant strain-rate test.

The constant strain-rate test method has been applied to study SCC mechanism in mild steels by Humphries et al [1],² in titanium alloys by Powell et al [2], Adepoju et al [3], and in austenitic stainless steels by Hoar et al [4-6], Takano et al [7,8], Vermilyea et al [9,10] and others [11-13]. Orman [14] also utilized this method for both aluminum and titanium

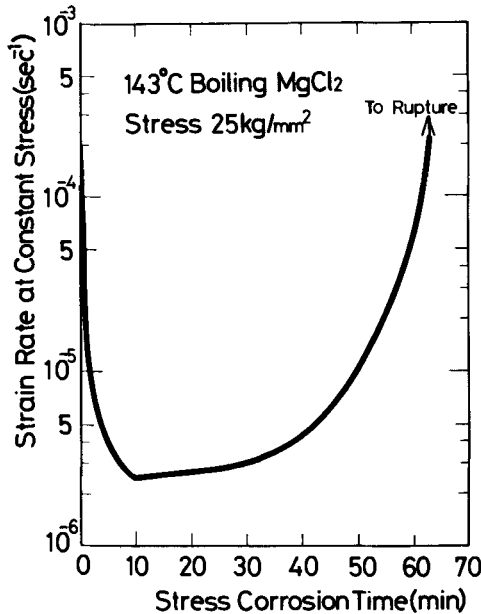


FIG. 2—The strain rate change during SCC of Type 304 stainless steel in 143°C boiling MgCl₂ solution.

²The italic numbers in brackets refer to the list of references appended to this paper.

alloys and showed that SCC susceptibilities could be expressed in terms of the change of fracture strain in corrosive environments.

In this paper, a revised susceptibility index, I_{SCC} , is presented based on the previously proposed one [15] for austenitic stainless steels both in transgranular SCC (TGSCC) in chloride environments, and intergranular SCC (IGSCC) in high temperature water. Then the index is compared with the time to fracture obtained by constant load test.

Experimental

Since apparent strain rates observed during constant load test are found between 10^{-6} s^{-1} and 10^{-3} s^{-1} for Type 304 stainless steel in 143°C boiling magnesium chloride (MgCl_2) solution under the stress of 25 kg/mm^2 as shown in Fig. 2, a tension test machine is employed so that strain rates can be controlled in the range between 10^{-6} s^{-1} and 10^{-1} s^{-1} .

Studies on the susceptibility to TGSCC in 143°C boiling MgCl_2 solution and IGSCC susceptibility in oxygenated high temperature water at 300°C were undertaken.

The chemical compositions of the specimens are listed in Table 1. The specimens were machined from 1-mm-thick cold rolled sheets. The cross section of specimens was $1 \times 4 \text{ mm}$ and the gage length was 20 mm. The specimens for TGSCC test were solution annealed at 1100°C for 30 min, and subsequently water quenched. The specimens for IGSCC were also solution annealed at 1100°C for 30 min and sensitized at 600°C for 24 h. Load-elongation curves during the SCC test were recorded both in 143°C boiling MgCl_2 solution and in high temperature water. After the SCC test, the whole fracture surface was examined by a scanning electron microscope (SEM) to measure the ratio of the area of SCC fractured surface to that of the mechanically fractured surface.

Results and Discussion

Effect of Strain Rate on Stress-Strain Curves

Figure 3 shows typical stress-strain curves of sensitized Type 304 stainless steel at the strain rate of $4.17 \times 10^{-6} \text{ s}^{-1}$ in high temperature water saturated with 1 atm oxygen gas and without oxygen at room temperature. The stress-strain curves in high temperature water without oxygen are almost identical with those in an argon gas atmosphere at 300°C . On the other hand, quite different stress-strain curves are found in the oxygenated high temperature water. The fracture strain is decreased to less than 10 percent in comparison with 50 to 60 percent in oxygen-free high temperature water. This drastic reduction of the fracture strain is ascribed entirely to IGSCC which occurred during the constant strain-rate test.

TABLE 1—Chemical compositions of the specimens.

No.	Cr	Ni	Mn	Si	C	P	N	S	O	Mo	Remark
Type 304	18.52	9.88	1.28	0.54	0.070	0.027	0.0259	0.008	0.0142	0.05	TGSCC, IGSCC
T-1	19.78	19.79	<0.01	<0.01	0.003	0.002	0.0033	0.006	0.0302	<0.01	TGSCC
T-2	20.09	19.87	<0.01	<0.01	0.002	0.007	0.0033	0.003	0.0301	<0.01	TGSCC
T-3	19.65	19.29	<0.02	<0.01	0.001	0.038	0.0038	0.003	0.0265	<0.01	TGSCC
T-4	19.40	19.92	<0.01	<0.01	0.003	0.003	0.2318	0.003	0.0297	<0.01	TGSCC
T-5	19.23	19.41	<0.01	<0.02	0.007	0.003	0.0069	0.007	0.0202	0.98	TGSCC
I-1	18.54	11.23	1.20	0.54	<0.002	0.003	0.0035	0.007	0.013	<0.01	IGSCC
I-2	18.50	11.50	1.17	0.58	<0.002	0.025	0.0040	0.012	0.013	<0.01	IGSCC
I-3	18.58	11.17	1.25	0.59	0.008	0.005	0.0014	<0.003	0.0014	<0.01	IGSCC
I-4	18.45	11.14	1.21	0.58	0.031	0.004	0.0048	<0.003	0.0010	<0.01	IGSCC

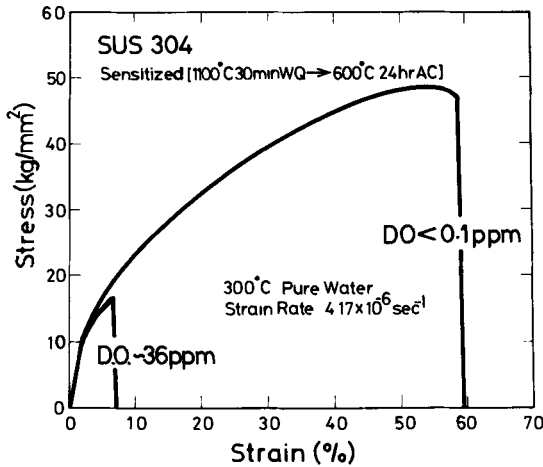


FIG. 3—Typical stress-strain curves of sensitized Type 304 stainless steel in oxygenated and oxygen free high temperature water. (DO = dissolved oxygen).

The strain rate dependence of the strain at the maximum stress $\epsilon\sigma_{max}$ is shown in Fig. 4; $\epsilon\sigma_{max}$ decreases with the decrease of strain rates both in TGSCC in 143°C boiling MgCl₂ solution and in IGSCC in oxygenated high temperature water. This tendency of $\epsilon\sigma_{max}$ suggests that SCC susceptibilities increase inversely proportional to strain rate, as confirmed by SEM observation of fracture surfaces. Based on the data shown in Fig. 4, the strain rates, $1.67 \times 10^{-5} \text{ s}^{-1}$ in TGSCC test and $8.34 \times 10^{-6} \text{ s}^{-1}$ in IGSCC test, respectively, were used hereafter.

SCC Susceptibility Index, I_{sc} , in Constant Strain-Rate Test

The SCC susceptibility has been simply stated by Eqs 1 and 2, where the relative change in the fracture strain in noncorrosive and corrosive environments is used as a criterion as shown in Fig. 5.

$$\Delta\epsilon = \epsilon_{mech} - \epsilon_{sc} \tag{1}$$

$$I = \Delta\epsilon / \epsilon_{mech} \tag{2}$$

where

- ϵ_{mech} = fracture strain in noncorrosive environments,
- ϵ_{sc} = fracture strain in corrosive environments, and
- I = simple expression for the susceptibility.

However, the susceptibility indexes indicated by these equations are not

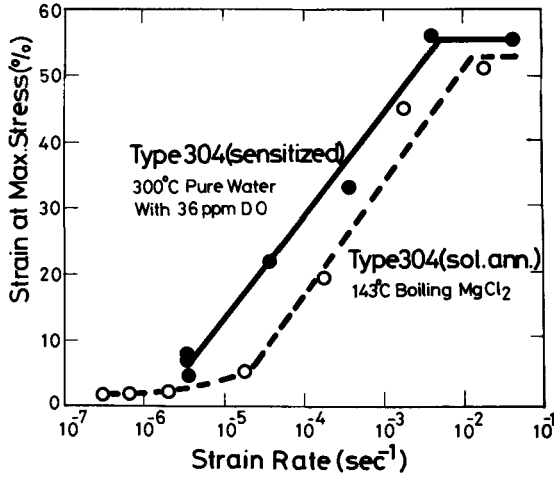


FIG. 4—Strain rate dependence of the strain at maximum load in stress-strain curves of Type 304 stainless steel in 143°C boiling MgCl₂ solution and in oxygenated high temperature water.

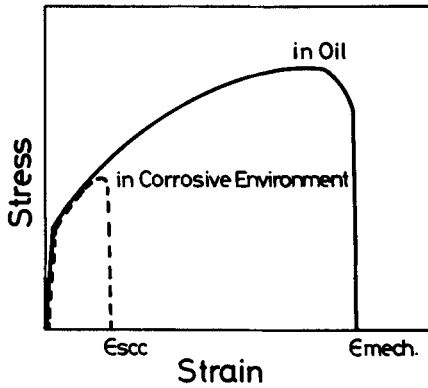


FIG. 5—Schematic stress-strain curves in noncorrosive environments and in corrosive environments at the same temperature.

suitable to compare the susceptibility of various alloys whose ϵ_{mech} differ in large amount.

In this study, it is found that the ratio of the area of the SCC fractured surface to that of the mechanically fractured surface is the most useful parameter applicable to various alloys regardless of ϵ_{mech} value. That is, the SCC susceptibility index, I_{scc} , is best defined by the equation

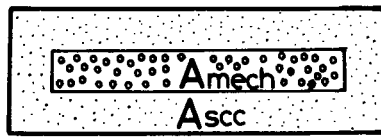
$$I_{scc} = A_{scc}/A_{mech} \tag{3}$$

where A_{sc} and A_{mech} are the areas of SCC fractured surface and the mechanically fractured surface, respectively, as shown in Fig. 6. I_{sc} described here is determined experimentally measuring A_{sc} and A_{mech} by SEM.

Strain Rate Dependence of I_{sc}

I_{sc} depends on the strain rate as shown in Fig. 7. The dependence of I_{sc} consists of three regions as follows: Region I where the strain rate is too high for SCC to occur and the fracture surface is dimple, Region II where I_{sc} increases as the strain rate decreases from 0 to about 2.4, and Region III where I_{sc} stays constant independent of the strain rate. The boundary values of the three regions depend on SCC susceptibilities of alloys in a given environment.

The dependence of I_{sc} on carbon contents in sensitized Type 304 stainless steel was studied at the strain rate of $4.17 \times 10^{-6} \text{ s}^{-1}$ in high temperature



$$I_{sc} = A_{sc} / A_{mech}$$

FIG. 6—Schematic illustration of the fracture surface in the constant strain-rate SCC test.

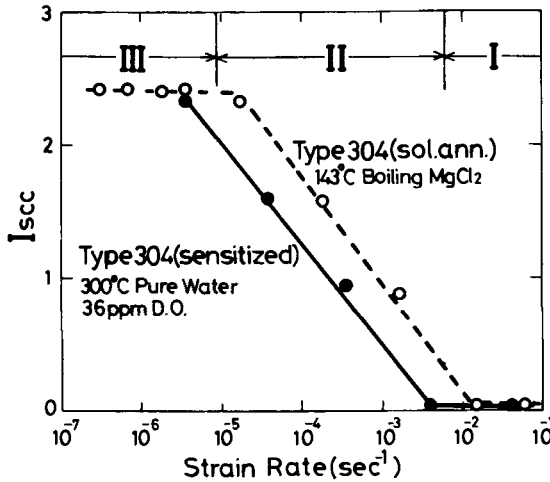


FIG. 7—The strain rate dependence of I_{sc} in TGSCC and IGSCC.

water as shown in Fig. 8. I_{sc} is close to 2.4 regardless of the carbon content above 0.008 weight percent. As the carbon content decreases below 0.008 weight percent I_{sc} shows a steep decrease, and it becomes zero at the carbon content less than 0.002 weight percent. These results suggest that when the carbon content is higher than 0.008 weight percent, the strain rate, $4.17 \times 10^{-6} \text{ s}^{-1}$, is in Region III, and it is in Region I that the carbon content is below 0.002 weight percent. However, the fact that I_{sc} is zero in the extra low carbon alloy at the strain rate, $4 \times 10^{-6} \text{ s}^{-1}$, may suggest that it is immune to SCC.

In order to make a judgment on the possibility of SCC in a given combination of material and environment in a limited time, the test at a very slow strain rate of the order of 10^{-6} s^{-1} to 10^{-7} s^{-1} is more suited, whereas other test methods face various difficulties such as time consuming experiments, especially at lower applied stresses or strain.

On the other hand, SCC susceptibilities of various alloys can be compared in Region II with conventional SCC susceptibility indexes such as the time to fracture in constant load test. The strain rates of $1.67 \times 10^{-5} \text{ s}^{-1}$ in TGSCC and $8.34 \times 10^{-6} \text{ s}^{-1}$ in IGSCC were chosen to get the correlation between I_{sc} and the time to fracture in constant load test.

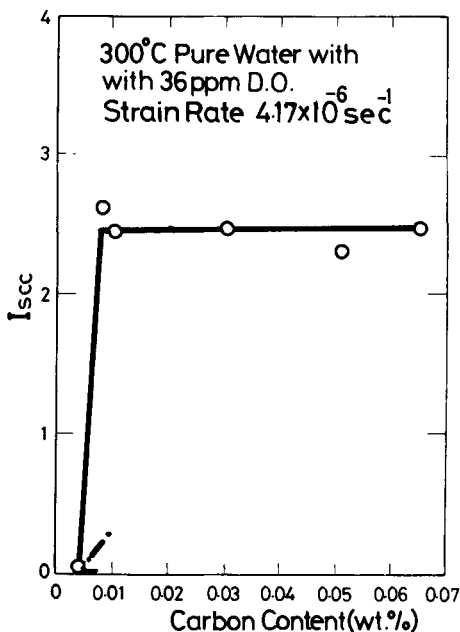


FIG. 8—The effect of carbon content on I_{sc} of sensitized Type 304 stainless steel in high temperature water.

Correlation between I_{sc} in Constant Strain-Rate Test and Time to Fracture in Constant Load Test

Figure 9 shows the correlation between I_{sc} and the time to fracture in TGSCC of various alloys in 143°C boiling MgCl₂ solution. It is clear that an excellent correlation exists between these two susceptibility indexes. Figure 10 also indicates the correlation between these two indexes in IGSCC of sensitized Type 304 stainless steel with different carbon content in oxygenated high temperature water. Although only some data are useful owing to the lack of the available data in constant load test [16], a fairly good correlation is still found between them.

These results demonstrate that I_{sc} defined by Eq 3 is applicable both to TGSCC and IGSCC.

Derivation of I_{sc} from Stress-Strain Curves

Derivation of I_{sc} has been done from stress-strain curves in corrosive and noncorrosive environments. The final expression is given by

$$I_{sc} = \frac{1 + \epsilon_n}{1 + \epsilon_{n\ sc}} \cdot \frac{P_n}{P_{n\ sc}} - 1 \tag{4}$$

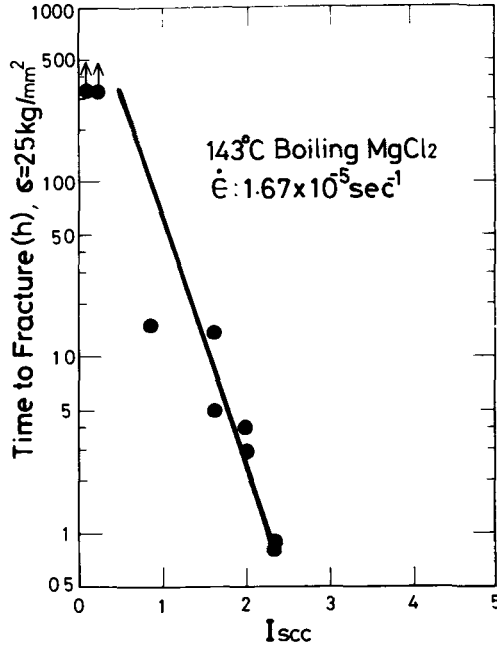


FIG. 9—The correlation between I_{sc} and the time to fracture in 143°C boiling MgCl₂ solution.

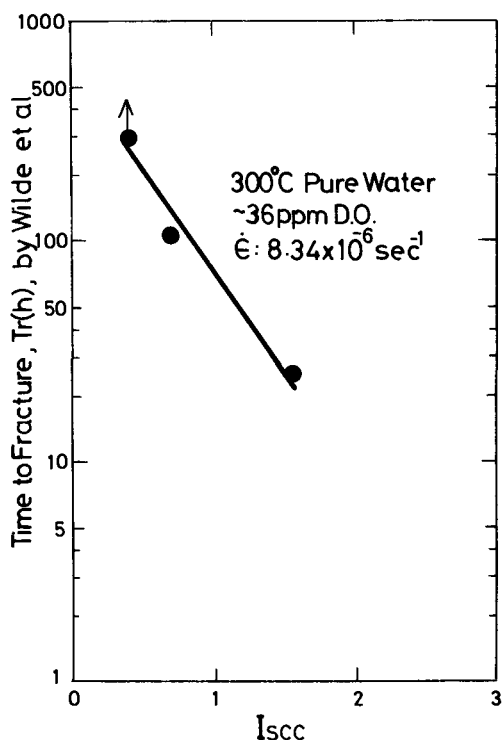


FIG. 10—The correlation between I_{scc} and the time to fracture in high temperature water. (The time to fracture in constant load test is referred to Ref 16).

where

ϵ_n, P_n = strain and load at maximum load in load-elongation curves obtained in noncorrosive environments, and
 $\epsilon_n^{scc}, P_n^{scc}$ = strain and load at maximum load in load-elongation curves obtained in corrosive environments.

It is confirmed that there is a linear correlation between I_{scc} obtained from the fractured surface and those calculated by Eq 4. The detailed discussions on the derivation of Eq 4 will be published elsewhere.

Summary

The validity of constant strain-rate test or slow extension rate test as a useful means to evaluate the SCC susceptibility is presented. The SCC susceptibility index, I_{scc} , is proposed both for TGSCC in chloride solutions and IGSCC in oxygenated high temperature water. The obtained results are summarized as follows.

1. The SCC susceptibility index, I_{scc} , is defined as the ratio of the area of SCC fractured surface to that of mechanically fractured surface under given test conditions.

$$I_{\text{scc}} = A_{\text{scc}}/A_{\text{mech}}$$

I_{scc} determined from fractured surface observation exhibits a linear relation with those calculated from stress-strain curves.

2. A linear correlation is found between I_{scc} in constant strain-rate test and the time to fracture in constant load test.

3. I_{scc} is applicable both to TGSCC and IGSCC.

4. The SCC susceptibility can be determined by a constant strain-rate test in a very short test period with higher accuracy as compared with conventional methods.

Acknowledgments

The authors would like to acknowledge the valuable suggestions by H. Okada, Director, S. Nagashima, Former Director, and T. Murata, Fundamental Research Laboratories, Nippon Steel Corporation.

References

- [1] Humphries, M. J. and Parkins, R. N., *Corrosion Science*, Vol. 7, 1967, p. 747.
- [2] Powell, D. T. and Scully, J. C., *Corrosion*, Vol. 24, 1968, p. 151.
- [3] Adepoju, T. and Scully, J. C., *Corrosion Science*, Vol. 15, 1975, p. 415.
- [4] Hoar, T. P. and West, J. M., *Nature*, Vol. 181, 1958, p. 35.
- [5] Hoar, T. P. and Scully, J. C., *Journal of the Electrochemical Society*, Vol. 3, 1964, p. 348.
- [6] Hoar, T. P. and West, J. M., *Proceedings of the Royal Society*, Vol. 268, 1962, p. 304.
- [7] Takano, M. and Shimodaira, S., *Transactions*, Japan Institute for Metals, Vol. 9, 1968, p. 294.
- [8] Takano, M., *Corrosion*, Vol. 30, 1974, p. 441.
- [9] Vermilyea, D. A., *Corrosion*, Vol. 29, 1973, p. 442.
- [10] Vermilyea, D. A. and Diegle, R. B., *Corrosion*, Vol. 32, 1976, p. 26.
- [11] Murata, T. and Staehle, R. W. in *The Theory of Stress Corrosion Cracking in Alloys*, J. C. Scully, Ed., North Atlantic Treaty Organization, 1970, p. 223.
- [12] Buhl, H., 6th International Congress on Metal Corrosion, Sydney, Australia, 1975.
- [13] West, J. M., *Corrosion Science*, Vol. 1, 1961, p. 178.
- [14] Orman, S., *Corrosion Science*, Vol. 9, 1969, p. 849.
- [15] Okada, H., Hosoi, Y., Abe, S., and Yamamoto, S., *Nihon Kinzoku Gakkaishi*, Vol. 38, 1974, p. 646.
- [16] Wilde, B. W. and Weber, J. E., *British Corrosion Journal*, Vol. 4, 1969, p. 42.

A. J. A. Mom,¹ R. T. Dencher,² C. J. v.d. Wekken,² and
W. A. Schultze²

Some Aspects of the Stress Corrosion Testing of Austenitic, Martensitic, Ferritic-Austenitic and Ferritic Types of Stainless Steel by Means of the Slow Strain-Rate Method

REFERENCE: Mom, A. J. A., Dencher, R. T., Wekken, C. J. v. d., and Schultze, W. A., "Some Aspects of the Stress Corrosion Testing of Austenitic, Martensitic, Ferritic-Austenitic, and Ferritic Types of Stainless Steel by Means of the Slow Strain-Rate Method," *Stress Corrosion Cracking—The Slow Strain-Rate Technique*, ASTM STP 665, G. M. Ugiansky and J. H. Payer, Eds., American Society for Testing and Materials, 1979, pp. 305-319.

ABSTRACT: The stress corrosion cracking (SCC) susceptibility of six different types of stainless steel (AISI 304, 316 and 431, and Uranus 50, Orion 26-1, and Orion 28-2 from Creusot Loire) was tested in concentrated magnesium chloride (MgCl₂) solutions by means of the slow strain-rate (SSR) method. The effects of strain rate, chloride concentration, testing temperature, electrode potential of the specimen, and the presence of inhibitors have been investigated. Test results are compared with literature data. The ferritic steel Orion 26-1, expected to be immune to SCC, was found to show some susceptibility in SSR tests. In the present SSR tests, some inhibitors were found to be completely effective in preventing SCC in MgCl₂ solutions in concentrations considerably lower than reported in the literature for constant strain-type testing conditions.

KEY WORDS: stress corrosion cracking, stress corrosion testing, stainless steels, slow strain-rate method, evaluation

While the slow strain-rate (SSR) method of stress corrosion cracking (SCC) susceptibility testing has the advantage over constant load and

¹National Lucht-en Ruimtevaartlaboratorium, Emmeloord, The Netherlands.

²Delft University of Technology, Laboratory of Metallurgy, Delft, The Netherlands.

constant strain methods of providing fast information, the correlation between the results obtained by the SSR method and other testing methods, as well as the correlation with SCC susceptibility under service conditions in actual practice in many cases, remains to be established.

In the present investigation the method of testing the SCC susceptibility of stainless steels in chloride environments by means of SSR tests in hot magnesium chloride (MgCl_2) solutions is evaluated. The effect of the concentration of the test solution, the temperature, and the employed strain rate is investigated in order to establish suitable test conditions. The ability of the SSR test to differentiate between stainless steels of varying SCC susceptibility is then tested on six different types of steel, and the results are compared with available literature data from constant load and constant strain tests.

Finally, the usefulness of the SSR method for determining the effect of a number of inhibitors in the test solution is investigated, and a critical potential for preventing SCC in AISI 304 is measured under SSR conditions. The results are compared with published results obtained under constant strain type testing conditions.

Experimental Procedure

Test Apparatus

The test apparatus was similar to that originally designed by Parkins. The crosshead speed could be varied in decade steps from 6.5×10^{-2} to 6.5×10^{-7} mm/min. For the employed specimen size, this corresponds to relative strain rates of $6.4 \times 10^{-5}/\text{s}$ to $6.4 \times 10^{-10}/\text{s}$, respectively. The tensile load on the specimen was measured by means of a calibrated strain gage bridge that was designed to compensate for the effect of temperature variations and was mounted on a rigid load carrying beam of the tensile apparatus. The output of the strain gage bridge was registered on a $x-t$ recorder.

Specimen Preparation

The compositions of the six different stainless steels used in this investigation are given in Table 1. Two of the steels, AISI 304 and AISI 316, have an austenitic structure. Type AISI 431 is martensitic. Uranus 50 is ferritic-austenitic, and Orion 26-1 and Orion 28-2 have a ferritic structure. The latter three types of stainless steel were supplied by the French company Creusot-Loire. The heat treatment shown in Table 1 for AISI 304 and AISI 316 was performed on the machined specimens in the laboratory. The other steels were heat treated by the supplier.

The effective gage length of the machined 10-cm-long cylindrical speci-

TABLE 1—Composition in weight percent, heat treatment, and structure of the various types of steel.

	C	Mn	Si	Ni	Cr	Mo	Cu	Ti	N	Al	S	P	heat treatment	structure
AISI 304	0.052	1.05	0.64	8.94	16.69	0.46			0.042				0.5h 1050°C water quenched	austenite
AISI 316	0.064	1.78	0.34	11.26	17.41	2.01			0.045				0.5h 1050°C water quenched	austenite
AISI 431	0.17	0.48	0.23	1.69	16.71	0.29			0.033				0.5h 1050°C annealed at 630-720°C	martensite
uranus 50	0.030	0.71	0.48	8.05	20.60	2.65	1.52	0.11	0.056				20min 1100°C air quenched	ferrite- austenite
orion 26-1	0.001	0.01	0.24	0.08	26.2	1.20			0.010		0.010	0.011	20min 900°C air quenched	ferrite
orion 28-2	0.0014 0.0017	0.06	0.11	0.22	27.98	2.25	0.034		0.0118	0.320	0.013	0.010	20min 900°C air quenched	ferrite

mens was 17 mm, with a corresponding specimen diameter of 2.5 mm. Before the tests, the specimen surface was abraded, using subsequently 320, 400, and 600 grit silicon carbide paper, followed by a polish with type 3/0 and 4/0 emery paper. The surface was then cleaned with alcohol, rinsed in distilled water, and dried in air.

Test Solution

Most tests were carried out in $MgCl_2$ solutions that were saturated at 25°C. These solutions were prepared by lengthly stirring in the presence of an excess of $MgCl_2 \cdot 6H_2O$, while the temperature was controlled at $25 \pm 0.1^\circ C$. The obtained solution has a concentration of 35.5 weight percent. Unless otherwise stated, the solution was employed at a testing temperature of 123°C, a few degrees below the boiling point at one atmosphere of 126.5°C. The advantage of a testing temperature below the boiling point is that evaporation losses are reduced, and consequently the concentration of the solution is better maintained. Less concentrated solutions were prepared by adding the required amount of water to the 35.5 weight percent $MgCl_2$ solution. Glycerine, which is easy to remove since it is water soluble, was used as an inert testing medium. Test results in glycerine were found to be identical to those obtained in paraffin.

Test Cell

The test cell consisted of a glass cylinder with trifluoroethylene resin bottom and top pieces. The sealing between the various parts was accomplished by means of rubber O-rings. A heating coil was mounted in a glass tube. The temperature of the test solution could be recorded and controlled, within $\pm 1^\circ C$, using a thermocouple that was mounted in a thin quartz tube. In addition, the temperature was measured with a precision thermometer. In order to maintain a constant concentration of the test

solution, evaporation losses were eliminated as much as possible by means of a water cooled reflux condenser.

Electrochemical Measurements

A saturated calomel reference electrode was placed in a beaker glass filled with the test solution and connected to the test cell via a salt bridge. Temperature differences of about 100°C in the electrode potential measuring circuit introduce an unknown electromotive force (emf). In the present study the measurement of electrode potential variations is not affected by the presence of this constant emf. Electrode potentials were measured by means of a millivolt meter. A recorder was connected to the low impedance output channel of the millivolt meter. After mounting the specimen it took about 30 min for the solution to reach the testing temperature. The SSR tests in this investigation were then started about 30 min after the test solution had reached its operating temperature. This time was needed for the electrode potential to become fairly steady. The mounting of a graphite counter electrode made it possible to perform potentiostatically controlled measurements.

Results and Discussion

Effect of the Chloride Concentration

Tests were carried out on specimens of the austenitic steel AISI 316 in 10, 25, and 35.5 weight percent MgCl_2 solutions, in distilled water and in glycerine. The testing temperature was 100°C. The employed strain rate was $6.4 \times 10^{-6}/\text{s}$. It will be shown in a later section that the fracture strain is a more sensitive measure for the SCC susceptibility than the maximum load. The observed fracture strain values are presented in Fig. 1.

Differences between the values measured in glycerine and in distilled water are probably due to experimental scatter. The tests indicate that at 100°C a MgCl_2 concentration of at least 25 weight percent was required to find evidence of SCC in the values of the fracture strain. Going from 25 weight percent to a concentration of 35.5 weight percent resulted in a large reduction in the fracture strain. Similar large changes in the aggressiveness of the test solution in this concentration range are evident from the log time to failure versus $1/T$ plot for constant load tests, as measured by Kohl [1].³ While Kohl [1,2] found that at 120°C the time to failure increased by a factor 3 for X5CrNi1810 and X5CrNi189 (AISI 304) on changing the concentration of the test solution from 45 to 33 weight percent MgCl_2 , no difference in the time to failure was observed for X5CrNiMo2215 as well as

³The italic numbers in brackets refer to the list of references appended to this paper.

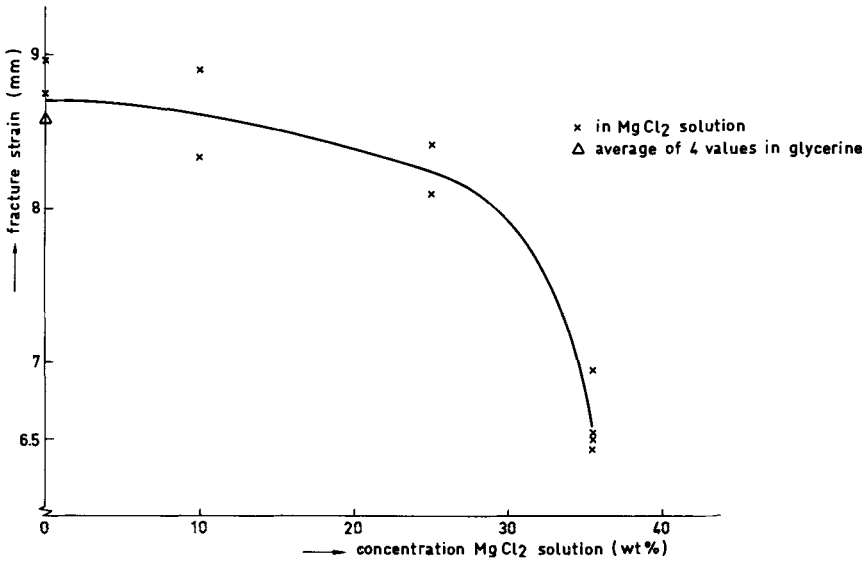


FIG. 1—The fracture strain as a function of the $MgCl_2$ concentration for AISI 316 specimens. The strain rate was $6.4 \times 10^{-6}/s$, the testing temperature $100^\circ C$.

for X5CrNiMo1812. Considering the magnitude of the experimental scatter, Thomas et al [3] found no significant differences in the time to failure for X5CrNi189 tested at $100^\circ C$ in 23 and in 36 weight percent $MgCl_2$ solutions. It appears that the effect of changes in the chloride concentration is strongly dependent on the type of steel.

Effect of the Testing Temperature

Figure 2 shows some results obtained for AISI 316 at 100, 120, and $123^\circ C$ in the 35.5 weight percent $MgCl_2$ test solution, using a strain rate of $6.4 \times 10^{-6}/s$. Again the fracture strain is compared to its value in glycerine at the same temperature.

A quantitative comparison between the SSR test results and results of constant strain tests is not possible. The present data indicate that the aggressiveness of a solution increases strongly with increasing temperature, in agreement with results from other testing methods [1,2,4]. At higher temperatures the scatter in the results appears to increase.

Effect of the Strain Rate

Figures 3 and 4 show the load-strain curves for the materials AISI 316

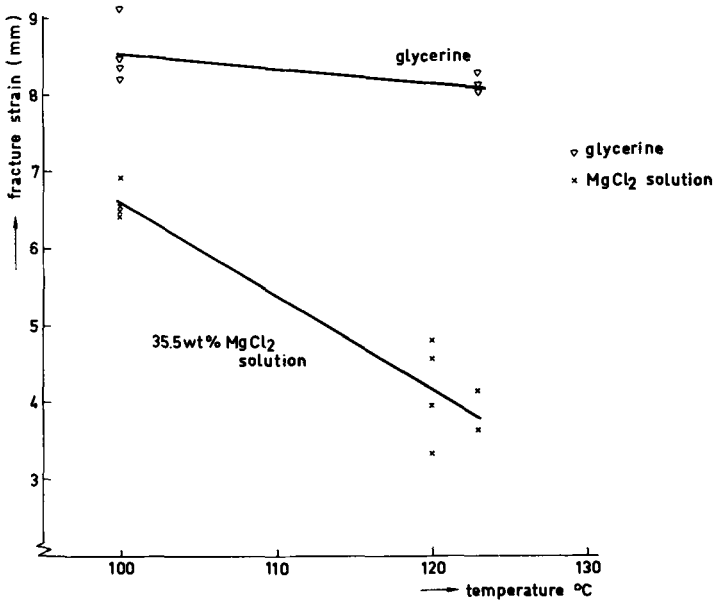


FIG. 2—The fracture strain as a function of the temperature for AISI 316 specimens. The strain rate was $6.4 \times 10^{-6}/s$, the $MgCl_2$ concentration 35.5 weight percent.

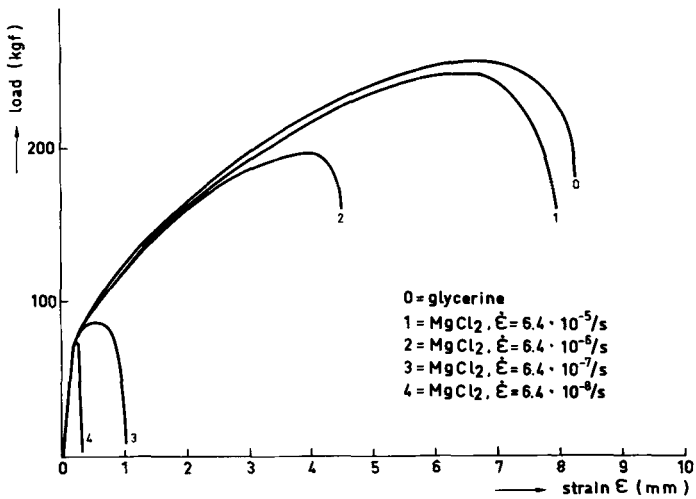


FIG. 3—The load as a function of the elongation for AISI 316 specimens, tested at 123°C in a 35.5 weight percent $MgCl_2$ solution, for different strain rates.

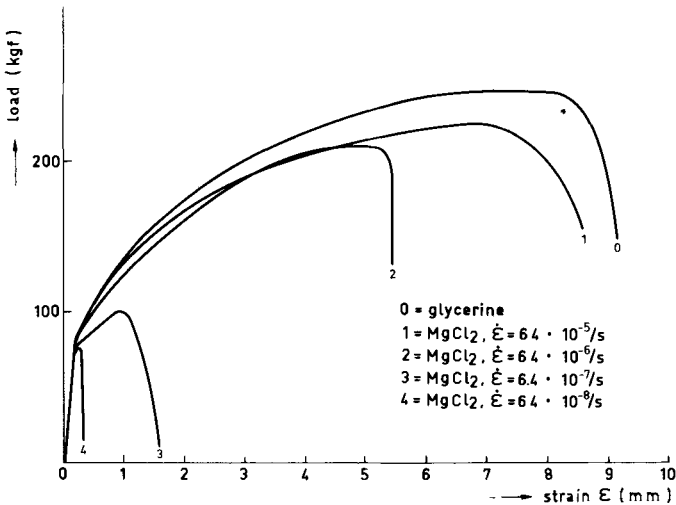


FIG. 4—The load as a function of the elongation for AISI 304 specimens, tested at 123°C in a 35.5 weight percent MgCl₂ solution, for different strain rates.

and AISI 304, for strain rates ranging from $6.4 \times 10^{-8}/s$ to $6.4 \times 10^{-5}/s$, the concentration of the test solution was again 35.5 weight percent MgCl₂, while the test solution temperature was 123°C.

Figures 3 and 4 also show that a strain rate of $6.4 \times 10^{-5}/s$ was too fast to clearly detect SCC in the susceptible austenitic steels AISI 304 and AISI 316. At a strain rate of $6.4 \times 10^{-6}/s$ the SCC process causes a clear reduction of the observed fracture strain, while the time to failure is less than 24 h. As will be shown later, the fracture strain results obtained, for example, on Orion 26-1, show that, using this strain rate and the above mentioned concentration and temperature, the testing method is able to detect the low susceptibility of this material. Therefore, there are no practical reasons to use lower strain rates. The lower rates remain of interest for theoretical reasons. At the employed strain rates in the range of $6.4 \times 10^{-5}/s$ to $6.4 \times 10^{-8}/s$, no evidence of a constant maximum load below a certain strain rate was detected. Such a plateau for the maximum load values was measured by Takano [5] for prenotched specimens. Some evidence of a minimum in the curves of the fracture energy as a function of the strain rate was found by Buhl [6] for AISI 304 and CrNiMoTi1810 in boiling MgCl₂ solutions at 144°C, at strain rates of $10^{-6}/s$ and $\approx 5 \cdot 10^{-5}/s$. The present load-elongation curves show that even at a strain rate of $6.4 \times 10^{-8}/s$, cracking did not start until the material had started deforming plastically. Tests at the next lower strain rate of $6.4 \times 10^{-9}/s$ are necessarily of very long duration, of the order of several weeks. For this reason,

and since without extra provisions it was not possible to maintain a constant concentration of the test solution during this period of time, attempts to use this low strain rate were abandoned.

SCC Susceptibility of the Various Stainless Steels

The load was measured as a function of the elongation for specimens of the various steels, in the 35.5 weight percent $MgCl_2$ test solution and in glycerine, at 123°C. The employed strain rate was $6.4 \times 10^{-6}/s$. The maximum loads, measured in glycerine (*left*) and in the $MgCl_2$ solution (*right*), are plotted in Fig. 5. The fracture strain data, obtained from the same tests, are plotted similarly in Fig. 6. The tests were performed in duplicate. The vertical bars represent the average of two measurements, while the difference between the two results, as shown in the figures, gives an indication of the reproducibility of the measurements.

A comparison of Figs. 5 and 6 shows that the well known SCC susceptibility of austenitic stainless steels in chloride environments is clearly demonstrated in the results of the slow strain-rate tests on AISI 304 and AISI 316. This follows from the maximum load data in the test solution as compared to the maximum load values in glycerine, as well as from the fracture strain data.

The situation is equally clear in the case of the ferritic steel Orion 28-2. Steels of this type, with high chromium and very low carbon and nitrogen content are generally considered not susceptible to SCC in chloride environments. No susceptibility was detected for this type of steel in $MgCl_2$ solutions at or above 140°C in constant load [7,8] or constant strain-type

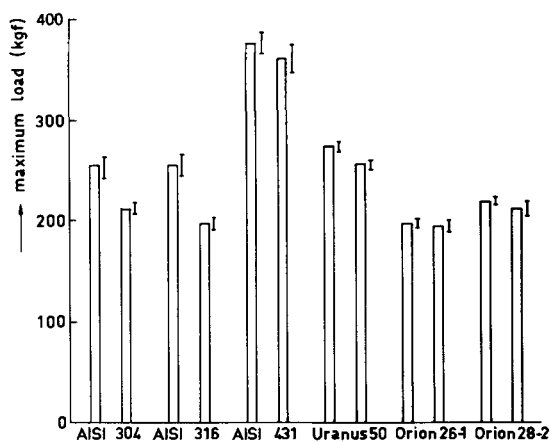


FIG. 5—The maximum load for specimens of various steels tested in glycerine (*left*) and in a 35.5 weight percent $MgCl_2$ solution (*right*), at a strain rate of $6.4 \times 10^{-6}/s$.

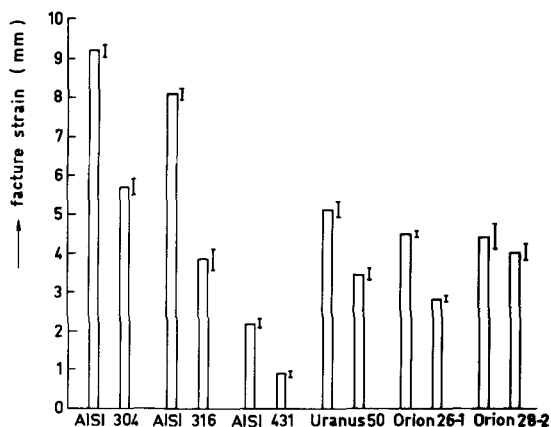


FIG. 6—The fracture strain for specimens of various steels tested in glycerine (left) and in a 35.5 weight percent $MgCl_2$ solution (right) at a strain rate of $6.4 \times 10^{-6}/s$.

tests [8]. The present SSR test results confirm that Orion 28-2 is not susceptible.

The ferritic steel Orion 26-1 might be expected to be similarly immune to SCC in chloride environments. The maximum load data represented in Fig. 5 suggest that SCC indeed does not occur in this type of steel. However, the fracture strain in the test solution is considerably lower than in glycerine. Stress corrosion clearly did occur during the SSR tests. This is further illustrated in Fig. 7, which shows a scanning electron microscope picture of part of the fracture surface of an Orion 26-1 specimen tested in the $MgCl_2$ solution. The surface exhibits river pattern features that are characteristic for SCC.

The ferritic-austenitic steels, as represented by Uranus 50 are generally considered to show little susceptibility [7] to SCC. This is confirmed by the present test results.

While martensitic stainless steels are known to show some susceptibility for SCC after heat treatments resulting in a high strength, the maximum load data do not indicate that AISI 431 is susceptible. On the basis of a fracture strain criterion, however, the martensitic steel AISI 431 can be termed susceptible to SCC in chloride environments.

From the above observations it can be concluded that in SSR tests on stainless steels in $MgCl_2$ solutions, the fracture strain (or time to failure) provides a more severe criterion for SCC susceptibility in chloride environments than the maximum load. On the basis of a fracture strain criterion, certain steels may be termed susceptible to SCC, while in most practical situations they may be sufficiently resistant to this type of failure. On the other hand, SCC susceptibility under severe service conditions can not be excluded on the basis of favorable SSR test results in $MgCl_2$ solutions,

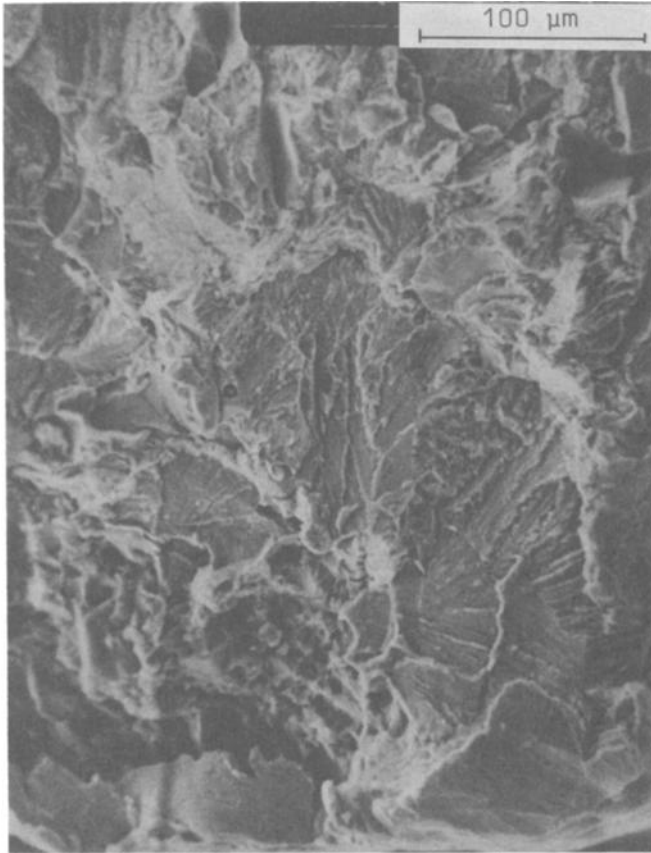


FIG. 7—Scanning electron micrograph of fracture surface of Orion 26-1 specimen after test in 35.5 weight percent $MgCl_2$ solution at $123^\circ C$ ($\dot{\epsilon} = 6.4 \times 10^{-6}/s$).

according to a maximum load criterion. Buhl [6] uses the fracture energy per unit volume of the strained part of the specimen to indicate the degree of SCC susceptibility. For cases where the maximum load is not lowered, but where the fracture strain is lower than in an inert medium, this criterion will correspond closely to the fracture strain criterion used in this investigation.

Effect of Some Inhibitors

Figure 8 shows the effects of small additions of sodium iodine (NaI) and sodium nitrate ($NaNO_3$) to the 35.5 weight percent $MgCl_2$ test solution. The employed strain rate was $6.4 \times 10^{-6}/s$, the temperature $123^\circ C$, and the material AISI 304.

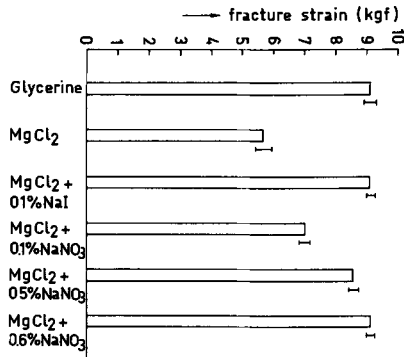


FIG. 8—The fracture strain for AISI 304 specimens, measured at 123°C in glycerine, in a 35.5 weight percent $MgCl_2$ solution and in this solution after addition of respectively 0.1 weight percent NaI, 0.5 weight percent $NaNO_3$ and 0.6 $NaNO_3$.

Complete inhibition against SCC was obtained by adding 0.1 weight percent NaI to the test solution. For a 0.5 weight percent $NaNO_3$ addition, the fracture strain values indicate that there is still some susceptibility to SCC, while 0.6 weight percent $NaNO_3$ addition provided completely effective protection. The nearly complete protection resulting from the 0.5 weight percent $NaNO_3$ addition is illustrated in the scanning electron microscope picture of the fracture surface, shown in Fig. 9. The above concentrations are considerably lower than the percentages of > 3 weight percent NaI and > 2 weight percent $NaNO_3$ reported by Uhlig and Cook [9] who used C-shape bend specimens in a $MgCl_2$ solution boiling at 130°C.

Electrode Potential Changes during the Tests

Figure 10 shows the load as a function of the strain for some of the tests just mentioned. The electrode potential changes recorded during the various stages of the tests, are shown in the same diagram.

Figure 10 shows that the NaI addition caused a rise of ≈ 30 mV in the electrode potential at the beginning of the test. For the $NaNO_3$ addition, the electrode potential rise is hardly significant. In the presence of the inhibitors, as well as in the uninhibited $MgCl_2$ solution, a drop in the electrode potential is associated with the onset of plastic deformation. This effect is similar to the potential drop measured by Graf and Springe [10] and by Stalder and Duquette [11] on straining stainless steel electrodes in boiling $MgCl_2$ solutions. This electrode potential drop appears to be the result of a film rupture process and the creation of active surface at the slip steps. The more or less constant value of the electrode potential in the next stage of the test can be interpreted as resulting from a situation where

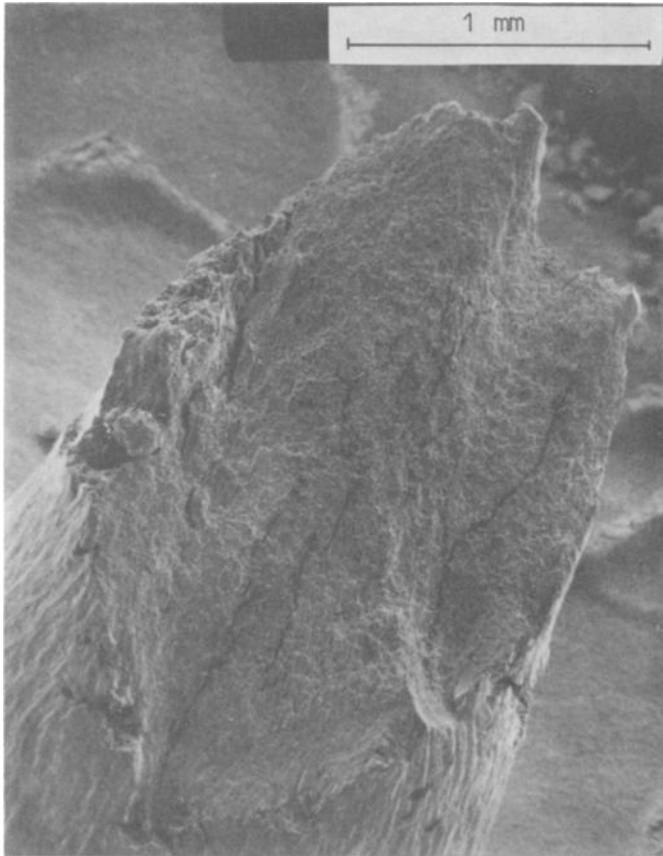


FIG. 9—Scanning electron micrograph of the fracture surface of an AISI 304 specimen, tested in the 35.5 weight percent $MgCl_2$ + 0.5 weight percent $NaNO_3$ solution at $123^\circ C$ ($\dot{\epsilon} = 6.4 \times 10^{-6}/s$).

the effect of the newly formed film free surface is compensated by the repassivation of earlier formed active surface. A large potential drop occurs, apparently due to crack formation in the case of the uninhibited solution and due to ductile rupture during the final stage of the test in the solution where the inhibitors are present. The electrode potential reaches a minimum when the specimen breaks and a maximum of active surface area is exposed to the test solution. As this newly exposed area becomes passivated, the electrode potential returns to its value before the test. In the solution where 0.6 weight percent $NaNO_3$ was present, some potential drop was measured after necking started. A similar electrode potential drop was not found for the NaI addition.

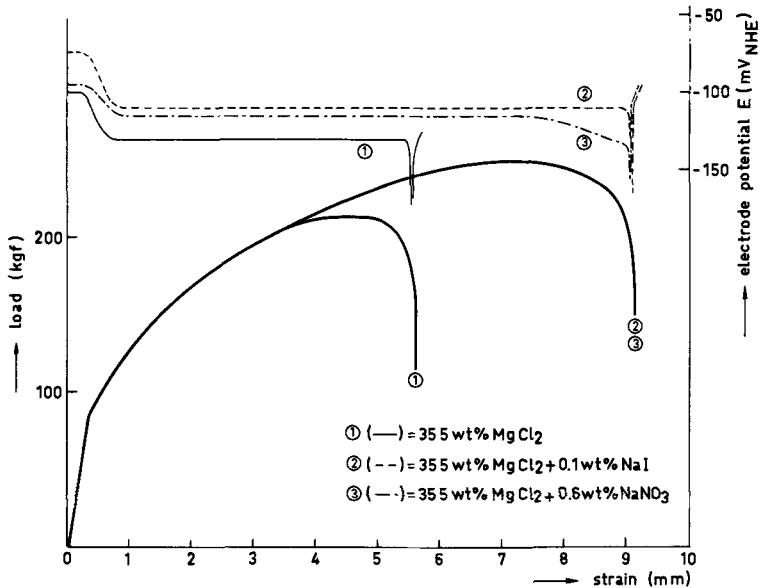


FIG. 10—The load and the electrode potential as a function of the elongation for AISI 304 specimens tested at a strain rate of 6.4×10^{-6} /s at a temperature of 123°C , in the uninhibited 35.5 weight percent MgCl_2 solution and in completely inhibited test solutions containing respectively 0.1 weight percent NaI and 0.6 weight percent NaNO_3 .

Potentiostatically Controlled Tests

Figure 11 shows the fracture strain as a function of the electrode potential for AISI 304, tested in the 35.5 weight percent MgCl_2 solution at 123°C and a strain rate of 6.4×10^{-6} /s.

A critical potential value for AISI 304 in the test solution of ≈ -135 mV (SHE) can be deduced from the data in Fig. 11. At and below this electrode potential there is no evidence of SCC. A comparison with curve 1 in Fig. 10 shows that this value is slightly below the electrode potential of ≈ -130 mV in the stage where a constant potential was measured under free corrosion conditions.

The presently found critical potential value can be compared to the value of -150 mV reported by Buhl [6] for the same material tested at a slow strain rate in a MgCl_2 solution boiling at 144°C , while Uhlig and Cook [9] found a critical potential of -140 mV for constant load tests in a MgCl_2 solution boiling at 130°C .

Conclusions

The SSR tests in MgCl_2 enable us to differentiate between stainless steels

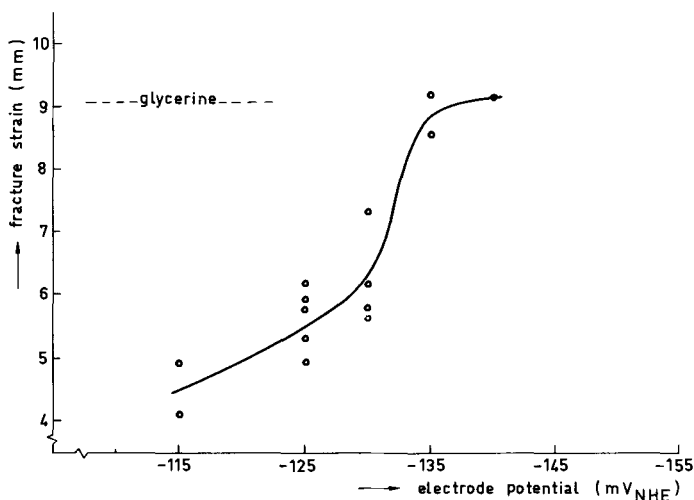


FIG. 11—The fracture strain of AISI 304 specimens, tested in glycerine and in the 35.5 weight percent MgCl_2 solution at 123°C , $\dot{\epsilon} = 6.4 \times 10^{-6}/\text{s}$, as a function of the electrode potential.

of differing SCC susceptibility in chloride environments. Under the presently used test conditions (strain rate $6.4 \times 10^{-6}/\text{s}$, testing temperature 123°C in a MgCl_2 solution boiling at 126.5°C) such tests take less than 24 h.

2. The SSR testing method gave results that are well comparable to the findings from other testing methods in tests of six different types of stainless steel. According to a criterion based on the fracture strain the ferritic steel Orion 26-1 showed a minor SCC susceptibility not found in other tests. This was confirmed by scanning electron microscope investigation of the fracture surface.

3. The SCC of AISI 304 under the above conditions of the SSR test could be avoided by adding 0.1 weight percent NaI or 0.6 weight percent NaNO_3 to the test solution or by decreasing the electrode potential to or below a value of -135 mV versus SHE.

References

- [1] Kohl, H., *Werkstoffe und Korrosion*, Vol. 16, 1965, p. 364.
- [2] Kohl, H., *Werkstoffe und Korrosion*, Vol. 19, 1968, p. 97.
- [3] Thomas, K. C., Ferrari, H. M., and Allio, R. J., *Corrosion*, Vol. 20, 1964, p. 89t.
- [4] Kohl, H., *Corrosion*, Vol. 23, 1967, p. 39.
- [5] Takano, M., *Corrosion*, Vol. 30, 1974, p. 441.
- [6] Buhl, H., "The Validity of the Slow Strain-Rate Method in the SCC Research Compared with Conventional Testing Techniques," this volume.
- [7] Combrade, P., Desestret, A., Cright, R. D. Mc., Gauthey, F., and Gres, C., *Revue de Metallurgie*, Vol. 71, 1974, p. 807.
- [8] Bond, A. P. and Dundas, H. J., *Corrosion*, Vol. 24, 1968, p. 344.

- [9] Uhlig, H. H. and Cook, E. W., Jr., *Journal of the Electrochemical Society*, Vol. 116, 1969, p. 173.
- [10] Graf, L. and Springe, G., "Fundamental Aspects of SCC," National Association of Corrosion Engineers, 1969, p. 335.
- [11] Stalder, F. and Duquette, D. J., *Corrosion*, Vol. 33, 1977, p. 67.

P. Suery¹

Detection of Heat Treatment Effects on Environmentally Induced Degradation of a Martensitic Stainless Steel and a Nickel-Base Alloy by the Slow Strain-Rate Method

REFERENCE: Suery, P., "Detection of Heat Treatment Effects on Environmentally Induced Degradation of a Martensitic Stainless Steel and a Nickel-Base Alloy by the Slow Strain-Rate Method," *Stress Corrosion Cracking—The Slow Strain-Rate Technique*, ASTM STP 665, G. M. Ugiansky and J. H. Payer Eds., American Society for Testing and Materials, 1979, pp. 320-332.

ABSTRACT: The response of slow strain-rate measurements to heat treatment of a cast, low carbon, martensitic stainless steel in 3 percent sodium chloride solution under cathodic and anodic polarization and Alloy 600 in 0.1 M sulfuric acid solution (poisoned with arsenic) under cathodic polarization has been investigated. The relative reduction of area evaluation was very sensitive to heat treatment and electrochemical polarization effects in both corrosion systems.

The reduction of area measurements on the stainless steel revealed a minimum and a maximum crack sensitivity after tempering at 873 K if the straining electrode were cathodically and anodically polarized, respectively. The test results are explained by hydrogen assisted cracking and active path cracking under cathodic and anodic polarization, respectively.

Alloy 600 samples in poisoned sulfuric acid showed a pronounced decrease in the relative reduction of area after a 50 percent cold deformation plus low temperature aging treatment at 673 K during 500 h. The same metallurgical state had been shown to be especially prone to caustic embrittlement at high temperature. It seems that the slow strain-rate test, as performed in this investigation, can be used as a sensitive method to detect variations in the susceptibility to environmentally induced degradation of Alloy 600 in high temperature caustic solutions.

KEY WORDS: steel castings, nickel alloys, stress corrosion cracking, hydrogen embrittlement, active path cracking, heat treatment, constant strain rate method, sodium chloride, sulfuric acid

¹Sulzer Bros. Ltd., Research and Development Department, CH 8401 Winterthur, Switzerland.

The susceptibility to environmentally induced cracking² of metallic materials usually is evaluated on the basis of long time tests at constant load or constant elongation. This procedure may be time-consuming, especially if extended incubation periods precede crack propagation. With the aid of the slow strain-rate method it is possible, even in such cases, to test a large number of heat treatment varieties of an alloy and to get useful information for comparative purposes about the susceptibility to brittle fracture under the influence of a certain environment.

Both martensitic stainless steels in chloride-containing media at ambient temperature and Inconel³ Alloy 600 in various high temperature aqueous solutions, under conditions known to produce SCC, frequently exhibit long crack initiation periods. The SCC behavior of martensitic stainless steels is strongly influenced by microstructural variations during heat treatment [1-5].⁴ Alloy 600, depending on its origin and preexposure history, may turn crack sensitive even at service temperatures typical of nuclear power plant steam generators [6-10].

The aim of this work is to show qualitative correlations between slow strain-rate and static stress corrosion test results on a cast, low-carbon, martensitic stainless steel and on a selected heat of Alloy 600 in several microstructural conditions known to influence the susceptibility to environmentally induced degradation.

For Alloy 600 the experimental conditions during slow strain-rate testing (for example, composition of electrolyte and test temperature) were not directly related to any service application or laboratory conditions which had resulted in crack formation. However, it was speculated that hydrogen uptake on a straining electrode of Alloy 600 from an acidic solution at ambient temperature could be structure sensitive, and this could modify the strain-to-rupture characteristics in a similar sense as had been observed in long time tests on bent beam specimens in high temperature aqueous solutions (for example, 50 percent sodium hydroxide (NaOH) solution at 553 K).

The relationship between heat treatment conditions and susceptibility to SCC in chloride-containing aqueous media is not yet well established for cast, low-carbon, martensitic stainless steels. Therefore, the results of slow strain rate measurements on a 13C + 4N bearing steel are discussed with reference to literature data on high carbon steels, for example, AISI 410 steel, and to own results on a similar, low carbon, cast steel examined with conventional longtime SCC test methods.

²The terms "environmentally induced cracking" (degradation) and "stress corrosion cracking" (SCC) are used as synonyms herein to denote a cracking process due to the conjoint action of stress (or strain) and a corrodent, irrespective of the cracking mechanism. "Hydrogen assisted cracking" (HAC) or "active path cracking" (APC) are terms used throughout this paper to denote cracking mechanisms if experimental data justify such a distinction.

³Tradename, International Nickel Co., Inc.

⁴The italic numbers in brackets refer to the list of references appended to this paper.

Procedure

Materials

The composition of the specimens is indicated in Table 1. The steel was received from the foundry in normal hardened plus tempered condition. Alloy 600 was taken from a commercially available lot in the mill annealed condition. A number of metallurgical operations were applied to the starting materials leading to the mechanical properties indicated in Table 2. The high strength stainless steel in the hardened condition shows a fully martensitic structure. The chemical composition of this material allows air hardening and suppresses the formation of deltaferrite. During tempering at 773 to 923 K, this alloy is softened through transformation of martensite to ferrite and chromium carbides of the Cr_{23}C_6 type. According to Table 2, annealing at 923 K gives rise to a partial reaustenitization with a subsequent martensite transformation leading to the observed rehardening effect. Alloy 600, in the solution annealed condition, showed a coarse-grained structure (grain size ASTM 4 to 5). Solution annealed plus 50 percent cold-deformed material was subjected to a low temperature heat treatment at 673 K. The latter procedure was shown to increase the tendency to environmentally induced cracking of smooth bent beam specimens from the same heat in a deaerated 50 percent caustic solution at 553 K during autoclave tests [11].

Specimen Preparation

Specimens used in the slow strain-rate experiments were of the plain tensile type with a circular test section of 4 mm diameter and a length of 36 mm. Samples were machined from the heat treated bars and ground on emery paper to a 5 μm surface finish. Specimen surfaces were covered by a silicon rubber paint, with the exception of a center part of about 10 mm length. This technique allows ruling out those specimens broken in painted regions from further consideration since in such cases the rupture would be purely mechanical. Furthermore, it is expected that any electrochemical quantity measured on the straining electrode can serve more sensitively as an indicator to rupture-induced corrosion phenomena if only the surface fraction undergoing contraction is exposed to the corrosive environment.

Method and Experimental Conditions

During the slow strain-rate experiments, the tension specimens were polarized to a constant potential with the aid of a potentiostat. The specimen was surrounded by a cylindrically shaped platinum gauze counter electrode. The saturated calomel reference electrode was connected to a capillary tube, the tip of which was directed to the noncoated surface area of the specimen.

TABLE 1—*Composition of investigated materials.*

	Chemical Composition, weight %								
	C	P	S	Si	Mn	Cr	Ni	Mo	Fe
Steel	0.036	0.012	0.006	0.46	0.70	12.1	3.7	0.27	bal
Alloy 600	0.026	0.008	0.007	0.33	0.23	16.3	bal	...	7.9

TABLE 2—*Metallurgical condition and mechanical properties of test materials at room temperature.*

Metallurgical Condition	R _p 0.2, MPa	R _m , MPa	A, ^a %	Z, ^a %	VHN 10
Steel					
1173 K/3.6 h					
+473 K/10 h	980	1040	17.5	62	330
+773 K/10 h	920	980	19	69	315
+873 K/10 h	660	820	22	68	250
+923 K/10 h	680	850	16.5	68	285
Alloy 600					
1373 K/1 h	175	530	52	70	115
solution anneal	no significant alteration of properties				
solution anneal +673 K/500 h	no significant alteration of properties				
solution anneal + 50% cold-reduced	820	950	9	33	280
solution anneal + cold-reduced + 673 K/500 h	no significant alteration of properties				

^aR_p = 0.2 yield strength,
R_m = tensile strength,
A = elongation, and
Z = reduction of area.

The upper side of the cell vessel (made of plexiglass) was open to the air. The whole assembly was placed in a specially designed, mechanically driven tensile machine with a crosshead speed range between 6.6 and 0.03 mm/h. The load versus elongation curves were electronically recorded. The unloaded specimens were prepolarized during 30 min in the aerated electrolyte solution. Then the slow strain-rate test was started.

Martensitic stainless steel specimens were examined in a 3 percent sodium chloride (NaCl) solution at ambient temperature. Polarization was either negative (-1.0, -0.75, and -0.50 V⁵) or positive (-0.10 and +0.30 V) with respect to the corrosion potentials. The latter were measured on separate nonstressed specimens. Breakdown potentials were determined potentiodynamically with a potential sweep rate of 0.084 mV/s, starting at the corrosion potential on tension specimens either at zero stress or after reaching the ultimate tensile strength values indicated in Table 2.

⁵All potential values with reference to the normal hydrogen electrode.

Alloy 600 specimens were investigated at room temperature in a 0.1 M sulfuric acid (H_2SO_4) solution containing 100 mg arsenic (as sodium arsenite (NaAsO_2)) per litre. This addition is known to enhance hydrogen entry into metallic lattices. The specimens were polarized to potential values between -0.80 and -0.40 V. The corrosion potential was approximately -0.30 V after 1 h in the acid solution.

The reduction of area was taken as the preferred quantity indicating any tendency to brittle fracture due to stress corrosion in the test environment. Additional evidence for environmentally induced failure was tried to get from an evaluation of specimen elongation and from maximum stress reached during the slow strain-rate experiment. All values obtained in test solutions were compared to corresponding values determined in oil at ambient temperature.

Results

Martensitic Stainless Steel

The variation in the reduction of area with applied strain rate on a specimen tempered at 773 K was determined at a potential of -1.0 V. The results are given in Fig. 1 as the ratio Z_c (reduction of area in presence of corrosive environment) to Z_o (reduction of area in oil), $Z_c/Z_o = 1$ indicating a nondetectable environmental effect. As can be seen from this figure, a lower shelf is reached at a speed of $6.0 \times 10^{-6} \text{ s}^{-1}$. Further reduction of the

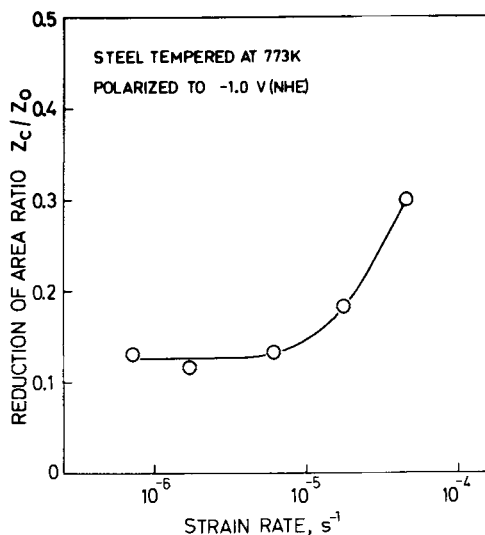


FIG. 1—Reduction of area versus strain rate measured on martensitic stainless steel in 3 percent NaCl solution.

strain rate did not enhance sensitivity. Thus, all the following results are based on a strain rate of $6.0 \times 10^{-6} \text{ s}^{-1}$.

The effect of tempering temperature on the reduction of area is shown in Fig. 2. The electrode potential is represented as a parameter within this graph. The evaluations of total elongation as well as time to rupture were in qualitative accordance with results from reduction of area measurements, whereas maximum attainable stress measured in presence of the corrosive environment and normalized to the value in oil was not significantly dependent on heat treatment and specimen potential.

Corrosion potentials scattered from about -0.3 to -0.2 V but were not influenced systematically by heat treatment, whereas breakdown potentials on nonstressed and stressed specimens depended on tempering temperature showing minima after tempering at 873 K (-0.10 and -0.20 V, respectively). Sample stressing corresponding to the ultimate tensile strength caused the breakdown potentials to shift by about 50 to 100 mV in the negative direction in all heat treatment conditions. The most positive potentials (approximately $+0.20$ V) were determined after tempering at 473 K.

At potentials more positive than open circuit value, irregular fluctuations of the anodic current on the straining electrodes were observed as soon as the

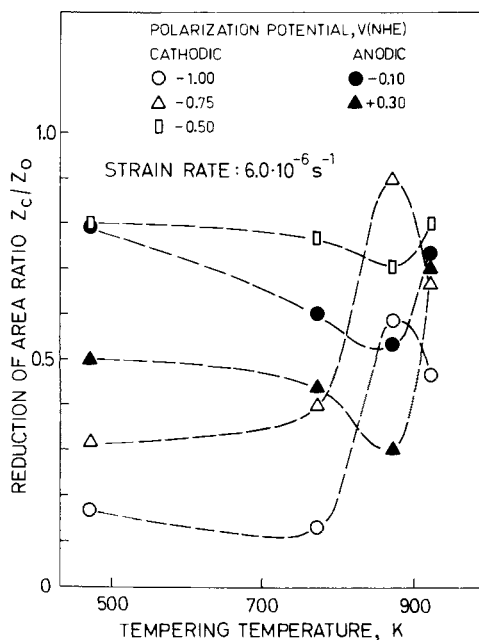


FIG. 2—Influence of tempering temperature and polarization on reduction of area of cast martensitic stainless steel in 3 percent NaCl solution.

plastic deformation region has been reached. This phenomenon is ascribed to passive oxide film rupture by plastic deformation.

Environmentally induced cracking was readily visible from the brittle inter- and transgranular fracture portion at the periphery of broken specimens detected by scanning electron microscope (SEM) fractography. There was no clear relationship between the depth of stress corrosion crack penetration and the reduction of area ratio. However, the intergranular portion of fracture reached a maximum on specimens tempered at 873 K, irrespective of the polarization potentials. In contrast to more negative potentials, cracks on specimens held at +0.3 V during straining were likely to start from pitting sites. This potential lies well above the breakdown potential of all investigated specimens in the stressed condition.

Alloy 600

Figure 3 shows the reduction of area ratio of Alloy 600 specimens in several metallurgical conditions at different cathodic potentials in poisoned H_2SO_4 . A previous evaluation of the influence of strain rate on reduction of area ratio showed a sufficiently pronounced effect at a speed of $1.7 \times 10^{-6} s^{-1}$. The effect of hydrogen absorption, again, was pointed out most clearly in the

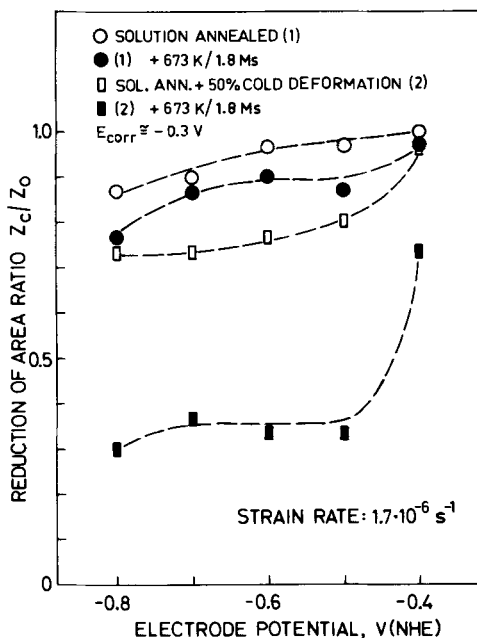


FIG. 3—Influence of metallurgical condition and polarization on reduction of area of Alloy 600 in H_2SO_4 .

reduction of area ratio while the time to failure and the total elongation were not as indicative. The cold-deformed plus 673 K tempered specimen revealed predominantly intergranular brittle fracture which was absent in the other metallurgical conditions. The cathodic current versus time relationship at the most positive potential investigated, -0.4 V, on the straining electrodes is represented in Fig. 4. The current density values indicated in this figure are corrected for the surface growth during specimen elongation.

Discussion

Martensitic Steel

As can be seen from Fig. 1, the reduction of area resulting from slow strain-rate experiments with a cast martensitic stainless steel in neutral NaCl solution is indicative of environmentally induced cracking during cathodic polarization. A strain rate of $6.0 \times 10^{-6} \text{ s}^{-1}$ was sufficient to detect susceptibility to this kind of environmental susceptibility. As shown in Fig. 2, cathodic polarization at -1.0 and -0.75 V leads to a remarkable loss of reduction of area on specimens at high strength levels (annealed at 473 and 773 K, respectively). In the softened condition (873 K) the reduction of area value is restored to a large extent. Specimens with reformed martensite

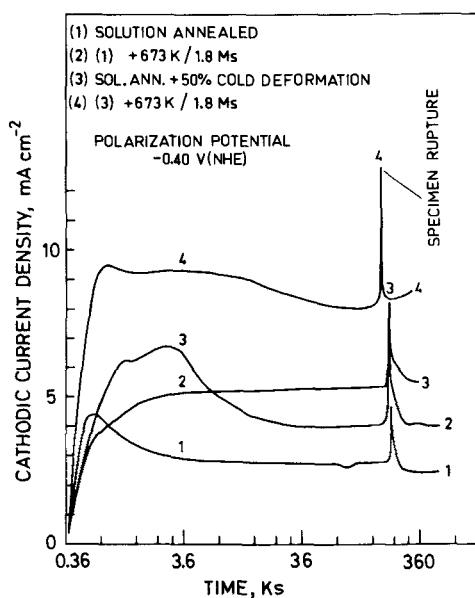


FIG. 4—Current density versus time curves on Alloy 600 electrodes during slow strain-rate test in H_2SO_4 .

(923 K) again reveal a tendency to brittle fracture in the corrosive environment. These findings are typical of HAC. Increasing amounts of non-transformed martensite in high strength steels generally reduce resistance to environmentally induced degradation under conditions leading to hydrogen evolution. The susceptibility to HAC of the investigated steel, according to the results of slow strain-rate measurements, follows the same qualitative trend with respect to the mechanical properties as it has been shown for AISI 410 steel in conventional stress corrosion tests using NaCl solutions poisoned with sulfide ions [2,12]. Additional work [13] on a cast steel with 0.032C, 13.2Cr and 4.2Ni has shown that the same sequence of susceptibility to HAC as a function of heat treatment is followed if time to failure is determined on four-point-loaded plain bent beam specimens exposed to a 5 percent NaCl solution under cathodic polarization.

From results of slow strain-rate tests in Fig. 2, it is concluded that heat treatment at 873 K leading to a hardness of 250 VHN 10 (23 HRC) does not eliminate completely the susceptibility to HAC during cathodic polarization. This observation is consistent with the generally accepted rule according to which HAC of high strength stainless steels is to be expected if hardness levels exceed 22 HRC.

The relative influence of tempering temperature on reduction of area at polarization potentials equal to or more positive than -0.50 V fundamentally differs from that measured at the more negative potentials, the reduction of area showing a minimum in the 873 K annealed condition. This minimum is very pronounced at $+0.3$ V. Such behavior may be explained by an APC mechanism which, in contrast to HAC, should be favored at more positive potentials. The active path is generated through Cr_{23}C_6 precipitation and related chromium depletion enhanced at prior austenite grain boundaries [2,14], reaching a maximum in the 870 K temper condition as has been proven on several heats of cast, low carbon stainless steels of similar composition [15]. After tempering at 923 K, the reduction of area is partly restored. Chromium depletion in this heat treatment condition is reduced to a large extent due to rapid chromium diffusion from the matrix into the grain boundaries.

Thus, the reduction of area measurement during slow strain-rate tests is thought to be a valuable method allowing rapid detection of susceptibility to either HAC or APC of high strength stainless steels in chloride media.

As mentioned above, breakdown potentials were more negative than $+0.30$ V in all cases. Therefore, it can be expected that corrosion pits on the straining electrodes precede crack formation at $+0.30$ V. This leads to the observed strong decrease in the reduction of area at all tempering temperatures except 923 K. The sharp rise at 923 K may be due to delayed pit initiation or decreased pit growth rates during the slow strain-rate experiment. Though SEM investigation did not reveal a significant difference in fracture surface topography between cathodically and anodically polarized

specimens, it is believed that the HAC mechanism sometimes postulated even for anodically polarized high strength steels undergoing pit corrosion is not effective at +0.30 V on the steel investigated in the present work. This hypothesis is supported by the fact that the tempering condition with the lowest amount of nontransformed martensite (873 K) shows a minimum in the reduction of area ratio.

From Fig. 2 it may be concluded that the loss of general corrosion resistance with increasing tempering temperature is the principal factor determining sensitivity of the investigated material to environmentally induced degradation if the specimens are anodically or only slightly cathodically polarized. The maximum SCC susceptibility is reached in a metallurgical condition prone to selective corrosion of prior austenite grain boundaries thought to be responsible for the observed maximum of brittle intergranular fracture by an APC mechanism.

If the reduction of area in the corrosive environment is taken as a generally valuable measure of sensitivity to environmentally induced cracking, our results at potentials near or above the open circuit value seem to contradict those reported by McGuire et al [12]. According to their work, the susceptibility to crack formation at anodic potentials should decrease with increasing tempering temperature as in case of strong cathodic polarization. The different behavior is probably explained by the fact that the NaCl solution used in Ref 12 has been poisoned with sulfide, inducing hydrogen absorption in growing pits even at relatively noble potentials. On the other hand, the K_{Isc} values of martensitic stainless steel AFC 77 in a NaCl solution reported by Webster [4] are in good qualitative agreement with our results from slow strain-rate experiments showing a continuous decrease with increasing tempering temperature up to 870 K by a sharp rise after annealing at about 1030 K.

As with anodically polarized specimens, annealing at 873 K favored intergranular SCC during the slow strain-rate tests conducted at -0.50 V down to -1.0 V. HAC, as the most probable mechanism of brittle fracture at these conditions, to our knowledge, is not significantly enhanced by chromium depletion at grain boundaries. Other microstructural changes at the latter therefore are considered to be responsible for HAC resulting in intergranular brittle fracture under the experimental conditions.

Alloy 600

From Fig. 3 it is concluded that Alloy 600 in poisoned H_2SO_4 shows a tendency to HAC particularly pronounced in the cold worked plus low temperature aged condition where intergranular fracture could be detected in the SEM. The 673 K heat treatment, applied to solution annealed material, did not affect the reduction of area to such an extent as was observed on cold-deformed material.

At a potential of -0.4 V, the highest cathodic current densities were reached on the straining electrode in the cold-deformed plus aged condition as shown in Fig. 4. The specimen rupture is indicated by a sharp current peak which again amounts to the highest value in the mentioned metallurgical condition. This peak may be explained by the sudden exposition of freshly created, plastically deformed, metallic material with an expectedly low overvoltage of the hydrogen evolution reaction (HER). Though not directly related to HAC, the relatively high cathodic current densities on the cold-worked plus annealed specimen demonstrates a relatively low overpotential of the HER during slow plastic deformation in H_2SO_4 .

Thus, slow strain-rate experiments, as performed in this investigation, can be applied to detect metallurgical reactions in Alloy 600 which are not readily visible from other low temperature corrosion tests (tests normally indicating susceptibility to intergranular corrosion failed to show preferred grain boundary attack in the "vulnerable" heat treatment condition).

The nature of the structural changes responsible for the environmentally induced cracking during cathodic polarization in acid solution is not yet known. Electron microscopical investigations with the replica technique were not successful in detecting any precipitations due to cold deformation plus low temperature annealing.

On the other hand, SCC tests performed with bent beam specimens four-point loaded to 90 percent of yield strength and exposed to deaerated 50 percent NaOH solution at 553 K revealed an increased sensitivity to environmentally induced cracking (predominantly intergranular) of the same heat of Alloy 600 if it were cold-deformed plus 673 K annealed and if the loaded specimens were galvanically coupled to a mild steel specimen (simulation of service conditions in nuclear steam generators). The detrimental effect of cold-deformation plus low temperature annealing was absent if the specimen were tested at their open-circuit potential. Similar effects of low temperature heat treatment on the SCC behavior of Alloy 600 in high temperature caustic solutions are reported in the literature [8,9]. These usually ascribed to an APC mechanism.

Since both slow strain-rate tests under conditions favoring HAC at ambient temperature and conventional SCC tests in high temperature caustic solution showed a remarkable correspondence with respect to the effect of a certain metallurgical treatment on cracking tendency and crack morphology it is hypothesized that intergranular HAC may be the cause of environmentally induced degradation of Alloy 600 in the particular structural condition even in the high temperature corrosive environment. Obviously, this hypothesis must be supported by further results from experiments pointing more directly to a HAC or APC mechanism of Alloy 600 degradation in high temperature caustic solutions. At least from thermodynamical data at 573 K, it can be concluded that the mild steel-Alloy 600 combination in the high

temperature 50 percent NaOH solution acts as a galvanic element with the anodic dissolution reaction proceeding on steel and evolution of hydrogen from the electrolyte concentrating on Alloy 600.

It was hypothesized that sulfur as an impurity element could exert a detrimental effect on SCC of Alloy 600 in high temperature water [6]. Other investigators [16] were not able to prove this hypothesis but have shown that carbon diffusion at grain boundaries in Alloy 600 is possible even at 590 K. Whether or not grain boundary segregation of such impurity elements at low temperature is responsible for service failures of steam generator tubes by intergranular SCC will certainly be a matter of further discussions.

Conclusions

The slow strain-rate test can be applied to cast, low carbon, martensitic stainless steels in chloride-containing media at ambient temperature and allows a rapid evaluation of the relative susceptibility to environmental cracking as influenced by heat treatment conditions. At a strain rate of about $6 \times 10^{-6} \text{ s}^{-1}$ heat treatment effects are clearly visible from reduction of area evaluations both on cathodically and anodically polarized straining electrodes. Hydrogen assisted cracking and anodic path cracking are readily discernible from each other on the basis of reduction of area versus tempering temperature curves at constant electrode potential.

The reduction of area as determined on a selected heat of Alloy 600 at ambient temperature in dilute H_2SO_4 poisoned with arsenic showed a marked decrease after a metallurgical treatment known to reduce the resistance of that particular heat to caustic cracking during long time conventional testing at high temperature if specimens were coupled to mild steel. It is presumed that the slow strain-rate experiment, as performed in this investigation, may be used as a sensitive and easily applied screening test to evaluate the susceptibility of Alloy 600 to environmental cracking in high temperature caustic solutions during cathodic polarization. Further tests on other heats of Alloy 600 are needed to verify this presumption.

References

- [1] Lillys, P. and Nehrenberg, A. E., *Transactions, American Society for Metals*, Vol. 48, 1956, p. 327.
- [2] Truman, J. E., Perry, R., and Chapman, G. N., *Journal of the Iron and Steel Institute*, London, 1964, p. 745.
- [3] Bressanelli, J. P., *Transactions, American Society for Metals*, Vol. 58, 1965, p. 3.
- [4] Webster, D., *Metallurgical Transactions*, Vol. 1, 1970, p. 2919.
- [5] Phelps, E. H., *Metals Engineering Quarterly*, May 1973, p. 44.

- [6] Coriou, H. et al, "Influence of Various Parameters Upon Intergranular Cracking of Inconel Alloy 600 and Inconel Alloy X 750 in Pure Water at High Temperature," Firminy Conference Preprint No. G-13, 1973.
- [7] Foster, G. G. and Taylor, J. W., "Stress Assisted Corrosion of Inconel 600 Heat Exchanger Tubing in High Temperature Water," Paper B, The Institute of Civil Engineers, London, 1971.
- [8] Spähn, H., Wagner, G. H., and Schenk, H., "Some Results on the Low Temperature Sensitization of Inconel 600, Discussion Contribution," Firminy Conference, 1973.
- [9] Weber, J. and Suery, P., *Materials Performance*, Vol. 15, 1976, p. 34.
- [10] van Rooyen, D., *Corrosion*, Vol. 21, 1975, p. 327.
- [11] Suery, P., unpublished work.
- [12] McGuire, M. F., Troiano, A. R., and Hehemann, R. F., *Corrosion*, Vol. 29, 1973, p. 268.
- [13] Suery, P., prepared for publication in *Werkstoffe und Korrosion*.
- [14] Truman, J. E., *British Corrosion Journal*, Vol. 11, 1976, p. 92.
- [15] Suery, P., prepared for publication in *Werkstoffe und Korrosion*.
- [16] McIlree, A. R., Michels, H. T., and Morris, P. E., *Corrosion*, Vol. 31, 1975, p. 441.

Validity of the Slow Straining Test Method in the Stress Corrosion Cracking Research Compared with Conventional Testing Techniques

REFERENCE: Buhl, H., "Validity of the Slow Straining Test Method in the Stress Corrosion Cracking Research Compared with Conventional Testing Techniques," *Stress Corrosion Cracking—The Slow Strain-Rate Technique*, ASTM STP 665, G. M. Ugiansky and J. H. Payer, Eds., American Society for Testing and Materials, 1979, pp. 333-346.

ABSTRACT: The appearance of a minimum in the susceptibility to stress corrosion cracking (SCC)/strain-rate curves obtained by slow strain-rate experiments has been examined carefully and a relationship between the repassivation rate of the material under investigation and the position of this minimum has been established.

For aluminum alloys, the results of the slow strain-rate experiments are not in complete agreement with the results of the conventional testing techniques. To explain this behavior, further experiments have to be carried out. At this moment, it seems to be doubtful whether the slow strain-rate testing technique is applicable to aluminum alloys.

The results with titanium alloys and high alloyed chromium- and chromium-nickel stainless steels obtained with different testing techniques (slow strain rate and constant load) are in very good agreement with each other.

KEY WORDS: stress corrosion cracking, tests, passivity

The slow straining testing technique has been developed by Parkins [1]² and has been applied for fundamental research mainly for iron materials [2-4]. More recently, other investigators have also used this test method [5,6] especially for fundamental research. However, for more practical application in the industry, the slow straining testing technique has not been introduced until now. The reason for this is possibly due to the assumption that the pulling of specimens to failure at low strain rates shows

¹Deutsche Forschungs- und Versuchsanstalt für Luft- und Raumfahrt E. V., Institut für Werkstoff-Forschung, Köln, Germany.

²The italic numbers in brackets refer to the list of references appended to this paper.

little relation to the occurrence of failures under practical service conditions. Another reason is the fact that there exist no comparable data of the results of different testing techniques including the constant straining technique up to now. In the following, the constant straining machine and the trifluoroethylene resin cell used is briefly described. Furthermore, a theoretical model for the explanation of the constant straining test results and some results of this test compared with these of conventional techniques are presented.

Experimental Procedure

Slow Straining Tension Test Machine

Figure 1 shows the complete machine with the synchronous motor as well as the gears on the right hand side and the tensile mechanism on the

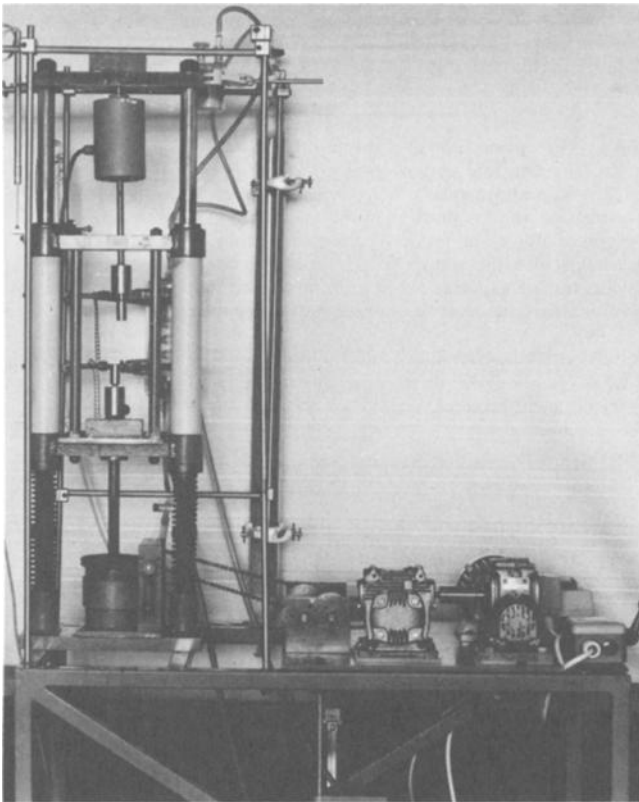


FIG. 1—Complete slow strain-rate testing machine without the cell.

left hand side. Between the two white tubes are the clampings for the specimen in the cell. Above the specimen there is the transducer for the load and on the left of the latter the inductive elongation meter. Beyond the clampings is a worm gear driven with a chain by the changeable gear in the middle of Fig. 1. This worm gear draws down the screw jack with the lower clamping.

Experimental Cell

The trifluoroethylene resin cell used for these experiments is shown in Fig. 2. In order to avoid contact corrosion, the clampings are isolated by a trifluoroethylene resin casing (8) slides in the threaded cap (7) and is sealed by an O-ring (7a). The specimen can be observed through a window (5) and the electrolyte, thermostated outside of the cell, circulates through the

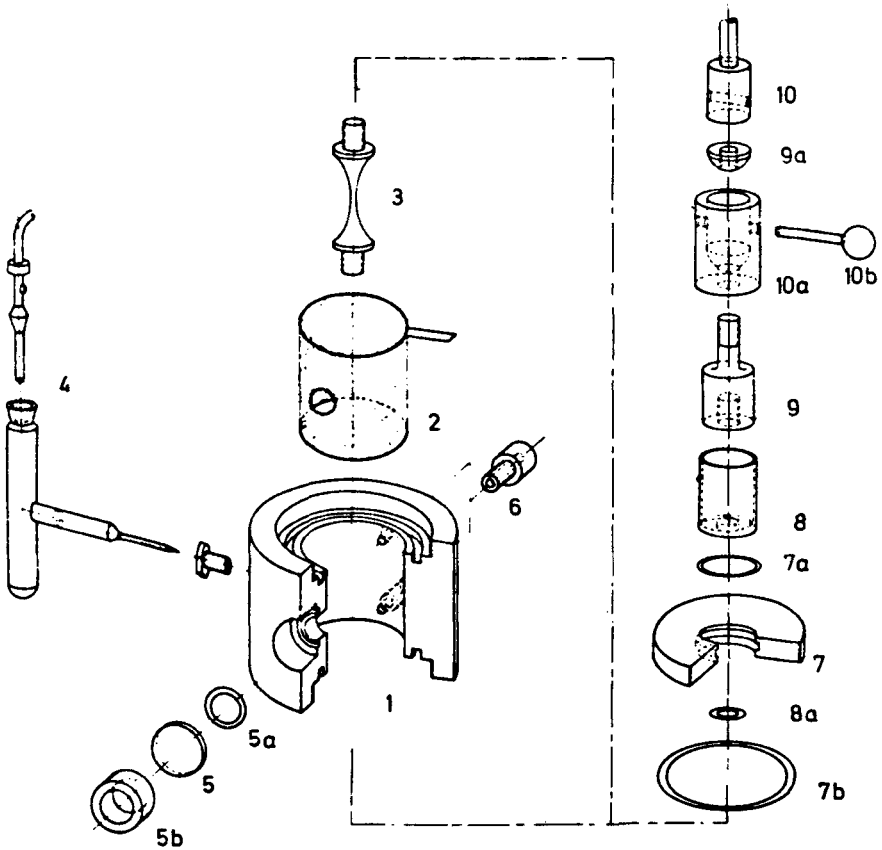


FIG. 2—Explosion drawing of the cell.

cell (6) at a relatively slow velocity. Inside the cell there are a counter electrode (2) and the reference electrode (4) which is connected with a capillary near the specimen.

Results and Discussion

Testing the Model for Explanation of the Appearing Minimum

The result of a slow straining experiment is a load-elongation curve which gives the usual parameters like ultimate tensile stress, yield strength, fracture elongation, reduction of area, etc. In the following, the area beneath the load-elongation curve, called "fracture energy," (E_F) is chosen to characterize the susceptibility of a given material to stress corrosion cracking (SCC). This value refers to the strained volume of the specimen in cubic centimetres. In the following figures, the explicit fracture energy in cal/cm³ is not plotted, but rather the ratio of it to the fracture energy measured in oil or air. This has the advantage of an easier comparison of different materials in different environments.

As shown in Fig. 3 the slow straining testing technique can give three types of E_F /strain-rate curves.

Curve 1 indicates that neither general corrosion attack nor stress corrosion cracking occurs.

Curve 2 displays a decrease of the E_F (env.)/ E_F (air) ratio with decreasing strain rate. This behavior may indicate an influence of stress corrosion cracking, but the same shape of curve can be obtained with general corrosion attack occurring. Lower strain rates are equivalent to a lower exposure time of the specimen in the environment. This can result in a decrease of the cross section and thereby in a decreasing E_F (env.)/ E_F (air) ratio. Further investigations to elucidate this type of curve are necessary in order to differentiate between SCC cracking and general corrosion attack. If stress corrosion occurs, the shape of the curve obtained should correspond to Curve 3. In the following, the reasons for the minimum appearing in this curve are briefly discussed.

At high strain rates (right side of Fig. 4) the corrosion process cannot keep up with the straining process, and the influence of corrosion attack is negligible. With decreasing strain rate, this latter influence becomes more and more important connected with a decreasing E_F (env.)/ E_F (air) ratio. The attack by the aggressive environment reaches a maximum at a strain rate where the repassivation can overtake the activation caused by straining. At further decreasing strain rates, active sites are repassivated or filmed before a corrosion attack can gain any influence. This must result in an increasing E_F (env.)/ E_F (air) ratio, as shown by Curve 3.

This model for the explanation of the minimum shall be proved as follows. The repassivation rate depends on numerous parameters, for example,

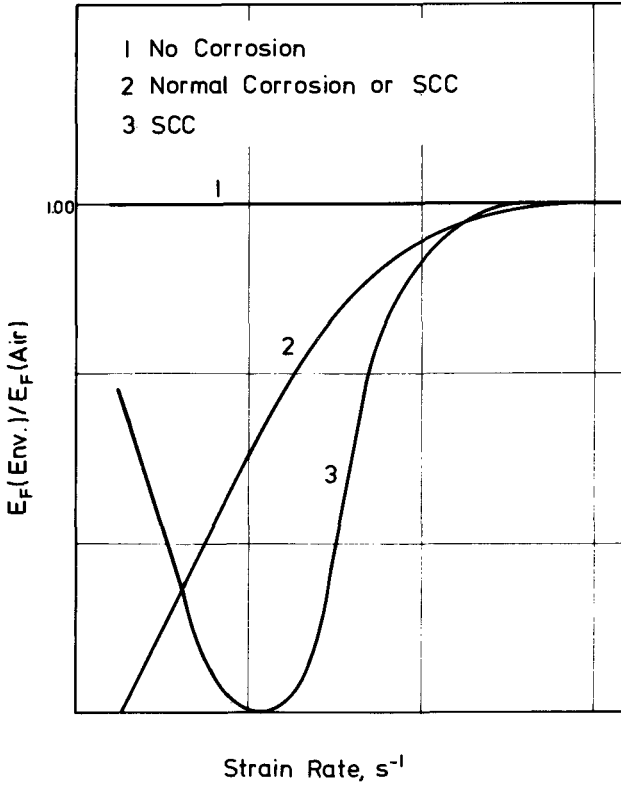


FIG. 3—Characteristic results of the slow strain rate testing technique. E_F means the fracture energy; this is the area beneath the stress-strain curve.

environment, material, solvent, aggressive or inhibiting ions, electrode potential, etc. If the repassivation rate is responsible for the appearance of this minimum, a variation of one of the parameters mentioned must shift the position of the minimum to a higher or lower strain rate.

The influence of formamide on the repassivation behavior of the titanium alloy Ti6Al4V has been described by Rätzer-Scheibe [7]. An increasing formamide ($HCO \cdot NH_2$) concentration (1 *N* sodium chloride (NaCl) solution) decreases the repassivation rate, until in 100 percent formamide solution the repassivation is completely stopped. Figure 4 shows the SCC behavior of a precracked Ti6Al4V specimen in 1 *N* NaCl solution in comparison with that of a smooth specimen of the same material in 1 *N* NaCl solution with 99.5 percent formamide as solvent. The reduced repassivation rate of the titanium alloy in the latter electrolyte results in shifting the minimum towards lower strain rates.

The influence of the material on the position of the minimum is shown

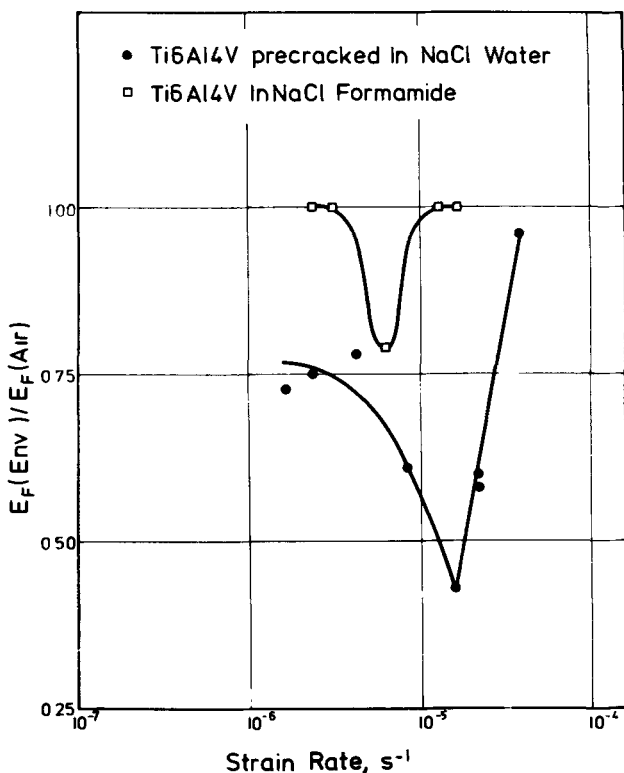


FIG. 4—Influence of the solvent on the position of the minimum for the titanium alloy Ti-6Al-4V. In aqueous solution a precracked specimen has to be used because a smooth specimen is not susceptible to SCC.

in Fig. 5. The minimum for the aluminum alloys is shifted to lower strain rates compared with the minimum for titanium alloys. Rätzer-Scheibe [8] has shown that the repassivation rate of aluminum alloys is evidently smaller than the repassivation rate of titanium alloys.

Another typical example of the influence of the material on the position of the minimum is shown in Fig. 6. Here the SCC-behavior of two austenitic stainless steels without molybdenum (X5CrNi 18 9) and with molybdenum (X10CrNiMoTi 18 10) is compared. It is well known that molybdenum in chromium-bearing stainless steels accelerates the repassivation rate. In agreement with this, the minimum for the molybdenum containing material with the higher repassivation rate is shifted to higher strain rates.

The same effect of repassivation, namely stopping or delaying the anodic dissolution of metals in an aggressive environment, can also be obtained by shifting the electrode potential to more negative values. This has been shown for 18/8-stainless steel (CrNi 18 9) by potentiostatic experiments in

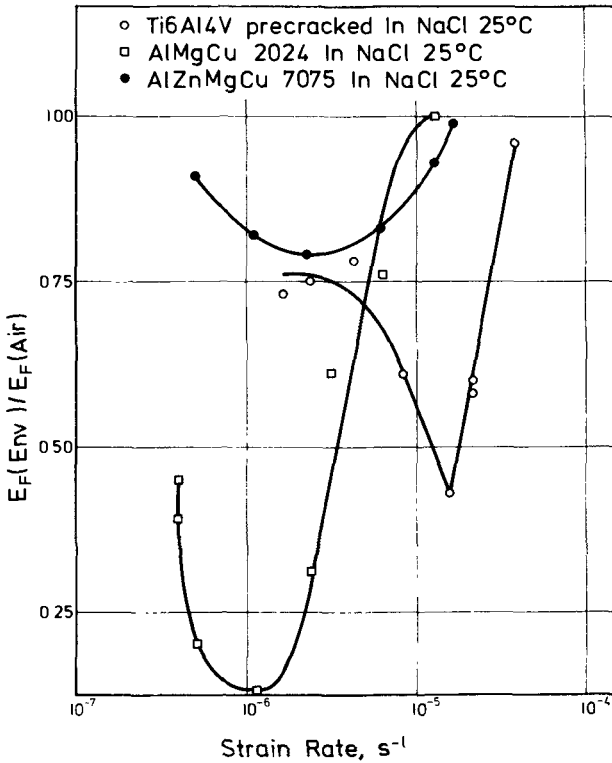


FIG. 5—Influence of the material on the position of the minimum.

boiling magnesium chloride ($MgCl_2$) solution. As Fig. 7 shows, this material is very susceptible to SCC at -120 mV_H and the position of the minimum indicates a very low repassivation rate, which is in agreement with results of Scully [9]. When the potential is fixed at -140 mV_H the susceptibility to SCC decreases and the minimum is shifted to higher strain rates in agreement with the given model.

The experimental results mentioned above show the strong dependence of the position of the minimum on the repassivation rate, which is required by the given model for the appearance of the minimum.

Comparison of the Results of Conventional Testing Techniques with Those of Constant Strain-Rate Tests

Because of the fundamental differences between the expressions for susceptibility of constant load tests (time to failure) and those of slow strain-rate tests (the above mentioned parameters or the fracture energy), a com-

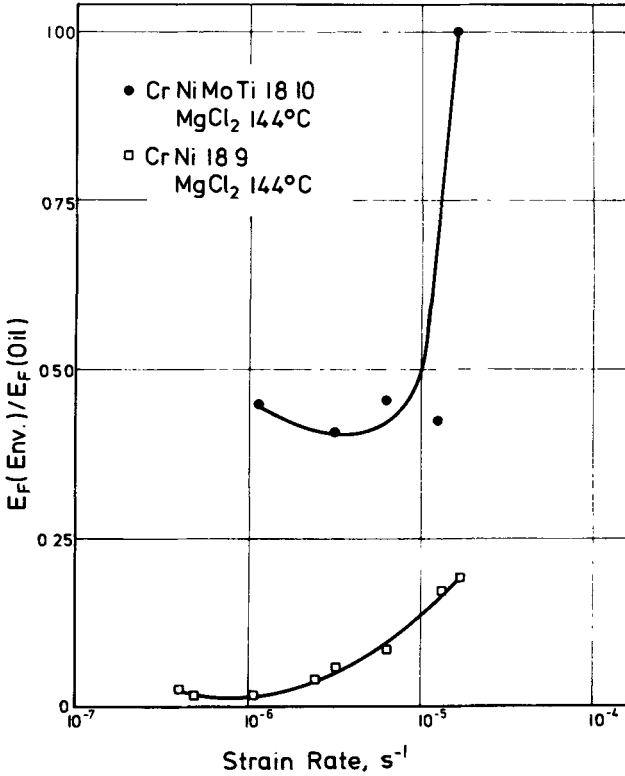


FIG. 6—Influence of the molybdenum content on the position of the minimum.

parison of the results of the different testing techniques can only be of a qualitative character. Therefore, the main features for such a comparison can be either the estimation of the degree of susceptibility to SCC of different materials in the same environment, or the possibility for determining critical potentials for SCC in a given environment. These critical potentials act simultaneously as protection potentials for the application of cathodic or anodic protection.

In the following a comparison of some materials based on the above mentioned topics is given.

Titanium Alloys—The well known fact that in aqueous NaCl solution the titanium alloy Ti-6Al-4V is susceptible to SCC only if a sharp crack exists has been confirmed by slow strain-rate experiments as shown in Fig. 8. The position of the minimum at a strain rate of $1.6 \cdot 10^{-5} s^{-1}$ indicates the high repassivation rate of this titanium alloy.

Aluminum Alloys—Brown and Gray [10] have investigated the three aluminum alloys DTD 5020A (similar 2014), DTD 5050B (similar 7075),

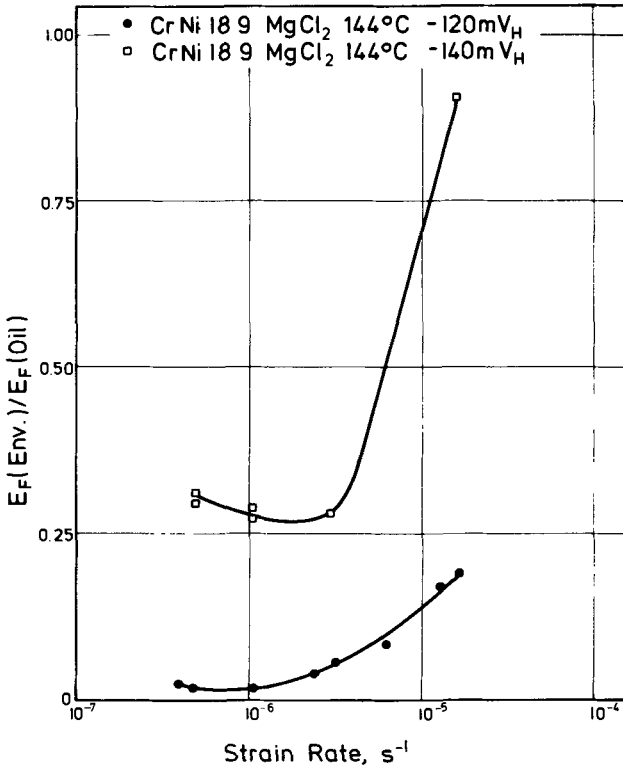


FIG. 7—Influence of the electrode potential on the position of the minimum of AISI 304.

and DTD 5090 (similar 2024) with the constant load as well as with the slow strain testing techniques. From the results the following threshold values were obtained

- 2014: 45 MPa
- 7075: 40 MPa
- 2024: 27 MPa

This gives the following sequence for SCC resistance: 2014 > 7075 > 2024. Corresponding slow strain-rate experiments with the same materials have been performed under free corrosion conditions and at the free corrosion potential under potentiostatic control. The latter has been achieved by variation of the controlled potential maintained by the potentiostat until the current became zero. When this value at the now fixed free corrosion potential had not altered for 1 or 2 h, the straining test began.

The experiments at the free corrosion potential without using a potentiostatic

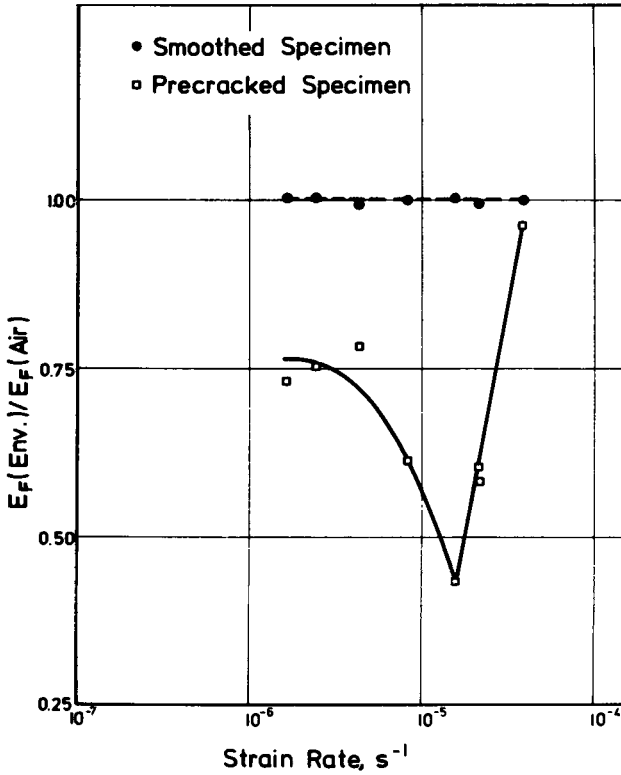


FIG. 8—SCC susceptibility of the titanium alloy Ti-6Al-4V in aqueous 1 N NaCl solution at 25°C.

stat do not give any reasonable results because of the high scatter of the obtained values. The results under potentiostatic control are given in Fig. 9. The sequence for the resistivity to SCC: 7075 > 2014 > 2024 is different from this given by Brown [10]. The results agree only in that the alloy 2024 is the most susceptible one of all. Until now the different results for the two aluminum alloys obtained by the different testing techniques cannot be explained. Presumably the fixed "free corrosion" potential is to be regarded as the reason for this disagreement.

Steels—In the AIG-Research Institute the SCC-susceptibility of the X20-Cr13-steel (AISI 416) in concentrated NaCl solution at room temperature has been investigated. The thermal treatments of the material were "as received" and 15 min at 1050°C, oil quenched, followed by annealing 2 h at 550°C, and air cooled. The results of this investigation with constant load testing techniques show that the annealed material is more susceptible to SCC than the material in the as-received condition. With regard to this

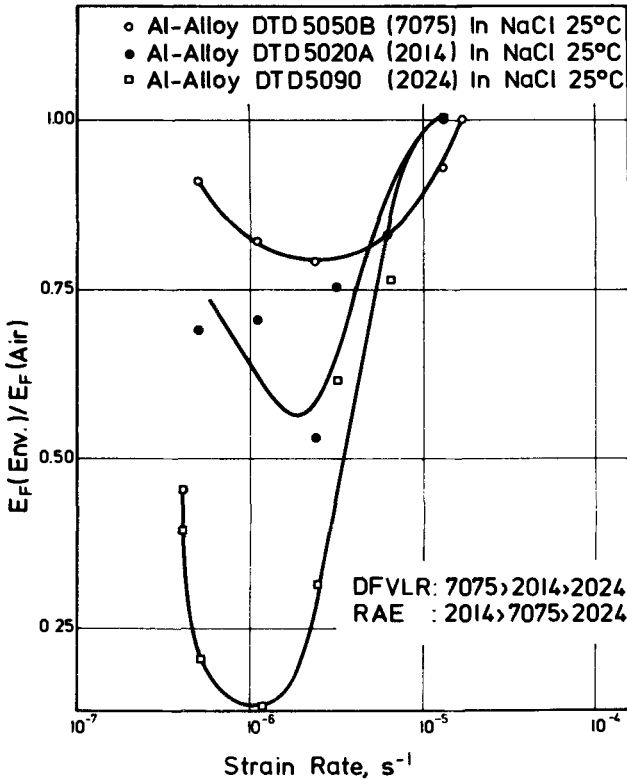


FIG. 9—SCC susceptibility of the three aluminum alloys in the same environment. The sequence of resistance to SCC of the various alloys does not agree with the results obtained by Brown [10] which are also given in the figure.

influence of the heat treatment, the results of the slow strain-rate tests performed with the same material and under the same experimental conditions are in full agreement with these of constant load tests (see Fig. 10).

The material X5 CrNi 18 9 (AISI 304) in the solution treated condition was tested with the constant load technique in boiling $MgCl_2$ solution under potentiostatic control in the Mannesmann Research Institute [11-14]. It was found that in this aggressive media the material was strongly susceptible to SCC with a critical potential at -130 mV_H . This potential, however, was not quite well established because all constant load tests were finished after approximately 300 h. Presumably with longer exposure times the critical potential would be found at more negative values.

By the slow strain-rate testing technique the high susceptibility of the 18/8 stainless steel was confirmed (see Fig. 8) and the critical potential for SCC in the 42 percent $MgCl_2$ solution was found at -150 mV_H as shown in Fig. 11. This seems to be a more correct value for the critical

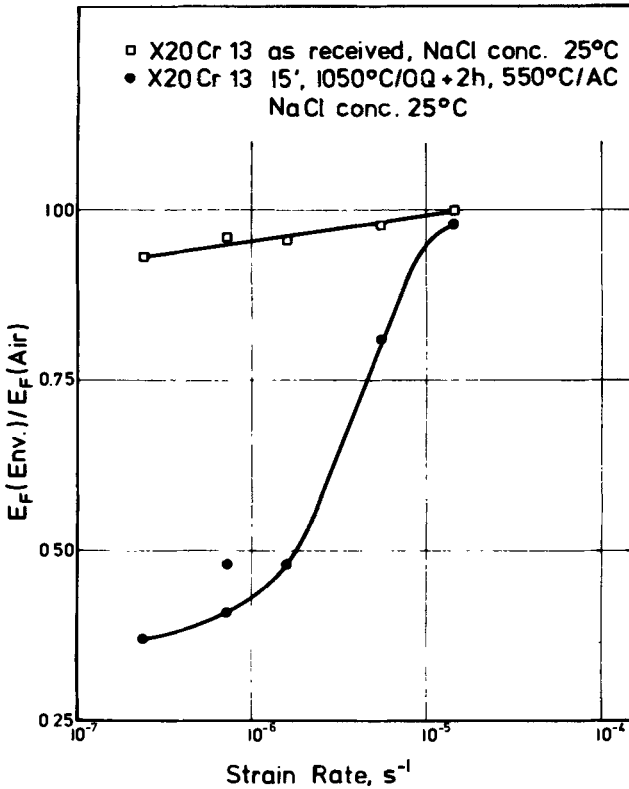


FIG. 10—SCC susceptibility of the chromium steel X20 Cr13 (AISI 416) in concentrated aqueous NaCl at 25°C.

potential than that obtained by constant load experiments and relatively short exposure times. An additional advantage of the slow strain-rate testing technique is the independence of the measured critical potential of the strain rate. Consequently this interesting potential, which may be also very important from the practical point of view (application of electrochemical protection) can be established very quickly by a few experiments with a high strain rate.

Conclusions

For titanium alloys and high alloyed chromium, and chromium-nickel stainless steels, the slow strain-rate tests give results which are in excellent agreement with those of conventional testing techniques (constant load, etc.).

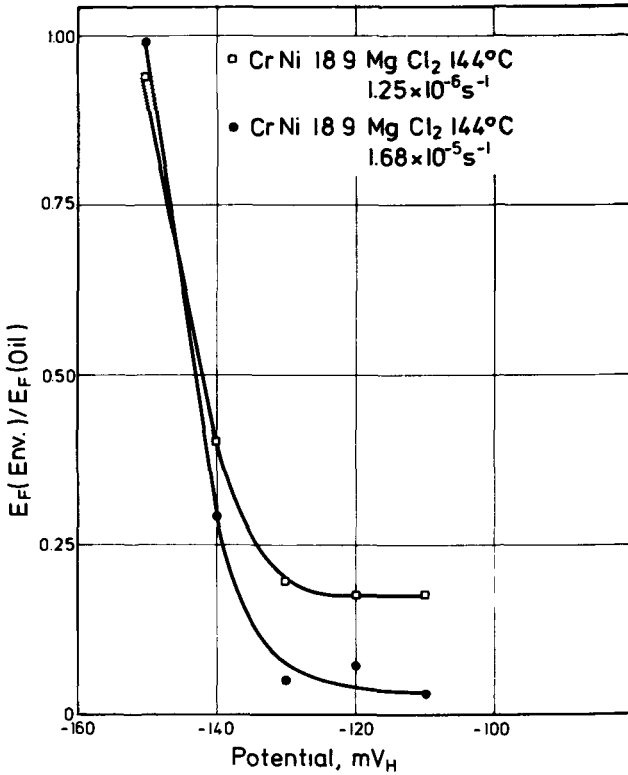


FIG. 11—Critical potential of the 18/8 austenitic stainless steel X5 CrNi 18 9 (AISI 304) in boiling MgCl₂ solution (144°C). At potentials more negative than the critical potential, no SCC occurs.

For aluminum alloys, the applicability of the slow strain-rate testing technique is still doubtful. More investigative work must be performed to get more information about the behavior of these alloys.

The given model for explanation of the appearing minimum has been confirmed.

Acknowledgments

Support of this study by the German Ministry of Research and Technology within the research program "Corrosion and Corrosion Protection" is gratefully acknowledged. The author wishes to thank Dr. Herbsleb (Mannesmann Research Institute), Dr. Horn (Bayer AG), and Dr. Glennly (Royal Aircraft Establishment) for providing the materials and helpful discussions as well as P. Kuhn and W. Amend for technical assistance.

References

- [1] Parkins, R. N., "Stress Corrosion Test Methods—The European Federation of Corrosion Contributions," AGARD Conference Proceedings, No. 98, p. 4-1.
- [2] Henthorne, M. and Parkins, R. N., *British Corrosion Journal*, Vol. 2, 1967, p. 186.
- [3] Humphries, M. J. and Parkins, R. N., *Corrosion Science*, Vol. 7, 1967, p. 747.
- [4] Henthorne, M. J. and Parkins, R. N., *Corrosion Science*, Vol. 6, 1966, p. 357.
- [5] Powell, D. T. and Scully, J. C., *Corrosion*, Vol. 25, 1969, p. 483.
- [6] Buhl, H. and Amend, W., "Untersuchung der Spannungsrißkorrosions-empfindlichkeit des Stahls X 3 CrNiMoN 17 13 5, W.Nr. 1.4439, mit konstanter Dehnungsgeschwindigkeit in CaCl_2 und NaCl ," DLR-FB 74-48, 1974.
- [7] Rätzer-Scheibe, H.-J. and Buhl, H., *Werkstoffe und Korrosion*, Vol. 26, 1975, S. 2.
- [8] Rätzer-Scheibe, H.-J., unpublished results.
- [9] Engseth, P. and Scully, J. C., *Corrosion Science*, Vol. 15, 1975, p. 207.
- [10] Brown, A. R. G. and Gray, J. A., "A Comparison of RAE Stress Corrosion Test Data on Aluminium Alloys Including the Merits of the Testing Techniques," Royal Aircraft Establishment Technical Report 74153.
- [11] Brauns, E. and Ternes, H., *Werkstoffe und Korrosion*, Vol. 19, 1968, S. 1.
- [12] Herbsleb, G. and Ternes, H., *Werkstoffe und Korrosion*, Vol. 20, 1969, S. 379.
- [13] Herbsleb, G. and Schwenk, W., *Werkstoffe und Korrosion*, Vol. 21, 1970, S. 1.
- [14] Herbsleb, G., *Werkstoffe und Korrosion*, Vol. 24, 1973, S. 867.

Comparative Findings Using the Slow Strain-Rate, Constant Flow Stress, and U-Bend Stress Corrosion Cracking Techniques

REFERENCE: Daniels, W. J., "Comparative Findings Using the Slow Strain-Rate, Constant Flow Stress, and U-Bend Stress Corrosion Cracking Techniques," *Stress Corrosion Cracking—The Slow Strain-Rate Technique*, ASTM STP 665, G. M. Ugiansky and J. H. Payer, Eds., American Society for Testing and Materials, 1979, pp. 347-361.

ABSTRACT: The testing of materials for stress corrosion cracking (SCC) in a use environment involves the risk that cracking may not be found by the test technique. When this happens, immunity to SCC may be incorrectly concluded. To avoid this type of error, the use of multiple testing techniques is recommended.

This report discusses the different findings for Type 304 stainless steel obtained by three SCC testing techniques: the slow strain-rate technique (SSRT), the constant flow stress (CFS) test, and the U-bend test. The comparative studies in 36.5 percent magnesium chloride solution show that the cracking mode has an electrochemical potential dependency. In sodium chloride solutions, in the range of 1 to 20 percent concentration, the studies show that the cracking has a critical strain-rate dependency.

KEY WORDS: strain rate, constant flow stress, U-bend, stainless steels, chloride stress cracking, stress corrosion cracking, evaluation

From a materials technology viewpoint, our desired test result was to find a method that would allow reliable assessment of the hazard of stress corrosion cracking (SCC) of a metal or alloy in a process environment. In the business sense, this result would mean that in the future more economical materials might be used with confidence that SCC failure will not occur.

The assessment of SCC risk, reliably and with confidence, is a common goal, and numerous test methods are used to achieve it. These include the U-bend specimen and test panel specimens containing residual stresses from dimpling and welding operations [1].² A newer method involves the

¹Principal engineering specialist, Monsanto Company, St. Louis, Mo. 63166; Mr. Daniels is presently senior research engineer, Shell Development Company, Houston, Tex. 77001.

²The italic numbers in brackets refer to the list of references appended to this paper.

slow, dynamic straining of tension specimens in the use environment [2]. However, each method introduces an unknown amount of uncertainty into the test results. Our investigation was directed at learning how to use the dynamic test method and other techniques as diagnostic tools. From comparative findings, we hoped to define areas of uncertainty for selected SCC test techniques. With this information, we proposed to lower the risk of overlooking SCC in testing by having used appropriate test techniques.

The SCC tests deal with two kinds of uncertainty. The first involves the metal-chemical environment. To be valid, the tests have to examine the probable metallurgical conditions and the chemical composition excursions that exist in the use environment. This uncertainty clearly concerns fabrication and process details. The second uncertainty concerns the testing technique itself. For example, the method of stressing and the length of testing time may affect the test result. Because of this latter uncertainty, the following basis was suggested for SCC-*no* SCC decisions.

The decision that a material can be used with confidence that SCC failure will not occur should be based upon either one of two experimental findings.

1. The material cracks, but with safe allowable changes in the use-environment, it does not crack. For example, the changes may be to: remove chlorides, add or remove oxidizing agents, or use anodic or cathodic protection.

2. The material does not crack in testing. Since a question exists whether the testing technique was appropriate and adequate, the criteria for *no* SCC in this case will be the agreement of multiple testing techniques.

Following the theme of this symposium, the results of our experience with the slow strain-rate technique (SSRT) will be detailed. Other techniques included in our study were: the constant flow stress (CFS) test [3,4] and the U-bend test.

Scope of Testing

To narrow the scope of our work, testing was limited to aqueous solutions at atmospheric pressure.

The factors chosen for the study of the test techniques were based upon the general understanding of the SCC mechanism. This mechanism involves the interaction of: (a) a susceptible metal or alloy to SCC, (b) a tensile stress, and (c) a SCC-inducing environment. Since the study was to compare test techniques, only the SCC-inducing environment factors were considered. The chosen factors were: (a) the electrochemical potential of the metal, (b) the composition and concentration of the chemical environment, and (c) the temperature of the test system. During the study, the test strain rate was shown to be an important factor and was given major attention in our study.

For rapid comparisons among techniques, alloy-chemical systems known to undergo SCC were tested. Based upon this reasoning, Type 304 stainless

steel was chosen for study in 36.5 percent magnesium chloride (MgCl_2) and in decreasing concentrations (from 20 to 1 percent) of sodium chloride (NaCl).

This paper summarizes our findings about the SCC of Type 304 stainless steel in these two chemical environments. The findings include a comparison of the alloy fracture modes produced by the various testing techniques.

Experimental Procedures

Materials

The Type 304 stainless steel used in this experimental program was tested in the as-received condition. Tables 1 and 2 list the heat numbers, certified analyses, and mechanical properties of heat tested. The 0.64 cm ($\frac{1}{4}$ in.) diameter bar stock was used for the SSRT specimens. The 0.09-cm (20-gage) and 0.30-cm (11-gage) sheet material were used for the CFS and U-bend specimens, respectively.

Specimens

Figure 1 shows the dimensions of the slow strain-rate tension specimens. These specimens have a machined gage section, 0.318 cm (0.125 in.) diameter by 1.27 cm (0.50 in.) length, and machined 2.54-cm (1.0-in.) radius shoulders to the rod stock diameter. In use, the 0.635 cm ($\frac{1}{4}$ in.) diameter stock was covered with a heat-shrinkable modified fluoroethylenepropylene resin tubing. This left only the machined portion or 3.67 cm² (0.57 in.²) exposed to the chemical environment.

The CFS specimen dimensions were 4.5 by 0.5 by 0.1 cm ($1\frac{3}{4}$ by $\frac{3}{16}$ by 0.04 in.). This specimen, its spring-loaded test fixture, and the test cell were patterned after the description given by Uhlig and co-workers [3,4]. The U-bend specimens were formed from 10 by 0.63 by 0.31 cm (4 by $\frac{1}{4}$ by $\frac{1}{8}$ in.) sheet material. These specimens were held in the plastically deformed condition during testing by a threaded Type 304 stainless steel rod and nut assembly.

Equipment

The slow strain rate test unit used in this study is similar to the unit used by Asphahani.³ However, our motor speed reduction-drive mechanism operated at crosshead speeds ranging from 9×10^{-8} to 9×10^{-11} m/s (3×10^{-6} to 3×10^{-9} in./s).

All tests were performed in glass equipment, and all test solutions were

³ See p. 277.

TABLE 1—Chemical analysis of Type 304 stainless steel tested.

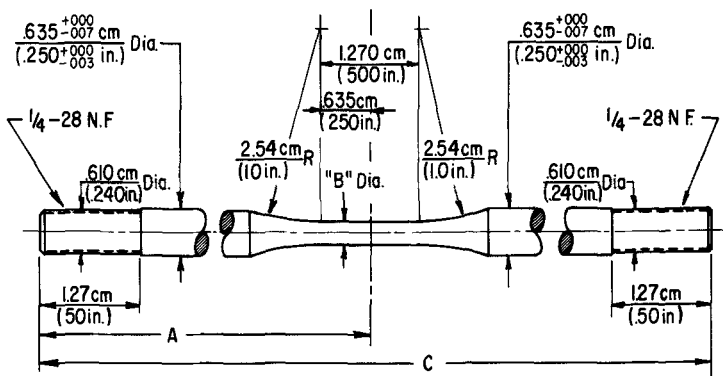
Heat Number	Form	Composition, %										
		C	Mn	P	S	Si	Ni	Cr	Mo	Cu		
x15311	0.64-cm dia bar	0.070	1.49	0.028	0.030	0.64	9.07	18.70	0.31	0.28		
G-8850	0.64-cm dia bar	0.061	1.52	0.017	0.024	0.62	8.32	18.65	0.34	0.10		
240397	0.09-cm (20-gage) sheet	0.055	1.46	0.023	0.013	0.70	8.79	18.63	0.17	0.22		
47780	0.30-cm (11-gage) sheet	0.067	1.66	0.021	0.016	0.47	8.68	18.64	0.17	0.14		

Conversion factor—1 cm = 0.39 in.

TABLE 2—Mechanical properties of Type 304 stainless steel tested.

	Heat Number			
	x15311	G-8850	240397	47780
Yield strength, MPa	586.0	449.0	273.0	317.0
Tensile strength, MPa	756.0	697.0	648.0	614.0
Percent elongation in 50.8 mm (2 in.)	41.0	41.0	55.0	57.5
Percent reduction in area	66.4	74.1
Rockwell B Hardness	96	95/97	82	84

Conversion factor—1 MPa = 145 psi.



Dash No.	A	Dia. "B"	C
- 1	10.80cm (4.25in.)	318cm (1.25in.)	22.86cm (9.00in.)

FIG. 1—Dimensions for SSRT specimen.

prepared from single distilled water and reagent grade chemicals. A heating mantle and mercury thermometer-temperature controller were used to keep the solution temperature within $\pm 2^\circ\text{C}$ (4°F) of the desired value. The SSRT and U-bend test cells had an adjustable luggin probe, and the CFS test cell had only a salt bridge. All cells had two platinum foil-counter electrodes having a total surface area of 6.3 cm^2 (0.98 in.^2). These latter provisions allowed the open-circuit or freely corroding potential (FCP) to be monitored and potentiostatically controlled potentials to be applied. All potentials were measured with respect to a saturated calomel electrode (SCE) reference located outside of the test cell at room temperature. The potentials in this

paper are reported with respect to the standard hydrogen electrode (SHE). The SCE is taken as 0.242 V more noble than the SHE.

Acquired Data, Reporting Methods, and Testing Procedures

In reporting results from SCC tests, three general types of data are involved: (a) the mechanical record, (b) the electrochemical record, and (c) the metallographic/fractographic record.

Mechanical Record

The mechanical record for the SSRT can take a number of forms. Our SSRT unit was instrumented to record on-line the tensile load versus crosshead displacement on an X-Y recorder. Load and displacement were measured in U.S. customary units, pounds and inches. Since this record is acquired with time, two important characteristics can be reported about a test: (a) the time to failure (tff), and (b) the crosshead displacement rate.

Frequently a test is terminated before ultimate failure by SCC or other mechanisms. Tests using the slowest strain rate were terminated prior to rupture when visual inspection and falling load suggested lengthy times to failure. These tests were conducted for times sufficient to develop specimen damage for a subsequent metallographic examination. In these cases, only test duration is reported.

Before cracking occurs, the crosshead displacement rate approaches the specimen strain rate. During cracking, the specimen stretches mainly at the crack(s); this is called yawning. Because of the localized nature of yawning, the specimen strain rate becomes indeterminate. As a consequence, the crosshead displacement rate relates only the experimental condition at yawning. For these reasons and the fact that strain rate depends upon the specimen gage length, the crosshead displacement rates (speed) reported are apparent specimen strain rates.

Of the remaining kinds of mechanical information, the most useful in our studies was the maximum load attained by the tension specimen during testing. In chemical environments, the maximum load divided by the original cross-sectional area of the specimen is not expected to give the ultimate tensile strength for the material. Among the several reasons for this are: corrosion, SCC, and embrittlement. Other diagnostic methods can determine which mechanism is operating.

The CFS and U-bend methods simplified the instrumental and mechanical equipment needs. In doing so, much of the mechanical test feedback was sacrificed. Only visual examination and cumulative testing time were monitored for these two tests.

Electrochemical Record

All three SCC test techniques acquired the same electrochemical information. Either the FCP or the applied current necessary to maintain a controlled potential was followed with time. At cracking, substantial electrochemical changes are seen sometimes. More often, changes in the applied current were a more sensitive indicator about events occurring on the specimen than the FCP record.

Metallographic/Fractographic Record

The purpose of the SSRT, the CFS, and U-bend tests was to find the conditions that cause cracking. Once found, it is also necessary to identify the cracking mode. To do this, either of two techniques can be used: metallographic or fractographic. When possible, both techniques were used.

Testing Procedures

In formulating the testing procedure, it was decided that all techniques test the specimens in the plastically deformed condition. This meant that the highest possible stresses, dictated by the yield strength for the material, would be imposed upon the specimen. Since materials are not designed for use at these stresses and because cracking does occur at lower stresses, this procedure was looked upon as an accelerating SCC test feature.

In practice, this meant manually stressing the SSRT tension specimen to about 75 percent of the material's yield strength in the empty test cell at room temperature. Hot solution was added then to the cell and heated to the test temperature. Dependent on the testing temperature, the thermal expansion relaxed the specimen prestress to about half the initial value. If a controlled potential was required for the test, it was established during this portion of the test start-up. At a stable temperature and stress, the specimen was then strained at the maximum crosshead speed of our unit. For slower crosshead speed tests, the maximum speed was reduced to the desired value at a stress of about 125 percent of the material's yield strength. This ensured testing in the plastically deformed condition at the slower crosshead speeds. Where elastic stresses were found to cause SCC, the specimen prestress was reduced to less than 25 percent of the material's yield strength.

The test procedure described is not that typically used by other investigators. The described procedure does introduce specimen prestress, relaxation, and anelastic recovery processes during the test. However, this procedure was found to be useful in scanning test conditions for a strain rate dependency for SCC.

Results

36.5 Percent Magnesium Chloride ($MgCl_2$) Solutions at 130°C (266°F)

The SCC studies of austenitic stainless steels date back to 1940 [5]. However, as evidenced by the literature of the 1970s, some SCC findings are controversial. For example, an intergranular (IG) cracking mechanism is reported for austenitic stainless steels in hot 36.5 percent $MgCl_2$ solutions where a transgranular (TG) cracking mechanism is expected [6-8].

Our results with 36.5 percent $MgCl_2$ solutions and as-received Type 304 stainless steel, at temperatures within 1 to 2°C (2 to 4°F) of the 130°C (266°F) boiling point, show that: (a) both intergranular and transgranular cracking modes occur, and (b) the cracking mode is electrochemical potential-dependent. Table 3 summarizes these results. At controlled potentials, depending on the test technique, more noble than the FCP, a transgranular cracking mode is found. Figure 2 shows a scanning electron microscope (SEM) photomicrograph for a SSRT specimen which typifies this fracture mode.

TABLE 3—Failure modes for Type 304 stainless steel in 36.5 percent $MgCl_2$ solutions at 130°C (226°F).

Potential, V SHE	SSRT Crosshead Speed, m/s		CFS	U-Bend
	10^{-7}	10^{-8}		
-0.058	TG, 2 h	TG, 2 h	TG, 1 h	...
-0.108	TG:IG, 3 h	TG:IG:TZ, 16 h	TG, 1 h	TG, 4 h
-0.133	TG:IG, 9 h	...
Freely corroding -0.136	IG:TZ, 22 h	IG, 22 h	TG:IG:TZ, 127 h	TG:IG:TZ, 48 h
-0.143	NF:100 h NF:137 h NF:199 h	...
-0.148	IG, 2 h	...	NF:10 h	TG:IG, 118 h
-0.158	ductile with IG, 21 h	IG, 42 h	...	TG:IG, 167 h

NOTE—

SHE = standard hydrogen electrode,

TG = transgranular cracking observed,

IG = intergranular cracking observed,

TZ = transition zone observed, transgranular cracking, at start of crack, then intergranular cracking,

NF = no (apparent) failure, and

h = total test time in hours.

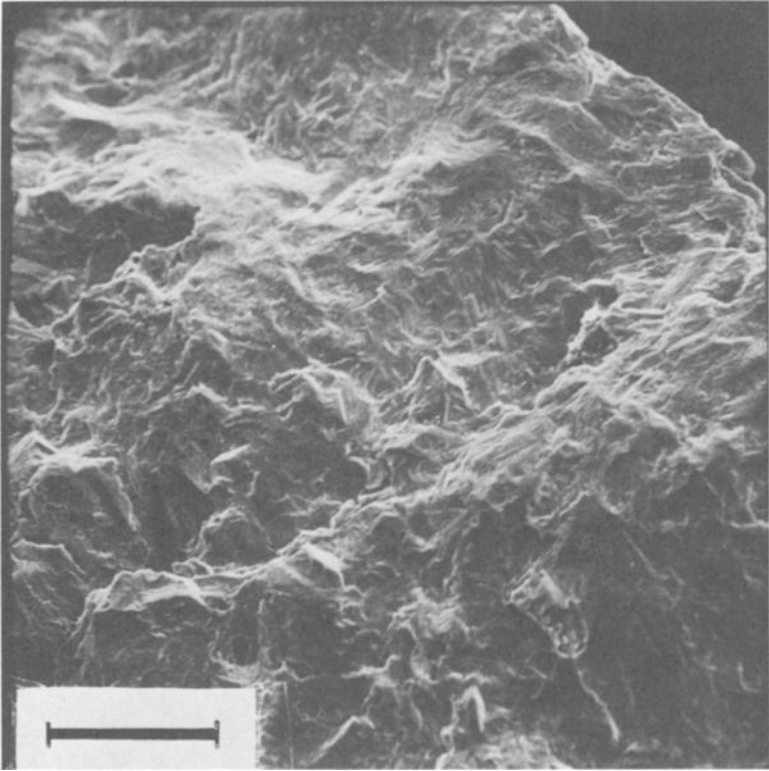


FIG. 2—SEM photomicrograph ($\sim \times 200$) of fracture surface of Type 304 stainless steel SSRT specimen showing TG cracking. Specimen was potentiostatically controlled at -0.058 V SHE in 36.5 percent $MgCl_2$ solution at $130^\circ C$ ($266^\circ F$), and strained at 2×10^{-10} m/s (9×10^{-9} in./s). Test period was ~ 2 h. (Scale mark indicates $100 \mu m$).

At the FCP (-0.135 ± 0.005 V SHE) the SSRT specimens tended to show predominately an intergranular cracking mode, whereas the bent strip specimens showed a mix of transgranular and intergranular cracking modes.

At controlled potentials more active than the FCP, different results were found for the three test techniques. The SSRT specimens showed intergranular cracking (Fig. 3) at crosshead speeds slow enough to minimize ductile fracture. No cracking was found, however, with the CFS specimens at cathodic potentials in the nominal 100-h test duration times. This finding is consistent with the results obtained by Uhlig and Newberg [4]. The U-bend specimens continued to show the mixed transgranular and intergranular cracking modes found at the FCP for this test technique.

Another aspect about the cracking of this system is illustrated in Fig. 4. This figure shows the maximum stress level attained in the SSRT test as a function of the controlled potential and crosshead speed. At -0.058 V SHE

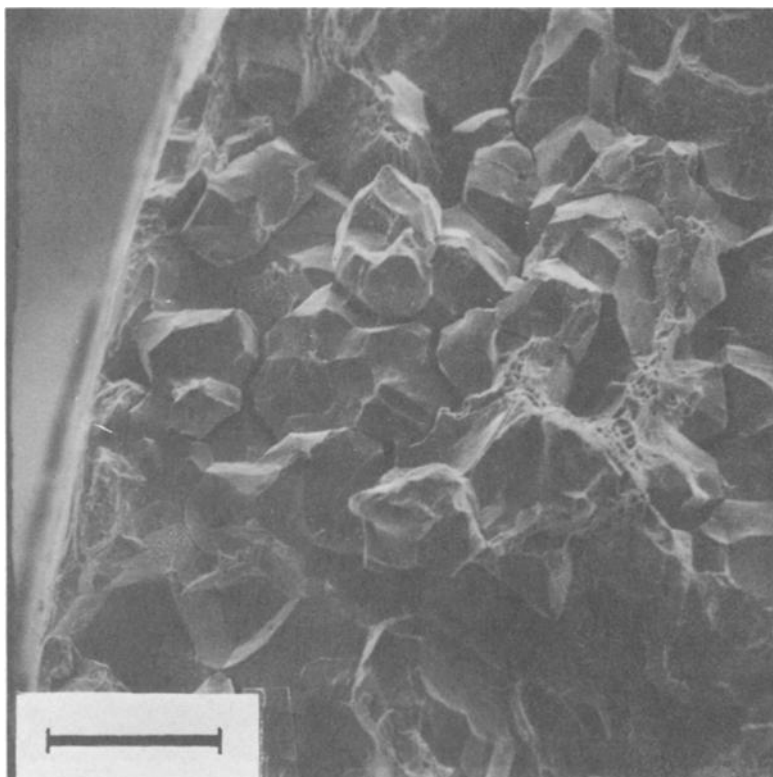


FIG. 3—SEM photomicrograph ($\sim \times 200$) fracture surface of Type 304 stainless steel SSRT specimen showing IG cracking. Specimen was potentiostatically controlled at -0.158 V SHE in 36.5 percent $MgCl_2$ solution at $130^\circ C$ ($266^\circ F$), and strained at 5×10^{-9} m/s (2×10^{-7} in./s). Test period was ~ 30 h. (Scale mark indicates $100 \mu m$).

(transgranular cracking mode), the maximum stress was found within the elastic region of the material's stress-strain behavior; at cathodically controlled potentials (intergranular cracking mode), the maximum stresses exceeded the yield strength for the material. In the vicinity of the FCP (mixed transgranular:intergranular cracking mode), intermediate values of the maximum stresses were found. These test results, within the diagonal band of Fig. 4, tended to be less repeatable. Table 3 and Figure 4 show that SSRT crosshead speeds of 9×10^{-8} m/s (3×10^{-6} in./s) cause cracking.

All three test techniques were monitored electrochemically. In controlled potential tests, where small current densities maintained the unbroken surface potential, crack initiation and propagation sometimes were accompanied by significant changes in the applied current. These changes started at loads slightly before the maximum load in the SSRT test. Similar current displays occurred with the CFS test, but these cannot be correlated to a

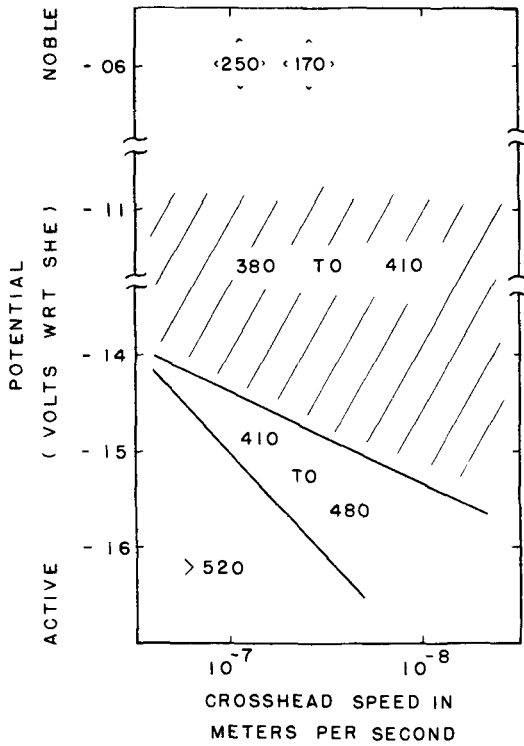


FIG. 4—Maximum stress in megapascals (MPa) for Type 304 stainless steel SSRT specimens in 36.5 percent $MgCl_2$ at $130^\circ C$ ($226^\circ F$) as a function of the potentiostatically controlled test potential and crosshead speed.

mechanical property. The U-bend test did not show this behavior because apparently cracks develop and propagate slowly.

Sodium Chloride (NaCl) Solutions, At $100^\circ C$ ($212^\circ F$)

In our test plan, dilute NaCl solutions were chosen as environments of low chemical aggressiveness. It was intended that seawater (3.5 percent) concentrations down to the parts per million range of NaCl be tested. But in the initial tests at 3.5 percent NaCl with the CFS method, cracking was not found. So, higher concentrations of NaCl solution were used in the tests. Our results with these solutions and as-received stainless steel, at $100 \pm 2^\circ C$ ($212 \pm 4^\circ F$), show that: (a) only the transgranular cracking mode is found, (b) decreasing crosshead speeds are required to find cracking with decreasing concentrations of NaCl, and (c) cracking is not found by the CFS technique in the 3.5 percent NaCl solution.

20 Percent NaCl Solutions—At controlled potentials, 10 to 20 mV more

noble than the FCP, the SSRT and CFS specimens exhibited both transgranular cracking and heavy pitting attack. Unlike the MgCl_2 test results, slower SSRT crosshead speeds of 1×10^{-9} m/s (4×10^{-8} in./s) were needed to find the transgranular cracking. These cracks were found at the ends of the gage length and in both smoothly increasing diameter shoulder sections.

All three SCC test techniques showed transgranular cracking at the FCP (-0.130 ± 0.005 V SHE) and less pitting attack. At cathodically controlled potentials, 10 to 20 mV more active than the FCP, the CFS specimens did not crack in the 100-h testing time. No SSRT test was run at cathodic potentials. The single U-bend test at -0.138 V SHE did find transgranular cracking.

10 Percent NaCl Solutions—These tests essentially repeated all but one of the findings for the 20 percent NaCl solution test work. The exception was that slower crosshead speeds of 9×10^{-11} m/s (3×10^{-9} in./s) were needed to find transgranular cracking at the FCP (-0.105 ± 0.005 V SHE). These cracks were localized at both shoulder regions of the specimen. The CFS specimens again showed transgranular cracking at the FCP and at -0.098 V SHE, but did not crack at controlled potentials 10 to 20 mV more active than the FCP for this system.

3.5 Percent NaCl Solutions—Although CFS specimens were tested at anodically controlled potentials in approximately 50-mV increments from the FCP (-0.083 ± 0.015 V) to $+0.142$ V SHE, where severe crevice corrosion and pitting occurred, cracking could not be found with this technique in the 100-h testing time. A single 1000-h CFS test at the FCP did not find cracking, nor did 100-h tests at controlled potentials 10 and 20 mV cathodic to the FCP.

Cracking was found, however, with the SSRT and U-bend tests. Transgranular cracks were found at the FCP and at an anodically controlled potential of -0.038 V SHE with the U-bend test. Controlled potential SSRT tests at -0.038 and -0.058 V SHE found cracking at crosshead speeds of 9×10^{-11} m/s (3×10^{-9} in./s), but did not at speeds ten times faster.

1 Percent NaCl Solutions—Our results with the SSRT in this solution show that a crosshead speed of 2×10^{-10} m/s (8×10^{-9} in./s) does find cracking at an anodic potential of 0.122 V SHE. This potential is approximately 20 mV more noble than the FCP. Figure 5 shows the location of these at the shoulder regions of this tension specimen. The fractographs of the fracture surface were not clear evidence for the fracture mode. General and localized corrosion distorted the fracture surface. However, intergranular attack is not suspected.

Discussion

The findings show that the three test techniques do not give identical results. An important criterion in comparing the techniques is whether the same failure mode results for specific conditions, exclusive of the ductile

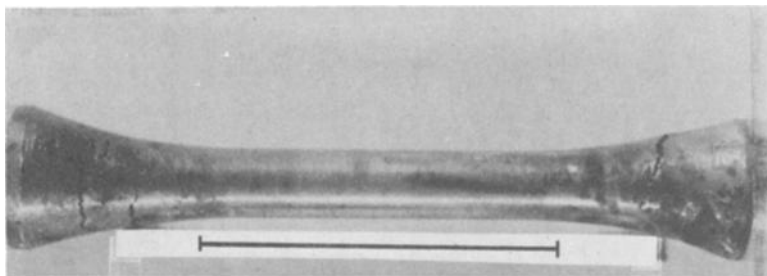


FIG. 5—Photomicrograph of Type 304 stainless steel SSRT specimen after 144 h exposure in 1 percent NaCl solution at 100°C (212°F). Specimen was potentiostatically controlled at 0.122 V SHE and strained at 2×10^{-10} m/s (9×10^{-9} in./s). (Scale mark indicates 1.3 cm).

failure mode possible with the SSRT. The findings for Type 304 stainless steel in the MgCl_2 and NaCl solutions show that whether or not failure occurs and its mode depend upon the test method.

In 36.5 percent MgCl_2 solutions at 130°C (266°F), all three testing techniques produce transgranular cracking at potentials more noble than the FCP. At the FCP, the SSRT produces predominately intergranular cracking; the CFS and U-bend techniques produce mixed transgranular and intergranular cracking.

At cathodic potentials for this alloy-chemical solution, the test results differed from one another. When the crosshead speed was slow enough to avoid ductile fracture, the SSRT specimens cracked by an intergranular mode. The bent specimen techniques, on the other hand, found cracking immunity with the CFS test and mixed transgranular and intergranular cracking modes with the U-bend test.

Additionally, the SSRT shows that macroelastic stresses are sufficient to produce transgranular cracking in this alloy-chemical system. With increasing amounts of intergranular cracking mode on the fracture surface, increasingly higher plastic flow stresses are needed to crack the alloy. All three techniques show that the cracking mode has an electrochemical potential dependency. The intergranular cracking, cracking immunity, and mixed mode cracking found for the three techniques at cathodic potentials show that while the electrochemical potential is an essential parameter, it alone does not control the cracking behavior of this system at these potentials. Figure 4 suggests, by the sloping band of intermediate (and less repeatable) values of the maximum stress, that the SSRT transition zone from transgranular to intergranular cracking has a strain-rate dependency.

Except for the SSRT finding at cathodic potentials, where a slower crosshead speed was needed to avoid ductile fracture and find intergranular cracking, this technique easily produced cracks at 9×10^{-8} m/s (3×10^{-6}

in./s). Last, the same total test time for SSRT tests at 9×10^{-8} and 1×10^{-8} m/s, at -0.058 V SHE, reported in Table 3 suggests that at this potential, crack growth velocity is more dependent on the electrochemical potential than on the crosshead speed.

Unlike the MgCl_2 studies, where cracking is easily found by the three techniques at most of the tested potentials, only the SSRT and U-bend tests found cracking in the more dilute tested NaCl solution studies.

The SSRT results suggest an explanation for this finding. These studies show that slow crosshead speeds (apparent strain rates) are required to crack Type 304 stainless steel in NaCl solutions. Further, slower crosshead speeds are needed to crack the alloy in lower concentrations of NaCl solution. This fact is substantiated by the measured crosshead speeds and by the location of the cracks on the tension specimens. In a 1 percent NaCl solution, the cracks occur well within the shoulders (Fig. 5) of the tension specimen, where the slowest strain rates occur for a dynamically straining specimen.

These studies suggest the following explanation for the 3.5 percent NaCl solution test technique results. If the creep rate for the thin, spring-loaded CFS specimen exceeds the critical slow strain rate for this alloy-chemical solution, cracking should not be found. On the other hand, cracks are found on the U-bend specimens because the creep rate for the thicker, plastically constrained specimen satisfies the critical slow strain rate for the alloy-chemical system.

Having demonstrated that strain rate can be a critical factor, it is recommended that SCC test programs use the SSRT to take advantage of the mechanical versatility of this method. Where the slowest strain rates are concerned, a statistically designed population of U-bend tests may be useful [9].

Last, SCC behavior has an electrochemical potential dependency. Consequently, experiments that couple the electrochemical and mechanical test techniques are more useful diagnostically.

Conclusions

1. The three studied techniques often give different results. Therefore, in order to predict SCC performance with confidence, one must use more than one test technique.

2. The findings for Type 304 stainless steel in 36.5 percent MgCl_2 solution at 130°C (266°F) show that: (a) the fracture mode of the alloy changes from transgranular (TG) to intergranular (IG) cracking with changes in the potentiostatically controlled potential, and (b) at cathodically controlled potentials, the SCC test result depended on the test technique used. The SSRT and U-bend tests found intergranular and mixed transgranular:intergranular cracking, respectively. No cracks were found with the CFS test.

3. The findings for Type 304 stainless steel in 1 to 20 percent solutions of NaCl at 100°C (212°F) show that: (a) decreasing strain rates are needed to

crack the alloy in decreasing concentrations of NaCl solution, and (b) cracks were found at all tested potentials using the SSRT and U-bend tests. Cracks were not found at cathodic potentials using the CFS test in 10 to 20 percent NaCl solutions, nor at any tested potential in the 3.5 percent NaCl solution.

Acknowledgments

The writer wishes to acknowledge the special contributions of H. J. Larigan, W. D. Dillon, E. W. Pittenger, and E. L. Seiler who designed and built our slow strain-rate and constant flow stress test units.

The writer also acknowledges the special contributions of J. D. Fairing and J. J. Ruprecht who performed the scanning electron microscopy work required for the fractographic analyses.

References

- [1] Craig, H. L., Sprowls, D. O., and Piper, D. E. in *Handbook on Corrosion Testing and Evaluation*, W. H. Ailor, Ed., Wiley, New York, 1971, Chapter 10, pp. 231-290.
- [2] Parkins, R. N. in *The Theory of Stress Corrosion Cracking in Alloys*, J. C. Scully, Ed., North Atlantic Treaty Organization, Brussels, 1971, pp. 449-468.
- [3] Lee, H. H. and Uhlig, H. H., *Journal of the Electrochemical Society*, Vol. 117, No. 1, Jan. 1970, pp. 18-22.
- [4] Newberg, R. T. and Uhlig, H. H., *Journal of the Electrochemical Society*, Vol. 120, No. 12, Dec. 1973, pp. 1629-1632.
- [5] Hodge, J. C. and Miller, J. L., *Transactions*, American Society for Metals, Vol. 28, 1940, pp. 25-82.
- [6] Takano, M., *Proceedings*, Fifth International Congress on Metallic Corrosion, National Association of Corrosion Engineers, Houston, 1974, pp. 355-359.
- [7] Ito, N. and Yoshino, M., *Proceedings*, Fifth International Congress on Metallic Corrosion, National Association of Corrosion Engineers, Houston, 1974, pp. 401-405.
- [8] Okada, H., Hosoi, Y., and Abe, S., *Proceedings*, Fifth International Congress on Metallic Corrosion, National Association of Corrosion Engineers, Houston, 1974, pp. 507-512.
- [9] Scharfstein, L. R. and Brindley, W. F., *Corrosion*, Vol. 14, No. 12, Dec. 1958, pp. 60-64.

J. F. Andrew,¹ J. T. Heron,¹ and J. Stringer¹

Some Comparisons of the Slow Strain-Rate Method with the Constant Strain and the Constant Load Methods of Stress Corrosion Testing*

REFERENCE: Andrew, J. F., Heron, J. T., and Stringer, J., "Some Comparisons of the Slow Strain-Rate Method with the Constant Strain and the Constant Load Methods of Stress Corrosion Testing," *Stress Corrosion Cracking—The Slow Strain-Rate Technique*, ASTM STP 665, G. M. Ugiansky and J. H. Payer, Eds., American Society for Testing and Materials, 1979, pp. 362-372.

ABSTRACT: Two practical stress corrosion investigations are outlined in which the results of slow strain-rate tests are compared with the results of other test methods. The possibility of formulating a specification to cover the slow strain-rate stress corrosion test method is considered.

KEY WORDS: stress corrosion cracking, strain rate, experimental data

The authors are concerned with the long term preservation of certain types of land service equipment and are necessarily involved with many facets of corrosion and protection of metals. The varied nature of the work coupled with time factors imposed by design and production authorities does not always allow for investigations to be carried out in depth; however, it does stimulate interest in rapid methods of assessment.

In the stress corrosion field, the authors' past approach has been to carry out constant strain or constant load tests on components or specimens with emphasis on the environments to which components will be exposed in practical situations. The drawbacks to these methods, for example, the duration and number of tests required to obtain reliable data, are well

*Copyright © Controller, Her Majesty's Stationary Office, London, England, 1977.

¹Principal scientific officer, senior scientific officer, and senior scientific officer, respectively, Royal Armament Research and Development Establishment, Kent, England.

known; and more recently, alternative more rapid test procedures, in particular the slow strain-rate method, have received attention.

The purpose of the present paper is to outline two independent investigations in which the slow strain-rate and either the constant strain or constant load stress corrosion test methods were used, thus enabling the results of different test methods to be compared.

Investigation 1

History

A 12Cr precipitation hardening stainless steel Kromar D70² (Table 1) in the form of strip, 0.75 mm thick, was selected for the large scale manufacture of a component with complex geometry. Parts of the component are stressed by bending at the assembly stage and remain in this state throughout the storage life of the component. The calculated maximum tensile stress in these parts of the component is 835 MPa and is parallel to the rolling direction of the strip.

It was envisaged at the developmental stage of the component that stress corrosion problems might arise and initially constant strain tests were carried out in a range of environments including those which could be met in service situations to assess this possibility. Slow strain-rate tests were carried out at a later stage.

Specimens

Stress corrosion and tension specimens were prepared from Kromar D70 bright annealed rolled strip with their long axes either parallel or normal to the rolling direction. Sets of specimens were heat treated for 3 h in a circulating air furnace at temperatures in the range 375 to 525 °C giving a range of tensile properties (0.1 percent proof stress, 1220 to 1790 MPa) (see Table 2).

Constant Strain Tests

Stress corrosion specimens were mounted in suitably protected test rigs designed to reproduce the exact stress levels experienced by stressed parts of the component after assembly. Sets of stressed specimens were exposed to each of the ranges of environment under consideration and were visually examined with a low power microscope ($\times 10$) for cracking at set time intervals up to 182 days from the time of exposure. The examination showed

²Supplied by British Steel Corporation. The material is not available in any other thicknesses or sections.

TABLE 1—Nominal composition of Kromar D70.

Element	%	
C	0	to 0.03
Mn	0	to 0.1
P	0	to 0.02
S	0	to 0.02
Cr	11.0	to 13.0
Ni	3.8	to 5.0
Mo	3.8	to 5.0
Co	11.0	to 13.0
Ti	0.2	to 0.4
Al	0.05	to 0.15
Si	0	to 0.2
Nb	0.100	} added
B	0.004	
Zr	0.020	

TABLE 2—Slow strain-rate test results on Kromar D70 strip, (crosshead speed 0.075 mm/h, temperature 80°C).

Aging Temperature, °C	Specimen Axis versus Rolling Direction, P = parallel, and N = normal	0.1% Proof Stress, MPa	Time to Failure, 3% NaCl	
			Time to Failure, Air	Time to Failure, Air, h
375	P	1225	1.02	37.7, 37.7
	P		1.03	
	N	1220	0.95	35.2, 35.3
N	0.96			
400	P	1320	0.98	43.6, 41.4
	P		1.00	
	N	1325	0.91	42.4, 37.7
N	0.95			
425	P	1440	0.40	47.2, 46.5
	P		0.42	
	N	1450	0.47	43.0, 42.6
N	0.48			
475	P	1610	0.44	37.6
	P		0.47	
	N	1630	0.37	36.6, 36.6
N	0.44			
525	P	1740	0.32	47.1
	P		0.33	
	N	1790	0.24	45.7
N	0.22			

that stress corrosion cracking, normal to the tensile stress in the outer fiber occurred only under salt droplet test conditions British Standard Performance Tests for Protective Schemes (BS 1391:1952) at elevated temperature, namely 60°C, and when the 0.1 percent proof stress of the material exceeded approximately 1400 MPa. This set of results are shown

in Fig. 1 in which average times to failure (3 results) are plotted against 0.1 percent proof stress.

Slow Strain-Rate Tests

The test equipment was designed and built by the Department of Metallurgy and Engineering Materials, University of Newcastle-upon-Tyne; aspects of test procedure have been described³ and are generally well known. Exploratory tests were carried out on the effects of crosshead speed and test temperature using specimens in a condition which on the basis of constant strain test results was known to be particularly susceptible to stress corrosion cracking in a warm chloride containing environment. A comparison of times to failure in 3 percent sodium chloride (NaCl) and in air at the same temperature (Table 3) suggested that a good indication of stress corrosion susceptibility could be obtained with a crosshead speed of 0.075 mm/h and a test temperature in the range 60 to 100°C.

The main part of the work was concerned with slow strain-rate tests in 3 percent NaCl and air at 80°C and at a crosshead speed 0.075 mm/h using specimens heat treated to produce a range of metallurgical conditions. These results (Table 2) were consistent with those obtained in constant

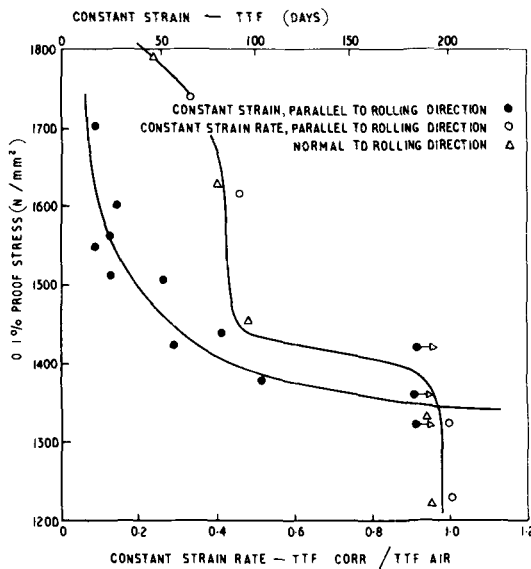


FIG. 1—Stress corrosion test results for Kromar D70 strip.

³Parkins, R. N., Mazza, F., Royuela, J. J., and Scully, J. C., *British Corrosion Journal*, Vol. 7, 1972, p. 154.

TABLE 3—Effects of crosshead speed and temperature on slow strain-rate test results for Kromar D70 strip (heat treated at 525 °C for 3 h).

Temperature, °C	Specimen Axis versus Rolling Direction, P = parallel, N = normal	Crosshead Speed, mm/h					
		2.5		0.075			
		Time to Failure, 3% NaCl Time to Failure, Air	Time to Failure, 3% NaCl Time to Failure, Air	Time to Failure, 3% NaCl Time to Failure, Air	Time to Failure, 3% NaCl Time to Failure, Air	Time to Failure, h	Time to Failure, h
60	P ^a	0.96	1.20, 1.33	0.35	47.2, 47.6		
	P	1.10		0.36			
	N ^b	1.06	1.11, 1.21	0.30	45.8, 46.6		
80	N	1.18		0.37			
	P	1.09	1.22	0.32	47.1		
	P	1.12		0.33			
100	N	1.11	1.19	0.24	45.7		
	N	1.14		0.22			
	P	1.06	1.14, 1.21	0.46	46.6, 46.9		
	P	1.23		0.50			
	N	1.07	1.22, 1.22	0.28	43.5, 44.9		

^a0.1% proof stress = 1740 MPa.

^b0.1% proof stress = 1790 MPa.

strain tests, see Fig. 1. The examination of fractured specimens showed that where evidence of stress corrosion was obtained, fractures were normal to the straining direction; in all other cases, fractures were of the shear type at approximately 45 deg to the straining direction. Detailed examination of the fractures by scanning electron microscope showed the shear type fractures had a dimpled structure typical of ductile failure; stress corrosion fractures were less readily examined owing to surface contamination with traces of corrosion product.

Investigation 2

History

Brass (70Cu, 30Zn) is an attractive constructional material, particularly in view of the degree of cold work it will withstand without fracture. It is well known that in the cold worked condition, this material is susceptible to season cracking, a phenomenon normally attributed to exposure to atmospheres containing traces of ammonia, unless a low temperature stress relieving heat treatment, for example 250°C for 1 h, is carried out.

In recent years, interest has been shown in brasses which can be readily cold worked and with greater strength in this condition than brass (70Cu-30Zn). Investigations have been carried out on the stress corrosion susceptibilities of these cold worked and heat treated materials in ammoniacal environments. One of these investigations covered a series of silicon brasses in which constant load and slow strain-rate test methods were used.

Specimens

Stress corrosion and tension specimens with their long axes normal to the rolling direction were prepared from 5 silicon brasses³ and brass (70Cu-30Zn) Defense Specification, Brass Strip for Cartridge Cases and for Caps (DEF 105), supplied in the form of strip 2.4 mm thick. The silicon brasses had been solution heat treated, water quenched, cold rolled, and finally low temperature heat treated; the brass (DEF 105) had been cold rolled to give a hardness of approximately 200 VHN and stress relieved at 250°C for 1 h. All specimens were cleaned by abrasion with wet pumice powder and washing with water and acetone. The results of mechanical tests on all the alloys and also their copper contents are given in Table 4.

Constant Load Tests

Stress corrosion specimens were stressed in tension at specific stress

⁴Detailed information on the compositions, mechanical treatments, and heat treatments of these alloys has been withheld owing to patent action.

TABLE 4—Mechanical properties^a and copper contents of silicon brasses 1 to 5 and brass (DEF 105).

Alloy	Tensile Properties, MPa				Copper Content, %
	0.2% Proof Stress	Tensile Strength	Elongation on 40 mm, %	VHN 20	
1	725	825	10	243	87.3
2	780	860	7	261	78.0
3	830	910	4	280	76.6
4	975	1100	2	295	76.2
5	835	935	10	268	86.1
Brass (DEF 105)	635	740	11	216	70.0

^aAverage of two determinations.

levels in constant load machines. The gage length of each specimen was exposed to a damp ammoniacal atmosphere at room temperature (approximately 20°C) and times to failure were recorded. The ammoniacal atmosphere was maintained by enclosing the gage length of each specimen with a 300-ml glass vessel containing 20-ml 1 *M* ammonium hydroxide (NH₄OH) in two small beakers; the ammonia solution was replaced with fresh solution each working day. It was calculated from published data⁵ that the ammonia concentration in the air space in the glass vessel was approximately 10-mg anhydrous ammonia (NH₃)/litre.

Most tests were carried out in triplicate, and the results obtained are shown in Fig. 2 in which applied stress is plotted against average time to failure. Both the silicon brasses and the brass (DEF 105) developed green-blue corrosion products and showed transgranular cracking.

Slow Strain-Rate Tests

The test procedure was related to that used in the previous investigation in that times to failure in test solutions and air were compared and considered in conjunction with the nature of the fractures obtained. The test solutions were prepared from a stock solution obtained by dissolving pure copper powder (average particle size 40 μm) in approximately 15 *M* NH₄OH. The stock solution was analyzed and the concentrations of copper and total ammonia in samples of this solution were adjusted by driving off ammonia by gentle heating followed by ammonia additions and dilution to give the required values, namely for solution 1—1 *M* NH₄OH containing 1-g copper/litre (pH = 11.9); for solution 2—4 *M* NH₄OH containing 4-g copper/litre (pH = 12.7). Both of these solutions produce black tarnish films on brass⁶ (DEF 105); filming of the silicon brasses was variable.

⁵Perman, E. P., *Journal of Corrosion Science*, Vol. 83, 1903, p. 1168.

⁶Pugh, E. N. in *The Theory of Stress Corrosion Cracking in Alloys*, J. C. Scully, Ed., North Atlantic Treaty Organization, Brussels, 1971, p. 418.

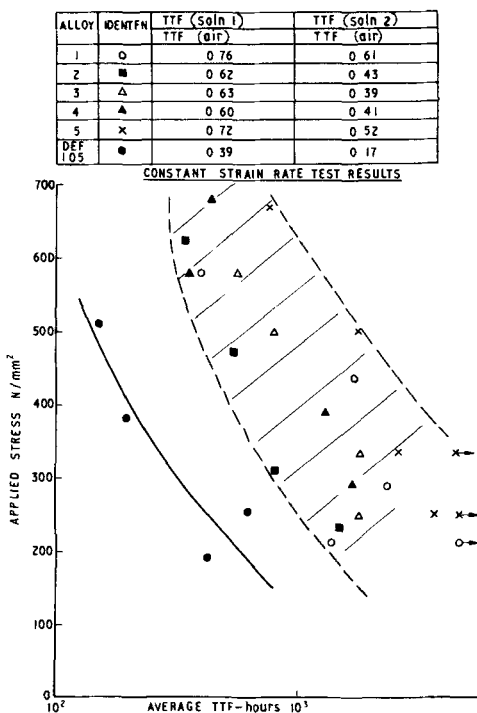


FIG. 2—Constant load and slow strain-rate test results for silicon brasses (alloys 1 to 5) and brass (DEF 105).

Preliminary experiments on the selection of a crosshead speed were carried out at $20 \pm 2^\circ\text{C}$ on brass (DEF 105) (see Table 5). A crosshead speed of 0.1 mm/h and test temperature $20 \pm 2^\circ\text{C}$ were used for the main part of the work and the results obtained (Table 6) are compared with those obtained in constant load tests in Fig. 2. Agreement between the two sets of results is good in that the silicon brasses were shown to be more resistant to stress corrosion cracking in certain ammoniacal environments than brass (DEF 105). The slow strain-rate results also suggest that there is a relation between the copper content of the alloys and their stress corrosion susceptibilities in the ammoniacal environments considered (see Fig. 3).

The fractures obtained in these tests showed a number of features. Thus those which occurred in the copper containing ammoniacal solutions were normal to the straining direction and showed a transgranular fracture mode. The failures of the alloys in air were related to their ductilities (Table 4); alloys 1, 2, 5, and brass (DEF 105) showed necking; alloys 3 and 4 showed a brittle type fracture with little reduction in cross-sectional area.

TABLE 5—Effect of crosshead speed on slow strain-rate test results for brass (DEF 105), temperature $20 \pm 2^\circ\text{C}$.

Crosshead Speed, mm/h			
1.0		0.1	
Time to Failure, Solution 2 ^a	Time to Failure, Air, h	Time to Failure, Solution 2 ^a	Time to Failure, Air, h
Time to Failure, Air		Time to Failure, Air	
0.34 0.34	3.42, 3.88	0.17	37.0

^a 4 M NH₄OH containing 4-g copper/litre.

TABLE 6—Slow strain-rate test results on silicon brasses (alloys 1 to 5) and brass DEF 105 (crosshead speed, 0.1 mm/h, temperature $20 \pm 2^\circ\text{C}$).

Alloy	Time to Failure Solution 1 ^a	Time to Failure Solution 2 ^b	Time to Failure, Air, h
	Time to Failure, Air	Time to Failure, Air	
1	0.80, 0.72	0.61, 0.60	33.42, 33.57
2	0.60, 0.63	0.42, 0.44	29.10, 31.13
3	0.59, 0.67	0.36, 0.41	29.00, 29.47
4	0.59, 0.61	0.41	25.33, 27.12
5	0.79, 0.64	0.51, 0.53	35.25, 35.90
Brass DEF 105	0.43, 0.35	0.17	37.0

^a 1 M NH₄OH containing 1-g copper/litre.

^b 4 M NH₄OH containing 4-g copper/litre.

Discussion

Two practical stress corrosion investigations have been outlined in which the results of slow strain-rate tests have been compared with the results of other stress corrosion test methods.

The first of these investigations was concerned with a 12Cr precipitation hardening stainless steel in strip form. Both slow strain-rate and constant strain test results led to similar conclusions concerning the strength of the material and its susceptibility to stress corrosion cracking in closely related hot aqueous chloride environments.

The second investigation was concerned with a comparison of the stress corrosion susceptibilities of a range of cold rolled and heat treated brasses in ammoniacal environments. Agreement between constant load and slow strain-rate test results was good in that the silicon brasses were shown to be less susceptible to stress corrosion cracking than brass (DEF 105).

The slow strain-rate test data also suggested that there was a relation

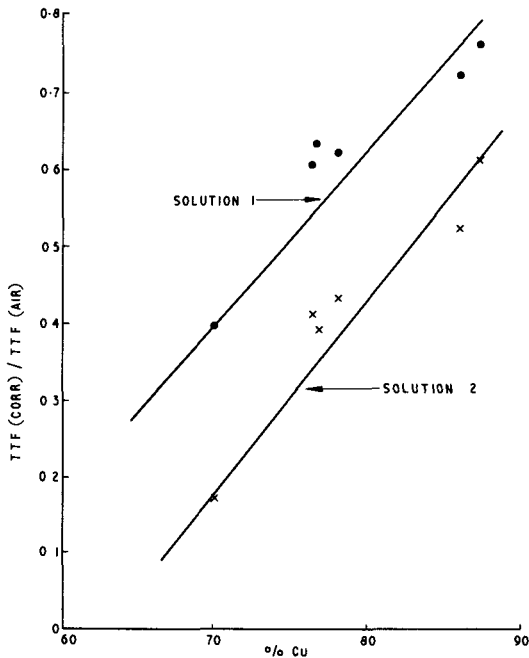


FIG. 3—Relationship between copper content of alloys and stress corrosion susceptibility in ammoniacal copper solutions.

between the copper content of the alloys and resistance to stress corrosion cracking (see Fig. 3) which was less obvious from constant load test results.

The relation between the environments used in the two types of test in the second investigation is not clear. However, it has been noted that the brasses exposed to a damp ammoniacal environment in constant load tests developed a green-blue corrosion product. On this basis, it is reasonable to assume that any condensed aqueous film on the metal surface will contain ammonia and have a high concentration of copper and be related to the tarnishing type of ammoniacal copper solutions⁵ used in the slow strain-rate tests.

A feature of the slow strain-rate tests described is that the work has been carried out using sheet or plate specimens with standard geometry and reference is made to the speed of the crosshead to which specimens are attached and not to rate of strain. This approach has been adopted both for simplicity of testing and also because in tests of this type, the precise strain rate is not readily obtainable. Thus the strain rate of the gage length of the specimen will be less than the maximum possible due to straining of the machine. Furthermore, since the machine is only subject

to elastic strain, the strain rate of the gage length of the specimen will increase with change from elastic to plastic strain.

Programs of work are being carried out on silicon brasses, precipitation hardening stainless steels, and high strength aluminium alloys using a similar approach to that described. As in the previous work, tests are being carried out at the free corrosion potentials and it is of interest to note that good agreement has been obtained between the results of slow strain rate and constant strain tests in 3 percent NaCl at 60°C for a high strength aluminium alloy supplied in two metallurgical conditions.

Finally, it is pertinent to consider whether slow strain-rate stress corrosion testing will become a standard test procedure in particular for sorting or quality assurance purposes. It is conceivable that as test data accumulate standard test procedures for a range of alloy systems can be agreed and published in the form of a stress corrosion specification. The formulation of such a document would require considerable collaborative effort involving standardization of test equipment and also specimen geometry, crosshead speeds, test environments, test temperatures, and methods of assessment. It would be an asset to organizations with an applied research background who are required to assist design, production, and quality assurance authorities on stress corrosion cracking problems.

Slow Strain-Rate Test Technique Equipment and Procedures

W. T. Nutter,¹ A. K. Agrawal,¹ and R. W. Staehle¹

Design and Construction of an Inexpensive Multispecimen Slow Strain-Rate Machine

REFERENCE: Nutter, W. T., Agrawal, A. K., and Staehle, R. W., "Design and Construction of an Inexpensive Multispecimen Slow Strain-Rate Machine," *Stress Corrosion Cracking—The Slow Strain-Rate Technique*, ASTM STP 665, G. M. Ugiansky and J. H. Payer, Eds., American Society for Testing and Materials, 1979, pp. 375-387.

ABSTRACT: The general considerations required in the design and construction of a slow strain-rate machine are discussed. A multispecimen machine built at the Ohio State University is illustrated, and the principal components used in this machine are listed. A four-specimen machine with a crosshead speed adjustable between 10^{-4} and 10^{-8} cm/s can be built for about \$5000.00.

KEY WORDS: slow strain rate, tensile machine, design, stress corrosion cracking

The slow strain-rate tensile machine has been recognized as a valuable tool in testing the susceptibility of metals to stress corrosion cracking (SCC) for more than ten years. Since its introduction in the early sixties, the slow strain-rate technique has received much attention and has increased in popularity to where it is now widely accepted as a viable method of experimentation. The fact that an American Society for Testing and Materials/National Association of Corrosion Engineers (ASTM/NACE) conference was held specifically to discuss this mode of testing attests to its importance.

This technique, in essence, requires a tension test machine of an adequate capacity and capable of providing a constant but extremely slow crosshead speed (10^{-4} to 10^{-7} cm/s), which is usually not found in ordinary commercial machines. The purpose of this paper is to share our experiences and acquaint the audience with the various components that are

¹Research associate, adjunct assistant professor, and professor, respectively, Department of Metallurgical Engineering, The Ohio State University, Columbus, Ohio 43210.

required in building such a machine to suit individual needs. The aim here has been to keep the machine simple and inexpensive while offering maximum versatility. Besides presenting the particulars of a machine, some generalities and constraints that are useful in the design are also outlined.

Machine Properties

Strain Rate

The optimum strain rate for testing the SCC susceptibility depends largely on the metal/environment system or the crack propagation rate (CPR). Usually, for a system in which the CPR is small, a low strain rate is required; and in cases where the CPR is high, a relatively fast strain rate is suitable. For example, the CPR in sensitized Type 304 stainless steel in pure water above 100°C is of the order of 10^{-9} m/s; a suitable strain rate for this system is in the range 10^{-6} to 10^{-7} s⁻¹. For admiralty brass in sulfate or nitrate solutions, the CPR is approximately 10^{-7} m/s for which a faster strain rate of 10^{-5} s⁻¹ is adequate. Since the metal/solution systems of interest in most laboratories is likely to change from time to time, it is imperative that a slow strain-rate machine be easily adaptable to the new systems without much effort. From our experience, the gage length of specimens is usually between 1 to 5 cm maximum; thus a machine with a crosshead speed adjustable in the range of 10^{-4} to 10^{-7} cm/s will be suitable for most metal/solution systems.

Capacity

The capacity of a machine is dictated by the ultimate tensile strength of the material to be tested and the specimen geometry. The ultimate strength of most materials, except the high strength alloys, is less than 7×10^8 Pa. If the gage cross section of the specimen is limited to 0.13 cm², the capacity of the machine should be at least 9000 N. The 0.13 cm² gage cross section corresponds to 0.4 cm gage diameter for a waisted round bar specimen, the type most commonly used, or to 1 cm gage width for a 0.13 cm thick hourglass-type strip specimen. A survey of literature has shown that most of the specimens used in SCC testing have dimensions smaller than those mentioned above. Therefore, it is reasonable to conclude that a machine with 9000 N capacity will be adequate in most cases. Limiting the capacity to 9000 N results also in a considerable cost saving, because it is one of the standard sizes in which many of the machine components, such as load cell and screw jack, etc., are available.

Space

The working space on a machine and the arrangement of the load frame are dependent on the size of the test cell which contains the test environment. The test environment is often an aqueous solution which may or may not be pressurized. The temperature of the solution could range from the room temperature to almost the critical point of water. However, a majority of the SCC tests are done in an unpressurized condition at or below the boiling point of the solution. The test cells in these cases are small, approximately 1 litre, and are made of either glass or tetrafluoroethylene. A high temperature, high pressure system requires an autoclave test cell.

The working space of about 30 by 30 by 30 cm will be sufficient, in most cases, for a nonpressurized cell and its accessories; but for a pressurized and refreshed cell the space requirement could be large, say, 50 by 50 by 60 cm for a furnace heated 4 litre autoclave. For a 1 litre size refreshed autoclave the space requirement on the machine is estimated to be 35 by 35 by 40 cm.

The specimen is invariably pulled from the top and against the autoclave head, via a jig, in the case of a pressurized system. With the glass or tetrafluoroethylene cells the specimen may be anchored at the top or bottom and pulled from the other end. However, pulling the specimen from its top offers an advantage; the drive train can be mounted on top of the machine frame and thus avoid damage to them from accidental solution spills from the cell.

Single or Multispecimen Machine

In order to describe completely the SCC susceptibility envelop (temperature, pH, and potential, etc.) of a metal/environment system, a rather large number of tests are required. The length of time required for conducting a SCC susceptibility test varies with the metal/environment system and the strain rate selected. A test with, say, admiralty brass in salt solutions at 10^{-5} s^{-1} is completed within two days, whereas one with high nickel alloys in high purity water at 10^{-7} s^{-1} may take as much as four to five weeks. An ordinary slow strain-rate machine has a limitation that only one specimen can be tested at a time. It is imperative that in order to cover a large test matrix, in a reasonable amount of time, one must work simultaneously with several machines. However, the cost of acquiring a number of machines may be prohibitive for many laboratories. In order to minimize the capital cost, the authors have built a multispecimen machine. This machine has the ability to strain four specimens simultaneously, and also has the same capabilities as a single specimen machine. The multispecimen

machine can be built for roughly half the cost of four single specimen devices.

Details of this machine and some general features of a single unit machine built in our laboratories is given in the following pages.

Major Components

A slow strain-rate tensile machine is a relatively simple device due to the fact that neither high speed, vibrations, acceleration, deacceleration, intermittent loading, or shocks are to be combated during its operation. The only function of the device is to apply a linear extension to the specimen at a predetermined rate. The principal components of a nonhydraulic machine are: (1) power drive, that is, electric motor; (2) speed reducers; (3) rotary to linear motion converter, that is, screw jack; (4) specimen alignment device, that is, universal joint; (5) load transducer; and (6) the machine frame. Some ancillary parts are timing belts and pulleys, or chains and sprockets, and a tachometer. The individual components are described in some detail in the following paragraphs; components are identified in Figs. 1 and 2.

One should refer to the appropriate trade literature of manufacturers for a complete detail of the functions and design parameters of the various components. It will be helpful also to consult any machine design handbook, such as *Kent's Mechanical Engineers Handbook*.

Power Drive

The principal power drive in a nonhydraulic machine of our interest is always a fractional horse power motor. The maximum power required in a machine will be at the highest load straining at the fastest speed, namely, 10^{-4} cm/s. Thus for a machine of 9000 N capacity the theoretical power required at the specimen end is 2.2×10^{-2} W. However, at this low speed, because of the practically static conditions, very high friction and inertial losses at every stage of the power transmission should be expected. In order to obtain low speeds, for example, from a 600 rpm motor, the number of transmission stages will be large, on the order of 7. If the efficiency of each stage is taken as 50 percent, then the power requirement at the motor shaft becomes $2.2 \times 10^{-2} \times (1/0.5)^7 \approx 3$ W. The power requirement of a multispecimen machine, pulling four specimens simultaneously at its maximum capacity of 9000 N each, would be $4 \times 3 = 12$ W. It is apparent that a one tenth of a horse-power motor will be adequate for either a single or multispecimen machine; such a motor will see practically no fluctuation in load from the start to the end of an experiment.

The motor which will maintain a constant speed during a test run and is

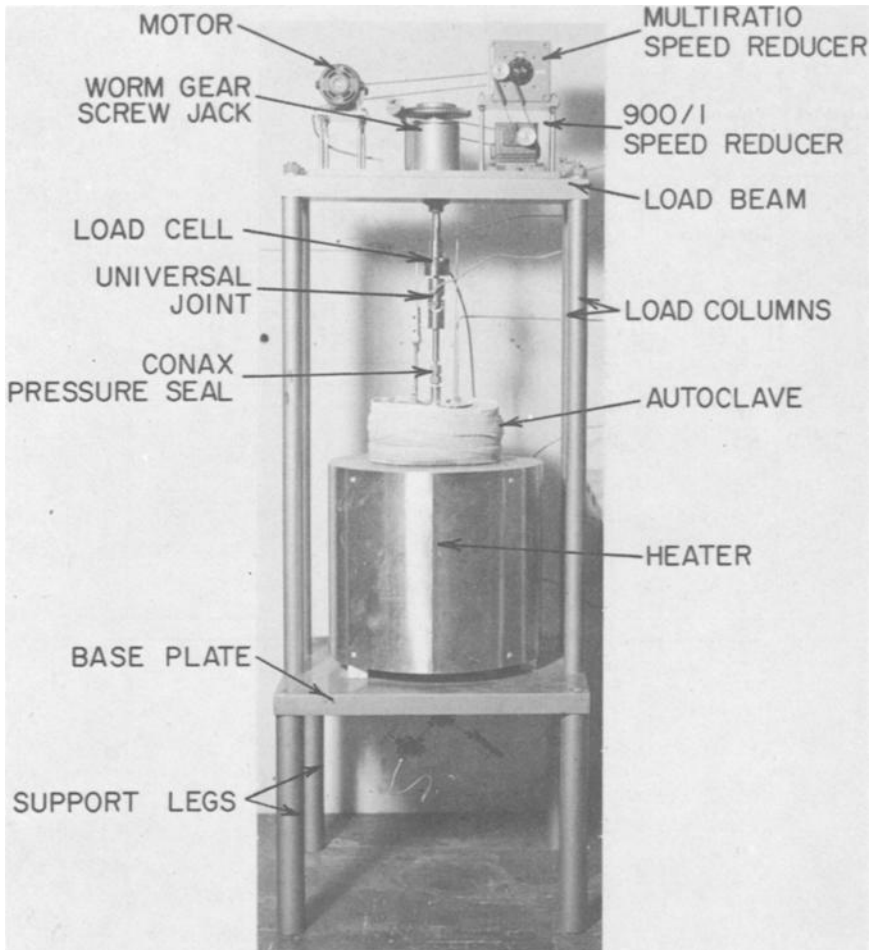


FIG. 1—A slow strain-rate machine with a furnace heated four litre autoclave.

not affected by the line voltage fluctuations will be suitable, for example, synchronous motor. However, recently shunt-wound direct-current motors with feedback control have become popular for constant speed operations. These have an additional advantage over a fixed speed synchronous motor. Their speed is adjustable within a specified range without affecting the torque. Another class of precision motors are available where the speed and torque are independently controllable. These consist of a motor with integrally wound generator and a transistorized feedback amplifier. The speed is adjustable precisely with a ten-turn potentiometer. The speed is maintained within 1 percent setting even with a ± 10 percent fluctuation

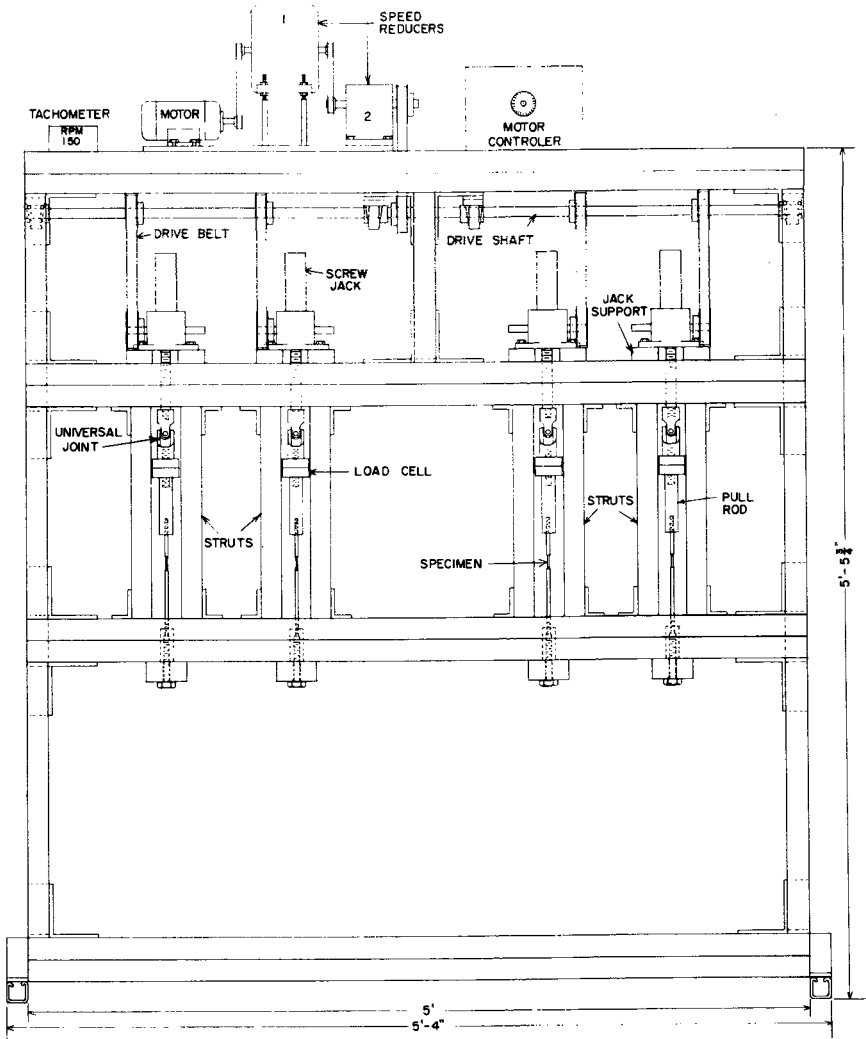


FIG. 2—Schematic drawing of a multispecimen slow strain-rate machine.

in the line voltage. The cost of such a motor-controller system is approximately \$500 as opposed to \$50 to 80 for a synchronous motor.

Speed Reducers

The methods of reducing the motor speed to meet the required low crosshead velocity are numerous: spur gear train, roller chain and sprocket

assemblies, timing belt and pulley assemblies, and commercial preboxed speed reducers, etc. Any of the above nonslip positive drive systems or a combination of systems can be used satisfactorily. The selection depends largely on the availability of the materials, compactness desired, the effort (machining of parts and alignment, etc.) required in assembly, and maintenance (lubrication, dusting, etc.). Personal preference and the cost can be deciding considerations. In the authors opinion, commercially available preboxed fixed and multiratio speed reducers offer the optimum choice. These units are compact and presealed with lubricants and are available in many sizes, speed ratios and torque ratings. Furthermore, these offer an "erector set" simplicity in building the machines. For coupling the motor, speed reducers, and the rotary to linear motion converters, the authors prefer timing belts and pulleys, which are also used in some of the well known tradename testing machines. Timing belts and pulleys are noiseless and require no lubrication; belt flexibility allows use of small diameter pulleys and imposes no stringent requirement on the alignment of shafts.

The important factors that need to be considered in selecting commercial speed reducers are output torque rating, maximum input speed, and input/output ratio. The total reduction needed, in order to obtain a cross-head velocity of 10^{-7} cm/s, is 6 decades, when using a 600 rpm motor and a 1 cm/100 turns screw jack. It is obvious that at least two reducers with, say, 1000/1 ratio are needed to achieve six decades of reduction. Since the torque is inversely proportional to the speed, the torque rating of the first reducer (motor end) will be a rather small, but that of the second reducer (jack end) will be relatively high. For enabling one to select the desired strain rate, over three orders of magnitude, 10^{-4} to 10^{-7} s $^{-1}$, we recommend a multiratio speed reducer for the first stage where the torque will be small, and a fixed ratio reducer for the second stage with larger torque.

Taking the example of a machine pulling 9000 N at 10^{-4} cm/s, the torque required at a 1 cm/100 turns screw jack of 20 percent efficiency will be 3.3 N/cm.

Thus, the output rating of the second speed reducer should be at least 4 N/cm or more for a single specimen machine, and 16 N/cm or more for a multispecimen machine. The torque rating of the first reducer would be less, by a factor equal to the input/output speed ratio of the second reducer, for example $16/1000 = 0.016$ N/cm for the multispecimen machine.

The timing belts for coupling, if a common type is used at all places, should be rated for the maximum force, that is corresponding to the maximum torque in the system. For a 16 N/cm case, assuming a 5 cm diameter pulley on the output shaft of the second reducer, the net pull on the belt will be $2T/D = 2 \times 16$ N/cm/5 cm = 6.4 N. If the tight to slack side ratio is two, then the belt strength should be 13 N minimum.

Screw Jack

One of the most convenient devices for converting a rotary motion into a vertical lift, with a simultaneous speed reduction, is a worm gear screw jack. The desired features in a jack, meant for use in a slow strain-rate machine, are capacity, large number of worm turns per centimeter of lift, keyed screw to prevent rotation during lift, no backlash, efficiency, compactness, and a sufficient vertical travel. The worm gear ratio and efficiency of jacks with identical capacity varies from make to make. A compact 9000 N jack with 20:1 worm gear ratio may have efficiency anywhere from 10 to 50 percent. A 6 to 12 cm vertical travel of the screw is sufficient in most cases.

Load Transducer

The simplest load indicating device in a testing machine is a load cell. However, a calibrated load cell with its accessories can be the most expensive item (\$500 to 700). An alternative is to install a strain gage on the pull rod and calibrate it. The load cell can be mounted either between the crosshead and the specimen or between the fixed bed of the frame and the specimen, depending upon the convenience. In selecting a load cell, the points to consider are: capacity, accuracy ~ 0.1 percent, linearity of response ~ 0.1 percent, low profile, and cost. A sealed and temperature compensated unit is preferred, since it is likely to be exposed to the corrosive vapors from the test environment. A low profile compact cell saves working space on the machine and thereby reduces the size of the frame.

Universal Joint

The purpose of a universal joint in the machine is to correct the alignment problem resulting from a slight mismatch of the vertical axes of the specimen and the pull rod in the jack. The universal joint is preferably mounted between the pull rod and the specimen, and it could also be mounted between the anchored end of the specimen and the machine frame. A cup and ball joint and a roller chain have also been used in the absence of a universal joint.

Machine Frame

Once the load capacity and the working space needed on a machine have been fixed, the shape of a frame is a matter of choice and structural materials available. The primary concern in a frame is its rigidity under maximum load, especially of the two, top and bottom, members which support the tensile load. The total deflection of these members under load

should not exceed a few hundredths of a millimetre. Any deflection, if present, will modify the strain rate.

The shape of a frame, as will be shown later, can be a simple rectangle supported on a steel base plate, a two-tier table, or a three-tier rack. The drive components of the machine carry little weight, and all can be assembled on a separate small plate, say, 30 by 45 cm, and placed on top of the frame, away from the work space.

Practically, any structural steel shape of proper dimensions, round or flat bars, I-beams, U-channels, and plates, etc., can be used in construction of a machine frame. However, a design which requires least effort, that is, welding, machining, etc., will be the most economical. As the loads involved in a slow strain-rate machine are of the order of only 9000 N erector set type framing members, such as U-channels, can be easily used in a frame. These offer considerable amount of flexibility in design, and avoid welding and machining operations. When using erector type members, careful attention must be given to the rigidity of the frame as a whole and the load bearing members in particular. Suppliers of such materials usually provide enough engineering information to enable one to make such checks.

Machines

In order to illustrate the points discussed earlier, a single-specimen machine is shown in Fig. 1, and a schematic drawing of multispecimen machine is shown in Fig. 2. The latter machine is for use with 0.5 to 1 litre cells, whereas the other machine is for use with a 4 to 6 litre autoclave. These two machines have been built and used extensively at the Ohio State University.

The frame of the single-specimen machine is a two-tier table. Table plates which bear the load are supported on round columns. The autoclave in Fig. 1 is anchored with three studs to the base plate. A clearance of about 2 cm is left between the autoclave and the base plate for asbestos pads which insulate the autoclave and prevent heating of the plate. The complete drive train assembly is mounted on a separate 1 cm thick plate which sits on the upper tier. The tension specimen inside the autoclave is held in a jig; the specimen is connected via a pull-rod to a universal joint and a load cell. The load cell in turn is connected to the screw jack in the drive assembly. A pressure seal around the pull rod prevents leakage from the autoclave, but allows free movement of the rod. The capacity of this machine is over 10 000 N.

The multispecimen machine in Fig. 2 is assembled on a three-tier rack which was erected with channels, angle brackets, nuts, and bolts. The vertical members of the rack are U-channels, while the stronger horizontal

members are H-channels. Struts are placed between the load bearing middle and lower tiers to eliminate flexure of these horizontal members during testing.

The portable drive train assembly is similar to that in Fig. 1; the assembly is mounted on the top tier of the rack. A variable speed motor (motor-generator) is the principal driving unit in the train, the speed of which is adjustable between 20 and 2000 rpm with an electronic motor controller. The motor drives a multiratio speed reducer which has 10 selectable reductions 1,2,5,10,20...1000/1. The next reducer in the train is a 900/1 fixed ratio speed reducer. All the interconnections between the various components of the train and the machine are made with nonslip timing belts and gear pulleys.

The fixed ratio speed reducer powers a shaft (2 cm diameter by 152 cm) which is supported on four pillow blocks underneath the top tier. The shaft, in turn, powers the four screw jacks that are positioned on the middle tier. The lift screw in the jacks moves 2.5 cm for every 100 turns of the worm. The screw is keyed to prevent its rotation during pull. The pulling capacity of the jacks is 9000 N. A tension specimen is connected to the lift screw via a pull rod, a load cell, and a universal joint. The lower end of the specimen is anchored, with a coupling nut, at the center of an anchor bar (4 by 8 by 31 cm) which is fixed under the lowest tier.

A safety feature not shown in Fig. 2 is a pointer arm attached to one of the pull rods. This pointer when moving upward crosses a set high limit where it mechanically actuates a power cut-off switch and stops the motor. This prevents the machine from self destruction in unattended operations.

The machine in Fig. 2 is capable of pulling four specimens simultaneously at the same rate. The crosshead speed is infinitely adjustable over a wide range, 10^{-4} to 10^{-8} cm/s. The speed is adjusted by selecting a proper combination of motor speed and one out of the ten input/output ratios in the multiratio speed reducer. The capacity of the machine is 9000 N for each specimen. The cost of materials, including four load cells, for the machine is approximately \$5000.00.

The principal components of the above machine and their model numbers are listed below:

Power Drive and Control System: Model No. TR9020,

Minarik Electric Company, Los Angeles, Calif.

Multi-ratio Reducer: Model No. 2611

Geartronics Corporation, North Billerica, Mass.

Fixed-ratio Reducer: Cat. No. TW113A-900-DMS

Boston Gear Division, North American Rockwell, Quincy, Mass.

Screw Jack: Model No. 2500, Series 1800

Duff-Norton Company, Charlotte, N. C.

Load Cell: Type U2M1, Capacity 2000 lb

BLH Electronics, Waltham, Mass.

Frame: Built from channel Nos. P1000 and P1001
Unistrut Corporation, Wayne, Mich.

Summary

In this paper, basic concepts for designing and building a multispecimen slow strain-rate machine have been outlined. The principal components used in building one such machine are also listed.

Acknowledgments

This work was partially supported by the Electric Power Research Institute, Palo Alto, Calif. on Contract No. RP-311-1. The authors also acknowledge the help of Paul Carter, of our laboratories, in drawing, assembling, and testing the various machines.

DISCUSSION

C. R. Crowe¹—One can easily modify a standard floor model Instron with a push-button speed selector to provide crosshead speeds of interest.² In the standard floor model Instron, the crosshead speed is controlled by a reference servo in the Selsyn drive unit. This reference servo is normally driven by a constant speed motor through appropriate gearing in the Selsyn unit. If one wishes to change the crosshead speeds, an external constant speed motor can be mounted to the front of the push-button speed selector and attached through gearing to the reference servo in the Selsyn unit as shown in Fig. 3. External speed control is then possible using the "special high" and "special low" push-button selectors. Figure 3 shows a 15 rpm constant speed motor attached to the Instron through a 2:1 gear reduction train. The gears are the standard sets provided with the Instron strip chart recorder. This setup produces a crosshead speed of 1.6×10^{-6} in./s in the low speed mode. Slower motors or lower gearing, or both, provide proportionally slower crosshead speeds.

As wired, there is a 10:1 speed difference between the high and low modes. This ratio can be changed by rewiring the clutches in the speed selector box. Figure 4 shows the necessary modifications to obtain a 5:1 speed ratio. The switches are provided to allow the unit to operate normally as well as in the modified mode. The switches are also visible on the front panel in Fig. 3.

¹Naval Surface Weapons Center, White Oak, Silver Spring, Md. 20910.

²Crowe, C. R. and Arsenault, R. J., *Acta Metallurgica*, Vol. 24, 1976, pp. 925-938.

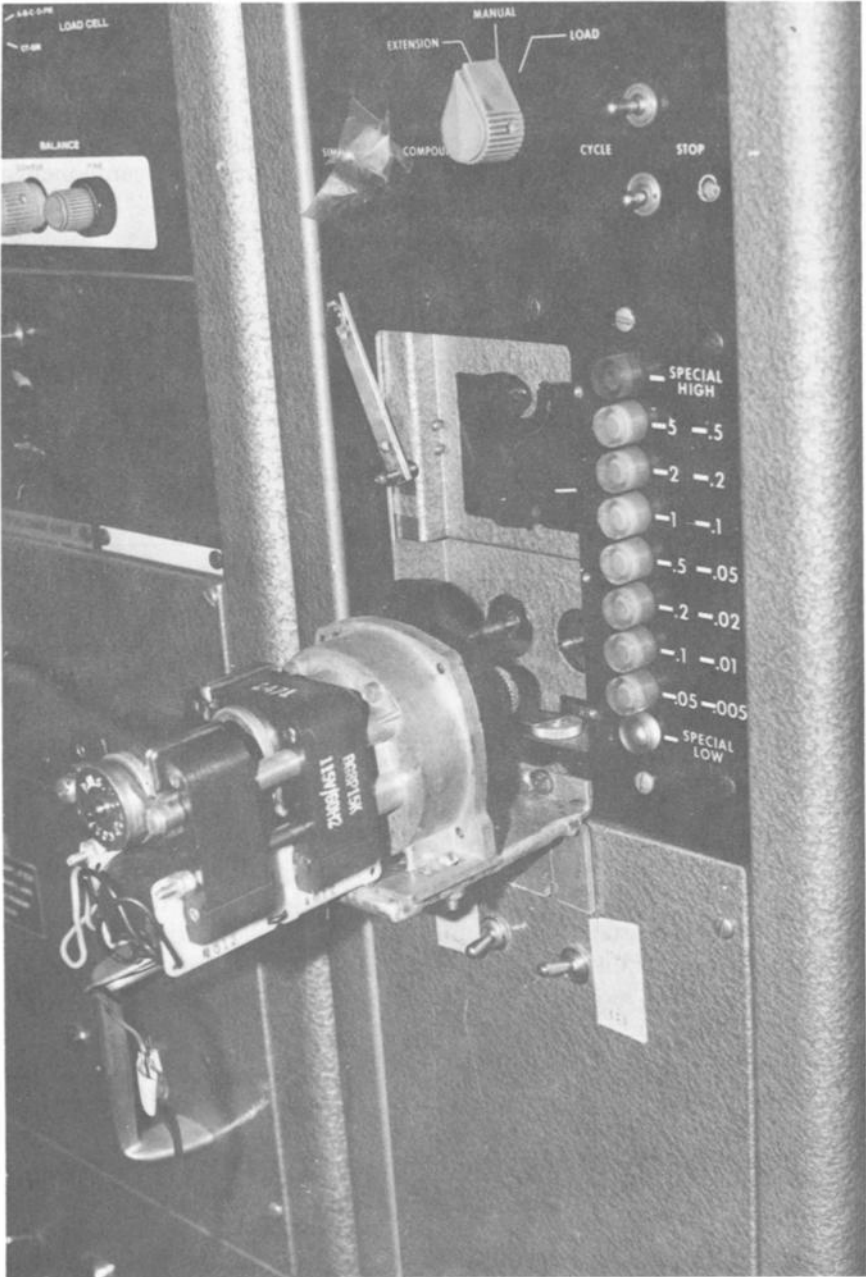


FIG. 3—A 15 rpm constant speed motor attached to Instron.

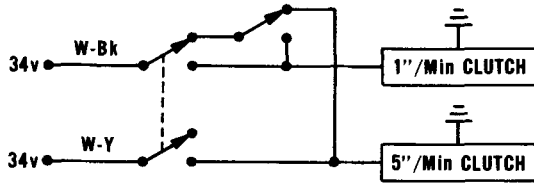


FIG. 4—Wiring modifications to select speed ratio.

W. T. Nutter, A. K. Agrawal, and R. W. Staehle (authors' closure)—No comment.

Multispecimen Test Facility for High Temperature, High Pressure Slow Strain-Rate Testing

REFERENCE: Lyle, F. F., Jr. and Norris, E. B., "Multispecimen Test Facility for High Temperature, High Pressure Slow Strain-Rate Testing," *Stress Corrosion Cracking—The Slow Strain-Rate Technique*, ASTM STP 665, G. M. Ugiansky and J. H. Payer, Eds., American Society for Testing and Materials, 1979, pp. 388-398.

ABSTRACT: This paper describes a slow strain-rate test facility in which 6 tension specimens may be tested simultaneously and load-versus-displacement curves for each specimen may be recorded. The facility is designed to operate at a maximum temperature of 500 K (450°F) and a maximum pressure of 28 MPa (4 ksi). Constant crosshead displacement rates ranging from 2.5×10^{-6} to 2.5×10^1 cm/s (10^{-6} to 10^1 in./s) may be obtained. Studies of hydrogen sulfide (H₂S)-induced stress corrosion cracking (SCC) of low alloy steels exposed to simulated sour gas well environments (hydrogen sulfide-carbon dioxide-water (H₂S-CO₂-H₂O)) are described. Use of the technique to determine H₂S-induced SCC susceptibility of various steels as a function of temperature is shown.

KEY WORDS: stress corrosion cracking, strain rate, high temperature tests, high pressure tests, multispecimen test facility, low alloy steels, sour gas well environments, temperature

During the past 5 to 10 years, use of the slow strain-rate technique for stress corrosion cracking (SCC) susceptibility testing has become widespread because of its positive nature and the economics in time and expense it provides.

Many such tests have been conducted at low temperature and pressure using one specimen per test machine, thereby negating some of the economy in testing time gained from the test technique. This paper describes a high temperature, high pressure test facility in which 6 specimens may be tested simultaneously, thereby permitting replicate tests to be conducted and different materials to be tested in the same environment.

¹Senior corrosion engineer and manager of mechanical properties section, respectively, Department of Materials Sciences, Engineering Sciences Division, Southwest Research Institute, San Antonio, Tex. 78284.

Tests conducted in this facility to determine the susceptibility of low alloy steels to SCC in sour-gas well environments are described.

Description of Test Facility

General

The facility is designed to operate to a maximum temperature of 500 K (450°F) and a maximum pressure of 28 MPa (4 ksi). It consists of an autoclave mounted in an 890 kN (200 000 lb) tension test machine. In the configuration described below, a maximum load of 44.5 kN (10 000 lb) can be applied to each of 6 individual pull rods. Constant crosshead displacement rates ranging from 2.5×10^{-6} to 2.5×10^1 cm/s (10^{-6} to 10^1 in./s) may be obtained. The facility was designed initially for the testing of low alloy steels in aqueous environments containing substantial quantities of hydrogen sulfide (H₂S) and carbon dioxide (CO₂), and small quantities of sodium chloride (NaCl). Materials of construction were selected for compatibility with this type of environment.

Test Vessel and Internals

A schematic drawing of the test vessel and internals is shown in Fig. 1. The vessel is a commercially available 3.8 litre (1 gal) Type 316 stainless steel autoclave. An internal liner made of nickel-chromium-cobalt-molybdenum (Ni-Cr-Co-Mo) alloy (MP35N) is used to protect the autoclave body. The autoclave head is penetrated by 6 Type A286 stainless steel pull rods. The pull rods are sealed with spring-loaded radial seals coated with an elastomer. The seals are cooled by water circulation through channels in the head. A Type 316 stainless steel specimen mounting frame is attached to the head by 6 Type A286 stainless steel rods. Flat tension specimens with 2.5 cm (1 in.) gage lengths and 0.30 cm² (0.05 in.²) cross-sectional areas are attached to the pull rods and frame with 13 mm (0.5 in.) diameter Type A286 stainless steel dowels. Figure 2 shows the assembled components with specimens in place.

Loading and Control

Loading is provided by an independent servocontrolled hydraulic actuator. A block diagram of the servocontrol loop is shown in Fig. 3. A ramp function generator drives the loading crosshead at the desired constant rate. Crosshead displacement is measured by a capacitance-type transducer mounted between the crosshead and the autoclave head; an output signal from this transducer is fed into an error detector where it is compared to the ramp generator output signal and modifies the signal, if necessary, to maintain the required constant rate of displacement. The pull rods are coupled in-

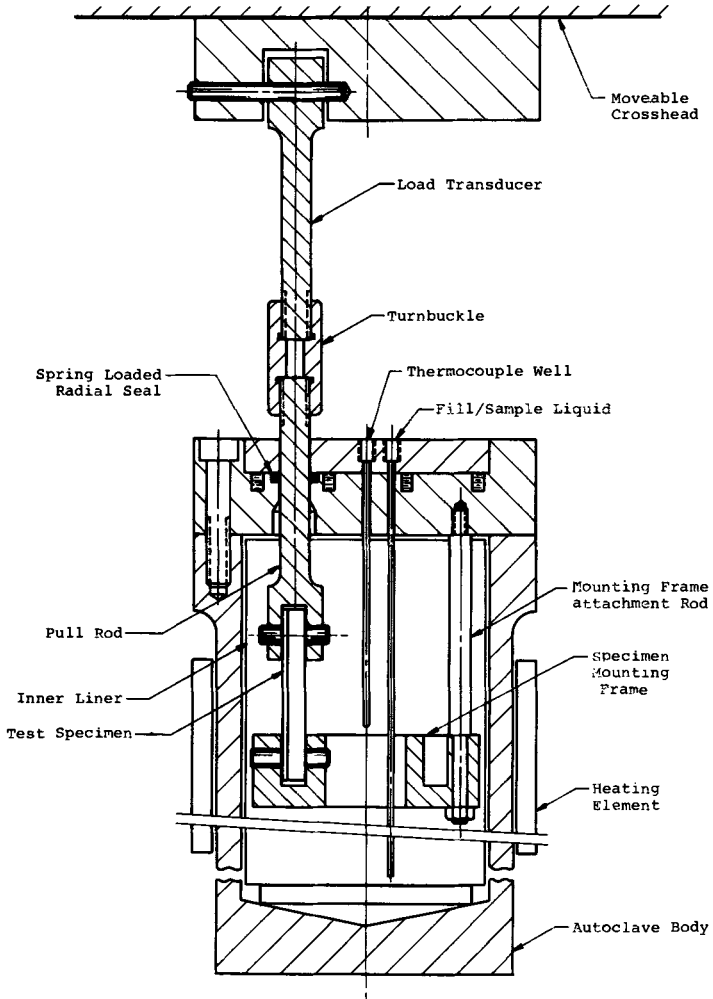


FIG. 1—Schematic drawing of test vessel.

dividually through 6 full-bridge strain-gage load transducers to the cross-head, thereby permitting the load on each specimen to be independently monitored. Output signals from the 6 load transducers and the displacement transducer are fed into a multichannel chart recorder which produces individual load versus displacement curves for each specimen. Yield, ultimate, and fracture strength for each specimen may be obtained from these curves.

Experimental Results

One of the major sources of natural gas available in the United States is

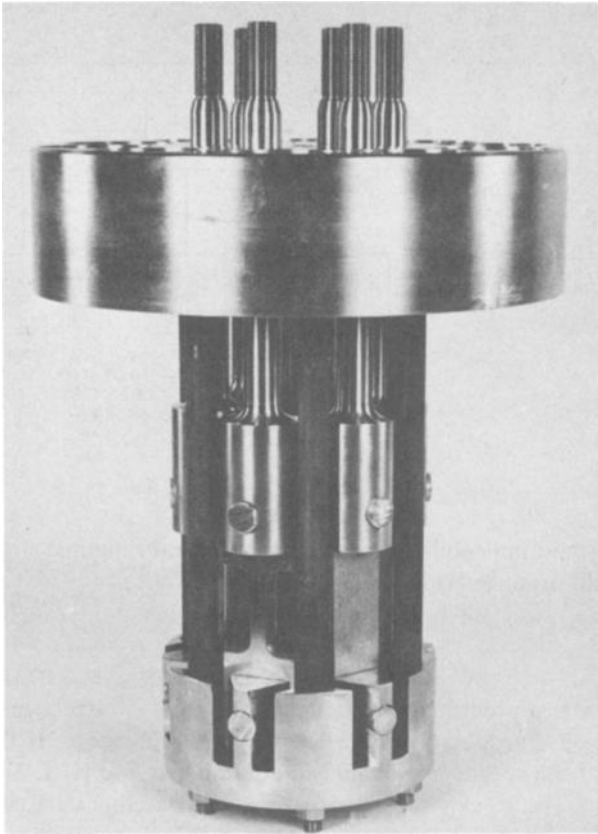


FIG. 2—Assembled components with specimens mounted for testing.

very deep, hot, high pressure sour-gas formations (that is, formations containing significant concentrations of CO_2 and H_2S). Because of the depth of the formations (some formations are more than 6 km (20 000 ft) below the surface) it is desirable to use high strength, low alloy steels for casing and tubing to minimize weight. These steels are known to be susceptible to H_2S -induced SCC at ambient and slightly higher temperatures and to be immune at more elevated temperatures. It is important to the petroleum industry to know the threshold temperatures for individual grades of casing and tubing steels in order that an intelligent selection of materials can be made for use at various depths within sour-gas wells.

A literature survey revealed no reported applications of the slow strain-rate technique to the study of H_2S -induced SCC or to other forms of hydrogen-induced SCC. Therefore an experimental program was undertaken to

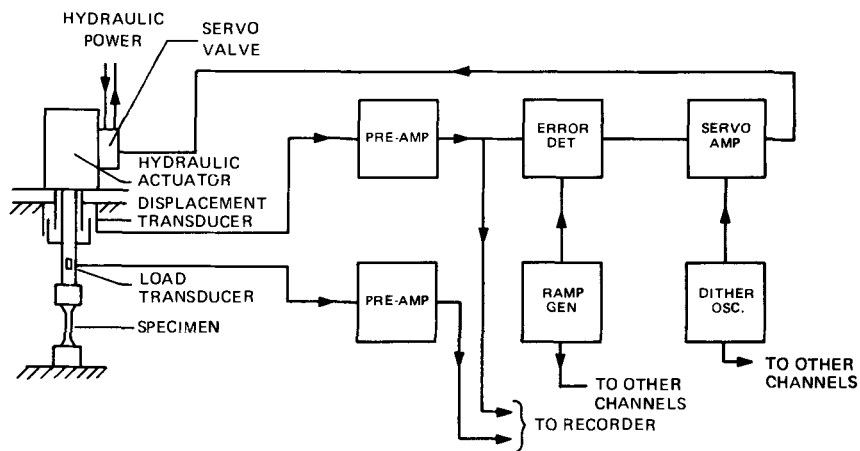


FIG. 3—Block diagram of servocontrol loop.

demonstrate the applicability of the slow strain-rate method under conditions known to produce H_2 -induced SCC.

Initial Tests

In the initial test program, six specimens of AISI 4130 steel heat treated to essentially three hardness levels (HRB 75, HRC 28, and HRC 32) were tested. Two of the specimens (quenched and tempered to HRC 27 and HRC 32, respectively) were exposed in air to provide baseline data. Two of the specimens (one quenched and tempered to HRC 28 and one annealed to HRB 75) were tested in 10 percent sulfuric acid (H_2SO_4) saturated with arsenic trioxide (As_2O_3), a solution known to promote rapid hydrogen-induced SCC. The purpose of this test was to demonstrate the ability of the slow strain-rate method to distinguish between a susceptible and a non-susceptible steel. The other two specimens (quenched and tempered to HRC 29 and HRC 33, respectively) were exposed in aqueous solutions containing 0.5 percent acetic acid (CH_3COOH) plus 5 percent NaCl, saturated with H_2S , a solution being used as a standard by the National Association of Corrosion Engineers for evaluation of the susceptibility of steel to H_2S -induced SCC. The test solution was prepared by bubbling nitrogen through the acidified salt solution overnight (about 15 h) to remove oxygen and then bubbling H_2S through for an hour prior to the test and continuously during the test. A slow strain rate of $2 \times 10^{-6} s^{-1}$ was employed.

Specimens were loaded rapidly to 90 percent of their yield strength and then to fracture at the slow strain rate. The test results are given in Table 1. The test time shown is the amount of time elapsed between initiation of slow

TABLE 1—Results of slow strain-rate tests on AISI 4130 steel in three environments at 298 K (75°F) ($\dot{\epsilon} = 2 \times 10^{-6} s^{-1}$).

Test Media	Hardness, HRC	Ultimate				Elongation, % in 25.4 mm	Reduction in Area, %	Time to Failure, ks
		Tensile Strength		0.2% Yield Strength				
		MPa	(ksi)	MPa	(ksi)			
Air	27	820	(119)	724	(105)	13.8	53.1	57.60
Air	32	1100	(160)	1048	(152)	11.0	39.2	49.68
H ₂ SO ₄ + As ₂ O ₃ ^a	75 (HRB)	563	(82)	363	(53)	21.6	29.4	84.24
H ₂ SO ₄ + As ₂ O ₃ ^a	28	896	(130)	645	(94)	4.5	7.6	14.40
H ₂ S ^b	29	938	(136)	931	(135)	4.0	6.4	1.44
H ₂ S ^b	33	1050	(153)	1040	(151)	4.0	7.7	2.88

^a10 percent H₂SO₄ with As₂O₃.

^b5 percent NaCl — 0.5 percent CH₃COOH solution saturated with H₂S.

straining and fracture. The elongation to failure of the quenched and tempered steel (HRC 28) was distinctly lower in the $\text{As}_2\text{O}_3\text{-H}_2\text{SO}_4$ solution than it was in air and secondary cracks were present in the specimen gage section, indicating the susceptibility of the steel to SCC in this environment. The annealed steel specimen was not expected to be subject to hydrogen-induced SCC and, as shown in Table 1, retained excellent ductility. Both of the quenched and tempered specimens exposed to the acidified H_2S salt solution cracked rapidly with severe loss of ductility and with secondary cracking present. The fact that the HRC 33 specimen displayed slightly better ductility and a slightly longer time to failure than did the HRC 29 specimen was attributed to data scatter and is inconsequential when results of the H_2S tests are compared with the results of the air tests. Elongation, reduction of area, and time to failure were found to be sensitive indicators of SCC. These tests readily demonstrated the ability of the slow strain-rate method to discriminate between susceptible and nonsusceptible steels in environments known to cause SCC under conditions which promote hydrogen entry.

Tests in Sour-Gas Well Environments

An additional series of tests was conducted then in a simulated sour-gas well environment to demonstrate that a temperature threshold above which a high strength steel would be immune to H_2S -induced SCC could be determined by the constant strain-rate techniques.

The test environment consisted of a deoxygenated 1000-ppm NaCl solution equilibrated with a gas phase containing 3.24 MPa (470 psi) partial pressure of CO_2 and 207 kPa (30 psi) partial pressure of H_2S . Specimen material consisted of AISI 4340 low alloy steel quenched and tempered to a hardness of 32 HRC. Tests were conducted in this environment at 298, 344, 366, and 394 K (75, 160, 200, and 250°F) and in air at 298 K (75°F). Duplicate specimens were exposed at each temperature.

The test results are given in Table 2. Time to failure, percent elongation, and percent reduction of area versus temperature curves are shown in Fig. 4. Data scatter was considerably greater for percent reduction of area because of difficulties in accurately measuring the cross-sectional area of fractured specimens. Ductility parameter values and time to failure increased with increasing temperature above approximately 344 K (160°F), indicating a decreasing susceptibility to SCC. This observation was confirmed by low power microscopic inspection of the specimens which revealed large numbers of secondary cracks in the gage length of specimens tested at 298 and 344 K (75 and 160°F), but only a few secondary cracks in the gage lengths of specimens tested at the higher temperatures.

Therefore, these tests did not define a temperature above which this particular steel was immune to H_2S -induced SCC. However, the trend of the data was sufficient to demonstrate the applicability of the technique.

TABLE 2—Results of slow strain-rate tests on AISI 4340 steel in H₂S-CO₂ environment^a at four temperatures ($\dot{\epsilon} = 2 \times 10^{-6} s^{-1}$).

Test Media	Temperature		Hardness, HRC	Ultimate Tensile Strength		0.2% Yield Strength		Elongation, % in 25.4 mm	Reduction in Area, %	Time to Failure, ks
	K	°F		MPa	(ksi)	MPa	(ksi)			
Air	298	(75)	32	1103	(160)	1048	(152)	11.0	39.2	49.68
H ₂ S-CO ₂	298	(75)	31	939	(136)	932	(135)	4.2	4.2	16.56
H ₂ S-CO ₂	298	(75)	31	892	(129)	892	(129)	2.4	6.2	14.04
H ₂ S-CO ₂	344	(160)	32	900	(131)	858	(125)	4.2	8.9	16.20
H ₂ S-CO ₂	344	(160)	32	900	(131)	862	(125)	4.2	1.4	12.96
H ₂ S-CO ₂	366	(200)	32	976	(142)	870	(126)	4.9	10.1	27.72
H ₂ S-CO ₂	366	(200)	33	950	(138)	877	(127)	5.3	7.1	25.20
H ₂ S-CO ₂	394	(250)	32	975	(141)	851	(123)	6.5	14.4	40.68
H ₂ S-CO ₂	394	(250)	32	930	(135)	816	(118)	6.5	7.4	34.00

^aDeoxygenated 1000-ppm NaCl solution overpressured with 3.24 MPa (470 psi) CO₂ and 207 kPa (30 psi) H₂S.

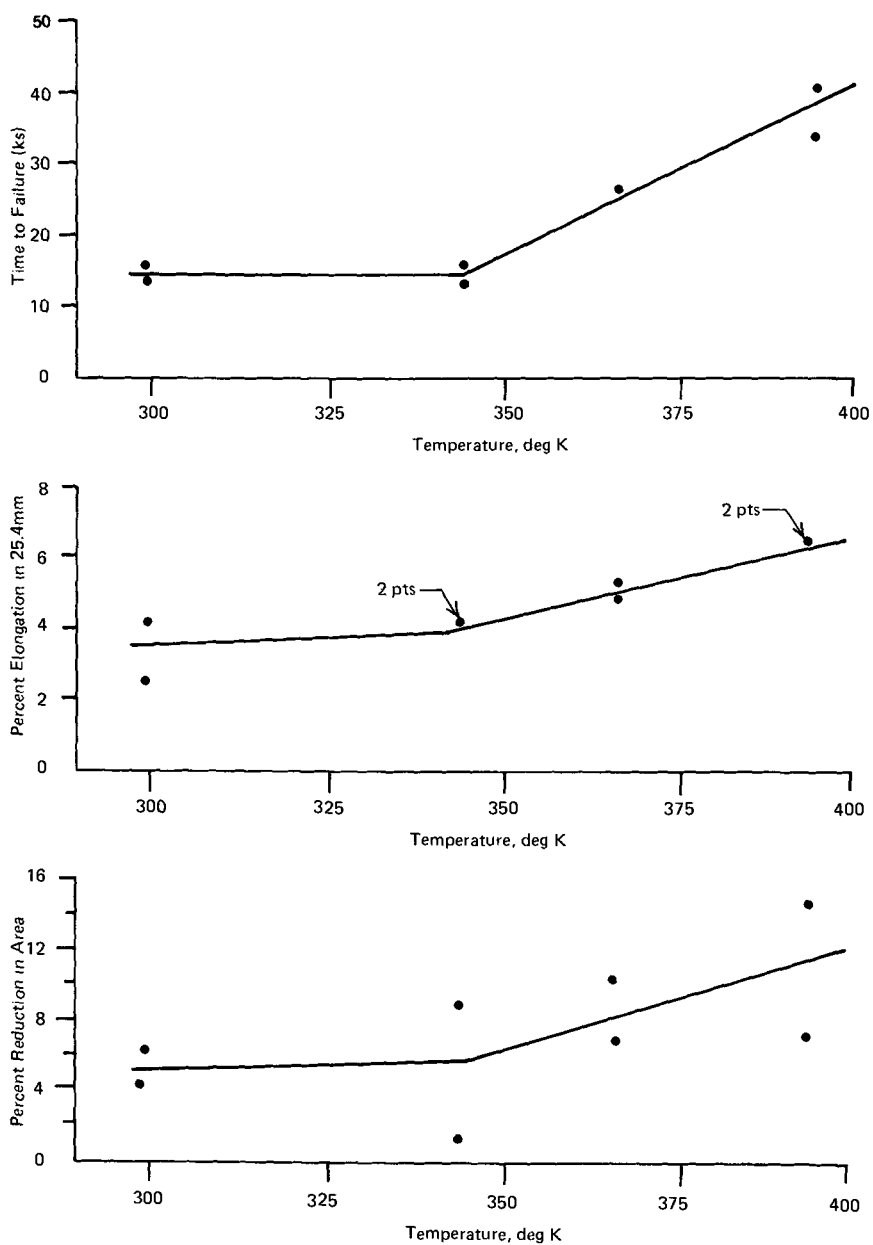


FIG. 4--Time-to-failure and ductility of AISI 4130 steel in H_2S-CO_2 environment versus temperature.

Following these preliminary studies, the multispecimen test facility was used to determine H₂S-SCC temperature thresholds for 25 different grades of casing and tubing steels ranging in yield strength from 570 to 1090 MPa (82.5 to 158.0 ksi). Results of a series of tests on a quenched and tempered steel with a yield strength of 1090 MPa (158.0 ksi) are shown in Fig. 5. A slow strain rate of $2 \times 10^{-6} \text{ s}^{-1}$ was used. Three test environments were employed: (1) H₂O—deaerated, deionized water plus a 3.45 MPa (500 psi) overpressure of N₂ gas; (2) CO₂—a deaerated brine solution (1000 ppm NaCl) plus a 3.45 MPa (500 psi) overpressure of CO₂; and (3) H₂S—deaerated brine solution plus a 69 kPa (10 psi) overpressure of H₂S and a 3.38 MPa (490 psi) overpressure of CO₂. In the H₂O environment tensile elongation increased with increasing temperature as would be expected. In the CO₂ environment, tensile elongation paralleled that in the H₂O environment, at slightly lower values, up to a temperature of 395 K (250°F); at higher temperatures tensile elongation decreased with increasing temperature. In the H₂S environment severe H₂S-induced SCC occurred at temperatures below about 365 K (200°F), as evidenced by very low tensile elongation, and above this temperature, elongation increased with increasing temperature reaching a maximum at 395 K (250°F); at higher temperatures elongation decreased with temperature along the same curve as in the CO₂ environment. In both the CO₂ and H₂S environments metallographic sections through specimens exposed at 420 K (300°F) confirmed the presence of severe SCC. These

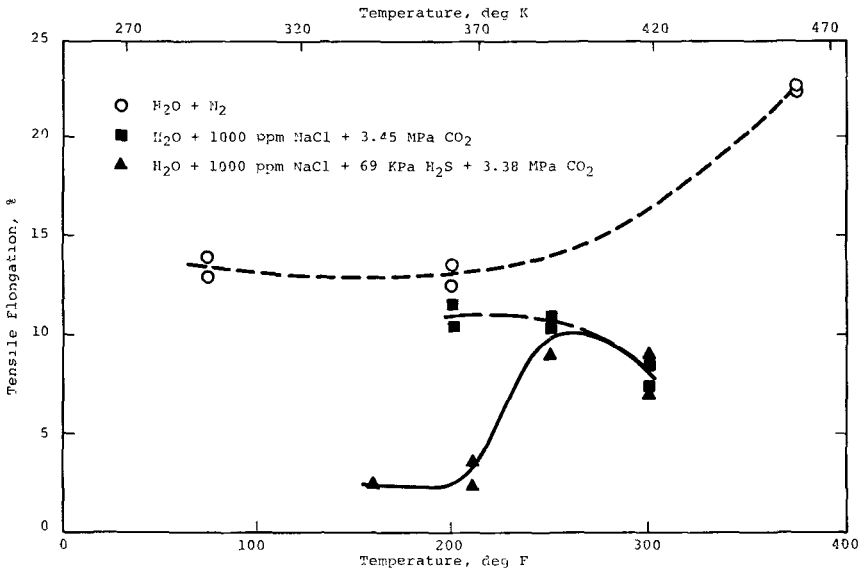


FIG. 5—Ductility of high-strength steel (0.2 percent yield strength = 1090 MPa) in three environments versus temperature.

results suggest that CO_2 induces SCC in this high strength steel at temperatures in excess of 395 K (250°F). A similar, although less pronounced behavior, was observed for a quenched and tempered steel with a yield strength of 900 MPa (130 ksi). Steels with yield strengths below 789 MPa (115 ksi) did not exhibit susceptibility to SCC at high temperatures. All of the lower strength steels tested were susceptible to H_2S -induced SCC at low temperatures and were immune at higher temperatures, with the transition temperature increasing in proportion to yield strength.

Conclusions

1. A multispecimen slow strain-rate test facility has been developed in which tests can be conducted at temperatures to 500 K (450°F) and pressures to 28 MPa (4 ksi) over a strain-rate range of 10^{-6} to 10^1 s^{-1} .
2. Applicability of the slow strain-rate technique to the study of H_2S -induced SCC has been demonstrated.
3. Use of the technique to determine H_2S -SCC susceptibility transition temperatures for low alloy steels exposed to sour-gas well environments has been demonstrated.
4. Results of tests in H_2S - CO_2 containing environments on low alloy steels with yield strengths of approximately 900 MPa (130 ksi) or higher indicate these steels are susceptible to SCC, apparently induced by CO_2 , at temperatures above approximately 395 K (250°F).

Discussion

*H. D. Solomon*¹—How do you correct or compensate for the failure of one of the six specimens which are being run in parallel?

F. F. Lyle, Jr. and E. B. Norris (authors' closure)—When one of the specimens fails, some unloading of the remaining specimens may occur, the degree of unloading depending upon the percentage of the total applied load carried by the various specimens. Following the failure of a single specimen, we have found that the other specimens reattain the loads they were carrying prior to the failure in a short time. Straining of the remaining specimens is continued then at the slow rate until all have failed.

¹General Electric Company, Corporate Research and Development Center, Schenectady, N.Y. 12301.

Portable Slow Strain-Rate Stress Corrosion Test Device

REFERENCE: Hauser, F., Abbott, S. R., Cornet, I., and Treseder, R. S., "Portable Slow Strain-Rate Stress Corrosion Test Device," *Stress Corrosion Cracking—The Slow Strain-Rate Technique*, ASTM STP 665, G. M. Ugiansky and J. H. Payer, Eds., American Society for Testing and Materials, 1979, pp. 399-407.

ABSTRACT: A portable test device has been constructed for determining the stress corrosion cracking (SCC) characteristics of process environments. The device may be inserted and retrieved from laboratory, plant, and field equipment operating at pressures up to 13.8 MPa (2000 psi) and temperatures not exceeding 204°C (400°F) without shutting down the system. Specimens are loaded by the slow strain-rate method which has the advantage of producing SCC in a short period of time. The device is small enough to be inserted through a 2.54 cm (1 in.) diameter valve. A hydraulic cylinder, which requires a compressed gas supply as a power source, loads the specimens.

Initial testing was performed using low carbon steel specimens in air at room temperature. The hydraulic method of specimen loading performed smoothly and allowed constant strain rates as low as $4 \times 10^{-7} \text{s}^{-1}$ to be maintained ± 5 percent at a hydraulic system pressure of 2.76 MPa (400 psi).

Tests with AISI Type 304 stainless steel specimens in boiling (45 weight percent) magnesium chloride at 155°C (311°F) confirmed the applicability of the device for SCC studies. Indicators used include time to fracture, ultimate tensile strength, percent elongation, and visual observations for secondary cracks.

KEY WORDS: strain rate, portable tension tester, stress corrosion cracking, magnesium chloride, austenitic stainless steels, stress corrosion tester

The slow strain-rate method developed by Parkins² for evaluating the susceptibility of a metal to fail by stress corrosion cracking (SCC) in a specific environment is widely used. Its primary advantages over other methods are (a) it permits strain rate to be studied as a factor in SCC, and (b) it permits a positive answer on susceptibility to SCC to be obtained

¹Professor, research assistant, professor, and senior development engineer, respectively, Department of Mechanical Engineering, University of California, Berkeley, Calif. 94720.

²Parkins, R. N. in *The Theory of Stress Corrosion Cracking of Alloys*, J. C. Scully, Ed., North Atlantic Treaty Organization, Brussels, 1971, pp. 449-468.

in a relatively short period of time. A principal disadvantage has been that the apparatus required a tension testing machine of such a size that it was necessary to bring the corrosive environment to the machine by containing it in a small test cell which surrounded the specimen. Study of SCC in many complex environments of interest such as process streams was not possible because of the difficulty of reproducing the temperature, pressure, flow, and composition variables in a small test cell appended to a large testing machine.

This paper describes a slow strain-rate apparatus which is portable and which permits tests to be made in laboratory equipment (for example, autoclaves), process equipment (for example, process vessels and piping), and field equipment (for example, storage vessels). This greatly increases the scope of application of the slow strain-rate technique. Following a description of the mechanical features of the apparatus and factors controlling the reliability of the strain-rate measurements, applicability of the device for SCC studies is demonstrated by tests made with AISI Type 304 stainless steel in boiling 45 percent magnesium chloride ($MgCl_2$) solution at 155°C (311°F).

Description of Apparatus

A schematic drawing of the equipment used to make a slow strain-rate test is shown in Fig. 1. The apparatus consists of a specimen mounted in a SCC test device which contains a probe connected to a double acting hydraulic cylinder which is operated by a hydraulic control circuit pressurized by nitrogen. Specimen strain is measured by the cylinder tension

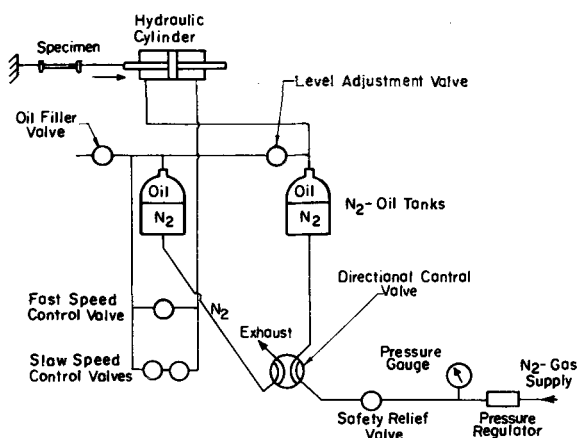


FIG. 1—Schematic diagram of portable SCC device.

rod displacement, and specimen load is measured by the differential pressure across the cylinder piston.

SCC Test Device

The test device is shown in Fig. 2. The SCC specimen can be inserted into and retrieved from a pressure system without shutting down the system. Two devices have been designed to allow the specimens to be inserted into either a low (up to 13.8 MPa (2000 psi)) or a high (up to 34.5 MPa (5000 psi)) pressure process system. To date, only the low pressure device has been constructed and tested.

The device consists of a double acting hydraulic cylinder attached on one end to a tension rod. The tension rod is concentric with and slides in another tube, the probe. An extension to the probe contains the specimen. With one end of the specimen attached to the nonmoving probe and the other end fixed to the tension rod, the specimen then can be loaded as desired. The method of hydraulic loading of the specimen can provide a smooth steady motion with variable strain rates. This system is simpler, lower in cost, and of less weight than a mechanical drive. The performance of the test device in an environment under pressure was experimentally determined to be indistinguishable from its performance when at atmospheric pressure. The only requirement necessary to ensure correct load readings was that the transducer amplifier/indicator for differential pressures be balanced while the probe was under pressure. The device has been designed to allow for insertion of the probe tube into a 25.4-mm (1-in.) gate valve. Electrical insulation of the specimen is achieved by ceramic spacers. In the device shown, all parts that would come into contact with the corrosive environment were made of Hastelloy C-276. All other parts were made of AISI Type 304 stainless steel. The device can be used in process systems where the temperature does not exceed 204°C (400°F). A detailed drawing of the probe assembly is given in Fig. 3.

The cylinder tension rod displacement is measured by a linear variable differential transformer (LVDT). A pressure transducer mounted across the hydraulic cylinder measures the differential pressure across the cylinder piston. The differential pressure times the effective piston area gives the load on the specimen. The displacement and pressure signal outputs are amplified and recorded on a dual pen strip chart recorder.

The device weighs 25.4 kg (56 lb). The housing diameter is 12.7 cm (5 in.), and the overall length of the device is 85 cm (33.5 in.). The length of the probe is 35.1 cm (13.8 in.), and the diameter of the probe is 2.4 cm (0.94 in.). The probe is designed to fit onto the flange of a valve.

Specimen

Specimens were machined to have a gage length of 5.72 cm (2.25 in.) and

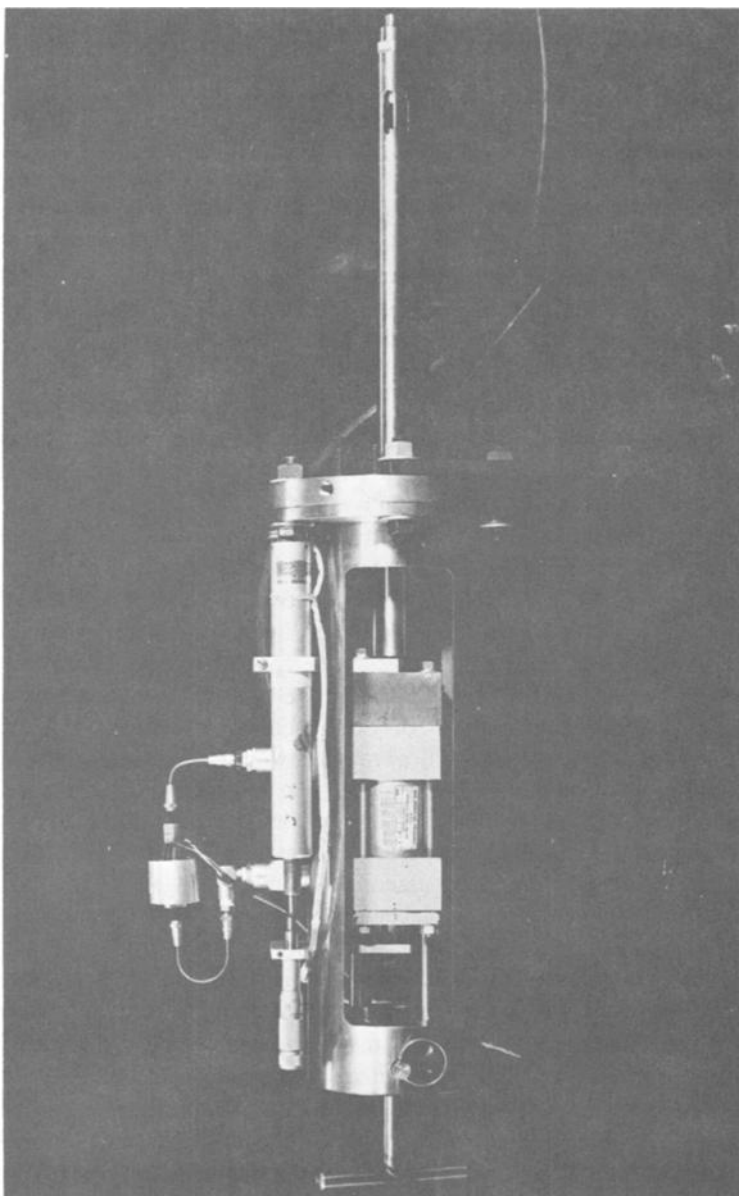


FIG. 2—Test device assembly. Overall length is 85 cm (33.5 in.); probe length is 35.1 cm (13.8 in.); and probe diameter is 2.4 cm (0.94 in.).

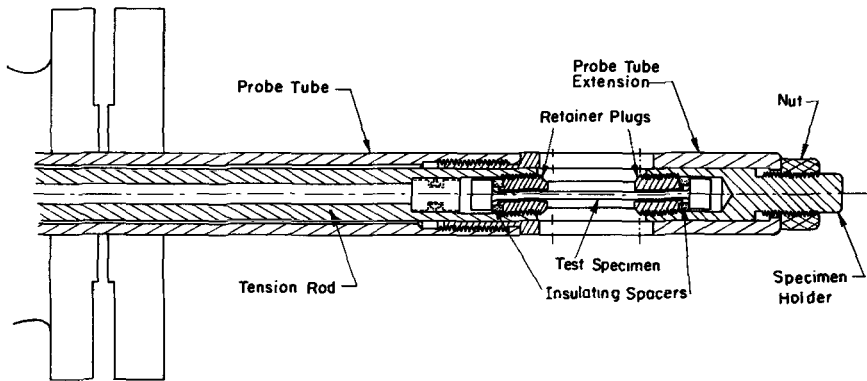


FIG. 3—Probe assembly details.

a diameter of 0.254 cm (0.10 in.). For large grained materials where a larger diameter specimen would be desirable, the overall size of the probe would have to be increased.

Hydraulic Control Circuit

A steady hydraulic oil pressure is applied to one side of the piston in the hydraulic cylinder while the flow rate of oil from the other side of the piston is metered to achieve the proper strain rate. The system operates as follows. Nitrogen is brought into the directional control valve that allows selection of which side of the hydraulic cylinder is to be pressurized. The nitrogen-oil tanks are used to convert nitrogen pressure into oil pressure. The fast speed control valve allows rapid positioning of the piston. The slow speed control valve is a very fine adjustment needle valve used to meter out the oil at the proper rate from the hydraulic cylinder. The maximum allowable pressure for the circuit is 11.0 MPa (1600 psig). The control circuit is mounted as a unit on a board measuring about 33 by 30½ cm (13 by 12 in.) and weighs about 13.6 kg (30 lb). It is connected by hoses to the nitrogen cylinder and to the SCC test device.

Results of Apparatus Evaluation Tests

Initial tests performed with low carbon steel specimens showed the device to be controllable and reliable. These tests were conducted in air at room temperature. Tests were made at hydraulic cylinder pressures ranging from 1.38 to 3.45 MPa (200 to 500 psig) to determine the effect of cylinder pressure on the specimen strain rate.

At the lower cylinder pressures, less than 2.07 MPa (300 psig), a con-

stant strain rate was not achievable during the specimen loading. At 3.45 MPa (500 psig), the strain rate remained constant during loading; however, it was necessary to close almost completely the single metering valve used initially in controlling the oil flow rate from the hydraulic cylinder to obtain a strain rate as low as 10^{-6}s^{-1} . A cylinder pressure of 2.76 MPa (400 psig) resulted in only a small (± 5 percent) variation of the strain rate and did not require the metering valve to be nearly shut off to obtain low strain rates.

Next, specimens were tested at strain rates from 4×10^{-7} to $1.4 \times 10^{-5}\text{s}^{-1}$. A recorder plot of the test made at the latter strain rate is shown in Fig. 4. The plot shows the displacement and the load versus time for a specimen. In the figure the initial starting points of the load and elongation plots are displaced slightly as the strip chart recorder could not begin both plots at the exact same point.

The measuring and recording devices were calibrated and exhibited less than 0.5 percent error within the ranges needed. The slow speed metering valve in the hydraulic control circuit was used to control the rate of displacement. Extreme care was taken when initially charging the control circuit with hydraulic oil to remove air and dirt particles completely.

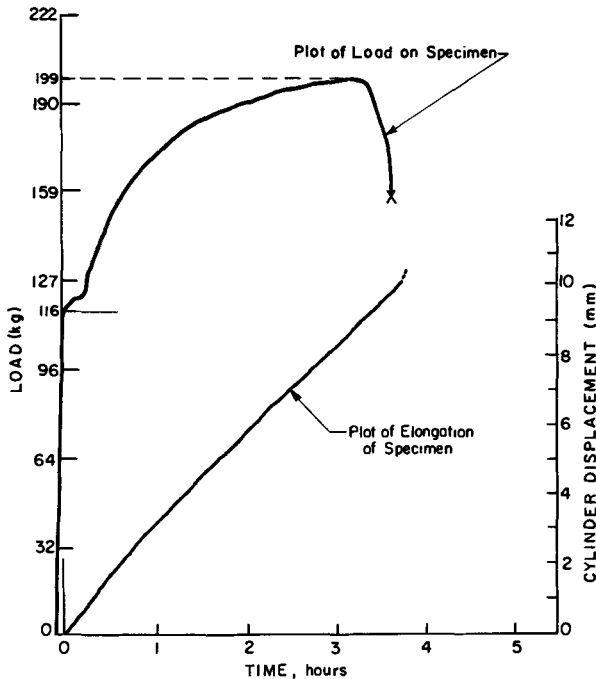


FIG. 4—Load and displacement versus time. This recorder plot represents a strain rate of $1.4 \times 10^{-5}\text{s}^{-1}$.

The degree of nonlinearity of the time-elongation measurements was studied to determine how to achieve the closest approach to a constant strain rate. The major factor affecting the shape of the time-elongation curve is due to the load of the specimen on the load applied by the hydraulic cylinder. It was determined that the curve could be straightened significantly by applying a pressure to the cylinder such that the applied load at that pressure exceeds the maximum load of the specimen by a factor of 2. The resulting line showed less than 5 percent deviation from the mean. For specimens such as the low carbon steels, there were no problems in the range of strain rates needed. However, for steels with tensile strengths greater than 0.621 GPa (90 ksi), it became necessary to use cylinder pressures above 3.45 MPa (500 psig), and strain rates less than $5 \times 10^{-6} \text{s}^{-1}$ were not obtainable with the present control circuit. As a compromise for the less than linear curves, it was decided that the slope at the midpoint best represented the strain rate for a given test.

Three solutions to the problem of testing high strength steels are available. The first is to reduce the cross-sectional area of the specimens. However, this might present problems in machining.

The second alternative is to use a larger hydraulic cylinder. The present device uses a 5-cm (2-in.) bore cylinder. A 10-cm (4-in.) bore cylinder was determined to be adequate for testing alloys with tensile strengths up to 1.38 GPa (200 ksi).

The third alternative is to use a pressure regulator in series with the needle valve to maintain a constant low pressure across the valve.

The repeatability of strain rates with the same control valve settings was poor in the present system. In practice, control could be accomplished by manual correction of the fine control valve setting during the initial part of the test.

SCC Test Results

The SCC tests were made with AISI Type 304 stainless steel specimens in boiling 45 percent MgCl_2 solution at 155°C (311°F) according to ASTM Recommended Practice for Performing Stress-Corrosion Cracking Tests in a Boiling Magnesium Chloride Solution (G 36).^{3,4} Figure 5 shows typical specimens before and after the test, together with a specimen that had been tested in air at room temperature. The specimen from the MgCl_2 test shows the secondary cracks and low reduction of area typical of SCC tests by the slow strain-rate technique.

The relationship between the strain rate and the percent elongation in Fig. 6 clearly illustrates the SCC effect of a boiling MgCl_2 solution on an

³Casale, I. B., *Corrosion*, Vol. 23, 1967, pp. 314-317.

⁴Streicher, M. A. and Sweet, A. J., *Corrosion*, Vol. 25, 1969, pp. 1-6.

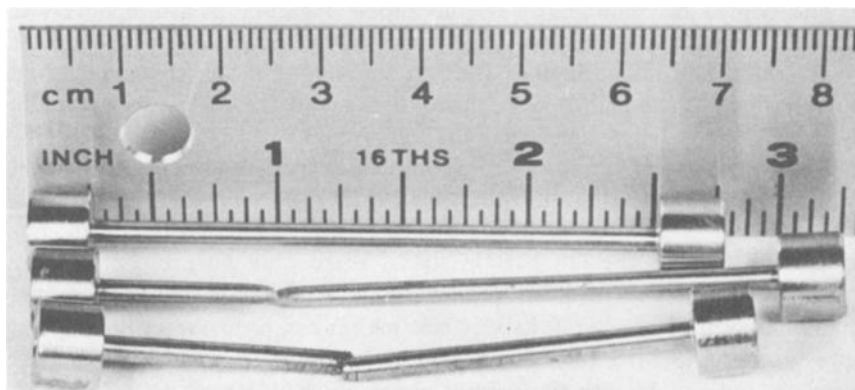


FIG. 5—Specimens before and after test. Top: before test; middle: air at room temperature; and bottom: $MgCl_2$ at $155^\circ C$ ($331^\circ F$) (note secondary cracks).

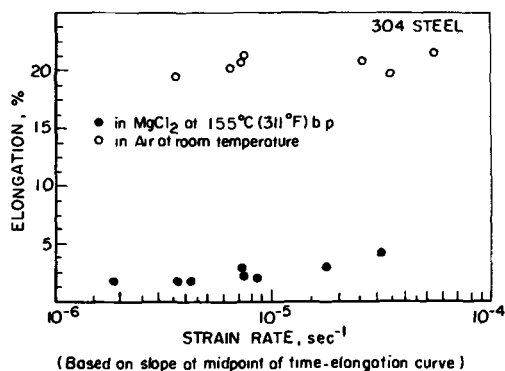


FIG. 6—Elongation versus strain rate.

austenitic stainless steel. The reduction in the percent elongation for $MgCl_2$ versus air exceeds 75 percent. Accuracy was determined to be within 5 percent for the elongation. In Fig. 7 the effect of a boiling $MgCl_2$ solution on the ultimate tensile strength was equally pronounced. This figure also illustrates the tendency for the $MgCl_2$ and air test results to converge as larger strain rates are used. The higher strain rates allow less time for corrosive action to occur and, hence, the tendency is for ductility to dominate the failure mode.

Conclusions

The portable test device was shown first to operate successfully based upon initial tension tests on low carbon steel specimens.

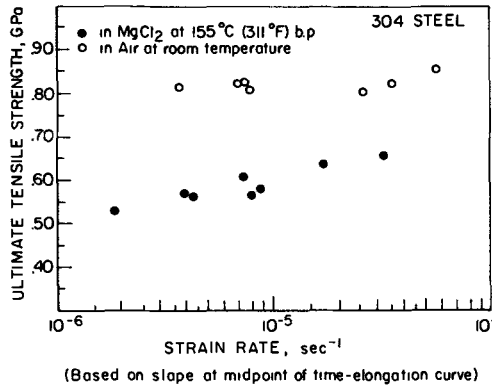


FIG. 7—Ultimate tensile strength versus strain rate.

Preliminary testing for SCC on AISI Type 304 stainless steel in boiling $MgCl_2$ have shown the new test device to be quite useful in SCC studies. Clear indicators of SCC failure are the time to fracture, the ultimate tensile strength and the percent elongation, and visual observations for secondary cracks.

Acknowledgments

The authors acknowledge with appreciation the support of Shell Development Company, research contributions of D. A. Low and V. A. Tejada, and many helpful discussions with E. Haycock.

Bryan Poulson¹

A Bursting Tube, Slow Strain-Rate Stress Corrosion Test

REFERENCE: Poulson, Bryan, "A Bursting Tube, Slow Strain-Rate Stress Corrosion Test," *Stress Corrosion Cracking—The Slow Strain-Rate Technique*, ASTM STP 665, G. M. Ugiansky and J. H. Payer, Eds., American Society for Testing and Materials, 1979, pp. 408-424.

ABSTRACT: The construction of a facility to perform slow strain-rate stress corrosion tests by slowly increasing the pressure in a tubular specimen is described. Advantages of this bursting tube stress corrosion test are outlined and preliminary results reported.

KEY WORDS: stress corrosion cracking, strain rate, bursting, failure, ductility, high pressure, high temperature

The origins of slow strain-rate stress corrosion cracking (SCC) tests are rather obscure but Nikofova [1]² appears to have been first to suggest their use. However, it is due to Parkins et al [2-4], and Scully et al [5,6] that slow strain-rate SCC tests have become accepted as an important technique. Historically, the work by Parkins et al developed from experiments to determine the stress at which cracks first initiate; the work by Scully et al evolved from the faster straining electrode electrochemical technique developed at Cambridge [7].

Indig and Vermilyea [8] appear to have been first to extend the use of slow strain-rate SCC tests to high temperature and pressures. Their apparatus consisted of a modified tensometer mounted on top of an autoclave pulling the specimen inside through a sliding seal; the specimen was insulated from the grips by oxidized zirconium. Numerous other cells have since been designed and these can be of the three basic types as shown in Fig. 1. The problems in using such cells is that polytetrafluoroethylene (PTFE), which is the most versatile material for the sliding seal, is limited

¹Group leader, Corrosion, NEI, Clarke Chapman Power Engineering Ltd., Advanced Technology Division, Gateshead, Tyne and Wear, England.

²The italic numbers in brackets refer to the list of references appended to this paper.

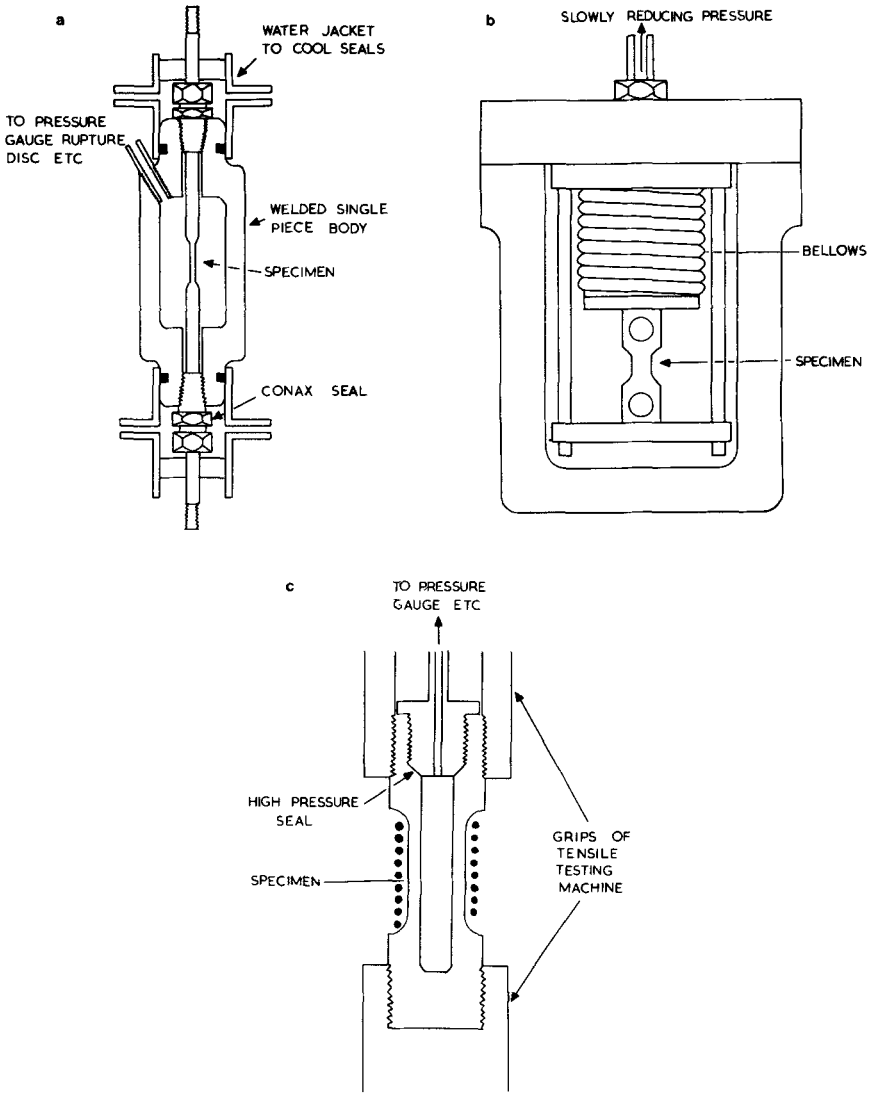


FIG. 1—Types of slow strain-rate cells for high pressure, high temperature applications: (a) sliding seal cell, (b) bellows arrangement, and (c) stressed autoclave design.

to about 537 K while insulation using oxidized zirconium is only suitable for relatively mild environments. However, a more basic limitation is that the environment of interest must be brought to and contained in a special cell on a suitable tensometer. This is quite suitable where the environment of interest is known and can be reproduced, but in many situations it would be advantageous to perform *in-situ* SCC tests. Simple side-stream

nonreturnable loops have been used, for example, to bring liquid ammonia to a slow strain-rate test facility [9], but are in general rather limited.

Bearing these technical and practical limitations in mind, it was decided to develop a facility which would allow the pressure in a tubular specimen to be slowly increased until failure occurred, for example, a bursting tube stress corrosion test [10].

Experimental

To achieve the very slow rates of pressure increase required to cause cracking, a pressurizing system was designed around a piston screw pump capable of generating 207 MPa (30 000 psi); this is shown in Figs. 2 and 3. The pressure generator is driven by a geared-down motor fitted with a time switch. This allows bursting times of between 900 and 28 800 s (15 min and 20 days) to be obtained. The output (0 to 5 V) from the pressure transducer is recorded on a chart recorder and a data logging system. The rupture disk, high pressure connectors, and other components are rated at 207 MPa (30 000 psi) or higher. The entire system, except the drive to the pressure generator and the stem of the pressure relieving metering valve, is contained in a safety enclosure. Initial tests were carried out with the environment around the specimen contained in a flat bottomed flask. Preliminary high pressure, high temperature tests under freely corroding conditions utilized a simple capsule type containment (Fig. 4). All other tests were performed in a Nimonic 75 autoclave with the specimen insulated

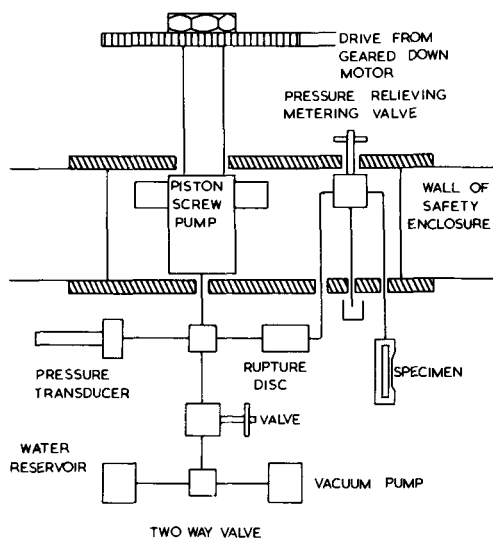


FIG. 2—Schematic diagram of bursting tube SCC facility.

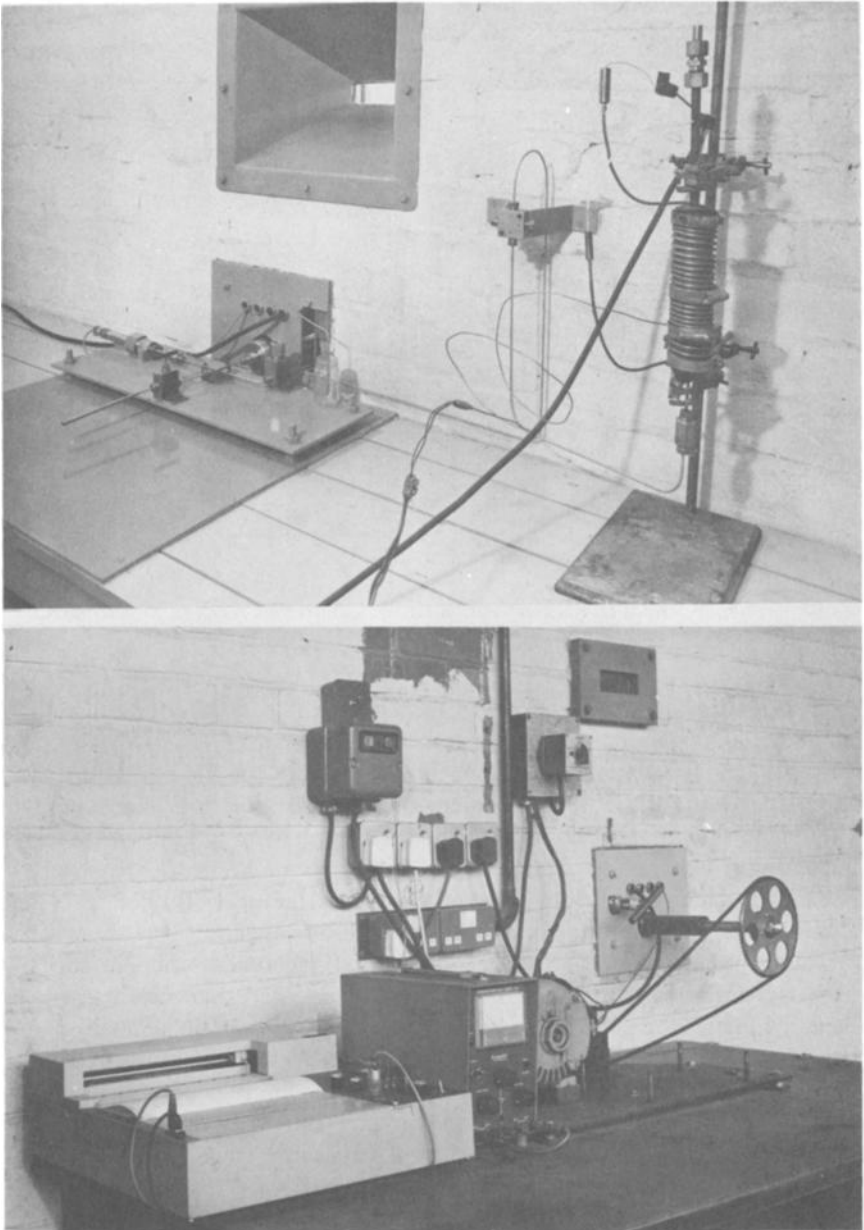


FIG. 3—View inside (top) and outside (bottom) safety enclosure showing bursting tube facility.

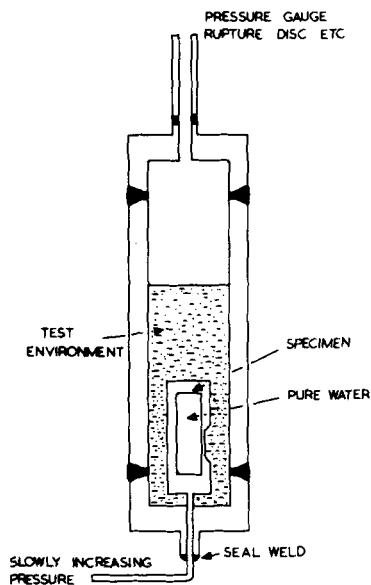


FIG. 4—Simple capsule type of containment for preliminary high pressure, high temperature tests.

from the autoclave by a cold PTFE seal and with facilities for controlling its potential available.

A tubular specimen, with a machined flat on one side (Fig. 5), was used. It is more difficult to calculate the bursting pressure of the tubular specimen, than it is a conventional specimen having a uniform reduced gage length (where the "thin walled" formula can be used). However, it is easy to machine accurately and it eliminates the possibility of specimen fragmentation and minimizes the required pump capacity.

The components of the capsule were first machined, the pressurizing tube was brazed in, the capsule was welded up, and then heat treatment began. Finally, the gage area was polished down to grade 600 emery paper prior to electropolishing for 600 s at 30 V in acetic acid plus 10 percent perchloric acid, and metallographically examined before being tested.

Prior to the start of the test, the pressurizing circuit was thoroughly evacuated and filled with pure water. During the time for the external environment to heat up, the pressure rise in the pressuring circuit—due to the thermal expansion of the water—was controlled using the metering valve. When the external conditions were stable, the motor drive was started. On specimen failure, a microswitch on the recorder operated a relay which turned off the power.

The analysis and mechanical properties of the Type 316 stainless steel

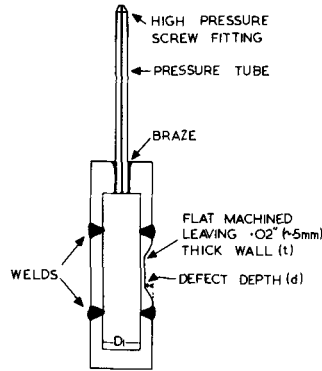


FIG. 5—Specimen design.

and the 9Cr-1Mo steel tested are shown in Table 1. The Type 316 stainless steel was solution annealed at 1323 K for 1800 s in flowing argon; the 9Cr-1Mo steel was tested as normalized (1800 s at 1223 K) or after subsequent tempering for 1800 s at 1023 K. The environments used in this investigation are detailed in Table 2.

Results

Typical pressure-time curves are shown in Fig. 6. Such curves are very similar to load-time curves obtained in conventional slow strain-rate tests. These are however two interesting features: (a) the pressure-time curve does not bend over just prior to fracture, and (b) after the initial leak, surprisingly high pressures can still be supported.

The results of all the bursting tube tests are collected in Table 3. Tests in which SCC occurred and the time to fail ratio (Tf ratio = time to fail in test environment/time to fail in inert environment) was small were as expected, associated with little or no bulging (Fig. 7). This is equivalent to a low reduction in area in a conventional slow strain-rate test.

Metallographic and fractographic features of failures (Fig. 8) were typical of what would be expected in a normal SCC test. It is interesting that no damage to the fracture surface appears to have been caused by the escaping high pressure liquid.

Discussion

Bursting Pressures and the Possibility of Fragmentation

The specimen used in this work (Fig. 5) is essentially thin walled over a small area with the rest of the specimen providing a restraining influence.

TABLE 1—Analysis and mechanical properties of steels used.

	C	Mn	Si	S	P	Ni	Cr	Mo	$\sigma_{0.2\%PS}$	MPa	σ_{UTS}
Type 316 stainless steel	0.05	1.58	0.5	0.012	0.025	12.04	17.63	2.53	260	600	600
9Cr-1Mo normalized	0.1	0.47	0.44	0.017	0.017	...	9.02	1	1188	1394	1394
Normalized and tempered	0.1	0.47	0.44	0.017	0.017	...	9.07	1	520	660	660

NOTE—

PS = proof stress, and

UTS = ultimate tensile strength.

TABLE 2—Solutions used.

Solution Designation	Composition	Temperature, K
MgCl ₂	MgCl ₂ boiling at 427 K ~ 45 weight %	427
8 M NaOH	320 g/litre NaOH, deoxygenated	573
0.5 M NaOH	20 g/litre NaOH, deoxygenated	573
Pure water	initially conductivity < 0.1 μ S, (Cl ⁻) < 2 ppb to which is added 20 ppb N ₂ H ₄ and NH ₄ OH to pH 9.1 to 9.5	573
Pure water + O ₂	as pure water but oxygenated with pure O ₂ for 3600 s prior to test	573

NOTE—

N₂H₄ = hydrozene, and
 NH₄OH = ammonium hydroxide.

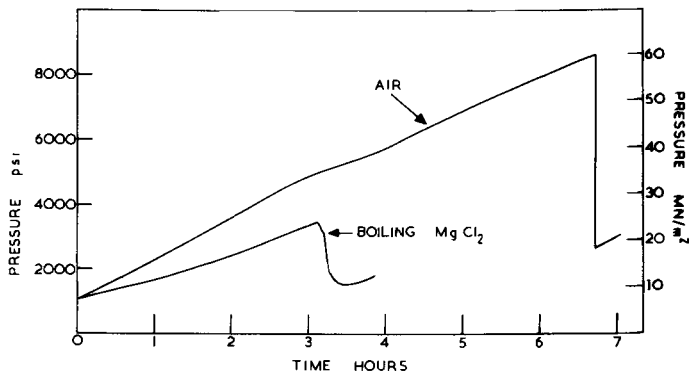


FIG. 6—Typical pressure-time curves.

Bursting pressures have been calculated using four different formulae; these pressures are compared with observed values in Table 4. The reproducibility of experimental bursting pressures is good. All the calculated bursting pressures are lower than the experimental value, the thick walled with longitudinal notch formula giving the best correlation. This poor correlation between calculated and measured bursting pressures is probably due to the thin walled region being restrained by the rest of the specimen. It does not invalidate the test in any way but makes prediction of bursting pressures for a given wall thickness less accurate. Even with the normalized and hard (VHN 460) 9Cr-1Mo steel specimen fragmentation did not occur (Fig. 9).

Comparison with more Conventional Tests

Although the tests reported here are of a preliminary nature, some comparison with more conventional tests can be made. The time to fail ratio

TABLE 3—Results of bursting tube SCC tests.

Alloy	Environment	Time to Fail, s	Time to Fail, (h)	Time to Fail Ratio	Maximum Pressure, MPa	Failure Mode
Solution annealed, Type 316 stainless steel	air	24 120	(6.7)	...	59.3	ductile
	MgCl ₂ boiling at 427 K	11 160	(3.1)	0.4	22.7	SCC with no bulging exten- sion cracking
	pure H ₂ O	28 080	(7.8)	1	58.6	ductile
	0.5 M NaOH } at 573 K	25 200	(7)	0.9	57.2	some bulging but extensive surface SCC
Normalized and Tempered 9Cr-1Mo	8 M NaOH	8 280	(2.3)	0.29	24.8	extensive SCC, no bulging
	pure H ₂ O at 573 K	50 400	(14)	1	86.8	ductile
Normalized 9Cr-1Mo	pure H ₂ O + O ₂ at 573 K	50 040	(13.9)	1	84.1	ductile
	air	72 000	(20)	...	135.1	ductile
	8 M NaOH at 573 K	34 550	(9.6)	0.48	70.3	no bulging, single crack

NOTE—Time to fail ratio = (time to fail in test solution)/(time to fail in inert environment).

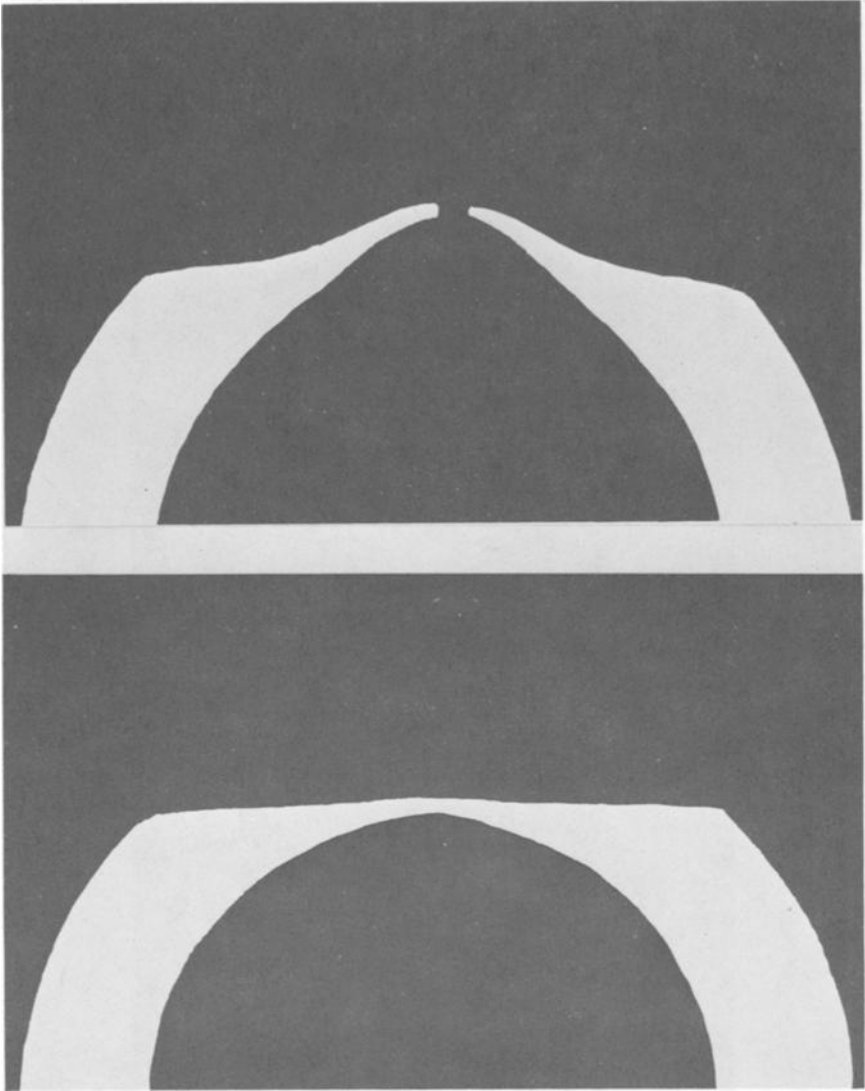


FIG. 7—Photomicrographs of Type 316 stainless steel specimen after a bursting tube test in: (top) air, and (bottom) $MgCl_2$ boiling at 427 K.

(Tf ratio) of bursting tube tests (Tf ratio = 0.46) and conventional slow strain-rate tests at $10^{-5} s^{-1}$ (Tf ratio = 0.39) for Type 316 stainless steel in magnesium chloride ($MgCl_2$) boiling at 427 K is similar. The low resistance (Tf ratio = 0.5) of hard and possibly sensitized normalized 9Cr-1Mo steel to cracking in 8 M caustic solution at 573 K under freely corroding conditions is in accordance with the available data [12], as is the

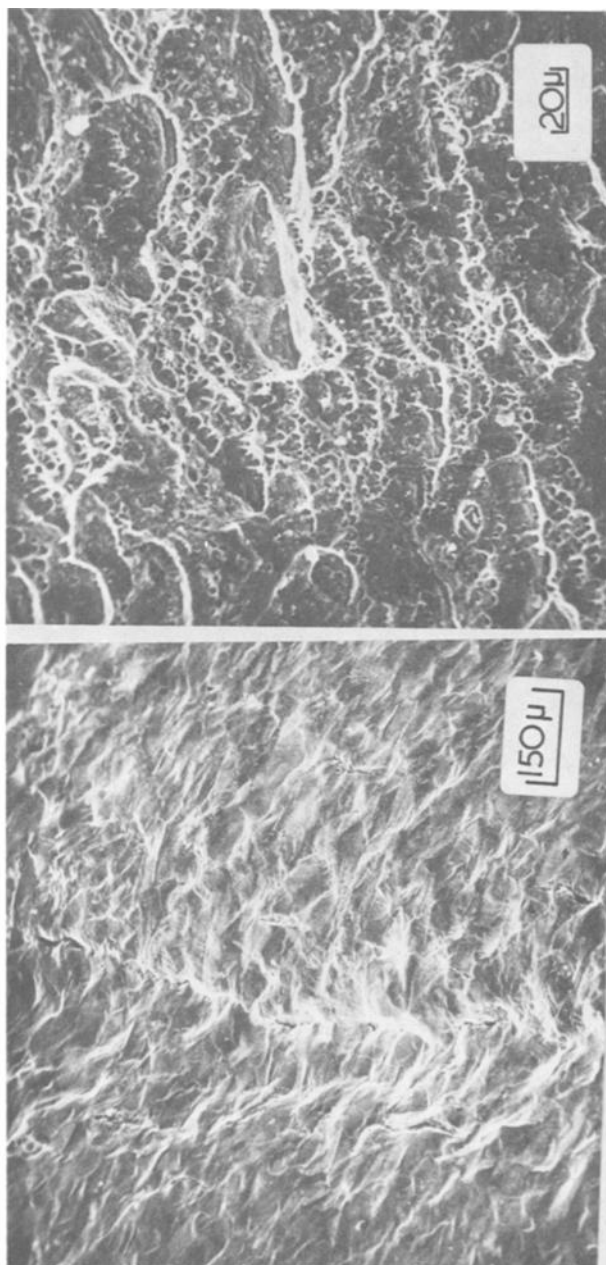




FIG. 8—Typical metallographic and fractographic features of Type 316 stainless steel specimens burst in air (a), (b) $MgCl_2$ boiling at 427 K, (c), (d).

TABLE 4—Experimental and calculated bursting pressures.

Material	Experimental	Thin Walled	Thick Walled with Longitudinal Notch [13]	Lames Equation	Faupels Relationship
	MPa (psi)	$P_b = \frac{\sigma_{UTS} \times 2 \times t}{D_i}$	$P_b = 1.08(\sigma_{UTS} - \sigma_y)F$	$P_b = \sigma_{UTS} \frac{K^2 - 1}{K^2 + 1}$	$P_b = \frac{2}{\sqrt{3}} \cdot \sigma_y \left(2 - \frac{\sigma_y}{\sigma_{UTS}} \right) \ln K$
Type 316	59.2 (8600) 58.6 (8500)	47 (6850)	45 (6800)	46 (6700)	36 (5200)
Normalized 9Cr-1Mo	135 (19600)	88 (12700)	114 (16460)	86 (12500)	98 (1420)
Normalized and Tempered 9Cr-1Mo	86.2 (12500) 86.8 (12600) 84.1 (12200)	42 (6100)	51 (7520)	41 (6000)	45 (6600)

NOTE—

K = outer radius/inner radius,

t = wall thickness,

P_b = bursting pressure,

D_i = inside diameter,

K_m = mean diameter,

C = half defect length,

R = mid-wall radius,

σ_y , σ_{UTS} = 0.2% proof stress and ultimate stress,

d = defect depth, and

M = stress magnification at crack tip, defined by Folias [14] which contains a term C^2/Rt .

$$F = \left\{ \frac{\frac{t}{d} - 1}{\frac{t}{d}} \times \frac{2t}{\frac{t}{d} - 1} \times \frac{Dm}{M} \right\}$$

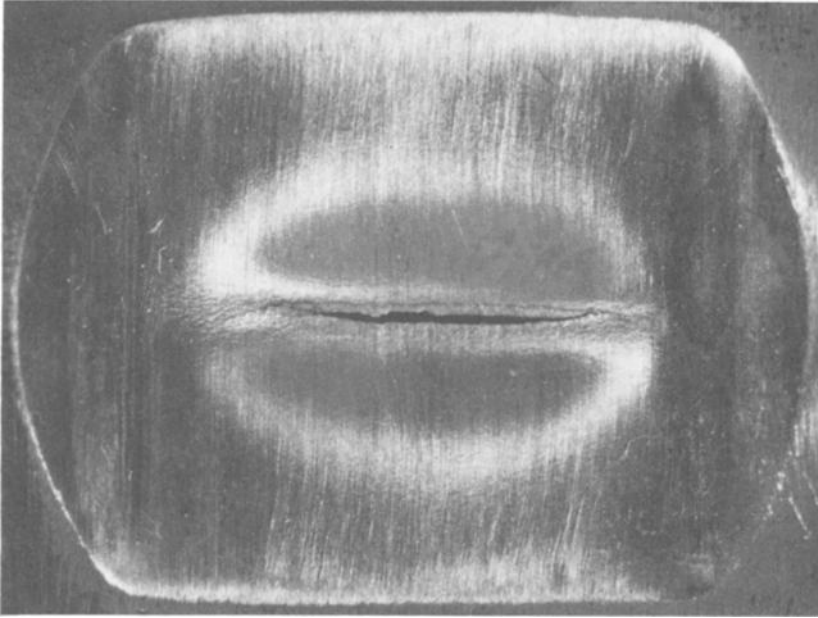


FIG. 9—*Lack of fragmentation in normalized 9Cr-1Mo specimen.*

high resistance of the same steel, when normalized and tempered, to cracking in "pure water" at 573 K. The high susceptibility of Type 316 stainless steel to 8 M sodium hydroxide (NaOH) at 573 K is also in accordance with both practical [15] and experimental [16] results. Finally, the metallographic and fractographic features were identical to those observed in normal SCC tests.

Advantages and Applications

A facility has been designed in which slow strain-rate tests are carried out by increasing the pressure inside a tubular specimen until it bursts. As indicated earlier this has the advantage over conventional high temperature, high pressure tests that the problems of a sliding seal and insulation are eliminated. Furthermore, this type of test has the advantage that it could be used as a rapid and severe *in-situ* SCC test. Probably a more suitable test for monitoring the possibility of cracking over long period would be to use a thin walled capsule at a high mean stress with a small cyclic stress superimposed. Parkins [17] has showed that for mild steel in carbonate-bicarbonate environments, small cyclic stresses promote intergranular SCC. This effect has only been examined in a limited number of material-environment combinations [18] but is to be expected to be a

general finding. In such a specimen, initiation would be nearly synonymous with failure and could be detected by a pressure sensor fitted with an alarm. Both types of tests could utilize a pressure balanced type of access fitting to allow on-line insertion and retraction of the specimen.

Since the specimen is hollow, it should prove possible to install a high energy heater inside and examine the effect of heat transfer. A further extension would be to form a layer of porous corrosion products on the specimen. This would allow wick boiling [11] and thus solute concentration to occur. The bursting tube type of test could also be used to generate the much higher strain rates which are used in yielding electrode [7] or strain transient studies. In this type of test, a specimen is usually held at constant potential and the current recorded while it is rapidly strained. The strain rates utilized (Fig. 10) are much too rapid to allow stress corrosion to occur but its possible occurrence can usually be predicted from the current increase obtained during straining. Such rapid strain rates could be achieved by a minor modification to the existing equipment, and we are also examining the possibility of building up a high pressure in an accumulator and then suddenly opening this to the specimen to provide a more rapid strain transient. A further modification, which will be incorporated in the near future, is a feedback loop. This will measure the pressure rise in the specimen and compare and adjust this if it deviates from the required rate of increase. Finally, the facility was of a similar cost to

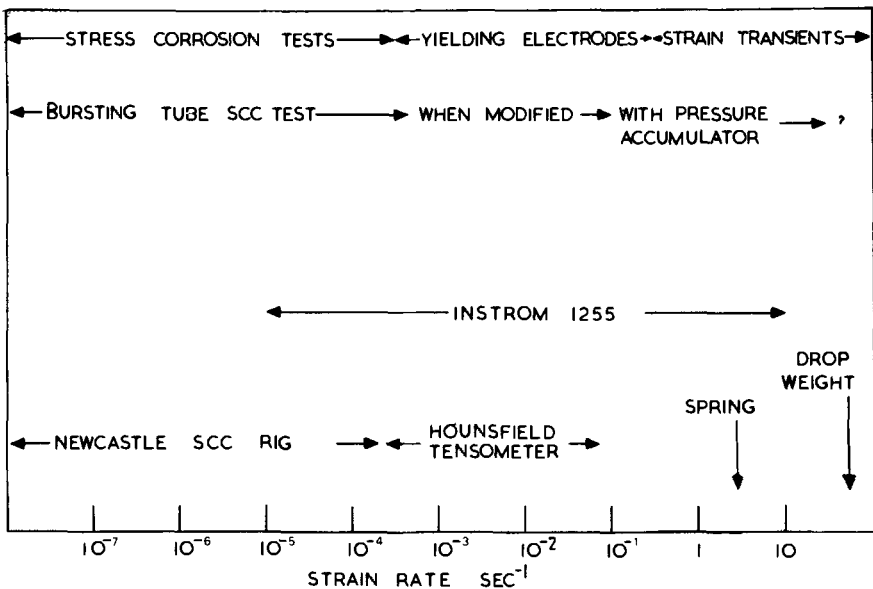


FIG. 10—Range of strain rates utilized in: slow strain-rate tests, yielding electrodes and strain transients.

a conventional slow strain-rate tensometer plus load cell. However, for high-pressure high-temperature applications it has the advantage that it only needs a simple modification to an existing autoclave to allow it to be used.

Conclusion

A new form of slow strain-rate SCC test has been designed in which the pressure in a hollow cylindrical specimen is slowly increased until it ruptures. A facility has been constructed which allows these "bursting tube" SCC tests to be performed. Preliminary results appear in reasonable agreement with more conventional tests. Advantages of this test are the elimination of the insulation and sliding seal problems of conventional high temperatures slow strain-rate SCC tests. More importantly the "bursting tube" SCC test offers the possibility of performing *in-situ* slow strain-rate tests with the opportunity of incorporating heat transfer effects and concentration processes due to "wick boiling."

Acknowledgments

The author thanks the management of Clarke Chapman Limited and the Central Electricity Generating Board, who have been associated with this work, for permission to publish the outcome of the development and the results.

References

- [1] Nikofoorova, K. in *Stress Corrosion of Metals*; Romanov, V. V. Israel Program for Scientific Translations, Jerusalem, 1961, Office of Technical Services, U.S. Department of Commerce, Washington, D.C.
- [2] Henthorn, M. and Parkins, R. N., *Corrosion Science*, Vol. 6, 1966, p. 357.
- [3] Humphries, M. J. and Parkins, R. N., *Corrosion Science*, Vol. 7, 1967, p. 747.
- [4] Syrett, B. S. and Parkins, R. N., *Corrosion Science*, Vol. 10, 1970, p. 197.
- [5] Powell, D. T. and Scully, J. C., *Corrosion*, Vol. 24, 1968, p. 151.
- [6] Scully, J. C. and Powell, D. T., *Corrosion Science*, Vol. 10, 1970, p. 371.
- [7] Hoar, T. P. and West, J. M., *Proceedings*, Royal Society, Vol. 268A 1962, p. 304.
- [8] Indig, M. E. and Vermilyea, D. A., *Proceedings*, International Conference on High Temperature and Pressure Electrochemistry, R. W. Staehle et al, Eds., National Association of Corrosion Engineers, Houston, 1977.
- [9] Poulson, B. and Arup, H., *Proceedings*, 7th Scandinavian Corrosion Conference, SINTEF Trondheim, 1976.
- [10] Poulson, B., Paper presented at Conference on Corrosion Testing and Monitoring, London, 1977, to be published by Institution of Corrosion Science and Technology.
- [11] Mann, G. M. W., CERL Report RD/L/N124/75, Central Electricity Generating Board, 1975.
- [12] Poulson, B., *Proceedings*, British Nuclear Energy Society Conference on Ferritic Steels for Fast Reactors, London, 1978.
- [13] Guest, J. C. and Hutchings, J. A. G., "Creep and Fatigue in Elevated Temperature Applications," Institution of Mechanical Engineers, Conf. Paper C221/73, London, 1974.

- [14] Folius, E. S., Aerospace Res. Labs. Report ARL-64-17, Oct. 1964.
- [15] Rosendahl, C. H., The Swedish Ironmasters Information Meeting, May 1960.
- [16] Poulson, B. and Gartside, H., submitted to *British Corrosion Journal*, Dec. 1977.
- [17] Parkins, R. N., paper published on 5th Symposium on Line Pipe Research, American Gas Association, Cat. No. L30174, 1974.
- [18] Greenwell, B., Ph.D. thesis University of Newcastle-upon-Tyne, 1977.

*R. S. Treseder*¹

General Discussion—Historical Note on the Slow Strain Testing of Solder

This is a historical note describing an early experience of Aaron Hachter, Ross Miller, and the writer with slow strain-rate stress corrosion testing. In 1945 there was some concern about the possibility of stress-related corrosion effects on the soldered joints in automobile radiators when sodium nitrite was used as a corrosion inhibitor in the radiator coolant. The accepted method of determining stress corrosion cracking (SCC) susceptibility in those days was to make tests using U-bend specimens. Obviously, this technique was not compatible with the mechanical properties of solder. Therefore, a test method was devised; this method was called a creep corrosion test. The specimen was a 50.8 mm long by 3.2 mm (2 by $\frac{1}{8}$ in.) diameter rod of 50-50 solder (50Sn, 50Pb) with brass end pieces. The specimen was loaded in tension by a 0.34 kg (0.75 lb) steel weight. Figure 1 shows the simple apparatus that was used.

In a typical test with tap water at 65°C (149°F), the load resulted in a specimen elongation of about 80 percent in 19 days. The test was ended when the weight reached the bottom of the glass cylinder. The load on the specimen corresponded to an initial stress of about 0.3 MPa (50 psi), and the average strain rate of about $5 \times 10^{-7} \text{ s}^{-1}$. The specimen had uniform elongation with no visible cracks. With sodium nitrite present, the specimen showed numerous transverse cracks. Figure 2 shows results of tests in air, tap water, and sodium nitrite solutions.

Using this test method it was learned that the cracking of solder in sodium nitrite solutions did not occur if there was no galvanic coupling with other metals. It was also found that cracking could be inhibited by the addition of disodium phosphate at a concentration about equal to the sodium nitrite concentration.

¹Consulting corrosion engineer, Oakland, Calif. 94611.

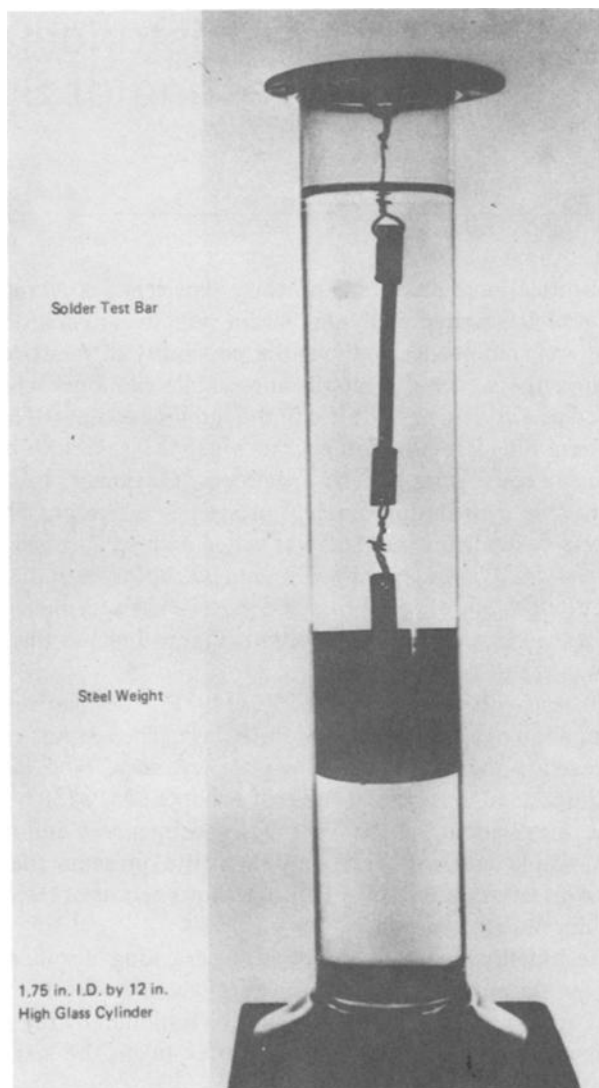


FIG. 1—Apparatus for stress corrosion test of solder. (1 in. = 25.4 mm.)

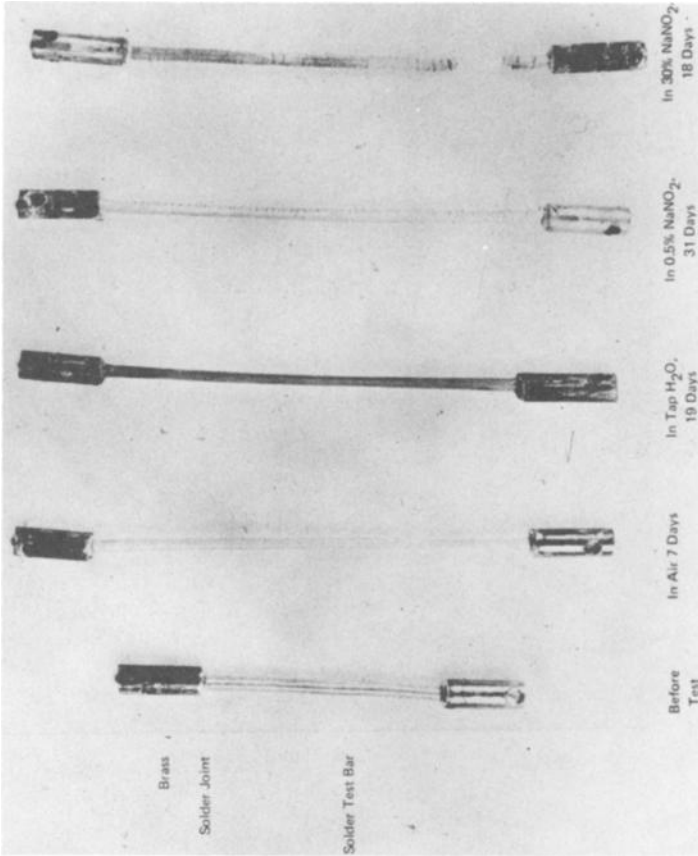


FIG. 2.—Test bars from stress corrosion tests of solder.

Summary

Summary

The papers in this publication are divided into four sections based on their principal subject matter. First, papers are presented which deal primarily with the background and interpretation of the slow strain-rate test technique. Second, applications of the slow strain-rate test to specific environments and, in particular, industries are described. Third, application of the slow strain-rate test to specific metals and alloys are described, and fourth, slow strain-rate test equipment and procedures are discussed. Thus, the reader is guided from a general treatment of the theory and practice of the slow strain-rate test technique through specific applications, and finally to a description of the test method itself.

An excellent treatment of the role of strain in the stress corrosion cracking (SCC) process is presented by Parkins. The concept of critical strain rate is developed, and the contribution of plastic strain to SCC in constant load tests is recognized. The relationship between slow strain-rate tests and constant load tests is discussed. Papers by Diegle and Boyd, and Hishida et al discuss the role of two other principal phenomena in the SCC process, namely, film rupture and anodic dissolution at the crack tip. The evaluation and interpretation of slow strain-rate tests is discussed by Payer et al. Several parameters to quantify SCC susceptibility are presented.

Applications of slow strain-rate tests to SCC in specific environments and specific industries are presented in the second section. Theus and Cels discuss caustic SCC studies related to nuclear steam generator and fossil boiler materials. Favorable comparisons were found between slow strain-rate tests, U-bend tests, and service experience. Kim and Wilde discuss SCC of carbon steel in ammonia. Ugiansky and Johnson describe slow strain-rate tests in gaseous atmospheres at elevated temperatures from 450 to 600°C. Slow strain-rate tests of stainless steels in high temperature, high purity water are discussed by Solomon et al. Clarke et al discuss the slow strain-rate test for rapid screening of susceptibility to intergranular SCC in high purity, oxygenated water at 289°C. Slow strain-rate test results are correlated with long term, constant load test results. Indig presents slow strain rate results for Incoloy Alloy 800 and 21/4Cr-1Mo steel in 5 or 10 percent sodium hydroxide (NaOH) at 316°C. The results are applied to materials selection for liquid metal fast breeder reactor (LMFBR) steam generators. Ondrejcin presents results of slow strain-rate tests used to select temperature and composition limits for storage of nuclear wastes in carbon steel tanks. Payer et al

describe the extensive use of slow strain-rate tests to prevent and control SCC of carbon steel in gas transmission pipelines. The technique was used to evaluate the temperature and composition limits of SCC, and it contributed to the identification of SCC inhibitors and development of pipeline coatings for SCC control.

In the third section, papers deal primarily with applications to specific metals and alloys. A broad range of alloys were studied. Scully presents results for titanium, brass, and zircaloy. Ugiansky et al studied SCC of aluminum alloys and compared slow strain-rate results with more conventional constant load test results. The effects of oxyanions and chloride on SCC of admiralty brass were determined by Kawashima et al. The effects of strain rate, solution temperature, and solution composition on the SCC of nickel-base and cobalt-base alloys was determined by Asphahani. Abe et al applied slow strain-rate technique to the study of SCC of sensitized stainless steel in high temperature water. Mom et al studied the effect of solution parameters and inhibitors on the SCC of austenitic, martensitic, duplex ferritic-austenitic, and ferritic stainless steels. The effect of heat treatment on SCC of a cast, low carbon, martensitic stainless in 3 percent sodium chloride was determined by Suery. Buhl compared slow strain-rate test results with constant load test results for several alloys and found good agreement for titanium alloys, high alloyed chromium stainless steels, and chromium-nickel stainless steels. Daniels compared slow strain-rate test results with other SCC tests for austenitic stainless steel in chloride solutions. Andrew et al describe applications of the slow strain-rate test technique for 12 percent chromium precipitation hardening stainless steel and 70-30 brass.

Equipment for slow strain-rate testing is described in the final section. Multiple-specimen test equipment is described in papers by Nutter et al and Lyle and Norris. Hauser et al describe a portable slow strain rate test device for use in the laboratory or a plant. Poulson describes a bursting tube test technique.

Certain general remarks also seem appropriate. Perhaps the first thing to point out is that if there was a perfect test method for stress corrosion cracking, we would all be using it exclusively. The fact that we use a variety of testing methods indicates that there is not a single, perfect method. The slow strain-rate technique is not the answer to every SCC problem. It is, of course, really no greater in its impact than that of the effort that is put into it by the user.

Many of the problems associated with slow strain-rate testing are dealt with in several of the papers in this volume. It is worth reminding ourselves that many of the points made could be made equally well for many other methods of testing. The problems that we get into with slow strain-rate testing are not necessarily uniquely a function of that test method. There are other methods where essentially the same problems exist. This is pointed out here because there is always the chance with a new technique like slow strain-

rate testing that some people will expect too much of the test. We have gone through this exercise before in relation to, for example, the precracked, fracture mechanics type test for SCC. There are very obvious limitations on slow strain-rate testing as observed in practice. For example, it does not give a stress or stress intensity at least in simplest form that the engineer can use directly in design calculations. The very difficult problem that remains is that of trying to relate the slow strain-rate type of testing to practical or engineering decisions. This is obviously an area on which we will still have to continue to work.

In spite of the challenges present for improving the slow strain-rate technique, it is an extremely powerful technique as is attested to by the many papers in this volume. One of the major advantages of this test is the fact that results are obtained very quickly, in a matter of a couple of days. Certainly if progress continues with slow strain-rate testing as it has in the last few years, this technique will contribute greatly to our knowledge of the mechanisms for SCC and will give us a rapid test method for SCC testing.

We gratefully acknowledge the contributions of Professor R. N. Parkins to the slow strain-rate technique, to the symposium, and to this publication.

G. M. Ugiansky

National Bureau of Standards, Washing-
ton, D.C. 20234; editor

J. H. Payer

Battelle Columbus Laboratories, Columbus,
Ohio 43201; editor

INDEX

A

- Alternate immersion test, 254
- Aluminum alloys
 - DTD 5020A, 340
 - DTD 5050B, 340
 - DTD 5090, 341
 - 2124 aluminum alloy, 255, 257
 - 2124-T851 aluminum alloy, 256, 257, 258, 260, 261, 262
 - 7075 aluminum alloy, 255, 258, 259, 263, 264
 - 7075-T6 aluminum alloy, 261, 265
- Ambient environment, 172
- Anodic dissolution, 47
 - Rates, 54, 55

B

- Beam deflection, 12, 14, 15
- Boiling water reactor materials performance, 149
- Box-Behnkin series, 214
- Brass, admiralty in
 - Nonammoniacal aqueous solutions, 266
 - Various solutions, 273
 - Anodic polarization behavior of, 273
 - Cracking mode of, 270
 - Current response of, 274
- Brass, admiralty
 - Photomicrographs of fractured specimens, 271
- Brass, unstressed admiralty, anodic polarization curves of, 269

Brass, 70Cu-30Zn

- Constant load tests on, 367
 - In solution of 1.5 *M* total ammonia and 0.04 *M* total copper, 241, 246, 247
 - Slow strain-rate tests, 368
- Brass, DEF 105
 - Effect of crosshead speed on slow strain-rate test results, 370
- Brass, silicon (alloys 1 to 5) and brass (DEF 105), 367, 369,
 - Constant load and slow strain-rate test results for, 370
 - Mechanical properties and copper contents of, 368
- Brittle fracture, 88
- Brittle mode, 64
- Buried pipelines, 223
- Bursting tube, slow strain-rate stress corrosion test, 408
 - Comparison with conventional tests, 415
 - Facility, schematic diagram, 410
 - Results of, 416

C

- Cathodic, current density, effects of, on hydroxide stress cracking of, 290
- Caustic stress corrosion cracking, 81, 95, 170
- Chemical environment, identification of, 223
- Chloride concentration, effect of, 308

- Cladding, corrosion resistant, 166
 Coal gasification candidate materials, 121
 Coatings, 227
 Quality, 223,
 Cobalt-base alloys, 279
 Constant beam deflection rate tests, 6, 20
 Constant flow stress, 347, 348
 Constant load cantilever beam tests, 12
 Constant load method, 362
 Constant load test, 13, 20, 296, 301, 302
 Constant strain-rate tests
 Calculated environmental effects in, 53
 Comparison of results with conventional testing techniques, 339
 Current densities in, 54
 In 4 *N* sodium nitrate (NaNO_3), 8
 Results on Type 304 stainless steel, 51
 Theoretical analysis, 48
 Copper-beryllium alloys, 238
 Corrosion fatigue, 19
 Crack growth rate, 47, 55
 Crack propagation, 11, 31, 64
 Crack tip, 18, 19, 28, 36, 38, 43, 209
 Region, 13, 16
 Strain rate, 15, 19, 242
 Unfilmed, 31
 Crack velocity, 9, 69, 232, 247
 Cracking kinetics, function of the dissolved oxygen content, 161
 Cracking response, 6, 12
 Creep
 Corrosion test, 425
 Rate of, 12, 20
 Response, 12
 Crevice chemistry effects, 146
 Crosshead speed, 239
 Cross-section metallography, 105
 C-shape specimens, tested in NaOH, 289
 Cyclic loading, 20
- D**
- Dislocation cross slip, 39
 Ductile, 212, 145
 Alloys, 23
 Failure, 17, 18
 Fracture, 6, 55, 247, 359
 Metal, 28
 Rupture, 88
 Steel, 63
 Ductility, 69, 73, 100, 119, 212, 214, 258
 Loss of, 64
 Ductility, specimen, measurement of, 69
 Dynamic strain, 105, 107, 109, 154
 Test, 9, 104, 153, 167
 Dynamic straining stress
 Corrosion test, 149
 Corrosion test facility, 151
 Tests (quality control tool), 167
- E**
- Effective strain rate, 7
 Elastic interactions, 23
 Electrochemical activity, 42
 Conditions for cracking, 12
 Reactions, 18
 Reactivation technique, 155
 Tension test, 206, 210, 214
 Electrochemical factors, 289
 Electrochemical potential, 248
 Electrode potential, 42
 Dependence of, 40
 Elongation to fracture, 247
 Engineering alloys, 27
 Environment, effect of, 224

Environmental deterioration rate,
change of with potential, 48
Environmental stress cracking, 279
Environmentally induced cracking
susceptibility, 321
Environmentally induced degradation,
320

F

Failure mode, effect of potential on,
90, 91
Fatigue precracked specimens, 7
Film formation for, 104
Austenitic stainless steels, 28
Brass, 27
Low strength ferritic steels, 29
Noble metal alloys, 30
Reaction films on alloys, 27
Titanium and titanium alloys, 29
Film, anodic rupture mechanism, 27
Film, chromium-containing passive,
28
Film, rupture, 43, 105
Repetitive, 35, 36, 38
Role of, 26, 38
Film, rupture, classic, 34
Films, corrosion, 26
Fractographic technique, 353
Fractography, 62, 68, 72
Fracture, alloy mode, 349
Fracture, mechanics approach, 55
Mode, 146
Surface, 101

G

Gas transmission pipeline, 223
Glycerine, 307, 308

H

Hastelloy Alloy C-276, 280
C-shape specimens tested in
NaOH, 289
Effects of cathodic current density
on the hydroxide stress
cracking, 290
Effects of cold work, 288
Effects of heat treatment on the
hydroxide stress cracking,
287
Effects of stress level and direc-
tion, 286
Hastelloy Alloy B, 280
Haynes Stellite Alloy No. 6B, 280
C-shape specimens tested in
NaOH, 289
Effects of cathodic current density
on the hydroxide stress
cracking, 290
Effects of cold work, 288
Effects of heat treatment on the
hydroxide stress cracking,
287
Effects of stress level and direc-
tion, 286
Heat treatment effects, detection of,
320
Helium and argon environments, as
"normalizing" environ-
ments, 118
High temperature
Anodic electrochemical studies,
185
Description of test facility, 389
High pressure slow strain-rate
testing, 133, 388
Schematic drawing of test vessel,
390
High temperature water, slow strain-
rate testing procedures in,
133
Hydrogen embrittlement, 26, 36

Hydrogen-induced cracking, 108

Hydrogen, on steel, cathodic charging of, 69

I

Inclusions, 66

Incoloy-800 alloy, 115, 171, 199

Caustic cracking, 184

Polarization curves, 191, 192, 193

Slow strain-rate testing, 183

Straining electrode experiments, 197

Incoloy Alloy 825, 280

Inconel 600, 39, 64, 73, 137

Inconel 671

Optical micrograph, 128

Scanning electron micrograph, 128

Inconel X750, 176

Inhibitors, 226

Effect of, 314

Inhibitors, corrosion, 226

Inhibitor-containing coatings, 227

Instron tension testing machine, 239

Intergranular corrosion, 66

Alloys, resistant to, 157

Intergranular crack, 17

Lengths, 17

Velocities, 19

Intergranular cracking, 21, 22, 55,

119, 141, 146, 147, 359

Intergranular fracture, 18, 121, 247

Intergranular propagation, 64

Intergranular stress corrosion cracks, 12, 13, 21, 39, 132,

214, 296

Propagation, 64

Resistance, 158

Susceptibility, 296

Ionic concentrations, 214

L

Liquid metal fast breeder reactor, steam generator, 170

Load cycling, 19

Load versus specimen elongation, 71

M

Magnesium-aluminum alloy, 13

In $\text{CrO}_4\text{-Cl}$ solution, 15, 17

Manganese-aluminum alloy in $\text{CrO}_4\text{-Cl}$, 18

Metallographic examination, 214

Technique, 353

Treatments, 174

Metallography, 62, 68, 69, 72

Optical, 64, 68

Metals in gaseous atmospheres, 113

Multispecimen test facility, 388

Design and construction of machine, 375

N

Nickel Alloy 600

Current density versus time curves, 327

Electrodes in H_2SO_4 , 85, 88

In NaOH solution, 324, 326, 329

Cracking zone for, 89

Effect of, 89

Influence of metallurgical condition and polarization on reduction of area of, 326

Nickel Alloy 671, stress-strain curves for, 124

Nickel Alloy 800, 85, 88, 119

In NaOH solution

Cracking zone for, 92

Effect of, 89

Scanning electron micrograph, 127

Stress-strain curves, 123

Titanium stabilized, 93
 Nickel alloys, 73
 Nickel-base alloy, 279, 320
 Ni-Co-Cr-Mo alloy, MP35N, multi-phase C-shape specimens tested in NaOH, 289
 Nitrate, alkaline radioactive wastes, polarization curves, 210
 Nitrate stress corrosion, 209, 214
 Nitronic 50 alloy, 155, 167
 Noble metal alloys, 30
 Nonpropagating cracks, 15, 16, 20, 23
 Significance of, 15
 Nonpropagating surface phenomena, 63

O

Oxidizing condition, effect of, 228
 Oxyanions and chloride ion, effect of, 266

P

Passive oxide film rupture, 326
 Passive potential region, 55
 Pipeline coatings, 227
 Pipeline steel, 222
 In caustic solution
 Effect of strain rate, 233
 Effect of temperature and strain rate, 232
 In potassium dichromate, effect of, 226, 227
 In 1 N Na₂CO₃ + 1 N NaHCO₃, 107
 Intergranular stress corrosion cracking range, 225
 Pitting corrosion, 66
 Plackett-Burman series
 Experiments, 212
 Results, 212, 213

Plastic crack tip, 55
 Plastic deformation, 28, 238
 Plastic displacement, 19
 Time dependent, 20
 Plastic strain, 16
 Plastic zone, 7, 15
 Polarization curves, 51, 177
 For 2¼Cr-1Mo alloy, 188, 189, 190
 Polarization tests, 54
 Portable slow strain-rate stress corrosion test device, 399
 Description of apparatus, 400
 Schematic diagram, 400
 Potential, applied, effect of, 102
 Potential control tests, 86
 Potential, corrosion reactions, effects of, 207
 Potentiostatically controlled tests, 317
 Pourbaix diagrams, 54, 267
 Precracked specimen, 19
 Predicting threshold stresses, 14
 Prenotched cantilever-beam specimen, 109
 Purex (221-F) specimen, 214

R

Radioactive waste, 209
 Composition of, 209
 Solutions, 204
 Supernates, ionic concentrations, 210
 Synthetic, analyses of, 211
 Tanks, 209
 Reference electrode, 85
 Repassivation rate of aluminum alloys, 338

S

Sanicro 30, 84
 In NaOH, effect of potential, 93

- Secondary stress corrosion cracks, 66, 68
- Sensitization, 119, 138
- Sensitization resistant alloys, 124
- Shallow surface penetrations, 65, 66
Interpretation of, 65
- Shot peening, 144, 145
- Slow dynamic strain, 5, 12
- Solution heat treatment after welding, 164
- Sour-gas, simulated well environment, 394
- Static load test, 23, 88
- Static loading, 19, 20
- Steel
- AISI 304, 73, 307
 - In $MgCl_2$, fracture strain, 315
 - In $MgCl_2$, specimens, 405
 - Load as a function of elongation, 311
 - AISI 316, 307
 - Fracture strain as a function of temperature, 310
 - AISI 431, 307
 - Chromium (X20-Cr13), in NaCl solution, 342, 344
 - AISI 4130, 392
 - In H_2S-CO_2 , slow strain-rate test results, 395
 - In H_2S-CO_2 , time-to-failure and ductility, 396
 - A202 Grade B, in liquid ammonia, 106
 - A285-B
 - Effect of $NaNO_2$ and NaOH, 219
 - Fracture characteristics of, 216
 - Intergranular cracking of, 215
 - A517 Grade F
 - In air-contaminated ammonia, 109
 - In air-contaminated metallurgical-grade ammonia, 100
 - In liquid ammonia, 106
 - In water-inhibited air contaminated metallurgical-grade ammonia, 100
- Annealed
- $2\frac{1}{4}Cr-Mo$, 195
- Carbon, 63, 70, 73, 227
- ASTM A285-B, 208
 - Base metal, 94
 - In carbonate-bicarbonate solution, alloying additions effect, 231
 - In $1 N Na_2CO_3 + 1 N NaHCO_3$, 11, 65
- Carbon (285-B)
- Anodic potentiodynamic polarization of, 207, 212
 - Variation of strength, 214
- Carbon, annealed, 103
- Carbon-manganese, 9, 10, 14, 17
- In aqueous solution of sodium carbonate and bicarbonate, 12, 105
 - In CO_3-HCO_3 , 15, 17, 22
- Cast martensitic stainless in NaCl solution, influence of tempering temperature and polarization on reduction of area of, 325
- Chromium-molybdenum ($2\frac{1}{4}-1$), 271
- Caustic cracking in, 182
 - Slow strain-rate testing for, 179
- ERW Grade X46 line-pipe
- In air-contaminated metallurgical-grade ammonia, 101
 - In water-inhibited air-contaminated metallurgical-ammonia, 101
- Ferritic-austenitic alloy, 305
- Fracture strain as a function of $MgCl_2$ concentration, 309
- Fracture strain tested in glycerine for, 313
- Maximum load for, 312

- Load as a function of elongation, 310
 - Mild
 - Elongation-electrochemical tension test, 220
 - In 2 *N* (NH₄)₂CO₃, 102
 - Orion 26-1, 307
 - Orion 28-2, 307
 - Stainless
 - Alloy XM-19, 141, 142
 - Creusot-Loire ICL-473 (Type 304) alloy, 155
 - ICL-167 (Type 316), 157
 - ICL-473, 157
 - Kromar D70, 363, 365
 - Susceptibility of, 312
 - (X5CrNi 18 9), 338
 - Stainless, austenitic, 28, 73, 133, 138, 150, 238, 294, 305, 338
 - In MgCl₂ solutions, 308, 345
 - Stainless, martensitic, 305, 320, 323-325
 - In NaCl solution, reduction of area versus strain rate, 324
 - Stress-elongation curves for C-Mn, 8
 - Steel, Type 304 stainless, 48, 50, 59, 85, 88, 132, 153, 155, 157, 349
 - Chemical analysis of, 350
 - Constant strain-rate tests, 56, 57
 - Dynamic strain testing of, 163
 - Exposure to A262E, 144
 - Fracture surfaces of, 141, 146
 - In NaCl, 360
 - In NaOH, 92
 - Intergranular stress corrosion cracking, 165
 - Mechanical properties, 351
 - Polarization curves, 51, 52
 - Steel, Type 304, stainless, sensitized, 296
 - In 10 *N* H₂SO₄ + 0.1 *M* NaCl, 52
 - Steel, Type 308 stainless
 - Effect of heat treatment, 143
 - Exposure to A262E, 143
 - Steel, Type 310 stainless, 115, 119, 121, 124
 - In H₂O/H₂S, 120
 - Scanning electron micrograph, 125
 - Stress-strain curves, 121
 - Steel, Type 310S stainless, 115, 119, 124
 - Stress-strain curves, 122
 - Steel, Type 316 stainless, 153, 412
 - Steel, Type 347 stainless, 115, 119, 124
 - Stress-strain curves, 122
 - Steel, Type 446 stainless, 123
 - Stress-strain curves, 123
 - Steel, Uranus 50, 307
 - Stress-strain curves, 123
 - Steels, fracture strain for, 312
 - Maximum load for, 312
 - Steels, fracture strain for, 312
 - In 4 *N* NH₄NO₃, 9, 10
 - Steels, stainless, susceptibility of, 312
 - Straining electrode, 83
 - Annealed 2¼Cr-1Mo steel, 194
 - Straining electrode experiment, 37, 177, 186
 - Strauss test, modified, 138
 - Stress relaxation, 44
 - Stresses, macroelastic, 359
- T**
- Temperature, effect of, 231, 309
 - Tensile machine, 375
 - Capacity, 376
 - Major components, 378
 - Multispecimen, 377, 380
 - Power drive, 378
 - Schematic drawing, 379, 380
 - Single specimen, 377, 379

- Space, 377
 - Strain rate, 376
 - Tensile strength, 247
 - Tension specimen, diagram of, 208
 - Threshold strain rates, concept of, 16
 - Threshold stress, 13, 18
 - From creep data, 13
 - Time-to-failure studies, 70, 73
 - Time to fracture, 302
 - Titanium alloy, 241
 - In NaCl formamide, 338
 - Precracked in NaCl water, 338
 - Ti-5Al-2.5Sn in NaCl, 42
 - Ti-6Al-4V, 337, 340
 - In aqueous NaCl, 342
 - Titanium-base alloys, 241
 - Titanium-oxygen, 242, 243, 244
 - In aqueous NaCl solution, 242
 - In CH₃OH/HCl solution, 243, 244
 - Ti-13Cr-11V-3Al
 - In CH₃OH/HCl solution, 245
 - Transgranular cracking, 21, 22, 39, 64, 141, 359
 - Transgranular fracture, 18
- U**
- U-bend stress corrosion test, 347, 348
 - Ultimate tensile strength, 212
- W**
- Weld metal, 85, 94
 - Weldments, 158, 172
 - Type 304 stainless steel, 155
 - Type 308L, dynamic strain testing, 158
- Z**
- Zircaloy-2, 245

